Department of Civil Engineering

On structure and rate dependence of Perniö clay

Igor Mataić

Aalto University

DOCTORAL DISSERTATIONS

Aalto University publication series
DOCTORAL DISSERTATIONS 8/2016

On structure and rate dependence of Perniö clay

Igor Mataić

A doctoral dissertation completed for the degree of Doctor of Science (Technology) to be defended, with the permission of the Aalto University School of Engineering, at a public examination held at the lecture hall R2 of the school on 15 January 2016 at 12.

Aalto University
School of Engineering
Department of Civil Engineering
Geoengineering

Supervising professor
Professor Leena Korkiala-Tanttu, Aalto University, Finland

Thesis advisor
Professor Minna Karstunen, Chalmers University of Technology, Sweden

Preliminary examiners
Professor Stefan Larsson, Royal Institute of Technology KTH, Sweden
Professor Vikas Thakur, Norwegian University of Science and Technology NTNU, Norway

Opponent
Professor Tim Länsivaara, Tampere University of Technology TUT, Finland

Aalto University publication series
DOCTORAL DISSERTATIONS 8/2016

ISBN 978-952-60-6617-2 (printed)
ISBN 978-952-60-6618-9 (pdf)
ISSN-L 1799-4934
ISSN 1799-4934 (printed)
ISSN 1799-4942 (pdf)
http://urn.fi/URN:ISBN:978-952-60-6618-9

Unigrafia Oy
Helsinki 2016

Finland

441 697
Printed matter

Aalto University

Abstract

Aalto University, P.O. Box 11000, FI-00076 Aalto www.aalto.fi

Author
Igor Mataić

Name of the doctoral dissertation
On structure and rate dependence of Perniö clay

Publisher School of Engineering

Unit Department of Civil and Environmental Engineering

Series Aalto University publication series DOCTORAL DISSERTATIONS 8/2016

Field of research Soil Mechanics and Foundation Engineering

Manuscript submitted 12 February 2015 **Date of the defence** 15 January 2016

Permission to publish granted (date) 18 December 2015 **Language** English

☒ **Monograph** ☐ **Article dissertation (summary + original articles)**

Abstract

Thesis evaluates effects of anisotropy, bonding and viscosity of soft sensitive Perniö clay. These key features were examined in relation to sample disturbance, strain-rate, and stress ratio conditions in consolidation.

Experimental evaluations form the basis of the study. The comprehensive sampling and laboratory testing programmes on soft sensitive Perniö clay comprised of three sampling techniques and numerous advanced oedometer and triaxial tests on natural and reconstituted specimens, resulting in a unique experimental database. Experimental results were interpreted in terms of physical parameters enabling detailed evaluation of the key features of soft soil behavior.

Firstly, the study explained effects of structure and sample disturbance on compressibility and consolidation characteristics in incrementally loaded oedometer tests (ILOT). Commonly accepted paradigm of c_α/c_c being constant under one dimensional consolidation conditions was yet again questioned. Secondly, the study explained effects of sample disturbance and strain-rate on compressibility characteristics in constant rate of strain oedometer tests (CRS). Utilizing advanced interpretation approaches the influence of strain-rate on slope in compression was clarified. With regards of triaxial testing, the stress ratio in anisotropically consolidated triaxial tests (CAD) was proven decisive for compressibility and destructuration response. Creep coefficient and c_α/c_c under triaxial test conditions were shown to be related to consolidation stress ratio and load increment ratio. Furthermore, the study explained the effects of sample disturbance, consolidation history and strain-rate on the clay response in undrained triaxial compression tests (CAUC). Undrained shear resistance and strength were found to be influenced by the strain-rate and destructuration. On the basis of characteristic points, advanced approach for defining strain-rate influence on undrained shear response was introduced.

Based on experimental results on Perniö clay, creep characteristics in one dimensional and triaxial test conditions are strongly related to sample disturbance and consolidation stress history. Furthermore, study clarified effects of sensitivity and destructuration. Approaches in interpretation of strain-rate effects on compressibility and undrained shear are extended. This is important to account for in any future sampling and testing programmes, in particular if the testing is aimed at improving advanced constitutive modelling of soft natural clays. Grounded on thesis findings, guidelines for enhancement of constitutive models for soft structured clays are set with emphasis on effects of structure and rate dependency on compressibility and strength.

Keywords soft clay, anisotropy, bonding, destructuration, rate dependence, creep

ISBN (printed) 978-952-60-6617-2 **ISBN (pdf)** 978-952-60-6618-9

ISSN-L 1799-4934 **ISSN (printed)** 1799-4934 **ISSN (pdf)** 1799-4942

Location of publisher Helsinki **Location of printing** Helsinki **Year** 2016

Pages 350 **urn** http://urn.fi/URN:ISBN:978-952-60-6618-9

Acknowledgements

Study presented herein was made as a part of research project; Modelling of progressive failure of the embankments and slopes funded by Academy of Finland, Grant 128459 2009-2013, and Aalto University, 2013-July 2014.

I would like to express my highest gratitude to my advisor Prof. Minna Karstunen (Chalmers University of Technology) for support and guidance during the research work. Prof. Minna Karstunen has helped me greatly by her critical comments; in discussions over a number of years, she has forced me to clarify results of research presented herein.

Also, I would like to express my highest gratitude to my supervisor Prof. Leena Korkiala-Tanttu (Aalto University) for guidance and encouragement during writing of the thesis, and for support in the final stages of the research which greatly helped the completion of the thesis.

Furthermore, I am grateful to Aalto University professors emeritus Pauli Vepsäläinen and Olli Ravaska for guidance during the initial stages of the research.

My thanks and appreciations also go to current and former personnel of Laboratories of Geotechnics at Aalto University, Tampere University of Technology and University of Strathclyde, for their help in various stages of research.

I would like to thank opponent Prof. Tim Länsivaara (Tampere University of Technology, TUT), as well as preliminary examiners Prof. Stefan Larsson (Royal Institute of Technology, KTH), and Prof. Vikas Thakur (Norwegian University of Science and Technology, NTNU), for evaluating my research results and providing valuable suggestions for improving quality of the thesis.

Also, I wish to thank to Prof. Predrag Kvasnička (University of Zagreb) for encouragement during the doctoral studies.

I would like to thank friends Mari Jaakonaho, Dušan Sovilj, Eric Halbach and Heidi Peltonen for solidarity.

Finally, I am indebted to my family; baka Tonka, Tata, Mama, Ečika, Ilonka, Ela and Tomika for their help and understanding during this long period of education.

Kutina, December 21st 2015

Igor Mataić

Contents

List of Abbreviations and Symbols

A_r	area ratio
C	inner clearance
Cl	clay content
D_e	external diameter of the sampler
D_i	internal diameter of the cutting edge of the sampler
G	shear modulus
G_o	initial shear modulus
G'_o	slope of the shear destructuration line
G_L	limit shear modulus
G_s	specific gravity
H_f	final height of the reconstituted sample
H_i	initial height of the reconstituted sample
Hm	organic content
ΔH	total settlement of the reconstituted sample
I_C	consistency index
I_L	liquidity index
I_P	plasticity index
K	bulk modulus
K'	bulk modulus number
K_L	limit bulk modulus
$K_Ø$	initial bulk modulus
$K'_Ø$	slope of the bulk destructuration line
K_o^{NC}	coefficient of earth pressure at rest
L_c	length of the cutting edge
M	compression modulus

M'	compression modulus number
M'_i	compression modulus intercept
M_L	limit compression modulus
M_o	initial compression modulus
M'_o	slope of the destructuration line
M'_{oi}	intercept of the destructuration line
$M_{o\ max}$	maximum value of the compression modulus in reloading
R1,…R4	reconstitution batch
S_r	degree of saturation
S_t	sensitivity
$S_{t\ max}$	initial sensitivity of the specimen defined with approach c
V_i	initial volume of the reconstituted sample
a	compression modulus exponent at high stress levels
a_o	destructuration rate coefficient
c_c	compression index
c_u	undrained shear strength
c_{ur}	undrained shear strength of the remoulded material
$c_{\alpha e}$	secondary compression coefficient
$c_{\alpha e\ max}$	maximum secondary compression coefficient
$c_{\alpha e\ i}$	intrinsic secondary compression coefficient
c_α/c_c	secondary compression coefficient to compression index ratio
d	particle size
e	void ratio
$\dot{e}$	rate of change in void ratio
e_f	final void ratio of the reconstituted sample
e_o	initial void ratio
e_r	remoulded void ratio
e_s	void ratio in undrained shear
$\Delta e/e_o$	specimen quality criterion
h	absolute elevation
m	mass
m_i	initial mass of the reconstituted sample
p'	mean effective stress

p'_p	mean effective stress at yield
p'_m	size of the yield curve
q	deviator stress
q_{max}	maximum deviator stress
q_p	deviator stress at yield
t_c	sampling cylinder thickness
t	time
z	depth
v_o	initial specific volume
v_i	specific volume at σ'_1=1 kPa related to intrinsic compressibility
v_R	specific volume at σ'_1=1 kPa related to NC compressibility of re-constituted specimen
w	water content
w_o	initial water content
w_f	final water content of the reconstituted sample
w_L	water content at liquid limit
w_P	plastic limit
w_r	remoulded water content
w/γ	specimen quality criterion
M	critical state stress ratio
α	yield curve orientation
β	strain-rate coefficient
γ	unit weight
γ_r	remoulded unit weight
ε_1, ε_3	principal strains
$\dot{\varepsilon}_1$	axial strain-rate
ε_{1F}	axial strain at failure
ε_d	shear or deviatoric strain
ε_v	volumetric strain
η	deviator to mean effective stress ratio
η_F	stress ratio at failure
η_α	stress ratio corresponding to p'_{max} in undrained shear
κ	slope of the intrinsic swelling line in e-ln $\sigma'1$ plane

κ_o	slope of the primary reloading line in v-ln σ'_1 plane
λ	the highest slope of the compression curve in v-ln σ'_1 plane
λ_i	slope of the intrinsic compression in v-ln σ'_1 plane
λ_R	slope of the NC line in v-ln σ'_1 plane on reconstituted specimen
μ	fluidity parameter
ν	viscosity
σ'_1, σ'_3	principal effective stresses
σ'_{1C}	vertical effective stress following triaxial consolidation
σ'_C	consolidation stress
σ'_L	limit stress
σ'_o	initial effective stress
σ'_p	preconsolidation pressure
$\sigma'_{p\ low}$	preconsolidation pressure at strain-rate $<3 \cdot 10^{-7}$ s^{-1}
σ'_{un}	unloading vertical effective stress in oedometer test
σ'_v	vertical effective stress
σ'_{vo}	effective overburden stress
φ'	effective friction angle
EOP	end of primary consolidation
GW	ground water
IL	incremental loading
LIR	load increment ratio
LOI	loss of ignition
LVDT	linear variable differential transducer
MAP	moving average period
NC	normally consolidated
NGI	Norwegian Geotechnical Institute
OC	overconsolidated
PMMA	polymethyl methacrylate (plexiglas)
S-2009	Perniö deposit sampling works in 2009
S-2010	Perniö deposit sampling works in 2010
SGI	Swedish Geotechnical Institute
TUT	Tampere University of Technology

Author's Contribution

This doctoral thesis is a monograph. The Author has himself performed sampling, laboratory testing, analysed the results, and written the thesis.

1. Introduction

1.1 Engineering aspects of soft soil behavior

Understanding the behavior of soft sensitive clay is important for evaluation of uncertainties inherent in geotechnical design. Due to increased urbanization, coastal sites characterized by soft marine clay deposits are increasingly used for construction purposes. To avoid unnecessary risks, overuse of building materials and energy, there is a need for accounting for main features of soft clay behavior in geotechnical design, eg. structure: anisotropy, bonding, destructuration; and rate dependency: aging, creep, viscosity, thixotropy. The results of research work presented herein aim to explain and quantify stress-strain-strain-rate effects governing the behavior of soft sensitive Perniö clay, and highlight the effects of sample disturbance to the soil response.

The behavior of soft clay is very complex. Its structure consists of fabric (arrangement of particles) and interparticle bonding (particle contact). Additionally, the behavior is rate dependent. Consequently, soft natural clays exhibit features such as:

- A significant degree of anisotropy developed during their deposition, sedimentation, consolidation history and any subsequent straining (changes in fabric) [Tavenas & Leroueil 1977, Burland 1990, Wheeler et al. 2003];
- Apparent bonding which is progressively lost during straining (destructuration) [Leroueil et al. 1979, Leroueil & Vaughan 1990, Burland 1990];
- Rate dependent stress-strain response which has a significant influence on the shear strength and the preconsolidation pressure (creep and strain-rate effects) [Bjerrum 1967, Mesri & Godlewski 1977, Vaid & Campanella 1977, Graham et al. 1983, Leroueil et al. 1985, 1988].

Combined effects of the above stated mechanisms are responsible for common problems of geotechnical design on soft soils, such as excessive settlements of foundations and delayed failure of embankments and slopes.

Comprehension of rate dependent soft clay behavior is essential for optimum design, i.e. long term functionality and stability of geotechnical structures on soft soils. Clay fabric in natural clay deposits is strongly anisotropic. Hence, its strength and strain response to stress variations reflects the arrangement of the particles and their contacts [Tavenas 1981]. Beneath the structure, destructuration may cause decrease in the undrained shear strength of sensitive clays, yet a common assumption is that the undrained shear strength increases due to consolidation [Karstunen & Koskinen 2004]. Effects of rate dependence such as creep are important for accurate evaluation of settlements in soft soils,

while strain-rate has a profound influence on shear strength of soft soils [Leroueil et al. 1985]. These aspects, responsible for eg. progressive failure of slopes, are commonly ignored in conventional geotechnical practice.

1.2 Constitutive modelling of soft soils

Complex features of soft clays, such as structure and rate dependency should be accounted for in geotechnical design. Constitutive modelling in conjunction with finite elements has proven to be viable approach for representing delayed phenomena of soft soils [Potts & Zdravković 1999]. Indeed, with some constitutive models it is possible to model some of these essential features [Tavenas & Leroueil 1977, Whittle & Kavvadas 1994, Hinchberger 1996, Potts & Zdravković 1999, Dafalias & Manzari 2006].

The results of laboratory tests performed in this study are used to evaluate formulation of two existing constitutive models; elastoplastic SCLAY1S developed by Karstunen et al. [2005], which accounts for modelling of anisotropy and destructuration based on fabric tensor approach by Wheeler et al. [2003] and intrinsic yield surface concept of Gens & Nova [1993]; and elasto-viscoplastic AniCreep developed by Yin et al. [2011], including options for modelling strain-rate effects and creep based on the overstress theory by Perzyna [1963]. These models include options to represent anisotropy, destructuration and viscosity, are among the finest constitutive models available for representing stress-strain-strength response of structured clays. Performance of the models still needs improvement, in particular concerning effects of destructuration process and effects of creep and viscosity.

1.3 Aim and objectives of the research work

The aim of the research was to get comprehensive quantitative data to understand how the complex stress-strain-strain-rate dependent response of soft natural clays is affected by sampling and testing procedures. Namely, an essential part of model development and validation is comparison of constitutive model formulation and predictions to high quality laboratory and in situ measurements [Näätänen & Lojander 2000]. In situ and laboratory testing performed on Perniö soft sensitive clay thus presents continuation of previous efforts with an agenda to enhance understanding and improve modelling capabilities of soft clay behavior [Korhonen & Lojander 1987, Wheeler et al. 2003, Karstunen et al. 2008b, Yin et al. 2011, Koskinen 2014]. Although previous research uncovered the importance and principal mechanism of destructuration and viscous effects in soft sensitive clay behavior, the effect of rate dependency of stress-strain behavior is still an area of considerable uncertainty. Namely, constitutive modelling of soil behavior via finite element analyses requires the highest quality sampling and testing methods so to ensure representativeness and comparability of laboratory results obtained [Clayton et al. 1982]. However, due to low values of undrained shear strength and sensitive structure, obtaining undisturbed samples in soft clays is highly demanding [Hvorslev 1949]. Consequently, most of the earlier studies with the aim of de-

velopment of constitutive models were based on partially disturbed specimens. As a result, constitutive formulation of destructuration effects is often quantitatively underrated. This fact has a profound effect on models ability to represent rate dependent aspects.

To explain and quantify stress-strain-strain-rate effects governing the behavior of soft sensitive Perniö clay, and thus provide solid basis for development of improved constitutive models, main emphasis of this study was on sampling and testing quality. The objectives of the research were:

1. To obtain undisturbed samples of Perniö soft sensitive clay. A major sampling programme including several sampling techniques was implemented. Sampling techniques used were Swedish standard ST II, Norwegian piston sampler NGI 54 mm, and Norwegian piston sampler NGI 86 mm [Kallstenius 1971, Andresen & Kolstad 1980].
2. To perform a major programme of advanced laboratory tests on Perniö clay examining crucial features of soft soil behavior. The testing programme included specific soil tests performed in conventional oedometer and triaxial apparatuses, namely;
   - Incrementally loaded oedometer tests (ILOT);
   - Oedometer tests at constant strain-rate (CRS);
   - Anisotropic triaxial consolidation tests (CAD);
   - Undrained triaxial tests in compression (CAUC), and
   - K_o triaxial tests.

   The tests were performed on natural and reconstituted specimens under conditions of varying rates of loading, applied constant stresses as a function of time (creep), and constant strain-rates, thus enabling detail examination of effects of creep and strain-rate on structure and progressive destructuration of bonds during straining.
3. To interpret the experimental results in terms of physical parameters representing effects of anisotropy, destructuration and creep, with special attention to understand how specimen quality affect these results. A secondary focus was on defining the influence of strain-rate on destructuration process, in the context of the SCLAY1S and AniCreep constitutive models.

1.4 Outline of the research work

Research work is presented in the following manner: Chapter 2 elaborates crucial aspects of soft sensitive clay behavior in the perspective of origin, sampling and laboratory testing. Chapter 3 introduces Perniö deposit and explains characteristics and implementation aspects of sampling techniques used. Chapter 4 elaborates sample preparation procedure for natural and reconstituted specimens and defines test conditions, objectives, and testing methodology used in specific tests of this study. Chapter 5 reports sampling and specimen preparation results and elaborates geotechnical conditions of Perniö deposit. Chapters 6 and 7 present and discuss experimental results obtained in oedometer and triaxial tests. Interpretation procedures in evaluation of anisotropy, bonding, and strain-rate effects are described in detail. Chapter 8 summarizes main findings of the study and makes recommendation for future work.

2. Theory survey

2.1 Origin of soft sensitive clay

Sensitivity of clay is defined as the ratio of the undrained shear strength in an undisturbed and completely remoulded condition at the same water content [Terzaghi 1944, Skempton & Northey 1952, Rosenqvist 1953, Bjerrum 1954, 1967, Crawford 1968, L'Heureux et al. 2014]. Commonly used classifications of soft sensitive clays and quick clays are given in Table 2.1 [Bjerrum 1954, Rankka et al. 2004]. Term soft sensitive clay identifies clays that exhibit sensitivity above unity. Characteristic of clay being sensitive indicates presence of fragile clay structure, resulting from complex interaction of microscopic flaky particles and physical-chemical bonds existing between them. Quick clay is a form of highly sensitive clay with a tendency to change from a relatively stiff and brittle material to a viscous liquid mass when disturbed [Torrance 1983, Thakur et al. 2011]. According to SGI, quick clay is defined as a clay with a sensitivity of 50 or more and a fully remoulded shear strength of less than 0.4 kPa [Rankka et al. 2004].

Table 2.1 Classifications of clays with respect to sensitivity according to Bjerrum [1954] and Ranka et al. [2004].

Sensitivity, S_t	Classification [Bjerrum 1954]	Sensitivity, S_t	Classification [Rankka et al. 2004]
<2	slightly sensitive	<8	low sensitivity
2-4	medium sensitive		
4-8	very sensitive		
8-16	slightly quick	8-30	medium sensitivity
16-32	medium quick		
32-64	very quick	>30	high sensitivity
>64	extra quick		

Geotechnical properties of subsoil are result of the geological history of the deposit [Bjerrum 1954]. During the Pleistocene age Scandinavia was cowered by ice masses [Bjerrum 1954]. Prior to and following the withdrawal of the glaciers, soil and crushed rock deposited on the sea bed and formed late glacial and postglacial sediments [Bjerrum 1954, Gardemeister 1975]. When deposited in sea water characterised by high ion concentration (i.e. low electro-kinetic potential), clay particles may flocculate, leading to sedimentation of large aggregates and resulting with flocculated structure characterised by high void ratio/water content [Rankka et al. 2004]. Following deposition, clay sediments

consolidate under their own weight resulting with formation of soft marine clay deposits [Bjerrum 1954]. However, withdrawal of the glaciers had additional effect, being that of unloading of the underlying rock, resulting with isostatic uplift, leaving the clay deposits located above sea water level [Bjerrum 1954]. Moved above sea water level, clay deposits became exposed to long term processes associated with the change in original depositional environment, such as leaching and weathering.

Leaching is one process associated with increase in electro-kinetic potential, and is one of the factors leading to the development of quick sensitive clay [Rosenqvist 1978]. Due to leaching the ion concentration in the pore water changes, by a process of gradual removal of substances such as dissolved salt ions from the soil [Rankka et al. 2004]. The explanation of the high sensitivity of Scandinavian marine clays as a result of leaching out of the salt has been given by Rosenqvist [1946]. Original salt content, i.e. average salt concentration of the deepest water of the sea in which the clays were laid down, is estimated to 35 g/l [Bjerrum 1954]. Leaching causes decrease of the original salt content in the pore water; by infiltration of rain (and snow) water, artesian water pressures in underlying permeable soil or rock, and by diffusion of salt towards zones with lower concentration [Rankka et al. 2004]. Reduction of salt content in the pore water is accompanied by a decrease in Atterberg limits, which in turn results in increased sensitivity [Bjerrum 1954]. Therefore, low salt content in Scandinavian marine clays is a precondition for high sensitivity [Söderblom 1969]. Leaching affects the forces between the particles but normally not the flocculated structure as such [Brand & Brenner 1981]. However, it strongly affects the ability of particles to re-flocculate after remoulding [Rankka et al. 2004]. If flocculated clay is subjected to leaching, electro-kinetic potential will increase, and a re-flocculation after remoulding may not be possible [Rankka et al. 2004].

Changes in sensitivity, Atterberg limits and shear strength during leaching have been studied by many researches, Bjerrum [1954], Rosenkvist [1955], Osterman [1964], Söderblom [1969], Torrance [1974] etc. If pore water salinity of marine clay decreases, considerable change in the clay plasticity will occur [Bjerrum 1954]. In fact, main effect of reduction in salt content is decrease in the activity of the clay minerals. Namely, decrease in salt content to concentrations below 15 g/l is accompanied by the plastic and liquid limit values being lowered [Bjerrum 1954]. However, for a certain decrease in pore water salt concentration, plastic limit changes only slightly, while that of liquid limit decrease is considerable (see Figure 2.1). A larger decrease in liquid limit than in plastic limit results in decrease of the plasticity index [Hight et al. 1987, Rankka et al. 2004]. Thus if the salt is washed out of clay, the plasticity of clay will decrease due to reduction in activity of clay minerals [Bjerrum 1954]. If during the process of leaching water content remains approximately constant, the consequence of clay plasticity reduction will be increase of liquidity index leading to rise of sensitivity [Hight et al. 1987]. Increase of liquidity index affects shear strength properties of leached clay. Namely, leaching out of the original salt in marine clays is accompanied by a reduction in the shear strength of the

undisturbed clay [Bjerrum 1954]. However, prevailing effect of the leaching is that of great reduction of remoulded undrained shear strength whilst the reduction in undisturbed shear strength is small [Bjerrum 1954]. In addition to effects on shear strength, important consequence of clay plasticity reduction is increase in compressibility [Hight et al. 1987, Rankka 2004].

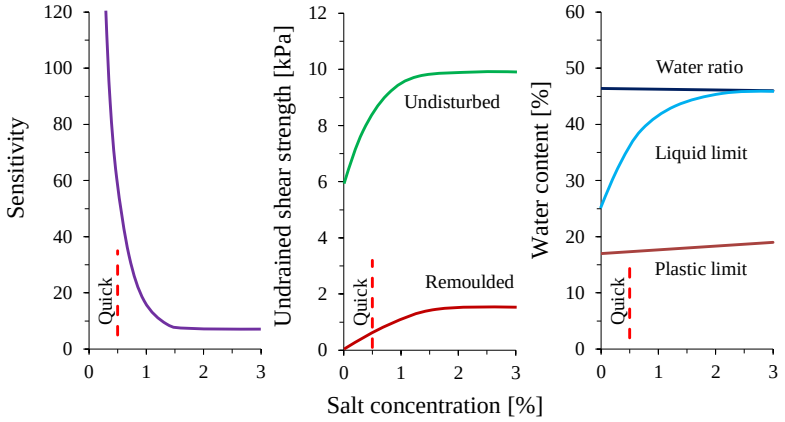

Figure 2.1 Changes in sensitivity, shear strength and consistency as functions of salt concentration in pore water during leaching [Bjerrum 1954]

2.2 Causes of disturbance of soft sensitive clay

Soft sensitive clays are materials very susceptible to disturbance. Thus, results of the laboratory tests on soft sensitive clay are to a large extent influenced by sample quality. To obtain samples of reasonable quality it is important to understand nature and extent of the factors and mechanisms influencing quality of the samples. Sample disturbance is not caused only by the sampling activity. Indeed, disturbance of soft sensitive clay can occur during various stages prior to start of a specific laboratory test, i.e. during sampling, packing, transport, storage and finally during specimen preparation. During each of these stages special attention is necessary in order to keep the extent of disturbance at an acceptable level. Causes of sample disturbance are divided into several groups in terms of the conditions and mechanism under which disturbance occurs, i.e. stress release, mechanical deformation, change in water content, chemical changes and temperature changes [Hvorslev 1949, Clayton et al. 1982]. It is important to understand that these mechanisms are interrelated.

2.2.1 Stress release

Independent of sampling technique used, upon retrieval and exposure to atmospheric pressure samples will be subjected to stress release. Thus, by removal of the sample from the stress conditions in situ, stress release and consequent disturbance of the material sampled is inevitable. Effects of stress release vary considerably depending upon the sampling depth and initial clay

properties. If material has substantially low permeability, negative pore pressures develop retaining effective stress level unchanged. On periphery of the sample suction will remain for a fairly short period. Thus, a non-uniform release of stresses occurs and the thin surface layer of clay progressively loses inherent structure tending to remoulded consistency [La Rochelle et al. 1981]. Due to this change in capillary suction, initial structure of the clay can be considerably modified and consequently mechanical properties of sample can be greatly affected. The remoulding at the surface is believed to be the cause of the fast release of the negative pore pressures [La Rochelle et al. 1981]. Thickness of this remoulded zone depends on the characteristics of the sampling method used [Hvorslev 1949, La Rochelle et al. 1981].

2.2.2 Mechanical deformation

Mechanical deformation occurs as a result of the abrupt change of the effective stresses of the sample, and is divided to primary and secondary component. Primary mechanical deformations of the sample occur during sampling stages and are caused by the sampling tool [Kalstenius 1971, Andresen & Kolstad 1980]. In addition to those caused by the sampler, shocks, heavy vibrations after sampling and disturbances occurring in laboratory preparation of specimens are major sources of mechanical disturbance as well. Due to their origin they are referred as secondary mechanical disturbances [Kalstenius 1971].

Primary mechanical disturbance depends upon the sampling technique implemented and to a large extent upon the expertise of the personnel in charge of the sampling process. Certain sampling tools do cause significantly more mechanical distortions of the sample than other. The most common effects of the mechanical deformation are displacement, compaction and extension of the sample. Mechanical deformations caused by the manoeuvring of the sampling tool can cause large changes in total stresses and large variations in pore pressure. The pore pressures are either positive or negative at different stages of the sampling operations [La Rochelle et al. 1981]. If the total stress and pore pressures are large enough, the stress path during sampling can reach the limit state curve. If stress path touches the limit state curve the structure of the clay is disturbed and its mechanical properties are greatly affected [La Rochelle et al. 1981].

Main causes of secondary mechanical deformations are either time dependent effects or incorrect handling and storage of the samples [Andresen & Kolstad 1980]. Mechanical distortions can occur during transportation stage if the samples are not isolated from negative effects of vibrations and shocks. Each sample should be placed in a separate rigid container and surrounded with packing material to prevent it from moving [Den Haan 2001]. Significant cause of secondary mechanical disturbance is the process of specimen preparation for laboratory testing. It depends upon the conditions of sample storage and characteristics of the specific testing device for which specimens are prepared.

2.2.3 Change in water content

Both aspects of change in the initial water content, i.e. water loss and swelling, are important mechanisms of sample disturbance. Change in the water content is very common cause of disturbance. The most significant changes are expected during sampling and sample storage. Susceptibility for change in the water content largely depends upon the composition of the material sampled.

In fully saturated low permeability clays, change in the water content is closely related to long term effects of stress release and mechanical disturbance. Disturbance during sampling occurs at essentially constant water content; the two main causes are the mechanical distortion associated with sampling operations and the release of total in situ stress [Leroueil & Jamiolkowski 1991]. Non-uniform release of stresses enhanced by existence of severely mechanically disturbed surface layer leads to variance in pore pressures that trigger long term exchange of the water content within the sample. With time pore water may migrate from the remoulded external zone to the intact central core [La Rochelle et al. 1981]. The mechanism of exchange in water content within the sample is enhanced if sampled material contains swelling minerals. This effect is responsible for difference in water content between periphery and core of sample. If sample contains swelling minerals it is essential to avoid contact with water during the specimen preparation. If exposed to water, specimen will expand as a consequence of water suction.

Considerable variations in initial water content might occur due to high differences in permeability of the material sampled. Silty clays are to a much larger extent susceptible to change in initial water content than clays of low permeability. Within silty zones pore pressures caused by sampling dissipate rapidly, reducing the ability to retain in situ effective stresses upon stress release. Rapid stress release is followed by considerable or complete destructuration of the sample. Capillary forces and the corresponding change of the pore water pressures following the stress release will vary from layer to layer [Hvorslev 1949]. Variation in the pore pressures within the sample can cause drainage of the water from clayey layers towards silty inclusions during long storage period. In addition, porewater contained within the silty layers of the sample is easily lost during sample extraction and preparation for testing.

Following sampling and transport sampled material is typically stored within the laboratory up to several months prior to being tested. To preserve initial moisture content, it is essential to ensure water-tight conditions during the storage. By what means are the samples preserved primarily depends upon sampling technique used. Testing should be avoided if the samples are stored for periods above 7 weeks, i.e. priority should be given to fresh samples.

2.2.4 Temperature change

Significant oscillations in temperature affect the stress-strain conditions of clay samples and therefore have an impact on disturbance level of the material sampled. Temperature changes are primarily avoided to prevent drying and wetting of the sample. To ensure minimal changes in water content and me-

chanical conditions in long term, samples should be stored at the constant temperature and relative humidity conditions as in their average natural environment [Andresen & Kolstad 1980]. To avoid freezing of the samples, temperature in a storage room should never drop below +4 °C [Den Haan 2001]. Freezing leads to formation of ice lenses causing destruction of the sample structure and attracting the moisture [Clayton et al. 1982].

2.2.5 Chemical changes

During long term storage chemical changes influencing the initial properties of the samples can occur. Change in the pore water chemistry can have serious effects on soil behavior such as decrease in sensitivity level [Clayton et al. 1982]. Thus, storage conditions should be such that the activation of chemical processes such as electrolysis, change in pH and salinity are prevented.

The most severe chemical changes can occur if the soil samples are stored in steel, copper, brass or zinc containers for long periods. Electrolysis due to contact between the soil and metal containers can produce a decrease in compressibility and an increase in plasticity and shearing resistance of the soil. If salty clay samples are stored for several months in metal and especially steel containers, strong adhesion between sample and container may develop with the force required for sample extraction being several times higher that required shortly after sampling [Hvorslev 1949, Berre et al.1969]. Electrolytic action is prevented by usage of water and air-tight sealing caps made of electrically inert materials [Hvorslev 1949].

Changes in the initial pH or salinity of the sampled material can occur if the samples are exposed to liquids with different pH or salt content compared to those of the pore water. The soil close to the bottom of the borehole may be affected by the pH or salts in the wash water or the drilling fluid, but the penetration is generally slight except in the pervious soil [Hvorslev 1949].

2.3 Undisturbed sampling techniques

Obtaining undisturbed samples in soft sensitive clays is a very challenging task. Soft clays are prone to distortion as they are water saturated materials whose consistency can easily change by an influence of mechanical action. Even a small mechanical intervention can trigger progressive modifications of clay structure and initial sensitivity level, and consequently, severely influence the accuracy of laboratory test results. In addition, sensitive soft clays are essentially brittle materials characterised by an occurrence of very clear failure surfaces and therefore prone to formation of weakened zones within the sample. Furthermore, soft sensitive clays are often characterised with very frequent occurrence of silty inclusions. Due to the common and considerable changes in the permeability, materials ability to contain initial structure, by build-up of negative pore pressures resulting from total stress release upon sample retrieval, can vary considerably. Changes in permeability cause additional difficulty in achieving and maintaining water content representative of that in situ. Problems related to moisture loss in sample zones characterised

with silty inclusions are common, and values of water content measured on the material sampled can vary drastically. Again, changes in the water content trigger further modifications of the stress level present within the sample and vice versa. Thus, it is very difficult to obtain material of uniform initial properties even if the material is sampled at the same depth, using identical sampling procedure.

Main factor influencing sample quality is the selection and implementation of particular undisturbed sampling technique. By undisturbed sampling, a technique causing least modification of initial properties, such as structure, consistency and particle content is considered. If undisturbed samples are to be obtained, effective stress during and after sampling must remain within the limit state surface [La Rochelle et al. 1981]. Methods enabling retrieval of larger samples are usually associated with less disturbance and minor modifications of initial properties. Among the various sampling techniques used, methods suitable for undisturbed sampling of clays can be divided into two major groups: block sampling and tube sampling.

Block sampling techniques are characterised with samples of considerable size, and are the most suitable when undisturbed samples are wanted. Block sampling is typically based on open type of pre-excavation and careful carving of the selected mass of material making it rather difficult to implement, particularly as the sampling depth is limited. Certain modifications, such as those of Shearbroke sampler, enable concept of block sampling being implemented using large diameter borehole [Lefebvre & Poulin 1979]. One of the main concerns of block sampling is adequate conservation of the large samples. It is usually achieved by coating with cling film and wax mixtures. Provided that pre-excavation of the material and careful carving around selected material and conservation are successfully made, laboratory test results on material so obtained indicate block sampling being the most suitable method for obtaining undisturbed samples representable of the in situ material.

Tube sampling method encompasses a large variety of sampling techniques based on various mechanisms, including cylinders to which material is pushed into and retrieved to surface by means of pre-existing boreholes. Displacement of soil caused by penetration of the sampler has two main effects; effective stresses of the soil are changed as a result of pore pressure increase, and bonds between the soil particles are broken [Clayton et al. 1982]. Quality of the samples obtained varies depending on the properties of material sampled and technical parameters of the sampler. All of the tube sampling methods include tube/cylinder being pushed into the material. What determines suitability of the sampler and quality of the material obtained is the rule of least mechanical action/disturbance caused by sampler/cylinder during its penetration and retrieval. Factors such as area ratio, cutting edge angle, inner clearance and sample length to diameter ratio are extremely important. Main design concerns are firstly, selection of the least possible tube thickness and area ratio to ensure minimum mechanical disturbance during sample penetration, and secondly, selection of as large diameter of the sampling tube as possible because the extent of sample disturbance is more pronounced if the diameter of the

sample is relatively small [La Rochelle et al. 1981]. Since the sampling is based on the retrieval of the samples through pre-existing boreholes, tube sampling methods are more suitable in obtaining the samples from greater depth compared to those of block sampling approach.

2.3.1 Area ratio

The area ratio of the sampler is crucial parameter influencing sample disturbance. It is defined by Equation 2.1, as ratio of the volume of displaced soil to volume of the sample:

$$A_r = \frac{D_e^2 - D_i^2}{D_i^2} \tag{2.1}$$

where; D_e and D_i respectively represent external and internal diameter of sampler cutting edge (Figure 2.2) [Hvorslev 1949]. Samplers with high area ratio come with increased sample disturbance and remoulding, increased penetration resistance, and possibility of entrance of the excess soil from the area immediately beneath the cutting edge [Clayton et al. 1982]. Area ratio is reduced by usage of thinner sampling cylinders.

2.3.2 Tube thickness and quality

In soft sensitive clays thin walled large diameter samplers are associated with the least disturbances during sampling (Figure 2.2). Thickness of sampling tube varies typically from 1.0 to 5.0 mm. Additional factor important in this perspective is quality of the sampling tubes. Poorly produced and poorly handled cylinders differ in their cross-sectional area along the longitudinal axis. Sampling cylinders of rolled steel are often characterised by oval cross sections. Similar effect might be a result of improper care of the cylinders. Thin sampling cylinders tend to be very fragile. Commonly, old sampling cylinders have deteriorated shape or cutting edge especially if used in granular materials. As a result gaps can occur between the sample and cylinder.

2.3.3 Cutting edge angle

Sampling disturbance, in particular those caused by large area ratio, can be reduced by introduction of cutting edge on the outer side of the sampling cylinder, as shown on Figure 2.2. Appropriate design of the cutting edge being that of 5 to 15 degrees, i.e. $L_c > D_e/4$ [La Rochelle et al. 1981], reduces the disturbance caused by sampling during penetration by enabling cutting of the material sampled instead of compressing it. If the angle of the attack of the cutting edge is small enough, the material displacements and eventual changes of volume caused by penetration of the sampler occur towards the outside of the cylinder, and the influence of the area ratio on the sample disturbance is minimised [La Rochelle et al. 1981]. Nevertheless, displacement and in some cases compression of the material sampled does occur resulting with increase of unit weight of the material.

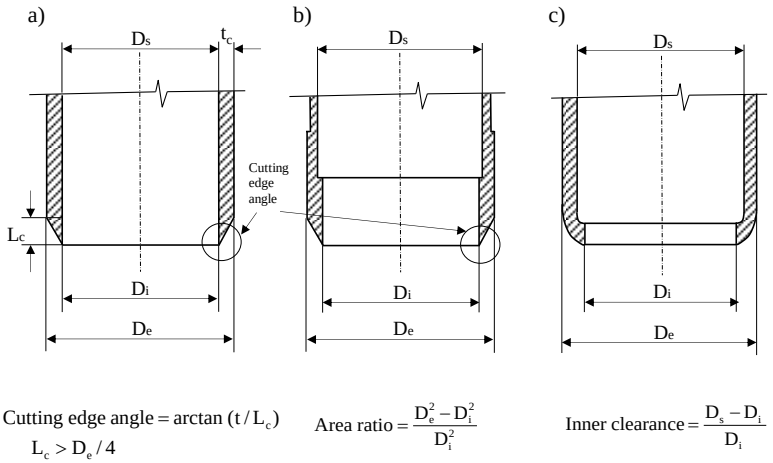

Figure 2.2 Tube sampler parameters; a) cylinder without inner clearance, b) sampler with screw on cutting shoe, and c) cylinder with rolled and reamed cutting edge [modified from Clayton et al. 1982].

2.3.4 Inner clearance

Some tube samplers include inner clearance in their design. Due to the mechanical action of the sampler, in situ stress-field is modified in terms of stress concentration primarily around the cutting edge of the cylinder. Figure 2.3 shows typical stress field so created. Magnitude of the stress concentration is proportional to the material disturbance and volume displacement caused by sampling tube, and is therefore proportional to the sampler area ratio, tube thickness and friction occurring between the sample and inner area of the tube. In overconsolidated clays friction between sample and tube can be considerable. In such cases sample undergoes severe compaction, with length of the sample recovered being less than the distance of the tube driven as shown on Figure 2.3 b) [Hvorslev 1949, Clayton et al. 1982]. Inner clearance is sometimes introduced to avoid this effect (see Figure 2.2 b & c). Inner clearance is given by Equation 2.2:

$$C = \frac{D_s - D_i}{D_i} \tag{2.2}$$

where; D_s is inner diameter of sampling tube and D_i is internal diameter of cutting shoe. Inner clearance is usually less than 4 %. It reduces friction between the sample and cylinder during penetration and has favourable effect on sample retrieval. Negative effect of inner clearance is that it allows sample to swell and deform laterally within the cylinder. Inner clearance is not recommended in sampling of normally consolidated or slightly overconsolidated soft sensitive clays. In soft sensitive clays and quick clays jamming is not of the primary concern. However, samplers with large area ratio can remould material underneath the sampler that can uncontrollably enter the sampling cylinder as shown on Figure 2.3 a). Material so obtained is not representable of the undisturbed sample. The effect cannot be observed by comparing the sample

length recovered with that of the tube driven. Indeed, with tube being filled with material, loss of bearing capacity underneath the sample cannot be noticed during sampling.

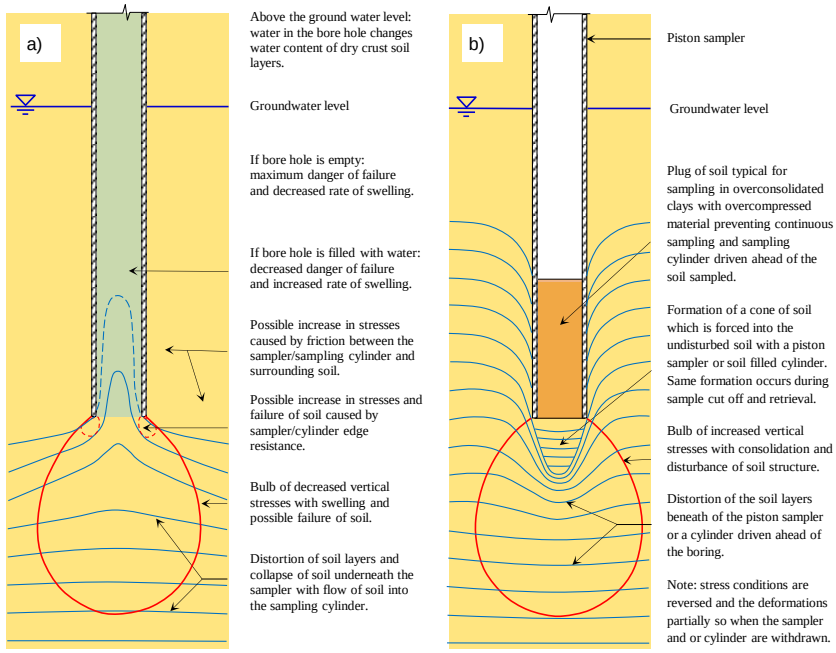

Figure 2.3 Stress changes and deformations in sampling, a) structural collapse and sampling of remoulded material, and b) plug formation within the cylinder [modified after Hvorslev 1949].

2.3.5 Length to diameter ratio

In soft sensitive clays the ability for sample retrieval is one of the most important concerns. Ability to retrieve sample from certain depth is restricted by the adhesion between the sample and the inner area of the sampling cylinder, and suction occurring within the cylinder. The resisting force containing the sample is proportional to the inner area of the cylinder activated during sampling. If the length to diameter ratio is inappropriate, the sample will slip out of the sampling cylinder. Sample loss is common occurrence during sampling and since it depends upon the unit weight of the material sampled applicability of sampler in situ is material dependent. Soft sensitive clays are typically characterised by the high water content which is favourable factor in terms of their retrieval. However, they are also characterised by creation of thin remoulded zones on contact with the sampling cylinders. Thus, due to nature of soft sensitive clay the contact between the sample and inside tube area is self-lubricating [La Rochelle et al. 1981, Clayton et al. 1982].

2.3.6 Sample diameter

The sample diameter is decisive parameter governing extent of sample disturbance. Figure 2.3 and Figure 2.4 show stress field and strains caused by the

tube penetration. In addition to compression immediately underneath of the cutting edge, when within the sampling cylinder the material sampled is firstly subjected to extension and later to additional cycle of compression. Consequently, it is common that the sample within the cylinder is not of the uniform quality. With sensitive clay being a brittle material, random failure surfaces within the sample can occur. Furthermore, due to the material displacement and friction between the cylinder and the sample, sample periphery is disturbed the most. In soft soils, outer layer of a sample is in a remoulded state and it is subjected to different pore pressures than the core of the sample, mainly resulting from higher sampling strains experienced [Casagrande 1936]. In the outer 5 mm moisture content is typically several percent lower than at the centre. Generally, the core of the sample is of the highest quality. To reduce influence of above negative effects and to increase the sampler performance sample diameter should be as large as possible.

Strains during sample penetration are inevitable. Extent of the sample disturbance is proportional to displacements and pore pressures occurring in penetration and retrieval. By careful selection of sampler characteristics and throughout understanding of stress changes during sampling, disturbances can be reduced to an acceptable level.

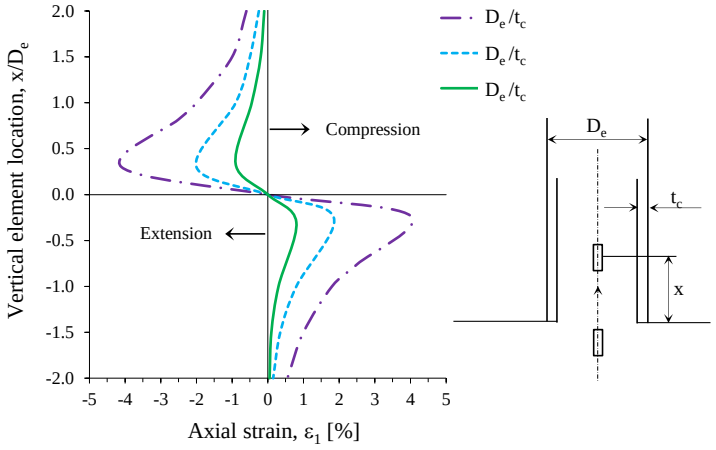

Figure 2.4 Axial strain history at the centre line of a sampling cylinder [modified after Baligh et al. 1987].

2.4 Oedometer test

2.4.1 Incrementally loaded oedometer test ILOT

The structure of natural soft clays includes interparticle bonding [Leroueil & Vaughan 1990]. When plastic straining occurs the bonding degrades, referred to as destructuration [Leroueil & Vaughan 1990]. Comparison of stress-strain curves obtained on intact and reconstituted specimens allows insight to the effects of structure and progressive destructuration of bonds during inelastic strains. As shown on Figure 2.5, oedometer test results on natural clay exhibit

compression curves above the intrinsic compressibility defined by the reconstituted material, with the post yield compression curve gradually converging with the intrinsic compressibility as the bonding is progressively lost [Burland 1990].

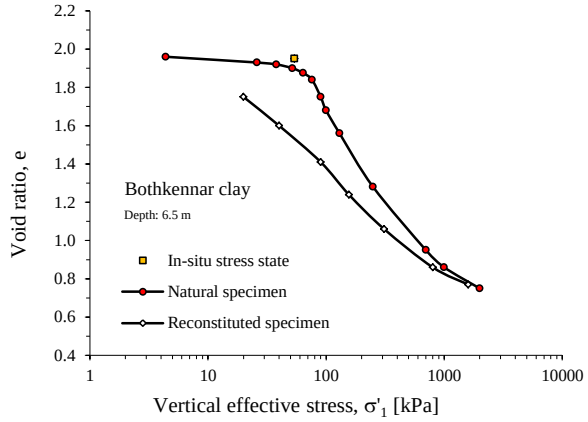

Figure 2.5 Compressibility of natural and reconstituted clay, Bothkennar clay [modified after Burland 1990].

Apparent preconsolidation pressure represents maximum pressure to which soil can be subjected without causing large settlements [Crawford 1986]. In accordance with the Cam-Clay theory, values of the preconsolidation pressure are determined by adopting bilinear approach (see Figure 2.6), with yield defined as the intersection of reloading line and normal compression line in a semi-logarithmic plot of vertical effective stress and void ratio [Schofield et al. 1968]. The results are confirmed in corresponding linear stress-strain plots, i.e. using modified bilinear approach [Koskinen et al. 2003].

In order to be able to compare directly results from oedometer test with those from triaxial tests, somewhat unconventional definitions of compression parameters are adopted. As shown in Figure 2.6, specimen compressibility is defined by compression indices in reloading κ_o (Equation 2.3), and normally consolidated range λ (Equation 2.4). The indices represent slopes of the lines fitted to the elastic (lowest gradient) and plastic portion (highest gradient) of the stress-strain curve, respectively [Koskinen et al. 2003]. Due to absence of bonding, the gradient of the normal compression line of reconstituted specimens is rather uniform and lower than that of natural specimens [Koskinen et al. 2004]. Exceptions to this rule are salty clays such as Mexico City clay. Two additional coefficients are important, the slopes of intrinsic compression line λ_i and swelling line κ. Slope of the intrinsic compression line defined by Equation 2.5, is obtained from stress range following considerable plastic straining and indicates compression characteristics similar to that of reconstituted specimens. Swelling index defined by Equation 2.6 represent specimen response in unloading. Reloading and swelling indexes are commonly of uniform values except for highly structured specimens when due to destructuration, swelling index κ tends to higher values compared to that of reloading index κ_o.

$$\kappa_0 = \frac{c_r}{\ln 10} = \frac{\Delta e}{\Delta \ln \sigma'_1} \qquad (2.3)$$

$$\lambda = \frac{c_c}{\ln 10} = \frac{\Delta e}{\Delta \ln \sigma'_1} \qquad (2.4)$$

$$\lambda_i = \frac{\Delta e}{\Delta \ln \sigma'_1} \qquad (2.5)$$

$$\kappa = \frac{c_s}{\ln 10} = \frac{\Delta e}{\Delta \ln \sigma'_1} \qquad (2.6)$$

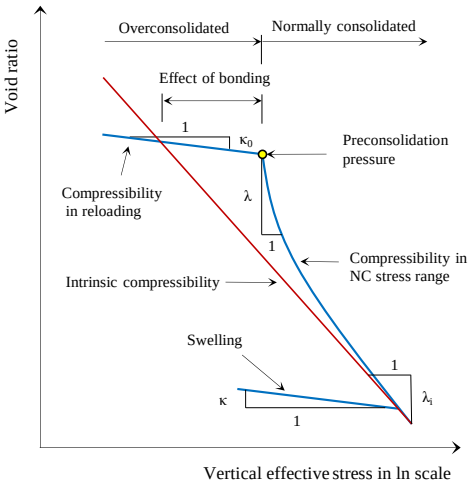

Figure 2.6 Idealized compressibility characteristics in one dimensional compression [modified after Leroueil & Vaughan 1990].

Effect of sensitivity is additional soil resistance to yielding resulting from interparticle bonding. Commonly, sensitivity values are determined with fall cone test, i.e. as ratio of the intact shear strength c_u, to the corresponding remoulded shear strength c_{ur}, at the same water content [Thakur et al. 2011]. Moreover, Karstunen et al. [2005] and Yin et al. [2011] suggested ratio of preconsolidation pressure of natural and reconstituted specimen as a measure of sensitivity.

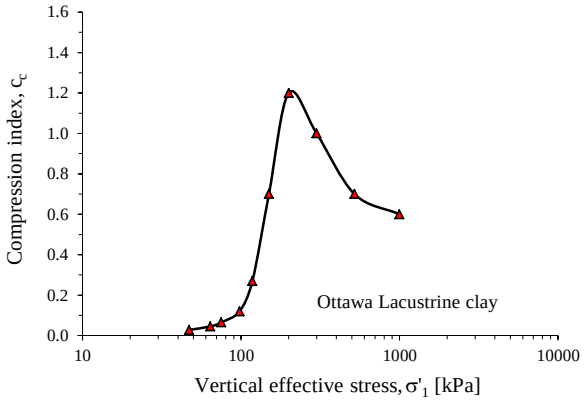

Figure 2.7 Stress dependency of slope in compression, Ottawa lacustrine clay [data after Graham et al. 1983].

In contrast to that of the reconstituted material, the natural sensitive clay specimens are characterised with change in compressibility within normally consolidated range as a result of progressive destructuration process. Thus, compression characteristics of natural sensitive clay specimen within normally consolidated range are strain dependent. If compression coefficients are related to vertical effective stress levels of each loading increment, a curve is ob-

tained such as shown on Figure 2.7 [Graham et al. 1983]. The curve represents the evolution of the destructuration process with accumulated strain due to stress level increase.

Important objective for oedometer testing is examining interrelation between destructuration process and secondary compression. Traditionally, secondary consolidation or creep is defined as the reduction in volume of a soil mass, caused by application of a sustained load to the mass and due to the adjustment of the internal structure of the soil mass, after most of the load has been transferred from the soil water to the soil solids [Crawford 1986]. As presented on Figure 2.8, pure creep is defined using the secondary compression coefficient $c_{\alpha e}$ given by Equation 2.7, as the slope of the final portion of log time-void ratio curve obtained for each loading increment, i.e. the compression per log cycle of time after pore pressures have essentially dissipated [Crawford 1986].

$$c_{\alpha e} = \frac{\Delta e}{\Delta \log t} \qquad (2.7)$$

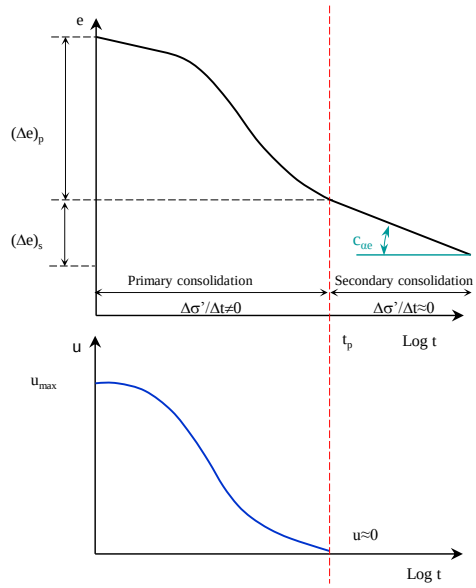

Figure 2.8 Definition of secondary compression coefficient in IL test [modified after Hight et al. 1987].

Figure 2.9 represents time-compression curves obtained under various intensities of constant vertical load in both recompression and normally consolidated domain. Shape of the time resistance curve is related to both consolidation process and different degree of mobilisation of reserve resistance against compression [Bjerrum 1967]. Evidently, secondary compression coefficient is not constant but highly stress dependent [Ladd 1972]. Consequently, it is possible to define creep behavior by relating secondary compression coefficient $c_{\alpha e}$ at each log cycle of time to stress level of corresponding load increment. With $c_{\alpha e}$ values plotted vs. vertical effective stresses curve shown on Figure 2.10 is obtained.

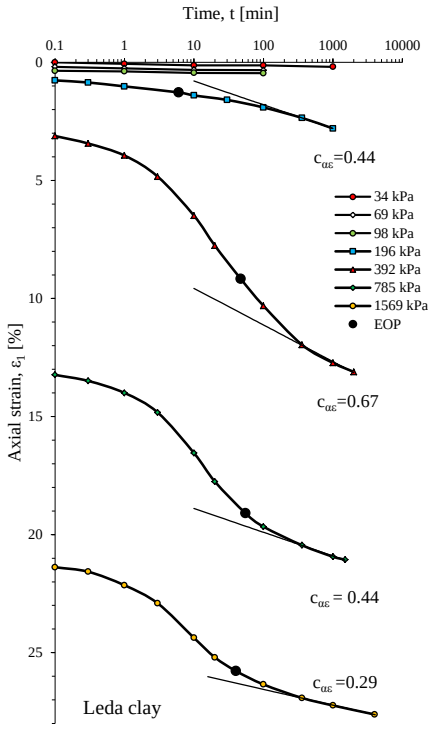

Figure 2.9 Time compression curves and secondary compression coefficients in IL test, Leda clay [data after Crawford 1986].

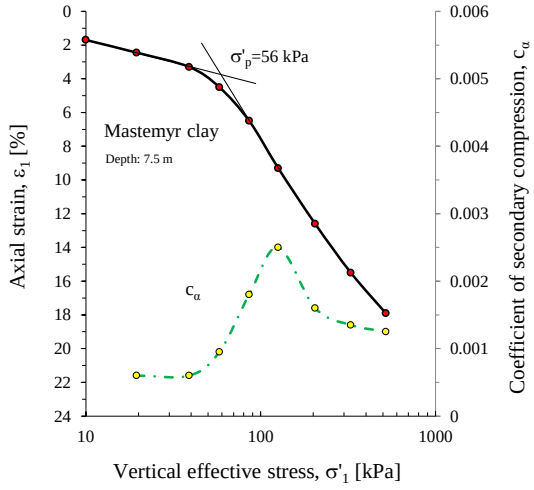

Figure 2.10 Stress dependency of secondary compression coefficient, Mastemyr clay [data after Clausen et al.1985].

Important parameter relating stress-strain to time-strain soil characteristics is that of $c_{\alpha e}/c_c$. Mesri et al. [1987] suggested the ratio $c_{\alpha e}/c_c$ is constant for a given soil, with values occurring between 0.04 and 0.08. However, if ratio of

$c_{\alpha e}$ over c_c is evaluated for each increment of a single oedometer test as the stress increases (see Figure 2.11), $c_{\alpha e}/c_c$ is observed to be significantly higher at stresses close to preconsolidation pressure [Graham et al. 1983]. In addition, results by [Leroueil et al. 1985] and recent results by [Yin et. al. 2011] show $c_{\alpha e}/c_c$ not being constant in soft sensitive clays.

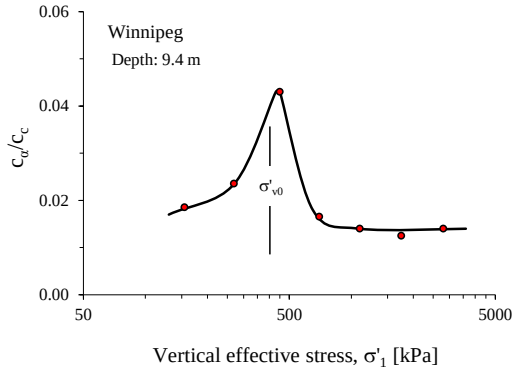

Figure 2.11 Stress dependency of c_α/c_c coefficient, Winnipeg clay [data after Graham et al. 1983].

One common approach in evaluation of compressibility is Tangent Modulus concept [Janbu 1963, Janbu 1967]. Tangent or compression modulus defined by Equation 2.8, is a measure of resistance against deformation and is crucial parameter for evaluating extent of clay structural resistance to compression.

$$M = \frac{\partial \sigma'_1}{\partial \varepsilon_1} \tag{2.8}$$

Based on extensive amount of experimental evidence Janbu [1967] identified principles of tangent modulus vs. vertical effective stress response of clays and quick clays shown on Figure 2.12.

Figure 2.13 presents strain and compression modulus response to vertical effective stress increase in IL oedometer tests on normally consolidated clay and quick clay. Janbu [1967] identified compression modulus of clays and quick clays in the overconsolidated range of IL test being constant. Furthermore, in the effective stress range of material being normally consolidated, both clay and quick clay response is characterised by continuous modulus increase with effective stress, defined by constant proportionality M'. However, in quick clays a marked drop in compression modulus is observed near preconsolidation stress level, signifying abrupt break down of the structural resistance of the clay skeleton [Janbu 1969]. Although most of the measured data presented in early works indicated half period sinusoidal pattern of compression modulus response in reloading, Janbu [1967, 1968] identified the compression modulus in overconsolidated range being constant, and undergoing instant transition in its intensity at the level of preconsolidation pressure. The interpretation approach is based on limited amount of data resulting from IL procedure.

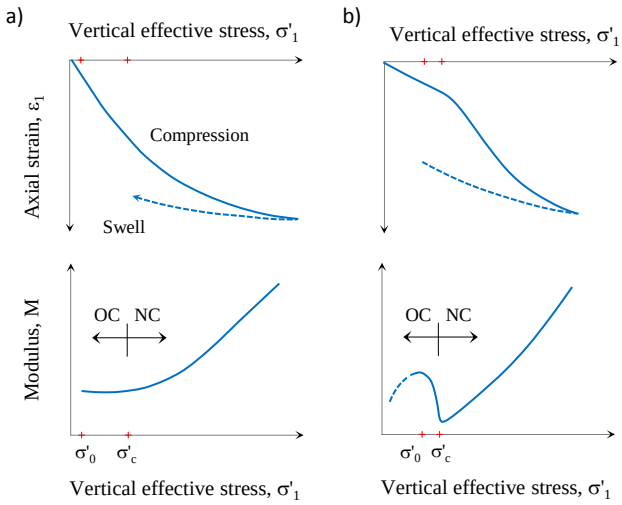

Figure 2.12 Typical strain and tangent modulus stress dependency curves obtained in oedometer test, a) clay, and b) quick clay [modified after Janbu 1967, Janbu 1998].

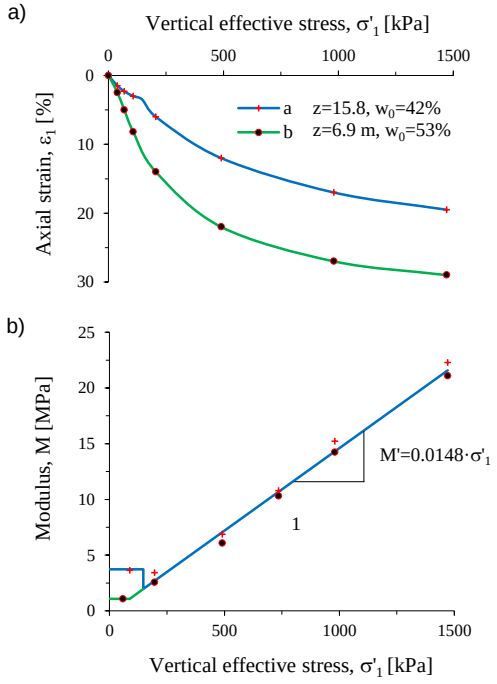

Figure 2.13 Stress-strain and stress-tangent modulus curves for normally consolidated clay and quick clay, Skabo clay [data after Janbu 1967].

Duration of the load increment influences stress-strain and time-strain characteristics of clay under oedometric test conditions [Taylor 1942]. Widely accepted model defining the effects is that developed by Bjerrum [1967] presented on Figure 2.14, based on concepts of young and aged normally consolidated

clay. The model defines material response in compression and swelling, i.e. current void ratio, being function of effective stress and time, R (σ'_v, e, t)=0 [Leroueil 2006]. Thus, a clay material subjected to constant vertical effective stresses undergoes the process of delayed compression with extent of compression proportional to the duration of loading. During prolonged periods under constant effective stress specimen continues to compress reaching a more stable arrangement of the particles resulting with reserve resistance against further compression, $\sigma'_p \geq \sigma'_o$ [Crawford 1986]. Settlement does not approach any ultimate value but continues at a decreasing rate [Hawley et al. 1973].

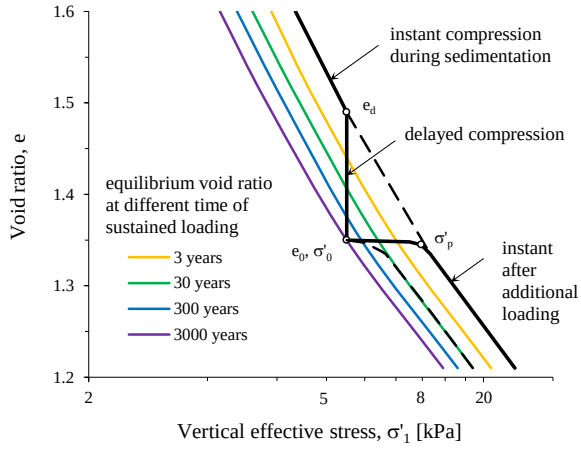

Figure 2.14 Compressibility and shear strength of a clay exhibiting delayed compression [modified after Bjerrum 1967].

Figure 2.15 shows effects of load increment duration on stress-strain behavior of clay in incrementally loaded oedometer test [Crawford 1964]. In long duration tests specimens are enabled to compress and consolidate for substantially longer period, i.e. are exposed to longer periods of delayed compression. During each load increment strain-rate progressively decreases with time of loading. With specimen being subjected to constant load during longer period, destructuration of inherent bonds is more pronounced and consequently effects of destructuration under each value of constant axial load are clearly exposed. Compression curve obtained in long duration tests are therefore placed underneath those obtained in 24 h incrementally loaded oedometer test.

Based on studies of loading time duration on compression characteristics and secondary compression coefficient [Mesri et al. 1977], and by adopting delayed compression concept by Bjerrum [1967], Mesri [1997] suggested stress-strain response in delayed compression being governed by model presented on Figure 2.16. According to EOP concept, effect of loading time on compression characteristics of clay materials is related to time period elapsed following the end of primary consolidation t/t_p [Watabe et al. 2012]. Perquisite for the validity of EOP concept is c_α/c_c parameter being constant.

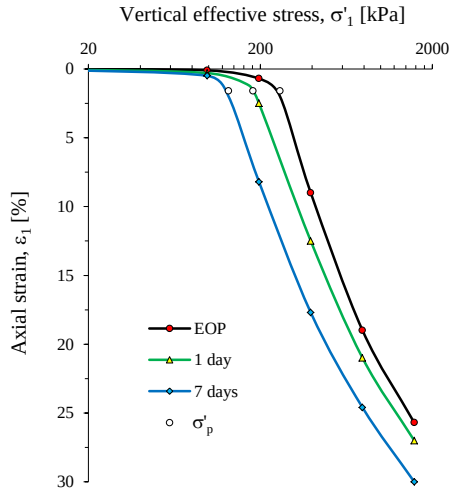

Figure 2.15 Oedometer test stress-compression curves for conventional and long term incremental loading [data after Crawford 1964].

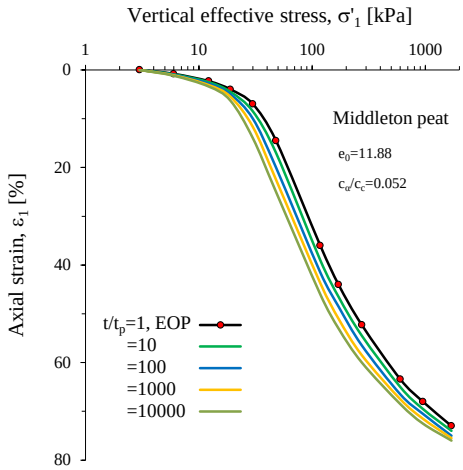

Figure 2.16 Influence of loading time duration on secondary compression response in oedometer test predicted by EOP concept, Middleton peat [adapted from Mesri et al. 1997].

Destructuration and duration of the load increment have important influence on material compression characteristics. Some IL odometer test results examining influence of loading step duration and load increment ratio LIR on compressibility are shown in Figure 2.17 [Graham et al. 1983]. Scatter of the results identified LIR and load increment duration having marked influence on the c_c response, especially in the normal consolidation range. Nonetheless, maximum c_c values were regularly identified at the stress level of preconsolidation pressure.

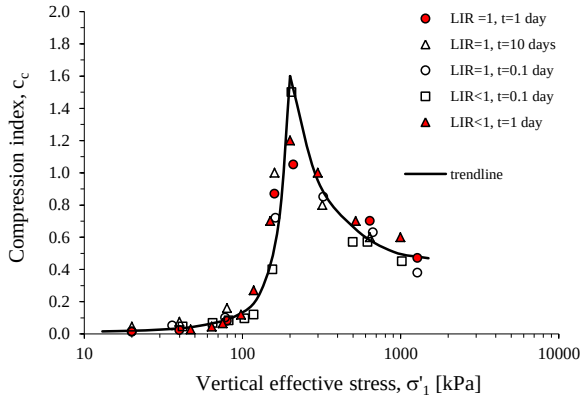

Figure 2.17 Influence of load step duration and load increment ratio on compression index, Ottawa lacustrine clay [Graham et al. 1983]

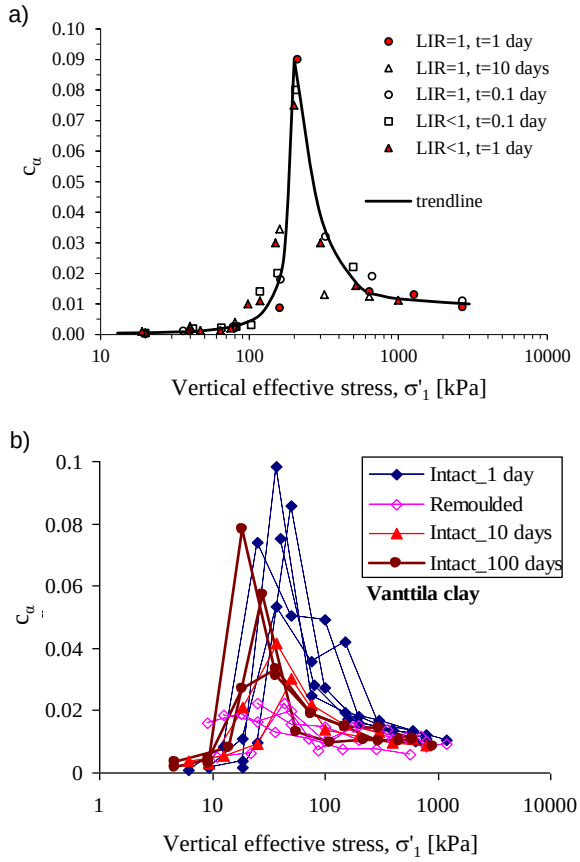

Figure 2.18 Influence of load step duration and load increment ratio on secondary compression coefficient, a) Ottawa lacustrine clay modified after [Graham et al. 1983], and b) Vanttila clay [Yin et al. 2011].

Figure 2.18 shows results of Graham et al. [1983] and Yin et. al [2011] examining effects of loading conditions in incrementally loaded oedometer test on secondary compression response. Secondary compression coefficient measured in long duration oedometer test is not a constant value. Since 24 h is suf-

ficiently long period for the complete dissipation of excess pore pressures under described incrementally loaded test conditions, the effect is mainly governed by influence of present level of structure and continuously changing strain-rate. Furthermore, results indicate considerable influence of structure, LIR and load step duration on magnitude of consolidation coefficient at certain effective stress level. However, the results are not evaluated in the perspective of specimen quality and sensitivity resulting with inconsistency in effects observed.

Effects of structure and loading conditions on compressibility in incrementally loaded oedometer test should be clearly observed if specimen response is evaluated in terms of c_α/c_c. Such efforts are presented on Figure 2.19 [Graham et al. 1983]. Although remaining within the commonly accepted limits of 0.04 and 0.08, Ottawa clay c_α/c_c results in Figure 2.19 a) exhibit considerable scatter and indicate stress dependent peak values. Figure 2.19 b) shows c_α/c_c values measured on Belfast clay contrasted to vertical effective stress normalized with effective overburden. The c_α/c_c values increase in reloading up to peak values corresponding to the level of preconsolidation pressure. With further increase of normalized effective stresses c_α/c_c values progressively decline.

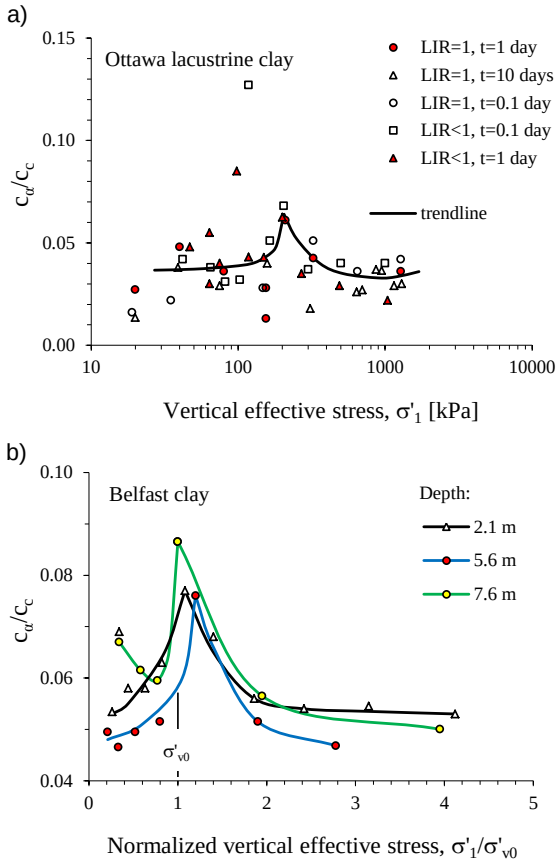

Figure 2.19 Influence of load step duration and load increment ratio on c_α/c_c stress dependence; a) Ottawa lacustrine clay, and b) Belfast clay [data after Graham et al. 1983].

The incrementally loaded oedometer test results above indicate loading conditions and destructuration being important parameters for reproduction of clay stress-strain-time behavior. Unfortunately, the results have not been related to specimen quality. Consequently, considerable uncertainty upon the nature of these effects still exists.

2.4.2 Constant rate of strain oedometer test CRS

Strain-rate is a crucial parameter governing compressibility of soft sensitive clay. Extending the work of Taylor [1942], Šuklje [1957] conducted systematic research aiming to identify effect of strain-rate on compressibility of geomaterials. Based on results, Šuklje [1957] proposed isotache concept illustrated on Figure 2.20. According to isotache concept, soil compressibility characteristics in void ratio vs. effective stress plane are represented by set of isotache curves ė=const., indicating unique relation between the effective stress, void ratio, and rate of change in void ratio, R (σ'_v, e, ė) [Leroueil 2006]. In line with isotache approach, creep occurs during the entire consolidation process, while time dependent strains are influenced by the thickness of the clay layer, permeability and drainage conditions [Claesson 2003, Degago et al. 2011].

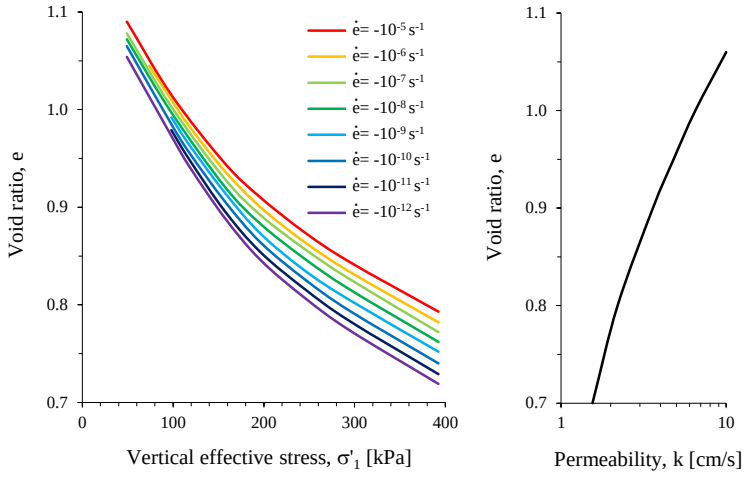

Figure 2.20 Isotache model representing isotache for clay of high compressibility [data after Battelino 1973].

Rate of strain has a significant influence on compressibility and yielding of clays, with preconsolidation pressure being considerably lower for slow tests than for fast ones [Crawford 1986]. Due to their viscous nature, the position of stress-strain curve in e vs. ln σ'_1 plane is determined by strain-rate imposed, with curves obtained at higher strain-rates being proportionally displaced to higher stress level indicating higher structural resistance (see Figure 2.21). The effect has been reported by Crawford [1965a], Sällfors [1975], Leroueil et al. [1985], Marques [1996] and Claesson [2003] to name just a few. As shown on Figure 2.22 a), by conducting CRS tests under different constant strain-rates and determining preconsolidation pressure at each strain-rate, confident definition of yield pressure strain-rate interaction can be attained [Ladd 1971,

Leroueil et al. 1985]. Moreover, as shown on Figure 2.22 b), in the selected range of strain-rates a linear relationship between the logarithm of normalized yield stress and the logarithm of strain-rate can be established [Yin et al. 2011].

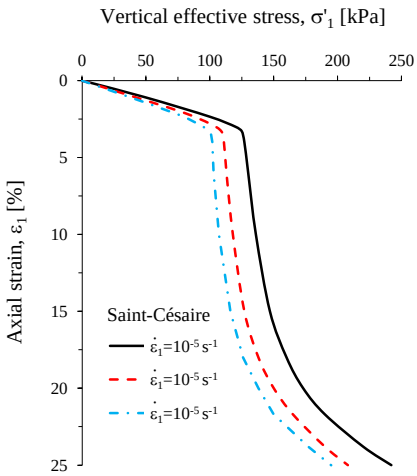

Figure 2.21 Effects of strain-rate on one dimensional compression, Saint-Césaire clay [Leroueil 1988].

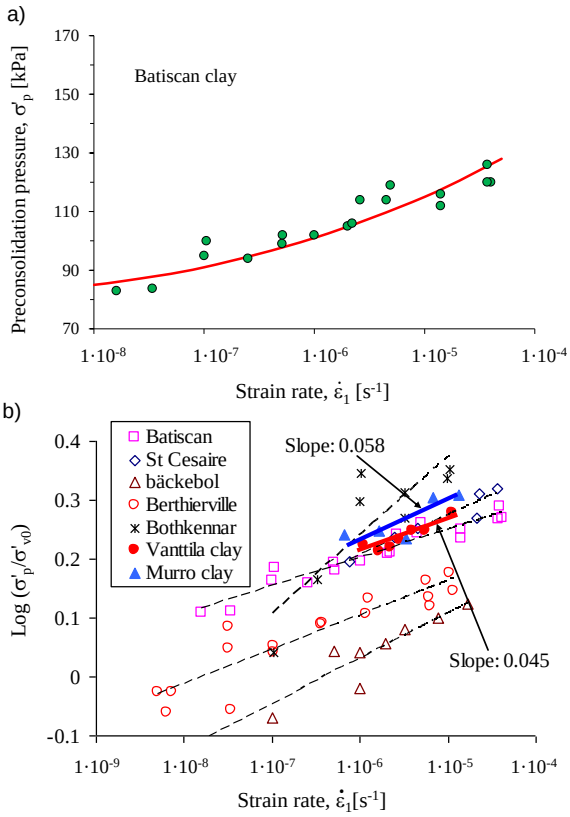

Figure 2.22 Effect of strain-rate on preconsolidation pressure in CRS oedometer test, a) in semilogarithmic [modified after Leroueil et al. 1985], and b) double log scale [Yin et al. 2011].

In evaluation of strain-rate effects on compressibility characteristics it is important to account for initial quality of the specimens. Continuously loaded CRS tests result with continuous stress-strain curve. Consequently, stress dependency of compression index, i.e. destructuration, can be clearly evaluated. Figure 2.23 presents CRS compression curves obtained on Bothkennar clay together with stress dependency of compression index [Tanaka 2000]. Test results presented are obtained on specimens compressed at identical strain-rate. The difference in compressibility response is not caused by strain-rate effects, but the difference in specimen quality resulting from implementation of different sampling techniques. Specimen obtained with sampler of better performance exhibits less deformation in reloading and higher compressibility following the yield [Tanaka 2000]. With rise of effective stresses both specimens tend towards unique value of intrinsic compression index.

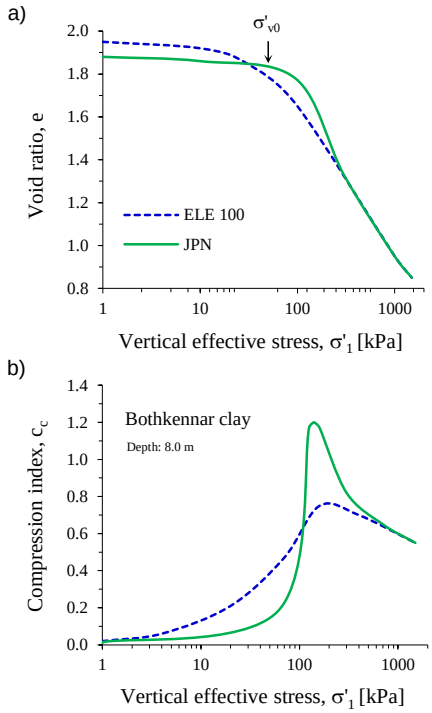

Figure 2.23 CRS test results on Bothkennar clay, a) stress compression curves and b) stress dependency of compression index [data after Tanaka 2000].

Compared to IL, a smooth loading procedure is more favourable from the viewpoint of reduced sample disturbance and consequently allows more accurate determination of both preconsolidation pressure and compression indices [Janbu et al. 1981]. In IL oedometer tests, for a short period after loading the rate of compression is at its maximum and is several million times faster than that experienced in the field [Crawford 1964a]. Shock-loading has an influence on specimen condition such as destroying or diminishing the viscous structural resistance of the soil skeleton at large stress-rates. This effect is expected to be significant on highly structured specimens of sensitive clay [Šuklje 1957].

Consequently, carefully conducted and systematically evaluated results of CRS tests performed at various levels of strain-rate can provide valuable information on nature of the destructuration process.

Figure 2.24 represents idealised compression modulus-stress curve based on continuous loading oedometer tests results on overconsolidated clay [Janbu et al. 1981]. In reloading, compression modulus increases up to stress level corresponding to effective stress of the specimen following stress release σ'_o, where it remains at fairly constant value M_o [Janbu et al. 1981]. With further increase of vertical effective stresses structural breakdown is initiated and marked by compression modulus decline until the preconsolidation stress level. At normally consolidated stress range compression modulus is linearly stress dependent with stress intercept at σ'_o indicating new virgin origin. The stress range characterising structural breakdown varies with type of soil and testing procedure [Tokheim et al. 1976].

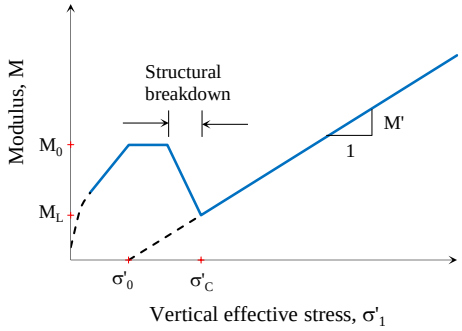

Figure 2.24 Idealized compression modulus stress dependency curve, overconsolidated Risvollan clay [modified after Janbu et al. 1981].

Effects of structural breakdown are to some extent recognized in Swedish practice [Larsson & Sällfors 1986, Larsson et al. 1997]. Improved compression modulus stress dependency interpretation presented on Figure 2.25 includes two constant compression moduli M_o and M_L, separated by linear but not instantaneous compression modulus change at stress levels prior yield. Instead of unique minimum, Swedish practice identifies constant compression modulus M_L for stress range defined by consolidation pressure σ'_C, and limit pressure σ'_L. It is only above σ'_L that the modulus linearly increases as an effect of the breakdown of the remaining structure and densification with rise in stress level [Larsson & Sällfors 1986, Åhnberg 2006].

Sällfors [1975] reported set of compression modulus vs. vertical effective stress curves obtained at different values of constant strain-rate (see Figure 2.26). The results imply intensity of initial compression modulus within an overconsolidated range being strongly and proportionally strain-rate dependent. Effects of destructuration in reloading seem to be rather uniform with compression modulus decrease prior yield being governed by similar stress-destructuration mechanism, i.e. slope of compression modulus versing vertical effective stress appears to be independent of rate of strain. Sällfors [1975] reported less compression in reloading at higher rates of strain. Furthermore,

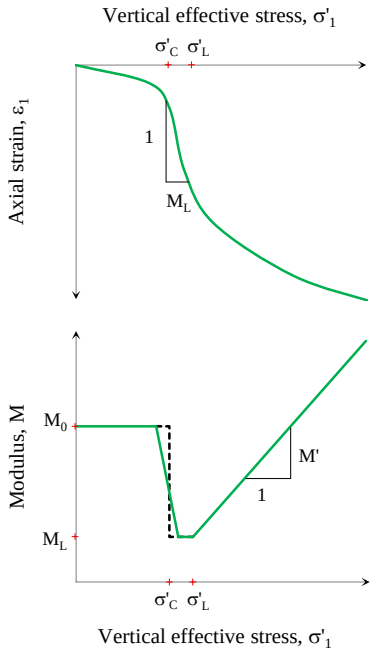

Figure 2.25 Swedish practice interpretation of the compression modulus in CRS test [after Larsson & Sällfors 1986].

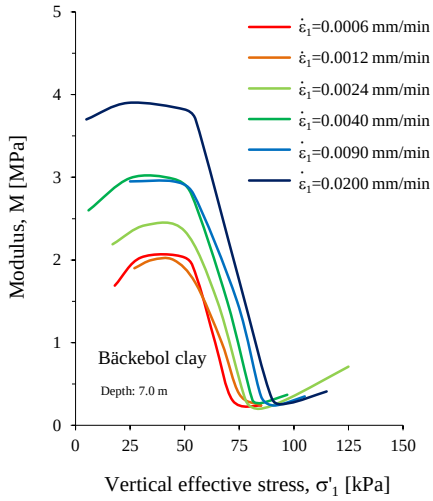

Figure 2.26 Compression modulus vs. vertical effective stress in CRS test, Bäckebol clay [data after Sällfors 1975].

according to Sällfors [1975] compression moduli curves, performed at low strain-rates, reach minimum compression modulus at lower vertical effective stress level compared to those obtained at high strain-rate intensities. The results are presented until rather low values of effective stress. Quality of the specimens used in the study is not reported, and it remains unclear to what extent presented results are influenced by sample disturbance.

2.5 Triaxial test

2.5.1 Incremental anisotropic consolidation triaxial test CAD

Previous research of clay compressibility under triaxial test conditions has revealed behavior of natural clay being strongly dependent upon the stress path in compression or extension. Indeed, stress ratio in consolidation has a major influence on specimen compressibility and yield. Figure 2.27 shows compression curve obtained in incremental triaxial consolidation test on natural clay specimen at constant stress ratio path K_o^{NC}=0.5 [Leroueil et al. 1983]. The load increment ratio is varied prior and after yield. Besides being clearly manifested, yield at K_o^{NC} stress ratio path corresponds to effective overburden stress [Tavenas et al. 1977]. However, for specimens consolidated under various constant stress ratio paths, yield stress is not a unique value.

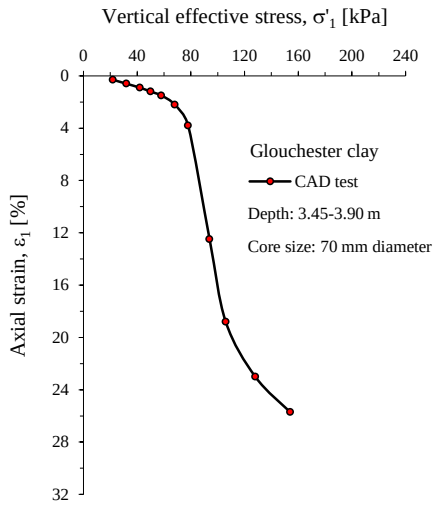

Figure 2.27 Anisotropic triaxial consolidation test, Gloucester clay [data after Leroueil et al. 1983].

By performing triaxial tests on reconstituted kaolin, Roscoe et al. [1968] showed yield stresses of isotropically consolidated specimens in q vs. p' plane forming an ellipse symmetrical to p' axis. This experimental finding shown in Figure 2.28 is the basis of the Modified Cam-Clay theory [Roscoe et al. 1968]. However, microstructure of most natural clays is anisotropic due to inherent structure formed during the sedimentation process and the subsequent self-weight consolidation [Koskinen et al. 2002, Koskinen et al. 2003]. Based on triaxial tests on natural clay specimens consolidated at various constant stress ratio paths, it was experimentally proven that yield stresses closely resemble pattern of inclined ellipse in q vs. p' plane [Tavenas et al. 1977, Tavenas et al. 1978, Tavenas 1981].

Figure 2.29 shows yield points obtained on natural specimens of Finnish clays consolidated along radial stress paths [data from Koskinen et al. 2002,

Karstunen & Koskinen 2004, Karstunen et al. 2008b]. Depending on stress ratio conditions imposed, specimens exhibit different values of yield stress. Using the yield points measured in consolidation at stress ratio paths -0.6<η<0.95, Author interpreted corresponding yield surfaces. Inclination of the elliptic yield surface manifests initial anisotropy of clay developed under K_o conditions.

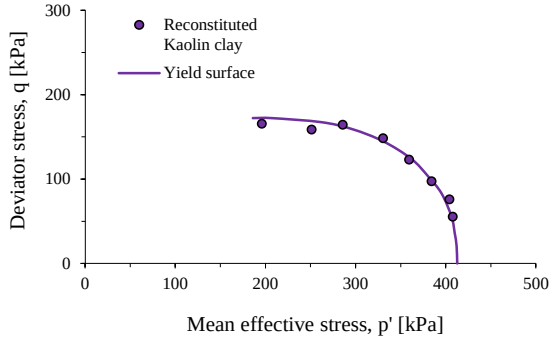

Figure 2.28 Yield surface of isotropically consolidated reconstituted Kaolin clay [modified after Roscoe et al. 1968].

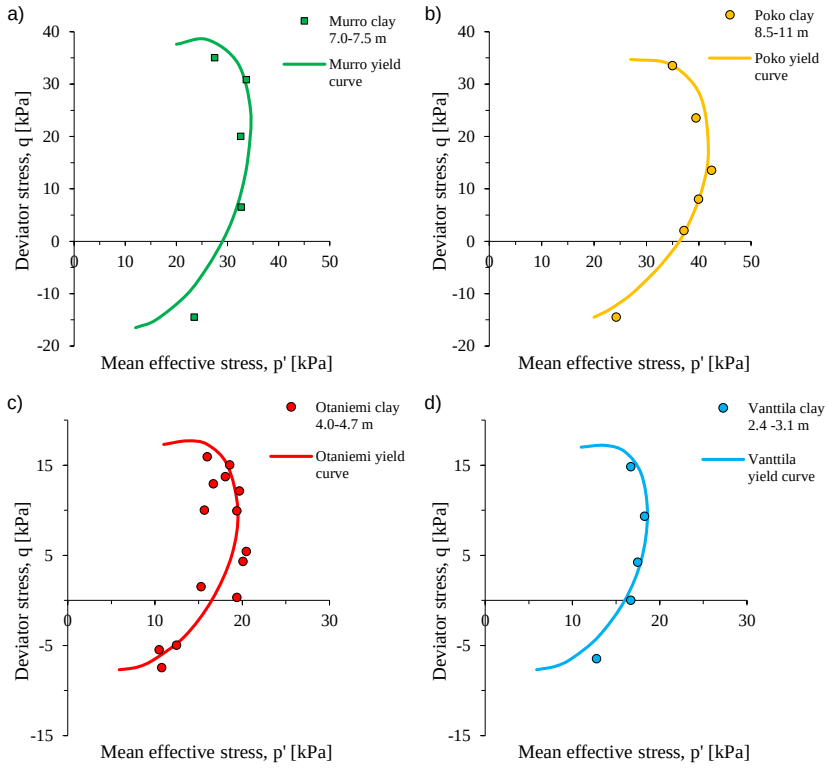

Figure 2.29 Yield surfaces of natural clays, a) Murro, b) Poko, c) Otaniemi, and d) Vanttila clay [data from Koskinen et al. 2002, Karstunen & Koskinen 2004, Karstunen et al. 2008b].

Besides initial anisotropy and stress ratio path characteristics, compressibility of clay in triaxial consolidation is highly dependent upon specimen sensitivity. The effect is presented on Figure 2.30, comparing compression response in triaxial CAD tests on natural and destructured clay specimens [Leroueil et al. 1979]. Compared to destructured, natural specimen exhibit additional resistance manifested by higher values of apparent preconsolidation pressure.

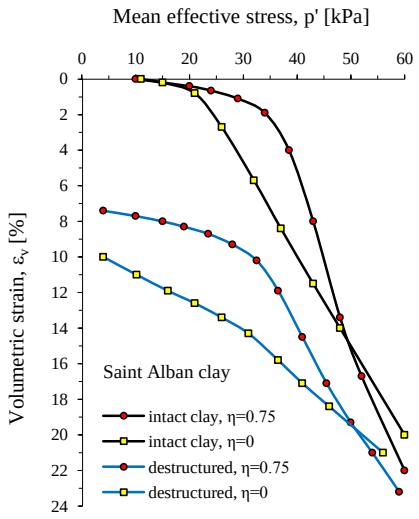

Figure 2.30 Compression curves in CAD triaxial tests, natural and destructured Saint Alban clay [data after Leroueil et al. 1979].

Effects consolidation stress ratio and specimen structure are not restricted to magnitude of yield only. Figure 2.31 presents reloading and post yield compression gradients in triaxial consolidation tests at various intensities of constant stress ratio on natural clay specimens [Koskinen et al. 2004, Karstunen et al. 2008b]. In triaxial stress space, the rate at which compression curve converges towards intrinsic compression line depends on the stress ratio imposed [Koskinen et al. 2004]. Thus, rate of destructuration is manifested by different gradient of the post yield compression curve. For nearly isotropic stress paths, natural specimens exhibit minor destructuration and values of λ are low. In contrast, at high stress ratios, destructuration is significant, and hence the values of λ are high. Effects of destructuration on swelling response are quantitatively much less notable compared to strains in virgin loading. Stress ratio dependency of compression indices presented on Figure 2.31 is characterised by the considerable scatter indicating significant variance in the initial quality of specimens evaluated.

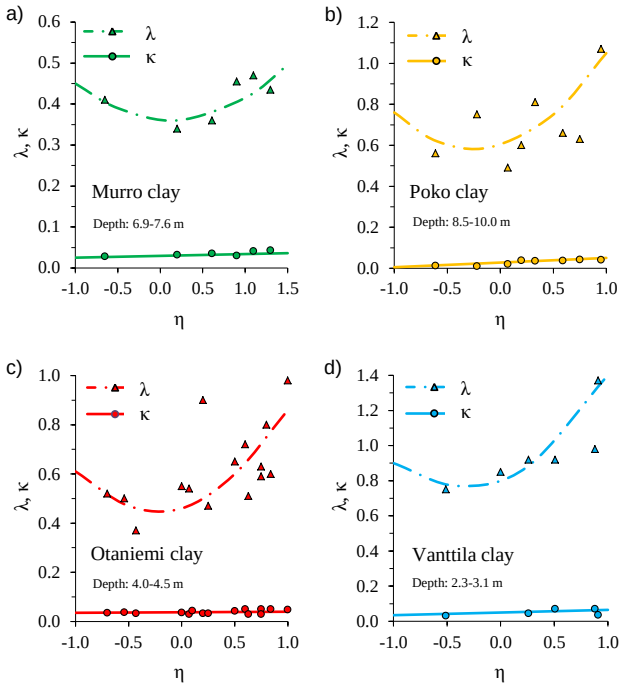

Figure 2.31 Influence of stress ratio in triaxial consolidation on κ, λ and λ_i of natural clay, a) Murro, b) Poko, c) Otaniemi, and d) Vanttila clay [data after Koskinen et al. 2004, Karstunen et al. 2008b].

2.5.2 Undrained triaxial compression test CAUC

Shear strength and strain response of clay is highly influenced by structural characteristics of the specimens as well as by the strain-rate conditions imposed in testing. Figure 2.32 contrasts triaxial undrained compression response of natural specimens with those obtained on specimens destructured in consolidation well beyond their yield stress [Leroueil et al. 1990]. The differen-

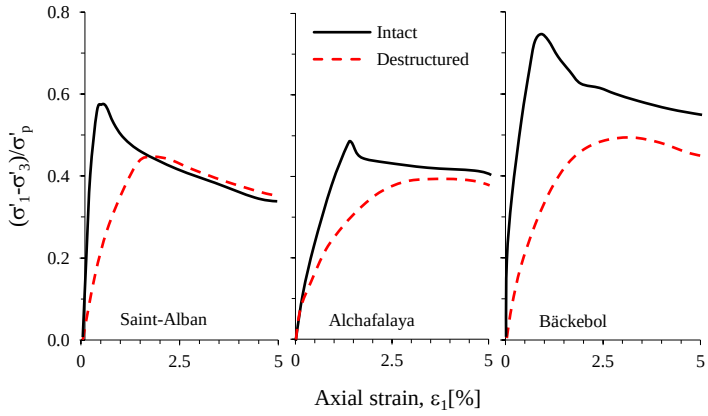

Figure 2.32 CAUC tests on natural and destructured Saint-Alban, Atchafalaya and Bäckebol clay [data after Leroueil & Tavenas 1985].

ces in stiffness and strength manifesting the effects of destructuration correspond with those caused by various extent of sampling disturbance presented in Figure 2.33 and Figure 2.34. Being less stiff, destructured clay exhibits reduced peak strength at larger failure strain [Leroueil et al. 1990]. Consequently, the yield surface identified based on destructured specimens is smaller in size. Results thus show failure envelope for the destructured clays being positioned lower than that for the natural structured clays [Leroueil et al. 1990].

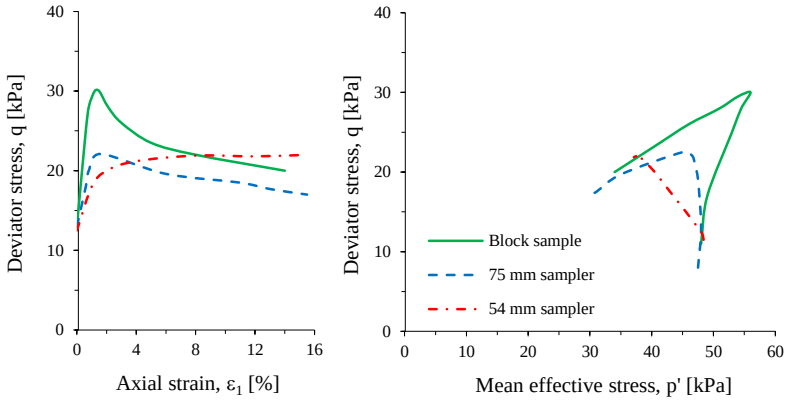

Figure 2.33 Effect of sample disturbance on CAUC test results, Lierstranda clay [data after Lunne et al. 1997].

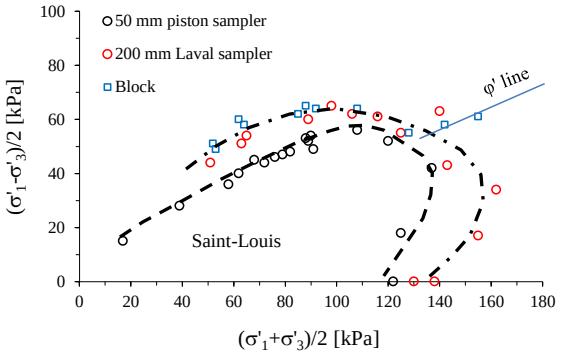

Figure 2.34 Effect of sample disturbance on yield surface, Saint-Louis clay [data after La Rochelle et al. 1981].

Besides destructuration, strength and stiffness of sensitive clay is a function of time. Figure 2.35 presents results of CAUC tests following consolidation to in situ stresses. Provided that the identically consolidated specimens of uniform quality are considered, triaxial undrained shear test under several constant strain-rate conditions provide clearly distinctive results. Results show specimen stiffness and strength being proportional to strain-rate imposed [Graham et al. 1983]. However, it remains unclear to what extent the results are influenced by specimen disturbance and consolidation conditions.

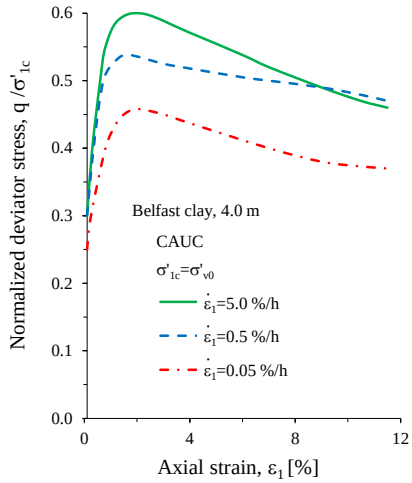

Figure 2.35 CAUC test results at constant strain-rate, Belfast clay [data after Graham et al. 1983].

Strain-rate variation during undrained shear alters stress-strain response of the specimen. As presented in the Figure 2.36, when the strain-rate is increased, the stress-strain response moves from the curve corresponding to the former strain-rate to that matching the new strain-rate [Vaid & Campanella 1977]. Thus, rise in strain-rate transfers stress-strain curve to a zone of higher apparent stiffness, while opposite effect occurs if strain-rate is reduced [Leroueil et al. 2003].

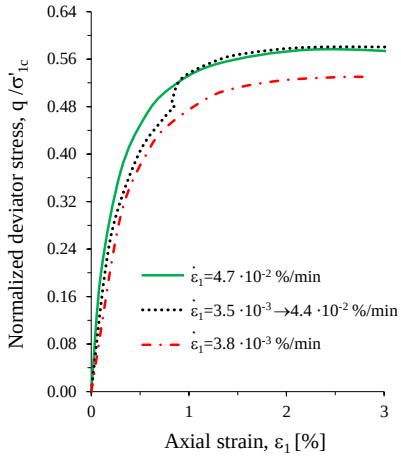

Figure 2.36 Influence of the strain-rate change in CAUC test, Haney clay [data after Vaid & Campanella 1977].

Effects of strain-rate on stress-strain response expose yield surface of natural clay being a function of strain-rate [Tavenas et al. 1979]. Indeed, size of the yield surface is proportional to the rate of undrained compression. Figure 2.37 illustrate influence of strain-rate on undrained compression stress path in q vs.

p' stress plane. Undrained compression tests performed on NC clays at rapid strain-rate are characterised with steeper stress paths and higher strength compared to those in slow tests. The steepness of the stress paths is direct manifestation of pore pressure build-up in undrained compression. Rise of pore pressure is more pronounced in tests at slow strain-rate, and vice versa. Consequently, strength of the specimen will differ depending on strain-rate resulting with distinctive yielding, exposing the yield surface for rapid loading being larger than that detected in slow loading [Graham et al. 1983, Leroueil et al 2003b]. The effect of strain-rate on size of the yield surface was experimentally proven by CAD tests at constant strain-rate shown in Figure 2.38. Yield curves obtained in consolidation at different strain-rates exhibit same shape, yet those representing results at rapid strain-rate are displaced to higher stress levels [Leroueil et al. 1985].

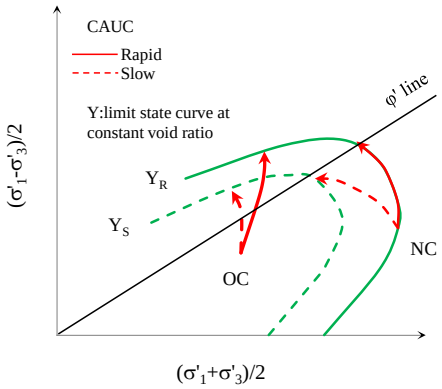

Figure 2.37 Stress paths for rapid and slow undrained compression test and corresponding yield surfaces [after Leroueil et al. 2003b].

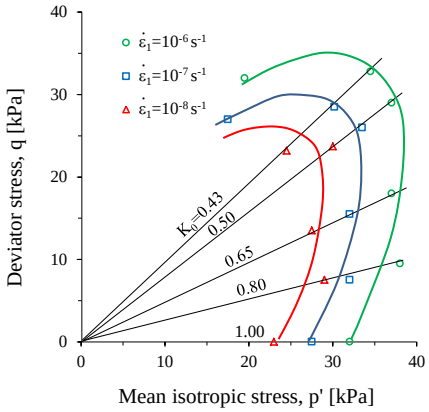

Figure 2.38 CAD tests at constant strain-rate and effects of strain-rate on yield surface, Berthville clay [data after Leroueil et al. 2003b].

With destructuration and strain-rate having opposite impact on shape and size of the yield surface, both effects need to be considered when defining rate dependence of stress-strain-strength behavior of soft sensitive clays.

3. Perniö site and sampling programme

3.1 Perniö soft sensitive clay deposit

The tests of this study are performed on Perniö clay, a soft sensitive marine clay of postglacial origin. Perniö clay deposit is situated in the south-western Finland, about 140 km west from Helsinki nearby the city of Salo (Figure 3.1). Detailed map of Perniö clay sampling site is presented in Appendix 1. Lithostratigraphic conditions of the sampling location include dry crust and stiff clay layer underlain by soft clay strata. Thickness of the soft clay formation alternates with hills of bedrock and moraine [Lehtonen 2011]. Within soft clay thin silty layers occasionally occur. Groundwater level at the location corresponds to -1.0 m below the surface.

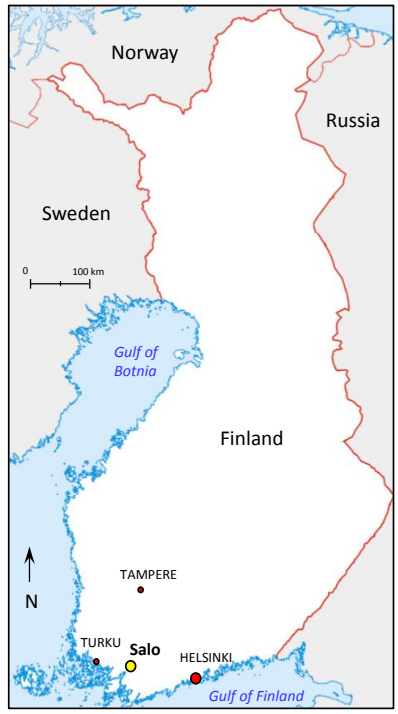

Figure 3.1 Location of Perniö clay deposit.

Geotechnical properties of Perniö soft clay are presented in Table 3.1. Undrained shear strength is typically very low, 10 to 20 kPa. Unit weight of the

material appears to be at about γ=14.7 kN/m^3 and specific gravity is of G_s=2.7 in average. Sensitivity values mostly appear in a range from 10 to 40. Initial void ratio values vary considerably between 1.8 and 2.6, corresponding to broad range of initial water content of the Perniö soft clay material i.e. from 60 to 111 %. Organic content of 1.4 % in Perniö clay is moderate. Typical value of initial plastic limit measured is between 29 and 37 % and liquid limit is of 46 to 101 %. According to the plasticity chart these values position Perniö clay above A-line among inorganic clays of high plasticity.

Table 3.1 Geotechnical properties of Perniö soft clay.

Material	Perniö clay
Sampling depth, z [m]	2.0-7.0
Unit weight, γ [kN/cm^3]	13.9-16.1
Undrained shear strength, c_u [kPa]	10.0-20.0
Sensitivity, St	13.8-41.9
Specific gravity G_s	2.7
Water content, w [%]	58.8-110.7
Clay content, Cl [%]	52.0-77.0
Organic content, Hm [%]	1.4
Plastic limit, w_P [%]	29.3-36.5
Liquid limit, w_L [%]	46.1-101.3
Void ratio, e_o	1.83-2.56

3.2 Perniö test embankment

In October 2009 Tampere University of Technology and Finnish Transport Agency initiated a full scale stability test project with an agenda of performing in situ test of Perniö railway embankment being brought to failure [Mansikkamäki et al. 2011]. Main objective of the failure test was to collect data for development of stability calculation methods and to test the technical suitability of different monitoring approaches [Mansikkamäki et al. 2011]. Results of preliminary research of Perniö deposit revealed presence of very soft sensitive clays. Consequently, Aalto University research of rate effects in structured soft clays was directed toward sampling, laboratory testing and constitutive modelling of soft sensitive Perniö clay.

Detailed map of Perniö site including location of old Perniö embankment is shown in Appendix 1. Furthermore, cross sections of the Perniö embankment A-A', B-B', C-C', D-D', E-E', F-F', and their location are presented in the Appendix 2 and Appendix 3, respectively. The height of the sand fill of the embankment was ~0.50 meters and varied depending on the cross section considered. In the section B-B' the highest elevation of embankment crest was measured, +8.62 m. Slope of the embankment was about 1:3. In addition to the embankment geometry, Appendix 3 contains results of preliminary investigation works including Swedish weight sounding and vane shear test.

Perniö test embankment and activities during the failure test are presented in Figure 3.2. Over the old sand fill, new 550 mm thick crushed rock layer was

constructed [Mansikkamäki et al. 2011]. To reduce the load required for failure and to control the location of the failure surface, ditch has been excavated ~7 m from the embankment on the future sliding side [Mansikkamäki et al. 2011]. The depth of the ditch was 2 m, and the side slope was 2:3. Within the area between the embankment and the ditch, a top surface layer of dry crust of 0.3 to 0.6 m was removed and placed as a counter weight on the opposite side [Mansikkamäki et al. 2011]. Field monitoring consisted of pore pressure and earth pressure gauges, automatic inclinometers, different displacement measurements and laser scanner [Mansikkamäki et al. 2011]. Loading of the embankment was achieved by means of large containers filled with sand using conveyor belt [Mansikkamäki et al. 2011]. Loading was increased in less than 36 hours from 0 to 87 kN/m^2, with failure occurring two hours after the loading ended [Mansikkamäki et al. 2011]. Failure of Perniö test embankment in a delayed manner complied with the viscous characteristics of sensitive soft clays. Due to time dependent behavior and strain softening of the clay, deformations and pore pressures continued to increase after the loading had ended and under conditions of constant external load were followed by displacement increase at an accelerating rate prior to failure [Mansikkamäki et al. 2011, Lehtonen 2011]. For more information on Perniö test embankment research reader is referred to Lehtonen [2011] and Mansikkamäki [2015].

Figure 3.2 Perniö test embankment.

When soft sensitive clays are subjected to stresses above their in situ overburden they undergo complex process of progressive loss of structure continuously altering their shear strength and compressibility characteristics. Inherent structure of soft clays is very sensitive in its nature. Since the destructuration process is often started already during sampling and is manifested by the sample disturbance, special attention needs to be given to the sampling of such materials. Inherent structure of sensitive clays is often erased by poor sampling procedure. Consequently, most of the published results describing behavior of natural clays are performed on more or less disturbed samples. Structure has important influence on stress-strain-strain-rate behavior of clays, such as creep and strain-rate effects. Moreover, rate dependence and

destructuration are closely interlinked processes, often with opposite manifestations on stress-strain characteristics of clays. In order to capture this effects complex and carefully performed laboratory tests are necessary.

3.3 Sampling programme objectives

Laboratory tests used as a basis for development of constitutive models should aim the highest quality samples so to ensure recording of material stress-strain-strain-rate response that represents the material's in situ behavior [Clayton et al. 1982]. To evaluate and quantify the influence of various aspects of sampling disturbance on the quality of laboratory test results on Perniö clay, three different sampling techniques are implemented; Swedish standard STII 50 mm, NGI 54 mm and NGI 86 mm sampler. Methods chosen are stationary piston tube sampling methods yielding samples different in size/diameter. Although better alternatives such as Laval and Sherbroke sampler were considered, they were not used because of unavailability of equipment and lack of research funds. Sampling is carried out with small scale drilling machine typically used for sampling and in situ sounding tests.

Aim of the sampling programme is to quantify effects of sampling on initial state parameters and stress-strain-strain-rate characteristics measured in the laboratory. Evaluation of sampler performance in soft sensitive Perniö clay has two major objectives. First objective is to compare and evaluate the performance and the influence of sampling techniques implemented on quality of results of laboratory tests conducted on rather homogenous material of same stress history, representative of in situ greenfield conditions. Second objective is to evaluate effects of secondary disturbances on quality of results of laboratory tests obtained on material with the same depositional, yet different in situ consolidation stress history. In order to meet later objective NGI 54 mm sampling technique is used for sampling of overconsolidated material and material subjected to partial destructuration process due to the influence of the construction works. This part of the sampling programme is in further text referred as S-2009. In the additional part of the sampling programme S-2010, selected sampling methods are implemented on a relatively narrow sampling area in order to enable evaluation and comparison of samplers' performance without significant influence of the variation of in situ stratigraphical conditions. Results of this complex sampling programme should yield with both clear evaluation of samplers performance in terms of their design limitations, and in addition clear evaluation of effects indicating poor sampling technique such as sampling caused overconsolidation or unloading.

Detailed plan of sampling works within the S-2009 is shown on Figure 3.3. Sampling profiles 44 and 47 are positioned so to enable sampling of material overconsolidated as a result of dry crust removal, while profiles 43 and 45 aim sampling of material influenced by the partial destructuration as a result of load caused by the embankment. Since it is the effect of the overconsolidation and destructuration processes in situ on sampling results that is of concern, single sampling method NGI 54 mm is sufficient to derive conclusions on the

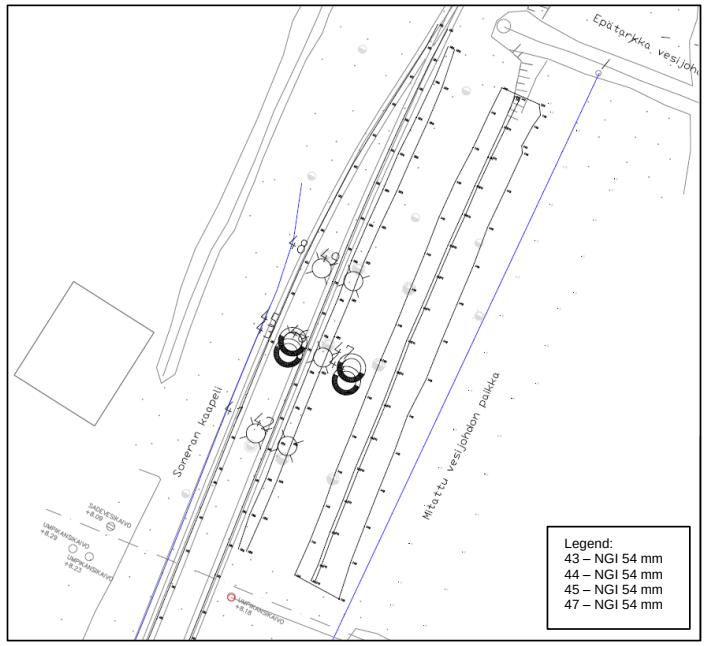

Figure 3.3 Location of sampling boreholes in sampling programme S-2009.

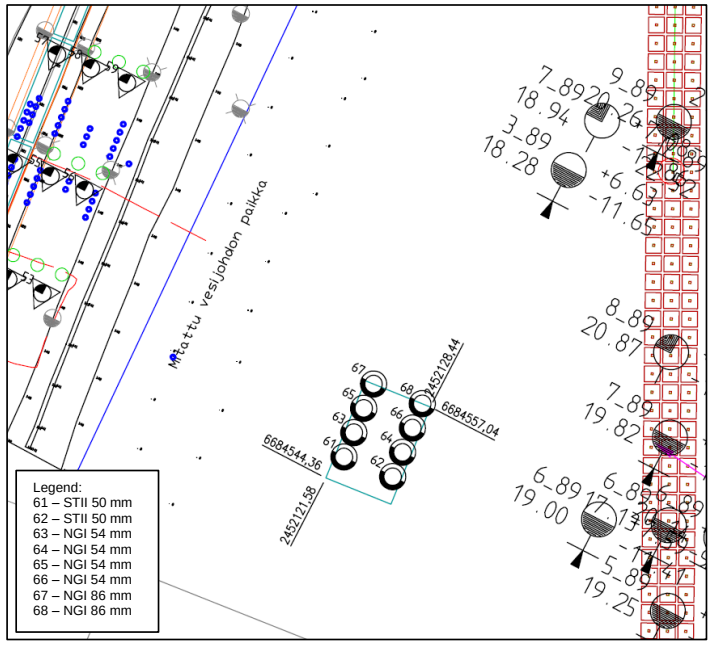

Figure 3.4 Location of sampling boreholes in sampling programme S-2010.

effects of interest. In addition, the sampling programme should clearly reveal stratigraphical conditions of the location. Two corresponding profiles in terms of material consolidation stress history and sampling depths are provisioned so to enable confirmation of sampling results. Sampling profiles 44 and 47 are located between the test embankment and excavated ditch. Within the area

surface layer of dry crust has been removed. Consequently, underlying material was subjected to unloading compared to the greenfield conditions. This fact is expected to influence test results obtained on material from these two boreholes. Profiles 43 and 45 are located at the toe of the Perniö test embankment. Additional stresses caused by the embankment are expected to cause modifications in structure and initial water content and thus marked effects on results of laboratory tests.

The location of sampling area with distribution of sampling techniques implemented within S-2010 is shown on Figure 3.4. Eight sampling boreholes are distributed within an area of 7.0 x 9.0 m. To exclude effects of crude errors in sampling each sampling method is used on at least two profiles. Sampling profiles are positioned close enough in order to reduce influence of differences in site stratigraphy. In parallel, sampling profiles are reasonably distanced with the intention of avoiding influence of works on one sampling profile on results obtained on profiles in its vicinity. Minimum distance between boreholes is 3 m. The profiles are positioned so to enable construction of two 7 m distanced cross sections representing in situ stratigraphical conditions. Sampling depths are chosen in such a manner that performance of various sampling techniques can be compared for every stratigraphical unit in situ. The location of the S-2010 sampling area is far enough from constructions existing on site in order to obtain sampling data representable for initial in situ conditions.

GPS coordinates of the sampling profiles are presented in Appendix 4. At each sampling profile a sample is taken at every metre of depth down to a depth of 7 m. In addition, position of the bedrock is determined on at least two boreholes within S-2010. The samplers selected and methodologies of their implementation are described in detail in the following.

3.3.1 Stationary piston sampler STII with 50 mm liner

Stationary piston sampler STII with 50 mm liner or Swedish standard sampler in Figure 3.5 is the most commonly employed sampling method in Finnish geotechnical practice. STII is fixed piston tube sampling method, as well as NGI 54 mm and NGI 86 mm. However, unlike NGI samplers, Swedish standard sampler has no inner extension rod. Instead, the sample cylinder is pressed downwards by rotation of the extension pipes, i.e. transfer of rotational to linear motion threw a screw and nut mechanism [Andresen & Kolstad 1980]. Internal diameter of sampler cutting edge is 15.12 mm with cutting edge angle of 5.7° and external diameter of 59.89 mm. Thus the resulting area ratio is considerable (30 %). The sampler knife has no inner clearance. ST II sampler essentially enables continuous sampling with sample obtained in three liners (tubes) contained within the sampler body. Liners made out of PMMA (Plexiglas) material have external and internal diameter of 54.0 mm and 50.3 mm, respectively. Length of each tube is 170 mm and thickness of the side walls is 1.70 mm. Only the part of the sample in the intermediate tube is suitable for shear strength and compressibility testing [Jakobson 1954]. Samplers' robust construction allows sampling of soft to stiff cohesive soils and silts.

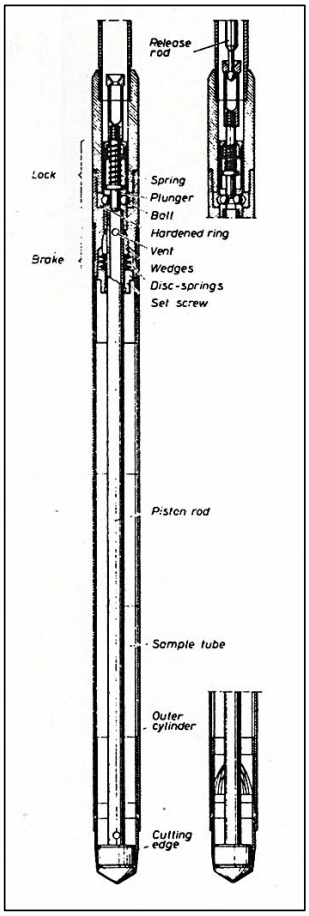

Figure 3.5 Stationary piston sampler, technical [Kallstenius 1971].

STII method is robust yet lengthy sampling technique involving complex mechanical processes in sampling. Prior to sampling the cutting edge (Figure 3.6 c) is removed and by means of relatively complex procedure plastic liners (Figure 3.6 e) are filled into the sampling body and locked by specially designed ring (see Figure 3.6 d). During the liner filling lubricant spray is used. By default this sampling technique utilises steel retainer preventing material loss during the sampler withdrawal. The retainer is a cylinder with number of steel-stripes attached to the lower end of the tube and is entering the sampler just above its lower end [Jakobson 1954]. With the sampler refilled, the cutting edge is screwed back on the bottom of the sampling body. Sampler is lowered into the predrilled borehole and pushed until the selected sampling depth. Thereafter, the samples are cut by rotation of the inner rods causing systematic withdrawal of piston so to enable entrance of the material into the liners. After achieving sufficient penetration depth and with liners filled, sampler is redrawn to the surface where cutting knife, retainer and mechanical parts are removed and liners taken out from the sampler by backward rotation of rod with piston. Each liner is released by cutting of the sampled material with thin metal wire. Following their release, liners are sealed on both ends using plastic

foil and rubber caps. Thus PMMA liners, which are favourable for water content prevalence, are used as the final container of the sampled material.

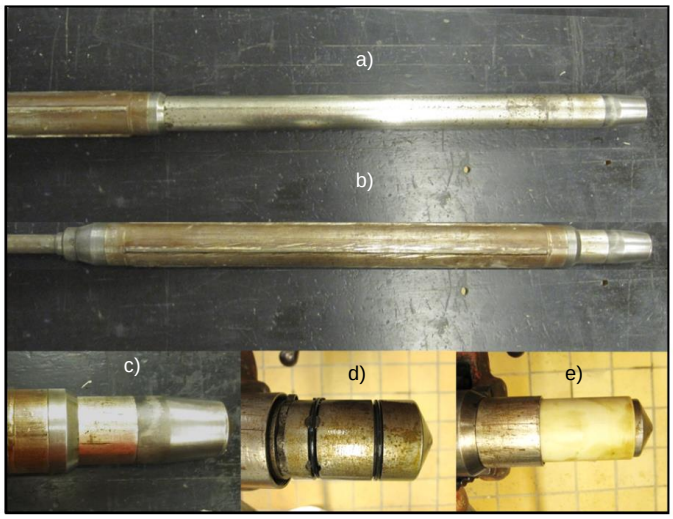

Figure 3.6 STII sampler with a 50 mm liner; a) after punching, b) before punching, c) cutting edge, d) mechanical lock ring, e) PMMA liners.

The STII sampling method yields rather poor sampling results owing to small size of the samples, robust sampler dimensions and lengthy sampling process. Considering that most of the time-consuming work during sampling involves connecting disconnecting, lifting up and lowering down drilling rods, pipes and tools, rather than the sampling action per se, complicated mechanism and system of sampler preparation prior sampling makes this method inappropriate from the perspective of sampling efficiency. Another disadvantage of this sampling method is in sampler being characterised by large area ratio causing considerable disturbance [Andresen & Kolstad 1980]. The main disadvantage of the sampling technique is the possibility of rotation of the entire sampler during the sample collection process unless the sampler body is fixed by in situ lateral stresses. If sampler is rarely used momentum employed to rotate the extension pipes can be substantial and possibly larger than torsional resistance of soft clay. ST II sampler is encompassed by Finnish geotechnical investigation and testing standard SFS-EN ISO 22475-1:2006E.

3.3.2 Norwegian Geotechnical Institute 54 mm piston sampler

At Aalto University, NGI 54 mm stationary piston sampler is routinely used for sampling of soft clays. The first model of the sampler, developed at Norwegian Geotechnical Institute in 1952 on the basis of Hvorslev's [1949] suggestions, is shown on Figure 3.7 [Andresen & Kolstad 1980]. The five main parts of the sampler are extension pipes, inner extension rods, sampler body with fixed piston and removable sampling cylinders. During the sampling, numbers of cylinders are used since they also have a function of a container. The piston of the sampler is of a fixed type and is directly connected to the inner rod while

the sampler body is connected by means of the extension pipes. Consequently, piston position can be modified by relative movement of inner rods and outer pipes. In two extreme positions, pistons conically shaped tip is either next to the sampler body (see Figure 3.8 b) or alternatively, it is outdrawn so that its tip position corresponds with cutting edge of the cylinder (Figure 3.8 c). In extreme positions piston is fixed by means of screws between inner rod and outer extension pipe. Originally designed Norwegian type 54 mm fixed piston sampler (Figure 3.7) has 54 mm internal diameter and 1.3 mm cylinder thickness. It is characterised with inside clearance of 0.9 %, area ratio of 12 %, and angle of edge of cutting shoe of 10°. Original form included two types of cylinders, 400-600 and 800-1000 mm long. For 800 mm samples length to diameter ratio is 15 [Andresen & Kolstad 1980]. Average thickness of the cylinders used in this study is 1.25 mm. Inside clearance was removed from Aalto University cylinders. Average internal diameter of the cylinders is 54.56 mm and their length is 880 mm. Average outer diameter of sampling cylinders is 57.00 mm, area ratio is 8.5 % and length to diameter ratio is 14.3. Optimum sample length of 780 mm means nearly continuous sampling [Andresen & Kolstad 1980]. The sampler is primarily designed for taking undisturbed samples in very soft to stiff clay [Andresen & Kolstad 1980, Leroueil & Hight 2003].

Sampling process is rather straightforward and time-efficient, if compared to sampling process using ST II. Prior to sampling, cylinder is connected to the sampler body by means of three locking nuts and entire assemblage is lowered into borehole by means of extension pipes and inner extension rods. In initial stage entrance of material into the cylinder is prevented by an outdrawn position of piston. Therefore, during driving of the sampler to the required depth, the piston rod is locked in its outdrawn position by means of a left-hand threaded spindle, so that position of the tip of the piston corresponds to the lower open end of the sampling cylinder [Andresen & Kolstad 1980]. In this configuration sampler is placed in the by auger pre-drilled borehole, and it is pushed downwards through the soil until tip of sampling cylinder reaches appropriate sampling depth. At selected sampling depth piston is released and withdrawn upwards by turning the inner rod, consequently opening the sampling cylinder and enabling entrance of the soil. In its upper position the piston is fixed directly underneath the sampling body by left hand spindle lock of the piston rod consequently carrying the entire weight of the inner rods. With the inner rod secured at the surface cutting of the soil can start [Andresen & Kolstad 1980]. In the following stage, entire assemblage is slowly pushed downwards by means of outer extension tubes with thin walled steel cylinder penetrating soil material and sample being cut into the cylinder. Groundwater or bentonite slurry trapped above the sample escapes threw the hollow piston valve. The penetration speed should be kept constant and adjusted to an optimum rate [Andresen & Kolstad 1980]. Based on NGI experience, 1.0 to 3.0 m/min penetration rate is recommended [Andresen & Kolstad 1980]. If the penetration speed is reduced below 0.1 m/min, adhesive forces start to build up causing severe disturbance [Andresen & Kolstad 1980]. During penetration there is no rotation of the cylinder with respect to its vertical axis in order to minimize disturbance of material sampled. When sampler's downward move-

ment reaches 780 mm or ~80 % of the cylinder length, movement is stopped. Thereafter, sample is cut off from the deposit by torsional stresses induced at the bottom of sampling cylinder by slow rotation of the sampler three to five times around its vertical axes. Finally, sampler is slowly redrawn to the surface. During sampler retraction, downward movement of the sample initiates vacuum underneath the piston [Berre et al. 1969]. This vacuum together with the friction between the sample and the cylinder prevents the sample from falling out [Berre et al. 1969]. Upon retrieval vacuum is released by opening piston valve and sampling cylinders are disconnected from the sampler [Andresen & Kolstad 1980]. Sampling cylinders serve as sample containers and need to be sealed on both ends by plastic bags and rubber caps in order to prevent moisture loss. Finally, sample containers are carefully transported in vertical position in order to avoid secondary mechanical disturbance.

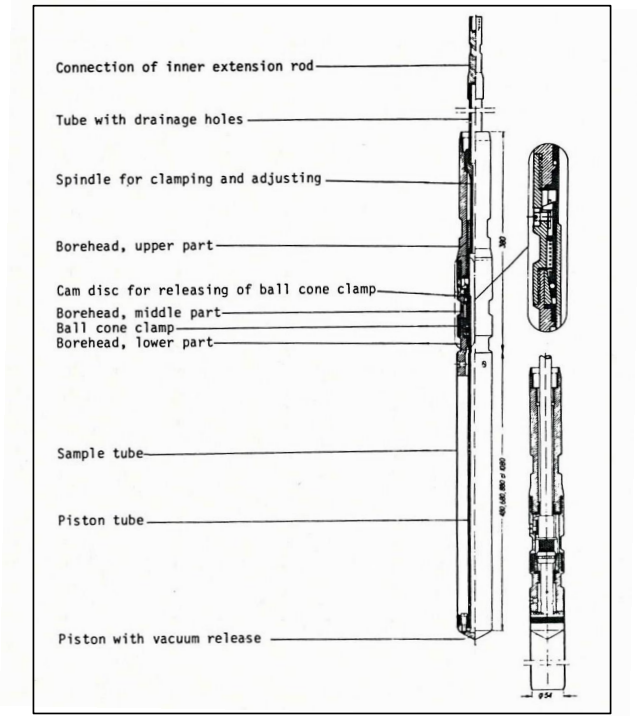

Figure 3.7 Original NGI 54 mm piston sampler, technical [Andresen & Kolstad 1980].

Inherent problems related to small diameter thin wall samplers such as NGI samplers are strength properties and possible tolerance imperfections during production. Possible cross sectional variations along the cylinder can knead and remould the sample while inside clearance sufficient to compensate for these variations will however enable sample to swell [Andresen & Kolstad 1980]. Furthermore, the edge of the cutting shoe can be easily damaged. Stainless steel cylinders used for sample storage can interfere with sample quality if stored for long period of time [Andresen & Kolstad 1980]. Due to characteristics of the sampling technique certain volume of the material immediately underneath the final sampling depth is severely disturbed by the penetration and

Figure 3.8 NGI 54 mm sampler, a) Aalto University version of NGI 54 mm sampler, b) sampling cylinder and outdrawn piston position, c) sampling cylinder and withdrawn piston position.

rotation of the sampler. To avoid sampling of a priori disturbed material, successive sampling levels should start at least 0.2 m deeper than maximum penetration depth reached in previous sampling stage. The lower and upper 10-15 cm of each sample are ordinarily disturbed and are therefore used for index and remoulded tests rather than shear strength and oedometer tests [Andresen & Kolstad 1980]. Laboratory test results on soft sensitive silty clay of intermediate plasticity from depths greater than 15 m indicate disturbance increasing with depth [Andresen & Kolstad 1980]. Need for inner extension rods roughly doubles the time needed for sampler lowering and sample retrieval. Inner extension rods typical for NGI samplers give better control of the piston movement.

3.3.3 Norwegian Geotechnical Institute 86 mm piston sampler

Aalto University NGI 86 mm sampler shown in Figure 3.9 is very rarely used under excuse of poor sample retrieval ability. Compared to NGI 54, NGI 86 mm sampler is modified in terms of sampling cylinders and sampler body dimensions in order to enable retrieval of samples larger in diameter. The sampling operation with NGI 86 mm piston sampler are carried out in the essentially identical manner as with the NGI 54 mm. Average thickness of thin walled steel cylinders is 1.50 mm. Average inner diameter of the cylinders is 85.88 mm and their length is 650 mm. Cylinders do not have inner clearance. The external diameter of sampling cylinders is 88.94 mm in average, and angle of cutting edge is 12° (10.0-14.0°). Area ratio of NGI 86 is favourably slightly lower compared to that of NGI 54 sampler being 6.8 %. Sampler has rather low material recovery. Maximum sampling length is 450 mm and after the upper and lower disturbed portions are removed about 250-300 mm of material can be considered undisturbed depending on the sampling methodology.

In some clays, especially fine sandy and silty clays, it may be difficult to convey large diameter samples to the ground surface in spite of that negative pressure which would arise with sample downward movement [Jakobson 1954, Andresen & Kolstad 1980]. To prevent losing samples, some overdriving during cutting of the sample has been practiced in silty and coarse materials [Andresen & Kolstad 1980]. This is not recommended in cohesive materials, because compression of the sample will cause disturbance [Andresen & Kolstad 1980]. In order to improve sampler performance when recovering samples in cohesive materials it is recommended to allow sample to reconsolidate for 5 to 10 min prior pulling up the sampler [Andresen & Kolstad 1980]. With the sampler at the surface the cylinder must be separated from the sampler without creating of a negative pressure between the piston and the sample. Negative pressure between the sample and the piston is released by opening the screw plug on the piston [Berre et al. 1969]. The suction that might arise tends to stretch material at the top of the sample [Andresen & Kolstad 1980].

Figure 3.9 NGI 86 mm sampler, a) Aalto university version of NGI 86 mm sampler, b) sampling cylinder and outdrawn piston position, c) sampling cylinder and withdrawn piston position.

Table 3.2 summarises main properties of the samplers selected. Recommendations for undisturbed sampling of soft soils are: area ratio less than 12 %, angle of cutting edge between 5 and 7°, internal diameter >100 mm [La Rochelle et al. 1981, Leroueil & Hight 2003]. Thus, among samplers used, NGI 86 mm sampler has the most favorable properties. Properties of the sampler however, do not concent with those optimal for undisturbed sampling of soft soils.

Table 3.2 Summary of properties of the samplers.

Sampling method	Cutting edge angle [°]	Area ratio [%]	Internal diameter [mm]	Cylinder wall thickness [mm]	Sampling length [mm]	
					Total	Undisturbed
STII	5.7	30	50.12	1.70	510	170
NGI 54 mm	14-22	8.5	54.56	1.25	780	480
NGI 86 mm	10-14	6.8	85.88	1.50	450	250

4. Experimental testing programme

4.1 Testing programme objectives

The testing programme, developed in collaboration with the University of Strathclyde, aims to facilitate examination of effects of anisotropy, structure and strain-rate on soft sensitive Perniö clay behavior. The laboratory tests are performed at Soil Mechanics and Foundation Engineering Laboratories at Aalto University and Tampere University of Technology. The testing programme comprises of advanced tests performed in oedometer and triaxial apparatus, namely; 24 h incrementally loaded oedometer tests (ILOT), oedometer tests at constant strain-rate (CRS), incrementally loaded anisotropically consolidated triaxial tests (CAD), undrained triaxial compression tests (CAUC) and continuously loaded triaxial K_o tests. The tests are performed on both natural and reconstituted specimens under conditions of varying rates of loading, constant applied stresses by time, and constant applied rate of strain.

Conditions during IL and CRS oedometer tests were defined to provide clear insight in; a) compressibility and structure characteristics of soft clay, i.e. sensitivity characteristics, progressive destructuration of bonds during inelastic strains, and interrelation between destructuration process and secondary compression coefficient; b) rate dependent compressibility characteristics of soft clay such as influence of strain-rate level on the preconsolidation pressure and destructuration process.

Triaxial CAD and CAUC tests were defined so to provide data concerning: a) influence of anisotropy on compressibility and structure characteristics of soft clay, such as definition of yield points corresponding to several consolidation stress ratios together with influence of destructuration on shape and size of yield surface; b) influence of shearing strain-rate and structure on undrained behavior and strength of soft clay, including effects of destructuration on position of failure envelope and clear insight on influence of strain-rate on strain softening.

The test results should enable simultaneous analysis of main aspects of soft clay behavior being: initial and induced anisotropy, bonding and destructuration, as well as creep and strain-rate effects on stress-strain response, and thus form an adequate base for defining true rate dependency of stress-strain-strength response of soft structured Perniö clay. Tests and testing procedures used are described in the following.

4.2 Specimen preparation

Terminology soil sample denotes amount of soil that is selected or prepared for evaluation of its properties, while that of soil specimen denotes certain amount of soil sample that is prepared for specific laboratory test.

4.2.1 Natural samples

Purpose of the natural sensitive clay specimen preparation is to reduce material sampled to adequate test dimensions and to set specimen into testing apparatus. While being set in the testing device, specimen geometry, stress state and water content should remain unchanged [Germaine et al. 1988]. Although efforts in retaining sample quality differ from one laboratory to another, preparation procedures typically include several stages; sample retrieval, shaping to adequate dimensions, transport and mounting of the specimen to the testing apparatus. Natural samples are retrieved from storage containers. Consequently, retrieval technique depends largely upon the sampling method used. Furthermore, dimensioning and test apparatus mounting highly depends upon the initial properties of the material tested, test conditions and characteristics of the testing device for which the specimen is prepared. During each of these stages there are several crucial steps when sample can be easily disturbed.

The main requirement of soft sensitive clay preparation is that during all phases of the laboratory work sample should be completely and rigidly supported and never subjected to shear strains throughout the entire process of specimen preparation [Landva 1964]. Generally defined causes of disturbance in sampling are valid for specimen preparation process as well. Although methods and equipment used to cut and mount samples of natural clay are relatively simple, completing specimen preparation process without causing specimen disturbance is equally complex task as undisturbed sampling itself. Preparation of specimens from undisturbed samples is often crudely accomplished in comparison to the techniques used for field sampling and as a result the tests are often performed on disturbed specimens [Landva 1964]. In following, techniques and equipment used for preparation of natural clay specimens for oedometer and triaxial test at Aalto University are briefly outlined.

Preparation of natural clay specimens for oedometer test include; retrieval of the sample from the sampling cylinder, shaping of the specimen using oedometer ring and wire saw, and fixation of the ring with the specimen into the oedometer cell and oedometer apparatus.

In tube sampling where material is stored within the hollow cylinders, sample is retrieved by means of horizontal piston extruder, i.e. by hydraulic or manual movement of the piston threw the horizontally fixed hollow cylinder until sample sufficient in length is extruded on the opposite side.

Mounting of the sample into the oedometer ring is achieved by placing a thin walled steel oedometer ring with external cutting edge on top of the sample and continuously pressing it by means of a press device until the ring is filled with material. Prior penetration oedometer ring inner area is covered with thin layer of silicone grease thereby reducing friction between material and steel

walls. The oedometer ring is then positioned upside down under a yoke fixed to two guiding rods [Sandbaekken et al. 1986]. During cutting oedometer ring penetration rate is kept constant and low. Excess amount of peripheral partially disturbed material is carefully cut away whereas the oedometer ring itself is progressively filled with the undisturbed material. The cutting edge of the oedometer ring must remain in the horizontal plane throughout the cutting process. If this condition is not fulfilled thin gap between specimen peripheral area and ring occurs. The cutting procedure is stopped when the top of the sample protrudes 3-5 mm above the oedometer ring [Landva 1964]. Finally, excess material on both sides of the ring is removed by performing several cuts directly above and below the oedometer ring using steel wire saw.

For the purpose of avoiding air under the specimen, oedometer ring with the specimen is placed into the oedometer cell containing thin layer of de-aired water [Tokheim et al. 1976]. Saturated filter paper and filter plates are placed above and below of the specimen while the entire system is locked in position by means of external guiding ring and three screws. Finally, oedometer cell is placed between the pedestal and piston of the oedometer apparatus and is filled with water just prior to the test.

Preparation of the natural specimens for triaxial test involves; sample retrieval from the storage cylinder, trimming of the sample to a suitable size, placement of the drainage stripes and mounting of the specimen into the cell of triaxial apparatus.

Sample retrieval from the storage cylinder is identical as in the oedometer test preparation with one exception being extrusion of longer sample.

Sample is reduced to an adequate cylindrical dimension by wire saw trimming in the specially designed trimming frame and cutting cradle. Positioned vertically within the trimming frame between two circular plates with hinges sample is freely rotated without subjection to undesirable torsion [Andresen et al. 1957]. The edges of the frame act as trimming guides and control specimen diameter while the sample is trimmed by movement of the wire saw along the edges of the frame from top to bottom. After each slice sample is rotated and new cut is made until desired polygonal cross section is achieved [Andresen et al. 1957]. A metal cradle supports the sample in horizontal position while its ends are trimmed. Its length determines the specimen height and its edges assure end cuts parallel and perpendicular to the vertical axis of the specimen [Andresen et al. 1957]. Being shaped to test dimensions, the specimen is wrapped with spirally positioned filter stripes accelerating drainage during triaxial consolidation [Leroueil et al. 1988a].

Using the cradle specimen is carried and placed on triaxial device pedestal, and sealed by means of piston cap, rubber membrane and rubber O rings with saturated ceramic filter stones positioned directly underneath and above the specimen. The function of the rubber membrane and rubber O rings is to allow transmission of the radial stress to the specimen and to establish the boundary between cell fluid and pore fluid [Germaine et al. 1988]. A suction cylinder holding the rubber membrane and the rubber O rings is necessary tool used to seal the specimen [Landva 1964]. The rubber membrane is placed inside the suction cylinder with its ends folded over cylinder edges and by suction drawn

tight to the cylinder [Andresen et al. 1957]. With carefully positioned specimen and top cap in place, suction cylinder with the membrane is lowered over the specimen [Andresen et al. 1957]. When the cylinder is in optimal position, the suction is released and rubber membrane is unfolded over the cap and the pedestal. Later, rubber O rings stretched over the suction cylinder are released under and above the specimen ensuring water tight connection of the membrane and cap/pedestal. The final operation is setting the top of the cell in place, filling triaxial cell with water, and installing triaxial cell piston. With upper cell section being lowered into position and with the three wing bolts tightened, the cell is filled with water [Andresen et al. 1957]. Finally, piston is carefully lowered through the top of triaxial cell and into the loading cup until contact with the specimen is achieved, and locked by control screw so to prevent axial straining of the specimen prior the start of the test [Landva 1964]. With the specimen placed in the water filled triaxial chamber and with the piston being brought into contact with the specimen, loading bar for controlled axial loading is mounted upon the piston and loading process is initiated.

4.2.2 Reconstituted samples

Reconstituted samples are obtained by remoulding of natural Perniö clay material. The aim of remoulding procedure is to erase initial structure of the clay while that of reconstitution is to ensure destructured material being consistent enough to be mounted to the testing device. Although important effects of post-depositional processes such as aging, leaching, and that of variations in composition and fabric are erased, advantages of testing reconstituted clays are that ambiguous and substantial effects of sampling disturbance in natural clays and their natural inhomogeneity can be eliminated [Hight et al. 1987].

Remoulding is performed by mixing of the natural Perniö clay material to a slurry at water content above the liquid limit, i.e. 1 to 1.5 w_L [Burland 1990]. With reconstituted samples obtained by remoulding natural material, behavior in reconstituted state is comparable with response of the Perniö clay in natural state [Karstunen & Koskinen 2008a]. After mixing, material is fully saturated and is in a liquid state, i.e. has no shear strength. To obtain material of uniform properties after reconstitution, particularly in terms of void ratio, consistent remoulding procedure regarding mixing efficiency and amount of water added is applied. Ideally, the water used in remoulding should have chemistry similar to that of pore fluid [Fearon & Coop 2000].

Following the remoulding, i.e. mixture reaching smooth texture and preferred fluidity, slurry is poured to acrylic cylinders 50 or 70 mm of inner diameter and 200 mm high. If slurry has low fluidity air bubbles form, leading to errors in measurement related to weak zones or closure of artificially created voids. Formation of air bubbles is avoided by pouring the slurry along the walls of the cylinder. Thereafter material is allowed to consolidate, while being stored in a period of minimum 30 days under uniaxial load of 15 kPa at constant temperature of +6°. During storage remoulded material is allowed to drain by means of geotextile and porous stone while reduction in height is

measured once a day. Final duration of consolidation is monitored based on Taylor's [1942] square root of time method and it varies from 1 to 3 months.

After the reconstitution, steps for oedometer test preparation are identical as those for natural clay, while in preparation for triaxial tests, specimen dimensioning procedure is modified. Namely, trimming of the sample is restricted only to actions ensuring adequate height of the specimen using wire saw and trimming cradle. Because soft consistency of reconstituted samples does not allow excessive trimming operations, cylinders used in reconstitution are of such diameter that trimming of the sample along the vertical planes is avoided.

4.3 Oedometer tests

4.3.1 Incrementally loaded oedometer tests ILOT

To obtain clear insight into compressibility, structure and creep characteristics of Perniö clay, incrementally loaded (IL) oedometer tests [Terzaghi 1925] with 24 h loading periods are performed on both natural and reconstituted clay specimens. IL oedometer test is a common model test in which a specimen of soil is subjected to pressure in order to predict the deformation that would occur to a stratum of soil under similar pressures in the ground [Crawford 1986]. Geonor and Aadex oedometer test apparatuses used at Aalto University are shown on Figure 4.1. During the test daily increments of vertical load are applied to a submerged specimen contained within the rigid ring and drained via porous stones above and under the specimen [Crawford 1986]. Due to IL methodology, compression curve is defined on the basis of final settlement data obtained after regular 24 h periods.

IL oedometer test conditions implemented are summarised in Table 4.1. Altogether, 63 IL oedometer tests are performed, nine of which are made on reconstituted material. The IL oedometer tests are performed on cylindrical specimens identical in size, i.e. 20.0 mm initial thickness and 50.0 mm in diameter. During the tests, specimen is loaded step-wise with load increment ratio LIR=1, i.e. each load step doubling total load of previous. The loading frame of the oedometer apparatuses has 10:1 lever arm [Sandbaekken et al. 1986]. Several loading patterns are used, herein defined by the intensity of initial axial load being: 2.42, 3.06, 3.67, and 4.28 kPa, i.e. weight of 50.0, 62.5, 75.0 and 87.5 g, respectively. Four distinctive groups of load increments ensure sufficient amount of reference points for clear interpretation of compressive behavior. Entire loading procedure is performed with free drainage conditions enabled by top and bottom filter stones [Sandbaekken et al. 1986]. Average duration of the test is 14 days. 24 h load step duration implemented ensures excess pore pressure dissipation during each load step. Tests are performed until considerable axial stress levels with target defined by loading value closest to 1000 kPa, being 1237.70, 783.36, 940.03 and 1096.70 kPa for distinctive loading patterns 1 to 4, respectively. After maximum load is reached, the samples are unloaded in several steps so to evaluate sample swelling behavior. Unloading is performed under LIR of 1/2, i.e. total load reduced

by half in each step, until stress levels corresponding to preconsolidation pressure which for sampled Perniö clay varies in a range from 20 to 50 kPa.

Main objectives of IL oedometer tests are to determine yielding points and identify sensitivity characteristics of natural and remoulded Perniö clay specimens. Furthermore, IL oedometer tests are used to re-evaluate destructuration, compressibility and consolidation response of Perniö clay specimens with various initial level of structure.

Figure 4.1 IL oedometer apparatuses at Aalto University.

Table 4.1 Test conditions in IL oedometer tests.

Test series	Test group	no. of tests	Test type	Material	Initial step load [kPa]	Load increment ratio	Load step duration [days]	Thickness [cm]
I	A	1	ILOT	Natural	2.42	1	1	2
	B	5	ILOT	Natural	2.42	1	1	2
II	A	9	ILOT	Natural	3.06	1	1	2
	B	17	ILOT	Natural	3.06	1	1	2
III	B	6	ILOT	Natural	3.67	1	1	2
	C	4	ILOT	Natural	3.67	1	1	2
IV	A	4	ILOT	Natural	4.28	1	1	2
	C	2	ILOT	Natural	4.28	1	1	2
V	D	6	ILOT	Reconstituted	3.06	1	1	2
VI	D	3	ILOT	Reconstituted	3.67	1	1	2

4.3.2 Testing methodology in IL oedometer test

IL oedometer tests at Aalto University are made using manual system of loading, while specimen vertical strains are acquired by digital data logging system.

Manual loading is achieved by placement of the weights on loading plate of the oedometer apparatus deadweight hanger following predefined intervals. Although time consuming, manual loading has one important advantage compared to automated step motor based loading. Dead load based loading ensures truly constant axial load on top of the sample during each loading step interval, while that achieved using step motor introduces conditions resembling dynamic loading. Because of the importance of loading duration on effects defining soft sensitive clay behavior, i.e. destructuration and creep, the IL oedometer tests carried out within this study are implemented strictly following 24 h load step duration.

To improve measuring accuracy and ensure sufficient amount of data for accurate interpretation of test results, digital data logging system is introduced. Data logging system implemented includes a linear variable differential transducer LVDT (Solartron displacement transducers DP10S and DP20S), connected to the computer monitoring unit via USB port using Orbit support pack for Excel. Calibrated measuring range of LVDT's is 10 and 20 mm providing the accuracy of measurement of +/-1.2 μm and +/-2.44 μm, respectively. During the test, vertical displacement of the specimen is continuously recorded in one minute intervals and stored to excel worksheet. The acquired data is in a real time displayed on a computer monitor using Excel software and user defined diagrams, enabling clear and effective monitoring of the specimen response. Automatic data logging system yields substantial amount of data recorded that is effectively reduced to specific readouts only, i.e. those after 1, 2, 3, 4, 5, 10, 20, 30 min, and followed with readouts made after every hour until the end of load increment interval. Thus, amount of data during every load interval of conventional oedometer test is reduced to 31 readings. Under various test conditions, automated data logging ensures readings at identical time sequences. Digital data acquiring system implemented is favourable both in terms of accuracy of readouts and amount of data recorded, and it ensures comparability of data recorded under various test conditions.

4.3.3 Constant rate of strain oedometer test CRS

To analyse viscous effects of soft clay behavior and relation between preconsolidation pressure and strain-rate, constant rate of strain oedometer test (CRS) [Hamilton et al. 1959] are performed on natural and reconstituted samples of soft sensitive Perniö clay. Automated oedometer apparatuses used for CRS testing are shown on Figure 4.2. During this mode of oedometer testing, submerged laterally constrained specimen with free upper drainage boundary is one dimensionally compressed under constant rate of displacement. The CRS tests were initially performed at Tampere University of Technology. In later stage of the study, additional CRS test were made at Aalto University.

Figure 4.2 CRS oedometer apparatuses at Aalto University.

Table 4.2 summarises conditions implemented in CRS oedometer tests on Perniö soft clay. Tests are performed on two types of specimens with respect to their size, being that of 20.0 mm thickness and 50.0 mm diameter and alternatively of 15.0 mm initial thickness and 43.7 mm in diameter. During axial loading at constant rate of strain, laterally constrained cylindrical specimen is drained to the top while at its impervious base pore pressures are measured [Tokheim et al. 1976]. Besides enabling evaluation of strain-rate effects on material compressibility, resulting pore pressure response is evaluated as well. CRS oedometer test provides a continuous compression curve, and it is overall less time consuming then IL testing. The smooth loading procedure is also favourable from the viewpoint of reduced sample disturbance and allows more accurate determination of preconsolidation pressure [Janbu et al. 1981]. Important perquisite for successful measurement of material response in CRS testing is to ensure sufficiently broad range of constant strain-rate levels applied. Considering previously conducted CRS tests [Sällfors 1975, Alén 2009, Yin et al. 2011] as an optimum, following strain-rate values were selected; 0.05, 0.03, 0.01, 0.001, 0.0002, 0.0001 mm/min yielding with $1{\cdot}10^{-5}$, $1{\cdot}10^{-6}$, $1{\cdot}10^{-7}$ s^{-1} for specimens of 15.0 mm thickness, and $4.2{\cdot}10^{-5}$, $2.5\ {\cdot}10^{-5}$, $8.3{\cdot}10^{-6}$, $8.3{\cdot}10^{-7}$, $1.7{\cdot}10^{-7}$ and $8.3{\cdot}10^{-8}$ s^{-1} for specimens of 20.0 mm initial thickness. A total of 56 CRS tests are performed within this study with 7 tests made on re-

constituted Perniö material. The tests are divided into ten test series each consisting of at least three tests made under distinctive constant rate of strain conditions. Tests are performed up to the maximum total stress level allowed by the loading frame of the apparatus, i.e. 900 kPa. Together with response in compression each test series includes tests examining swelling response. Following maximum compression, in at least one test within each series, specimen is unloaded in single load step. Time required for test completion varies significantly depending upon specimen compressibility and rate of strain imposed, starting from 2 h for fast tests up to more than 800 h (35 days) for tests at the lowest strain-rate.

Table 4.2 Test conditions in CRS oedometer tests.

Test series	Test group	no. of tests	Test type	Material	Thickness [cm]	Displacement rate [mm/min]
I	63A	1	CRS	Natural	2	0.001
		1		Natural	2	0.05
		1		Natural	2	0.0002
		1		Natural	2	0.03
		2		Natural	2	0.01
II	65A	1	CRS	Natural	2	0.05
		2		Natural	2	0.1
		1		Natural	2	0.0001
		1		Natural	2	0.001
		1		Natural	2	0.01
III	67A	2	CRS	Natural	2	0.0002
		2		Natural	2	0.001
		2		Natural	2	0.01
		1		Natural	2	0.05
IV	44B	3	CRS	Natural	1.5	0.009
		2		Natural	1.5	0.0002
		2		Natural	1.5	0.0009
V	63B	2	CRS	Natural	2	0.001
		1		Natural	2	0.0002
		2		Natural	2	0.01
VI	65C	2	CRS	Natural	2	0.03
		2		Natural	2	0.01
		1		Natural	2	0.0002
		1		Natural	2	0.001
VII	66C	1	CRS	Natural	2	0.0002
		1		Natural	2	0.0001
		3		Natural	2	0.001
		3		Natural	2	0.01
VIII	68C	1	CRS	Natural	2	0.0001
		1		Natural	2	0.01
		2		Natural	2	0,001
IX	A28D	1	CRS	Reconstituted	2	0.001
		1		Reconstituted	2	0.0002
		2		Reconstituted	2	0.01
X	A19D	1	CRS	Reconstituted	1.5	0.01
		1		Reconstituted	1.5	0.001
		1		Reconstituted	1.5	0.0002

Main objective of CRS oedometer tests on Perniö clay is to define strain-rate influence on yield and compressibility. In the interest of examining effects of destructuration, test at various strain-rate are performed on natural specimens with different level of structure.

4.3.4 Testing methodology in CRS oedometer test

Automated oedometer testing apparatus used is fully automated testing device designed and constructed at Tampere University of Technology [Kolisoja et al. 1987]. The apparatus can run various kinds of oedometer tests based on three different loading procedures being that of incremental loading (IL), constant rate of strain (CRS), and constant pressure ratio (CPR) [Kolisoja et al. 1989]. The automated oedometer test apparatus employs accurate and easy to use testing methodology enabling test execution independent on working hours [Kolisoja et al 1988]. Due to these advantages automated apparatus is viable alternative to manual incrementally loaded oedometer testing.

In addition to oedometer cell and loading frame containing an electromechanical press and transducers to record vertical load and pore pressure, apparatus consists of control unit, data logger and a microcomputer [Kolisoja et al. 1987]. Deformations are accomplished by stepping motor and mitre gear thus transferring the rotation of the motor to a vertical motion in order to compress the test sample against the load cell (Kiowa LC-200kg) attached to the rigid load frame [Kolisoja et al. 1987, Sandbaekken et al. 1986]. The base of the specimen is impervious, but contains porous stone connected to a pressure transducer (Cell 1 Honeywell 19 c 030 PG4K, 200 kPa, Cell 2 Sensor technics PS 100 GC, 700 kPa). During the test, loads acting on the specimen and pore pressure at the bottom of the specimen are measured at short intervals using electronic strain-gauge transducers, thus transforming quantities of interest to digital signals collected by data logger [Kolisoja et al 1989, Kolisoja et al. 1987]. Speed of the rotary motion of the stepping motor is controlled via a control unit by a microcomputer based on previous measurements, while the resulting compression of the sample is indirectly calculated from the number of steps of the stepping motor [Kolisoja et al. 1987, Kolisoja et al. 1989]. Apparatus allows testing of unloading response, however, unloading is not strain-rate controlled.

Measured data is transferred to the microcomputer unit for storage, computations and plotting of standard diagrams [Sandbaekken et al. 1986]. Altogether, microcomputer continuously logs the data of; time, total axial pressure, excess pore pressures at specimen bottom and axial deformation of the specimen, in automatically chosen intervals ranging from 5 to 10 min throughout the loading stage of the test. Hence, time derivatives of these quantities are also known being load-rate, strain-rate and pore pressure-rate [Tokheim et al. 1976]. In the automated interpretation, recorded data is used for calculation of compression modulus and coefficient of consolidation utilizing solutions of the continuous loading oedometer test introduced by Janbu et al. [1981].

The loading procedure calls for very little manual intervention. At the onset of the test control program gives the operator a choice of input parameters defining loading procedure. In CRS test those are; deformation rate, maximum

axial load, maximum relative deformation and minimum unloading stress level. Current status of the test is monitored by control programs also utilised to display relevant data on test in progress [Sandbaekken et al. 1986]. Control unit stops the test when pre-set limitations are reached, i.e. predefined deformation or load level [Tokheim et al. 1976].

4.4 Triaxial test

4.4.1 Incremental anisotropic consolidation triaxial tests CAD

Triaxial test is a widely used test for evaluation of strength, compressive and extensive behavior of soil materials [Rendulic 1937, Bishop et al. 1957]. In this study it is used for anisotropic consolidation and undrained compression tests. Anisotropic consolidation triaxial tests CAD, are performed to examine influence of consolidation stress ratio and structure on compressibility of Perniö clay. The CAD test is stress controlled triaxial test with consolidation of the specimen taking place under condition $\sigma'_1 \neq \sigma'_3$ [Head 1986]. Typical procedure for IL CAD test includes increments of vertical and radial stress applied to specimen under open drainage valve conditions [Karstunen & Koskinen 2008a]. Triaxial test apparatuses Wykeham Farrence, Tristar 500 kg used for CAD tests are shown on Figure 4.3.

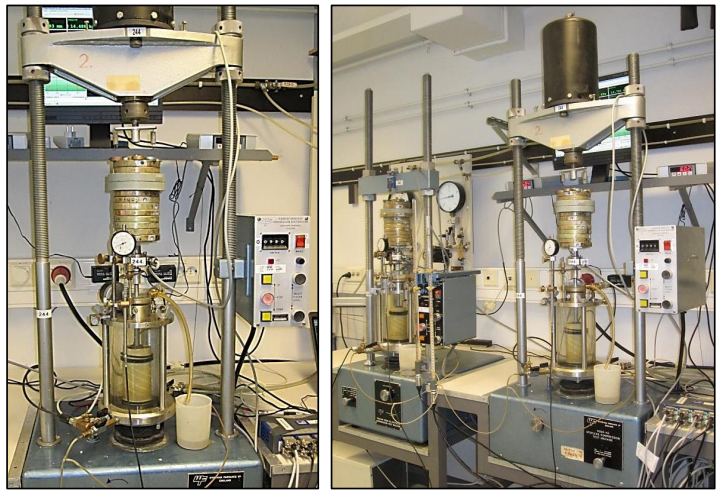

Figure 4.3 CAD test in triaxial apparatuses at Aalto University.

Conditions governing triaxial consolidation tests on natural and reconstituted specimens of Perniö clay are listed in Table 4.3. Tests were performed on cylindrical specimens of 50 mm diameter and 100 mm height. Altogether, 35 CAD tests are performed on natural, and 13 on reconstituted material. Specimens are consolidated by stepwise increase in cell pressure followed with additional increase in vertical load [Andresen et al. 1957]. Since the specimen is allowed to drain via spirally placed filter stripes on the periphery and porous stones on top and bottom, specimen consolidates laterally as well as vertically

[Andresen et al. 1957, Head 1986]. Depending upon the specimen type and consolidation conditions imposed, tests are conducted within five test series, each subdivided to three groups. In tests within particular series, the ratio between horizontal and vertical stresses is kept constant corresponding to a predetermined value, i.e. $\eta=q/p'=0.4$, 0.6 and 0.85 or $\sigma'_3/\sigma'_1=$ 0.68, 0.57, and 0.46, respectively. Based on preliminary estimates, critical state of Perniö clay in compression is $\eta=q/p'=1.32$. Thus, consolidation stress ratio $\eta=0.85$, corresponds to NC value of earth pressure coefficient at rest, $K_o^{NC}=0.46$. The intention is to reproduce stress level similar to that in situ [Karstunen & Koskinen 2008a]. Testing procedure used in the remaining test series is the same, with an exception of consolidation stress ratio imposed, i.e. $\eta=0.6$ or $\eta=0.4$. Test series comprise three test groups noted by A, B and C. Specimens of a particular group are loaded along the identical stress ratio path to same stress state [Karstunen & Koskinen 2008a]. The final stress state in consolidation is defined by maximum cell pressure imposed, i.e. 20, 40 or 60 kPa. Consolidation period following loading is 24 h, except in final step prolonged for 36 or 48 h to ensure dissipation of excess pore pressure prior to undrained shearing. Consolidation under controlled stress ratio requires application of many small increments of vertical and radial stress [Germaine et al. 1988]. To moderate specimen disturbance from shock loading and ensure sufficient amount of stress-strain points for consistent identification of yield, LIR in consolidation is varied. Loading conditions along radial stress paths are controlled by cell pressure increase of 3 kPa prior, and 10 kPa with yield exceeded, i.e. σ'_3 = 5, 8, 11, 14, 17, 20, 23, 26, 29 and 40, 50 and 60 kPa. Thus, IL at certain η comprises two sets of axial and radial stress increments corresponding to reloading and virgin loading stress range. A test of this type lasts from 6 to 14 days, depending on the stress ratio, final cell pressure, and duration of the consolidation period under the final load.

Table 4.3 Test conditions in CAD triaxial tests.

Test series	Test group	no. of tests	Test type	Material	Sample type	Consolidation stress ratio	Cell pressure [kPa]
I	A	3	CAD	Perniö	natural	0.4	20
	B	5		Perniö	natural	0.4	40
	C	5		Perniö	natural	0.4	60
II	A	3	CAD	Perniö	natural	0.6	20
	B	5		Perniö	natural	0.6	40
	C	3		Perniö	natural	0.6	60
III	A	3	CAD	Perniö	natural	0.85	20
	B	6		Perniö	natural	0.85	40
	C	2		Perniö	natural	0.85	60
IV	A	2	CAD	Perniö	reconstituted	0.4	20
	B	2		Perniö	reconstituted	0.4	40
	C	2		Perniö	reconstituted	0.4	60
V	A	3	CAD	Perniö	reconstituted	0.85	20
	B	2		Perniö	reconstituted	0.85	40
	C	2		Perniö	reconstituted	0.85	60

Main objective of the CAD tests is to examine influence of consolidation stress ratio on specimen compressibility and destructuration. Special attention is given in evaluating effects of structure and consolidation stress ratio on yield stress and shape and size of yield surface. To examine destructuration mechanism, the tests consider specimens of various initial sensitivity levels.

4.4.2 Testing methodology in CAD tests

IL anisotropic consolidation tests at Aalto University are performed using manual loading, while specimen response is measured digitally.

Anisotropic stress conditions are achieved by additional axial load via piston, in excess to isotropic loads imposed by cell pressure [Andresen et al. 1957]. Load increments are kept small to minimise straining due to undrained shear, and long enough to allow full consolidation. At the end of each increment the changes in length and volume are used to calculate the present area and dead load in the following step [Germaine et al. 1988]. Triaxial cell pressure is imposed via system composed of compressed air source, manual air pressure regulator (Fairchild, Model 10) and air/water constant pressure cell, and is controlled by means of on cell 400 kPa gauge pore pressure transducer (EuroSensor EPT 3100-A-00400-B-4-A) via the digital process indicator (DS Europe AN-401). Ideally, cell pressure and axial dead load should be increased simultaneously. In reality, cell pressure precedes application of vertical load. To reduce specimen exposure to shock loads and excessive strain-rates, if considerable, total axial load of increment is implemented in stages. Due to importance of time and strain-rate effects, 24h loading intervals were obeyed.

Being IL under controlled stress ratio, total stress conditions are known while specimen axial and volumetric deformations are measured. Vertical deformation of the specimen is measured using LVDT (Solartron displacement transducer AX/10/SH), with the measurement range of +/-10 mm and tolerance of +/-10 μm. Volume of expelled pore-water is measured with 7 kPa gauge pressure transducer (Druck PDCR 4010) registering hydrostatic pressure of pore-water in the burette. Measurements are made in 20 sec intervals and continuously logged using 8 channel data acquisition unit (HBM, Quantum XMX840A). Data acquired is in a real time shown on the monitor of computer unit using Catman AP software, enabling control of specimen response.

Within this study CAD tests are interpreted from digitally acquired data. Problems encountered in interpretation are excessive amount of data recorded, and necessity for manual input of stress conditions in the interpretation files. Raw measurements logged in 20 sec interval are reduced in interpretation by filtering readouts after 1, 2, 3, 4, 5, 10, 20, 30 min, followed with those at hourly intervals until the end of load increment. Approaches in interpretation of CAD data correspond with those in IL oedometer. Manual input of incremental stress conditions was highly time consuming. To solve this issue, testing equipment was modified by installing load cell (HBM U2ED1) on top of the piston and underneath the axial loading bar [see Kuwano et al 1999]. Under described configuration dead weight imposed via the loading bar is continuously logged together with corresponding specimen deformation. Disad-

vantage of the modification is increase in weight of the new compound piston to 700 g, i.e. minimum axial load in consolidation is increased. The modification affected test series II, III, IV and V. By this modification, problem of recording loading conditions is only partly solved. Pore pressure transducer measuring cell pressure via digital process indicator should be connected to the data logging device as well. Under described preferences, complete set of the data essential for effective CAD test interpretation would be readily available in digital form. Cell pressure logging was omitted in the present study due to the lack of the equipment. Presently, triaxial test data acquisition is organised using two data logging devices, each limited with 8 input channels. Additional data logging device (HBM, Quantum XMX840A, 8 channels) is necessity. Besides enabling logging of the entire set of data relevant for interpretation, such configuration would increase the flexibility of the measuring systems with each triaxial apparatus equipped for independent testing process.

4.4.3 Undrained triaxial compression tests CAUC

Initiated at various consolidation states, undrained triaxial compression tests (CAUC) on natural and reconstituted Perniö clay are performed at several constant strain-rates. The tests are performed to examine influence of structure, consolidation stress ratio and strain-rate on specimen response. Undrained triaxial compression is a strain controlled test with specimen subjected to controlled axial deformation under constant confining pressure, with change in water content of the specimen prevented [Andresen et al. 1957]. As a result of deformation rate imposed, axial load rises until failure due to maximum shear strength of the specimen being overcome [Head 1986]. With specimens drainage prevented, pore pressures rise as the load increases leading to reduction of effective stresses [Head 1986]. Shear at constant axial strain-rate prevents abrupt failure of the specimen enabling measurement of softening response. Aalto University triaxial apparatuses in CAUC tests are shown on Figure 4.4.

Figure 4.4 CAUC test in triaxial apparatuses at Aalto University.

Table 4.4 Test conditions in CAUC triaxial tests.

Test series	Test group	no. of tests	Test type	Sample type	Consolidation stress ratio	Cell pressure [kPa]	Strain-rate [%/h]
I	A	1	CAUC	natural	0.4	20	6
		1		natural	0.4	20	0.6
		1		natural	0.4	20	0.06
	B	2		natural	0.4	40	6
		2		natural	0.4	40	0.6
		1		natural	0.4	40	0.06
	C	3		natural	0.4	60	6
		1		natural	0.4	60	0.6
		1		natural	0.4	60	0.06
II	A	1	CAUC	natural	0.6	20	6
		1		natural	0.6	20	0.6
		1		natural	0.6	20	0.06
	B	2		natural	0.6	40	6
		2		natural	0.6	40	0.6
		1		natural	0.6	40	0.06
	C	1		natural	0.6	60	6
		1		natural	0.6	60	0.6
		1		natural	0.6	60	0.06
III	A	1	CAUC	natural	0.85	20	6
		1		natural	0.85	20	0.6
		1		natural	0.85	20	0.06
	B	1		natural	0.85	40	6
		1		natural	0.85	40	0.6
		2		natural	0.85	40	0.06
	C	1		natural	0.85	60	6
		1		natural	0.85	60	0.6
IV	A	1	CAUC	reconstituted	0.4	20	6
		1		reconstituted	0.4	20	0.6
	B	1		reconstituted	0.4	40	6
		1		reconstituted	0.4	40	0.6
	C	1		reconstituted	0.4	60	6
		1		reconstituted	0.4	60	0.6
V	A	1	CAUC	reconstituted	0.85	20	6
		1		reconstituted	0.85	20	0.6
	B	1		reconstituted	0.85	40	6
		1		reconstituted	0.85	40	0.6
	C	1		reconstituted	0.85	60	6
		1		reconstituted	0.85	60	0.6

Undrained compression tests are onset following anisotropic consolidation conditions described in chapter 4.4.1. As presented in Table 4.4, V distinctive CAUC test series comprise 15 test groups, each including at least two tests. CAUC tests within series I are performed on natural clay specimens anisotropically consolidated at η=0.4, to distinctive cell pressure levels of 20, 40 and 60 kPa representable of test groups A, B and C. Following consolidation, σ'_3 is kept constant and specimens are failed in undrained shear by increasing axial load at constant axial strain-rates of 0.1, 0.01 or 0.001 mm/min, i.e. 6, 0.6, and 0.06 %/h. Tests on natural specimens within series II and III are per-

formed under the same conditions as those of series I, with exception of undrained shear being onset following consolidation to η=0.6 or 0.85. Remaining CAUC tests in series IV and V consider reconstituted specimens consolidated to η=0.4 and 0.85. Reconstituted specimens are sheared undrained at constant strain-rate of 0.1 and 0.01 mm/min (6 and 0.6 %/h) at confining pressures of 20, 40 or 60 kPa. With reconstituted specimens of series IV and V tested in an identical manner as natural of series I and III, contrast of the results at equal strain-rate allow identification of effects of induced anisotropy and destructuration in undrained shear. Shear is performed until considerable strain levels so to examine specimen response with pore pressures tending towards stable values. Finally, at least one test of each group examines specimen response in relaxation, i.e. pore pressure and strain response under constant axial load. In total, 45 CAUC tests in compression are performed. Duration of the undrained shear tests varied from 1 to 14 days, depending on the strain-rate applied, target axial strain and relaxation period.

Main objectives of the CAUC tests are to quantify influence of anisotropy, structure and shearing strain-rate on strength and compressive behavior of Perniö clay. As a result of induced anisotropy, i.e. distinctive consolidation conditions and consequent extent of destructuration, test results of each series manifest different strength and compression characteristics. The CAUC tests thus enable identification of effects of strain-rate on undrained shear strength, softening response and position of failure envelope in compression.

4.4.4 Testing methodology in CAUC tests

Modification of triaxial apparatuses necessitated change in methodology of undrained shear of CAUC test. Procedures used are outlined in the following.

Undrained conditions are set with gauge pore pressure transducer (EuroSensor EPT 3100-A-00400-B-4-A) connected to the specimen. Previously the piston was locked to enable removal of dead weights from the loading plate. Thereafter, load cell (HBM U2ED1) was installed underneath the loading frame. Next, manual adjustment wheel was used to press the piston against triaxial loading frame via load cell, until axial load corresponding that in anisotropic consolidation was achieved. Then, piston was released and axial loading at constant strain-rate was imposed. Upward movement of the cell pedestal is governed by stepping motor of triaxial apparatus while the specimen is sheared until a definite failure, i.e. ε_1>15 %. Later, the step motor is stopped to investigate specimen response in relaxation. With test completed, specimen is removed from the apparatus, photographed, measured, and sectioned for evaluation of water content and dry weight [Germaine et al. 1988].

Above defined procedure for undrained compression tests is crude, leading to stress conditions at the onset of undrained shear differing that in consolidation. Being manually adjusted, axial stresses are easily exceeded causing pore pressure increase up to ~2 kPa, and rapid decrease of axial load up to ~0.5 kg. Thus, just prior the undrained shear, sample stress conditions are altered triggering new consolidation. Decline of axial stress displaces initial stress state to lower deviator stress, while rise in pore pressure reduces mean effective stress

level. Instead from consolidated state, test is started with certain initial pore pressure to which excess pore pressure due to application of the deviator stress is added [Head 1986]. The error influences both stress-strain path and undrained strength measured. Bearing in mind magnitude of strain-rate effects on undrained shear strength, above defined testing procedure is inappropriate.

To ensure accurate measurement, undrained shear testing methodology is modified by installing load cell on top of the piston [Kuwano et al. 1999]. Following the consolidation and with undrained conditions being set, dead load weight is kept compressing the specimen. Then, triaxial cell pedestal is raised until loading bar of the piston is positioned underneath the triaxial loading frame. Thereafter, movement of triaxial cell pedestal at constant strain-rate is started. As shown on Figure 4.5, undrained compression is onset when loading bar containing dead load comes into the contact with the triaxial loading frame. Load cell measures load imposed by dead weight and that caused by piston being pressed against loading frame. The testing procedure ensures onset of undrained shear at exact stress level to which the specimen is consolidated, i.e. with initial pore pressure being zero. Disadvantage of the new testing methodology is that in present configuration measure of undrained shear resistance is not allowed to drop below values defined by axial load in consolidation.

Figure 4.5 Detail of CAD and CAUC in triaxial test apparatus.

In triaxial testing digital data acquiring system is used. Problems inherent to data logging in CAD are present in undrained shear tests as well. Monitoring of triaxial test requires measurements of five quantities: piston force, cell pressure, pore pressure, axial deformation and volume change [Germaine et al. 1988]. In current practice cell pressures are not digitally logged. Since they are maintained constant throughout the undrained shear, cell pressure data logging is less important than in CAD test. However, due to poor state of valves and cell water leakage, cell pressure in undrained shear does oscillate, particularly in lengthy tests. The continuous logging of cell pressure would enable faster interpretation and ensure changes in strength and stiffness due to cell

pressure oscillations being easily recognised. It is for this reasons that implementation of additional data logging device is necessary. Finally, triaxial apparatuses should be equipped with double acting pneumatic actuator capable of providing constant piston force. Loading based on dead weight should be replaced with that provided by double acting cylinder and electronic pressure regulator enabling automation of compression and extension loading of the specimen.

4.4.5 Continuous loading triaxial K_o test

To measure coefficient of earth pressure at rest of Perniö clay deposit, continuous loading triaxial K_o tests were performed. Triaxial K_o test is a type of anisotropic consolidation test in which consolidation stresses are conditioned by specimen's lateral strains remaining null. Under the condition horizontal to vertical effective stress ratio corresponds to K_o^{NC}. To maintain $\varepsilon_3=0$, triaxial apparatus necessitate return algorithm specifying the adequate change in axial strain and radial stress conditions. K_o triaxial tests within this study are performed at Tampere University of Technology using automated triaxial apparatuses shown in Figure 4.6.

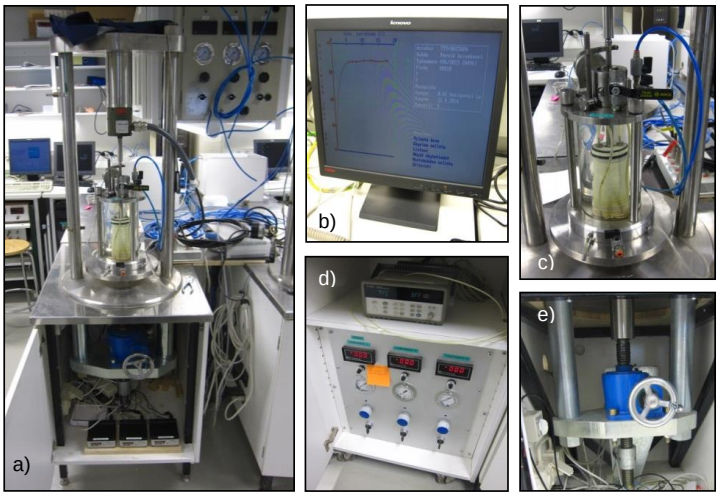

Figure 4.6 Automated triaxial apparatus at Tampere University of Technology, a) triaxial apparatus, b) test monitoring, c) triaxial cell, d) pressure controller, and e) step motor.

K_o triaxial tests are performed on specimens with 35 mm in diameter and 80 mm height. The specimen with open top drainage boundary is continuously loaded under variable axial and radial stress conditions ensuring zero radial strain. Continuously logged measurements are used to provide means for adequate change in transient loading conditions. Thus, loading conditions are adjusted in frequent intervals in order to maintain $\varepsilon_3=0$. Being continuously loaded test, in low permeability materials high testing rate leads to development of considerable excess pore pressures [Länsivaara 1993]. To maintain drained conditions during consolidation, testing rate is controlled by pore pressure measurements at the specimen undrained bottom [Länsivaara 1993].

Realising true K_o^{NC} conditions is not possible without a rigid horizontal boundary [Head 1986]. Due to triaxial specimen end restraints vertical effective stress varies along the specimen axis inevitably causing non uniform lateral deformation under axial load. For stress ratio to be constant, horizontal effective stresses would have to vary with specimen height, yet within triaxial cell only uniform radial stress via confining pressure can be applied [Head 1986]. However, if radial strains are kept fairly constant and if axial strains are not large, ratio of horizontal to vertical effective stress corresponds to K_o^{NC} reasonably well [Head 1986]. Duration of continuous loading triaxial K_o test lasts up to 7 days, depending upon specimen permeability and size.

Objective of the K_o triaxial tests was to determine coefficient of earth pressure at rest for Perniö soft sensitive clay. Figure 4.7 contrasts K_o^{NC} consolidation techniques in incrementally and continuously loaded triaxial tests. Continuous loading procedure under the stress conditions fairly representing that in situ minimalizes disturbance of specimen structure. The K_o^{NC} so determined is used to specifying test conditions in remaining triaxial tests on Perniö clay.

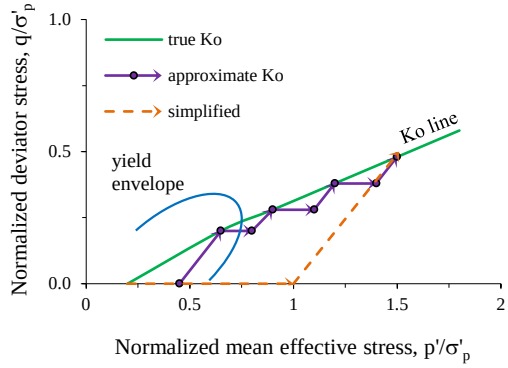

Figure 4.7 Incremental and continuous loading CAD techniques [after Germaine et al. 1988].

4.4.6 Testing methodology in K_o test

K_o tests are performed using automated triaxial test apparatuses developed at Tampere University of Technology. The apparatus is enhanced version of automated oedometer apparatus enabling fully automated stress and strain controlled triaxial tests [Kolisoja et al. 1989]. Thus, most of the testing methodology regarding loading and data acquiring is identical to that in CRS testing. Herein, aspects related to triaxial test execution are addressed. Additionally to conventional triaxial tests, the equipment enables execution of stress controlled tests along any linear stress path in positive q-p' plane, K_o consolidation tests and α test (ε_d=0) [Länsivaara 1993]. Following the input of specimen and test control parameters, tests are governed by microcomputer operated control program without manual intervention [Kolisoja et al. 1989].

Additionally to stepping motor operated loading capable of both accurate axial stress and strain control, triaxial test apparatus includes automated cell pressure application and control unit. With the triaxial apparatus connected to a pressure source, cell pressure is controlled using stepping motor operated

pressure regulator with accuracy of 0.2 kPa [Länsivaara 1993]. In K_o^{NC} consolidation radial strains are indirectly calculated on the basis of continuously measured volumetric and axial strains using Equation 4.1. Zero radial strains are maintained by adjusting axial strain to make them equal to volumetric strain at each sequence of the test ($\varepsilon_1=\varepsilon_v$) [Länsivaara 1993]. Thus, microcomputer evaluates measurements logged and adjusts axial deformation and radial stress based on the data collected [Kolisoja et al. 1989].

$$\varepsilon_3 = (\varepsilon_v - \varepsilon_1)/2 \tag{4.1}$$

Beside quantities measured in automated oedometer testing, automated triaxial testing apparatus includes continuous measurement and log of cell pressure, back pressure and volume change of the specimen [Länsivaara 1993]. Measurements of cell pressure and back pressure are provided using strain gauge pressure transducer, while measurements of volumetric strains of the saturated specimens are made using electronic balance, weighing the amount of water going in and coming out from a specimen [Kolisoja 1990]. At any sequence test progress can be examined in diagrams relating deformation to load, volume change or pore pressure. Besides bringing ease of operation and enabling execution of advanced stress and strain controlled tests, results gained are proven equivalent to those of traditional methods [Kolisoja et al. 1989].

5. Sampling and specimen preparation

5.1 Soil sampling results

5.1.1 Sampling performance

ST II sampling results
Sampling with STII sampler (see Figure 5.1) was chosen to obtain samples of quality representable for Finnish geotechnical practice and to investigate the influence of the considerable area ratio on the extent of sample disturbance. Due to the characteristics of STII sampling process, and enhanced by its robust construction, certain volume of the material underneath the final sampling depth is severely disturbed by the sampler penetration. Area ratio of the sampler relevant at the start of sampling is 118 % [Andresen & Kolstad 1980].

Figure 5.1 Sampling with STII; a) piston mechanism, b) PMMA cylinders, c) filling, and d) closure of the sampler.

The main objection to the sampling performance with STII was related to the use of retainer which should be avoided in sampling of soft clay. Retainer introduced severe deformations along the sample surface (see Figure 5.2 a). Furthermore, PMMA cylinders, characterised with development of considerable shear resistance along the internal area of liners, caused additional damages of the sample (Figure 5.2 c and d). Using this sampling method, there was no clear peripheral remoulded zone. Instead, as shown on Figure 5.2, sample sur-

face was regularly characterised by severe deformations in form of channels and cavities indicating overconsolidation [Clayton et al. 1982]. In addition, STII sampler in its function employs complex set of mechanical parts shown on Figure 5.1 a). Besides resulting with laborious sampling process, sampling with STII demanded usage of lubricant. Consequently, samples were often covered with layer of grease evident during sample extraction (see Figure 5.2 b). Due to the extent of disturbance, considerable amount of material had to be trimmed off reducing the size of samples already small in diameter. Consequently, STII obtained samples were unsuitable for preparation of specimens with 20 cm² of cross sectional area, commonly used in laboratory testing.

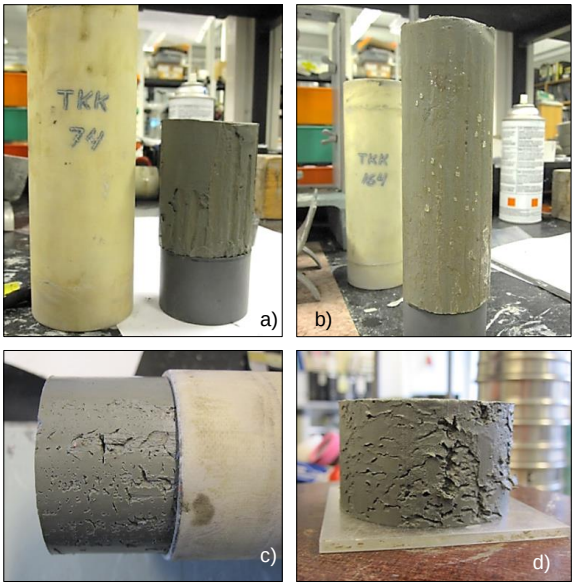

Figure 5.2 Sample disturbances with STII; a) influence of sample retainer, b) influence of lubricant, c) PMMA related friction during sample extraction, and d) sample disturbance in the form of channels and cavities.

The STII sampler due to the mode of sampler penetration can be used in much stiffer materials compared to NGI fixed piston samplers. PMMA cylinders used in Swedish standard samplers are more favourable for sample storage compared to steel cylinders [Andresen & Kolstad 1980].

NGI 54 mm sampling results

Main problems associated with quality of sampling using NGI 54 mm sampler shown on Figure 5.3, were related to the quality and the condition of sampling cylinders. The NGI 54 mm steel cylinders were of low quality in terms of thickness of thin walls varying along the circumference. Several groups of cylinders with respect to average wall thickness were used, i.e. 1.0, 1.25 and 1.5 mm. Furthermore, steel cylinders were in poor condition in terms of quality of the cutting edge. Due to their inappropriate application in stiff cohesionless soils, cutting edges of the cylinders were often damaged (Figure 5.4). In most of the cases cutting edge was restored, however, frequently out of plane while

the cutting angles reproduced varied considerably. Some cylinders had oval cross section caused by impacts. Presence of oval cross section led to squeezing of the sample upon the rotation of the cylinder, resulting with thick disturbed zone along the periphery of the sample. To evaluate applicability, it is important to perform soundings in the vicinity of the future sampling profile. This sampling technique is not suitable for sampling in coarse sands and gravels. Furthermore, equipment was not designed to withstand severe impacts. Poor condition of the cutting edge and poor accuracy of cylindrical shape was responsible for sample disturbances shown in Figure 5.4 a) and b), while disturbances in Figure 5.4 c) were caused by impact.

Figure 5.3 Sampling with NGI 54 mm, a) prior penetration and b) following extraction.

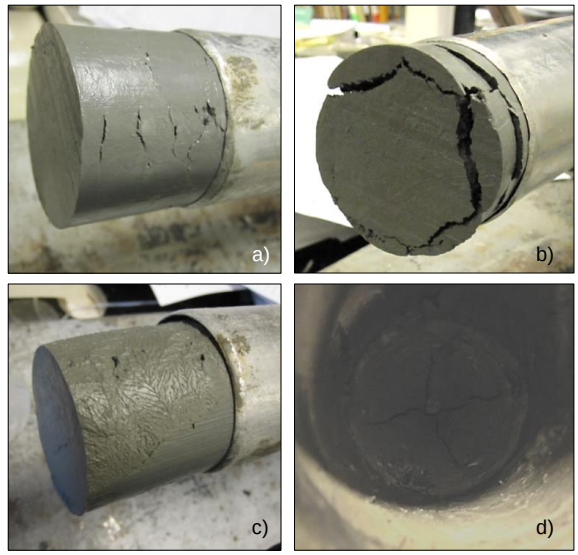

Figure 5.4 Sample disturbances with NGI 54 mm; a) friction caused disturbance during sample extraction, b) influence of the damaged cutting edge, c) effect of impact, and d) effects of drying.

Due to characteristics of the sampling process, samples were not of uniform quality along the cylinder length. About 100 mm of material in the upmost part of the cylinder was disturbed by the action of piston. Systematic evaluation of sample quality at the upmost part of cylinder revealed the material often being remoulded. If the piston was not properly locked prior to sampler

extraction, the disturbed zone was considerably thicker resulting from the action of piston and inner rod weight on top of the material sampled. The material so obtained cannot be considered undisturbed. Sample cut-off procedure prior to the extraction of the sampler, i.e. application of torsion underneath sampling cylinder and suction initiated upon sampler withdrawal, introduced severe disturbance of the material at the bottom of the cylinder. Indeed, final 100 mm was not representative of the undisturbed material and its testing was avoided. Therefore, out of 800 mm of the material that can be obtained in one cylinder, only 600 mm can be in the best case considered undisturbed. Indeed, within remaining 600 mm of sample, considerable variation in quality can occur in the case of poor condition of the cylinder, or eventual deviations from optimum sampling procedure such as inappropriate depth of the sampler, speed of penetration etc. Finally, variation in the extent of sample disturbance along cylinder length was highly influenced by the lithostratigraphic conditions in situ. In soft sensitive clays characterised with silty inclusions, drastic variation in sample quality along the sample length were common.

NGI 54 mm sampler provided satisfactory performance in terms of sample retrieval. The mass of the material contained within cylinder in the case of successful application that varied from 2.5 to 2.7 kg, was very often successfully maintained within the cylinder by friction on 0.134 to 0.125 m^2 of activated inner area. The minimum shearing resistance necessary for sample retrieval is independent of the length of cylinder filling and amounts 0.20 kPa. To increase quality of the samples, speed of penetration during sampling was minimised to 0.1 to 0.2 m/s. Low speed was maintained at the onset of retrieval of the sampler to minimise suction at the bottom of the sample. After 1 m of slow upward movement retrieval speed was increased to about 0.5 m/s.

NGI 86 mm sampling results

NGI 86 mm sampler (see Figure 5.5) has proven to be of very poor performance in the terms of sample retrieval. The reasons for the malfunction were twofold, and were related to sampler design and poor condition of the equipment. During retrieval, sample is withheld within the cylinder by combined action of friction between the sample and the cylinder walls, and suction created between piston and material on top of the sampling cylinder.

In comparison to NGI 54, NGI 86 mm sampler dimensions are more unfavourable in terms of parameters influencing sample retrieval. Due to large diameter, mass contained within the cylinder in the case of successful filling was considerable, and varied from 3.3 to 3.8 kg. The corresponding active contact area between the cylinder and sample varies from 0.10 to 0.12 m^2, respectively. Thus, minimum shearing resistance between sample and steel walls required for successful retrieval was 0.31 kPa, i.e. 55 % higher than that for NGI 54.

Additional reason for poor retrieval was the poor condition of the sampler. Aalto University NGI samplers do not have pressure valve securing the suction upon sampler retrieval. Furthermore, external diameter of the section of the sampler to which cylinders are connected is slightly smaller than the internal diameter of the cylinders, while the rubber rings designed to ensure tight con-

nection are old and damaged. Consequently, two problems arouse. When mounted upon sampler, cylinders could deviate angularly with respect to vertical axis. This fact had a negative influence on sampling quality and it resulted with formation of gaps between cylinder and sample Figure 5.6 a). Due to nonexistence of the pressure valve and poor connection between the cylinder and sampler, once the upward movement was initiated, pressure created within the cylinder freely dissipated. Thus, sample retrieval with NGI 86 sampler was impossible because rather heavy sample was withheld only by shear resistance between steel cylinder and layer of remoulded material along sample periphery (Figure 5.6 c).

Figure 5.5 Sampling with NGI 86 mm; a) upon sampler retrieval exhibiting sample cut-off cone and, b) prior to removal of sampling cylinder.

The problem has been solved in situ by implementation of overdriving technique, and by implementation of several layers of self-adhesive tape ensuring water tight connection between the cylinder and sampler. Discouraged by negative retrieval results on initial large diameter profile, i.e. profile 68, overdriving method was initiated. Penetration of the sampler was continued for ~10 cm following the depth of sampling cylinder being completely filled. Since the stress field underneath filled cylinder corresponds to that during sampler penetration with cylinder closed by piston, the procedure had a negative effect on the quality of the samples obtained. Underneath the cylinder, failure of underlying soil occurs, while the material at the bottom of cylinder was exposed to increased compression stresses. Implementation of overdriving severely decreased the length of the undisturbed portion of the sample. For this reason upper 100 and lower 150 mm of the sample, obtained on S-2010 profile 68, were omitted from testing. In the later stage of NGI 86 sampling, self-adhesive tape was implemented on the contact of sampler and cylinder so to substitute for the nonexistence of the pressure valve. The air trapped within the sampling cylinder was allowed to exit during material penetration, while upon sampler retrieval, tape ensured water/airtight conditions. This modification improved the performance of the sampler with successful sample retrieval becoming almost regular (>90 %). Following the tape application, considerable suction at the upmost portion of the cylinder was registered during cylinder removal, especially at higher sampling depths. With retrieval becoming almost regular, primary cause of the sampler malfunction was resolved. Indeed, remaining

large diameter sampling works on profile 67 were performed without overdriving. Moreover, suction registered ensured successful sample retrieval while its intensity indicated that following the pressure valve installation, no further problems related to successful retrieval with NGI 86 mm are to occur.

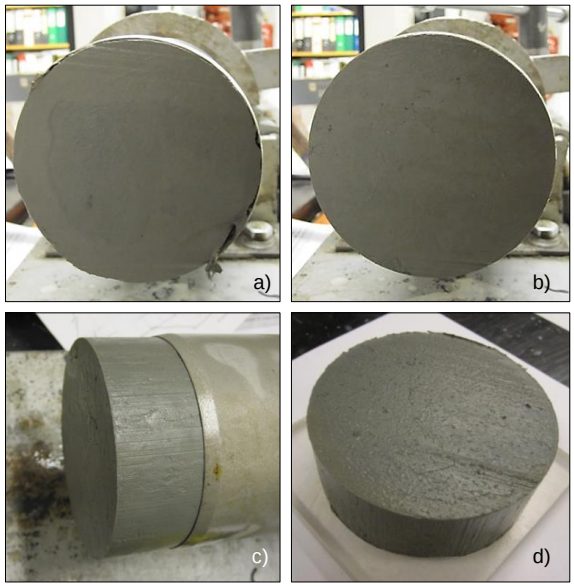

Figure 5.6 Sample disturbances with NGI 86 mm; a) disturbed periphery and gap between sample and cylinder, b) cutting edge quality, c) friction in sample extraction, and d) high quality sample and pore pressure release bubbles on freshly cut surface.

NGI 86 mm cylinders were in better condition compared to NGI 54 mm, including quality of the cutting angle and centricity. By careful examination of cross section of the samples obtained by NGI samplers, i.e. see Figure 5.4 a) and Figure 5.6 b), it was possible to identify zones of the intact core and that of disturbed/remoulded material. The remoulded zone was about of the same thickness for both NGI samplers. Thus, the diameter of the undisturbed core was larger with NGI 86 compared to that of NGI 54, identifying the main advantage of large diameter sampling in soft soils. Furthermore, in the case of out of centricity penetration of the sampler, remoulded zone occurred on the opposite side to that of gap between the sample and cylinder (Figure 5.6 a).

To conclude, NGI 86 mm sampler should be examined and repaired by providing pressure valve and ensuring tight connection of cylinder to the sampler. By doing so, the problems related to sample retrieval will be solved without the need for overdriving. With valve activated minimum pressure on top of cylinder required for successful recovery (0.31 kPa) can be easily achieved. Furthermore, if the cylinder is prevented from inclining during sampling, possibility for appearance of gaps between cylinder and sample is reduced.

Transport and storage

Unlike in 2009, following the sampling in 2010, special care was taken so to improve transport conditions. During transport, sampling cylinders were se-

cured in vertical position on a compressible base created by layers of canvas and foam mattresses. Techniques used for securing water tight conditions were enhanced by additional layers of plastic wrap and impermeable tape.

In storage, typical procedure was implemented. At Aalto University samples were stored in the cold room with controlled temperature of +6 °C. Cylinders were kept in upward position under water sealed conditions within the specific containers depending upon the sampling technique used. Following extrusion of the samples, remaining material was promptly sealed back again and stored in temperature controlled room. In the present study no attention was given to changes in chemical conditions since the laboratory did not employ equipment for measuring or monitoring chemical changes of the samples stored.

Additional efforts implemented in this study, prevented impact caused disturbances and prolonged usability of the samples in terms of representativeness of initial water content and void ratio.

5.1.2 Stratigraphic conditions

Results of sampling programmes with respect to stratigraphic characteristics and material distribution are elaborated in the text that follows. Sampling results revealed stratigraphic conditions in the vicinity of the Perniö embankment differing from those at the location of the sampling programme in 2010. Consequently, the stratigraphic conditions are elaborated separately.

Sampling Programme S-2009

Sampling works in 2009 using NGI 54 mm, aimed defining stratigraphy of Perniö deposit in the vicinity of the embankment and obtaining soft clay material influenced by stress changes of the in situ conditions. Altogether, S-2009 included four sampling profiles, i.e. 43, 44, 45 and 47. Sampling profiles 43 and 45 were made next to the embankment toe, while profiles 44 and 47 were located several meters from the embankment on the future sliding side. Sampling profiles corresponded to the location of the cross section D-D'. Detail location of the S-2009 sampling works is presented on Figure 3.3 and in Appendix 1. One NGI 54 mm cylinder sample was obtained for each meter of the deposits until final sampling depth of 6 m, dry crust and stiff clay included. Based on sampling results obtained on profiles 43, 44 and 45, and Swedish weight sounding and CPT results along profile D-D', stratigraphic conditions underneath of the embankment were established.

Stratigraphic conditions interpreted are presented in Figure 5.7 and Table 5.1. According to the cross section D-D', elevation of the ground surface at the location of profiles 43 and 45 was +8.53 m absolute. Dry crust layer was registered up to 2.53 m and was followed by stiff clay layer up to 2.93 m of depth. Thereafter, 2.1 m thick sulphide containing soft clay strata occurred up to 5.03 m of depth, and was succeeded by heavily stratified (fissured) stiff silty clay material until the final depth of investigation, i.e. 6.03 m of depth (+2.5 m absolute). The elevation of the ground surface on the position of profiles 44 and 47 was estimated on the basis of data on profile D-D' to be +7.56 absolute. On profiles 44 and 47, dry crust material was registered up to 1.66 m of depth.

Beneath dry crust, 0.4 m thick stiff clay layer occurred. Soft clay stratum that followed was thicker than on profiles 43 and 45, starting from 2.06 and continuing until 5.56 m of depth, i.e. between +5.5 and 2.0 m absolute. Thereby, until final sampling depth of 6.56 m of depth (+1 m absolute) stiff clay was registered. Groundwater level was positioned at 1.83 m beneath the embankment and at 0.86 m of depth on profiles 44 and 47, i.e. +6.7 m absolute.

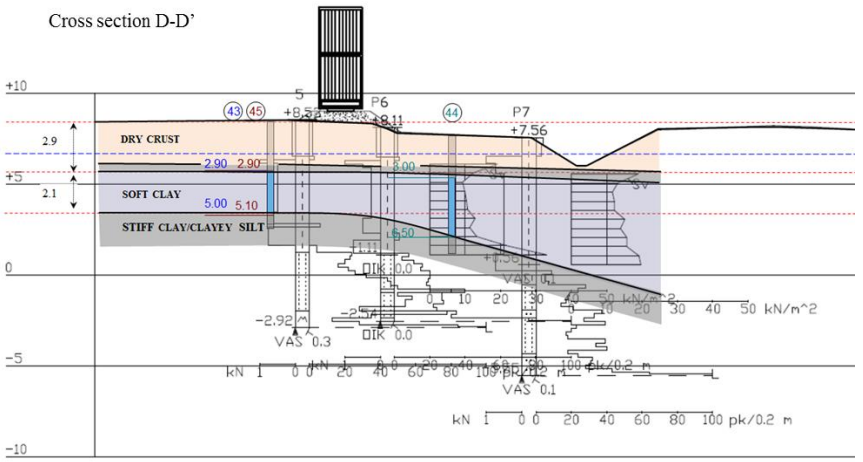

Figure 5.7 Stratigraphic conditions beneath the Perniö embankment, cross-section D-D'.

Results obtained in S-2009 complied with the previously performed investigations at the location (TUT), i.e. CPT and Swedish weight sounding results on profiles 5, P6 and P7. Measurements next to the embankment indicated stiff clay layer appearing until +1.1 absolute, and being followed by silt stratum until -2.0 m and -2.4 m absolute on profiles 5 and P6, respectively. In comparison, on profile P7, silt layer appeared between -0.4 and -4.4 absolute. Furthermore, on respective profiles 5, P6 and P7, bedrock was registered at -2.92, -2.54 and -5.5 absolute, confirming existence of local ridge underneath of the embankment, above which ~1 m thick layer of moraine exists.

Sampling Programme S-2010

Sampling works aiming to evaluate performance of STII, NGI 54 and NGI 86 mm samplers included eight sampling profiles set on seven meter distanced cross sections A-A' and B-B'. Sampling works targeted soft clay and were performed for each meter of soft clay strata up to 7 m of depth. Detail location of the S-2010 sampling works is shown in Figure 3.4 and Appendix 1. Owing to this arrangement, variation in the results due to natural variability in soil properties was expected to be equal for all samplers [Jakobson 1954].

Results of the sampling programme S-2010 on cross sections A-A' and B-B' are shown in Table 5.1 and Figure 5.9. Average elevation of the ground surface at the location of S-2010 sampling field is +7.5 m. Due to vicinity of sampling profiles, results obtained were almost identical. Typical borehole profile consisted of 0.3 m of humus, followed by dry crust layer up to 1.4 m of depth. Dry crust was followed by layer of stiff clay with 0.5 m average thickness, i.e. be-

tween +6.1 to +5.6 absolute. Auger facilitated removal of the dry crust and stiff clay material enabled penetration of samplers into underlying very soft clay subsoil (Figure 5.8). Sulphide bound soft clay strata was onset at 1.9 m of depth, i.e. +5.6 absolute (Figure 5.10). Thin silty inclusions shown on Figure 5.10, occasionally occurred on profiles 63, 65, 66, 67 and 68 at depths between 4.0 and 6.5 m, i.e. +1.0 to +3.5 absolute. Sounding on profiles 61 and 67 revealed soft clay presence until 11.7 m of depth (-4.2 absolute), thus considerably thicker than underneath Perniö test embankment. A soft clay stratum was succeeded by 1.1 m thick continuous layer of silt and 0.7 m thick layer of moraine, positioned just above bedrock (profile 61). Bedrock was evidenced at 13.5 and 13.1 m of depth on profiles 61 and 67, i.e. -6.07 and -5.6 m absolute, respectively. Field data indicated position of groundwater at ~1 m of depth, however, following the laboratory examination of the sampled material, zero pore pressure level was set to depth of 0.8 m (+6.7 absolute).

Figure 5.8 Auger facilitated removal of dry crust and stiff clay, a) dry crust, 0-1 m, b) stiff clay, 1-2 m, and c) soft clay at 2-3 m of depth.

Laboratory investigation following the S- 2010 revealed Perniö soft clay stratum being consistent of three distinctive sublayers (see Figure 5.9). Zone A, following stiff clay layer, appeared continuously from +5.6 to +3.8 m absolute. Between +3.8 and +1.2 m above sea level, Perniö soft clay was characterised with increased content of silt, i.e. zone B. Finally, zone C was registered for elevation levels underneath +1.2 m absolute.

Aalto University practice includes determination of initial properties of material in each sampling cylinder immediately following the sampling. The parameters typically determined are: water content, liquid limit, undrained shear strength, undrained remoulded shear strength and sensitivity. With an exception of water content, the parameters are determined using fall cone test. Furthermore, parameters of plastic limit, specific gravity, loss of ignition, organic content, particle distribution curves and clay content are sporadically evaluated. Following S-2010, unit weight, initial void ratio, plasticity index, liquidity index, consistency index and activity were evaluated as well. Among parameters listed, only water content, liquidity index, undrained shear strength and sensitivity were suitable for evaluation of the performance of the samplers, while remaining parameters were used to define stratigraphic conditions.

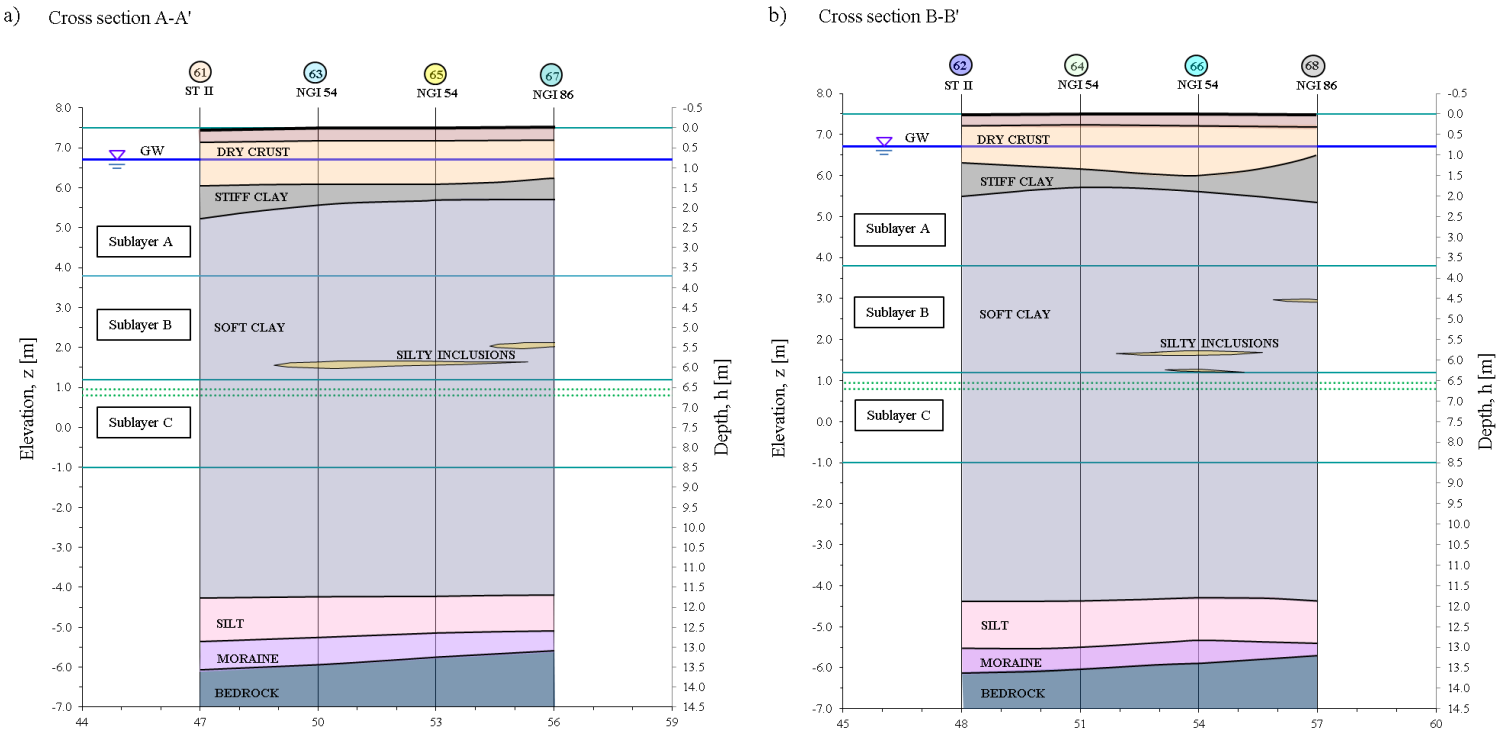

Figure 5.9 Stratigraphic conditions beneath S-2010 sampling field, a) cross section A-A' and b) cross section B-B'.

Table 5.1 Stratigraphic conditions of sampling fields' S-2009 and S-2010.

		Material	Depth z [m]	Absolute depth h	Thickness d [m]
S-2009 Profile 44	h0=+7.56	dry crust	0.00 - 0.86	7.56 - 6.70	0.86
		dry crust sub.	0.86 - 1.66	6.70 - 5.90	0.80
		stiff clay	1.66 - 2.06	5.90 - 5.50	0.40
		soft clay	2.06 - 5.56	5.50 - 2.00	3.50
		stiff clay	5.56 - 6.56	2.00 - 1.00	1.00
S-2009 Profile43 and 45	h0=+8.53	dry crust	0.00 - 1.83	8.53 - 6.70	1.83
		dry crust sub.	1.83 - 2.53	6.70 - 6.00	0.70
		stiff clay	2.53 - 2.93	6.00 - 5.60	0.40
		soft clay	2.93 - 5.03	5.60 - 3.50	2.10
		stiff clay	5.03 - 6.03	3.50 - 2.50	1.00
S-2010 Profile 61....68	h0=+7.5	dry crust	0.00 - 0.80	7.50 - 6.70	0.80
		dry crust sub.	0.80 - 1.40	6.70 - 6.10	0.60
		stiff clay	1.40 - 1.90	6.10 - 5.60	0.50
		soft clay A	1.90 - 3.70	5.60 - 3.80	1.80
		soft clay B	3.70 - 6.30	3.80 - 1.20	2.60
		soft clay C	6.30 - 8.50	1.20 - -1.00	2.20

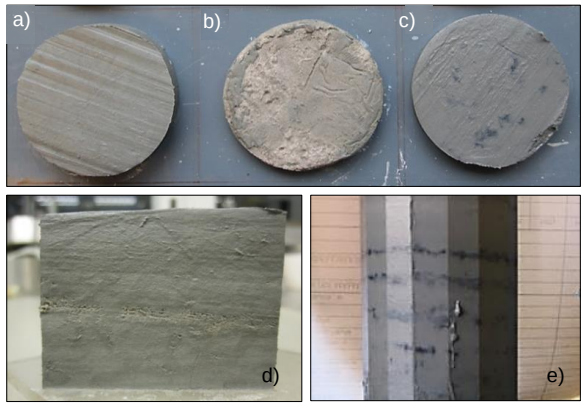

Figure 5.10 Perniö deposit materials; a) soft clay, b) and d) silty clay, c) and e) sulphide content.

5.1.3 Initial state parameters

Initial state parameters considered for preliminary identification purposes are: water content, initial void ratio, unit weight and overburden effective stress. The parameters depend upon depositional conditions including initial density of the sediment, rate of deposition and water chemistry; and post depositional processes such as stress history, chemical history, time related changes and fabric [Hight et al. 1987]. These conditions can change during sedimentation and subsequent consolidation, leading to large variance in initial water content, void ratio and unit weight within a deposit. Gravimetric water content was obtained based on total and 24 h, 100 °C, oven dried sample weight. Ini-

tial unit weight and void ratio values after sampling were calculated based on initial volume of the sample. The initial volume was defined by inner area of the sampling cylinder and provisional length of the sample. In the case of poor sampling gap between sample and cylinder may occur. Consequently, volume used in determination of unit weight and void ratio may overestimate the real volume of the sample. The effect leads to underestimation of unit weight and overestimation of initial void ratio values. However, since the gap between sample and cylinder is merely a result of poor sampling performance, it is that these values represent in situ properties more accurately than measurements based on real volume of the sample. Furthermore, poor sampling performance may cause considerable densification of the sample leading to underestimation of void ratio and overestimation of unit weight measured compared to those in situ. These two effects of poor sampling thus have opposite manifestations. Among parameters determined after the sampling, magnitude of initial water content was used as a reasonable basis for the evaluation of the sampling performance. The values of unit weight and initial void ratio were used primarily for defining stratigraphic conditions. Large scatter in initial void ratio and unit weight values however, implied poor sampling performance.

Initial water content

In Figure 5.11 a), water content values after S-2009 and S-2010 are related to sampling depth. Following the S-2010, average w_o of dry crust and stiff clay amounted 40 and 89 %, respectively. In soft clay strata, w_o values varied broadly from 60 to 110 %. Average w_o of 99.6 % in zone A, 83.6 % in zone B, and 103.7 % in zone C implied existence of three distinctive units of Perniö soft clay. Within zone A, the lowest w_o identified profiles 61 and 62 (STII), and profile 68 (NGI 86). The highest values of 107 %, were obtained on profiles 64, 66 (NGI 54) and 67 (NGI 86). In zone B, w_o varied broadly from 58.8 to 110.5 %. Samples with high silt content exhibited the lowest w_o. In contrast, occasional soft clay samples on profiles 64 (NGI 54) and 67 (NGI 86), exhibited very high w_o equivalent to those in zone A and C. High scatter in zone B reflected considerable permeability variations and difficulties related to high quality sampling in silty clays. Within zone C, w_o above 106 % identifying upmost section of the zone were independent of the sampling method used. Somewhat reduced values on profiles 61 (STII) and 65 (NGI 54), characterised greater depths of the zone. In contrast to S-2010, water content values measured following the S-2009 were considerably less. Representable w_o values in dry crust and stiff clay were 33.0 and 53.5 %, respectively. At elevation corresponding to zone A and B, S-2009 sampling works returned average w_o of 76 % and 62 %, respectively. Lower water content values in 2009 were largely a result of the influence of Perniö embankment and the consequent increase in overburden stress over a long period of time. Moreover, decreased values may have also been related to poor sampling performance in 2009.

Initial void ratio

Figure 5.11 b) presents initial void ratio values of Perniö soft clay evaluated following the S-2010. As the material was fully saturated, e_o profile reflected that of w_o values, i.e. for $S_r=1$, $e_o=w \cdot G_s$. In zone A, average e_o was 2.9, while the

highest values identified mid of the zone. Within zone B characterised by considerable scatter, average e_o amounted 2.4. Samples containing silt exhibited low e_o. Finally, zone C was characterised with overall the highest e_o, amounting 3.1 in average. The highest values occurred in upmost portion of the zone.

Unit weight

Figure 5.11 c) relates unit weight of Perniö deposit materials to sampling depth. Unit weight data representing dry crust and stiff clay (S-2009) indicated respective values of 18.5 kN/m^3 and 16.8 kN/m^3. Values determined on soft clay following S-2010 varied from 13.9 to 16.1 kN/m^3. In zones A and C, results were uniform and amounted 14.4 kN/m^3 in average. In contrast, unit weight data in zone B were very scattered and generally higher, with average at 15.2 kN/m^3. Unit weight values obtained following S-2009 were overall the highest. Indeed, at elevation corresponding to zones A and B, S-2009 results were 1-1.5 kN/m^3 above S-2010 average.

Overburden stress distribution

Due to the significance of effective overburden stresses in evaluation of specimen quality, viscosity, and anisotropy effects, selection of the unit weight values and groundwater level was given high importance. Considering results of field investigations and laboratory test, zero pore pressure level was positioned at +6.7 m absolute, i.e. 1.83 m underneath of the embankment and at 0.8 m of depth at sampling field S-2010. Interpretation of the effective overburden stresses was based on unit weight values measured in laboratory testing and following the sampling. As shown in Table 5.2, average unit weight values were adequately reduced to compensate for the effects of sampling disturbance.

Table 5.2 Unit weight and overburden stress distribution of Perniö deposit.

		Material	Total u.w. γ_t [kN/m^3]	Effective u.w γ [kN/m^3]	Depth z [m]	Absolute elevation [m]	Overburden stress total σ_{v0} [kPa]	effective σ'_{vo} [kPa]
S-2009 Profile 44	h0=+7.56	dry crust	17.35	17.35	0.86	6.70	14.9	14.9
		dry crus sub.	17.35	7.35	1.66	5.90	28.8	20.8
		stiff clay	16.33	6.33	2.06	5.50	35.3	23.3
		soft clay	14.75	4.75	5.56	2.00	87.0	40.0
		stiff clay	18.37	8.37	6.56	1.00	105.3	48.3
S-2009 Profile43 and 45	h0=+8.53	dry crust	17.23	17.23	1.83	6.70	31.5	31.5
		dry crus sub.	17.23	7.23	2.53	6.00	43.6	36.6
		stiff clay	16.33	6.33	2.93	5.60	50.1	39.1
		soft clay	15.08	5.08	5.03	3.50	81.8	49.8
		stiff clay	17.61	7.61	6.03	2.50	99.4	57.4
S-2010 Profile 61,...68	h0=+7.5	dry crust	17.0	17.0	0.80	6.70	13.6	13.6
		dry crust sub.	17.0	7.00	1.40	6.10	23.8	17.8
		stiff clay	16.0	6.00	1.90	5.60	31.8	20.8
		soft clay A	14.15	4.15	3.70	3.80	57.3	28.27
		soft clay B	15.10	5.10	6.30	1.20	96.5	41.53
		soft clay C	14.15	4.15	8.50	-1.00	127.7	50.66

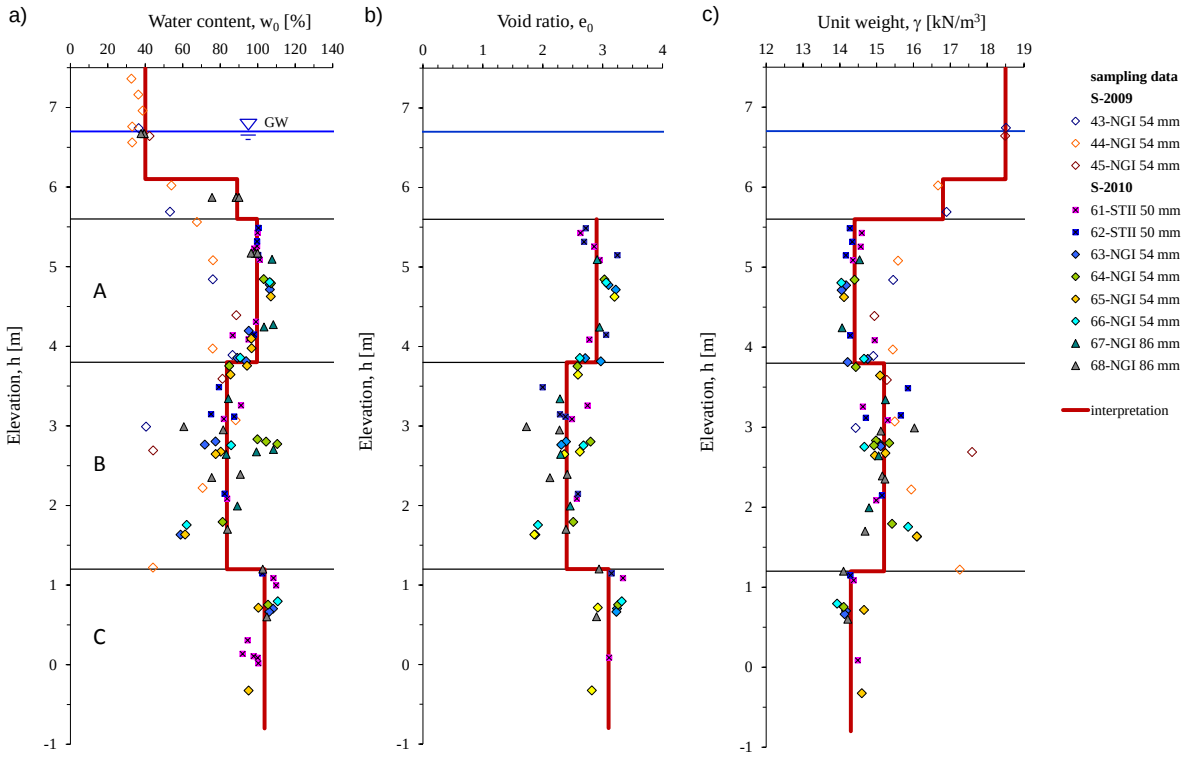

Figure 5.11 Initial state parameters of Perniö deposit; a) water content, b) void ratio, c) unit weight.

Water content to unit weight ratio w/γ

Relation of water content to unit weight is suitable approach for evaluation of quality of geotechnical investigation results [Leroueil et al. 1990]. In deposits with similar depositional conditions, by plotting w vs. γ continuous curve is obtained. Since both, water content and unit weight are influenced by sample disturbance, high magnitude of w/γ indicates high sample quality.

Figure 5.12 a) relates water content to unit weight values following the sampling. With an exception of sporadic data on profiles 43 and 45 (S-2009) and profile 65 (S-2010), resulting w/γ curve is continuous indicating Perniö clay materials being of similar geological origin. The relation is well represented by Equation 5.1.

$$w = 7.96 \cdot 10^{6} \gamma^{-4.23} \tag{5.1}$$

In Figure 5.12 b) w/γ values are plotted in relation to sampling depth. The resulting w/γ values varied broadly from 1.97 to 7.95 %/kN/m³, being the lowest for dry crust, followed by those of weathered clay, and finally by high values in soft clay and quick clay materials. Examined with respect to sampling method used, specimens characterised with the highest w/γ values were obtained on profiles 68, 67 (NGI 86) and 63, 64, and 66 (NGI 54). Considering S-2010 results obtained using NGI samplers representable values in stratigraphic units A, B and C amounted 7.5, 5.5 and 7.4 %/kN/m³, respectively.

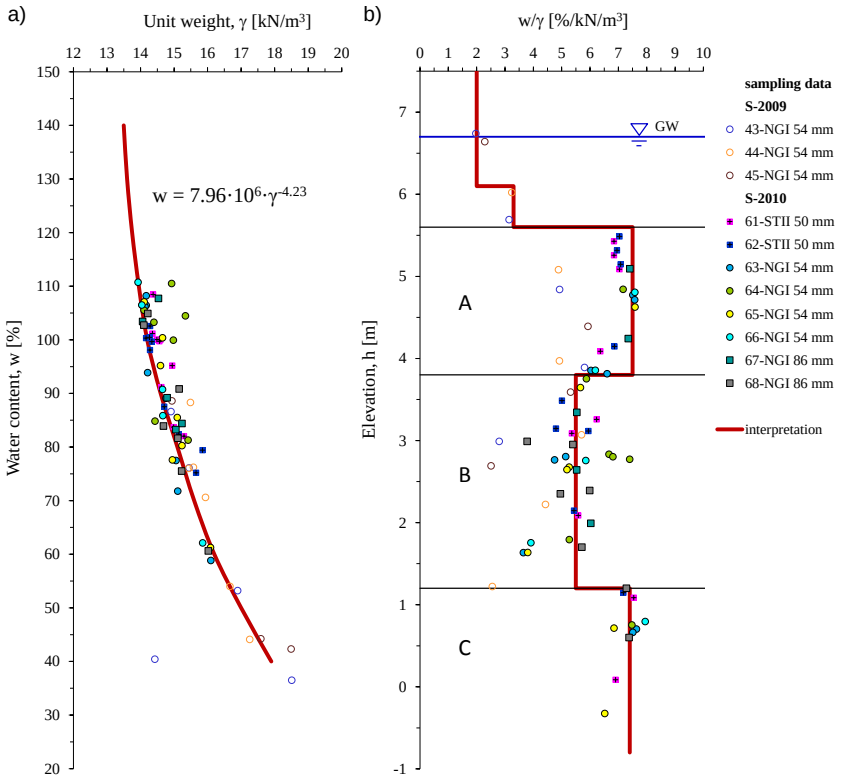

Figure 5.12 Perniö clay water content to unit weight data; a) w/γ curve, b) w/γ depth distribution.

5.1.4 Composition and compositional effects

Particle size distribution

Particle size distribution curves obtained for Perniö deposit materials are presented in Figure 5.13. All of the stratigraphic units of Perniö deposit were categorised as clays, containing above 40 % of clay size particles by weight of total mass of fines [ISO 14688-2:2004]. Dry crust contained up to 7 % of sand, and clay size particles in a considerable range from 38 to 64 %. Clay materials of zone A and B contained rather high proportion of clay size particles, typically between 52 and 64 %. Compared to zone B, grain size distribution curves of zone A were generally smoother due to higher percentage of fine sand and coarse silt, i.e. up to 10 % and 20 %, respectively. Silty clays of zone B contained up to 14 % of sand, and rather low content of clay particles, typically 42 to 46 %. In contrast, zone C was characterized with the highest clay content ranging from 70 to 76 % and rather low percentage of coarse silt, i.e. <9 %.

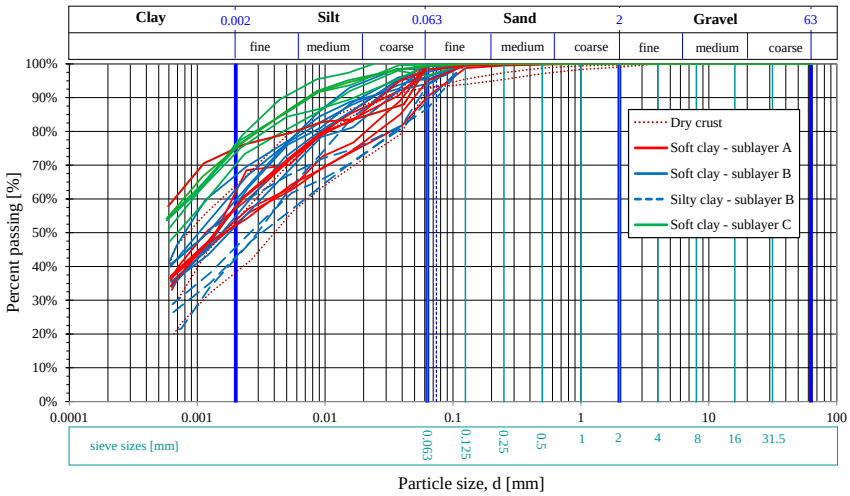

Figure 5.13 Particle size distribution of Perniö deposit materials.

Clay content

Content of clay sized particles in relation to depth at Perniö is shown in Figure 5.14 a). In dry crust and stiff clay materials clay content was estimated to be ~52 %. In soft clay strata, clay content increased with depth, being 56, 58 and 75 % by average in zones A, B and C, respectively. Clay content in zones A and B indicated materials of intermediate plasticity. Silty inclusions within zone B were evidenced by occasional very low clay content of <50 %. In contrast, zone C was characterized with very high and rather uniform clay content indicative of high plasticity clays.

Loss of ignition and organic content

Figure 5.14 b) and c) present loss of ignition and organic content in Perniö deposit. Limited amount of data available indicated loss of ignition in Perniö soft clay of 4.3 % in average. Somewhat lower values of 3.8 % occurred in zone

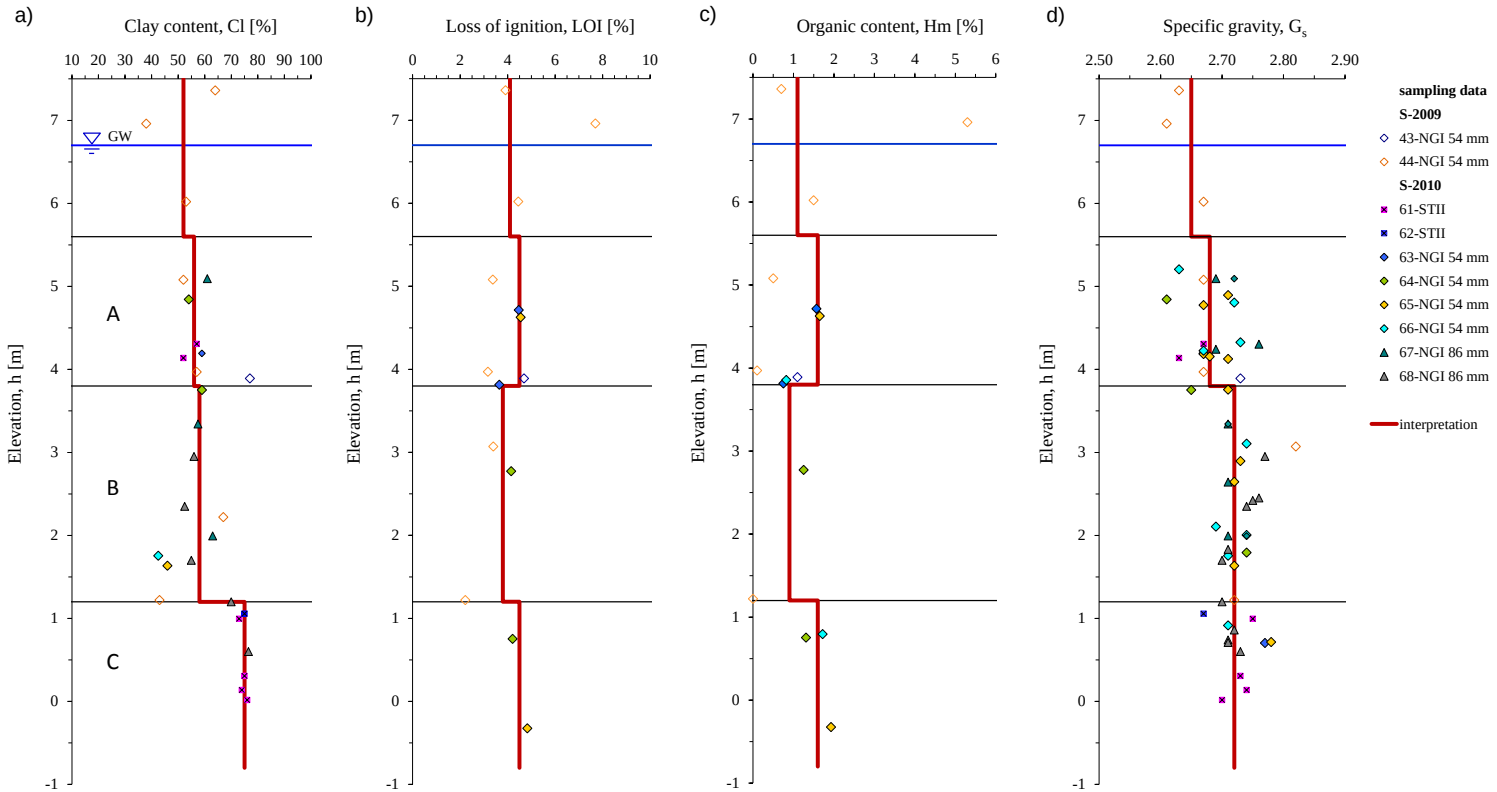

Figure 5.14 Compositional effects of Perniö soft clay; a) clay content, b) loss of ignition, c) organic content, and d) specific gravity.

B, while in zones A and C loss of ignition tended to 4.5 %. Same distribution pattern characterised organic content, being 1.4 % in average with tendency towards 0.9 % in zone B, and 1.6 % in zones A and C. Results obtained on material sampled in 2009 indicated generally lower values of both parameters. Dry crust and stiff clay materials were characterised with considerable scatter with loss of ignition of 4.1 % and organic content of 1.1 % being the probable targets. Finally, as shown on Figure 5.10, Perniö soft clay regularly exhibited dark sulphide bearing sediment in form of bands and spots, typical for fine grained soils in coastal region of south-western Finland [Gardemeister 1997]. The sulphide bearing black material oxidised rapidly after sampling and turned grey. Concentration of sulphide or its impact has not been evaluated within this study.

Specific gravity and mineralogy

Figure 5.14 d) shows results of specific gravity measurements of Perniö clay using Pycnometer. The specific gravity values varied notably from 2.61 to 2.78 being the lowest in dry crust. Presence of the silty inclusions had no influence the results obtained. Although results of zone A indicated slightly lower average specific gravity of 2.68 compared to 2.72 in zones B and C, after taking into consideration accuracy of the measurement and to simplify interpretation, a unique value of 2.70 was adopted for Perniö soft clay. The mineralogical composition of Perniö deposit materials was not tested, however, in the cool climatic conditions prevailing in the northern countries, the mineralogical development leads at fairly early stage to Illite clays, beyond which no significant changes take place [Gardemeister 1975]. The granular minerals are predominantly Quartz and Feldspar [Gardemeister 1975]. The main group of micaceous minerals consists of Illite, as well as in many instances, Chlorite [Gardemeister 1975]. The regional variation is slight [Gardemeister 1975].

5.1.5 Undrained shear strength and sensitivity

Following sampling, undrained shear strength and sensitivity values were measured. The results obtained are presented on Figure 5.15.

Undrained shear strength

The undrained shear strength c_u, classified Perniö clay material as soft clay of very low undrained shear strength [ISO 14688-2:2004]. The measurements were performed using ELE fall cone device with 100 g, 30° cone. Typically for NC soft marine deposits, undrained shear strength of Perniö clay increased with depth. As shown on Figure 5.15 a), c_u values obtained in 2010 ranged between 10.0 and 15.0 kPa at upper part of soft clay deposit, and rose with depth to values between 15.0 to 20.0 kPa in its lower portion. Exceptions were results in the upmost portion of zone A with values >18 kPa, corresponding to that of stiff clay and dry crust. Furthermore, the undrained shear strength values of material sampled in 2009 were clearly higher, particularly in zone B, and were characterised with considerable scatter of the results. The c_u values in zone A and B being 2.5 and 4.0 kPa higher compared to those in 2010, iden-

tify influence of Perniö embankment on the increase in the undrained shear strength. In OC clay, the water content is less than in the NC clay, while undrained strength, dependent on the water content is higher [Wood 1983].

Sampling technique used influenced resulting undrained shear strength. In S-2010, the lowest c_u were obtained on NGI 54 and NGI 86 sampled material. c_u values of material sampled with STII were notably the highest among 2010 results, especially within zone A. However, it was undrained shear strength of material obtained with NGI 54 in S-2009 that was the highest overall. The results indicated densification effects due to additional load by the embankment, and NGI 54 mm sampling in 2009 being poorly conducted.

Undrained remoulded shear strength

Due to the fact that soft clay, when remoulded has shear strength so low that it cannot reliably be measured by compression tests, the most suitable determination is carried out either by in situ or laboratory vane test, or fall cone test [Bjerrum 1967]. Figure 5.15 b) shows results of undrained shear strength obtained on remoulded soft clay of Perniö deposit measured with Geonor fall cone device using light, 10 g, 60° cone. Results obtained categorised undrained shear strength of remoulded Perniö clay being extremely low [ISO 14688-2:2004]. Depth distribution pattern of undrained remoulded shear strength c_{ur} generally resembled that of undrained shear strength c_u. Yet it was the c_{ur} values characterising zone B that were the lowest, while those of zone A were notably the highest.

Results showed undrained remoulded shear strength being influenced by sampling. The lowest values of undrained shear strength were obtained on remoulded material sampled with NGI 86 mm sampler, followed by NGI 54 and STII. Among NGI 54 data, profiles 44 and 63 exhibited higher values of c_{ur}, while the rest of the results were very uniform. Fact of c_{ur} on STII sampled material being the highest was related to disturbance effects in sampling.

Sensitivity

Figure 5.15 c) shows fall cone test determined sensitivity values of Perniö soft clay, obtained as the ratio of undrained and undrained remoulded shear strength of the same specimen (see Figure 5.16). Considerable oscillations in sensitivity indicated significant extent of initial bonding being destroyed in sampling, transport and sample extraction. Altogether, the results exhibited similar depth distribution pattern. The lowest values were obtained in the upper portion of zone A, and increased with depth until +2.0 m absolute within zone B characterised with overall the highest sensitivity. Thereafter, sensitivity slightly decreased, with values of zone C being somewhat lower than in zone B, yet significantly higher than in zone A.

STII sampling method overall gave the lowest sensitivity values, ranging between 10 and 35. Average values in zones A, B and C, were 14.0, 28.0 and 25.0, respectively. Scatter of sensitivity values gained was high, i.e. results on profile 61 significantly outperformed those of profile 62. Overall, the results were comparable with the lowest sensitivity values on material sampled with NGI 54 mm.

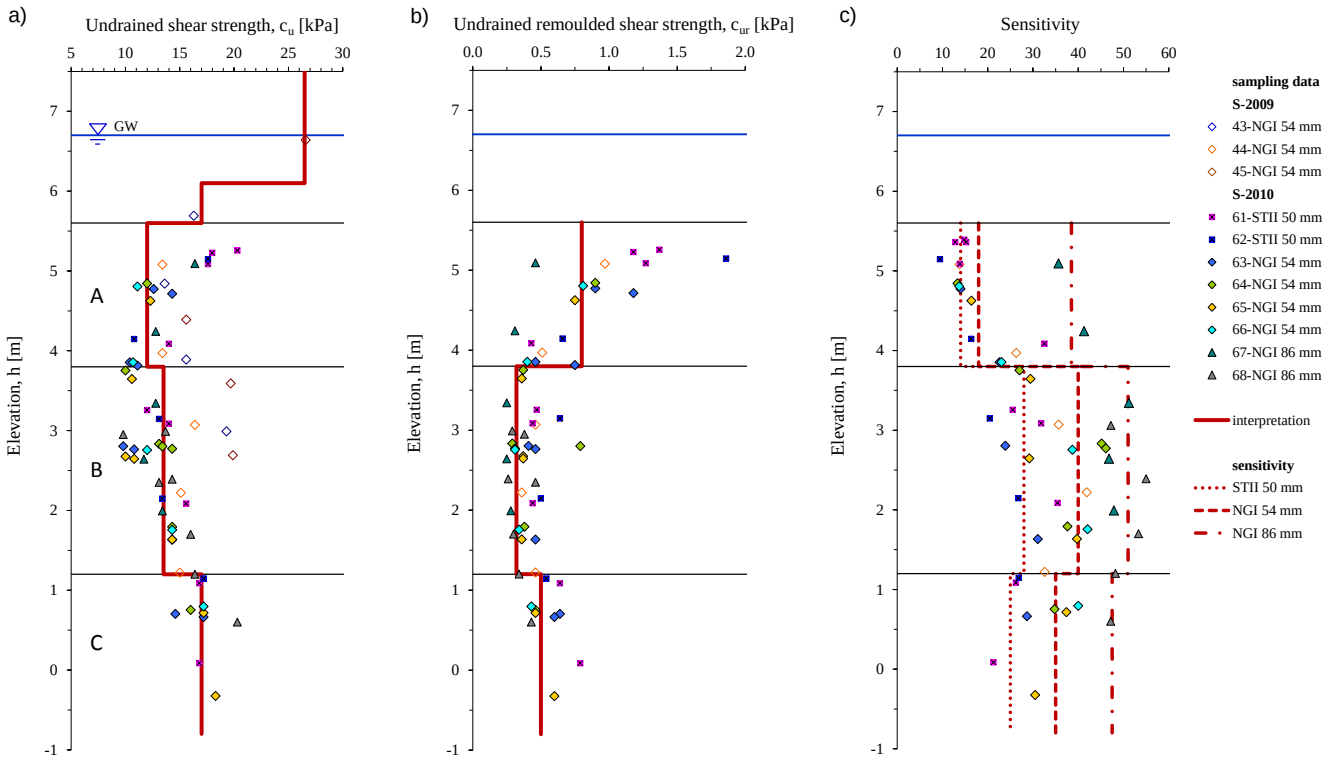

Figure 5.15 Shear strength and sensitivity of Perniö soft clay based on fall cone test, a) undrained shear strength, b) undrained remoulded shear strength, and c) sensitivity.

Sensitivity values obtained on material sampled with NGI 54 mm ranged from 13 to 47, and with an exception of those on profile 63, were rather regularly distributed with depth. Results obtained in 2009 were in very good correlation with 2010 sensitivity data. Average sensitivity values for zones A, B and C were 18.0, 40.0 and 35.0, respectively. Considering simplicity of the application, i.e. sampling works being straight-forward, this method gave samples of reliable quality and is suitable for standard engineering practice.

Sensitivity obtained on NGI 86 mm sampled material were considerably higher than those related to other samplers used in this study. The sensitivity values ranged from 35 to 55, with average in soft clay zones A, B and C being 38.5, 51.0 and 47.5, i.e. at least 10 units higher compared to those of other methods. Scatter of data was low and resulting values exhibited similar distribution as those related to other sampling techniques. Although this sampling method demanded considerable experience and skill for successful application, according to the fall cone test, it resulted with the least disturbance of the material sampled. In the absence of better alternative, the method should be regularly used when high quality samples for advanced laboratory testing are needed. Based on the results obtained on NGI 86 mm samples, Bjerrum's [1954] classification criterion identified all three sublayers of Perniö soft clay as very quick, i.e. $32<S_t<64$. Moreover, according to Swedish practice Perniö soft clay strata were classified as high sensitivity materials, i.e. $S_t>30$ [Rankka et al. 2004]. Furthermore, results obtained on NGI 86 mm sampled material of sublayer B categorised as quick clay, i.e. $S_t>50$ and $c_{ur}<0.4$ kPa [Rankka et al. 2004].

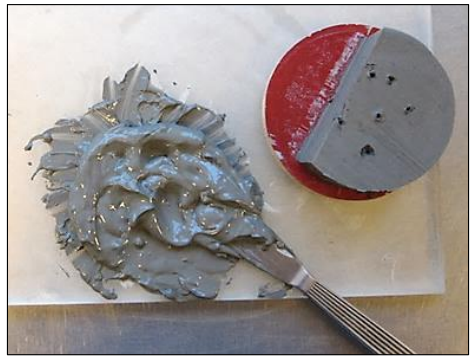

Figure 5.16 Remoulding of Perniö soft clay for sensitivity evaluation.

5.1.6 Atterberg limits

Understanding of the fundamental properties of clays requires a detailed study of the factors which control the plasticity [Bjerrum 1954]. In order to provide quantitative measure of Perniö clay plasticity, values of plastic limit and liquid limit were evaluated [Atterberg 1911]. Values of liquid and plastic limit determined as well as their relation to water content are presented on Figure 5.17 and Figure 5.18.

Plastic limit

Plastic limit w_p is a water content at which remoulded clay passes from brittle to plastic condition [Skempton 1967]. Plastic limit was determined as the moisture content of thread of soil rolled without breaking until only 3 mm in diameter. Plastic limit values of Perniö soft clay materials shown in Figure 5.18 a) were rather uniform. Indeed, limited amount of data available indicated slight decrease with depth, from 36.5 % in upper soft clay of zone A, to 30.5 and 29.5 % within zones B and C, respectively.

Liquid limit

Liquid limit w_L reflects the water holding capacity of the clay and is defined as a water content at which, in the remoulded state, clay passes from plastic to an almost liquid condition [Skempton 1967]. Liquid limit values of Perniö clay obtained by fall cone test varied broadly from 46.1 to 101.3 %. Based on the results shown in Figure 5.18 a), average liquid limits in zones A and C were 90.0 and 81.5 %, while that of zone B was 58.0 %. Liquid limit values measured in 2010 were slightly higher than those of material sampled in 2009.

Plasticity index

Plasticity index I_P, defining the range of water content over which the soil remains in a plastic condition is generally taken as an appropriate measure of soil composition [Hight et al. 1987]. According to Hight et al. [1987], effects of fabric on soil properties are not reflected on plasticity index. Detailed data on plasticity index versus depth is presented on Figure 5.18 b). Soft clay materials of zones A and C exhibited average plasticity indexes of 53.4 and 52.0 %, respectively. Silty clays within zone B had markedly lower average plasticity index of 29.3 %. However, occasional soft clay specimens within zone B exhibited very high values of plasticity index, i.e. as high as 58.3 %.

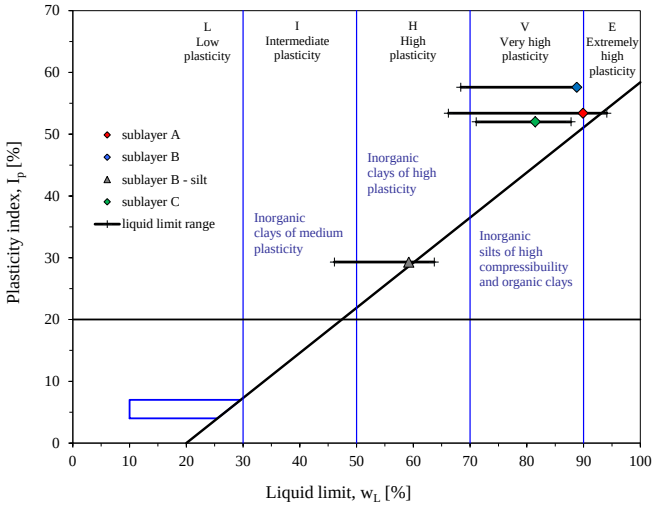

Figure 5.17 Plasticity chart; Perniö soft clay results.

On plasticity chart shown on Figure 5.17, Perniö clay plasticity indexes are related to liquid limits [Casagrande 1932]. Perniö soft clay materials being inorganic clays, positioned above A-line. The highest scatter of liquid limit values, i.e. from 66.2 to very high 94.1 %, was gained for materials of zone A. In plasticity chart, zone A material was classified as high plasticity to extremely high plasticity clay. In contrast, liquid limit values obtained in zone C were markedly narrower 71.1 to 87.8 %. Range of liquid limits determined in zone C correlates with very high plasticity. Liquid limit values for soft clay of zone B, ranged from 68.4 to 88.8 % indicating material of high to very high plasticity. However, in silty clay, being dominant material of this zone, liquid limits were exceptionally low 46.1 to 63.7 %, thus classifying zone B materials as inorganic clays of intermediate plasticity to inorganic silts of high compressibility.

Liquidity index and consistency index

In order to relate natural water content of Perniö soft clay materials with Atterberg limits, liquidity indexes have been calculated [Skempton 1953]. Despite the wide range in initial water content, liquidity index I_L [Terzaghi 1936] obtained for materials of a certain deposit and corresponding to different depositional conditions and post depositional processes, fall within a relatively narrow band of values. Soft clays have liquidity index near to unity, whereas stiff clays may have values near to zero. In quick clays however, liquidity index is greater than 1.0 [Lancellotta 1995].

Depth distribution of liquidity indexes of Perniö soft clay is presented in Figure 5.18 c). Perniö soft clay materials regularly displayed liquidity index above 1.0. In fact, results obtained within each stratigraphic unit occurred within relatively narrow range with average values of 1.26, 1.82 and 1.55 for materials of zone A, B and C, respectively. Since the sum of liquidity index and consistency index equals unity, Perniö soft clay displayed negative values of I_C, indicative of very low consistency materials with natural water content above liquid limit [ISO 14688-2:2004]. Furthermore, average consistency indexes in zone A, B and C of -0.26,-0.82 and -0.55, respectively, indicated zone B to be the stiffest and zone A the softest among Perniö soft clay materials. It is worth of noting that in specimen preparation soft clay of zone C was identified as highly brittle material, failing along very clear planes.

Liquidity index is used as simple mean for evaluation of soil sensitivity, since liquidity index values are shown to increase with increasing sensitivity at a given effective pressure [Skempton 1953, Bjerrum 1954, Lefebvre et al. 1988]. From the Figure 5.18 c), it is clear that distribution of liquidity index with depth resembled that of sensitivity values obtained using fall cone test, i.e. liquidity indexes of zone B were the highest. It is acknowledged that the highest values of liquidity indexes in all three stratigraphic units of Perniö soft clay were those obtained on material sampled with NGI 86 mm sampler, while the lowest values were those obtained on material sampled with STII 50 mm.

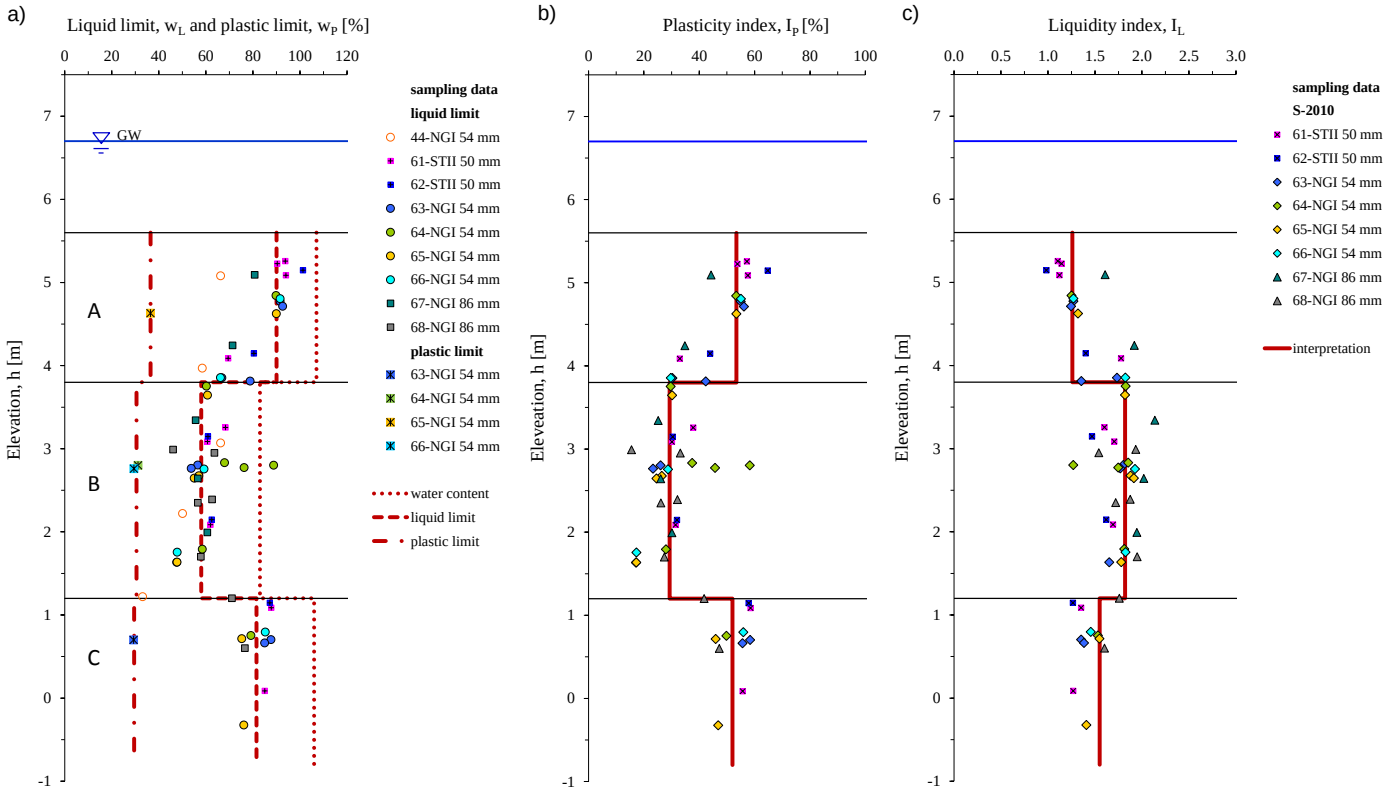

Figure 5.18 Atterberg limits of Perniö soft clay, a) liquid limit and plastic limit, b) plasticity index, and c) liquidity index.

Bjerrum [1954] and Kenney [1976] related liquidity index to logarithm of sensitivity. In addition to comprising Bjerrum's [1954] general classification of clays according to their sensitivity, Figure 5.19 compares data obtained on Perniö clay to that of Norwegian marine clays and Canadian varved clays. Correlation defined by Bjerrum [1954] is based on average liquidity indexes at certain sensitivity level obtained on large number of samples. Perniö results from sublayers A and B complied well with correlation reported by Bjerrum [1954], while data obtained on material C were characterised by lower liquidity indexes. Thus, at certain sensitivity level sublayer C data showed lower liquidity indexes, compared to those obtained on material from sublayer B. However, sublayer C results complied well with range obtained for Norwegian marine clays as reported by Kenney [1976].

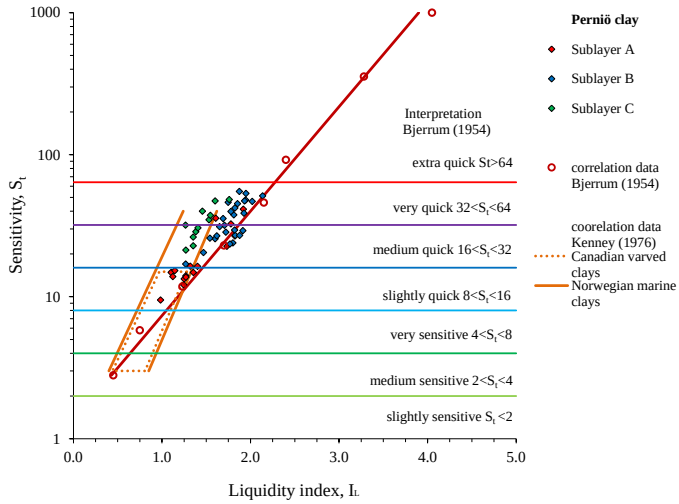

Figure 5.19 Relation of liquidity indexes with logarithm of sensitivity for Perniö clay, Norwegian marine clays and Canadian varved clays [data from Bjerrum, 1954, and Kenney 1976].

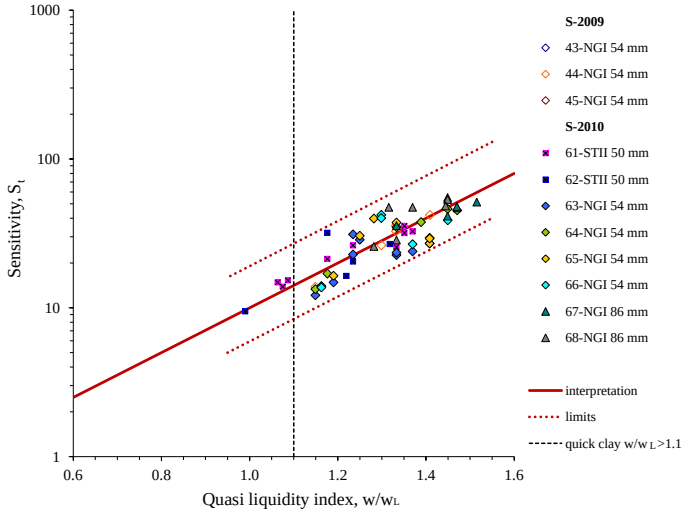

Figure 5.20 Quasi liquidity indexes of Perniö soft clay related to logarithm of sensitivity.

Swedish practice correlates sensitivity with quasi liquidity index defined as ratio of natural water content of undisturbed material over that at liquid limit [Osterman 1964]. As shown on Figure 5.20, when related to logarithm of sensitivity, quasi liquidity indexes occurred within narrow range for all Perniö clay materials, making this approach suitable for fast sensitivity evaluation. Furthermore, experience has shown quick clays being characterised by water content and liquid limit ratio higher than 1.15 [Rankka et al. 2004]. All zones of Perniö soft clay satisfied this criteria being in average 1.18, 1.43 and 1.30, in zone A, B and C, respectively.

Skempton and Northey [1952], Mitchell [1976], Wroth & Wood [1978], and Locat & Demers [1988] showed undrained remoulded shear strength correlating well with liquidity index. Results obtained on Perniö clay, placed undrained remoulded shear strength and liquidity index in limits set by Mitchell [1976], evaluating large variety of clays. As shown on Figure 5.21, data obtained on Perniö soft clay complied very well with Equation 5.2 formulated by Locat & Demers [1988] on the basis of data obtained on Canadian clays.

$$c_{ur} = \left(\frac{19.8}{L_I} \right)^{2.44} \tag{5.2}$$

It is worth of noting that Wroth & Wood [1978] showed relation between liquidity index and undrained remoulded shear strength being a projection of the critical state.

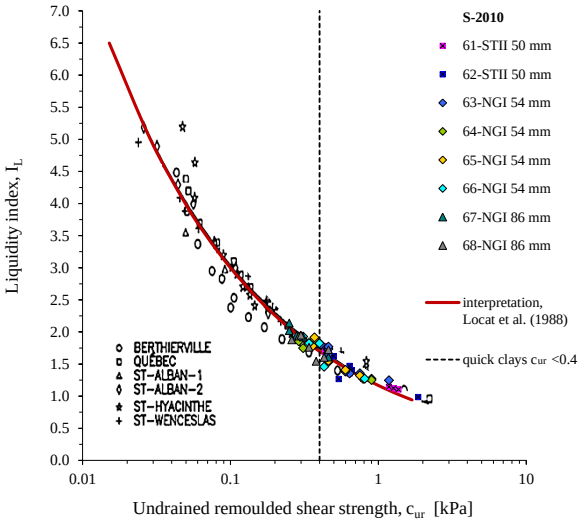

Figure 5.21 Correlation of undrained remoulded shear strength and liquidity index for Perniö and some Canadian clays [data modified after Locat & Demers, 1988].

Colloidal activity and viscosity

The higher the plasticity indexes, more pronounced are the colloidal properties of clay [Skempton 1953]. Moreover, the colloidal properties are contributed largely by the finest particles, i.e. clay fraction [Skempton 1953]. In order to examine colloidal properties of Perniö clay, colloidal activity determined as

ratio of plasticity index over clay content was evaluated [Skempton 1953]. Values obtained for soft clays in zone A, B and C amounted 0.95, 0.99 and 0.69, respectively. In silty clays of zone B, activity decreased up to 0.51. The values obtained classified soft clay material of zone A and B to normal clays with activities between 0.75 and 1.25, typical for marine clays with Illite as the predominant mineral [Skempton 1953, Bjerrum 1954]. Furthermore, activity of less than 0.75 in zone C and silty clay of zone B, identified inactive group typical for post glacial marine clays deposited in salty waters, which have subsequently been leached by percolation of fresh water following the isostatic uplift [Skempton 1953]. In addition to inactive minerals such as quartz and feldspar, Scandinavian clays contain appreciable amount of Illite. Activity of pure Illite is 0.90, i.e. considerably higher than of the other minerals [Skempton 1953]. Consequently, content of Illite mainly controls the plasticity of clay, i.e. clays with the highest activity typically show the highest Illite content [Bjerrum 1954]. For comparison, range of Perniö clay activity values was broader than that of Norwegian marine clays, typically occurring between 0.15 and 0.64 [Bjerrum 1954].

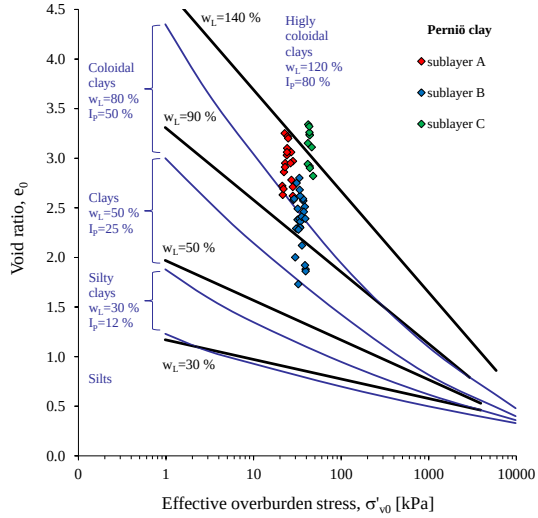

Figure 5.22 Estimation of Perniö clay compositional effects on void ratio-overburden effective stress relation [modified after Lambe & Whitman 1969].

Void ratio of a normally consolidated clay, at a given overburden pressure, depends upon the nature and the amount of clay minerals present [Skempton 1967], but also on the structural arrangement of the particles. Figure 5.22 adapted from Lambe & Whitman [1969] presents an attempt to relate initial void ratio and liquid limit of clays to soil composition. Approximate boundaries between clays of low, medium and high plasticity are represented by liquid limits of 30, 50, 90 and 140 % [Skempton 1967]. Furthermore, Figure 5.22 illustrates the change in virgin compressibility in e-log σ'_{vo} plane and increase in compressibility with plasticity index [Hight et al. 1987]. At higher stresses convergence to a single void ratio occurs. Initial void ratio of Perniö clay mate-

rials at corresponding effective overburden stress, confirmed existence of three distinctive units. Material of zone B mostly predominated area of colloidal clays, while that of zones A and C, characterised with the highest initial void ratio values, occurred within the area of highly colloidal clays.

Correlating liquidity index with rheometer measured viscosity, Locat & Demers [1988] gave Equation 5.3 suitable for estimation of the viscosity of a soil with values of liquid index between 1.5 and 6.

$$\nu = \left(\frac{9.27}{I_L} \right)^{3.33} \tag{5.3}$$

The equation has been used to estimate and compare viscosity of stratigraphic units of Perniö soft clay (see Figure 5.23). Based on values of average liquidity index, viscosity in zone A, B and C amounted 769, 226 and 386 mPas. It is important to emphasise that above derived values are estimates since for entire range of liquidity indexes, limits of viscosity were in limits 189 to 1750, 132 to 752 and 253 to 756 mPas in zones A, B and C, respectively. Nevertheless, it is possible to conclude that zone A was characterised with the highest viscosity, followed by zone C, and finally by that of zone B material.

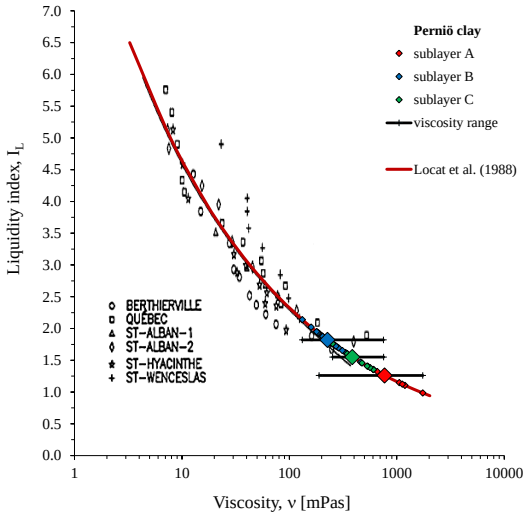

Figure 5.23 Estimation of Perniö clay viscosity on the basis of data for some Canadian clays [modified after Locat & Demers, 1988].

5.1.7 Stratigraphic conditions and sampling disturbance

Results obtained during, and immediately following the sampling of Perniö clay are used to firstly, discuss conditions of Perniö deposit with respect to depositional and post depositional processes, identify existence of distinctive stratigraphic units and allow definition and analyses of characteristic parameters for each stratum, and secondly; to discuss effects of sampler performance, influence of sampling quality on material properties and provide recommendations for sampler selection/use and selection of material for testing.

Stratigraphic conditions

In following, processes leading to formation of Perniö soft clay deposit are discussed. Main advantage is given to analysis of the factors determining mechanical properties of soft clays being: composition, fabric, stress-time history and chemical history [Hight et al. 1987].

Concentration of salt in the pore water varies from clay to clay depending on original salt content and the degree of leaching to which the clay has been subjected since sedimentation [Bjerrum 1954, 1967]. Analysis of the Perniö deposit sampling results suggest entire zone of soft clay material, i.e. underneath of +5.6 m absolute, being subjected to leaching process. However, extent of leaching differed mainly due to variation in geological conditions, i.e. variation in permeability and groundwater chemistry. The rate of leaching process depends on the hydraulic gradient and hydraulic conductivity characteristics of certain deposit [Torrance 1979]. Presence of permeable layers, such as sand and silt layers that enable connection to the surface water or other low salinity water conducting layers greatly enhances the possibility and rate of leaching [Rankka et al. 2004]. As in the case of Perniö deposit, there is often a permeable layer above, below or embedded in the layer of quick clay [Talme 1968]. Consequently, quick clay is found more often in clay deposits with moderate thickness and less frequently in thick deposits, where it only occurs close to permeable layers [Rankka et al. 2004]. Furthermore, outcome of the increase in electro-kinetic potential and subsequent reactions leading to emergence of sensitive clays depends upon chemistry of the groundwater. Leaching with soft groundwater results with highly sensitive quick clay, while clays leached with hard water are typically of low sensitivity [Brand & Brenner 1981].

In the case of Perniö clay deposit, leaching is caused by rain and snow water percolating the upper layers and frequent silty inclusions saturated with pore water low in salinity. As a result of different degrees of groundwater flow to which various sections of the deposit were subjected, Perniö clay sediments of similar mineralogy, grain size distribution and depositional history, today show different geotechnical properties [Bjerrum 1954]. If geotechnical properties of Perniö clay stratigraphic units are examined in the perspective of leaching effects, various degrees of leaching are clearly acknowledged. Compared to those in zone A, plastic limit values of zone B and C were lower (see Figure 5.18). Furthermore, the lowest liquid limit values occurred within zone B, followed by zone C, and finally, zone A. Consequently, plasticity index of zone B was considerably less than those of materials embedding it. Variation in clay plasticity was in accordance with the magnitudes of colloidal activity, being the highest in zone B, followed by zone C, and lastly by that of zone A. It is important to notice that within zone B only, activity of clay minerals decreased from rather high 0.99 to 0.51. Same relative order of magnitudes to those of activity can be noted by examining values of liquidity indexes and sensitivity values within distinctive sublayers (see Figure 5.18 and Figure 5.15). Lastly, depth distribution of liquidity index and sensitivity was confirmed by magnitudes of undrained remoulded shear strength, following the pattern of zone B,

C and A, from the lowest to highest. To conclude, within zone B, containing permeable inclusions, leaching process is the most advanced, and is followed by zone C, especially in its upper portion influenced by zone B permeability. Finally, zone A, satisfies some of the categorization criteria for quick clays, such as by sensitivity and liquidity values as defined by Bjerrum [1954] and magnitude of w/w_L ratio according to Swedish practice [see Rankka et al. 2004], however lacking the permeable zones and being close to surface, leaching in this sublayer is in its initial stages. Accordingly, quick clays in zone B and C are expected to have considerably lower total amount of ions compared to that of low sensitivity sublayer A [Rankka et al. 2004].

Section of Perniö deposit above +5.6 subjected to effects of drying and weathering has changed the upper layers to stiff crust. Indeed, dry crust and stiff clay (weathered clay) material, subjected to negative pore water pressures above water table and water table fluctuations (drying and wetting), are formed under influence of desiccation (evaporation, transpiration and infiltration), and weathering processes (reduction and oxidation) [Bjerrum 1954]. In contrast to leaching, weathering increases ions bounded to the clay minerals and therefore counteracts the leaching process [Hight et al. 1987]. Consequently, quick clay is newer found in or directly beneath weathered dry crust [Rankka et al. 2004]. As in the case of Perniö clay deposit, such materials typically behave as dense, highly overconsolidated materials with increased shear strength, and are typically characterised by reduced water content, increased plasticity index and reduced liquidity index [Hight et al. 1987].

Although the generally acknowledged effects associated with leaching comply with those measured in Perniö soft clay, distribution of initial water content/void ratio demands additional attention. Namely, sampling results of Perniö clay deposit indicate increased water content in materials embedding zone B (see Figure 5.11). Considering the fact that sublayer B was characterised with the highest sensitivity and highest extent of leaching (see Figure 5.15), reasons for reduced level of water content remain unclear. Supported by in situ experiences, it is expected that the water content during leaching remains unchanged [Bjerrum 1954]. Furthermore, laboratory experiments of leaching identified effects of; decrease of liquid limit and reduction of the shear strength of the remoulded clay, yet also that of water content values remaining almost unaltered [Bjerrum 1954]. There are three possible explanations for variation in the initial water content/void ratio within Perniö soft clay deposit.

Firstly, one may argue that materials of zone A and C, although saturated, continued to absorb water from more permeable zone B, leading to an increase of the volume of the soil mass and distinctively higher water content. Assumption of this mechanism would imply clay of sublayers A and C, and occasionally clayey layers within zone B being progressively softened by the water which increases the distance between the clay minerals leading to emergence of the colloidal properties (see Figure 5.22). However, beside the fact that material of zone A and zone B are similar in terms of particle size distribution, mineral composition of Perniö clay is dominated by non-swelling clay minerals, making the effects of mechanism suggested, negligible.

Secondly, possible mechanism leading to variation in the water content/void ratio results might be related to influence of sampling. Namely, in fine-grained materials and especially in those with considerable permeability (clayey silt, clayey sand), loss of water and consequent decrease of initial void ratio values might have occurred as a result of sampling disturbance, i.e. stress release, mechanical disturbance and drying (see Chapter 2.1 and 5.1). In favour of this mechanism goes the fact that the highest water content and void ratio values measured in sublayer B, corresponded to those in sublayers embedding it (see Figure 5.11). This mechanism, related to conclusions on sampler performances and its effects on sampled material properties is elaborated in detail in the following section.

Thirdly, variation in water content/void ratio values might be related to differences in depositional conditions. To explain higher water content in zone A and C compared to that in sublayer B, depositional and post depositional chemical history of the Perniö soft clay deposit needs to be discussed.

In accordance with geological evolution of the Baltic Sea, four types of fine-grained sediments occurring in Finish geological conditions are, from the oldest to the youngest, Baltic Ice Lake, Yoldia, Ancylus, and Littorina sediment [Gardemeister 1975]. Although, geological dating tests have not been made within the present study, correlation parameters such as clay content, organic content and water content, varying clearly in different types of sediment, direct to the conclusion of; sublayer C corresponding to that of Yoldia sediment; sublayer B corresponding to Ancylus sediment and finally; sublayer A corresponding to that of Littorina sediment. Furthermore, limited amount of data available on reddish, sandy sediment occurring above the bedrock indicates Baltic Ice Lake sediment. Following information suggests the sediment correlation with Perniö clay stratigraphic units; Yoldia and Littorina sediments are deposited in relatively high salinity marine environment of Yodial sea and Littorina sea, resulting with formation of rather homogenous and rather high void ratio structure. Furthermore, owing to the land uplift, in the intermediate of those two evolutionary stages, connection of the Yoldia sea with the ocean was broken, leading to formation of Ancylus lake, characterised as brackish, relatively low salinity depositional environment [Gardemeister 1975]. Thus, the lower water content in Ancylus sediment of sublayer B might be a result of higher electro-kinetic potential during deposition, leading to formation of relatively lower initial void ratio structure, compared to that formed during sedimentation of sublayers A and C. Furthermore, the maximum salinity typically occurs in Littorina sediment, and at present appear to be approximately one half of the original salinity, due to among others, diffusion and leaching processes [Gardemeister 1975]. In other types of sediments, salinity is considerably below the level met within Littorina sediment [Gardemeister 1975]. These statements comply with leeching effects established on Perniö deposit materials. Furthermore, organic content of zone A being 4.5 %, corresponds to that typically found in Littorina sediment, i.e. 4 % in average [Gardemeister 1975]. The average organic content in zone B and C is lower, yet above that typically found in Ancylus an Yoldia sediment, i.e. 1 to 1.2 %. However, in these types of

sediment, the classification properties are most significantly correlated with clay content [Gardemeister 1975]. Namely, as in the case of sublayer B, Ancylus sediment typically contains slight micro-varving resulting from variation in salinity of the sedimentary basin, i.e. mixing of fresh and saline waters [Gardemeister 1975]. On the other hand, as in the case of sublayer C of Perniö deposit, Yoldia sediment typically contains clayey materials in the largest amount [Gardemeister 1975]. Finally, sensitivity values corresponding to very and extra quick clays (S_t >32) measured in zone B and C, are typically contained primarily in Ancylus and Yoldia sediments [Gardemeister 1975]. Significant correlations in water content, organic content, clay content and sensitivity, justify categorization of distinctive units of Perniö soft clay deposit with types of fine grained sediment occurring in coastal areas of south-western Finland. However, it is important to note that initial water content and void ratio correlation parameters defined by Gardemeister [1975] were based on evaluation of material sampled with STII and neglected effects of sampling disturbance.

Influence of sampling disturbance on material properties

Sensitive soil can be thought as one which has water content that is too high to be good for it [Wood 1983]. The surplus of in situ void ratio to that of disturbed or remoulded sample is an indication of the amount of water that is released when the structure of the sample is disturbed and the soil tries to reach equilibrium under the new level of effective stress [Wood 1983]. Reduction in the water content during sampling, being a common manifestation of disturbance, is primarily dependent upon material type and sampling method implemented. Permeable soils such as that of silty clays within sublayer B, may be subject to appreciable volume changes during sampling [Hvorslev 1949]. However, in fully saturated soils of low permeability such as clays of sublayer A and C, significant volume changes during the sampling are unlikely to occur. Extent of volume change is in addition highly influenced by sampling per se. Poor sampling technique or poor sampling performance might lead to significant volume changes of the material sampled [Hvorslev 1949].

As the first estimate of sampling quality, Perniö clay samples were visually examined. STII samples were characterised by often and considerable fractures along sample periphery. In contrast to those gained by other two methods, samples obtained with STII indicated the material being subjected to considerable compression in sampling. In contrast, material obtained using both NGI samplers was generally of lower consistency compared to that obtained with STII. Among samples obtained with NGI samplers, main problems were related to poor condition of sampling cylinders, namely; gap between the sample and the cylinder caused by cylinders being out of centricity, and fractures along sample periphery caused by poor condition of the cutting edge. Furthermore, visual evaluation revealed ~10 mm thick zone of disturbed material along the cross-section periphery of the samples. Thus, the main advantage of NGI 86 mm sampler compared to that of 54 mm was larger diameter of the samples obtained, ensuring larger diameter of the undisturbed core. High quality samples were very brittle and failed along clear surfaces while those

disturbed were characterised by high plasticity. Furthermore, high quality samples exhibited small bubbles along the surface of freshly cut sample, resulting from considerable pore pressure release (Figure 5.6 d).

The effects discussed above were manifested in initial water content values measured. In zone A and C, the lowest water content values were regularly obtained on material sampled with STII. In zone B containing silty clays, the sampling performance evaluation in terms of initial water content was difficult. All three sampling methods yielded considerable scatter and relatively low resulting values. Nonetheless, samples obtained with NGI samplers occasionally exhibited exceptionally high initial water content values indicating specimens of relatively higher quality (see Figure 5.11). Furthermore, the main advantage of preserving high initial water content in NGI 86 mm sampling was manifested by the lowest values of undrained remoulded shear strength (see Figure 5.15). Indeed, the lowest remoulded shear strength was found in clays with the highest sensitivity. In contrast, undrained shear strength values obtained on both undisturbed and remoulded STII samples, were the highest, resulting from considerable densification and reduction of initial water content. In terms of initial state parameters and undrained shear strength, manifestations of poor sampling complied, although to a lesser extent, with the effects caused by the additional load of the embankment, i.e. decrease in water content, increase in unit weight, and increase in undrained shear strength.

Quantitatively, sampling quality of Perniö soft clay material has been examined on the basis of two independent approaches. First being that of sensitivity measurements using a fall cone test, and second, that of evaluation of liquidity index (see Figure 5.15 c and Figure 5.18 c). Both approaches identified samples obtained with NGI 86 mm being superior to those obtained with NGI 54 mm and STII. Sampling difficulties were quantitatively the most clearly exposed in clays of zone B with a high sensitivity and low activity. Although less indicative, in zone C characterised with high clay content, performance of samplers with respect to sensitivity, liquidity index and initial water content values obtained was consistent. Since sensitivity values determined with fall cone test are highly dependent upon sampling quality, sensitivity measurements on samples obtained with poor sampling method such as STII were highly misleading. With sensitivity of the specimens being proportionally related to amount of water they contain, reduced water content values in sublayer B suggest effects of sampling disturbance (see Figure 5.11). Thus, within sublayer B performance of all sampling methods used regularly led to significant sampling disturbance manifested by reduction in initial water content. Considering its present condition, as well as importance of sampling on resulting properties, improvement of sampling equipment is a work of major importance.

5.2 Specimen preparation results

Almost equally significant source of disturbance as sampling is the process of retrieval and mounting of the samples into testing devices, and the expertise of the personnel in charge of the specimen preparation. Procedures used in prep-

aration of sensitive natural clay specimens very susceptible to disturbance are of crucial importance. Specimen preparation from high sensitivity samples characterised by high brittleness is far more challenging compared to that from severely disturbed soft clay materials. Preparation of the reconstituted specimens demands care as well, particularly concerning the monitoring of sample characteristics during consolidation. For these reasons preparation of the specimens was given special attention in this study.

5.2.1 Natural samples

Common problem in oedometer specimen preparation are fractures and cavities of the material within the ring. The cavities produce serious error on oedometer results obtained, since the compressibility measured to some extent results from filling the cracks within the specimen.

The most critical part of the oedometer test specimen preparation is pressing of the ring and removal of the excess material on rings side. Oedometer ring properties, in terms of the cutting edge angle and wall thickness, differ depending upon the apparatus used. Thickness of ring walls used in IL and CRS oedometer tests of this study were 1.3 and 1.5 mm, respectively. Consequently, area ratio of the 50 mm diameter ring for IL oedometer tests was more favourable than that used in CRS testing. The difference had a profound influence on cutting of the samples into the ring, with specimens prepared with thicker CRS rings often being deteriorated by cavities. The best practice of soft clay oedometer specimen preparation is that of an undisturbed material being vertically pushed directly from the sampling cylinder into the oedometer ring [Sandbaekken et al. 1986]. At Aalto University however, sample was first extruded from the cylinder and later mounted into the oedometer ring, leading to unnecessary unsupported handling of the sample. Crucial factors influencing sample disturbance are fixation of oedometer ring in horizontal plane and the rate of sample filling [Sandbaekken et al. 1986]. In mounting of the sample, movement of the ring is maintained in the horizontal plane by means of guiding rods, while ring penetration of ~5 mm/min ensures minimum displacement of the specimen. Cavities most often occurred during mounting of high sensitivity samples obtained by large diameter 86 mm sampler. Since the samples were very brittle, it was necessary to implement pre-trimming to reduce amount and strength of the material trimmed off by the oedometer ring. Indeed, 86 mm samples had to be trimmed to 55 mm diameter, prior being mounted into 50 mm ring [Sandbaekken et al. 1986]. If sample diameter was not adjusted, fractures during oedometer ring mounting occurred regularly.

Important issue is adequate removal of the excess material above and underneath the ring. If the process is not skilfully done, very brittle soft sensitive clay samples often fail, resulting with fractures next to ring walls or surfaces cut being out of plane. Based on the experience in preparation of natural specimens of Perniö clay using 0.4 mm wire saw, it was impossible to shape high sensitivity specimen within an oedometer ring without occurrence of brittle failures. The problems in the oedometer specimen preparation were significantly reduced by replacing 0.4 mm steel wire, with one 0.2 mm in diameter,

according to the recommendation by Andersen et al. [1957], i.e. 0.1-0.2 mm. Using a thinner wire, sample was truly cut, i.e. displacement of the material remained within the desired plane. Since samples of natural sensitive clay are more brittle than those partially disturbed or remoulded, it is on high quality samples where the importance of the wire saw diameter is essential.

Issues related to testing equipment used that might lead to errors in measurement or effects similar to specimen disturbance were related to length of LVDT probe and delay in readouts. Namely, measuring range of LVDT's mostly used in oedometer testing was 10 mm. Settlement exhibited by high quality specimens generally exceeded these limits. Consequently, in order to enable complete measuring range, metal plates needed to be placed underneath the LVDT sensor. This procedure can introduce errors in measurements and complicates the interpretation of the results. Thus, Solartron LVDT DP10S used have to be replaced with LVDT DP20S.

Important aspects of triaxial specimen preparation procedure are extraction and trimming of the sample, and later, transport and placement of the specimen under appropriate conditions within the triaxial cell. The specimens are most easily disturbed during placement to the pedestal and during mounting of the rubber membrane and rubber O rings [Landva 1964].

By current practice, while extruded from the sampling cylinder, samples are manually supported using cradle allowing shear deformations to occur. In order to reduce sample disturbance, usage of fixed cradle should be examined. Trimming of the sample to the correct size with the wire saw subjects the sample to comparatively large vertical forces that cause them to strain vertically and to bend sufficiently to alter their behavior during the subsequent test [Landva 1964]. Extent of thin disturbed zone formed on the plane of the cut is proportional to the diameter of wire saw used. Transport of the specimen to the triaxial device was done using metal cradle. However, better support is provided using plastic wrap placed around the specimens' longitudinal axis, and should be preferably used.

Since essentially done without support, placement of the specimen to the triaxial test device involves several crucial steps during which specimen is easily bent, squeezed and displaced. Poor installation on the triaxial cell pedestal often results with top and bottom of the specimen being out of horizontal plane leading to uneven vertical stress distribution and possibly, bending of the specimen. The disturbance may affect results obtained in the beginning of the test, such as compressibility characteristics at the start of the consolidation. Furthermore, porous stones above and underneath the specimen were connected to the piston cap/pedestal using stiff rubber stripes. Since the connection is not fixed, regularly occurring voids introduced error in measurements. Thus, considerable settlements measured in the first loading increments during anisotropic triaxial consolidation were result of filling of the voids between specimen, porous stone and cap/pedestal rather than being relevant deformation characteristics of the specimen itself. To avoid errors, metal porous stones screwed to the cap and pedestal should be used, while plastic wrap should be used in supporting the specimen during placement.

Implementation of unguided suction cylinder endangers the specimen to disturbing forces while mounting the O rings [Landva 1964]. The suction cylinder used for installation of the rubber membrane and rubber O rings was during installation pushed over the specimen. Thus, unless special care is given it may displace specimen from the optimum position. Indeed, during membrane installation, rather crude rubber O rings were rolled off from suction cylinder onto the pedestal or top cap isolating the specimen within the membrane. Being unguided, suction cylinder can uncontrollably move displacing and bending the specimen. Poor triaxial specimen installation often results with bending of the specimen and consequently, displacement from the optimum position for lowering of the piston rod into the piston cap. In such cases specimen position needs to be readjusted in order to enable piston installation, introducing additional disturbance of the specimen. Implementation of cylinder guiding rods and less stiff rubber O rings in preventing pore water leakage should be examined.

5.2.2 Reconstituted samples

Remoulding results in a clay slurry, characterised by separated particles, and liquid, low viscosity consistence [Rankka et al. 2004]. Following the remoulding of quick clay, refloculation is not possible because of the repulsive forces between the particles. Instead, it is only possible to bring the particles into contact again after considerable reduction in the water content simultaneously resulting with aligned particle structure [Rankka et al. 2004]. Consequently, void ratios of reconstituted samples are considerably lower to that of the corresponding natural material, while structural sensitivity effects are completely erased resulting with substantial reduction in compressibility and strength of the reconstituted material.

Results of remoulding and reconstitution procedures implemented are shown in Table 5.3 and Table 5.4, respectively. Altogether, four reconstitution batches were made, i.e. R1, R2, R3 and R4. In order to keep high quality sensitive samples for evaluation of natural properties, material used for remoulding mostly originated from depth levels of the sublayer A, obtained using STII sampler. The material was cut into pieces and remoulded using standard food mixer. As shown in Table 5.3, the mass of clay material in remoulding, as well as the amount of water added during mixing varied. After mixing for ~10 min, water content was 90.8, 91.8, 84.1 and 97.8 %, for batches 1 to 4, respectively. Following the addition of water and application of additional mixing period for ~20 min, respective water content of homogenous slurry amounted 94.4, 101.0, 92.8 and 109.3 %. Average void ratio of remoulded material for batches R1,…R4, estimated under assumption of specific gravity of 2.7, amounted 2.55, 2.73, 2.51 and 2.95, respectively.

Equipment used in reconstitution consisted of moulding cylinders with filtering system and loading frame with loading rod and piston. Figure 5.24 a) and b) show triaxial and oedometer sample moulds prior reconstitution loading. In order to allow drainage of the sample while at the same time preventing

sample loss, both cylinder types used filtering system composed of filter paper, geotextile and porous stone placed under and above the sample. Besides differing in acrylic cylinder diameter, two types of moulding systems differed in connectivity details as well. Moulding system aiming samples for oedometer tests shown on Figure 5.24 b), including plastic cap on the cylinders bottom, is more robust and should be preferred. To ensure stability of the cylinders and restrict movement of the piston to vertical axis, loading frame shown on Figure 5.24 c) was used. Axial stress of 15 kPa was applied via piston fixed at the bottom of the loading rod by means of dead load, i.e. 3.05 and 5.51 kg for 50.0 and 68.5 mm diameter cylinders, respectively. The diameter of the piston, being ~1 mm less than that of the acrylic cylinders reduced friction between two, while friction between loading rod and metal frame was reduced by oiled plastic guides. Sample settlement, i.e. relative movement of loading rod to the steel frame, was measured daily using Vernier caliper.

Figure 5.24 Reconstitution; a) ∅50.0 mm moulding cylinders, b) ∅68.5 mm moulding cylinders, c) loading frame.

Table 5.3 Remoulding parameters.

Batch no.	Total mass m [kg]	Water content w [%]	Water added [ml]	Remoulded water content w_r [%]	Remoulded void ratio e_r	Remoulded unit weight γ_r [g/cm3]
R1	2.5	90.8	41	94.4	2.55	7.46
R2	2.3	91.8	150	101.0	2.73	7.11
R3	2.3	84.1	134	92.8	2.51	7.55
R4	3.7	97.8	200	109.3	2.95	6.70

Figure 5.25 shows time-settlement curves of the remoulded material in 50.0 and 68.5 mm diameter cylinders. Total settlement measured varied considerably from 27.1 to 36.0 mm, mainly reflecting variation in the initial sample

height and initial water content. Additional reason for variation in total settlement might have been related to variance in friction between the piston and acrylic cylinder of different moulds. Altogether, following the 40 days of reconstitution period, no significant settlement occurred.

In order to correlate settlements measured with change in water content during reconstitution, void ratio values are plotted against time on Figure 5.26. With time, void ratio progressively declined and following 40 days period converged toward target value well represented by average void ratio of material of the certain reconstitution batch. The average void ratio values after reconstitution on oedometer and triaxial test specimens reconstituted in batches R1,...R4 amounted 1.79, 2.03, 1.81 and 2.03, respectively.

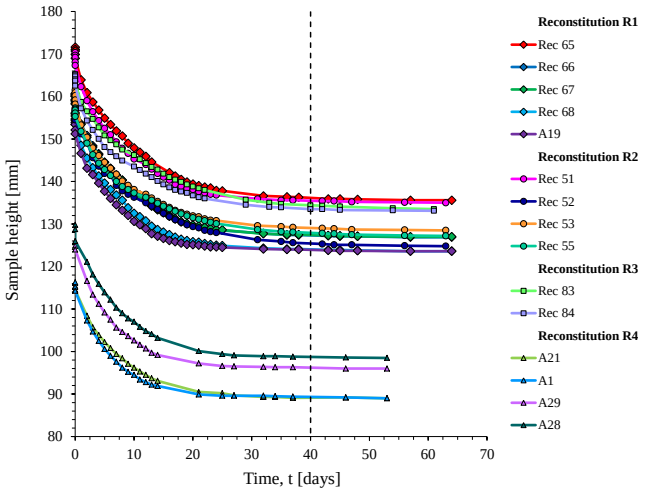

Figure 5.25 Change in sample height during reconstitution of Perniö clay.

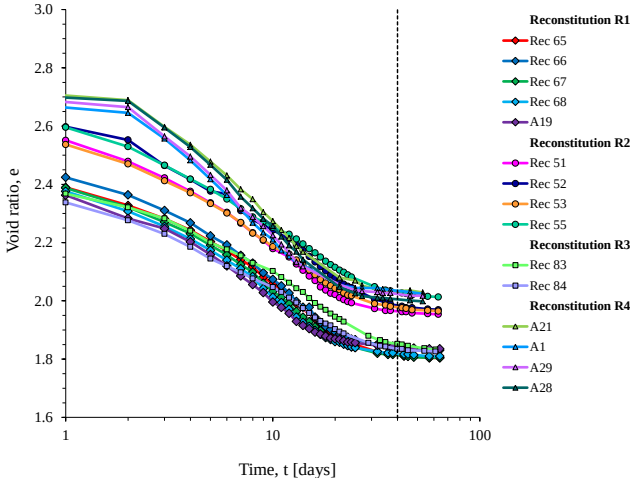

Figure 5.26 Time vs. void ratio curves in reconstitution of Perniö clay.

Since the initial height of the sample prior to consolidation was not measured, initial height values shown in Table 5.4, had to be evaluated by adding the total consolidation settlements to that of sample height following reconstitution. In order to allow estimation of friction between the piston and cylinder, as well as to quantify sample disturbance in preparation of reconstituted specimens, initial height of the material in certain cylinder prior reconstitution needs to be accurately measured. Initial sample height should be defined by known volume of the material being poured into the moulding cylinders using beaker.

Table 5.4 Reconstitution parameters.

Batch	Sample No.	Initial mass m_i [g]	Initial volume V_i [ml]	Initial height Hi [mm]	Total settlement ΔH [mm]	Final height H_f [mm]	Final water content w_f [%]	Final void ratio e_f	Water content prior testing w_0 [%]	Void ratio prior testing e_0
R1	Rec 65	523.8	336.8	171.6	36.0	135.6	66.8	1.80	67.9	1.80
	Rec 66	503.4	312.2	159.1	34.1	125.0	67.8	1.83	68.0	1.81
	Rec67	493.2	315.4	160.7	33.7	127.0	66.8	1.80	67.3	1.78
	Rec68	487.4	306.3	156.1	32.5	123.6	67.0	1.81	66.5	1.75
	A19	453.6	303.6	154.7	30.5	124.2	67.0	1.81	67.1	1.79
R2	Rec 51	461.8	334.2	170.3	35.3	135.0	72.4	1.95	72.4	2.00
	Rec 52	446.5	307.3	156.6	31.8	124.8	72.9	1.97	76.6	2.12
	Rec 53	438.4	316.9	161.5	33.5	128.0	72.3	1.95	59.8	1.81
	Rec 54	453.8	308.3	157.1	29.9	127.2	74.7	2.02	78.4	2.16
	Rec 55	465.0	308.7	157.3	31.7	125.6	73.2	1.98	75.2	2.07
R3	Rec 83	476.6	324.2	165.2	33.8	131.4	66.2	1.79	62.9	1.81
	Rec 84	482.5	324.0	165.1	33.2	131.9	66.7	1.80	68.6	1.81
R4	A28	730.9	478.1	129.8	31.3	98.5	74.0	2.00	76.1	2.00
	A29	649.7	463.0	125.7	29.7	96.0	74.7	2.02	75.1	2.02
	A1	725.3	428.4	116.3	27.3	89.0	74.9	2.02	75.6	2.02
	A21	720.4	427.6	116.1	27.1	89.0	75.1	2.03	76.7	2.06

An example of well-prepared reconstituted sample is shown on Figure 5.27. Following the reconstitution, i.e. during sample extraction, it was noticed that material in the upper portion of the cylinder was stiffer than that located at the bottom. Three reconstituted oedometer test specimens typically obtained from 68.5 mm diameter moulds, allowed comparison of the specimen consistency along the cylinder height. As shown in Figure 5.28, specimens located at the top generally exhibited lower void ratio compared to that of specimens originating from the bottom of the cylinder. Change in the consistency along the sample height was an effect related to the load application and relative distance of the drainage boundary. Material in the middle of the cylinder had longest drainage path. Furthermore, due to the concentrated action underneath of the piston, compared to that nearby the fixed pedestal, material at the top of the sample was subjected to relatively higher loads than that occurring at the sample base, and was more rapidly densified.

To conclude, if the reconstitution process is initiated on material remoulded in a single batch, results obtained are expected to be more comparable. In addition to accurate measurements of total settlement, it is essential to accurately determine initial volume of the remoulded material in moulding cylinders.

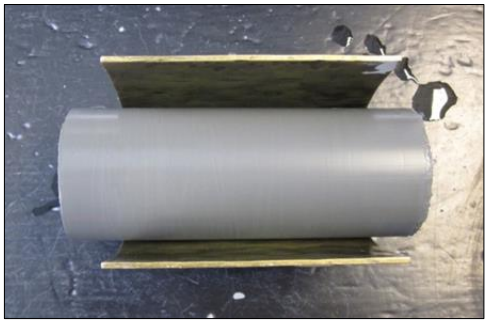

Figure 5.27 Reconstituted triaxial sample of Perniö clay.

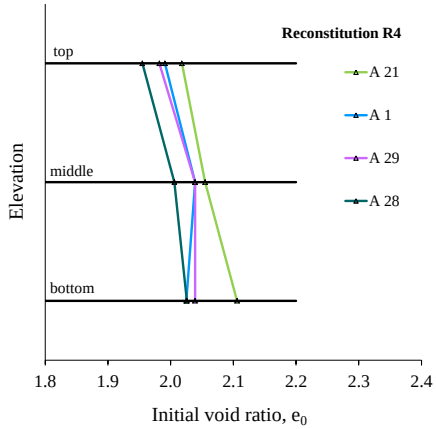

Figure 5.28 Initial void ratio values along moulding cylinder height.

Priority should be given to transparent cylinders, using connection system shown on Figure 5.24 b), being more robust and allowing better control of the consolidation process. Adequate attention should be given so to ensure accurate and identical external load conditions with rod and piston weight included. Following the 40 days of consolidation, samples are expected to be of suitable consistency for prepration of specimens for both oedometer and triaxial testing. In addition to compression and shearing behavior, reconstitution results should be examined by evaluation of Atterberg limits and viscosity of the soil produced.

6. Oedometer testing

6.1 IL oedometer test results

6.1.1 General overview

Compressibility response for the entire set of IL 24h oedometer tests on natural and reconstituted specimens of Perniö clay are shown in Figure 6.1. The results are firstly briefly outlined, and latter specific features are examined in detail, i.e. sample quality, compressibility, bonding, creep and strain-rate influence.

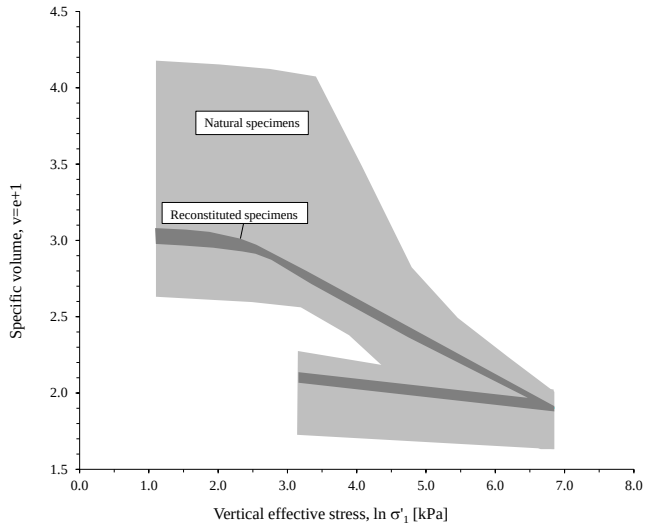

Figure 6.1 Compressibility of Perniö clay in incrementally loaded oedometer tests.

ILOT results on reconstituted specimens

Oedometer tests results on reconstituted specimens were rather uniform. Being obtained in a single batch R4, moulding cylinders A21, A1 and A29, initial void ratio values were similar, i.e. 2.03 in average (see Figure 5.28). Stiffness characteristics were very uniform, with an average slopes prior and following yield being κ_o=0.057 and λ_R=0.259, respectively. Compared to natural specimens, response of reconstituted material in normal compression was considerably stiffer, representing lower bound of Perniö clay compressibility overall. Swelling response with an average unloading slope κ=0.054 complied with

that in reloading. Preconsolidation pressures varied narrowly from 13.5 to 15.0 kPa, corresponding well to load level in reconstitution. Variations in σ'_p were probably related to differences in unknown friction between piston and acrylic cylinder, resulting with different samples of the same clay having slightly different stress histories at the start of test [Karstunen & Koskinen 2008a].

ILOT results on natural specimens

Oedometer test results on natural specimens were characterised with high variation in compression response. Scatter reflected natural variance of Perniö deposit and large variation in quality of the specimens evaluated. The tests were performed on material obtained with NGI 54 mm sampler on profiles 63, 64, 65 and 66, as well as on that using NGI 86 mm sampler on profiles 67 and 68. Initial void ratio values varied greatly from 3.18 to 1.64, with later value being less than that measured on reconstituted specimens. Slope in reloading κ_o varied from 0.011 to 0.079, while maximum slope in NC stress range λ, occurred between 0.249 and 1.122. Some results on natural specimens characterised by low λ, corresponded with those obtained on reconstituted specimens, indicating complete destructuration at the onset of test. The majority of compression curves however, exhibited high λ values, which following the stress increase asymptotically converged toward values representing compressibility

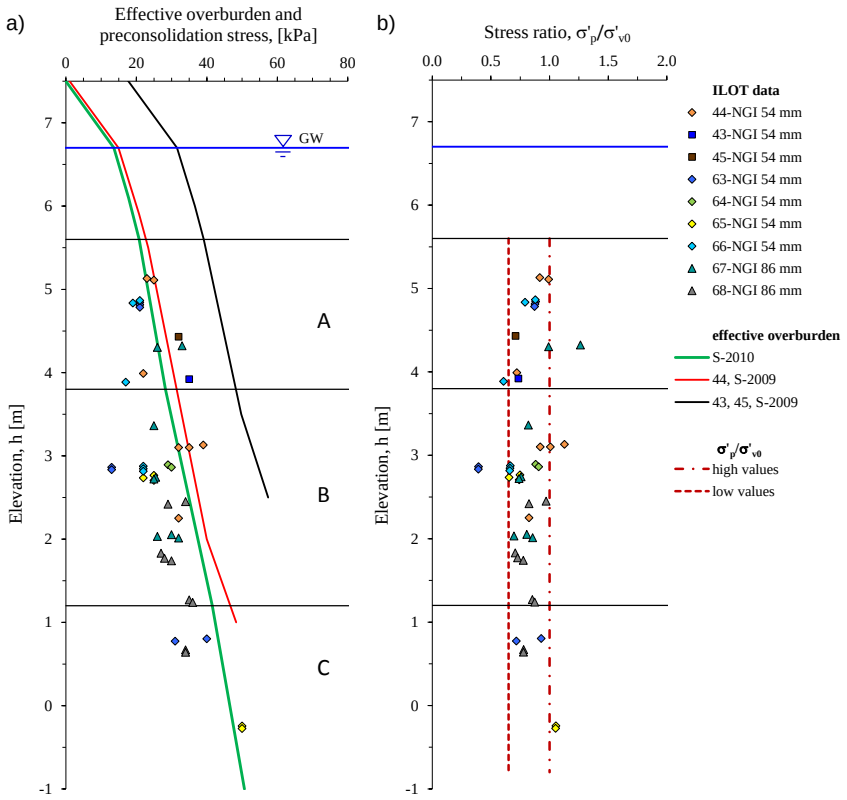

Figure 6.2 Overburden stress distribution and preconsolidation pressures in IL oedometer tests.

of reconstituted specimens. Parameters obtained after considerable straining were less, yet still considerably scattered, i.e. intrinsic compression slope λ_i, occurred between 0.188 and 0.371, while swelling slopes κ, varied from 0.028 to 0.079.

Figure 6.2 shows preconsolidation pressures obtained in IL oedometer tests on natural specimens as a function of depth. The results were characterised with considerable scatter at an arbitrary elevation. Due to variation in the specimen properties and test conditions, e.g. variations in the sampling depth and location, sampling disturbance, strain-rate, and loading pattern, some scatter at yield was expected [Koskinen et al. 2003]. However, variation in σ'_p values on natural specimens of Perniö clay was considerably high, i.e. $0.61<\sigma'_p/\sigma'_{vo}<1.05$. Indeed, only limited amount of σ'_p values corresponded to vertical effective stress in situ. Since the locational characteristics and test conditions were similar, the effect was indicative of considerable extent of sample disturbance. Clearly, no concise conclusions on Perniö clay compression behavior can be made prior to detailed evaluation of the results with respect to effects of structure and specimen quality.

6.1.2 Initial state parameters

Water content

Water content values determined on IL oedometer specimens are shown in Figure 6.3 a). Based on S-2010, average water content of IL oedometer specimens was 108.7, 89.0, and 103.2 % in respective soft clay sublayers. Thus, average w_o representing IL oedometer specimens resembled the results following the sampling. Within soft clay sublayers however, scatter of values was very significant. Water content distribution with depth was markedly different if the highest values were considered, i.e. 110, 119 and 106 % in respective sublayers A, B and C. In contrast, S-2009 IL oedometer specimens exhibited the lowest w_o.

Initial void ratio

Figure 6.3 b) relates e_o values of IL oedometer specimens with depth. Based on S-2010, IL oedometer specimens were represented by average values of initial void ratio of 2.9, 2.4 and 2.8 in sublayers A, B and C. Considering the highest values, e_o in respective soft clay sublayers amounted 3.0, 3.2 and 3.1, thus identifying the highest e_o in sublayer B. Results obtained on IL oedometer specimens sampled in 2009 were significantly less.

Unit weight

Unit weight values representing IL oedometer specimens are shown in Figure 6.3 c). Average γ values of S-2010 IL oedometer specimens amounted 14.1, 15.0, and 14.4 kN/m^3, in respective soft clay sublayers. Based on the lowest values, γ in soft clay sublayers was well defined by single value of 14.0 kN/m^3. In contrast, the highest γ values identified IL oedometer specimens sampled in 2009.

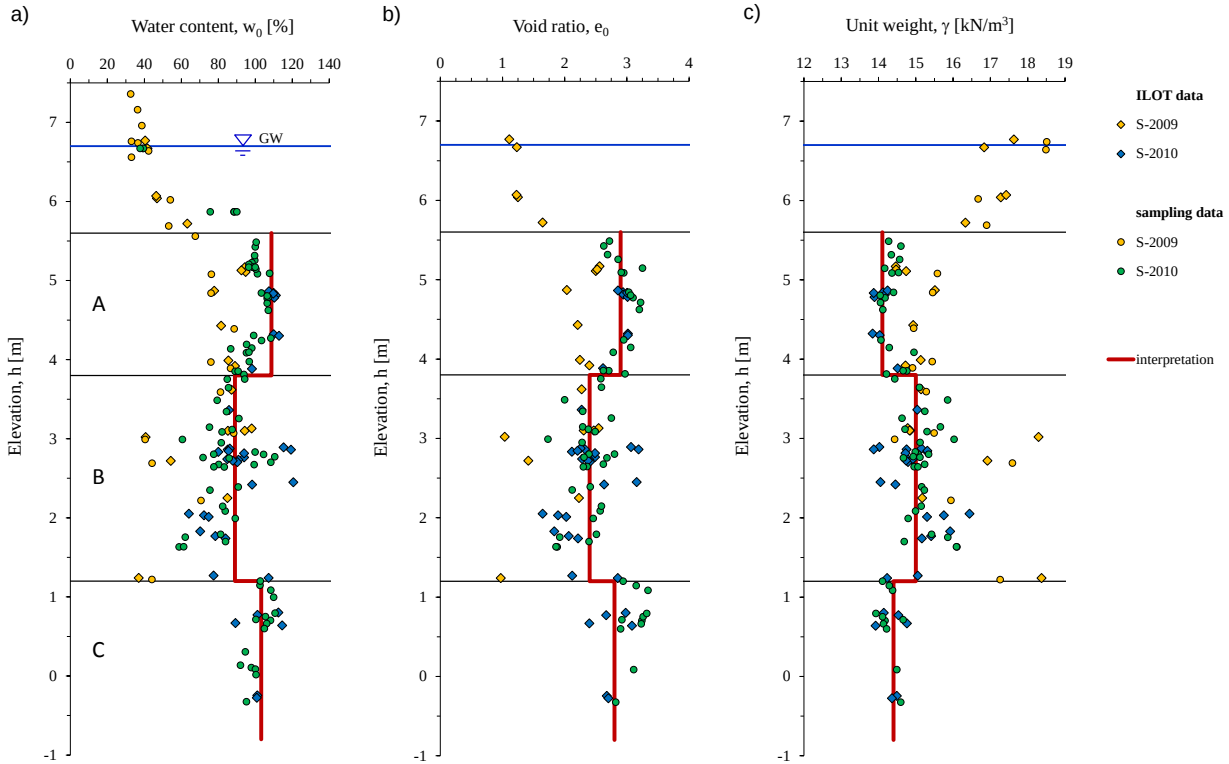

Figure 6.3 Initial state parameters of IL oedometer specimens, a) water content, b) void ratio, and c) unit weight.

6.1.3 Sample quality

In interpretation of laboratory tests, accounting for specimen quality is equally important as understanding effects of depositional and post depositional processes. High scatter in one-dimensional compression response of Perniö clay indicated substantial influence of sample disturbance on magnitude of parameters measured. To quantify disturbance of the specimens two independent criteria were used, $\Delta e/e_o$ and w/γ.

$\Delta e/e_o$ criteria

Evaluation of quality of oedometer test specimens quantified in terms of $\Delta e/e_o$ is shown in Figure 6.4 a). Namely, cumulative change in void ratio up to effective overburden pressure Δe, was scaled with initial void ratio of the specimen e_o [Lunne et al. 2006]. Since resistance to compression is influenced by initial structure, the ratio is reciprocal to quality of the specimen evaluated. The disadvantage of the method is that specimen needs to be subjected to consolidation for its quality to be quantified. Thus, the evaluation approach is applicable for specimens tested in oedometer or triaxial consolidation tests only. The specimen quality assessment includes disturbances occurring during specimen preparation as well as effects of testing methodology. Consequently, the approach might yield misleading conclusions on sampling technique performance. Indeed, high sampling quality results can be substantially reduced by poor specimen preparation, inadequate testing and differences in tests conditions. Finally, the specimen quality evaluation method is influenced by origin and composition of the material evaluated.

The $\Delta e/e_o$ results obtained on specimens aiming IL oedometer tests revealed most of the material being severely disturbed. Indeed, most of the specimens exhibited $\Delta e/e_o>0.07$, identifying poor sample quality. Furthermore, limited amount of specimens satisfied $0.07>\Delta e/e_o>0.04$, representing good to fair sampling quality, while number of very good to excellent samples with $\Delta e/e_o<0.04$ was none. Specimens quantified as fair to good, originated from profiles 63, 64 and 65 sampled with NGI 54, and profiles 67 and 68 sampled with NGI 86. Considering the overall representation of good to fair quality specimens obtained by two sampling methods, conclusion was negligibly better performance of NGI 86 sampler. Contrasted to results following sampling elaborated in Chapter 5.1, results for IL oedometer specimens indicated significant disturbance in laboratory preparation.

w/γ criteria

To access the effects of specimen preparation procedure, additional sample quality evaluation criteria was implemented. The approach is based on magnitude of initial state parameters, i.e. sample quality is expressed by water content to unit weight ratio $2.0<w/\gamma<10.0$ %/kN/m^3. With both parameters being influenced by sample disturbance, high w/γ values correspond to high quality samples. The ratio can be determined without subjecting specimen to test stresses. Indeed, the method is not inevitably influenced by disturbance in specimen preparation and during the tests itself. Consequently, w/γ is suitable approach for evaluation of sampling disturbance caused by various sampling

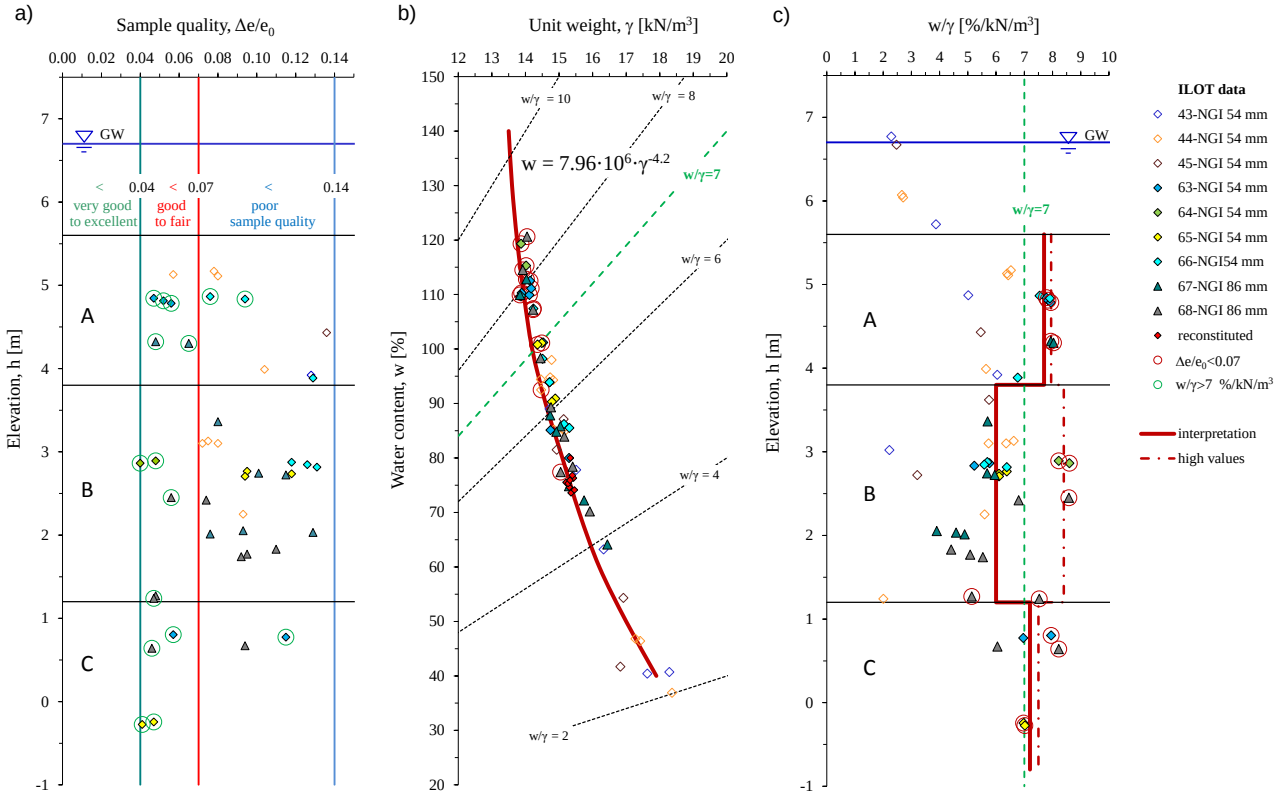

Figure 6.4 Specimen quality in IL oedometer tests on Perniö clay; a) $\Delta e/e_0$ criteria, b) w/γ curve, and c) w/γ criteria.

techniques. Furthermore, w/γ measured prior the specific test enable evaluation of disturbances in specimen preparation.

In Figure 6.4 b) water content values of IL oedometer specimens are related to unit weight. In addition, results identifying good to fair quality specimens according to $\Delta e/e_o$ criteria are highlighted. The resulting w vs. γ response complied that after sampling. The w/γ values varied from 2.0 to 8.6 %/kN/m³. Specimens of the highest quality exhibited the highest w/γ values. With an exception of two records, Perniö clay specimens characterised by $\Delta e/e_o<0.07$ corresponded to w/γ>7.0 %/kN/m³. The w/γ=7.0 %/kN/m³ was thus used as a threshold value to differentiate specimens of high to those of low quality. The highest quality oedometer specimens with w/γ>8 %/kN/m³ were obtained on profile 64 (NGI 54), and NGI 86 profiles 67 and 68 (S-2010). Results on S-2009 specimens were considerably less, i.e. w/γ<6.6 %/kN/m³. For reconstituted specimens average w/γ was 4.9 %/kN/m³. Dry crust materials and those with high percentage of silt generally exhibited w/γ<4 %/kN/m³.

In Figure 6.4 c), w/γ results obtained on IL oedometer specimens are related to sampling depth. In respective soft clay sublayers average w/γ values amounted 7.7, 6.0 and 7.2 %/kN/m³. The results complied fairly well with response measured following the sampling. Based on the specimens of the highest quality representative w/γ values were substantially higher, particularly within sublayer B, i.e. 8.0, 8.4 and 7.5 %/kN/m³, respectively. Within sublayer A, the highest values identified results on profiles 63, 66 (NGI 54), and 67 (NGI 86) in the mid of the zone. Exceptionally high values within sublayer B were obtained on specimens from profiles 64 (NGI 54) and 68 (NGI 86). In sublayer C, the highest w/γ values identified specimens on profiles 63 (NGI 54) and 68 (NGI 86).

Comparison of $\Delta e/e_o$ and w/γ sampling quality criteria

The fact that the $\Delta e/e_o$ cannot be determined unless one-dimensional or triaxial consolidation tests is undertaken, is the major disadvantage of the sample quality evaluation approach. Laboratory testing techniques do differ in terms of stress path and strain-rate conditions. Consequently, void ratio reduction up to the level of effective overburden in situ Δe, is affected by test conditions influencing the objectivity of sample quality results. The w/γ sample quality evaluation approach is not influenced by the limitation. Determination of both parameters is identical if done directly following sampling or on specimens prepared for testing. Consequently, resulting w/γ values are suitable for comparison of various sampling techniques, and evaluation of disturbances in specimen preparation. Finally, unit weight and water content can be monitored during the entire testing process. Thus, w/γ response under the specific test conditions can be correlated to specimen sensitivity allowing better insight in sample disturbance and destructuration effects.

6.1.4 Compressibility and preconsolidation pressure

Effects of sample disturbance on compressibility curve

Stress-strain response of natural specimens in one-dimensional compression revealed considerable scatter. To evaluate Perniö clay compressibility in rela-

tion to both specimen quality and sublayer of origin, Figure 6.5 examines change in specific volume vs. vertical effective stresses normalized with respect to preconsolidation pressure interpreted. Compression curves obtained on three distinctive soft clay sublayers A, B and C are shown separately. The results obtained on good quality, poor quality and reconstituted specimens are distinctively displayed.

Confirming the results in Figure 6.4 c), good quality specimens were characterised by higher initial specific volume. In addition, good quality specimens were distinguished by considerably steeper slope identifying compressibility within NC stress range. Slope of the normal compression line on reconstituted specimens fairly represented a tangent to normal compression behavior of both good quality and poor quality natural specimens at high stress levels. Thus, results on good to fair quality specimens were generally positioned above and were shifted towards higher σ'_1/σ'_p level compared to those obtained on specimens of poor quality. Since the strain-rates in IL oedometer tests were similar, shift of the normal compressive response toward lower values of specific volume was a clear manifestation of sampling disturbance.

Oedometer test results identifying high quality specimens characterised by high v_o and high λ, occurred within all soft clay stratigraphic units. Indeed, it was the highest quality specimens of sublayer B that exhibited the highest v_o and sharpest transition at yield. Unlike the results in Figure 6.5 a) and c) however, majority of the results on sublayer B exhibited considerably lower specific volume fairly represented by value of 3.3. Furthermore, responses on poor quality specimens of sublayers A and C were comparable to those on poor quality specimens of sublayer B. Thus, results shown in Figure 6.5 indicated variance in compression characteristics measured in soft clay sublayers being merely a result of sampling disturbance.

Considering the results presented, possible specimen disturbance mechanism can be set. Due to increased silt content, specimens of sublayer B were typically characterised with relatively higher permeability. When subjected to stress release, negative pore pressures dissipated rapidly. As the result of pore pressure dissipation, effective stresses were almost entirely reduced. Stress release of the specimen was coupled by substantial decrease in void ratio. Decline in void ratio was progressively accompanied by modification in clay structure and reduction in sensitivity. When the specimen was subjected to increase in vertical effective stress during testing, it was eventually restored to NC condition. In the process however, the specimen responded with additional and relatively high void ratio reduction. In low permeability specimens, changes in void ratio following the sampling related effective stress reduction were considerably less. Due to low permeability, the specimen tended to behave as “undrained” and stress reduction was coupled by development of considerable negative pore pressure (suction). The suction prevented decline in water content maintaining the initial structure of the specimen. When such specimen was reloaded, changes in void ratio prior to restoring in situ stress conditions were minor, and resulting stress-strain response was characterised by sharp transition from reloading to virgin compression conditions.

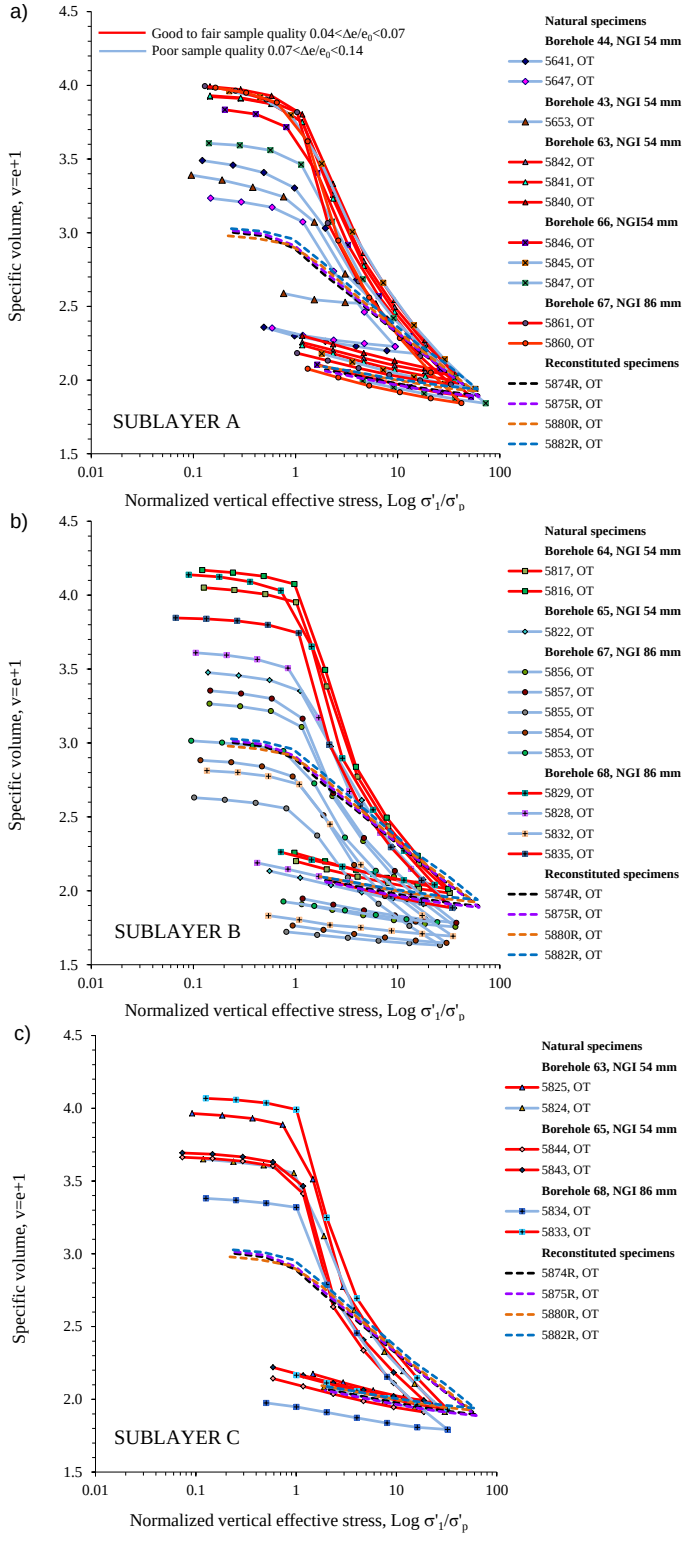

Figure 6.5 IL oedometer test results in σ'_1/σ'_p vs. specific volume plane for good quality, poor quality, and reconstituted specimens, a) sublayer A, b) sublayer B, and c) sublayer C.

Effects of sample disturbance on preconsolidation pressure

Because of being relatively incompressible up to the consolidation stress and very compressible at higher loads, accurate σ'_p determination of the sensitive clays is particularly important [Crawford 1986]. The σ'_p values were defined from ln σ'_1 vs. v plots using bilinear approach (see Figure 6.7). The methodology used was based on fitting two straight lines to the parts of the stress-strain curve exhibiting the lowest and the highest gradients. The intersection of the lines defined yield. The resulting values were confirmed by examining yield in linear stress-strain plots [Koskinen et al. 2003]. To evaluate influence of sampling disturbance on magnitude of the preconsolidation pressure, Figure 6.6 relates σ'_p/σ'_{vo} values to $\Delta e/e_o$ sampling quality criteria. The result was distinctive pattern well represented by Equation 6.1:

$$\Delta e / e_0 = 0.051 \cdot (\sigma'_p / \sigma'_{v0})^{-1.9} \qquad (6.1)$$

The specimens with the lowest $\Delta e/e_o$ values matched the highest σ'_p/σ'_{vo} response. Furthermore, in Figure 6.6 specimens characterised with $w/\gamma>7$ %/kN/m³ are highlighted. Among the specimens tested under identical conditions, those characterised with high w/γ exhibited higher σ'_p/σ'_{vo} values. Note that the stress ratio σ'_p/σ'_{vo} corresponds to terminology of the overconsolidation ratio OCR.

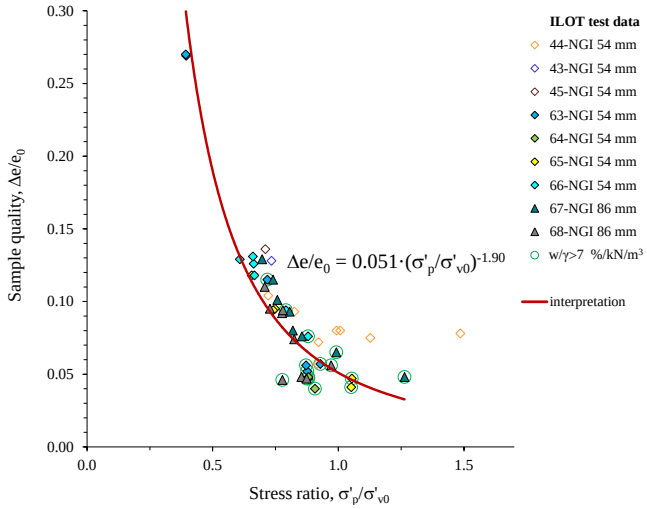

Figure 6.6 Preconsolidation pressure in IL oedometer tests related to specimen quality.

6.1.5 Compressibility -Cam-Clay parameters

To examine response of Perniö soft clay in IL oedometer test, measured compressibility characteristics were interpreted using Modified Cam-Clay theory parameters. The details on determination of the parameters are presented in Figure 6.7. In Figure 6.8 values obtained are related to sampling depth. Results identifying specimens of good quality with $\Delta e/e_o<0.07$ are highlighted.

Reloading κ_o and swelling behavior κ

The slope of reloading and swelling line is very sensitive to the stress range over which it is determined [Wood 1983]. Furthermore, the values are influenced by the hysteretic effect resulting from stress path dependency. Interpreted values of reloading κ_o and swelling slope κ are related to sampling depth in Figure 6.8 a) and b). The magnitude of reloading slope was markedly lower than that identifying swelling. Since Perniö clay was not of swelling type, this effect was primarily related to sensitivity, i.e. nature of clay structure present. According to Burland [1990], the ratio between swelling index and intrinsic swelling index is solid indicator of fabric and interparticle bonding in the natural soil. Thus, κ_o values being lower than κ indicated sensitive specimens whose natural structure added resistance to compression.

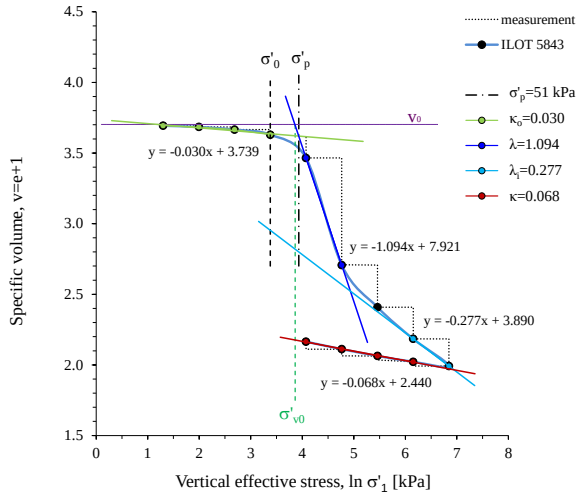

Figure 6.7 Interpretation of Cam-Clay compressibility parameters, ILOT 5843.

Reloading indices represented the highest initial slope without intersecting stress-strain path (see Figure 6.7). The κ_o were determined for similar stress range so to ensure comparability of results obtained. Although the values were generally low, i.e. κ_o<0.080, scatter of the data was considerable, particularly in the upper portion of Perniö soft clay deposit. Average κ_o values for materials of sublayer A, B and C, amounted 0.046, 0.030 and 0.023, respectively. Thus, results showed compression resistance in reloading increasing with depth. Good quality specimens with $\Delta e/e_o$<0.07, commonly exhibited lower κ_o.

The values of swelling slope were obtained for unloading stress range above the in situ preconsolidation pressure (see Figure 6.7). Average κ values in sublayers A, B and C, amounted 0.066, 0.050 and 0.070, respectively. Thus following compression to ~1000 kPa, κ values measured in sublayer B were lower than those in sublayers embedding it. Contrary to that in reloading, swelling slope was proportional to specimen quality. For good quality specimens alone, swelling response was well represented by value of 0.070 in all soft clay strata.

Therefore, while κ determined following considerable straining primarily depended upon the composition and stress history of the specimen, κ_o were mainly influenced by specimen disturbance. Sensitive clay specimens exhibited additional resistance to compressibility and consequently negligible extent of compression in reloading. Low values of κ_o indicated minor changes in initial state parameters compared to those existing in situ. In contrast, if the specimen was disturbed, its initial sensitivity was reduced and consequently, its compressibility in reloading increased approaching that in swelling.

Normal compression λ and intrinsic compression behavior λ_i

Progressive destructuration process in natural specimens is manifested by changes in the apparent slope of the compression curve. Slopes of the normal compression line λ, and that of intrinsic compression λ_i interpreted from IL oedometer test are related to sampling depth in Figure 6.8 c) and d).

Values of slope of the compression line in NC range λ, defined the highest inclination of the stress-strain response measured on natural specimens (see Figure 6.7). The resulting values exhibited very significant scatter, i.e. $0.39<\lambda<1.12$. The scatter reflected influence of the quality of specimens evaluated. Average λ values in respective soft clay sublayers were 0.70, 0.57 and 0.90, thus resembling distribution of w_o and e_o. However, based on these values, i.e. with impact of specimen quality neglected, resulting estimations of settlements would be erroneous. Indeed, considering specimens of the highest quality, λ was significantly higher, i.e. ~1.08 in all soft clay sublayers. The exceptionally high λ values were identified on NGI 86 profiles 67 and 68, and NGI 54 profiles 63, 64 and 65. Thus, sample quality should be studied so that results on high quality specimens are used to establish the true soil behavior.

Following considerable extent of straining apparent slope of the compression curve is reduced to intrinsic value λ_i. The parameter was defined by last two measurements in oedometric compression (see Figure 6.7). Average values of λ_i in sublayers A, B and C were 0.30, 0.25 and 0.30, respectively. The lowest values were identified on specimens from high sensitivity silty clay stratum. Furthermore, λ_i values measured in sublayer B were also characterised with the highest scatter. The results indicated destructuration process in oedometer test being influenced by initial characteristics of the specimen. Namely, due to common occurrence of silty lenses, material sampled within zone B differed from those of zone A and C in terms of reduced initial water content. Furthermore, within the zone B of high sensitivity obtaining high quality samples presented a considerable difficulty. Consequently, initial structure of most of the specimens originating from the zone was disturbed. Both facts influenced the destructuration process measured. Indeed, magnitude of λ_i values reached was proportional to the initial water content and initial sensitivity of the samples. The conclusion was confirmed by results on specimens of the highest quality. Represented by value of 0.32 in all soft clay sublayers, λ_i values identifying the specimens were the highest. Somewhat misleading were results in 2009, performed until lower level of σ'_1 in compression. High magnitude of the λ_i values reflected lower stress related extent of destructuration compared to that in S-2010 tests.

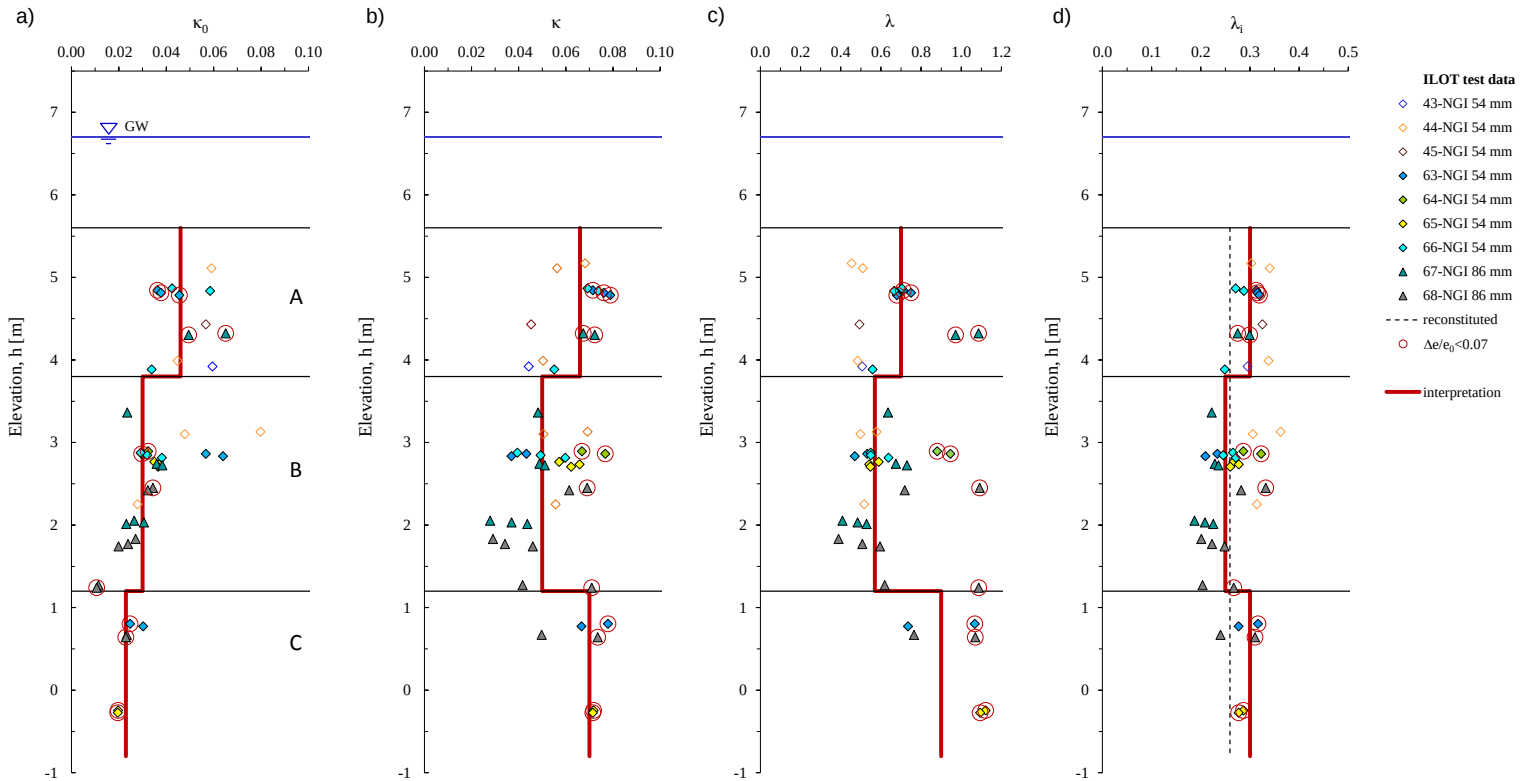

Figure 6.8 Cam-Clay compressibility parameters in IL oedometer tests; a) slope in reloading κ_0, b) slope in swelling κ, c) slope of normal compression λ, and d) slope of intrinsic compression line λ_i.

Figure 6.8 d) includes average value of normal compression slope determined on reconstituted specimens, i.e. λ_R=0.259. If compared with λ_i values obtained on destructured natural specimens, than λ_R represented intrinsic compressibility of natural specimens fairly well. Namely, average λ_R complied with λ_i values in sublayer B, yet was somewhat lower than λ_i measured in sublayers A and C. The effect reflected oedometer tests on reconstituted specimens being initiated at w_o lower than that of natural specimens.

Correlation of intrinsic parameters λ_i and κ

If slope of the intrinsic compression and that in swelling are determined on destructured specimens, the values obtained are representative of the material with similar properties and should consequently correlate. Some results relating the intrinsic compression and that of swelling have been presented by Burland [1990], when evaluating results of Samuels [1975]. Burland [1990] used the ratio to define susceptibility of clay to structural breakdown. Herein, relation between the slope of the intrinsic compression line and swelling line was evaluated based on IL oedometer tests on Perniö clay. Values of κ plotted vs. λ_i in Figure 6.9, show close correlation well defined by Equation 6.2:

$$\lambda_i = 2.5 \cdot \kappa + 0.12 \tag{6.2}$$

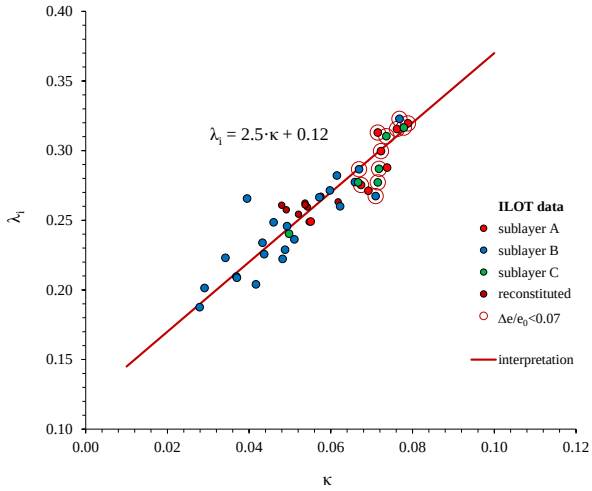

Figure 6.9 Relation of λ_i and κ in IL oedometer tests on Perniö clay.

Using the Equation 6.2 fairly accurate estimate of κ values can be obtained, provided λ_i is known. Correlation perquisite was sufficient level of destructuration. Thus, the expression was related to stress and void ratio levels at which λ_i was defined and to which specimen were subjected prior defining κ. The correlation was valid for the entire profile, thus independent of sampling depth. Results on high quality specimens typical of sublayer A and C positioned at the highest values of κ and λ_i. In contrast, data representing sublayer B typically exhibited rather low values of κ and λ_i. The results confirmed specimens of sublayer B being of considerably different destructuration character-

istics, represented by lower values of λ_i reached in oedometric compression compared to above and underlying zones. Since based on truly intrinsic properties of destructured material, the correlation was independent of the extent of specimen disturbance. The statement was confirmed by results on reconstituted specimens, satisfying the condition set by the correlation very well.

Stress dependency of slope in compression

To re-evaluate compression characteristics, slope of the compression path was related to vertical effective stress normalized with stress at yield. Thus, in addition to reloading κ_o, normal compression λ, and intrinsic compression λ_i, defined by distinctive values, Figure 6.10 enables evaluation of change in the compressive response with strain, i.e. following the stress increase.

Slope in compression stress dependency curves exhibited same general features. Prior to preconsolidation pressure, i.e. $\sigma'_1/\sigma'_p<1$, slope in compression rose at low rate, reflecting slight increase in reloading compressibility. At stress ratios following the preconsolidation, changes in compression characteristic were abrupt; at first rapid increase to maximum value, and later that of progressive decline reflecting compressibility decrease and changes in structure, i.e. destructuration process. The highest slope of the compression curve λ, was obtained at stress levels immediately following the preconsolidation. Towards the end of the test, slope of the compression curve asymptotically declined to stabilize at certain uniform level indicating intrinsic compressibility λ_i, i.e. compression characteristics of the destructured material.

Figure 6.10 shows that λ values were strongly dependent upon the incremental loading pattern implemented. Namely, due to limitations of IL oedometer test, in some tests λ values interpreted underestimated maximum compression of the specimen tested. Depending on the compliance of the preconsolidation pressure with that of closest loading conditions, resulting curve exhibited either clear peak or markedly reduced value. Overall, the highest λ values were obtained for $2<\sigma'_1/\sigma'_p<4$. However, clear peak value was exhibited for $2<\sigma'_1/\sigma'_p<3$, independent of the specimen quality. Outside this stress ratio range, slope in compression stress dependency curve was typically truncated. This disadvantage can be avoided by selecting appropriate loading pattern in relation to the effective overburden, or by modifying testing methodology by imposing additional loading increments at stresses close to preconsolidation.

To investigate influence of specimen structure, Figure 6.10 examines slope in compression stress dependency curves with respect to specimen quality. Following the preconsolidation pressure, i.e. $\sigma'_1/\sigma'_p>1$, reconstituted specimens exhibited fairly uniform slope of compression curve $\lambda_R= 0.259$. At $\sigma'_1/\sigma'_p>20$ slight decrease in compression slope was observed. On natural specimens however, variations in λ values were considerable. Thus, besides loading pattern implemented, magnitude of values of λ was highly dependent upon specimen quality. In tests performed on good quality specimens, load increments within stress ratio range $2<\sigma'_1/\sigma'_p<3$ produced both clear peak and markedly high λ value. Consequently, in tests satisfying both of the conditions accurate determination of compressibility response above effective overburden was en-

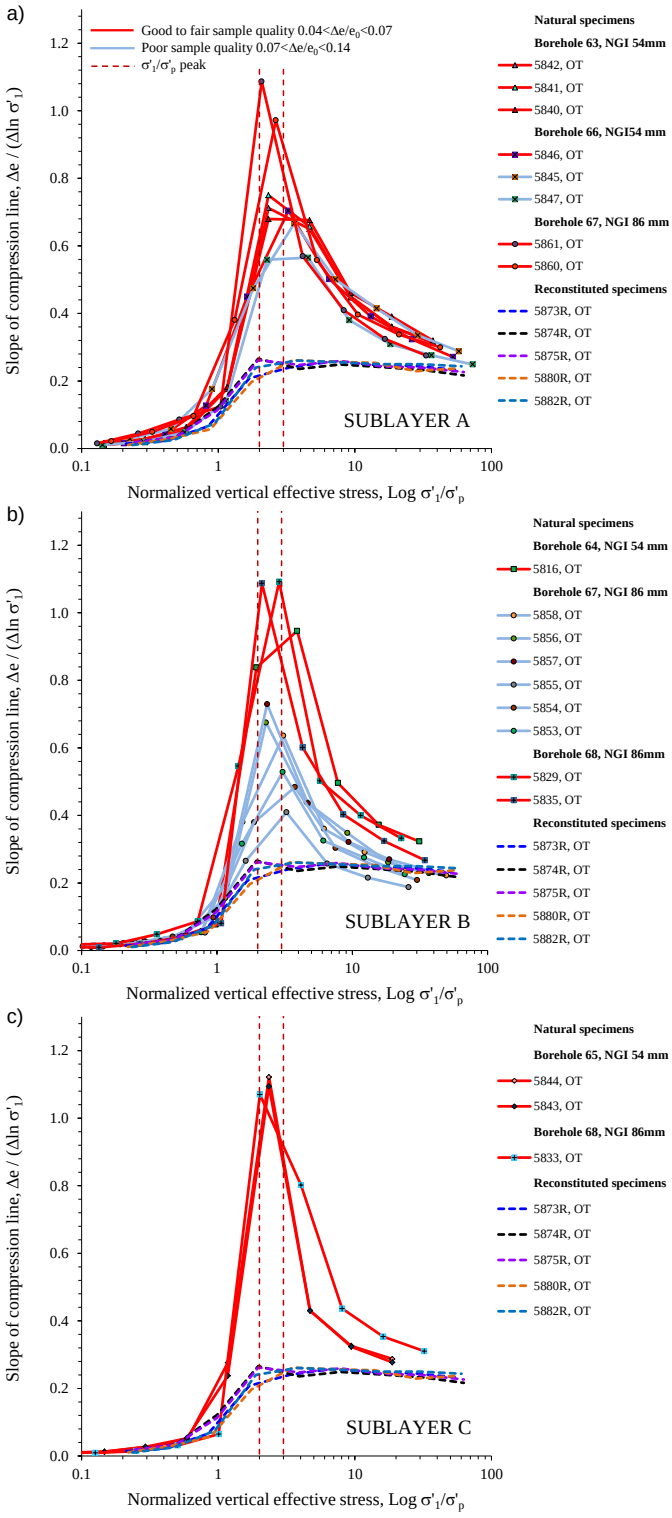

Figure 6.10 Slope in compression stress dependency in IL oedometer tests on Perniö clay; a) sublayer A, b) sublayer B, and c) sublayer C.

abled. Average λ value identifying poor quality specimens was 0.730, while values of λ obtained on good quality specimens were markedly higher, and for loading increments characterised by $2<\sigma'_1/\sigma'_p<3$, appeared in a narrow range from 1.4 to 1.6. Furthermore, intrinsic compression values λ_i, corresponding to those obtained on reconstituted specimens were in testing of poor quality specimens reached at markedly lower σ'_1/σ'_p, compared to that needed in testing of good quality specimens.

Values of λ interpreted without consideration of specimen disturbance are misleading. Fact that compression curves measured on high quality specimens exhibited uniform maximum independent of sublayer of origin, indicated variation in compressive response measured being merely a result of specimen disturbance. In soft clay specimens of sublayer B, being of the highest sensitivity, susceptibility for specimen disturbance was the highest, resulting with systematic underestimation of in situ compression characteristics.

6.1.6 Compressibility-Compression modulus parameters

Interpretation of parameters

To provide better insight on the compressibility of Perniö clay in IL odometer tests, the results were examined on the basis of Compression modulus theory [Janbu 1967]. Compression modulus parameters interpreted from measured data are presented as a function of vertical effective stress in Figure 6.11. Approaches used aimed consistency with Cam-Clay stiffness parameters. Initial constant compression modulus M_o, was set to comply with maximum compression modulus measured within the stress range preceding yield. Furthermore, initial vertical effective stress σ'_o corresponding to the maximum value of compression modulus in reloading $M_{o\,max}$, was consistently evaluated. Constant limit compression modulus M_L, was determined for the stress range defining slope of the normal compression line λ. Thus, consolidation stress σ'_C and limit stress σ'_L, were set to correspond to extreme values of stress range defining gradient λ. Due to the effects of IL procedure and semilogarithmic scale, in some tests stress range defining λ did not comply with that of minimum compression modulus. In those tests, stress range defining M_L was set to identify maximum compressibility in linear σ'_1 vs. specific volume plane. Values of σ'_C and σ'_L were adjusted accordingly. Transition from M_o to M_L was represented by the destructuration line interpolated to measured compression moduli for stress range between initial effective stress σ'_o and consolidation stress σ'_C. The destructuration line was thus defined by slope M'_o, and intercept M'_{oi}. Compression moduli values measured for stress range above σ'_L and prior provisionally set vertical stress of 500 kPa, were represented with line defined by modulus number M' (slope) and intercept M'_i. Final portion of the compression moduli curve for $\sigma'_1>500$ kPa was fitted to measured data using parameter a, in accordance with Equation 6.3 [Janbu 1967].

$$M = M' \cdot \sigma'^{\,1-a}_{v} \tag{6.3}$$

Compression modulus parameters and curves interpreted are presented in Figure 6.12 and Figure 6.14, respectively. The values obtained as well as general conclusions on compression modulus response are explained in following.

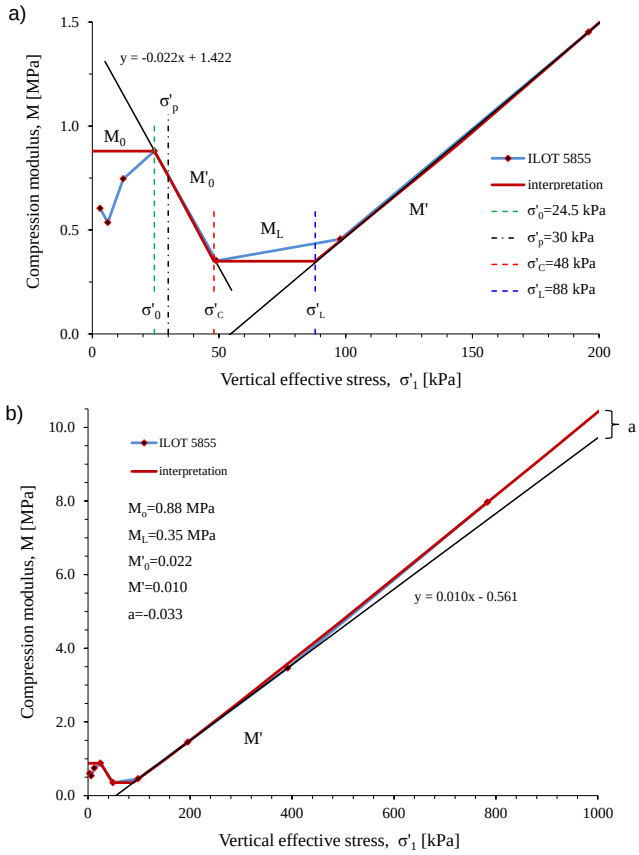

Figure 6.11 Interpretation of compression modulus parameters, ILOT 5855; a) detail on compression modulus response in reloading, and b) entire testing stress range.

Initial M_o and limit compression modulus M_L

Interpreted values of initial compression modulus M_o are related to sampling depth in Figure 6.12 a). Average M_o determined on natural specimens increased with depth amounting 0.65, 0.85 and finally very high 1.50 MPa in respective soft clay sublayers. In contrast, M_o on reconstituted specimens were 0.45 MPa in average, thus considerably less. These findings indicated magnitude of M_o being proportionally influenced by specimen structural characteristics, clay content, as well as by effective overburden stress. Average M_L values on natural specimens shown in Figure 6.12 b) were significantly smaller, i.e. 0.20, 0.26 and 0.25 MPa in soft clay sublayers A, B and C. Thus, distribution of M_L vs. depth identifying zone B as the material of the overall lowest compressibility complied with conclusions based on λ values in Figure 6.8 c). In contrast, M_L values on reconstituted specimens varied from 0.21 to 0.27 MPa, and were well represented by an average of 0.24 MPa. Majority of natural spe-

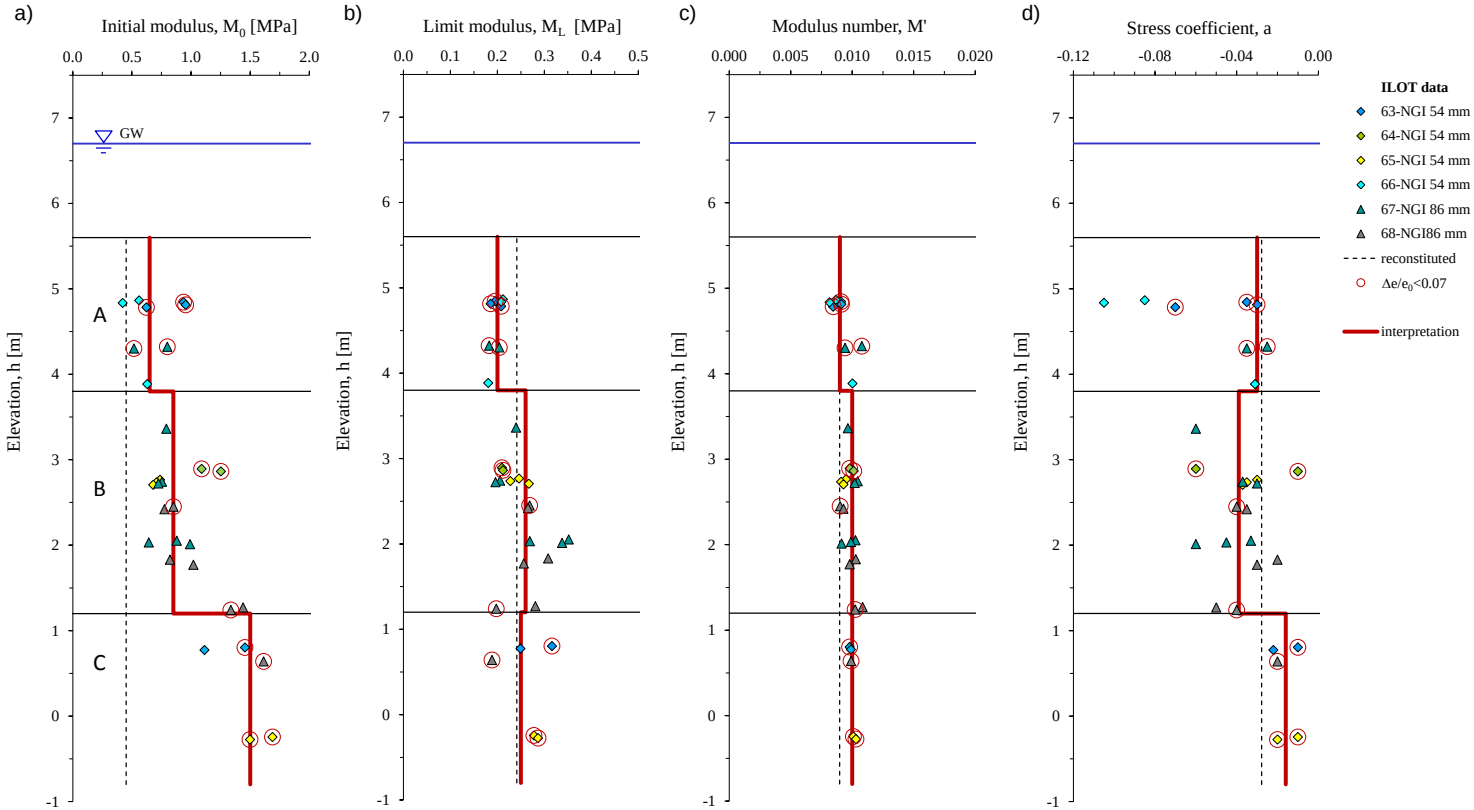

Figure 6.12 Compression modulus parameters in IL oedometer tests; a) initial compression modulus M_0, b) limit modulus M_L, c) modulus number M', and d) stress coefficient a.

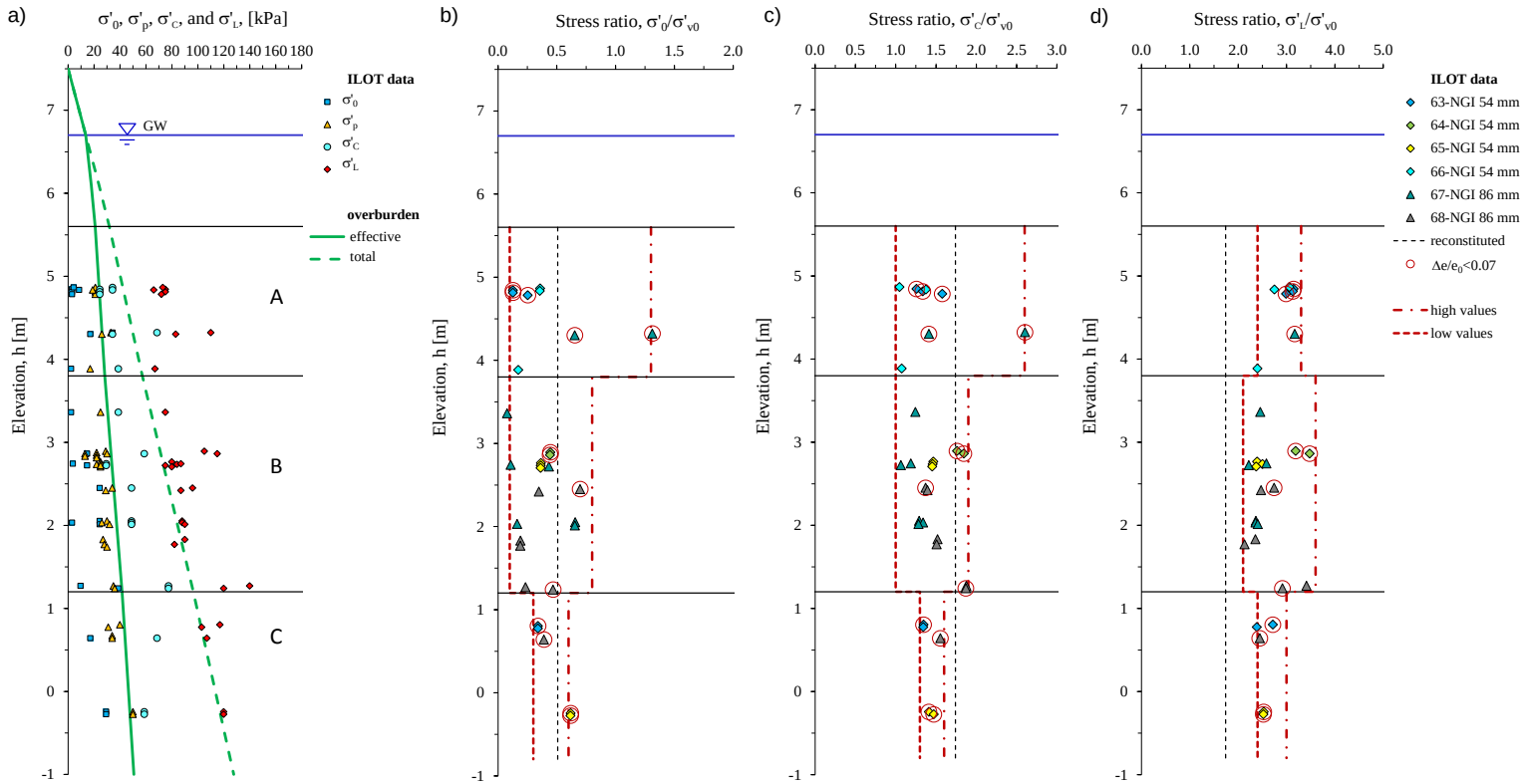

Figure 6.13 Evaluation of effective stress parameters characterising compression modulus curve in IL oedometer tests; a) initial effective stress σ'_0, compression stress σ'_C, and limit stress σ'_L, b) σ'_0/σ'_{v0}, c) σ'_C/σ'_{v0}, and d) σ'_L/σ'_{v0}.

cimens of good quality exhibited lower M_L values than reconstituted and those of poor quality. However, despite being evident by high scatter of M_L values determined for sublayer B and C materials, effects of sample disturbance on compressibility were less exposed compared to those based on values of λ. These results manifest effects of semi-logarithmic scale in interpretation of Cam-Clay parameters as well as limitations inherent of IL test procedure.

Modulus number M' and stress exponent a

Figure 6.12 c) and d) present depth distribution of modulus number M' and stress exponent a, defining compression modulus response above limit pressure σ'_L. Values of modulus number M' on natural specimens were found to be uniform in all soft clay sublayers. Overall, M' values varied from 0.008 to 0.012, and were well represented with value of 0.009 in sublayer A, and 0.010 in sublayers B and C. Average modulus number obtained on reconstituted specimens was 0.009. In contrast, values of stress exponent a identifying compression modulus response at high stress levels, were highly scattered ranging from -0.105 to -0.001. Values representable of sublayer A, B and C materials amounted -0.030, -0.039 and -0.016, respectively. Occasional stress exponent values in sublayers A and B were markedly lower.

Effective stress parameters σ'_o, σ'_C and σ'_L

Figure 6.13 evaluates stress parameters characterising compression modulus curve. Initial vertical effective stress $\sigma'_{o,}$ matching maximum compression modulus in reloading $M_{o\ max}$, increased with sampling depth. The parameter reflected unloading stress of the specimen strongly related to specimen quality [Janbu 1998]. Indeed, σ'_o exhibited by the specimen corresponds to a suction pressure and indirectly to water content maintained following the sampling and specimen preparation. At the initial stages of test loading, it was the suction pressure that resisted compression of the specimen, resulting in very low compressibility in the range of low stresses [Hong 2010]. Following normalization with effective overburden, resulting values mainly occurred within $0.1<\sigma'_o/\sigma'_{vo}<0.8$. Occasional data on high sensitivity specimens were among the highest. In contrast, the lowest values of σ'_o/σ'_{vo} identified poor quality specimens severely disturbed in specimen preparation. Finally, σ'_o/σ'_{vo} representing reconstituted material was 0.51, thus matching the average response on natural specimens. Effective stress parameters σ'_C and $\sigma'_{L,}$ increased with sampling depth as well. σ'_C somewhat exceeded σ'_p, while σ'_L response resembled distribution of total overburden stress. Furthermore, σ'_C/σ'_{vo} values mainly occurred in limits from 1.0 to 1.9. In contrast, σ'_L/σ'_{vo} values generally ranged from 2.1 to 3.6. Overall, σ'_C/σ'_{vo} and σ'_L/σ'_{vo} obtained on specimens of good quality were often the highest. Corresponding stress ratio identifying reconstituted specimens amounted 0.74.

Effects of sample disturbance on compression modulus curve

Figure 6.14 shows interpreted compression modulus curves for natural and reconstituted specimens evaluated with respect to specimen quality. The results obtained in respective sublayers are distinctively displayed. Overall, the

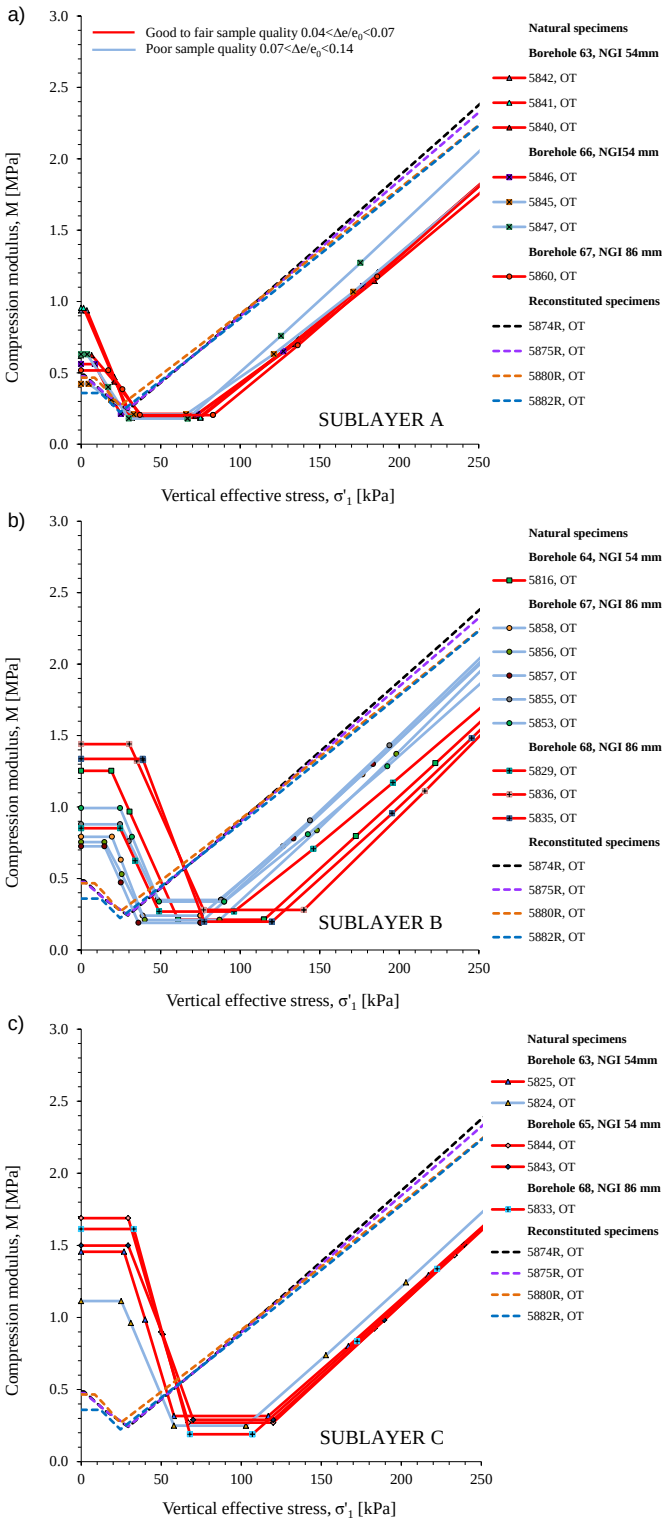

Figure 6.14 Interpreted compression modulus response in IL oedometer tests on Perniö clay; a) sublayer A, b) sublayer B, and c) sublayer C.

results confirmed M_o being highly influenced by specimen structural characteristics, yet also by sampling depth. Specimens of sublayer C showed the highest M_o, while those of sublayer B and finally sublayer A exhibited reduced values of the parameter. Contrary to those in sublayer A, M_L values identifying underlaying materials were more scattered. However, the lowest M_L values in all soft clay sublayers represented by value of 0.2 MPa, identified specimens of the highest quality. Gradients of the destructuration line M'_o defining transition between M_o and M_L, were similar for the entire set of IL oedometer tests on natural specimens. In contrast to natural, reconstituted specimens exhibited the lowest M_o values, and reduced magnitude of gradient M'_o. Furthermore, M_L of reconstituted specimens was reduced to a distinctive stress level corresponding to consolidation pressure. Thus, while reconstituted specimens exhibited reduction in compressibility following σ'_C, natural specimens continued to compress at high rate within the limit modulus stress range. Above σ'_L change in compressibility of natural resembled response of reconstituted specimens. Indeed, up to stress levels of 500 kPa modulus number was of similar magnitude independent of the specimen condition. Compression modulus curves obtained on good quality natural specimens however, were shifted toward higher stress levels reflecting higher σ'_L values. Thus, position of compression modulus curve in successive soft clay sublayers was defined by effective overburden and specimen quality. Both parameters were related to σ'_o, i.e. unloading stress of the specimen following the sampling and preparation.

6.1.7 Bonding parameters

Sensitivity

Determination of initial sensitivity of the specimen subjected to oedometric compression is based on comparing the response of a natural specimen with that of an equivalent reconstituted specimen. However, the determination of sensitivity is not a straight-forward task. In the following several procedures are argued and finally new method is suggested.

Consistent approach for sensitivity evaluation based on oedometric compression results was given by Yin et al. [2011] (Equations 6.4 and 6.5). Sensitivity is defined as ratio of preconsolidation pressure σ'_p, of natural specimen, and intrinsic preconsolidation σ'_{pi}, of reconstituted specimen, i.e. $S_t=\sigma'_p/\sigma'_{pi}$. Sensitivity interpreted depends upon method and accuracy of determination of the preconsolidation pressures. Determination of σ'_p of natural specimens was elaborated by Salford [1975] and is not considered herein. In this study, σ'_p was defined using bilinear and modified bilinear approach based on Cam-Clay theory [Koskinen et al. 2003]. The methods yield with lower limit of σ'_p. Problems in determination of intrinsic preconsolidation pressure σ'_{pi}, were more significant, and were related to reconstituted material response in oedometer tests. According to Yin et al. [2011], σ'_{pi} is stress state at intersection of normal compression line of reconstituted specimen, with that of primary reloading line of natural specimen in oedometric compression. Thus, in v-ln σ'_1 plane:

$$\sigma'_{pi} = e^{\frac{v_{\kappa 0} - v_R}{\lambda_R - \kappa_0}} \quad (6.4)$$

$$S_t = \frac{\sigma'_p}{e^{\frac{v_{\kappa 0} - v_R}{\lambda_R - \kappa_0}}} \quad (6.5)$$

where: λ_R and v_R define line representing reconstituted specimen response in NC stress range, i.e. slope and intersection with specific volume axis at unit pressure; κ_o and $v_{\kappa o}$ define primary reloading of natural specimen, i.e. slope and intersection of reloading line with specific volume axis at unit pressure.

Disadvantages of the approach are related to interpretation of reloading line and position of reference compressibility line of the reconstituted specimen.

a) Interpretation of reloading line; To calculate sensitivity using the Equation 6.5, primary reloading response of natural specimen needs to be defined. Since the position of the reloading line highly depends upon the stress range considered, systematic analyses of reloading response are uncommon. In this study, reloading slope was defined for stress range prior to σ'_o.

b) Specific volume range of reconstituted specimens; Ideally, initial water content of reconstituted specimen should correspond to that of natural specimen. However, due to the high natural water content of Perniö clay and effects of flocculated structure, it was impossible to prepare reconstituted samples at the same w_o as those of natural. Such specimens would have simply been too soft to handle and test [Karstunen & Koskinen 2008a]. Consequently, line defining compressibility of reconstituted specimen in NC stress range had to be extended to allow σ'_{pi} interpretation (see Figure 6.15).

c) Slope of the normal compression line of reconstituted specimen; Slope of the normal compression line of reconstituted specimen in IL oedometer test is proportional to the w_o of the specimen evaluated [Shibata & Nishihara 1999, Hong et al. 2010, Hong et al. 2012]. Reconstituted specimens tested in IL oedometer tests were obtained in a single reconstitution batch. Consequently, the specimens had similar w_o and resulting λ_R matched well (see Figure 6.1). However, slope representing normal compression of reconstituted specimens λ_R=0.259, was merely one of the possible responses valid for specimens at w_o of 76.0 %. Thus, adequate reference compressibility of reconstituted material in NC stress range should be obtained by normalization of compression lines measured on specimens tested at various w_o. Suitable approaches are that of representing normal compression line in normalized void ratio stress space as suggested by Shibata & Nishihara [1999], or that based on Burland's [1990] void index as suggested by Hong et al. [2012].

d) Position of the normal compression line for reconstituted specimen; As the natural specimen is destructured, its compressibility progressively converges to that of reconstituted specimens. However, problems with reference compressibility of reconstituted specimens were not restricted to slope only. As shown in Figure 6.5, positions of the destructured segment of the stress-strain curve of natural specimens varied considerably. Thus, to enable sensitivity interpretation, normal compression line representing reconstituted speci-

mens had to be translated so to tangent final portion of stress-strain response of natural specimen at high stress levels (Figure 6.15).

To overcome above stated disadvantages and improve the reliability of sensitivity determination, alternative approaches are suggested and evaluated. In Figure 6.15 they are referred as approach a, b and c.

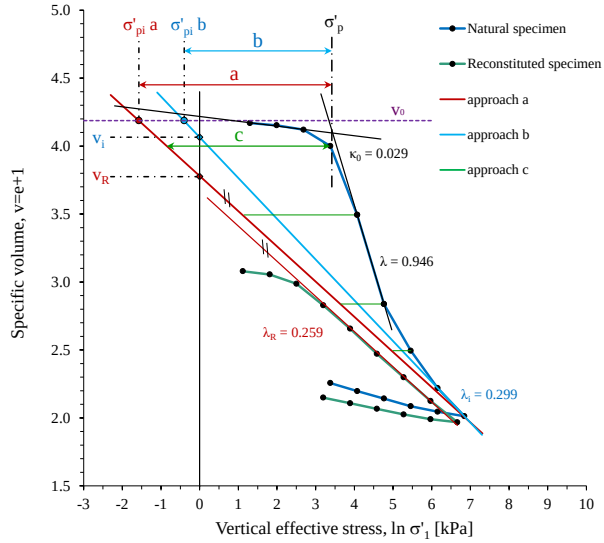

Figure 6.15 Sensitivity of IL oedometer specimen interpreted using approaches a, b, and c.

Approach a

By modifying determination of intrinsic preconsolidation pressure, approach a aims overcoming difficulties in interpretation of reloading behavior. Using the approach set by Yin et al. [2011], σ'_{pi} interpreted were regularly associated with specific volume above that measured on oedometer specimen prior testing. To overcome this problem, and additionally, to avoid discrepancies related to stress range used in interpretation of reloading behavior, approach a defined σ'_{pi} at the intersection of translated normal compression line of reconstituted specimen with line defining initial specific volume of natural specimen $v_o=e_o+1=$const. (see Figure 6.15). Approach a is defined with Equation 6.6:

$$S_t = \frac{\sigma'_p}{e^{\frac{v_0 - v_R}{\lambda_R}}} \tag{6.6}$$

For $\sigma'_{pi}<1$, quantitative effect of the modification on interpreted sensitivity values is considerable. Depth distribution of sensitivity values obtained using approach a are shown in Figure 6.16 a).

Approach b

Aiming to overcome problem of the initial water content effects on compressibility of the reconstituted specimen, approach b employed alternative reference to represent compressibility of destructured material. Instead with λ_R, compressibility of destructured material was based on intrinsic compression

response λ_i determined on natural specimens at high stresses (see Figure 6.15). In approach b therefore, σ'_{pi} was defined at the intersection of line representing compressibility of destructured natural specimen with line defining initial specific volume of the same specimen. Approach b is defined by Equation 6.7:

$$S_t = \frac{\sigma'_p}{e^{\frac{v_0 - v_i}{\lambda_i}}} \tag{6.7}$$

Using this approach, two problems arose:

a) For implementation of this technique, specimens need to be sufficiently destructured by testing to high stress levels. In IL oedometer tests of this study, intrinsic compressibility line was interpolated using two final settlement points obtained on specimens compressed to ~1000 kPa (see Figure 6.15). As a criteria for validity of λ_i determination, $\lambda_i/\lambda_R<25\%$ was used. All IL oedometer tests performed on S-2010 material satisfied the criteria.

b) Sensitivity obtained using approach b is influenced by sample disturbance. As stated by Hight et al. [1987], specimen disturbance following the sampling of leached clay is responsible for shift in the position of its virgin consolidation line. Thus, sample quality influenced not only magnitude of void ratio change yield, i.e. $\Delta e/e_o$, but strain response at high vertical effective stresses. As shown on Figure 6.8 b), λ_i obtained in soft clay sublayers A, B and C differed, i.e. natural specimens with low w_o showed lower intrinsic compressibility. The results support hypothesis of lower e_o values in sublayer B being an effect of sample disturbance. Choice of λ_i instead of λ_R, failed to overcome influence of the sample disturbance effects on sensitivity calculated. The S_t values obtained using approach b are related to depth in Figure 6.16 a).

Approach c

Sensitivity of the specimen is strain dependent. To capture change in sensitivity with increase of vertical effective stresses approach c was set. Using the approach, continuous sensitivity data were determined as an ratio of vertical effective stresses carried by natural and reconstituted specimen at the same magnitude of specific volume, i.e. $S_t = \sigma'_{Nn}/\sigma'_{Rn}$ at $v_n=e_n+1$ (see Figure 6.15). Approach c is defined by Equation 6.8:

$$S_t = \frac{\sigma'_{Nn}}{\sigma'_{Rn}} = \frac{\sigma'_{Nn}}{e^{\frac{v_i - v_R}{\lambda_R}}} \tag{6.8}$$

Advantages of the approach c are: a) sensitivity values were evaluated for the entire range of compressibility measured, with maximum sensitivity obtained taken as representable of initial sensitivity of the specimen; b) distinctive sensitivity values corresponded to specific magnitude of water content, c) being obtained directly from the measured compressibility data, sensitivity values were not influenced by interpretation of parameters such as κ_o or σ'_p, and d) approach c is actually the only method compatible with definition of intrinsic yield surface [Gens & Nova 1993], used in destructuration models, i.e. it being the imaginary yield surface for the same clay without bonds. The approach is weighted by several disadvantages: a) reference compressibility of reconstitut-

ed specimen in NC stress range, i.e. line with λ_R slope, needed to extrapolated and translated to enable sensitivity determination; b) compressibility of reconstituted specimen in NC range was influenced by its initial water content, and thus not unique reference, and c) since measured response of the specimen was directly used in interpretation, sensitivity values calculated were restricted to specific volumes marking the end of each load increment. Indeed, it is in continuously loaded tests that the approach c revealed its full potential.

Comparison of sensitivity obtained in oedometer test and fall cone test

Sensitivity results obtained using approaches a, b and c are shown in Figure 6.16. Ideally, the results representing IL oedometer specimens should correspond to sensitivity values in fall cone test following sampling.

Sensitivity values obtained with approach a (see Figure 6.16 a), exhibited the same sensitivity vs. depth pattern as fall cone test results. Beside well defined depth distribution pattern, the approach clearly distinguished high quality specimens from those of poor quality. Compared to values in fall cone test however, overall magnitude of resulting values was very high. Sensitivity defined with approach a closely corresponds to that set by Yin et al. [2011]. Indeed, values gained with Equation 6.5 would be somewhat higher than those in Figure 6.16 a). In sublayer A, S_t<14 characterised poor quality oedometer specimens sampled with NGI 54. High quality NGI 54 specimens exhibited S_t ~47. Sensitivity values obtained on NGI 86 specimens from the same sublayer were twice as high, i.e. S_t ~94. In sublayer B, values on poor quality specimens were much lower compared to those identifying specimens of high quality, i.e. ~11 for former, and as high as 150 for the later. Within sublayer C resulting values were scattered as well. High quality specimens exhibited 40<S_t<122, while for those of poor quality average S_t was ~22. Considering all soft clay sublayers, the highest S_t values identified specimens sampled with NGI 86.

Values obtained using approach b (see Figure 6.16 b), corresponded well with fall cone test results, both in terms of distribution with depth and magnitude. Within sublayer A, values on S-2010 oedometer specimens sampled with NGI 54 and NGI 86 resembled those obtained in fall cone test on respective materials. In sublayer B, most of the values identifying S-2010 oedometer specimens were very low, i.e. S_t~10. Considering limited number of high quality specimens on profiles 65 (NGI 54) and 68 (NGI 86), S_t varied from 20 to 46. Thus, sensitivity values corresponded in range with values obtained in fall cone test after sampling. Fairly independent of sampler type, S_t results within sublayer C ranged narrowly from 18.3 to 31.6. The values thus resembled fall cone test results on STII sampled material. Finally, S_t values identifying S-2009 sampled oedometer specimens (NGI 54 mm) were negligible indicating completely destructured material.

Figure 6.16 c), shows depth distribution of sensitivity obtained with approach c. The maximum sensitivity values determined with Equation 6.8 were taken as representative of initial sensitivity of the oedometer test specimens. The values closely corresponded to specific volume at preconsolidation pressure. Values obtained on oedometer test specimens in sublayer A, i.e. S_t~25 (NGI 54) and S_t~40 (NGI 86), matched average fall cone test results on corresponding materials. Values on poor quality specimens within sublayer B were

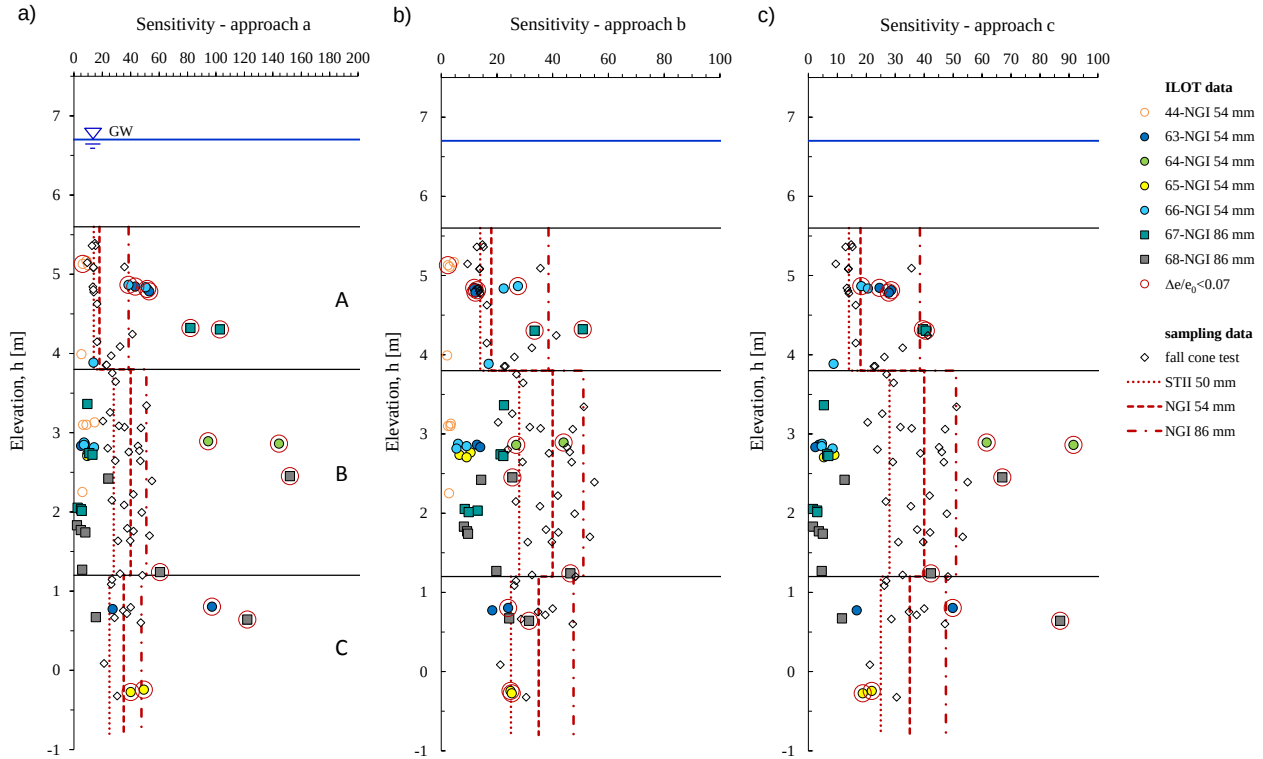

Figure 6.16 Sensitivity of IL oedometer test specimens compared to values obtained in fall cone test after sampling; a) approach a, b) approach b, and c) approach c.

~5, while those on high quality specimens ranged broadly from 42.6 to 91.6. Considerable scatter occurred in sublayer C as well, starting from ~14 in poor specimens and increasing with specimen quality up to 87.0.

Despite high difference in the magnitude of the results, the methods considered gave similar pattern of sensitivity vs. depth, analogous to that based on fall cone test. Results obtained using approach a exceed fall cone determined values by factor of ~3. In contrast, results of approaches b and c matched fall cone test results in magnitude fairly well. Unlike methods a and c, approach b identifies least scatter in sublayer C, being unrealistic. Using approach c, occasional very high sensitivity values on high quality specimens surpassed expected limits set by fall cone test. Overall, method c was the most valid approach as it represented well general pattern, magnitude, and finally clearly distinguished high quality specimens from those of poor quality.

Figure 6.17 shows sensitivity of IL oedometer specimens correlated from initial void ratio and slope of the normal compression line [Leroueil et al. 1983].

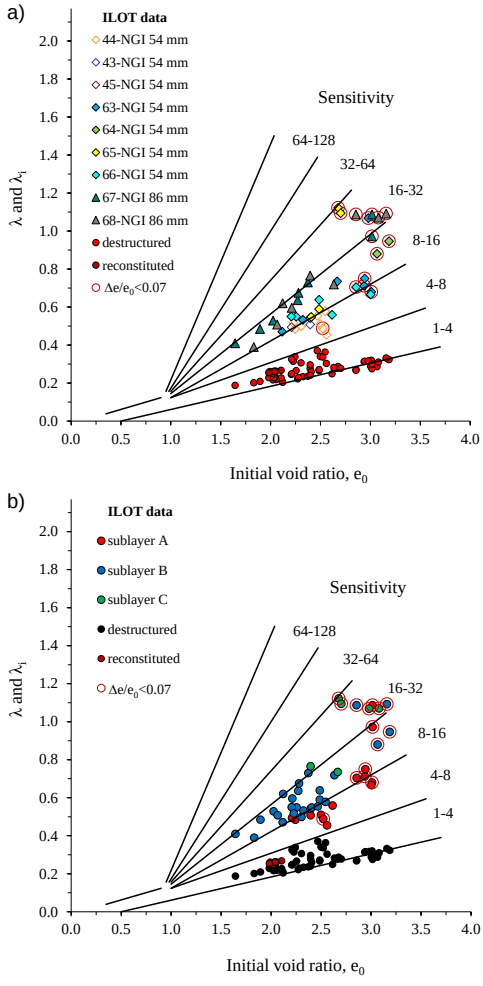

Figure 6.17 Sensitivity of IL oedometer test specimens correlated from e_0 and λ (λ_i); a) relation to sampling profile, and b) sublayer of origin [correlation after Leroueil et al. 1983].

In Figure 6.17 a) results obtained are related to specimen quality. Compared to those measured in fall cone test, correlated S_t values were significantly lower in all soft clay sublayers. The results obtained in S-2009 showed the lowest sensitivity among natural clay specimens, i.e. $S_t<8$. Most of the natural specimens displayed sensitivity in a range from 8 to 16. Specimens identified as being of good quality occurred within $8<S_t<32$ and were characterised with $e_o>2.8$. Limited amount of specimens characterised by $16<S_t<32$, originated from profiles 63 and 65 (NGI 54), and profile 68 (NGI 86). Reconstituted specimens and destructured natural specimens exhibited S_t between 1 and 4.

In Figure 6.17 b) results are evaluated with respect to sublayer of origin. The lowest sensitivity results $S_t<8$, identified poor specimens sampled in 2009 from sublayer A. Overall, most of the specimens of poor quality with $8<S_t<16$, originated from sublayer B. Finally, high quality specimens with $16<S_t<32$ were mostly represented by sublayer C specimens, and occasionally, by specimens of sublayers A and B.

Rate of destructuration

For structured clays, the term structure refers to size, shape and orientation of the particles and bonds between them [Crawford 1986]. During the IL oedometer test, structural characteristics of the specimen are changed in the process of destructuration. Continuous sensitivity data obtained using the approach c enabled evaluation of characteristics of the destructuration process.

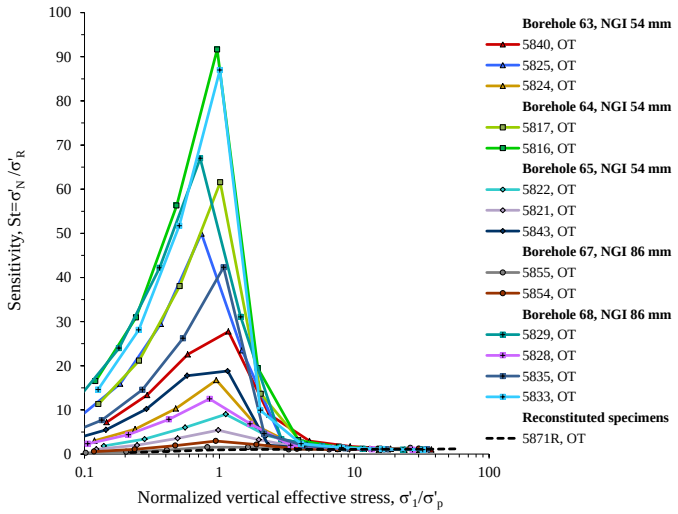

Figure 6.18 Sensitivity values in IL oedometer test related to σ'_1/σ'_p.

In Figure 6.18 sensitivity data of IL oedometer test specimens are related to vertical effective stress normalized with preconsolidation pressure. S_t was shown to rise in reloading, while within NC stress range it progressively declined. Sensitivity maximum complied with the preconsolidation pressures interpreted. Furthermore, due to characteristics of approach c, maximum sensitivity values complied with specific volume at yield. For these reasons $S_{t\,max}$ was taken as representable of initial sensitivity of the specimen.

Aiming to identify influence of specimen quality on rate of destructuration, S_t values are related to specific volume in Figure 6.19. Based on Perniö clay IL oedometer test results, rate of destructuration for high quality specimens was well represented by Equation 6.9, while that of poor quality specimens was defined by Equation 6.10. Thus in IL oedometer test, high quality specimens were more rapidly destructured.

$$S_{tHQ} = 0.0074\, e^{2.258v} \tag{6.9}$$

$$S_{tLQ} = 0.0809\, e^{1.2259v} \tag{6.10}$$

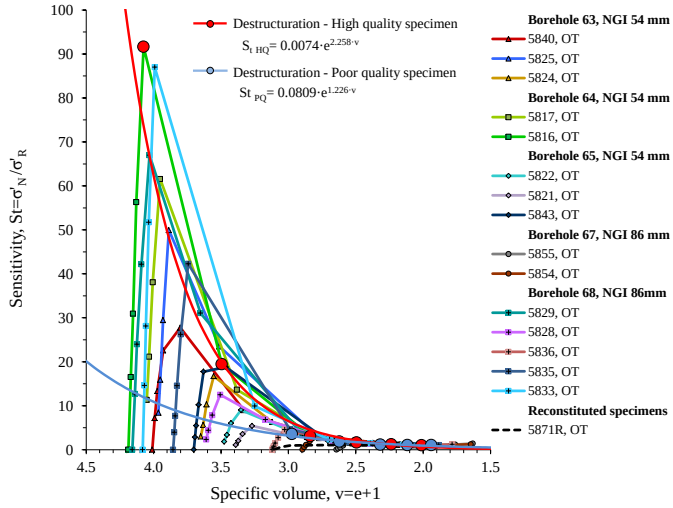

Figure 6.19 Sensitivity values in IL oedometer test related to specific volume.

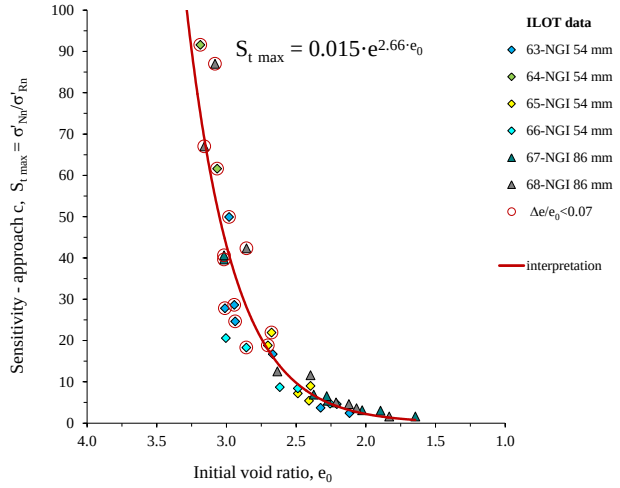

Figure 6.20 Maximum sensitivity values in IL oedometer test related to initial void ratio.

Figure 6.20, presents values of $S_{t\,max}$ defining IL oedometer test specimens plotted vs. corresponding values of initial void ratio. Unlike sensitivity values obtained using approach a and b, $S_{t\,max}$ showed clear exponential relation to e_o, well represented by Equation 6.11. The results thus showed sensitivity of the specimens being exponentially related to amount of water they contain.

$$S_{t\max} = 0.015\, e^{2.66 e_0} \tag{6.11}$$

6.1.8 Creep parameters

Implementation of automated measurement of specimen compressibility allowed adequate amount of data being gathered for explicit interpretation of creep behavior. In addition, load increments being implemented in regular 24 h periods ensured high accuracy of the results obtained. The data was used for interpretation of secondary compression coefficient. Furthermore, the creep response was related to the compression response of the specimen in terms of $c_{\alpha e}/c_c$ ratio. Finally, both secondary compression coefficient and $c_{\alpha e}/c_c$ were examined in relation to vertical effective stresses implemented in oedometer testing and related to stratigraphic characteristics of Perniö deposit and sample quality.

Secondary compression coefficient $c_{\alpha e}$

To examine compressibility of Perniö clay in relation to time, values of the secondary compression coefficient in IL oedometer tests were defined. The values were obtained for identical duration sequence from 6th to 24th h of each load step, when changes of void ratio with logarithm of time were linear (see Figure 6.21).

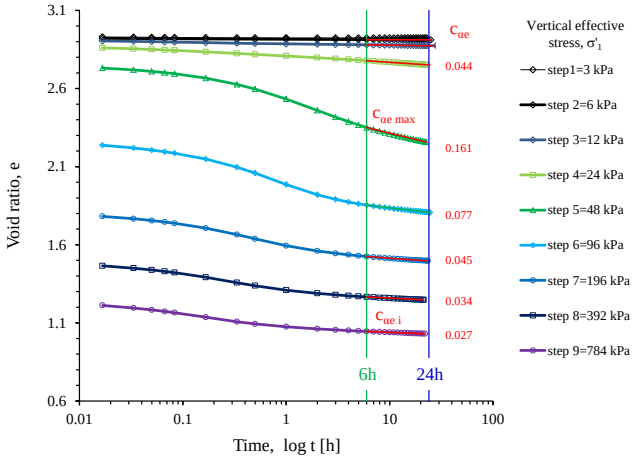

Figure 6.21 Interpretation of secondary compression coefficient, ILOT 5842.

The magnitude of the secondary compression coefficient depended upon the strain level, and indirectly stress level to which specimen was subjected [Graham et al. 1983]. Extreme values of secondary compression coefficient are re-

lated to depth in Figure 6.22. Maximum values of secondary compression coefficient $c_{\alpha e\ max}$, occurred at stress levels following the yield. Minimum values however, identified specimen response at high stress levels at the end of consolidation test, and were thus termed intrinsic $c_{\alpha e\ i}$.

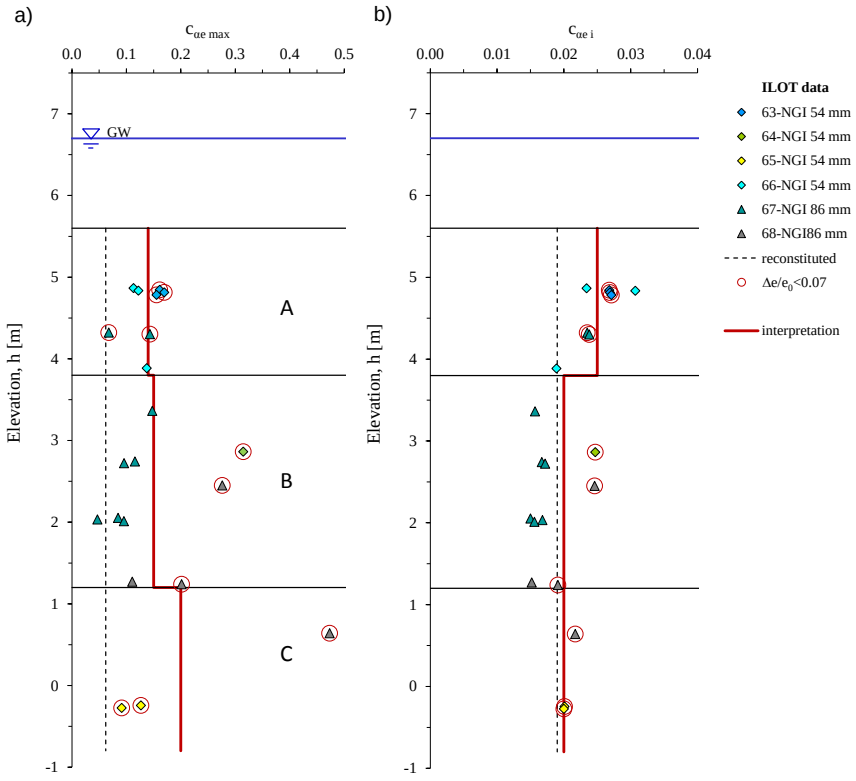

Figure 6.22 Secondary compression coefficient in IL oedometer tests; a) maximum secondary compression coefficient $c_{\alpha e\ max}$, b) Intrinsic secondary compression coefficient $c_{\alpha e\ i}$

Depth distribution of maximum secondary compression coefficients is presented in Figure 6.22 a). The magnitudes of $c_{\alpha e\ max}$ varied considerably from 0.047 to 0.47. Average $c_{\alpha e\ max}$ representing specimens of sublayer A was 0.14. In contrast to those in sublayer A, results within sublayers B and C were highly scattered. Furthermore, the results indicated quality of the specimens having considerable influence on magnitude of the values obtained. Average $c_{\alpha e\ max}$ within sublayer B was 0.15. Poor quality specimens however, regularly exhibited rather low $c_{\alpha e\ max}$ of ~0.11. In contrast, $c_{\alpha e\ max}$ representing specimens of good quality was 0.30. The highest scatter overall identified sublayer C, i.e. $0.127<c_{\alpha e\ max}<0.473$, with most probable target being ~0.20. In comparison, average $c_{\alpha e\ max}$ obtained on reconstituted specimens was 0.062.

Figure 6.22 b) shows values of intrinsic secondary compression coefficients vs. depth. Resulting values ranged narrowly from 0.015 to 0.030. The highest $c_{\alpha e\ i}$ were identified in sublayer A with an average of 0.025. Within sublayers B and C average $c_{\alpha e\ i}$ values were less, i.e. 0.20. The highest scatter occurred in

sublayer B. Low values of ~0.15 were exhibited by disturbed specimens, while high values identified on good quality specimens matched those in sublayer A. Finally, average $c_{\alpha e\,i}$ on reconstituted specimens was 0.019.

Overall, difference between maximum $c_{\alpha e\ max}$ and intrinsic secondary compression coefficients $c_{\alpha e\,i}$ in IL oedometer tests on Perniö clay was considerable. Based on specimens of the highest quality, secondary compression coefficient decreased in magnitude from 0.14, 0.30 and 0.47 in respective sublayers toward intrinsic values of 0.025 in sublayer A, and 0.020 in sublayers B and C.

$c_{\alpha e}$ stress dependency

Coefficient of secondary compression $c_{\alpha e}$, varies with the ratio of vertical effective stress σ'_1 and preconsolidation pressure σ'_p [Graham 1983]. Figure 6.23 examines stress dependency of $c_{\alpha e}$ measured on Perniö clay. The results include data on both reconstituted and natural specimens. The results are distinguished with respect to sublayer and related to sample quality using $\Delta e/e_o$ criteria. Overall, change in $c_{\alpha e}$ with σ'_1/σ'_p was similar for all of the specimens. In the overconsolidated range, $c_{\alpha e}$ was low, yet proportionally stress dependent. It was following the yield that the values of $c_{\alpha e}$ abruptly rose to maximum. With further increase in σ'_1/σ'_p, secondary compression coefficients gradually declined towards intrinsic value of similar intensity. Thus, while $c_{\alpha e\,i}$ complied well, $c_{\alpha e\ max}$ varied considerably. Examined with respect to sublayer of origin, response of low sensitivity sublayer A specimens was very uniform. Most of the curves exhibited peak $c_{\alpha e}$ corresponding to ~0.016, somewhat exceeding those on low quality specimens with $c_{\alpha e\ max}$~0.012. In contrast, results on specimens of sublayers B and C were highly scattered. Most specimens exhibited peak at 0.010. However, good quality specimens of both sublayers exhibited 2 to 5 times higher maximum $c_{\alpha e}$ response. The highest values $c_{\alpha e}$ >0.15, were measured on specimens from NGI 86 profile 68, and NGI 54 sampled profiles 64 and 63. Common feature in tests exhibiting high $c_{\alpha e}$ values was close match of load increment intensity and preconsolidation pressure level. In contrast to those on natural, $c_{\alpha e}$ values measured on reconstituted specimens were overall the lowest. Thus, specimen structural characteristics had the crucial influence on magnitude of creep response. Indeed, maximum $c_{\alpha e}$ values were related to the highest rate of destructuration exhibited around the preconsolidation pressure [Graham et al. 1983, Karstunen et al. 2008b, Yin et al. 2011]. The maximum $c_{\alpha e}$ occurred within $1.4<\sigma'_1/\sigma'_p<2.5$ for all the specimens considered. Thus, stress ratio range characterizing maximum $c_{\alpha e}$ values was less compared with that defining peak gradient in compression λ, i.e. $2.0<\sigma'_1/\sigma'_p<3.0$. To conclude, owing to more pronounced destructuration effect following yield, high quality specimens exhibited the highest $c_{\alpha e}$. For disturbed specimens in contrast, effect of $c_{\alpha e}$ stress dependency was less exposed. The values of $c_{\alpha e}$ converged to a constant value for high stress ratio levels when the interparticle bonds were destroyed [Yin et al. 2011]. Target value of $c_{\alpha e\ i}$ of 0.020 was reached by poor quality specimens at lower σ'_1/σ'_p compared to that required in tests on specimens of good quality.

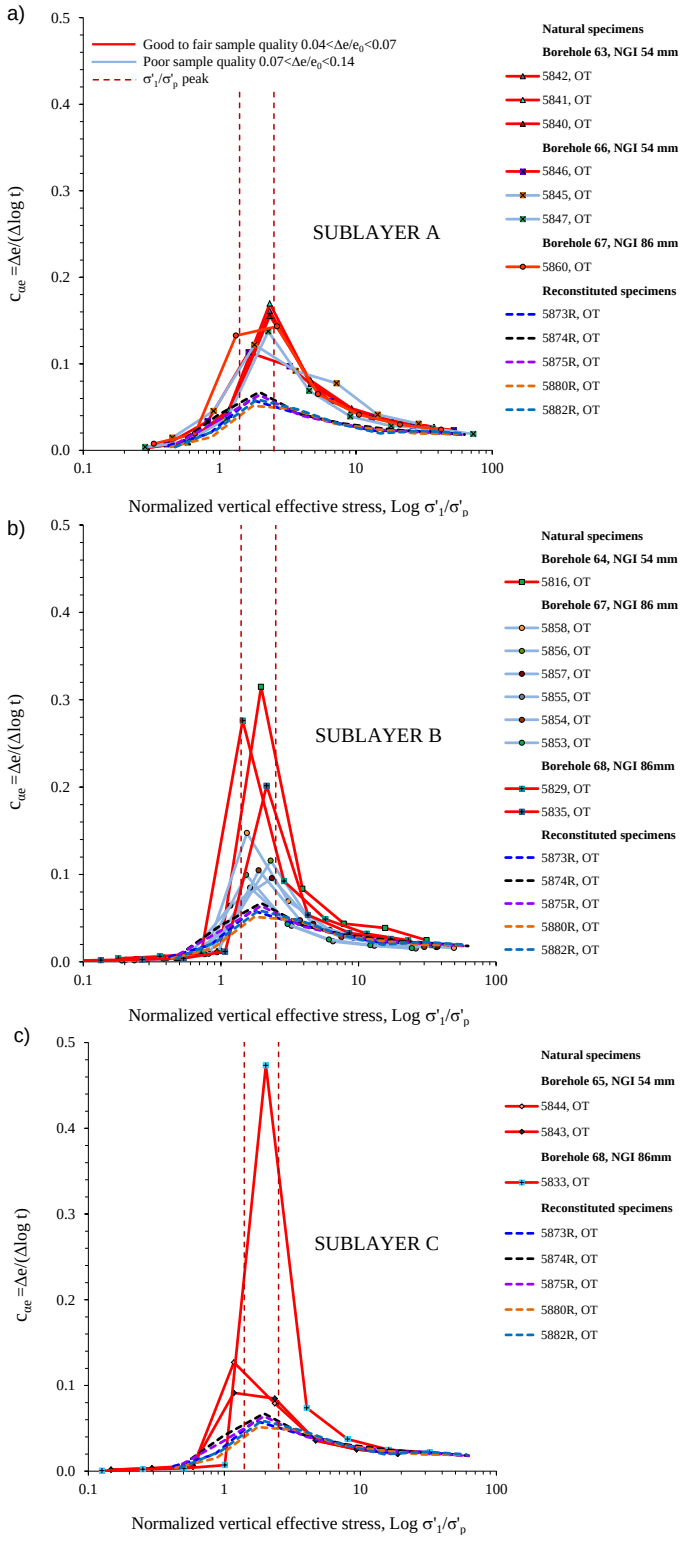

Figure 6.23 Stress dependency of secondary compression coefficient $c_{\alpha e}$ in IL oedometer tests on Perniö clay; a) sublayer A, b) sublayer B, and c) sublayer C.

c_α/c_c parameter

In order to relate creep response to that of stress related compressibility characteristics, secondary compression coefficients were scaled with compression indices and expressed with c_α/c_c relation. Because of unification of time and stress related characteristics the ratio has high importance in representing compression response of structured clay. It is commonly assumed that the c_α/c_c is fairly constant for a given soil, with values occurring between 0.04 and 0.08 [Mesri & Castro 1987]. However, if evaluated for each increment of oedometer test, c_α/c_c for clays is observed to be significantly higher at stresses close to yield [Graham et al. 1983, Graham 2006]. This fact has significant implications on compressibility of clays. If c_α/c_c is constant the compression curves for various load increment durations in IL tests, or strain-rates in CRS tests are parallel [Graham et al. 1983]. To define Perniö clay compressive response, c_α/c_c values were firstly evaluated with respect to sampling depth. Later, c_α/c_c stress dependency curves were examined in detail.

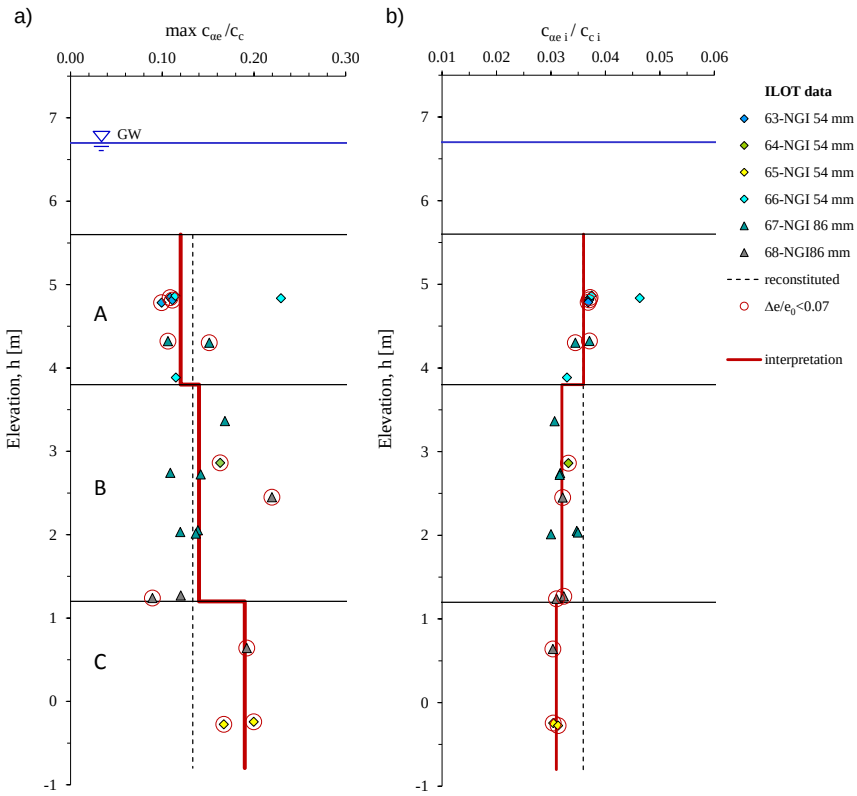

Figure 6.24 $c_{\alpha e}/c_c$ parameter in IL oedometer tests; a) maximum values of $c_{\alpha e}/c_c$, and b) intrinsic $c_{\alpha e\,i}/c_{c\,i}$.

Maximum and intrinsic c_α/c_c values obtained in Perniö clay oedometer tests are presented in Figure 6.24. Interpretation of c_α/c_c parameter demands ratio of component values to be evaluated at identical loading increment. As shown

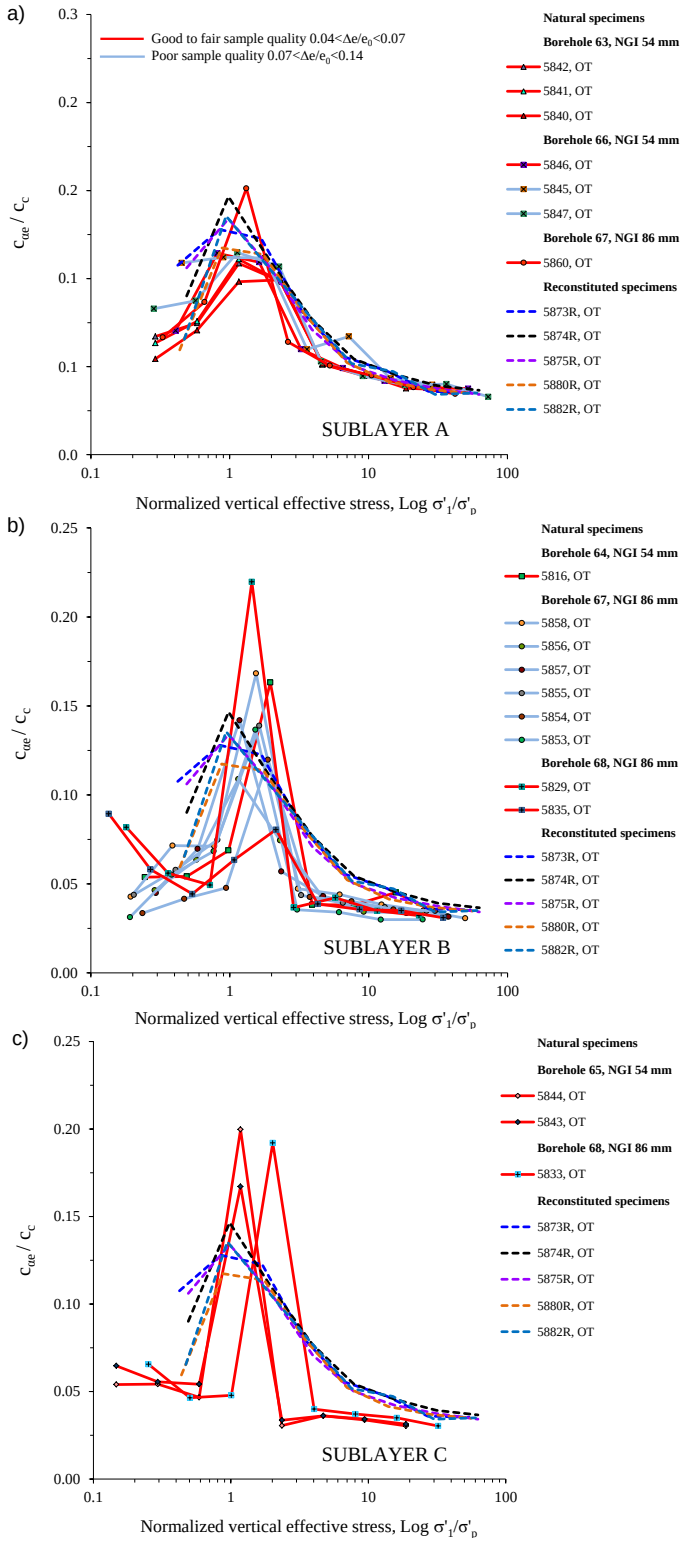

Figure 6.25 Stress dependency of c_α/c_c in IL oedometer tests on Perniö clay; a) sublayer A, b) sublayer B, and c) sublayer C.

in Figure 6.24 a), the maximum c_α/c_c values thus obtained amounted 0.12, 0.14 and 0.19, in respective soft clay sublayers A, B and C. In contrast, maximum c_α/c_c representing reconstituted specimens was 0.13. Thus, c_α/c_c values on natural and reconstituted Perniö clay exceed commonly accepted limits.

Intrinsic c_α/c_c values determined at final loading step when specimen was destructured are shown in Figure 6.24 b). The values appeared in narrow range amounting 0.036, 0.032 and 0.031, in respective soft clay sublayers. Thus, depth distribution pattern of intrinsic c_α/c_c opposed that of maximum c_α/c_c values. Intrinsic ratio representing response of the reconstituted specimens was 0.036, thus corresponding to c_α/c_c intrinsic obtained on low sensitivity natural specimens of sublayer A.

c_α/c_c stress dependency

Entire set of c_α/c_c values obtained during IL oedometer tests are in Figure 6.25 related to σ'_1/σ'_p. Responses measured in respective soft clay sublayers are distinctively presented. Overall, c_α/c_c in reloading stress range were low, typically <0.75, and rose with load intensity. Maximum values of c_α/c_c occurred at stress levels corresponding to yield or somewhat above, i.e. $1<\sigma'_1/\sigma'_p<2$. Thereafter, as a result of destructuration, ratio values decreased toward intrinsic c_α/c_c values of ~0.036. In low sensitivity sublayer A, maximum c_α/c_c values were the lowest. Furthermore, response of sublayer A specimens within NC was marked with asymptotic decrease of c_α/c_c, resembling that of reconstituted material. In contrast, maximum c_α/c_c values obtained in sublayers B and C were notably higher. Additional feature was also present, that of abrupt decline of c_α/c_c values toward intrinsic values. Thus, in contrast to specimens of sublayer A, peak c_α/c_c values were reduced in single load increment following the yield, while post peak c_α/c_c were fairly constant and less. Overall, maximum c_α/c_c values were proportional to specimen quality. Post yield c_α/c_c decline was the most rapid in high quality specimens, followed by poor quality specimens and finally being progressive in reconstituted specimens. Results of IL oedometer test at LIR=1 clearly show that c_α/c_c is not constant. Based on results presented herein c_α/c_c values varied from 0.22 after the yield, to 0.030 at high effective stress levels.

6.1.9 Strain-rate parameters

Isotache in IL oedometer test

Digital data acquisition during IL oedometer tests enabled interpretation of the results using isotache concept [Šuklje, 1957]. In the approach compressive behavior is evaluated based on strain-rates experienced by the specimen. Average rate of strain, considering entire IL test is typically rather low, i.e. <0.30 %/h, and depends on the factors such as magnitude of the loading increments and compressibility of the specimen. For example, average strain-rate in tests on reconstituted specimens is less than that experienced by natural ones, i.e.

0.20 %/h. However, if strain-rates are addressed as average during specific loading step, values obtained considerably exceed above defined. Indeed, average value during specific loading increment can rise up to 0.80 %/h. Finally, if strain-rates are evaluated for sequential readings during certain load increment, strain-rates experienced by the specimen range broadly, from ~4 %/h to 100%/h in the first minute of loading, to ~0.002 %/h at the end of one day. Thus, although the specimen in IL test compresses at an average rate not faster than 0.30 %/h, the actual strain-rates during the test vary considerably depending upon the intensity of applied load, specimen quality and time elapsed from load application.

Figure 6.26 a) presents entire set of sequential strain-rates measured during provisionally selected IL oedometer test 5860 on natural specimen. For loading steps within NC stress range, strain-rates at the onset of loading varied from 1 to $2 \cdot 10^{-4}$ s^{-1}. Furthermore, strain-rates reached following the 24 h period occurred between $2 \cdot 10^{-8}$ and $2 \cdot 10^{-7}$ s^{-1}, and were typically reciprocal to intensity of the load increment. In OC range, extreme strain-rates exhibited in 24 h loading steps were somewhat lower compared to those in NC range, and were overall proportional to intensity of load implemented.

Following the approach by Leroueil et al. [1985], sequential strain-rates were used to interpret isotache curves by identifying sets of specific volume data corresponding to strain-rates of $6 \cdot 10^{-5}$, $3 \cdot 10^{-5}$, $1 \cdot 10^{-5}$, $3 \cdot 10^{-6}$, $1 \cdot 10^{-6}$, $3 \cdot 10^{-7}$ and $1 \cdot 10^{-7}$ s^{-1}. The obtained isotache curves corresponding to NC stress range are presented in semi-logarithmic plot of vertical effective stress vs. specific volume shown in Figure 6.26 b). When evaluated in semi-logarithmic plot, isotache curves altogether progressively converged with decrease of specific volume. Furthermore, with decrease of strain-rate distance between isotache lessened. Stress-strain curve in IL testing closely corresponded to isotache obtained for $1 \cdot 10^{-7}$ s^{-1}. In Figure 6.26 c), isotache in NC stress range are related to vertical effective stresses in linear plot. Distance between isotache was revealed to be stress dependent. At stress levels following the yield, distance between isotache progressively increased with rise of vertical stress up to threshold value of 274 kPa, i.e. 7^{th} loading step. However, at stress levels above 274 kPa, isotache remain about parallel. The threshold vertical stress was indicative of level where sensitivity values interpreted according to approach C become less than 1. Furthermore, the threshold stress level normalized with yield corresponded to σ'_1/σ'_p of 10.55. In Figure 6.24 and Figure 6.25 examining c_α and c_α/c_c stress dependency, above σ'_v/σ'_p of 10.55 the parameters were about constant. These results confirm Nash [2010], i.e. if the isotache are parallel their position is not influenced by the destructuration process. Furthermore, results suggest normalization of isotache curves with preconsolidation pressure being limited to stress range prior complete destructuration. However, if plotted in semi-logarithmic vertical stress vs. specific volume plane, isotache curves at high stress levels will apparently coincide. Thus, hypothesis of unique compression response for normalized isotache curves is from practical point of view, acceptable.

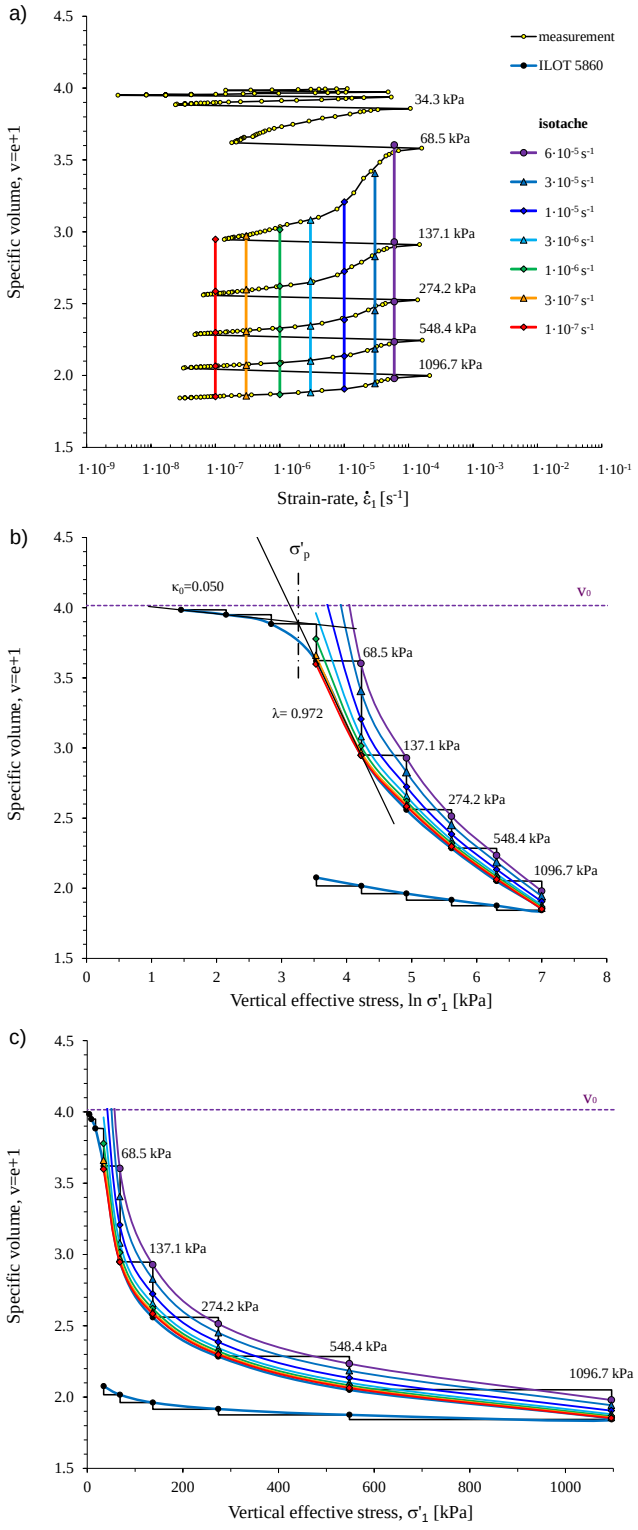

Figure 6.26 Isotache of Perniö clay in IL oedometer test 5860.

Strain-rate coefficient β

To account for strain-rate influence on stress-strain behavior of structured clays, Yin et al. [2011] identified two parameters; strain rate coefficient β, and fluidity index μ. Strain rate coefficient β is defined by Equation 6.12; where gradient λ_i represents compressibility of destructured/reconstituted specimen in NC stress range, κ_0 is slope of reloading line, and $c_{\alpha e\,i}$ is intrinsic secondary compression coefficient. The approach was used for examination of strain-rate effects in IL oedometer tests on Perniö clay. Compressibility of the destructured/reconstituted specimen can be defined in two equivalent ways, i.e. Equations 6.12 and 6.13. Both sets of results are critically evaluated.

$$\beta_1 = \frac{\lambda_i - \kappa_0}{c_{\alpha ei}} \tag{6.12}$$

$$\beta_2 = \frac{\lambda_R - \kappa_0}{c_{\alpha ei}} \tag{6.13}$$

In Figure 6.27 a) values of β_1 are related to sampling depth. Thus, compressibility of destructured material was defined by intrinsic slope of destructured natural specimen λ_i. The results were consistent and exhibited low scatter, i.e. $4.84<\beta_1<11.66$. Furthermore, the results identified β_1 in sublayer A being less, compared to those in underlying sublayers. Considering good and poor quality specimens, β_1 values in sublayers B and C complied in magnitude. Average β_1 value in sublayer A was 9.0, while that in sublayers B and C was 10.6. Finally, average β_1 value representing reconstituted material was 9.3, thus corresponded with that on sublayer A specimens.

Figure 6.27 b) shows distribution of β_2 values vs. sampling depth. Thus, compressibility of destructured material was defined by reconstituted specimen response in NC stress range λ_R. Scatter of resulting β_2 values was high, i.e. $6.8<\beta_2<15.14$. Average β_2 values in sublayers A, B and C, amounted 7.5, 12.0 and 9.5, respectively. Within sublayer B however, results were highly influenced by specimen quality. Based on poor quality specimens average β_2 was 13.5, while considering good quality specimens representative value was as low as 8.5. Thus, depending on specimen quality, β_2 distribution changed from sequential increase with depth, to that of β_2 values in sublayer B considerably exceeding values in sublayers embedding it. Finally, average β_2 value representing reconstituted specimens was 10.9.

To conclude, one of the main effects of sample disturbance is reduction of specific volume. Thus, tests on poor quality specimens were initiated from relatively lower specific volume. Consequently, in tests on poor quality specimens intrinsic compressibility λ_i was less compared to that measured on high quality specimens sampled at the same depth. The effect influenced β obtained using Equation 6.12, i.e. the effects of sample disturbance on resulting β values were reduced.

Fluidity parameter μ

According to Yin et al. [2011], fluidity index μ is defined by Equations 6.14 and 6.15:

$$\mu = \frac{c_{\alpha ei}\left(M_c^2 - \alpha_{K0}^2\right)}{\tau(1+e_0)(M_c^2 - \eta_{K0}^2)} \tag{6.14}$$

$$\mu = \dot{\varepsilon}_{vK0}^{r} \frac{\lambda_i - \kappa}{\lambda_i} \frac{M_c^2 - \alpha_{K0}^2}{M_c^2 - \eta_{K0}^2} \tag{6.15}$$

with:

$$\dot{\varepsilon}_{vK0}^{r} = \frac{\lambda_i}{\lambda_i - \kappa} \frac{c_{\alpha ei}}{(1+e_0)\tau} \tag{6.16}$$

where;

$\dot{\varepsilon}_{vK0}^{r}$

is reference strain-rate, M_c is slope of critical state line in compression, η_{Ko} is consolidation stress ratio and τ is test duration. Compressibility of destructured/reconstituted material in Equation 6.16 can be defined either with λ_R or λ_i. Depending on the approach, two sets of reference strain-rate data were obtained. Using λ_R instead of λ_i, the reference strain-rate values were negligibly higher. Using Equation 6.14 or 6.15 however, unique set of fluidity parameters were obtained. The main parameters defining magnitude of fluidity index are initial specific volume v_o, intrinsic secondary compression coefficient $c_{\alpha e\, i}$ and slope of the critical state in compression M_c. Furthermore, $c_{\alpha e\, i}$ and M_c are intrinsic parameters, while v_o is sample quality dependent. Since the v_o is related to the sampling disturbance, μ is influenced by sampling quality as well. Same conclusion is valid for strain-rate coefficient β, via κ_o. This results are opposed to conclusion of Yin et al. [2011] stating; uniqueness of stress-strain-strain rate behavior suggests that the viscosity parameters are independent of destructuration process, even when all the bonds are destroyed and the soil tends to reconstituted state.

Figure 6.27 c) shows values of fluidity index vs. depth. Results occurred within narrow limits $0.007<\mu<0.011$. Values of fluidity index decreased with depth, amounting in average 0.0095, 0.0083 and 0.0080 in soft clay sublayers A, B and C. Average fluidity index obtained on reconstituted specimens was 0.0093, thus closely corresponding to results in sublayer A. Results indicated magnitude of μ being proportional to sampling quality.

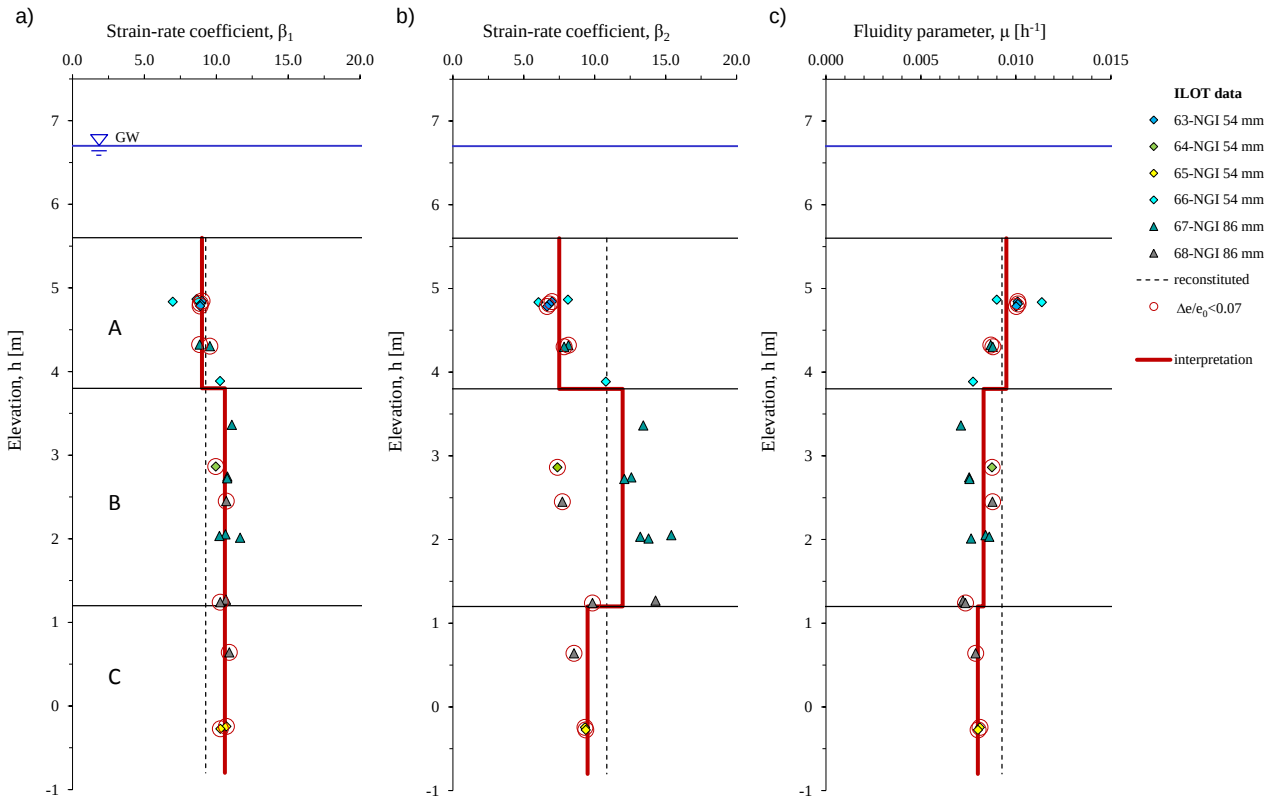

Figure 6.27 Strain-rate parameters in IL oedometer tests; a) strain-rate coefficient β_1, b) strain-rate coefficient β_2, and c) fluidity index μ.

6.2 CRS oedometer test results

6.2.1 General overview

Figure 6.28 presents compressibility response of entire set of CRS oedometer test performed on Perniö clay. In the following results are briefly outlined. Latter, specific features such as sample quality, compressibility, and bonding, are examined in detail with emphasis on the influence of strain-rate.

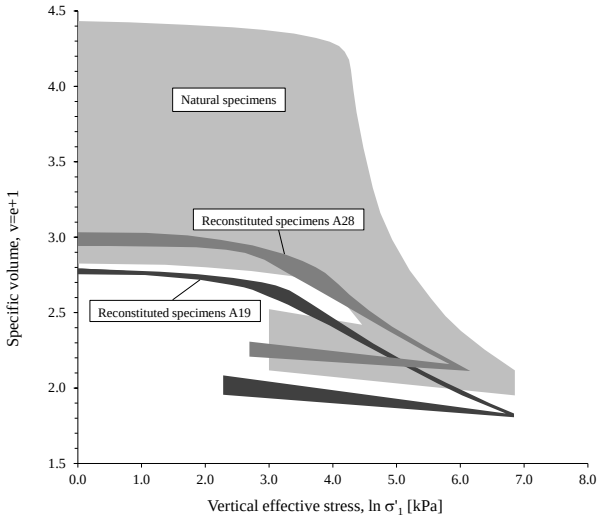

Figure 6.28 Compressibility of Perniö clay in constant rate of strain oedometer tests.

CRS results on reconstituted specimens

CRS tests on reconstituted specimens were performed on material from cylinders A19 and A28, obtained in distinctive remoulding batches R1 and R4. Reflecting water content following the reconstitution, average e_o amounted 2.00 and 1.79 for A28 and A19, respectively. Response of reconstituted specimens was evaluated at three distinctive constant strain-rate levels. Influence of strain-rate was manifested as proportional offset of the compression curve towards higher vertical effective stresses. The effect was the most pronounced at stresses slightly prior and following the yield. Average κ_o for A19 and A28 amounted 0.047 and 0.045 respectively, being less compared to 0.057 in IL oedometer tests. NC response in CRS tests identified reconstituted material being considerably stiffer than natural. Average λ of 0.231 and 0.270 for respective A19 and A28 material confirmed influence of initial water content on compression response [Hong et al. 2010]. Furthermore, λ for A28 complied with that on IL oedometer specimens remoulded within the same batch. Average slope in compression at high stress levels λ_i, amounted 0.192 and 0.231 for A 19 and A 28, representing ~84% of that following the yield. With maximum compression level reached, reconstituted specimens of certain test group were unloaded to identical level of vertical effective stress. Swelling response was

similar, except in tests at the highest strain-rate exhibiting distinctively higher values. Average κ for respective groups A19 and A28 amounted 0.043 and 0.036, thus negligibly less than κ_o. Proportionally to strain-rate, preconsolidation pressures of reconstituted specimens ranged from 12.5 to 21.0 in A19, and from 13.0 to 28 in A28. Distinction in σ'_p range was probably related to difference in size of the specimens, i.e. 1.5 cm thickness and 15 cm² area in A19 compared to 2.0 thicknesses and 20 cm² area in A28.

CRS results on natural specimens

CRS oedometer test results on natural specimens were characterised with considerable scatter in compression response. Additionally to natural variance of Perniö deposit and effects of sample disturbance, compression curves were influenced by magnitude of strain-rate implemented. To ensure comparability of the results, CRS oedometer tests were performed within 8 test groups with material of each group originating from the same sampling cylinder. Thus, dissimilarities in material properties were restricted to variance in sampling quality within the cylinder, and predominantly different extent of disturbance in specimen preparation. As shown in Table 6.1, CRS test groups evaluated all stratigraphic units of Perniö soft clay, i.e. 44B, 63A, 63B, 65A, 65C, 66C, 67A and 68C. Effects of the inhomogeneity of the deposit were considered by at least two test groups being performed on the material of the same sublayer. To assess influence of sampling quality, six groups were made on material obtained with NGI 54, while later two evaluated material sampled with NGI 86 mm sampler. To estimate effects of specimen size, 44B tests considered specimens 1.5 cm thick and 15 cm² in area, while remaining test groups examined samples of 2.0 cm thickness and 20 cm² area. To provide substantial amount of data for concise interpretation of strain-rate effects, each group included tests under conditions of at least three different constant strain-rate levels.

Table 6.1 Conditions in CRS oedometer testing of natural Perniö clay.

Test series	Sampling Point No.	Sublayer	Sampling method	Cylinder no.	Absolute depth h [m]	Thickness h_o [cm]	Diameter d [cm]	Area A [cm2]
I	63	sublayer A	NGI 54 mm	208	3.90 - 4.14	2.0	5.05	20
II	65	sublayer A	NGI 54 mm	55	4.10 - 4.28	2.0	5.05	20
III	67	sublayer A	NGI 86 mm	100	5.10 - 5.32	2.0	5.05	20
IV	44	sublayer B	NGI 54 mm	51	2.25 - 2.43	1.5	4.37	15
V	63	sublayer B	NGI 54 mm	33	1.67 - 1.79	2.0	5.05	20
VI	65	sublayer C	NGI 54 mm	67	-0.17 - 0.02	2.0	5.05	20
VII	66	sublayer C	NGI 54 mm	209	0.79 - 1.21	2.0	5.05	20
VIII	68	sublayer C	NGI 86 mm	88	0.71 - 0.86	2.0	5.05	20

Altogether, e_o of natural specimens varied considerably from 1.85 to 3.45. Compared to values in IL oedometer tests, reloading slope κ_o was generally higher, and varied from 0.024 to very high 0.158. Furthermore, slope of the normal compression line λ, varied from 0.421 to exceptionally high 4.032. Ex-

treme λ values, i.e. three times above maximum values in IL oedometer tests, represented 66C high quality specimens of quick clay registered at +0.79 to 1.05 absolute. Intrinsic compression slope of destructured specimens satisfying $\lambda_i/\lambda_R<25\%$, varied from 0.204 to 0.302, thus complied well with corresponding values in IL oedometer tests. Slope of the swelling line κ varied from 0.027 to 0.104. Defined with single unloading point to effective stress typically less than σ'_p, resulting κ values were less reliable than those in IL tests. Nevertheless, upper limit notably exceeded IL oedometer test values, while the highest κ were obtained on very sensitive specimens of 66C group.

Magnitude of strain-rate defined position of the compression curve. Significance of the strain-rate effects on compressibility of natural specimens is examined in Figure 6.29, where preconsolidation pressures are related to sampling depth. In CRS tests at the lowest strain-rates, σ'_p corresponded to effective overburden, i.e. $\sigma'_p/\sigma'_{vo}\sim1.0$. However, with σ'_p being proportionally strain-rate dependent, values on specimens compressed at high strain-rates occurred within $1.3<\sigma'_p/\sigma'_{vo}<2.3$, depending on the sublayer and quality of the specimen considered. In following, various aspects of compressibility are examined with respect to effects of structure and strain-rate imposed. In addition, stress, strain and strain-rate dependency of compression characteristics in selected high quality test groups; 63A, 63B, 65C and 66C, are elaborated in detail.

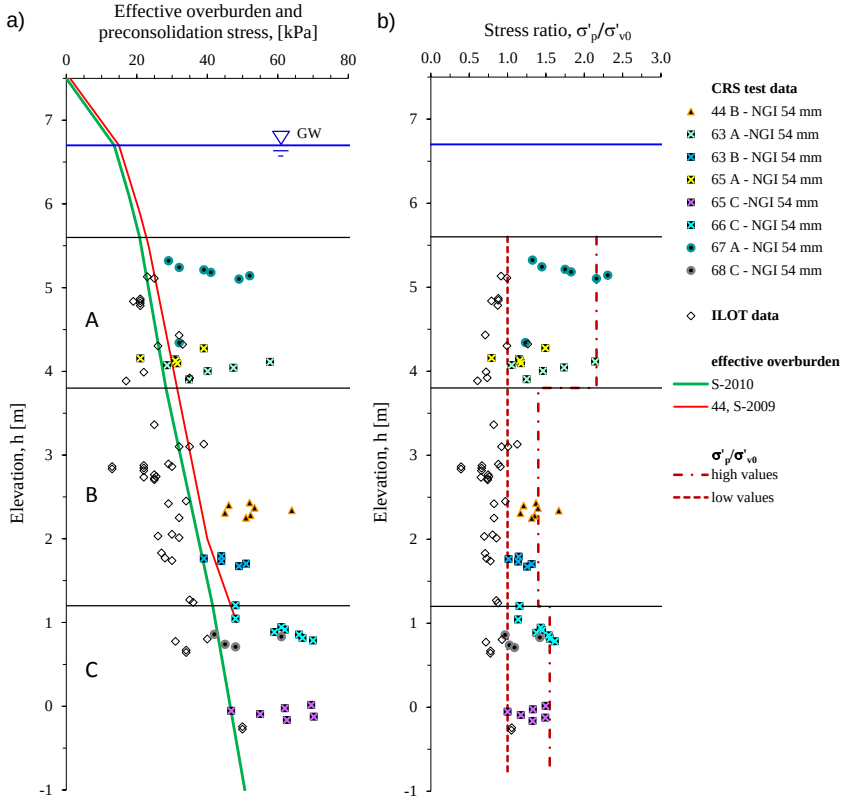

Figure 6.29 Overburden stress distribution and preconsolidation pressure in CRS oedometer tests.

6.2.2 Initial state parameters

Water content

In Figure 6.30 a), water content values of CRS specimens are related to sampling depth. S-2010 CRS specimens identified average w_o of 101.3, 79.0, and 106.8 % in respective soft clay sublayers. The results complied with data measured on IL oedometer specimens and those following the sampling. Some specimens within sublayers A and B exhibited markedly low w_o indicating considerable sample disturbance. In contrast, CRS specimens in the upmost segment of sublayer C were characterized with exceptionally high w_o>110%.

Initial void ratio

Initial void ratio values determined on CRS specimens are shown in Figure 6.30 b). Considering S-2010, average e_o of CRS specimens were 2.7, 2.1 and 2.9 in respective soft clay sublayers. High scatter of e_o reflected inhomogeneity of the deposit and considerable variation in specimen disturbance. CRS specimens within sublayer A exhibited 2.13<e_o<3.04, while those obtained at depths of sublayer B were 1.85<e_o<2.32. The highest e_o values overall were measured in sublayer C with 2.40<e_o<3.45. Exceptionally high e_o>3.0 identified quick clay material in the upmost portion of the zone C.

Unit weight

Initial unit weight values determined on CRS specimens shown in Figure 6.30 c), comply with general response identifying Perniö clay deposit. Based on S-2010 CRS specimens, average γ in sublayers A and C was 14.3 kN/m^3, while that in sublayer B amounted 15.3 kN/m^3. Within zones A and B, several specimens exhibited considerably higher γ values indicating sample disturbance. Lowest values overall identified upmost section of zone C with γ<14.0 kN/m^3.

6.2.3 Sample quality

$\Delta e/e_o$ criteria

Figure 6.31 a) relates $\Delta e/e_o$ determined on CRS oedometer specimens to sampling depth. The criteria identified majority of CRS specimens being of good to fair (0.04<$\Delta e/e_o$<0.07), and very good to excellent quality ($\Delta e/e_o$<0.04). Only three specimens were identified poor, i.e. $\Delta e/e_o$>0.07. The results thus indicated that CRS specimens were of substantially higher quality than those in IL oedometer test (see Figure 6.4 a). However, void ratio change up to the level of effective overburden Δe was highly dependent upon the strain-rate implemented in the actual test. Being influenced by testing conditions, $\Delta e/e_o$ approach was not appropriate for comparison of initial quality of the specimens or evaluation of sampling performance. The method adequately identified true measure of sample disturbance prior to σ'_{vo}. However, since the corresponding void ratio change was dependent upon the strain-rate, the method was suitable for comparison of specimens tested at identical strain-rate conditions only.

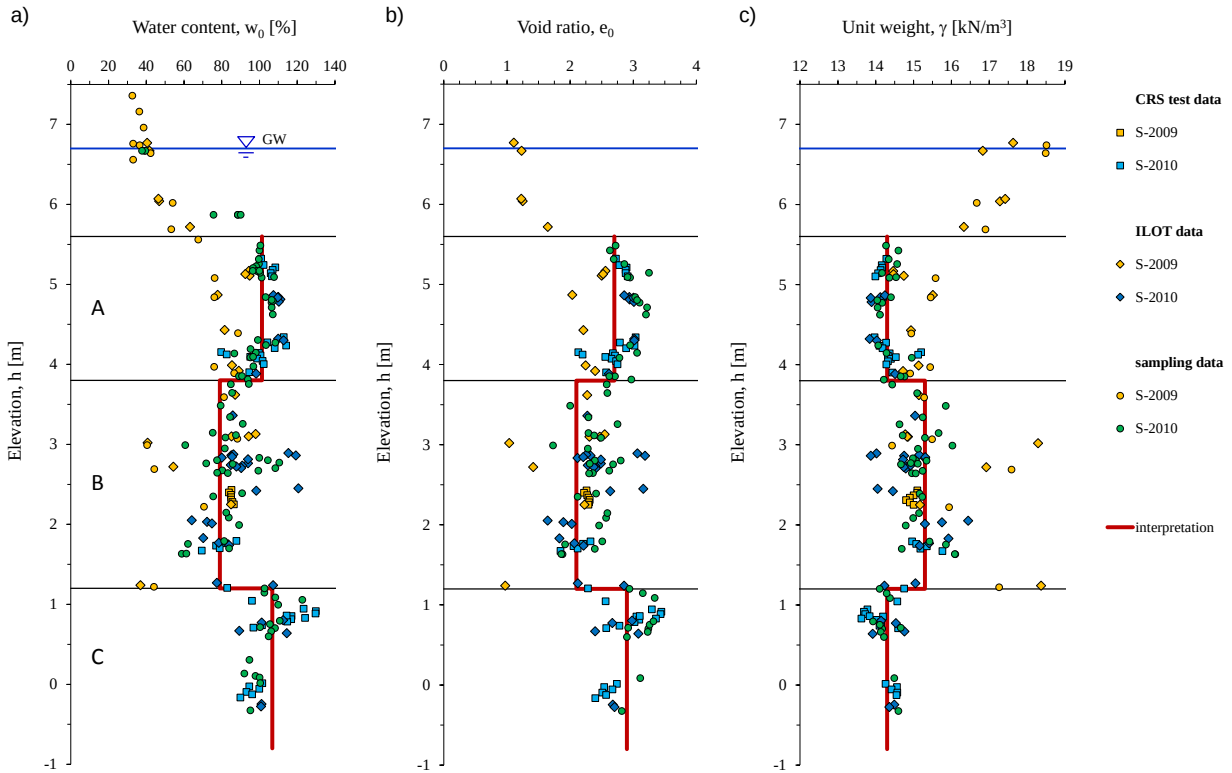

Figure 6.30 Initial state parameters of CRS oedometer specimens, a) water content, b) void ratio, and c) unit weight.

w/γ criteria

For saturated specimens with G_s of 2.7, w/γ is directly related to e_o. Thus conveniently, specimens satisfying w/γ≥7 %/kN/m³ are characterised with v_o≥3.71. Disadvantage of w/γ specimen quality criteria is in inability to recognise effects of in situ conditions on specimen initial properties. Although among specimens from zones A and C the criteria identified both poor and good quality specimens, all of the specimens in zone B were categorised as poor. If generally lower w_o of specimens in zone B was not caused by sampling, yet was instead an in situ characteristic of Perniö deposit, than w/γ identification of specimen quality is limited to corresponding depths. However, water content and unit weight values determined following sampling or prior testing are not influenced by test conditions. Thus, w/γ is reliable specimen quality classification if specimens subjected to various testing conditions are to be compared. If adequate attention is given to ensure consistent specimen preparation, w/γ values are to minimal extent influenced by processes other than sampling, transport and storage, and are therefore the values to be considered if meaningful sampler performance evaluation is to be made.

Figure 6.31 b) presents water content of CRS test specimens related to corresponding unit weight data. The resulting w/γ curve complied well with data measured following sampling and on IL oedometer test specimens. The w/γ values identifying CRS oedometer specimens varied from 4.2 to 9.5 %/kN/m³. The best sampling results were obtained on profiles 68, 67 (NGI 86) and 66 (NGI 54) with w/γ>8.0 %/kN/m³. Majority of the results obtained using NGI 54 sampler indicated lower w/γ values. Results on profiles 63A, 65A and 65C (2010) were mainly within 6.5<w/γ<7.2 %/kN/m³, while those on 63B (2010) and 44B (2009) exhibited w/γ<6.0 %/kN/m³. For reconstituted specimens w/γ was between 4.2 and 5.0 %/kN/m³.

In Figure 6.31 c), w/γ values for CRS specimens are related to depth. Consistent with evaluation of IL oedometer specimens, w/γ>7 %/kN/m³ was used to identify CRS specimens of high quality. Average w/γ values on CRS specimens amounted 7.1, 5.2, 7.5 %/kN/m³ in sublayers A, B and C, respectively. The values complied fairly well with data after sampling and on IL oedometer specimens. In sublayer A, w/γ results were represented by 63A, 65A and 67A CRS specimens. The values in the middle of sublayer A were the highest. Exceptionally high values w/γ>8.0 %/kN/m³, were obtained on occasional specimens of 65A (NGI 54) and 67A (NGI 86). Within zone B, NGI 54 sampled 44B CRS specimens (tested at TUT) exhibited very uniform w/γ~5.7 %/kN/m³. In contrast, results on 63B CRS specimens obtained with the same sampler were scattered from 4.4 to 5.7 %/kN/m³, and thus comparable to IL oedometer specimens of lower quality. The w/γ representing CRS specimens within zone C exhibited considerable scatter. Exceptionally high w/γ at elevation from +0.86 to +0.95 identified highly sensitive quick clay. Thus, the best sampling results within zone C, i.e. w/γ>8 %/kN/m³, were obtained on oedometer test specimens of 66C (NGI 54) and 68C (NGI 86). Lower section of the zone was represented by NGI 54 sampled 65C material with 5.4<w/γ<7.1 %/kN/m³.

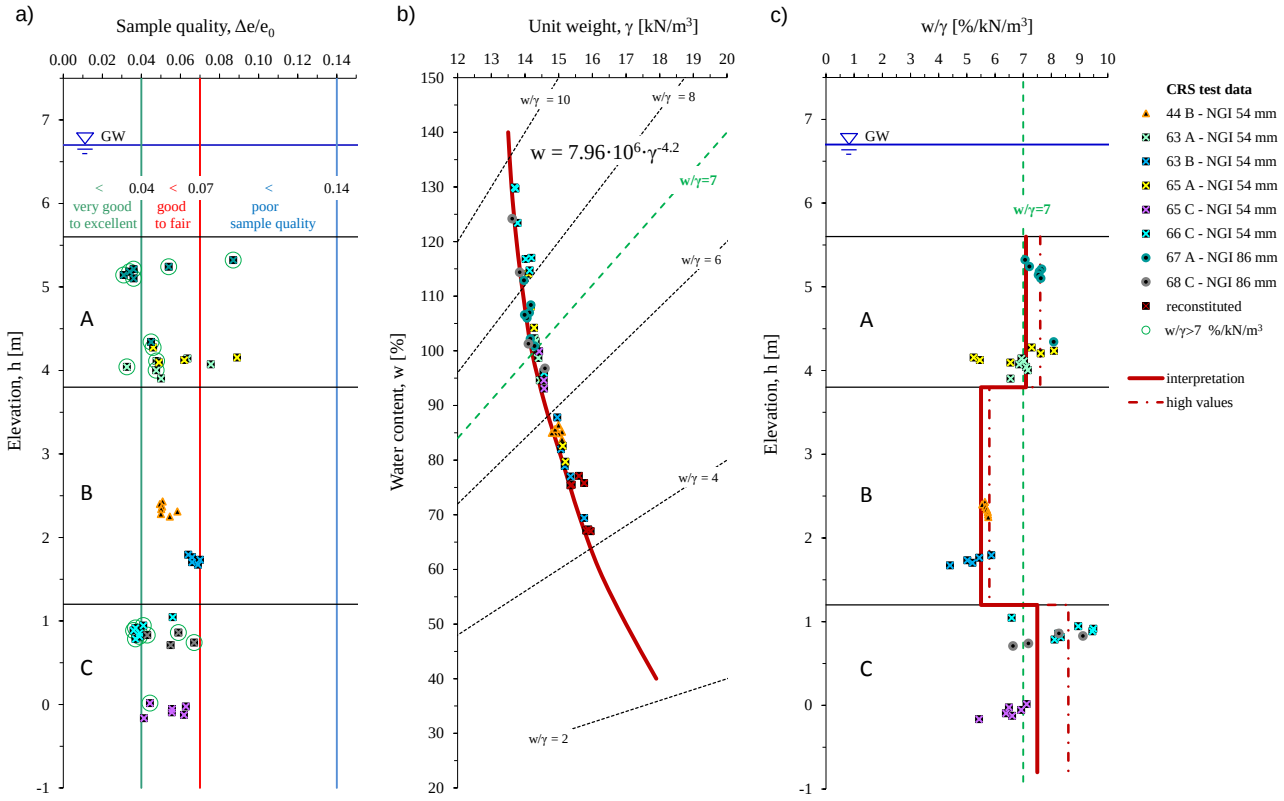

Figure 6.31 Specimen quality in CRS oedometer tests on Perniö clay; a) $\Delta e/e_0$ criteria, b) w/γ curve, and c) w/γ criteria.

Comparison of $\Delta e/e_o$ and w/γ sampling quality criteria

CRS test conditions have significant influence on $\Delta e/e_o$ values obtained. As shown in Figure 6.31 a), considerable amount of specimens identified as being of good and excellent quality, i.e. $\Delta e/e_o<0.07$, were discarded if $w/\gamma>7$ %/kN/m³ criteria was of concern. The w/γ criterion however, may have failed to recognise natural variation of water content and unit weight data, being systematically less on material from sublayer B. Thus besides sampling, w/γ values were influenced by initial structural characteristics, composition and stress history of the sample, e.g. magnitude of effective overburden stress in situ. Nonetheless, exceptionally high w/γ values clearly identified highly sensitive quick clay material of distinctive properties compared to overlaying and underlying materials. In contrast, the lowest values $w/\gamma<5.2$ %/kN/m³ obtained on reconstituted material reflected characteristics of destructured material. Thus, if instead of $\Delta e/e_o$ approach, the evaluation of sample quality was based on w/γ, the results were consistent and meaningful.

6.2.4 Compressibility and preconsolidation pressure

Effects of strain-rate and sample disturbance on compressibility curve

CRS oedometer test results on Perniö clay showed considerable scatter of compression response. In addition to sampling disturbance, scatter was caused by the magnitude of strain-rates imposed.

Influence of the strain-rate on compressibility is identified as proportional shift of the entire compression curve towards higher vertical effective stresses [Sällfors 1975, Leroueil et al. 1988b]. Strain-rate effects are commonly defined by linear or exponential proportionality between strain-rates imposed, and the preconsolidation pressures interpreted [Leroueil et al. 1985, Kobayashi et al. 2005]. The approaches evaluate compressibility in σ'_1 vs. ε_1 plane and neglect to consider specimen disturbance. If samples are not homogenous, preconsolidation pressures and absolute magnitudes of vertical strain are not comparable [Tokheim, Janbu 1980]. Indeed, with the effects of specimen disturbance being reciprocal to those of strain-rate, the approaches lead to uncertainties in deriving concise conclusions on compression response measured.

CRS results on good quality specimens characterised with high v_o, are shifted toward higher vertical effective stresses compared to those of poor quality. Moreover, high quality specimens indicate the highest compressibility in NC stress range. In order to explain effect of both, specimen disturbance and strain-rate, laboratory tests need to be performed at substantial range of strain-rates on specimens of similar quality, while resulting compression curves need to be evaluated in the perspective of effective stress dependent void ratio or specific volume change.

To ensure comparability of the results, tests need to be performed on specimens from similar depth. Sample quality may vary considerably depending upon the sampling method used. If tube sampling is used, tests need to consider material from the same sampling cylinder. Even with above condition satisfied, considerable variations in properties can occur due to the non-homogeneity of the deposit, local failures or variations in disturbance within the cylinder, and different extent of disturbance in specimen preparation.

Since this study aims defining both rate dependent and destructuration effects, CRS results on Perniö clay comprised groups of oedometer test at various strain-rates on material with different levels of sample quality and initial structure. In following, the compression curves are examined within the perspective of sublayer of origin, specimen disturbance, and strain-rates implemented. Selected tests on 63A, 63B, 65C, and 66C on natural, and A19 on reconstituted specimens are respectively presented in Figure 6.32-Figure 6.35.

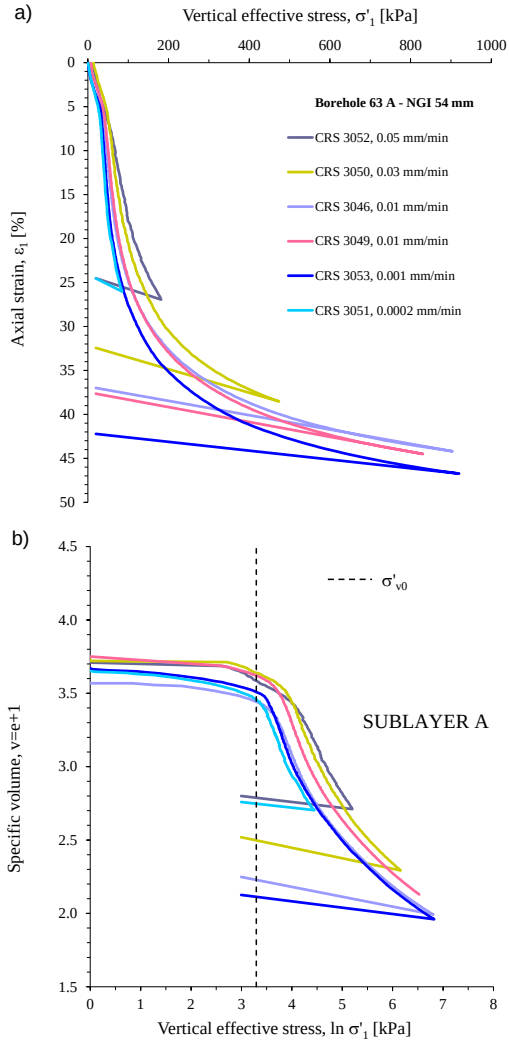

Figure 6.32 Compressibility in CRS oedometer test on 63A; a) σ'_1 vs. ε_1, and b) σ'_1 vs. specific volume.

Figure 6.32 presents CRS tests on sublayer A material sampled on profile 63 at elevation of +4.14 to 3.90, absolute. 63A test group comprised considerable range of strain-rates, i.e. 0.0002, 0.001, 0.01, 0.03 and 0.05 mm/min. Tests were performed on homogenous material of uniform quality characterised by narrow range of v_o, i.e. 3.57 to 3.75. The w/γ values varied from 6.55 to 7.16

%/kN/m³, identifying material of somewhat lower quality compared to average of 7.2 %/kN/m³ characterising sublayer A. Examined in σ'_1 vs. ε_1 and σ'_1 vs. v_o plots, results exhibited clear pattern of strain-rate dependence, with offset of the compression curves towards higher vertical effective stresses being proportionally strain-rate dependent. In σ'_1 vs. ε_1 plane, compression curve for CRS 3046 obtained at 0.01 mm/min on lowest quality specimen with w/γ of 6.55 %/kN/m³, deviated at high effective stress levels. Indeed, compared to CRS 3049 performed at identical strain-rate, CRS 3046 indicated somewhat lower compressibility. Furthermore, in σ'_1 vs. v_o plane compression curve for 3046 was positioned well underneath that of 3049. Due to higher extent of initial disturbance, compression curve for 3046, complied with 3053 curve obtained at lower strain-rate of 0.001 mm/min.

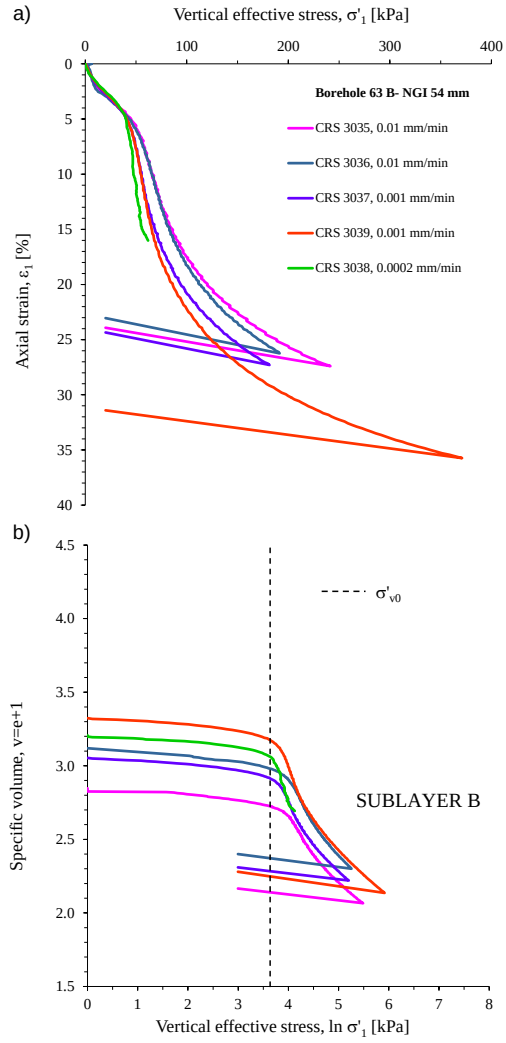

Figure 6.33 Compressibility in CRS oedometer test on 63B; a) σ'_1 vs. ε_1, and b) σ'_1 vs. specific volume.

CRS tests on 63B material, corresponding to absolute elevation of +1.67 to 1.79, are shown in Figure 6.33. The 63B group included tests at strain-rates of 0.0002, 0.001 and 0.01 mm/min. The specimens were characterised with high variation in generally low v_o ranging from 2.85 to 3.32. Corresponding w/γ varied from 4.40 to 5.87 %/kN/m^3, representing lower limits of zone B marked with average of 5.6 %/kN/m^3. Notable variations in initial properties were common feature of sublayer B specimens due to occurrence of silty inclusions and high susceptibility to disturbance. In spite of differences in initial properties, when examined in σ'_1 vs. ε_1 plane, strain-rate influence on 63 B compression response was consistent. However, pairs of tests at identical strain-rates enabled evaluation of results with respect to specimen quality, i.e. CRS 3035 and 3036 at 0.01, and 3037 and 3039 at 0.001 mm/min. Until ε_1~15 %, response of specimens compressed at corresponding strain-rates complied. With further increase of strain significant discrepancies occurred resulting with considerable deviation in stress-strain response at high stress levels. Specimens 3035 and 3037 with lower w/γ of 4.40 and 5.00 %/kN/m^3, were less compressible. Examined in σ'_1 vs. v_o plane, results on poor quality specimens positioned underneath corresponding compression curves 3036 and 3039.

Figure 6.34 shows CRS tests performed on 65C material sampled at elevation of -0.17 to +0.02, absolute. The tests were performed in a broad range of strain-rates including 0.0002, 0.001, 0.01 and 0.03 mm/min. Quality of material differed substantially, with w/γ varying from 5.44 to 7.12 %/kN/m^3 and overall being considerably less than average in zone C amounting 7.5 %/kN/m^3. Corresponding v_o values occurred in limits from 3.40 to 3.74. In σ'_1 vs. ε_1 plane results showed rather clear pattern of strain-rate dependence. At high strain levels though, influence of specimen quality on compression response was evident. Compression curves of poor specimens 3054 and 3056 exhibiting lower compressibility, introduced uncertainties in interpretation of compression response, eg. compression curve for 3056 obtained at 0.001 mm/min, at high stress levels placed above compression curve for 3058 compressed at 0.01 mm/min. Due to variance in quality of the specimens considered, in σ'_1 vs. v_o plane influence of strain-rate on compressibility was obscured. With an exception of tests at 0.03 mm/min, compression curves complied rather well, independent of the strain-rate imposed. However, careful evaluation of results obtained at identical strain-rates of 0.01 or 0.03 mm/min, revealed compression curves of poorer specimens placing underneath those of better quality.

To expose specimen disturbance mechanism in CRS tests, compression curves obtained on the highest quality quick clay specimens of 66C, were confronted with response of A19 reconstituted specimens. Considering both test groups, specimens evaluated were compressed at strain-rates of 0.0001, 0.0002, 0.001 and 0.01 mm/min. As shown in Figure 6.35, test results obtained on A19 represented lower bound of Perniö clay compressibility. Typically for reconstituted material, tests performed on A19 specimens exhibited uniform initial properties, characterised by w/γ of 4.20 to 4.25 %/kN/m^3, and the lowest v_o in Perniö clay amounting 2.77 to 2.80. Influence of strain-rate was consistent, and was the most prominent at stress levels following yield. As in IL oedometer tests, stiffness of reconstituted specimens in NC stress range

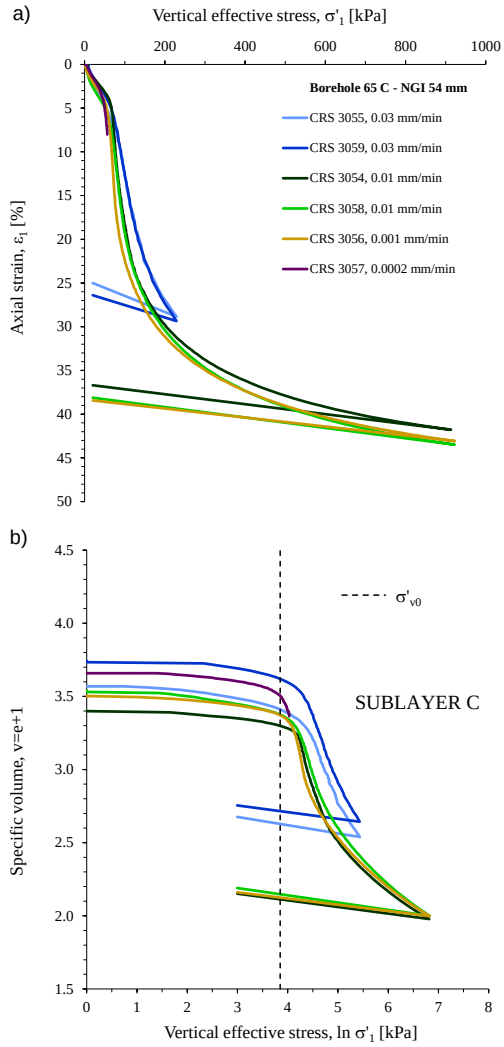

Figure 6.34 Compressibility in CRS oedometer test on 65C; a) σ'_1 vs. ε_1, and b) σ'_1 vs. specific volume.

corresponded with that of natural specimens at high stress levels. 66C material from upper portion of sublayer C relates to elevation between 0.78 and 1.21 (6.30–6.75 m of depth). Although from the same cylinder, 66C specimens were characterized with very significant scatter of v_o and S_t. While quick clay specimens exhibited the highest v_o encountered in testing of Perniö clay, i.e. 4.45, the values on poor specimens were considerably less. Test CRS 3007 was performed on relatively poor specimen with v_o of 3.56 and w/γ ratio of 6.59 %/kN/m³, while CRS 3045 was made on specimen with high percentage of silt, lowest v_o of 3.28 and w/γ of 5.62 %/kN/m³. Examined in σ'_1 vs. ε_1 plane, specimens with similar initial properties and compressed at identical strain-rates complied rather well. With an exception of 3045, compression curves exhibited proportional influence of strain-rate on the extent of compression curve translation toward higher effective stresses. Tests performed at 0.01 mm/min

on somewhat lower quality specimens, exposed to some extent stiffer response at high strain levels compared to the highest quality specimens of the group. Compression curve obtained on silty clay specimen 3045 compressed at the lowest strain-rate, was markedly stiffer, and intersected remaining compression curves at strain level of ~20%. In σ'_1 vs. v_o plane, the highest quality specimens tested at 0.001 mm/min, exhibited the highest compressibility. Response of somewhat lower quality specimens at higher strain-rate of 0.01 mm/min was stiffer, yet due to strain-rate influence, resulting compression curves were slightly shifted toward higher vertical effective stresses. In contrast, results in CRS 3007 and 3045 on specimens of markedly lower quality were positioned well underneath remaining compression curves. In addition of low v_o, compression curve obtained on silty clay specimen, exhibited markedly higher recompression slope, and overall the lowest compressibility.

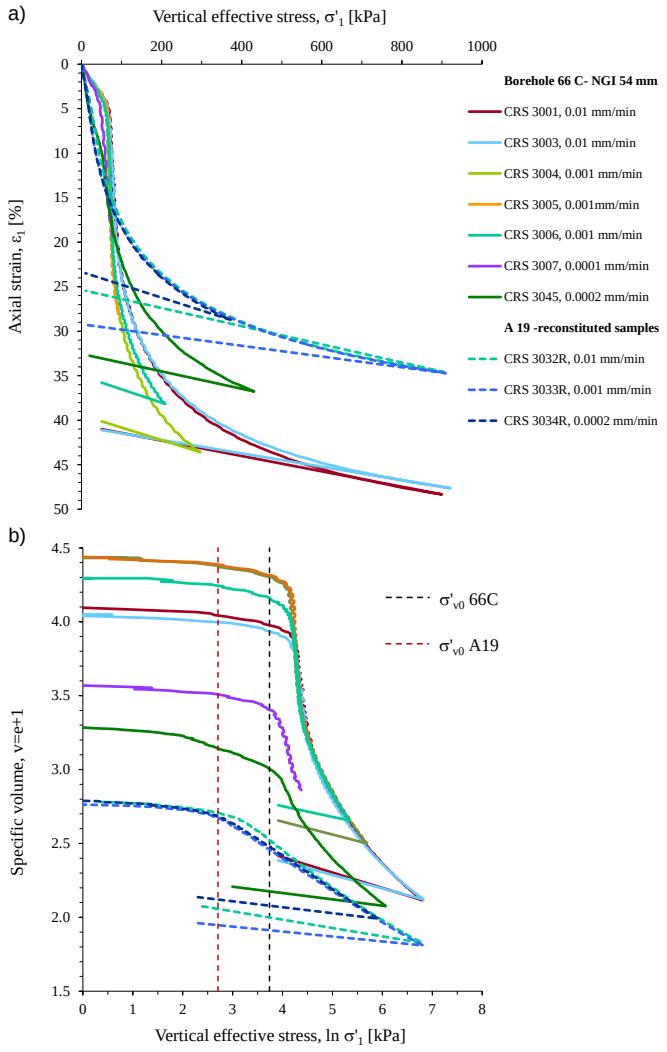

Figure 6.35 Compressibility in CRS oedometer test on natural 66C and reconstituted A19; a) σ'_1 vs. ε_1, and b) σ'_1 vs. specific volume.

CRS test results on Perniö clay showed effects of strain-rate intensity being reciprocal to those of specimen disturbance. Effects of specimen disturbance on compression response were considerable. Consequently, in interpretation of strain-rate effects, evaluation of quality of the specimens was essential. If tests are performed on non-homogenous material or on material varying in specimen quality, absolute magnitudes of vertical strain are not comparable [Tokheim, Janbu 1980]. Consequently, the advantage should be given to examination of compressibility in relation to compression measure influenced by specimen disturbance, such as specific volume or void ratio.

Effect of strain-rate on pore pressure

Pore pressure response of the specimen in CRS oedometer tests was dependent upon permeability and strain-rate imposed. Although pattern of pore pressure response was similar independent of the strain-rate, actual magnitude of pore pressures, as well as the rates of pore pressure development, were highly strain-rate dependent. Pore pressure response to vertical effective stress increase resembled that of compression moduli stress dependence. At the onset of test at a given rate, pore pressures exhibited exponential increase until stress level characterising maximum compression resistance in reloading σ'_o. With further increase in σ'_1, pore pressures either reached steady state level remaining almost constant, or somewhat decreased reaching minimum at preconsolidation stress level [Tokheim, Janbu 1980]. Following the yield, rapid transition occurred characterised by pore pressure and σ'_1 proportionality. For $\sigma'_C<\sigma'_1<\sigma'_L$, pore pressures rose almost linearly, while for $\sigma'_1>\sigma'_L$, stress increase was coupled with pore pressure build-up at decreasing rate.

Figure 6.36 presents results of pore pressure measurements obtained in selected CRS tests. With pore pressure being highly dependent upon the strain-rate imposed, maximum values measured ranged from several kPa at 0.0002 mm/min, up to several hundreds of kPa at 0.05 mm/min. Due to variance in permeability, specimens tested at identical strain-rate responded with considerably different pore pressures and compressibility. To elaborate response of Perniö materials, pore pressures measured on specimens compressed at 0.01 mm/min corresponding to stress level of 200 kPa were examined and compared. In tests CRS 3046 and 3049 on 63 A material, pore pressures measured at σ'_1 of 200 kPa corresponded well amounting ~58 kPa. At high stress levels, poorer quality specimen 3046 exhibited somewhat lower pore pressures. In tests CRS 3035 and 3036 on 63B, pore pressures varied considerably. At σ'_1 of 200 kPa, CRS 3035 exhibited pore pressure of 20 kPa, while that in 3036 was 34 kPa. Again, generally lower pore pressures were measured on specimen of poorer quality. 65C tests CRS 3054 and 3058 exhibited similar pore pressure response. At σ'_1 of 200 kPa the pore pressures were 82 and 86 kPa, respectively. Despite being of corresponding quality, 66C specimens 3001 and 3003 strained at 0.01 mm/min, differed in pore pressures registered. At σ'_1 of 200 kPa, respective pore pressures amounted 68 and 72 kPa. Furthermore, at high stress levels pore pressures were generally higher in CRS 3003. In contrast to

responses measured on natural specimens, A19 reconstituted specimen 3032 at σ'_1 of 200 kPa exhibited the highest pore pressures overall, i.e. ~90 kPa (see Figure 6.37).

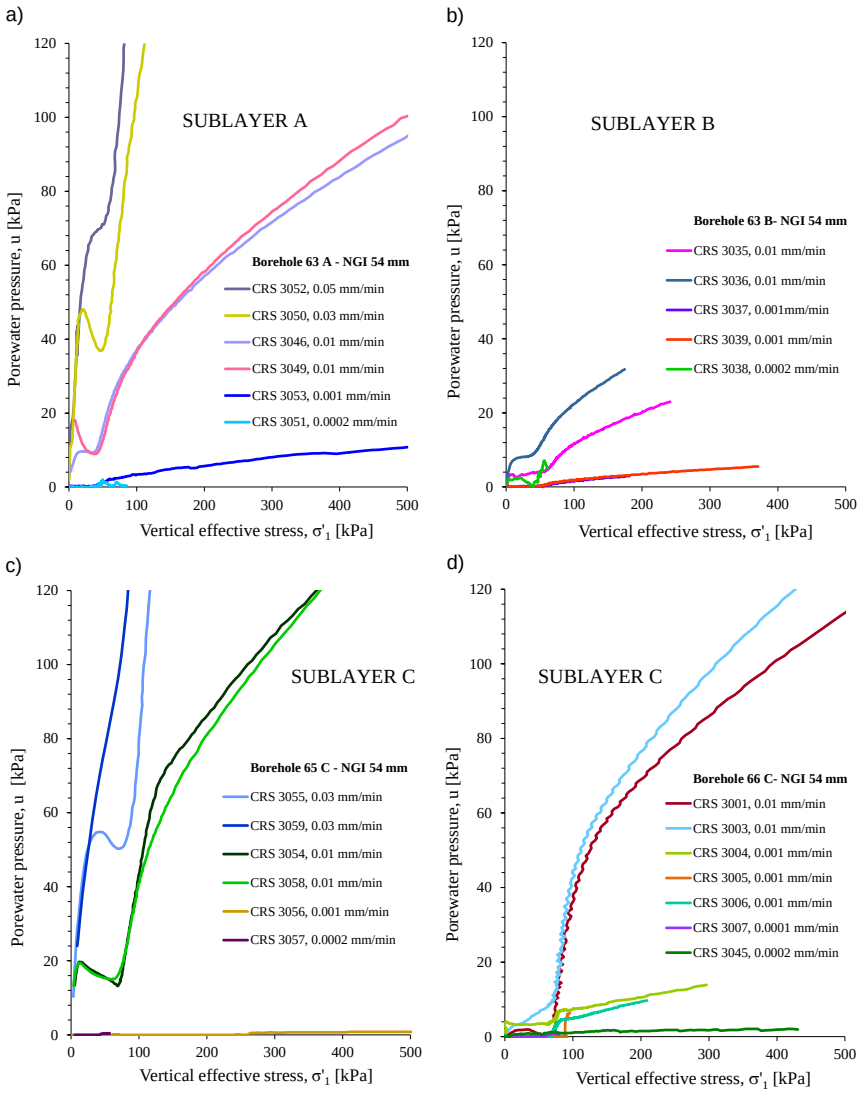

Figure 6.36 Pore pressure vs. vertical effective stress in CRS oedometer test on natural specimens; a) 63A, b) 63B, c) 65C, and d) 66C.

To conclude, considering specimens compressed at identical rate of 0.01 mm/min, silty clay specimens of sublayer B exhibited the lowest pore pressures and the highest scatter in values. Somewhat higher pore pressure response characterised material form sublayer A and C. Specimens of relatively poorer quality typically exhibited pore pressures relatively lower in magnitude. Overall, the highest pore pressures were measured on reconstituted specimen indicating the lowest permeability.

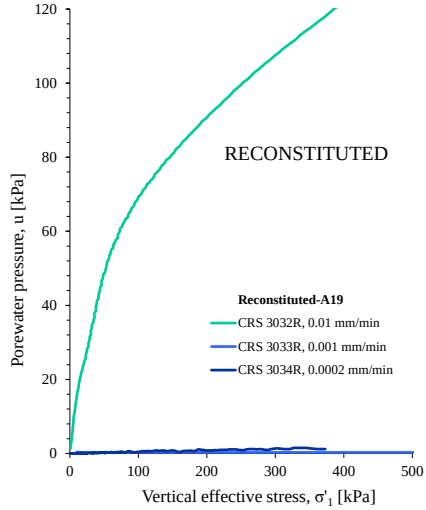

Figure 6.37 Pore pressure vs. vertical effective stress in CRS oedometer test on reconstituted A19 specimens.

Effect of strain-rate and sample disturbance on preconsolidation pressure

Values of preconsolidation pressure in CRS tests depended upon the specimen quality and strain-rate imposed. Approaches used in interpretation of σ'_p were consistent with those used in IL oedometer tests. Due to continuous loading however, σ'_p interpretation was more accurate than in IL tests [Tokheim, Janbu 1980]. In contrast to those in IL oedometer test, σ'_p values identified in CRS tests generally exceed effective overburden (see Figure 6.29). The effect was related to the proportional influence of the strain-rate. Only if the rate of strain was low enough, i.e. CRS of $2 \cdot 10^{-6}$ s^{-1}, the σ'_p obtained was about the same as for conventional IL test [Larsson & Sällfors 1986]. Furthermore, specimens of poor quality generally exhibited relatively lower values σ'_p.

In Figure 6.38, σ'_p/σ'_{vo} values are related to $\Delta e/e_o$ specimen quality criteria. Due to the influence of strain-rate on reloading response, $\Delta e/e_o$ values could not be directly related to initial quality of the specimens. Compared to those obtained in IL oedometer tests, CRS test data were overall positioned in relatively narrow range of $\Delta e/e_o$ values, while σ'_p/σ'_{vo} values were significantly higher. Despite the proportional strain-rate influence on σ'_p, results obtained in CRS tests complied with pattern of response in IL oedometer test, thus confirming exponential rise in σ'_p/σ'_{vo} values with decline of $\Delta e/e_o$. Considering both IL and CRS oedometer tests the relation was well represented by Equation 6.17:

$$\Delta e / e_0 = 0.065 \cdot \left(\sigma'_p / \sigma'_{v0}\right)^{-1.3} \qquad (6.17)$$

In the same Figure specimens characterised with $w/\gamma > 7$ %/kN/m³ are highlighted. Since based on initial parameters of the specimen, w/γ values were independent of the testing procedure. Specimens characterised with high w/γ generally exhibited higher values of σ'_p/σ'_{vo}, thus confirming the validity of w/γ sampling quality criteria.

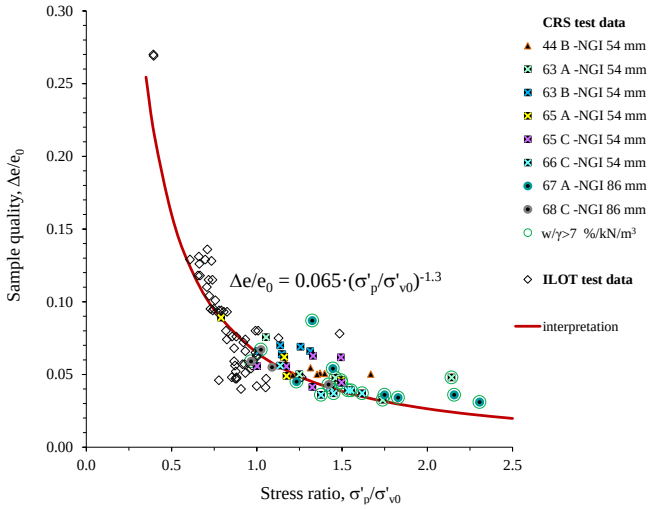

Figure 6.38 Preconsolidation pressure in CRS oedometer tests related to specimen quality.

Normalization of compression curves

Figure 6.39 to Figure 6.43 examine compression curves obtained in selected CRS tests in relation to vertical effective stress normalized with that at yield. Validity of the normalization was dependent upon the accuracy of the determination of initial specific volume and consistency of the preconsolidation pressure interpretation. Šuklje [1957] and Bjerrum [1967] showed that no unique stress-strain relation exists independent of time. Furthermore, Šuklje [1957] suggested set of relations, i.e. isotache, each valid for a certain strain-rate [Larsson & Sällfors 1986]. Works by Leroueil et al. [1985], Leroueil et al. [1988], Leroueil [2006], and recent findings by Watabe & Leroueil [2012] and Watabe et al. [2012], suggest compression curves normalized with σ'_p resulting with unique stress ratio-strain relation for a specific clay. CRS results on Perniö clay are used to evaluate validity of the unique compression concept and to identify influence of the destructuration on results of the normalization.

Previous studies evaluate unique compression concept in terms of axial strains, thus neglecting or omitting to elaborate initial quality of the specimens. Material inhomogeneity and variation in the quality of the specimens introduce discrepancies to the ability of relating absolute magnitudes of vertical strains [Tokheim, Janbu 1980]. Moreover, CRS results normalized with σ'_p are typically compared up to relatively low axial strains of ~20 %. With strain-rate influence on structural characteristics of the specimen being cumulatively related to the extent of specimen compression, it is necessary to examine unique compression concept by considering response at high stress ratio levels as well. By adopting constant scaling value, i.e. σ'_p, the normalization approach assumes rate of change in specimen's structure at certain strain-rate being constant. Effect of the strain-rate on the rate of change of structural characteristics of the specimen needs to be considered as well. Finally, normalized compression curves are typically displayed in terms of log σ'_1/σ'_p. The approach emphasises normalization effects at low stress ratios, while neglecting differences at high stress ratio levels. Normalized compression curves obtained on

Perniö clay at various magnitudes of strain-rate are herein examined with respect to both, ε_1 and v. Advantage was given to the later, i.e. v being a function of specimen disturbance. In evaluation of Perniö clay results, specimen quality was consistently related to the results obtained.

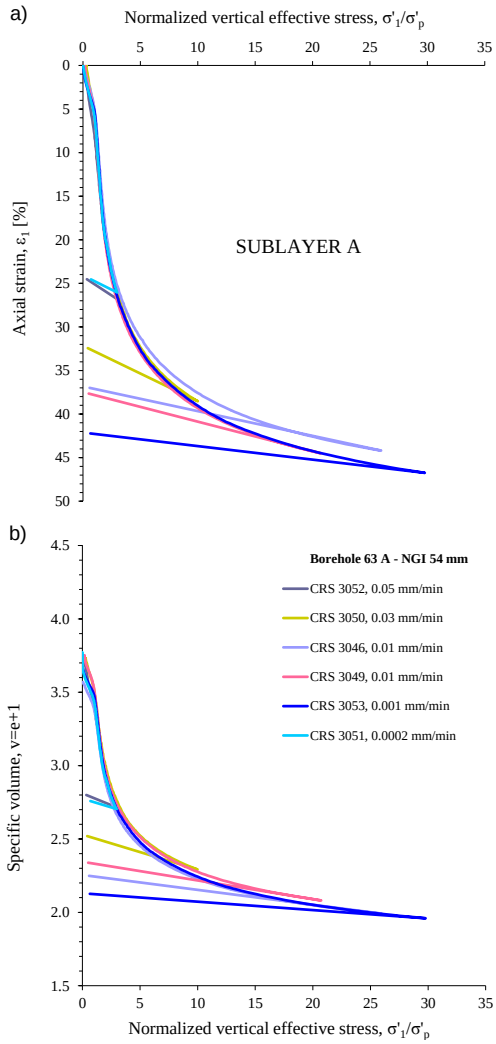

Figure 6.39 Normalization of 63A compression curves; a) σ'_1/σ'_p vs. ε_1, and b) σ'_1/σ'_p vs. specific volume.

CRS results of 63A test group shown in Figure 6.39 considered specimens of relatively low, yet fairly uniform sensitivity St~15-30. Consequently, in σ'_1/σ'_p vs. ε_1 plane, normalized compression curves complied very well. At ε_1>25%, normalized compression curve representing poor quality specimen 3046 (0.01 mm/min), progressively deviated with stress ratio increase plotting well above remaining curves. In σ'_1/σ'_p vs. v plane, resulting compression curves complied as well. Normalization discrepancies were magnified with increase of stress ratio. At high stress ratio levels tests performed on the highest quality speci-

mens 3049 (0.01 mm/min) and 3050 (0.03 mm/min), plotted somewhat above remaining curves indicating more pronounced strain-rate influence on compression characteristics measured. In contrast, normalized compression curve obtained for the lowest quality specimen 3046 (0.01 mm/min), was characterised by somewhat lower specific volumes overall. Regarding swelling response, normalized slope in swelling was proportional to specific volume reached in compression.

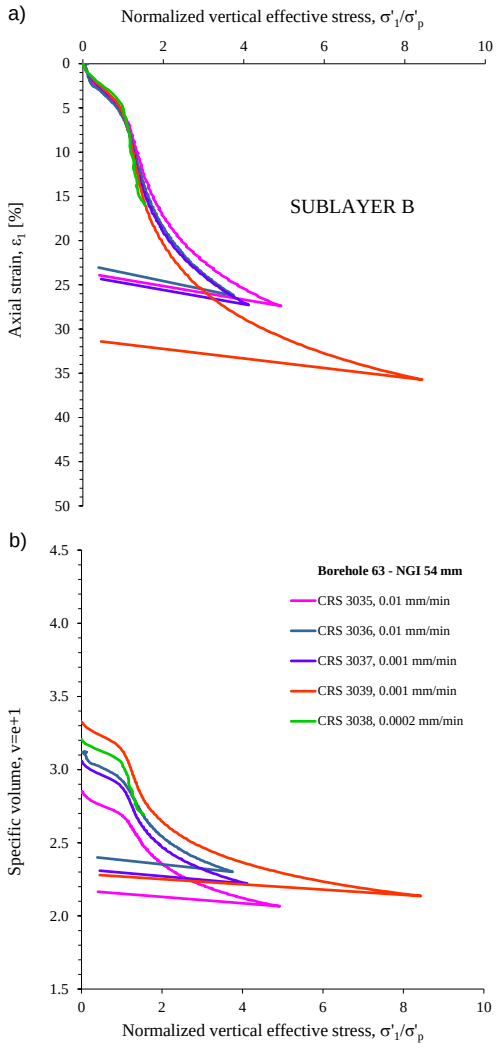

Figure 6.40 Normalization of 63B compression curves; a) σ'_1/σ'_p vs. ε_1, and b) σ'_1/σ'_p vs. specific volume.

Figure 6.40 presents normalized compression curves obtained for 63B test group. Sensitivity values of the specimens considered were generally very low, 4<St<12. In σ'_1/σ'_p vs. ε_1 plane, deviations in normalized compressibility were significant and intensified with the increase of stress ratio. Representing specimen of initially higher compressibility and higher σ'_p, normalized compression curve on the highest quality specimen 3039 (0.001 mm/min), plotted

underneath remaining curves. In contrast, curve obtained on the poorest quality specimen 3035 (0.01 mm/min), plotted above the rest. Normalized compression curves obtained in the remaining tests complied well. Examined in σ'_1/σ'_p vs. v plane, normalized compression curves did not correspond. Resulting curves were embedded by extreme responses obtained for tests CRS 3035 and 3039. Deviations in response intensified with increase in stress ratio. Normalized compression curves obtained on the poorest quality specimens 3035 and 3037, plotted well underneath the rest. Normalized compression curves in 63B are convenient for elaborating effects of the specimen quality. Tests CRS 3035 and 3036 were compressed at 0.01 mm/min, while CRS 3037 and 3039 were made at 0.001 mm/min. Compared to those obtained on lower quality specimens compressed at the same rate, results on specimens with higher w/γ 3036 and 3039, plotted above indicating somewhat more pronounced strain-rate influence on compression characteristics.

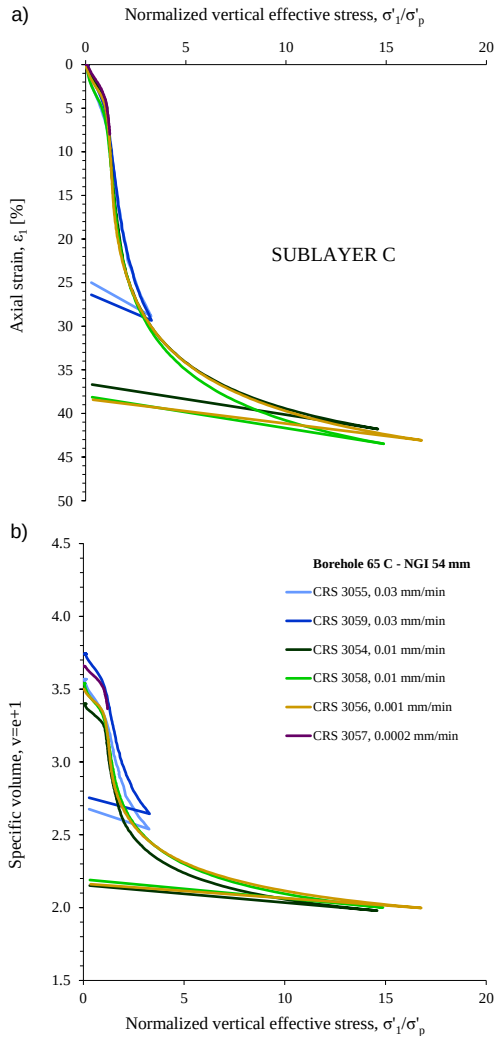

Figure 6.41 Normalization of 65C compression curves; a) σ'_1/σ'_p vs. ε_1, and b) σ'_1/σ'_p vs. specific volume.

Figure 6.41 shows normalization results of 65C test group. In σ'_1/σ'_p vs. ε_1 plane, results complied well. Slight deviations occurred at high stress ratio levels. Normalized compression curves for specimens of the highest quality compressed at the highest strain-rate, surprisingly, plotted above the other curves. Remaining results complied well for ε_1<30%. Later, the poorest specimens 3054 (0.01 mm/min) and 3056 (0.001 mm/min), exhibited relatively lower ε_1 at high stress ratio levels. Despite similar sensitivity St~15-26, when examined in σ'_1/σ'_p vs. v plane, normalization of 65C results was not concise. Results for CRS 3055 and 3059 compressed at 0.03 mm/min plotted well above indicating more pronounced strain-rate influence on compression characteristics measured. Normalized compression curve for the highest quality specimen 3059, plotted entirely above, while that obtained on 3054 (0.01 mm/min) with the lowest w/γ ratio, plotted beneath the remaining curves. Normalized slope in swelling was proportional to v at the onset of unloading.

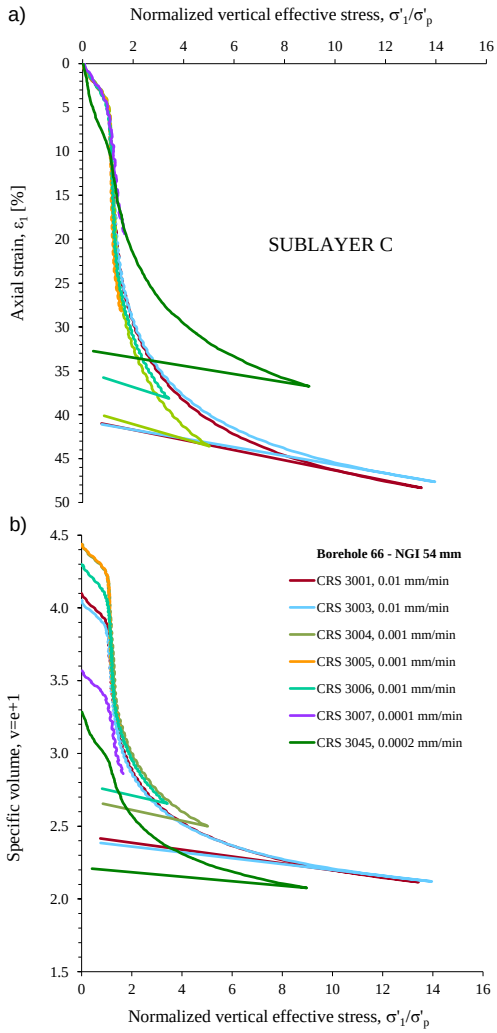

Figure 6.42 Normalization of 66C compression curves; a) σ'_1/σ'_p vs. ε_1, and b) σ'_1/σ'_p vs. specific volume.

Figure 6.42 presents normalized compression curves obtained for 66C. Specimens of the test group were generally characterised by exceptionally high w/γ and sensitivity St~125-165. Examined in σ'_1/σ'_p vs. ε_1 plane, response of silty clay specimen 3045 (0.0002 mm/min), significantly differed from the rest of the results. Remaining results complied very well up to ε_1 of 20%. Reflecting variation in initial properties, for ε_1>20% normalized curves diverged considerably. Those obtained on specimens of lower quality plotted significantly above results on high quality specimens. Examined in σ'_1/σ'_p vs. v plane, 66C results complied rather well. Exception were curves obtained on poor quality specimens at low strain-rates 3007 and 3045, indicating similar response, yet plotting at lower v. At high stress ratio values, normalized compression curves on the highest quality specimens tested at 0.001 mm/min, plotted somewhat above curves obtained at 0.01 mm/min. For entire set of 66C results, stress ratio related slope in swelling was proportional to v reached in compression.

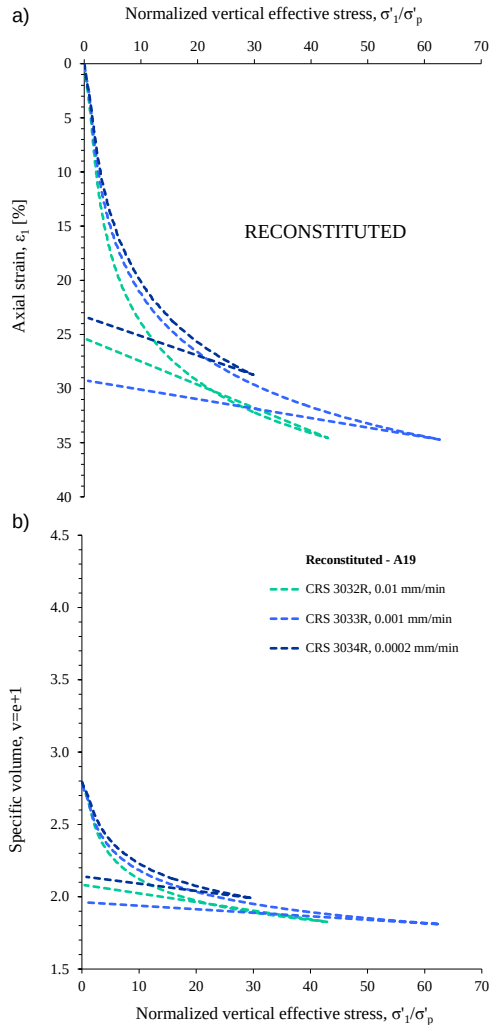

Figure 6.43 Normalization of A19 compression curves; a) σ'_1/σ'_p vs. ε_1, and b) σ'_1/σ'_p vs. specific volume.

Normalized compression curves representing reconstituted specimens of A19 test group are presented in Figure 6.43. The tests were performed on specimens of similar initial properties. Interestingly, normalized compression response opposed conclusions in CRS tests on natural specimens. In σ'_1/σ'_p vs. ε_1 plane, curves corresponded at low stress ratio. However, already at ε_1~10%, normalized compression curves progressively diverged with stress ratio increase. Results obtained at the highest strain-rate plotted underneath those at low strain-rates. In σ'_1/σ'_p vs. v plane, normalized compression curves progressively diverged with increase in stress ratio as well. In contrast to results obtained on natural specimens, normalized compression curve obtained at the lowest strain-rate related with the highest values of v and vice versa. Furthermore, compressibility results obtained on reconstituted specimens exhibited better normalizing results in σ'_1/σ'_{vo} vs. v plane. Using the approach, normalized compression curves at various level of strain-rate complied well in their final portion. However, with σ'_p values being proportional to strain-rate intensity, normalization with σ'_{vo} did not perform well following the yield. Same conclusions were valid for results on reconstituted specimens A28.

According to unique compression concept, normalized compression curves representing homogenous material compressed at various strain-rates, coincide. With stress ratio expressed in log scale and results compared for ε_1<20 %, normalization yields corresponding results even if sample disturbance is neglected. However, on specimens varying in quality results at identical strain-rate do differ. When normalized, the results oppose unique compression response, particularly at high stress ratio levels. In σ'_1/σ'_p vs. ε_1 plane, normalized compression curves diverge with increase in stress ratio, with high quality specimens plotting under those obtained on specimens of poor quality.

With v_o being a variable of specimen disturbance, in σ'_1/σ'_p vs. v plane specimen disturbance was accounted for by variance in v_o. Assuming the validity of unique compression concept, curves obtained on high quality specimens plot above, yet are parallel to normalized curves obtained on poor quality specimens at high σ'_1/σ'_p levels. However, if strain-rate influences compressibility and rate of the destructuration process outside the scope accounted by normalization with constant σ'_p, than at high stress ratio levels normalized compression curves representing specimens of variable quality are not parallel. Based on CRS results on Perniö clay specimens, latter statement was correct. Typical response characterising normalization of CRS results on natural specimens, was that of specimens tested at high strain-rates being somewhat more subjected to destructuration than what was accounted by normalization with yield pressure. Consequently, when normalized, the highest quality specimens tested at the highest strain-rates plotted somewhat above those tested at low strain-rates, while the difference in the response increased with increase of stress ratio. In contrast, normalized compression curves obtained on reconstituted specimens at high strain-rates were typically related to the lowest specific volumes, thus indicating less rapid destructuration at high stress ratio levels than accounted by σ'_p normalization. Thus, additionally to normalization with

σ'_p, Perniö clay results indicated necessity for strain normalization factor accounting for strain-rate influence on specimen destructuration rate.

To conclude; present view is that of unique compression concept being valid if homogenous specimens are compared. The concept should be extended by taking into consideration influence of sample disturbance and influence of strain-rate on the rate of destructuration. Following normalization with σ'_p relatively higher in magnitude, normalized curves representing high quality specimens in σ'_1/σ'_p vs. ε_1 plane plotted underneath remaining curves and vice versa. In σ'_1/σ'_p vs. v plane, results on natural specimens for $\sigma'_1/\sigma'_p>1$ indicated effectiveness of the normalization being influenced by the magnitude of strain-rate imposed. If tests performed at identical strain-rate were normalized with σ'_p, response for higher quality specimen plotted above those obtained on specimen poorer in quality. At high stress ratio levels normalized curves diverged significantly, indicating better quality specimens being relatively more exposed to strain-rate caused destructuration.

6.2.5 Compressibility–Cam-Clay parameters

Compressibility of Perniö clay in CRS oedometer tests was evaluated using Modified Cam-Clay theory parameters. Criteria in parameter determination are shown in Figure 6.44. Results obtained are related to sampling depth in Figure 6.45 and compared with those measured in IL oedometer tests. Values identifying high quality CRS specimens with $w/\gamma>7$ %/kN/m³ are highlighted.

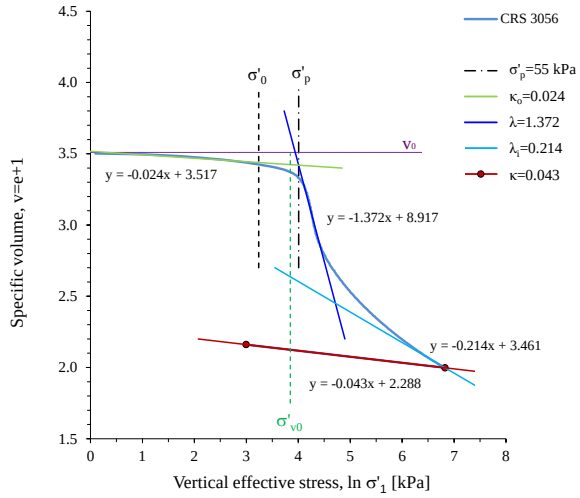

Figure 6.44 Interpretation of Cam-Clay compressibility parameters, CRS 3056.

Reloading κ_o and swelling behavior κ

In Figure 6.45 a) and b) values of reloading and swelling slope in CRS tests are related to sampling depth. Both κ_o and κ varied significantly even within CRS tests of the same group.

The slope of reloading κ_o was influenced by rate of compression, drainage conditions, and stress range over which it was defined. In IL oedometer tests,

rates of strain prior yield were similar for various loading patterns, and were generally low. In CRS tests however, strain-rates imposed ranged considerably, magnifying the influence on κ_o results. Furthermore, drainage conditions in IL and CRS test differed, i.e. CRS test specimen had only upper free drainage boundary. Thus, reloading at CRS was characterised by pore pressure increase reciprocal to the specimen permeability. Consequently, even the specimens compressed at apparently same strain-rate, may have differed in reloading response. Reloading behavior in CRS tests was defined from continuous data. Thus, κ_o interpreted were more accurate than those in the IL tests. However, since κ_o values are highly dependent upon the range of data considered, consistent load interval had to be used to ensure comparability of the results.

Figure 6.45 a) relates κ_o determined in CRS oedometer tests to sampling depth. Reloading indices were determined for the stress range prior maximum compression resistance in reloading (see Figure 6.44). Overall, the results were very scattered, i.e. κ_o<0.016. The highest scatter occurred in the upper portion of Perniö deposit, i.e. sublayer A. Average κ_o amounted 0.055, 0.044 and 0.053 in respective sublayers A, B, and C. Thus, unlike in IL oedometer tests where average κ_o values receded with depth, CRS results identified zone B with the highest compression resistance in reloading. Furthermore, κ_o values in CRS oedometer tests were generally higher, i.e. values in IL oedometer test complied with lowest κ_o in CRS tests. Specimens with w/γ>7 %/kN/m^3 showed high κ_o.

Values defining swelling response were influenced by destructuration and pore pressure level at the onset of unloading, as well as by stress range over which the κ was evaluated. Unloading in CRS apparatuses used is not strain-rate controlled. Instead, swelling response is defined by two points, marking σ'_1-v conditions at the onset and that at the end of unloading. With σ'_p being strain-rate and specimen quality dependent, ensuring consistent unloading stress range was difficult. Two unloading schemes in CRS tests of this study are depicted in Table 6.2. First scheme considered unloading to $\sigma'_{p\,low}/\sigma'_{un}$<1, while second comprised tests unloaded to stress levels $\sigma'_{p\,low}/\sigma'_{un}$>1.25, where σ'_{un} is unloading effective stress and $\sigma'_{p\,low}$ is the yield stress at strain-rate <$3\cdot10^{-7}$ s^{-1}. Influence of strain-rate on κ occurred indirectly, reflecting pore pressure and extent of destructuration at the onset of unloading. Stress and strain levels reached in CRS testing were typically less than those in IL oedometer tests. Consequently, the amount of sufficiently destructured CRS specimens, suitable for comparing κ indices with those in IL oedometer test, was limited. In addition, indirect manifestation of CRS conditions was variance in pore pressures at the onset of unloading. Considerable pore pressures occurring at high strain-rates, as well as drainage conditions and permeability of the material considered influenced unloading response measured.

As shown in Figure 6.45 b), scatter of κ values in CRS oedometer tests was considerable, i.e. 0.027 to 0.100. Average κ values in respective soft clay sublayers amounted 0.060, 0.045 and 0.070. Thus, the lowest κ characterised sublayer B of Perniö deposit. Compared to results in IL oedometer tests, average κ in sublayers A and B were somewhat lower. Considering sufficiently de-

structured CRS oedometer specimens, those with $w/\gamma>7$ %/kN/m^3 generally exhibited high κ. The highest magnitudes and the highest scatter of κ values characterised quick clay material of sublayer C, i.e. tests groups 66C and 68C unloaded to $\sigma'_{p\,low}/\sigma_{un}<1.0$.

Overall, κ_o and κ values in CRS were more scattered than in IL oedometer tests. Range in strain-rate and nature of its change, together with drainage conditions and pore pressure were the main reasons for high scatter of κ_o. Conclusions were valid for swelling response as well. However, since unloading was not strain-rate controlled, scatter of the values was caused by difference in destructuration and pore pressure level at the onset of unloading, and characteristics of the stress range over which κ was evaluated. Main conclusion based on IL oedometer test results, i.e. κ_o being typically less compared to κ, was valid in CRS testing as well. Thus, results of CRS tests confirmed effect of structure on ratio of reloading to swelling response [Burland 1990]. Only for material of relatively more permeable zone B very susceptible to sample disturbance, κ_o and κ values corresponded in magnitude.

Table 6.2 Unloading schemes in CRS oedometer tests on Perniö clay.

Test group	Unloading scheme I σ'_{un} [kPa]	$\sigma'_{p\,low}/\sigma'_{un}$	Test group	Unloading scheme II σ'_{un} [kPa]	$\sigma'_{p\,low}/\sigma'_{un}$
63A	20	1.43	44B	50	0.90
63B	20	1.95	65A	30	0.70
65C	20	2.34	66C	50	0.96
67A	15	1.93	68C	50	0.84
A19	10	1.25	A28	15	0.86

Normal compression λ and intrinsic compression behavior λ_i

Changes in slope of the compression curve manifest gradual destructuration and densification of the specimen. Compression response in CRS testing depended upon specimen quality, strain-rate, extent of deformation, and intensity of vertical effective stress to which specimen was subjected.

In Figure 6.45 c), λ values defining the highest compressibility in CRS tests are related to depth. Details on interpretation are shown in Figure 6.44. Significant scatter of the results manifested effects of strain-rate and specimen disturbance. Within 66C only, λ varied from 0.70 to 4.03. With an exception of extremely high values on quick clay in 66C, in respective soft clay sublayers A, B, and C, λ were well represented by 0.85, 0.70 and 1.15. Thus as in IL oedometer tests, the lowest λ values characterised zone B. Evaluated with respect to w/γ, high quality specimens generally exhibited high λ values. Influence of disturbance in specimen preparation was considerable, particularly in zone A, i.e. 65A and 67A. Overall, λ values in CRS tests exceeded those on IL specimens, i.e. the lowest λ in CRS tests complied with average λ in IL oedometer tests.

In Figure 6.45 d), λ_i values representing intrinsic slope of the compression curve in CRS tests are related to sampling depth. The values were defined by last ten measurements in oedometric compression (see Figure 6.44). The CRS

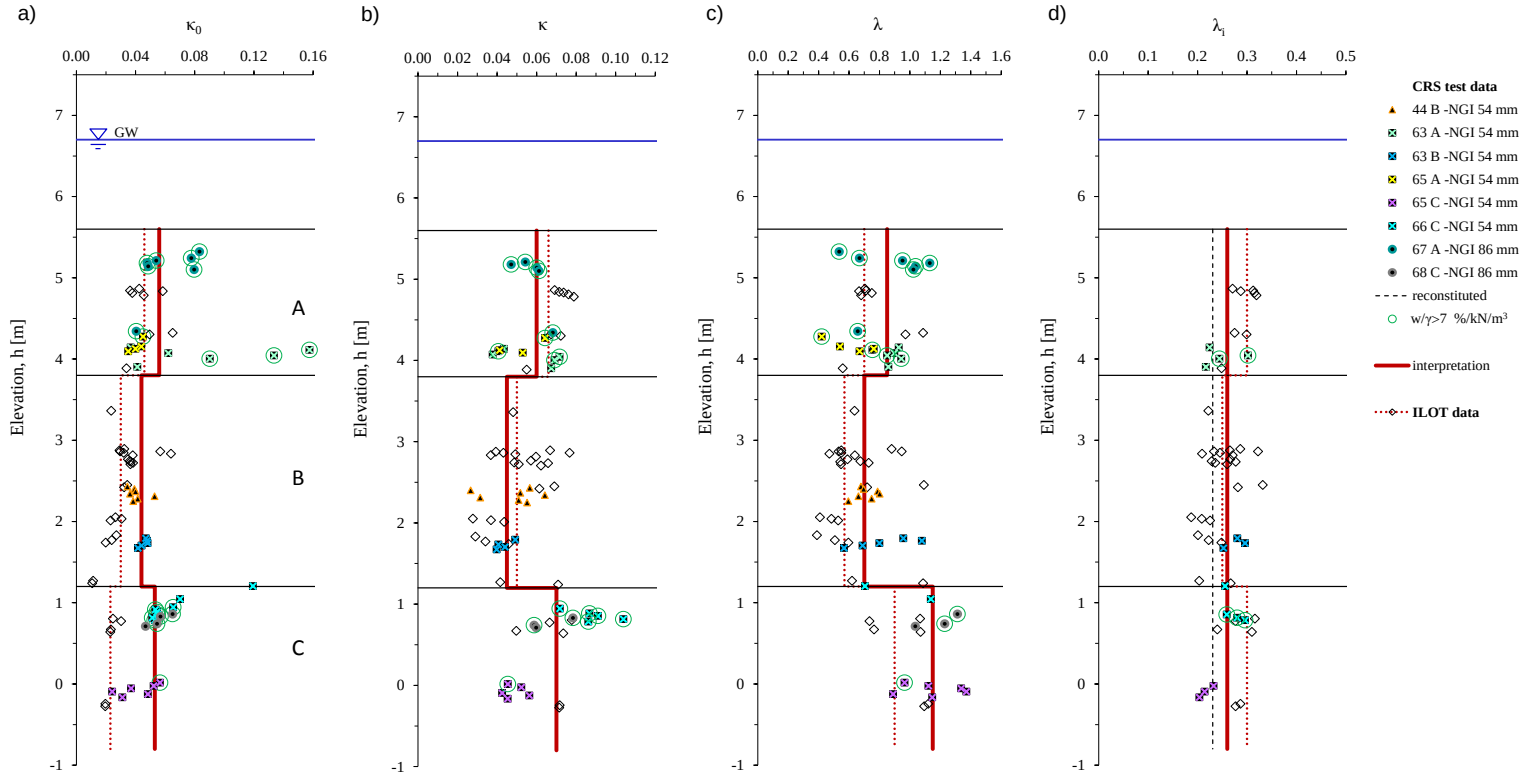

Figure 6.45 Cam-Clay theory compression indices in CRS oedometer tests, a) slope in reloading κ_0, b) slope in swelling κ, c) slope of normal compression λ, and d) slope of intrinsic compression line λ_i.

equipment used was calibrated to axial load of 900 kPa. Depending on the initial water content, strain-rate and sensitivity of the specimen, ε_1 reached at σ'_1 of 900 kPa varied from 35 to 50 % for reconstituted and natural samples, respectively. Although tests at high strain-rates reduce duration of oedometer testing considerably, obtaining representative intrinsic compression properties at low strain-rates was highly time consuming. Considering strain-rates implemented, i.e. 0.0001 to 0.05 mm/min, duration of the test providing sufficient level of destructuration (λ_i/λ_R<25%), varied from 3.3 h to 69.4 days. Due to time limits of the testing program, specimens compressed at low strain-rates were often terminated following period of 30 days. Consequently, amount of λ_i values suitable for comparison with those in IL oedometer tests performed until ~1000 kPa was limited. Considering sufficiently destructured CRS specimens, λ_i results ranged from 0.2 to 0.3. Overall the results were well represented by average value of 0.26 valid for all soft clay sublayers. Intrinsic compressibility of natural specimens corresponded well with λ_R measured on reconstituted material. Despite difference in strain-rate and drainage conditions, λ_i values matched those obtained in IL oedometer tests, i.e. results in sublayer B complied while those in sublayers A and C were somewhat lower. To allow for detail analyse of strain-rate influence, compression indices need to be evaluated in relation to linear stress scale.

Correlation of intrinsic parameters λ_i and κ

Figure 6.46 examines validity of the Equation 6.2, correlating compression and swelling response of the destructured material. Compared to those on IL specimens, CRS oedometer test results were more scattered. Scatter reflected variation in effective stress and strain level reached in compression, and effects of strain-rate including pore pressure. Due to difficulties in CRS testing at high stress levels, limited amount of CRS tests were performed until sufficient level of destructuration, i.e. λ_i/λ_R<25%. Swelling slope measurement approach and variance in unloading stress range contributed the scatter. Among sufficiently destructured specimens, results for A19, 65C and 63A complied with Equation 6.2. In contrast, results for 63B plotted above, while 66C and occasional 63A results plotted underneath the correlation. In tests on 63B maximum σ'_1 in compression was <380 kPa. Thus, 63B results plotting above correlation were unloaded from considerably lower stress level. Remaining CRS tests on natural specimens compressed until the σ'_1~900 kPa, complied with those in IL odometer tests. Exception were 66C specimens 3000, 3001 and 3003, and 63A specimens 3049 and 3046, plotting underneath the correlation. The CRS results addressed were performed on high quality natural specimens compressed at 0.01 mm/mm. Considering the entire set of tests performed at strain-rate of 0.01 mm/mm, relation was well defined by equation Equation 6.18:

$$\lambda_i = \kappa + 0.18 \tag{6.18}$$

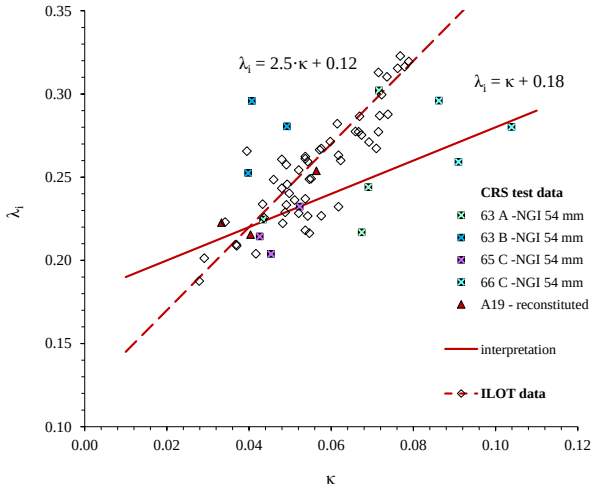

Figure 6.46 Relation of λ_i and κ in CRS oedometer tests on Perniö clay.

Thus, although characterized with higher scatter compared to those on IL specimens, results of CRS tests generally fit correlation representing behavior of destructured material. Results obtained at high strain-rate however, indicated strain-rate proportional shift of the trend-line toward lower λ_i and higher κ values.

Stress dependency of slope in compression

Continuous data in CRS oedometer test enabled detail evaluation of the change in the slope of the compression curve (see Figure 6.47). The data was used to define compression indices κ_o, λ and λ_i, identifying specimen response in reloading and NC stress range. Indices calculated from successively recorded data however, exhibited high oscillations in value. Oscillations were the highest in NC region, firstly, at stresses following the yield, and secondly, at stress level of ~4σ'_{vo}. Sequentially calculated λ following the σ'_p, varied from -3 to 15. Furthermore, at stress level of ~4σ'_{vo}, oscillations remained considerable, yet were characterised by positive values only. Although the oscillations correctly indicated material instability, to obtain representable compressibility indices moving average filtering technique was used. The aim of the filtering procedure was to select optimum range of data, i.e. large enough to exclude oscillations in the compression slope, jet narrow enough for accurate representation of compressibility. Filtering options considered moving average periods (MAP) ranging from 5 to 110 successive readings. Thus, the κ_o, λ and λ_i were defined as average slope within the certain period. The slopes obtained identified tangents on the compressibility curve. Optimum MAP depended on the magnitude of the oscillations. Due to considerable difference in compressibility prior and following yield, optimum MAP varied. In reloading, MAP of 5 sufficed, while optimum MAP in NC range varied between 40 and 90, depending on specimen sensitivity and strain-rate imposed. In this study compromise was found by merging optimally filtered curves in OC and NC stress range.

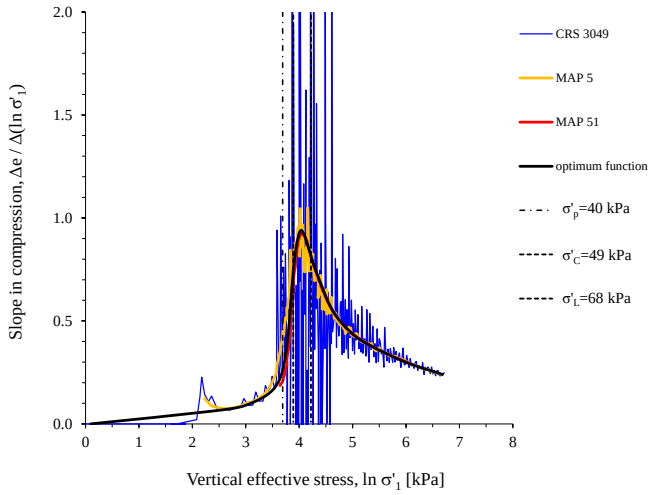

Figure 6.47 Interpretation of stress dependency of slope in compression, CRS 3049.

Figure 6.48-Figure 6.52 examine slope in compression stress dependency in selected CRS tests on reconstituted and natural Perniö clay specimens. Evaluation considered tests on A19, 63A, 63B, 65C and 66C. To examine effects of structure, results on natural specimens were contrasted with those on A19 reconstituted material. Successive values of slope in compression related to ln σ'_1, allowed evaluation of κ_o, λ and λ_i interpreted. In addition, slope in compression vs. σ'_1/σ'_p gave detail insight into stress and strain-rate influence on rate of change in compressibility, i.e. destructuration.

Unlike in IL tests on reconstituted samples in which similar κ_o and λ values were obtained, magnitude of the indices in CRS oedometer tests varied depending upon the strain-rate imposed. In tests at 0.01, 0.001 and 0.0002 mm/min, respective κ_o values within A28 amounted 0.045, 0.043, 0.047, while those in A19 were 0.043, 0.046, and 0.051. Thus, tests performed at lowest strain-rate exhibited the highest κ_o values. Furthermore, in A28 tests at 0.01, 0.001 and 0.0002 mm/min, λ values amounted 0.283, 0.250 and 0.231, respectively. In addition, A19 test performed at corresponding strain rates exhibited respective λ of 0.254, 0.223 and 0.216. Thus, influenced by the pore pressure build-up, λ values in tests on reconstituted specimens were proportional to strain-rate. Due to difference in size and initial water content of the specimens, λ values obtained in A28 tests were generally higher than those obtained within A19.

In Figure 6.48 a), slope in compression on A19 specimens is related to vertical effective stresses. Slope in reloading rose at rate reciprocal to the strain-rate imposed. Following yield, λ was the highest for test 3032 compressed at the highest rate, while at high stress levels, values of slope in compression coincided. Examined in relation to σ'_v/σ'_p in Figure 6.48 b), for $\sigma'_v/\sigma'_p<1$ rate of reloading slope increase was proportional to strain-rate. Within $1<\sigma'_v/\sigma'_p<10$, values of compression slope were proportional to strain-rate, while at high σ'_v/σ'_p influence of strain-rate was negligible.

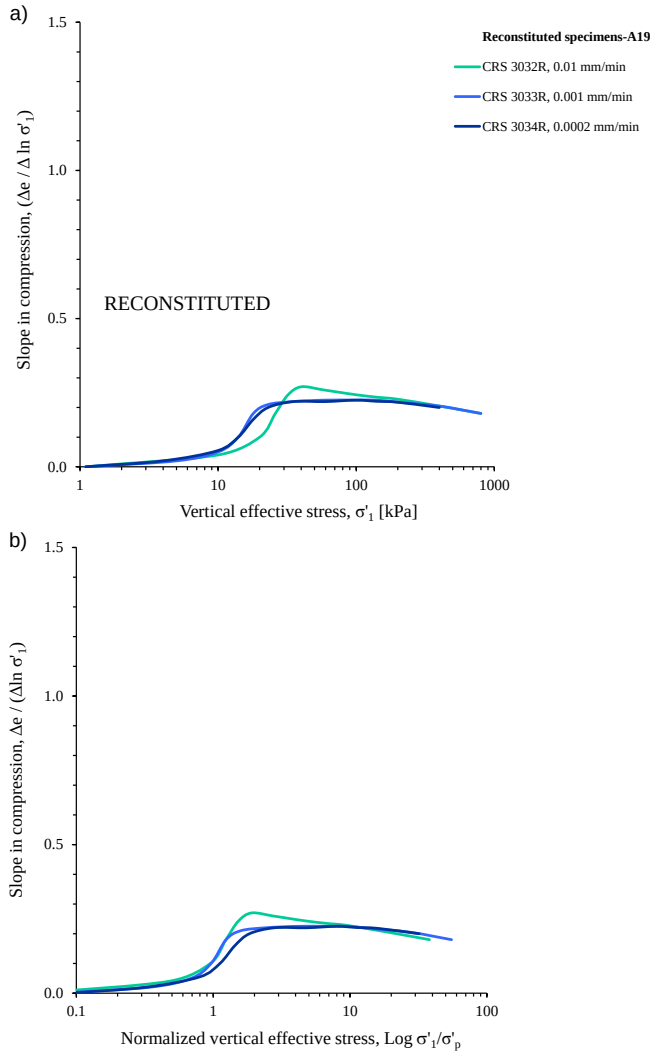

Figure 6.48 Slope in compression stress dependency for A19; a) slope in compression vs. ln σ'_1, and b) slope in compression vs. σ'_1/σ'_p .

Slopes in compression in tests on 63A are related to ln σ'_1 on Figure 6.49 a). Initial values of slope in reloading complied well with those obtained on reconstituted specimens. Following the yield, slope in compression rapidly rose to maximum value representing λ. Due to strain-rate influence, λ values occurred at different stress levels. Typical for low sensitivity specimens of uniform quality, λ values were similar in magnitude amounting 0.82 in average. Following the maximum, slope in compression progressively declined toward values obtained on reconstituted material. Rate of decrease was proportionally strain-rate dependent. Average λ_i at high stress levels amounted 0.29.

When normalized with σ'_p in Figure 6.49 b), curves defining slope in compression complied overall rather well. At certain stress ratio, curves obtained at high strain-rates generally exhibited higher slope in reloading. Compared to those on reconstituted specimens, slopes in reloading were greater. Following

the σ'_v/σ'_p=1, values of normalized slope in compression rose at similar rate, while maximum λ values occurred at similar stress ratio of 1.5. Finally, 63A curves merged with response of reconstituted specimens at σ'_v/σ'_p~20. Curves presented corresponded well with results on IL specimens of sublayer A.

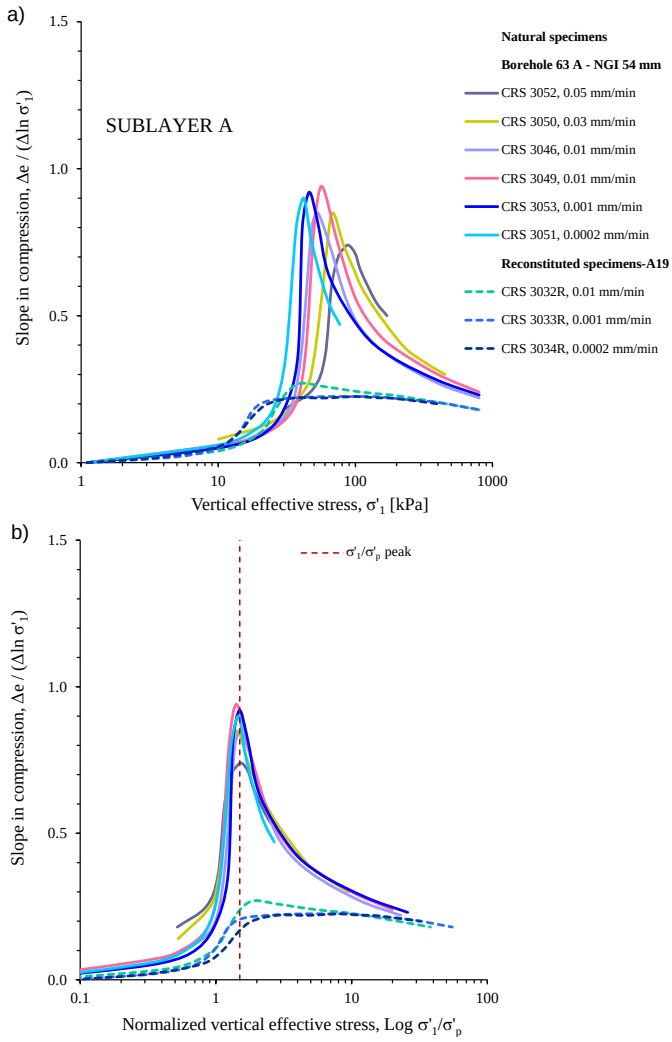

Figure 6.49 Slope in compression stress dependency for 63A; a) slope in compression vs. ln σ'_1, and b) slope in compression vs. σ'_1/σ'_p.

Slope in compression for 63B are related to ln σ'_1 in Figure 6.50 a). At low stresses, slopes in reloading were fairly uniform. Following the yield, slope in compression rose at rate reciprocal to strain-rate, being the highest for 3038 performed at 0.0002 mm/min, and the lowest for 3035 and 3036 compressed at 0.01 mm/min. λ values reached ranged from 0.57 to 1.08, and were reciprocal to strain-rate. In test compressed at identical strain-rates, λ values exhibited were proportional to specimen quality. Overall, λ in 63B exceeded values obtained in IL tests on material of sublayer B. Considering relatively low stress

level reached, final values of compression slope complied fairly well with those on reconstituted samples. Rate of compression slope decrease was proportional to strain-rate, while poor quality specimens reached λ_i at lower stress levels.

Normalization with σ'_p shown in Figure 6.50 b) revealed slope in compression in 63B being influenced by specimen quality and rate dependent destructuration process. Values of normalized slope in reloading were initially fairly similar, yet toward $\sigma'_v/\sigma'_p=1$, natural specimens exhibited distinctively higher slope in reloading compared to reconstituted. As a result of variation in magnitude of λ, following the $\sigma'_v/\sigma'_p=1$ values of normalized slope in compression rose at higher rate in tests compressed at the lowest rate. Stress ratio corresponding to λ varied from 1.25 in 3038 compressed at 0.0002 mm/min, to 1.4 in tests at 0.01 mm/min. Poor quality specimens reached intrinsic compressibility at σ'_v/σ'_p~5, while on those of high quality same effect was at σ'_v/σ'_p~10.

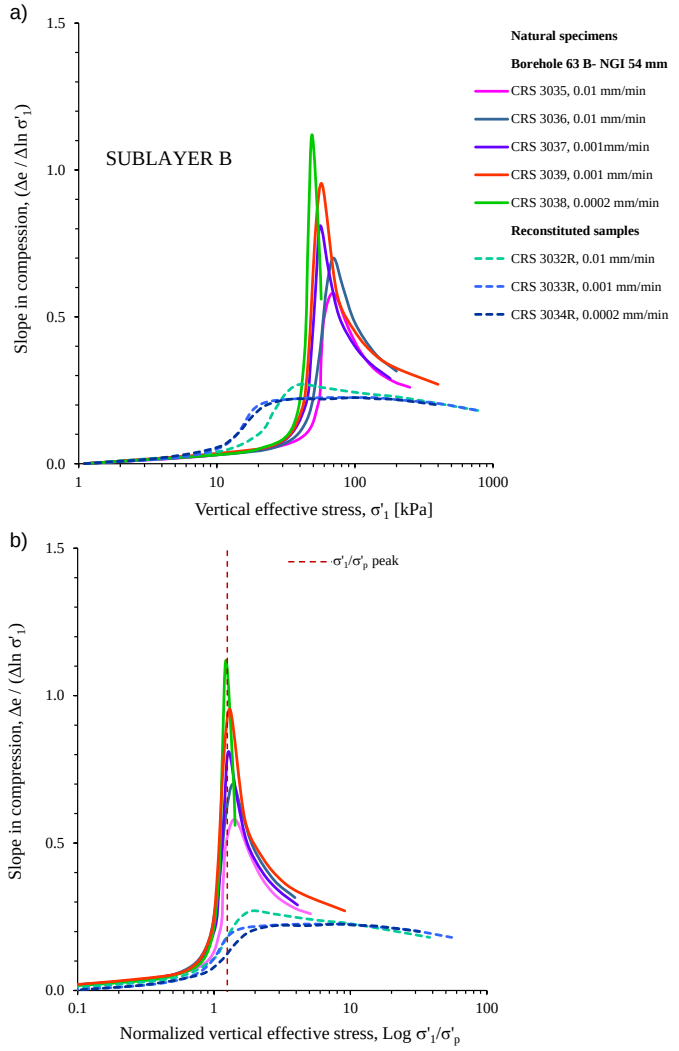

Figure 6.50 Slope in compression stress dependency curves for 63B; a) slope in compression vs. ln σ'_1, and b) slope in compression vs. σ'_1/σ'_p.

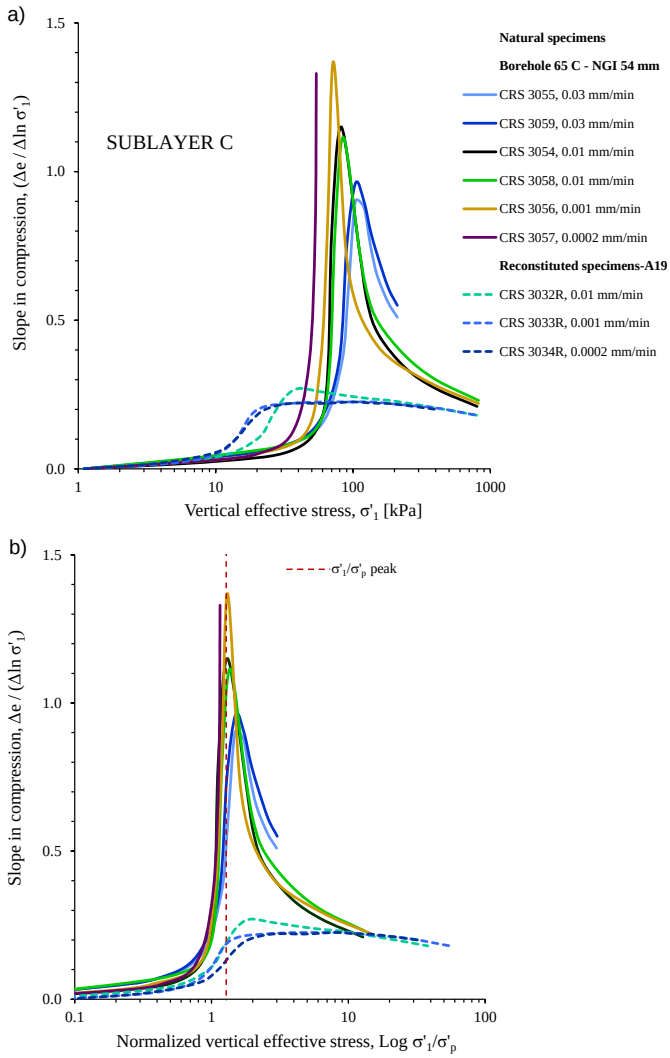

Figure 6.51 Slope in compression stress dependency for 65C; a) slope in compression vs. ln σ'_1, and b) slope in compression vs. σ'_1/σ'_p.

Results obtained on specimens 65C are shown in Figure 6.51 a). At stress levels prior and somewhat exceeding yield, rate of increase in compressibility was reciprocal to strain-rate implemented. In tests at high strain-rates, values of λ occurred at relatively higher stress levels. λ values varied significantly from 0.88 to 1.37, and were reciprocal to strain-rates imposed. Overall, λ in 65C exceeded those in IL tests on material of sublayer C. Rate of compression slope decrease was proportional to strain-rate imposed, while λ_i reached at high stress levels complied with those on reconstituted specimens.

When normalized with σ'_p, 65C curves indicated normalized reloading slope being proportional to strain-rate imposed. Typically for materials of high sensitivity, above $\sigma'_v/\sigma'_p=1$ rates of compression slope increase and magnitudes of λ were reciprocal to strain-rate implemented. Stress ratio values corresponding to λ varied from 1.28 in 3026 compressed at 0.001 mm/min, to 1.6 in 3055

performed at 0.3 mm/min. Overall, poor quality specimens reached intrinsic compression at somewhat lower σ'_v/σ'_p.

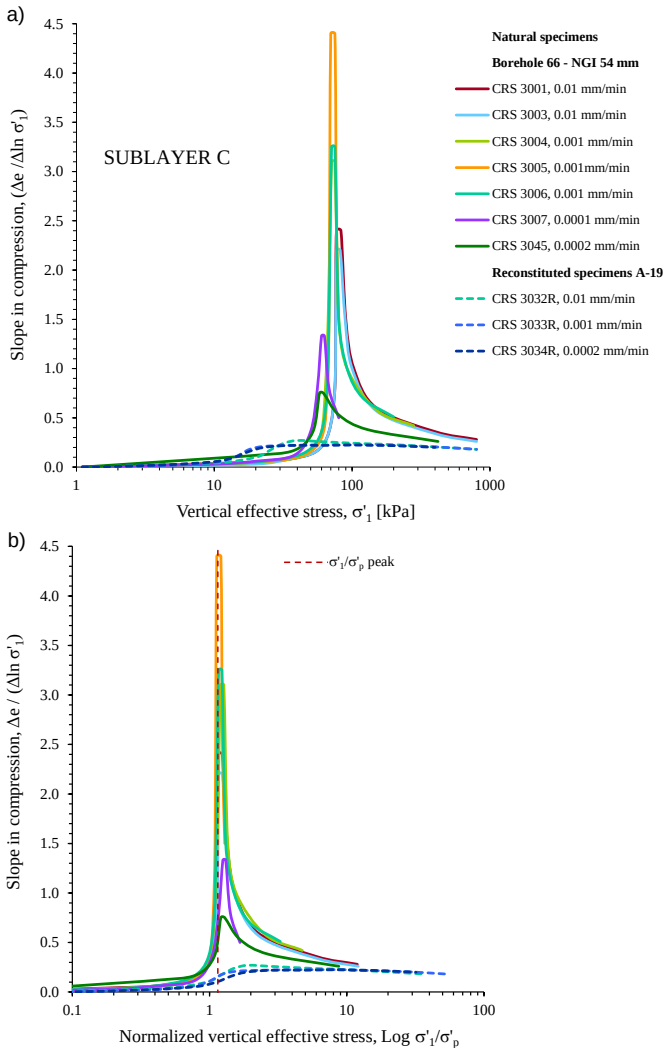

Figure 6.52 Slope in compression stress dependency curves for 66C; a) slope in compression vs. ln σ'_1, and b) slope in compression vs. σ'_1/σ'_p.

In Figure 6.52 a), slope in compression stress dependency curves on 66C are examined. Due to high sensitivity, λ values on 66C were the highest among IL and CRS test results. As for 63B and 65C, λ values were reciprocal to the strain-rate imposed. Exceptions were λ obtained on poor quality specimens 3045 and 3007. Considering tests performed at identical strain-rate, i.e. CRS 3000, 3001 and 3003 at 0.01 mm/min, and CRS 3004, 3005 and 3006 compressed at 0.001 mm/min, λ exhibited were proportional to w/γ. λ_i values at high stress levels complied with response of reconstituted specimens.

The 66C slope in compression curves normalized with σ'_p are shown in Figure 6.52 b). For high quality specimens, stress ratio corresponding to λ com-

plied, amounting 1.15, while for poor quality specimens corresponding σ'_v/σ'_p was somewhat higher. Again, poor quality specimens reached λ_i at relatively lower stress ratio.

Results presented exhibited consistent pattern of both strain-rate and specimen quality influence on compressibility. In tests on natural specimens, magnitude of maximum slope in compression λ, was reciprocal to strain-rate. Among specimens compressed at identical strain-rate, poor specimens exhibited lower value of λ. Prior to maximum, increase in compression slope was reciprocal to strain-rate, while following the maximum, compression slope declined proportionally to strain-rate imposed. In tests on reconstituted specimens, change in compression slope prior yield was reciprocal to strain-rate. In contrast to response obtained on natural specimens, magnitude of maximum slope in compression was proportionally strain-rate dependent.

Preconsolidation pressure normalized curves representing slope in compression are useful for evaluating validity of the unique compression concept [Leroueil et al. 1985, Leroueil et al. 1988b, Leroueil 2006, Watabe & Leroueil [2012] and Watabe et al. [2012]. According to the unique compression concept, slope in compression curves for tests performed at various compression rates, when normalized with respect of σ'_p, should coincide. However, results of CRS tests on Perniö clay expose limitations of the approach. In tests on natural specimens, resulting from strain-rate influence on magnitude of maximum slope in compression, rate of compression slope increase to maximum value was reversely proportional to strain-rate. Following the maximum slope in compression, specimens tested at high strain-rates exhibited lower rate of compression slope decrease. Influence of specimen disturbance was reflected by poor quality specimens reaching intrinsic slope in compression at relatively lower stress ratio. In tests on reconstituted specimens, for stress ratios prior $\sigma'_v/\sigma'_p=1$, as well as up to $\sigma'_v/\sigma'_p=10$, compression slope was proportionally strain-rate dependent, while for $\sigma'_v/\sigma'_p>10$, compression curves coincided. Based on slope in compression stress dependency curves for Perniö clay, destructuration process in tests at constant rate of strain was influenced by additional factors to those considered by stress normalization with respect to preconsolidation pressure. The discrepancy effects were proportional to strain-rate intensity and extent of specimen disturbance.

6.2.6 Compressibility–Compression modulus parameters

Interpretation of parameters

Perniö clay one dimensional compression results obtained under constant strain-rate conditions were examined using Compression modulus theory [Janbu 1967]. To enable comparison of the results, compression modulus interpretation approach initially used was consistent with that for IL oedometer test results. Later, implementation of alternative approach was examined, suitable for detail representation of compression modulus response in overconsolidated stress range. Resulting parameters were consistently related to those based on Cam-Clay theory. Premises of the interpretation approaches used are shown in Figure 6.53 and Figure 6.54 and explained in following.

Resulting from continuously loaded test procedure, CRS testing conveniently provided substantial amount of data. However, measured compression modulus data was characterised by oscillations. The effect had significant influence on analysis of the results, especially in the overconsolidated range. To enable consistent interpretation, measured data was filtered using moving average technique adopting various MAP. Optimum period was selected based on criteria ensuring representatives of compression modulus parameters.

When defining modes of σ'_1 vs. M response of clays and quick clays, Janbu [1967] identified compression modulus in reloading being constant. For quick clays constant compression modulus is defined as undergoing rapid decline to low extreme at preconsolidation pressure, while in NC stress range modulus continuously rises with vertical effective stresses. Although stating initial compression modulus being fairly constant, some experimental results presented by Janbu [1969] and Tokheim & Janbu [1976] indicated σ'_1 vs. M response of sensitive clays in reloading resembling parabola. Accuracy of the interpretation has direct impact on representatives of the results.

Parabolic response of compression modulus in reloading was to some extent recognized by Janbu et al. [1981], and Swedish practice [Larsson & Sällfors 1986, Larsson et al.1997, Claesson 2003], by adopting improved compression modulus curve including two constant compression moduli M_o and M_L, separated by linear yet not instantaneous compression modulus change at stresses prior preconsolidation. The linear decline in compression moduli from M_o to M_L is attributed to destructuration of soft clay. The change occurring over certain stress range rather than instantaneously indicates structure of sensitive material being progressively lost. Instead of continuous compression modulus increase following the yield, Swedish practice identifies stress range with constant compression modulus M_L. Thus, instead of unique minimum typical for response of reconstituted material, quick clays exhibit constant compression modulus M_L over certain stress interval following the yield. It is only with limit pressure σ'_L exceeded that compression modulus starts to rise.

To enable comparison with results of IL oedometer tests, Perniö CRS tests were interpreted on the basis of Swedish practice principles [Larsson & Sällfors 1986, Larsson et al.1997, Claesson 2003]. Details on interpretation approach used are shown in Figure 6.53 and elaborated in following.

Within overconsolidated region, natural Perniö clay specimens in CRS tests exhibited parabolic response in effective stress vs. compression modulus plane. Initially, compression modulus exponentially rose to peak value, and later gradually declined until σ'_p was reached. Thus, maximum value of compression modulus $M_{o\ max}$, separated two modes of compression behavior in reloading. Prior $M_{o\ max}$, specimen exhibited negligible strain, well represented by linear response in ln σ'_1 vs. v plane. The effect was used for consistent interpretation of reloading slope κ_o, calculated for stress range prior σ'_o.

Initial constant compression modulus M_o was defined as the maximum modulus measured within vertical effective stress range prior yield. Due to the considerable scatter of measured data, moving average filtering was used to obtain representable results. Namely, compression modulus data was evaluated using MAP from 3 to 21 subsequent readings. Values of M_o obtained con-

verged with the increase in MAP. Adequate value was selected by adopting criteria of change in maximum compression modulus for various averaging periods not exceeding $\Delta M_{o\ max}$ <0.15 MPa. With result set, vertical effective stress matching maximum value of compression modulus in reloading σ'_o was defined.

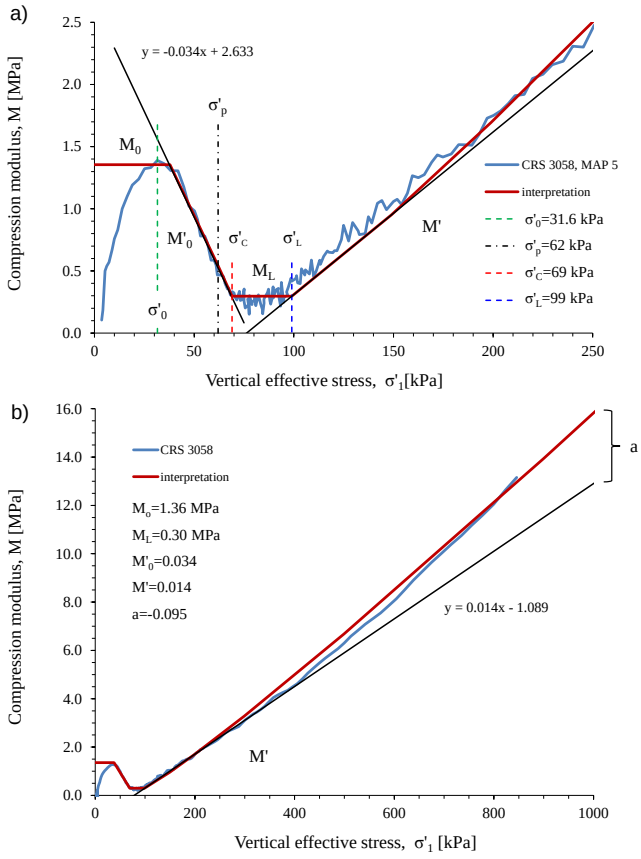

Figure 6.53 Interpretation of compression modulus parameters, CRS 3058; a) detail on compression modulus response in reloading, and b) entire testing stress range.

For stresses close to the preconsolidation pressure, the modulus drops until it again becomes constant and the stress-strain curve again becomes a straight line [Larsson & Sällfors 1986]. Thus, limit modulus M_L represented the lowest value of compression modulus measured on soft sensitive clay specimen. In CRS tests on natural specimens, stress range corresponding to M_L complied with that identifying maximum compression slope λ in v vs. ln σ'_1 plot. This fact was used for consistent interpretation of M_L stress limits σ'_C and σ'_L. Due to moderate oscillations in the measured compression modulus data, representative M_L value was obtained as an average modulus for stress range between σ'_C and σ'_L. Unlike in IL test where M_L was defined from one value only, in CRS tests entire set of data within the stress range was considered.

In accordance with Swedish practice, decline in compression moduli amid constant values of M_o and M_L, is linear. Herein, the transition was defined by

line interpolated on compression modulus data for stresses between σ'_o and σ'_p, with σ'_o denoting initial effective stress and σ'_p being the preconsolidation pressure. The destructuration line so obtained and identified by the slope M'_o and intercept M'_{oi}, idealises compression modulus change as an effect of destructuration in reloading. Position of σ'_p between constant moduli extremes is a meter of argument or definition [Tokheim, Janbu 1980]. Generally, bilinear definition of σ'_p in ln σ'_1 vs. v plane represented lower limit, while σ'_C in σ'_1 vs. M plot was representative of upper limit of the preconsolidation pressure.

Limit pressure σ'_L, is the vertical effective stress where the linear portion of stress-strain curve after the preconsolidation pressure ends, and the modulus starts to rise with increasing effective stress [Larsson & Sällfors 1986]. Increase of compression modulus in NC region was defined by a line of M' slope and M'_i intercept, interpolated for a stress range above σ'_L and prior to provisionally selected effective stress level of 500 kPa. Final segment of the compression modulus curve corresponding to σ'_1>500 kPa, was interpreted in compliance with Equation 6.3, using the parameter a.

Interpretation approach defined was made using algorithm, automatically identifying optimum parameters. Results of compression modulus interpretation of selected CRS tests on Perniö clay are presented in relation to vertical effective stresses in Figure 6.57 to Figure 6.61.

Beside above defined approach based on Swedish practice, alternative interpretation was examined (see Figure 6.54). True representation of compression modulus in overconsolidated region necessitated definition of both progressively increasing and decreasing compression modulus for stresses preceding and following σ'_o. Continuously measured data in CRS tests allowed interpolation of parabola, with apex corresponding to (σ'_o, $M_{o\,max}$). The approach enabled detail examination of strain-rate influence on compression modulus response in reloading. Material response prior $M_{o\,max}$, indicates mobilization of available structure without destructuration taking place, with σ'_o representing effective stress to which material was unloaded as a consequence disturbances in sampling, storage and specimen preparation. Gradual compression moduli decline following the σ'_o is attributed to progressive destructuration process prior yield. Influence of strain-rate on the rate of destructuration of sensitive clay material was evaluated by considering characteristics of the parabola interpolated. Namely, parabola was defined using quadratic Equation 6.19:

$$M = a_0 \cdot \left(\sigma'_v - \sigma'_0\right)^2 + M_{0\max} \tag{6.19}$$

where: a_o termed destructuration rate coefficient defined characteristics of the parabola with apex in point with coordinates σ'_o and $M_{o\,max.}$ For a_o<0, parabola opens downwards. Magnitude of a_o defined horizontal stretch, i.e. increase in a_o made the arms of the parabola moving closer together, while decrease in a_o made the arms spread out wider. Thus, relation of parameter a_o with strain-rates imposed allowed detail evaluation of strain-rate influence on rate of the destructuration. Remaining aspects of the interpretation approach were identical to those based on Swedish practice. Results of parabola based tangent modulus interpretation of selected CRS tests are presented in Figure 6.62.

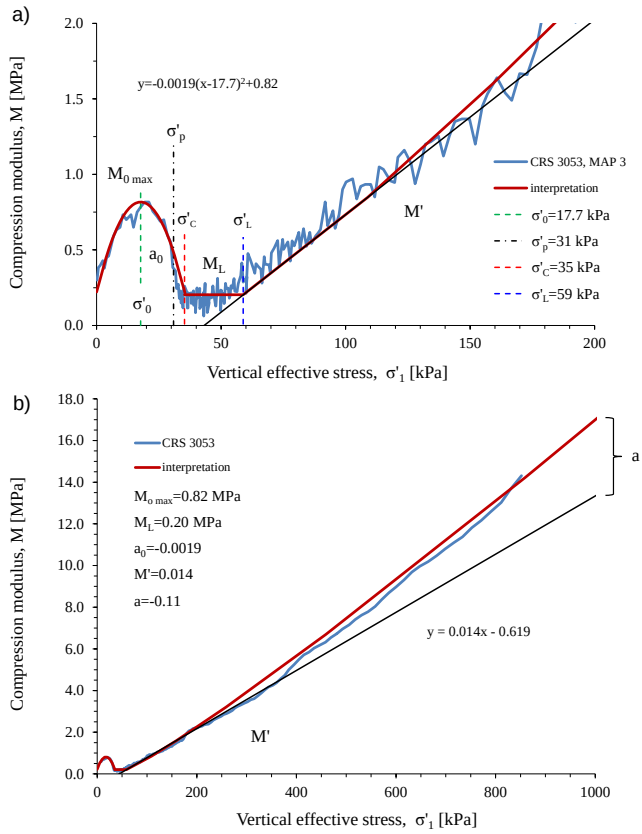

Figure 6.54 Alternative interpretation of compression modulus parameters, CRS 3053; a) detail on compression modulus response in reloading, and b) entire testing stress range.

Initial M_o and limit compression modulus M_L

Figure 6.55 a) shows values of initial compression modulus M_o, displayed vs. depth. Representable values of M_o in respective soft clay sublayers amounted 0.80, 1.20 and 1.60 MPa. Compared with those in IL oedometer tests, the M_o values exhibited similar response, yet were overall somewhat higher. Thus, the M_o values progressively increased with depth, indicating proportional relation to clay content and effective overburden stress. High quality specimens with $w/\gamma>7$ %/kN/m³, frequently exhibited high M_o. M_o values on reconstituted specimens were represented by average of 0.53 MPa, thus complying well with response of reconstituted material in IL oedometer tests. Based on the tests considered, strain-rate effects on magnitude of M_o were of low significance.

Values of limit compression modulus M_L are related to sampling depth in Figure 6.55 b). The results were characterised by average of 0.26 MPa, representative of soft clay sublayers overall. Due to influence of strain-rate M_L values exhibited moderate scatter. The results however, resembled those obtained on natural specimens in IL oedometer tests. Furthermore, M_L in CRS tests on reconstituted specimens were represented by an average of 0.29 MPa, being somewhat above 0.24 MPa obtained in IL oedometer tests. Specimens of high sensitivity exhibited the lowest M_L and thus the highest compressibility overall.

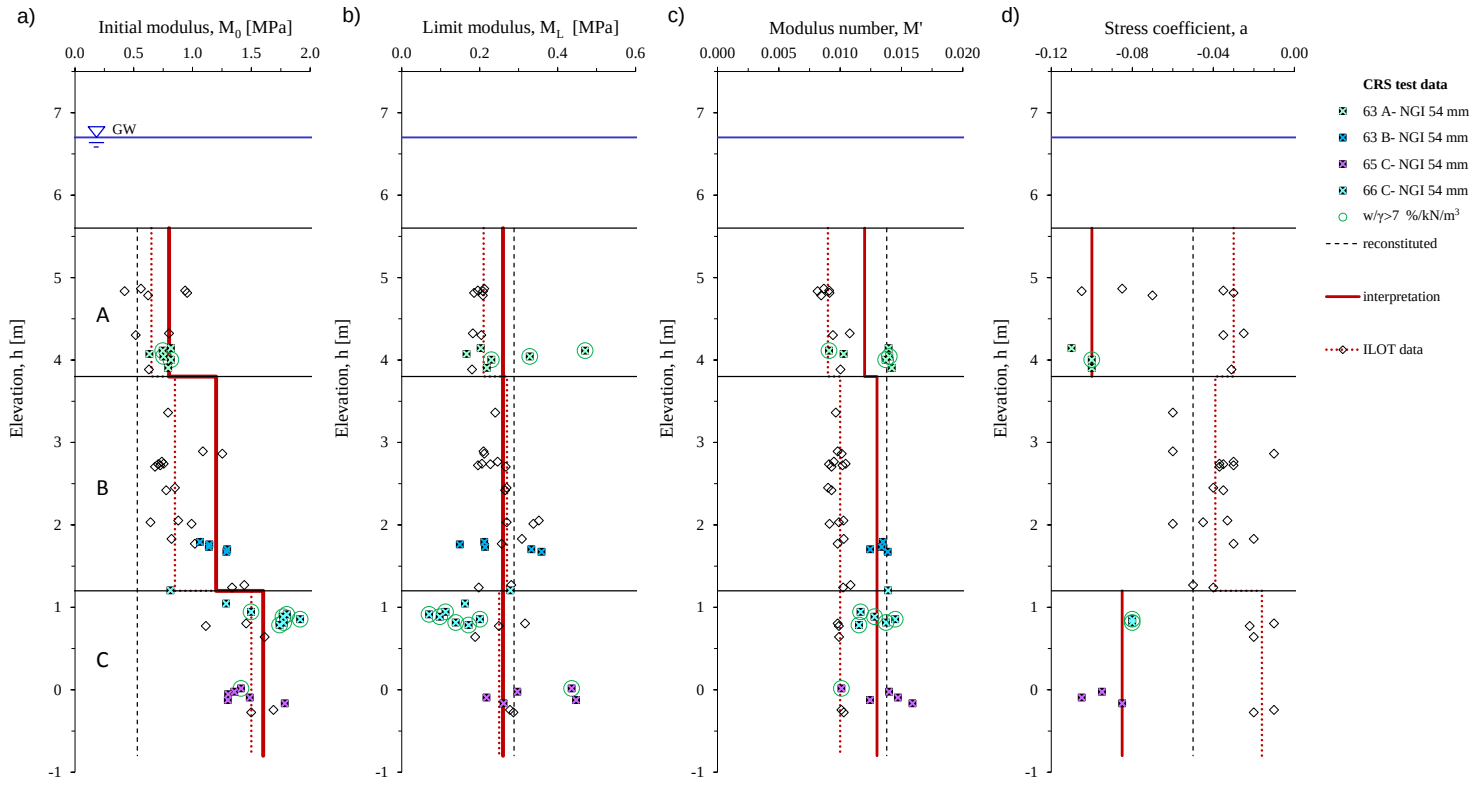

Figure 6.55 Compression modulus parameters in CRS oedometer tests; a) initial compression modulus M_0, b) limit modulus M_L, c) modulus number M', and d) stress coefficient a.

Modulus number M' and stress exponent a

As shown in Figure 6.55 c), modulus number M' in CRS tests on natural specimens were well represented by values of 0.012 in sublayer A, and 0.013 in sublayers B and C. Furthermore, M' characterising reconstituted material amounted 0.014. Overall, values of M' exhibited moderate scatter. Compared with results obtained in IL oedometer tests, resulting values were generally somewhat higher. The effect was related to difference in testing conditions.

Values of stress exponent a are related to depth in Figure 6.55 d). Compared with results in IL oedometer tests, main characteristic of compression modulus results in CRS tests was that of distinctively stiffer response at high effective stresses. At σ'_1 of 1000 kPa in IL oedometer test average compression moduli was ~10 MPa. At corresponding stress level in CRS tests, magnitude of compression moduli was significantly higher, amounting ~16 MPa. Stiffer response in CRS tests was manifested by a values considerably lower in magnitude. Limited amount of data allowed interpretation of response in zone A and zone C, only. The corresponding values of a amounted -0.100 and -0.085, respectively. In addition, average value of parameter a in CRS tests on reconstituted specimens was -0.050. The reasons for relatively low values of parameter a were related to difference in loading and drainage conditions in CRS testing.

Figure 6.56 examines effective stress parameters characterising compression modulus curve. Values of σ'_o increased with depth, confirming close relation with stress state of the specimen prior to testing, i.e. suction pressure. Due to negligible influence of strain-rate on specimen response prior to $M_{o\,max}$, scatter of the results was low. When normalized with effective overburden, resulting values mainly occurred within limits $0.5<\sigma'_o/\sigma'_{vo}<0.8$. Exception were high values in sublayer A with $\sigma'_o/\sigma'_{vo}\sim1.4$. In contrast, average σ'_o/σ'_{vo} on reconstituted specimens was 0.59. High quality specimens with $w/\gamma>7$ %/kN/m^3 generally exhibited the highest σ'_o/σ'_{vo}. Results obtained resembled those in IL oedometer tests. Lower limits of σ'_o/σ'_{vo} however, were generally higher indicating higher quality of CRS oedometer test specimens.

As in IL tests, effective stress parameters σ'_C and σ'_L, increased with sampling depth. The parameters were strongly influenced by strain-rate imposed. Consequently, results exhibited considerable scatter at corresponding elevation, i.e. tests indicative of high σ'_p exhibited increase in σ'_C and σ'_L. Despite occasional very high values within sublayer A, majority of σ'_C/σ'_{vo} values occurred between 1.2 and 1.8. The values corresponded well with results in IL oedometer tests. Furthermore, values of σ'_L/σ'_{vo} mainly occurred between 1.5 and 2.9. Again, some results in sublayer A exhibited somewhat higher values, i.e. 3.8. Compared with those in IL oedometer tests, σ'_L/σ'_{vo} values identifying CRS oedometer test specimens were generally less. Overall, specimens satisfying $w/\gamma>7$ %/kN/m^3 exhibited the highest σ'_C/σ'_{vo} and σ'_L/σ'_{vo}. In contrast to natural, for reconstituted specimen σ'_C was equal to σ'_L. Consequently, response of the reconstituted specimens was characterised by average stress ratio value of 1.52. The result complied with the lowest σ'_L/σ'_{vo} values identifying response of natural specimens.

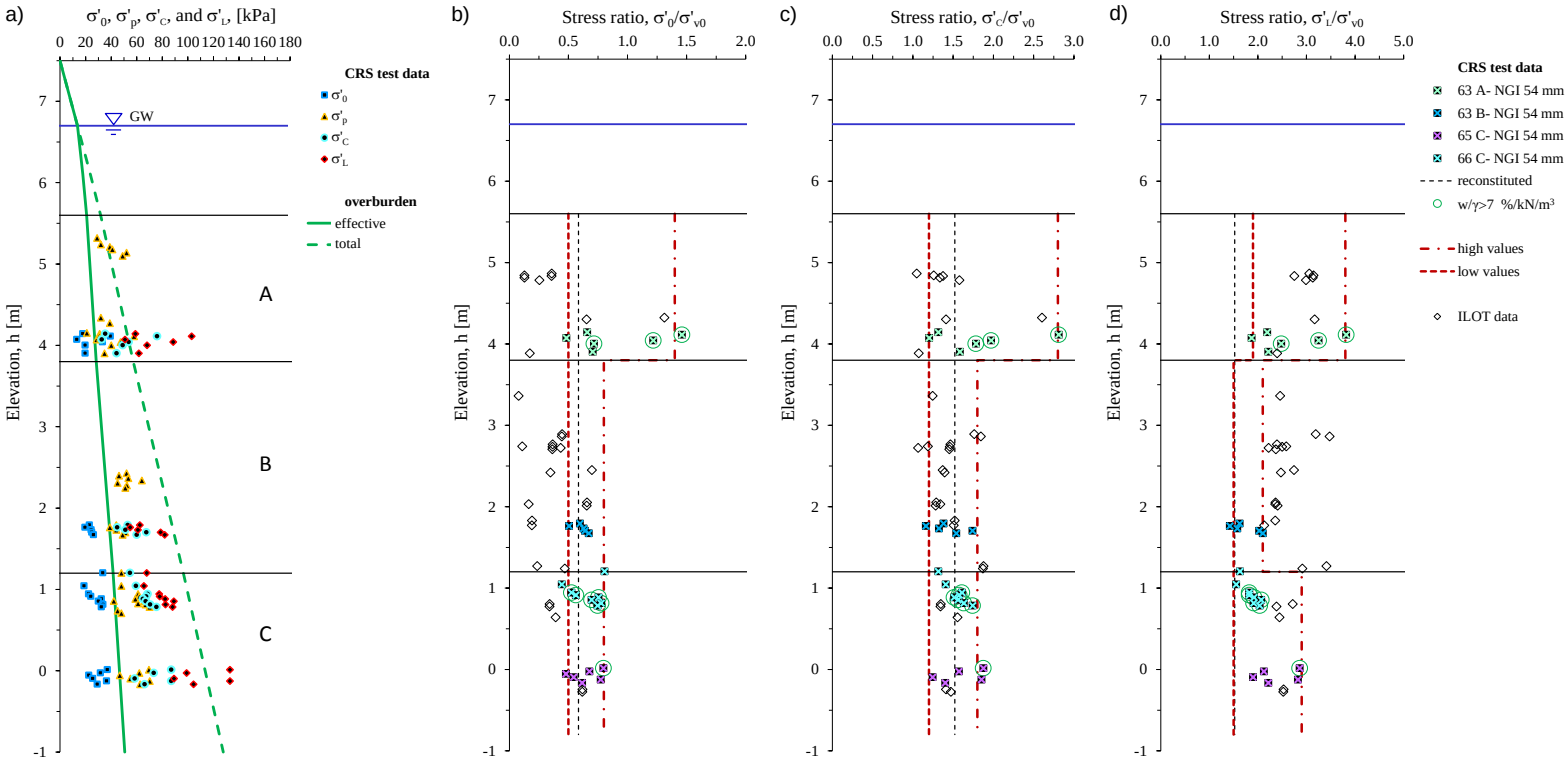

Figure 6.56 Evaluation of effective stress parameters characterising compression modulus curve in CRS oedometer tests; a) initial effective stress σ'_0, compression stress σ'_C, and limit stress σ'_L, b) σ'_0/σ'_{v0}, c) σ'_C/σ'_{v0}, and d) σ'_L/σ'_{v0}.

Effect of strain-rate and sample disturbance on compression modulus curve

Figure 6.57 to Figure 6.61 examine results of compression modulus interpretation for selected groups of CRS tests on Perniö clay. Emphases were given to identification of strain-rate and destructuration effects as well as to comparison of compression modulus parameters with respect to sampling depth.

Figure 6.57 presents compression moduli results obtained on A19 reconstituted specimens. Values of M_o were rather low, and varied from 0.47 to 0.60 MPa. Magnitudes of gradient M'_o were proportional to strain-rate imposed. Thus, transition from M_o to M_L occurred over the highest stress range in CRS 3032 at 0.01 mm/min. Typical for reconstituted material, M_L was reduced to a single stress level $\sigma'_C=\sigma'_L$. Considering results at various strain-rates, compression modulus response within NC stress range complied well. Indeed, responses above σ'_C were characterised by M' ranging from 0.013 to 0.014, and rather low stress exponent value of a=-0.05.

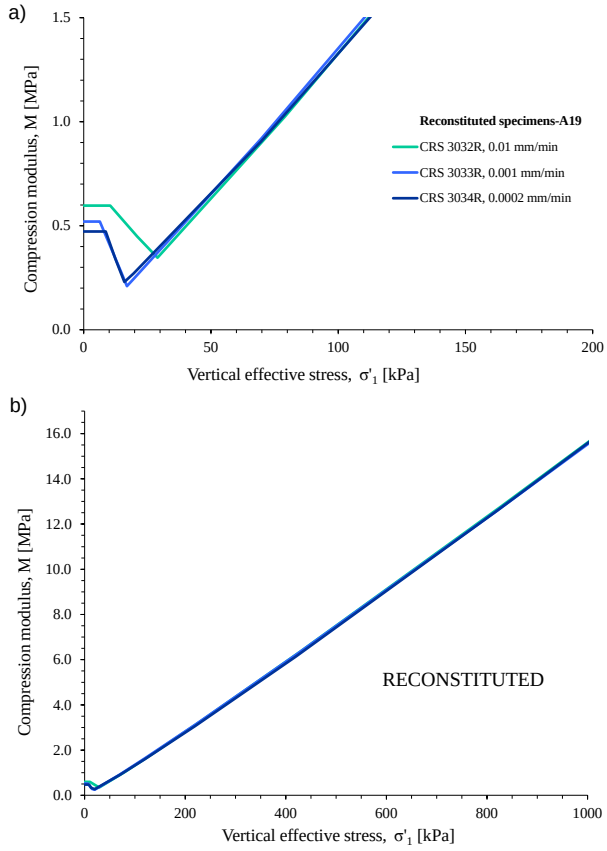

Figure 6.57 Compression modulus interpretation of A19 CRS oedometer tests, a) details on reloading, and b) entire stress range tested.

Results of compression modulus interpretation of 63A tests are shown in Figure 6.58. Due to narrow range of w/γ, values of M_o were uniform and amounted 0.76 MPa in average. Values of M'_o occurred between -0.051 and -0.013, and revealed proportional influence of strain-rate on compression mod-

ulus decline in reloading. The M_L values were proportionally strain-rate dependent as well, and ranged from 0.17 MPa at 0.0002 mm/min to 0.47 MPa at 0.05 mm/min. Thus, intensities of M_L confirmed proportional influence of strain-rate on specimen destructuration rate. Depending upon the strain-rate imposed, resulting σ'_L was proportionally translated toward higher vertical effective stresses. As for the entire set of CRS tests on natural specimens, values of M' appeared in a narrow range from 0.010 to 0.014. Finally, compression modulus responses at high stress levels identified low values of stress exponent, i.e. a=-0.010.

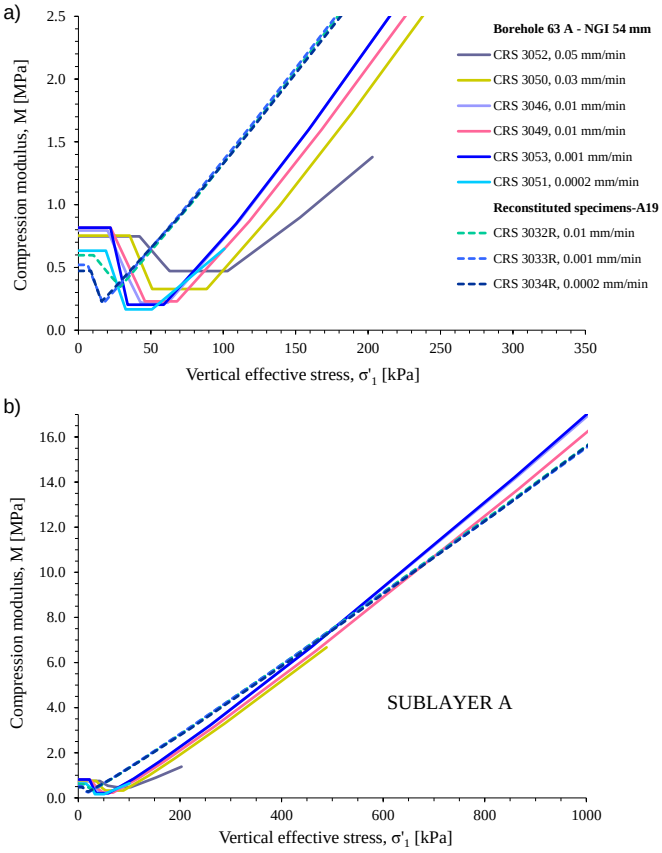

Figure 6.58 Compression modulus interpretation of 63A CRS oedometer tests, a) details on reloading, and b) entire stress range tested.

Figure 6.59 presents compression modulus results for 63B. Despite low w/γ overall, M_o values were relatively high, i.e. 1.06 to 1.30 MPa. Rate of compression moduli decline M'_o was proportional to strain-rate imposed, i.e. -0.049 in 3038 at 0.0002 mm/min to -0.026 in 3036 at 0.01 mm/min. Thus, destructuration prior yield was the most rapid in tests at low strain-rates. M_L values were proportional to strain-rate imposed as well. Furthermore, M_L values obtained at corresponding strain-rate complied in magnitude rather well. Effects of strain-rate on σ'_L were manifested by translation of compression modulus

curve to higher effective stress levels proportional to strain-rate imposed. For $\sigma'_L<\sigma'1<500$ kPa, modulus rose at fairly similar rate, corresponding well with that obtained on reconstituted specimens. 63B tests were not performed until sufficiently high stress level for evaluation of stress exponent.

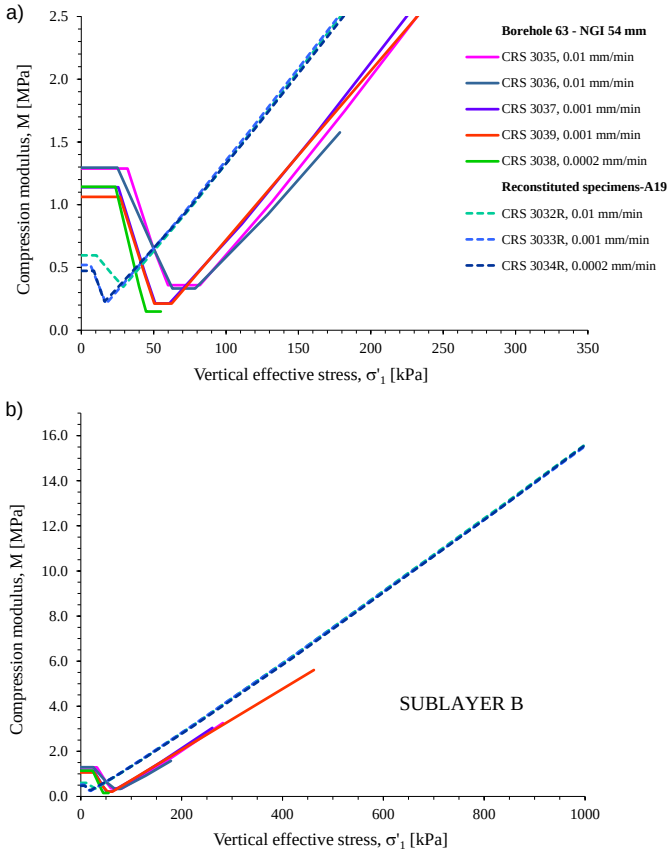

Figure 6.59 Compression modulus interpretation of 63B CRS oedometer tests, a) details on reloading, and b) entire stress range tested.

Interpreted compression moduli response for 65C is shown in Figure 6.60. Typically for sublayer C, M_o values were high and ranged from 1.30 to 1.78 MPa. Rate of destructuration in reloading was proportional to strain-rate imposed, with M'_o between -0.016 in 3055 at 0.03 mm/min, and -0.050 in 3056 at 0.001 mm/min. Values of M_L were strain-rate dependent as well, and varied from 0.22 in 3056 to 0.45 MPa in 3055. Proportional to strain-rate imposed, σ'_L values were offset to higher effective stress level. Values of M' varied considerably from 0.010 to 0.016, being the lowest in tests performed at high strain-rates. Stress exponent values ranged from -0.080 to -0.011.

Figure 6.61 presents compression modulus curves obtained for 66C. Due to large difference in specimen quality, M_o varied broadly from 0.81 in silty clay specimen 3045, up to very high values between 1.80 and 1.92 MPa on high quality quick clay specimens. M_L values were generally low and occurred over

narrow stress range. Considering high quality specimens only, M_L was proportionally strain-rate dependent and varied from 0.07 to 0.20 MPa. However, it was the poor quality silty clay specimen 3045 exhibiting the highest M_L overall, i.e. 0.28 MPa. Similarly to reconstituted specimens, increase in compression modulus above σ'_L was defined by M' between 0.011 and 0.015. At high stress levels however, compression curves approached those of reconstituted specimens at uniform and relatively high rate represented by a =-0.08.

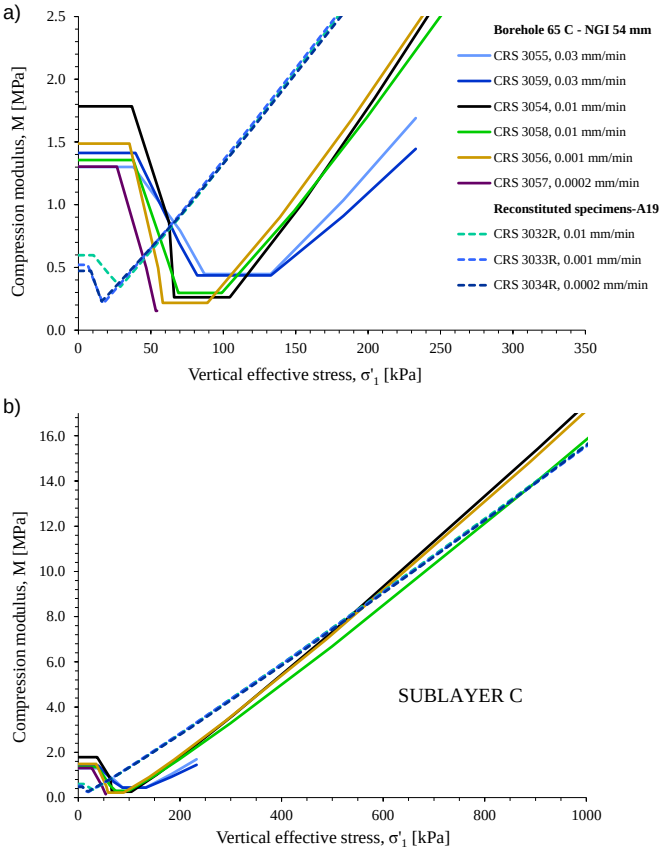

Figure 6.60 Compression modulus interpretation of 65C CRS oedometer tests, a) details on reloading, and b) entire stress range tested.

CRS test results interpreted in accordance with Swedish practice identified slope of the destructuration line M'_o, being proportional to strain-rate imposed. Linear representation of modulus decline however, was crude approximation of the true response. As an alternative, Figure 6.62 presents compression modulus stress dependency curves with reloading response represented by parabola interpolated to measured data. Apex of the parabola was set to coordinates (σ'_o; $M_{o\,max}$), identifying maximum compression resistance in reloading. According to Equation 6.18 magnitude of a_o identified rate of exponential compression moduli decline following $M_{o\,max}$. The approach enabled

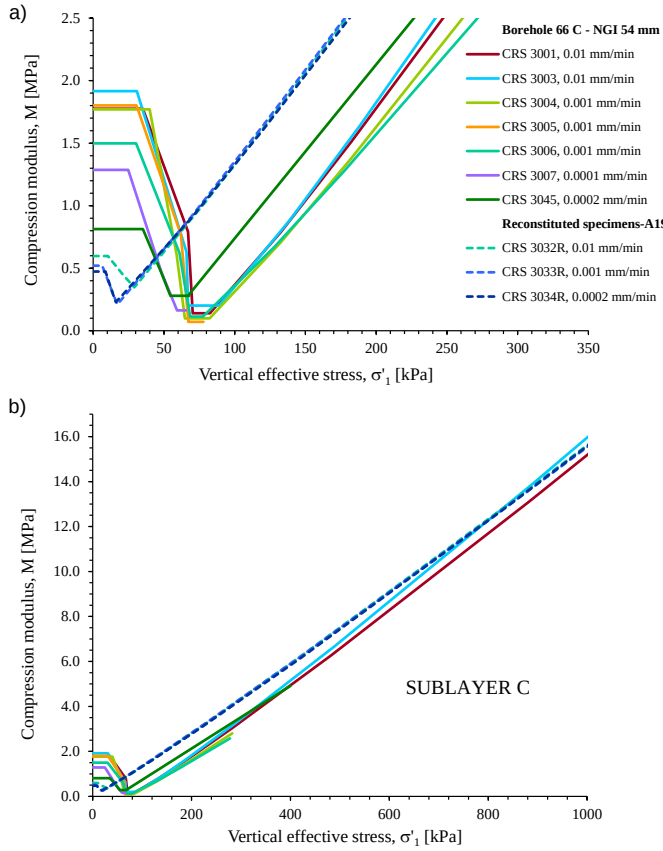

Figure 6.61 Compression modulus interpretation of 66C CRS oedometer tests, a) details on reloading, and b) entire stress range tested.

detail examination of strain-rate effects on destructuration in reloading. In Figure 6.63 values of destructuration rate coefficient a_o are related to strain-rates in CRS tests considered. Destructuration rate coefficient a_o was generally proportional to logarithm of strain-rate. The proportionality was clearly exhibited by sensitive clay specimens of 63B and 65C. Despite somewhat more pronounced scatter, same conclusion was valid for results on low sensitivity 63A material. Finally, the highest scatter and generally the lowest proportionality was exhibited by results of 66C.

Influence of strain-rate on M_L was studied by Larsson & Sällfors [1986]. According to the Authors, for strain-rates below some threshold value M_L is constant. However, if this rate is exceeded, the M_L increases with increasing rate of strain. Furthermore, the Authors suggested additional parameter for identification of strain-rate influence on compression moduli response following the σ'_p. The parameter, herein denoted by A, stands for vertical effective stress defined by the intersection of line representing linear increase in compression modulus above σ'_L, and effective stress axis, i.e. M=0. The Authors report A being approximately equal to the σ'_p of an undisturbed specimen, thus follow-

ing identical rate dependency as σ'_C [Larsson & Sällfors 1986]. Parameters A and M_L, being rate dependent, indicate σ'_L being rate dependent as well [Larsson & Sällfors 1986]. Results obtained on Perniö clay CRS tests confirmed magnitude of M_L, as well as corresponding stress limits σ'_C and σ'_L being proportionally strain-rate dependent. However, values of parameter A in CRS tests presented herein, although proportionally strain-rate dependent, were merely crude approximates of σ'_p interpreted. Based on Perniö clay CRS tests, it was the stress level defined by intersection of compression modulus response of natural, with that obtained on reconstituted specimen that corresponded with σ'_p of natural material.

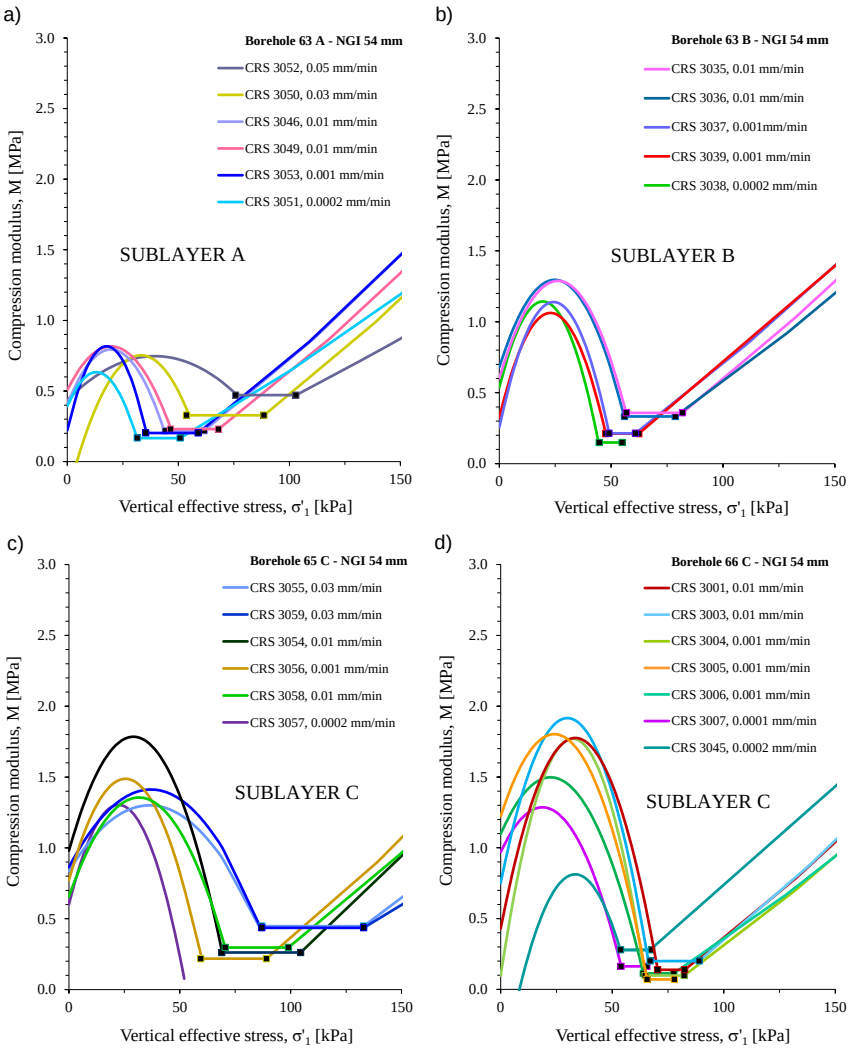

Figure 6.62 Compression modulus interpretation of CRS oedometer tests with reloading response represented by parabola; a) in 63A, b) 63B, c) 65C and d) 66C.

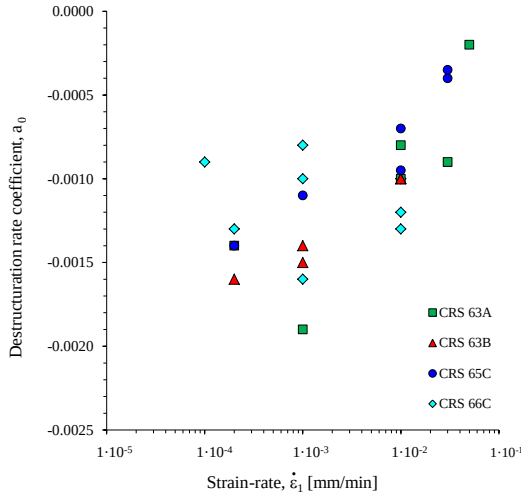

Figure 6.63 Relation of destructuration-rate coefficient to strain-rate in CRS tests.

6.2.7 Bonding parameters

Sensitivity

NC clay can exhibit an apparent preconsolidation pressure due to changes in interparticle forces resulting from chemical alterations, changes in salt concentration, replacement of pore fluid, long term secondary compression and thixotropy [Leonards & Girault 1961]. Furthermore, effect of strain-rate intensity is that of proportional offset of the oedometric compression curve toward higher vertical effective stresses. Compared to IL, disturbance during the continuous loading test are markedly diminished, while the rate of destructuration is dependent upon the strain-rate imposed. With the compression curve characteristics, i.e. κ_o, λ and σ'_p, influenced by both, bonding and strain-rate intensity, the resulting effects need to be considered when sensitivity parameters are interpreted. In following, sensitivity of specimens in CRS tests determined using approaches a, b and c are examined and compared (see Figure 6.64). In addition, issues related to determination of sensitivity from CRS compression curves are addressed.

Although characterised by similar values of λ_i, compressibility curves obtained on natural specimens at various strain-rates were at high vertical effective stress levels distinctively positioned. Consequently, for specimens with same initial specific volume, yet compressed at various strain-rates, sensitivity values could not be determined in relation to some average compression response of reconstituted material. To correspond with intrinsic compression characteristics of natural specimens of certain test group, several reference compression lines were used, depending upon the strain-rate within the actual tests. Ideally, for test on natural specimen performed at certain strain-rate, sensitivity and destructuration process should be evaluated in relation to destructured compression characteristics, obtained at corresponding strain-rate.

As well as being influenced by the strain-rate, compressibility of reconstituted specimen within NC stress range was dependent upon the initial water con-

tent. Reconstituted specimens in CRS tests originated from cylinders A19 and A28 obtained in distinctive reconstitution batches, i.e. R1 and R4. Average initial water content for A28 and A19 specimens amounted 76.0 and 67.1 %, respectively. At high stress levels where the influence of strain-rate was negligible, average compression slope in $\ln\sigma'_1$ vs. v plane was somewhat higher for A28 specimens amounting 0.231, compared to that of 0.192 for A19 specimens. Despite the difference in drainage conditions, average slope of the normal compression line on A28 specimens, i.e. 0.229, complied with that on IL oedometer test specimens reconstituted within the same batch R4.

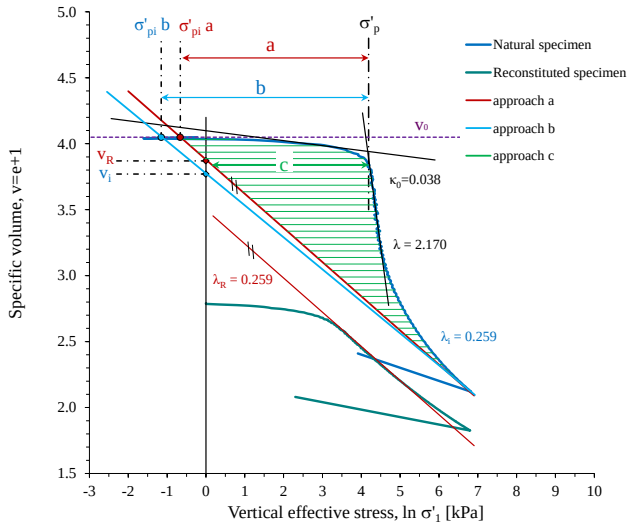

Figure 6.64 Sensitivity of CRS oedometer specimen interpreted using approaches a, b, and c.

Approach a

In approach a, sensitivity of specimens in CRS oedometric compression were calculated with Equation 6.6. Thus, reference line representing compressibility of destructured material was defined by average compressibility of reconstituted material within NC stress range (see Figure 6.64). To enable comparison with sensitivity in IL oedometer tests, λ_R of 0.259 was used. To compensate for strain–rate effects, line representing compressibility of reconstituted material was translated to tangent stress-strain response of natural specimens at high stress levels. Thus, reference lines differed in v_R, i.e. specific volume at intersection with specific volume axis. Translation of reference compression line had notable effect on sensitivity interpreted. In tests at low strain-rates, reference line positioned to fit compressibility of natural specimen at high stresses often intersected line of initial specific volume at $\sigma'_{pi}<1$. Consequently, specimens tested at lower strain-rates generally exhibited higher sensitivity values. Sensitivity obtained using approach a are in Figure 6.66 a) related to depth.

Approach b

In approach b, sensitivity was obtained using Equation 6.7. Thus, compressibility of destructured material was represented by line interpolated on data

defining compressibility of natural specimen at high effective stress levels, i.e. last ten readings (see Figure 6.64). If natural specimen was not compressed until sufficient level of strain, reference compression line could not be adequately positioned resulting with underestimation of sensitivity calculated. Unlike in IL oedometer tests, the amount of sufficiently compressed CRS specimens was limited. Indeed, due to considerable duration of tests at low strain-rates, sensitivity calculated often underestimated true values. Initial water content and quality of the specimen considered influenced strain response of natural specimens at high level of vertical effective stresses. Specimens of high quality exhibited higher intrinsic compressibility. However, reflecting the higher specific volume, high quality specimens generally resulted with the highest sensitivity values. Depth distribution of sensitivity values obtained with approach b, are presented in Figure 6.66 b).

Approach c

Approach c, defined by Equation 6.8, enables evaluation of strain-rate influence on rate of destructuration. As in the approach a, reference compressibility line representing destructured material was positioned to correspond with compressibility of natural specimen at high stress levels (see Figure 6.64). The line was thus defined by reconstituted specimen slope in compression $\lambda_{R,}$ and intercept v_R. Sensitivity was determined as ratio of vertical effective stress measured on natural specimen with that defined by reference compressibility of reconstituted material, evaluated at identical level of specific volume. Since CRS tests yield continuous compression curve, the interpretation approach provided continuous sensitivity data for the entire range of compressibility measured. Distinctive sensitivity values corresponded to specific level of water content. As presented in Figure 6.65, so obtained data related to vertical effective stress, void ratio or time, enable evaluation of the destructuration process under CRS conditions. Sensitivity values were not influenced by interpretation of preconsolidation pressures, since it was the maximum sensitivity that was considered representable for initial state of the specimen. Sensitivity obtained with approach c are related to depth in Figure 6.66 c).

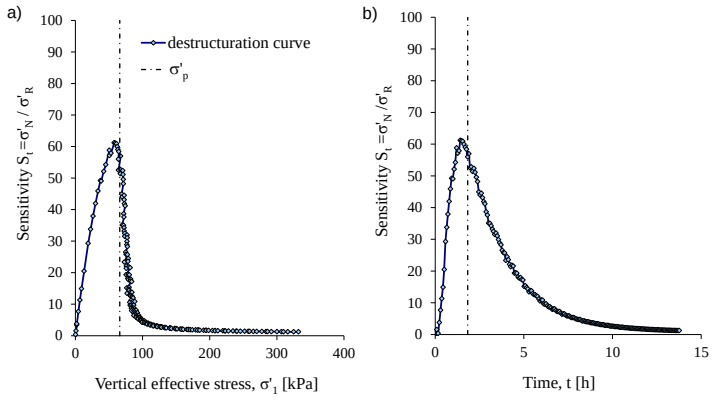

Figure 6.65 Continuous destructuration curve obtained using approach c; a) sensitivity vs. vertical effective stress, and b) sensitivity related to time.

Comparison of sensitivity obtained in oedometer test and fall cone test
In Figure 6.66, sensitivity interpreted from CRS test results on Perniö clay are related to depth and compared to values interpreted for IL oedometer tests and those obtained by fall cone test following the sampling.

Sensitivity values obtained using interpretation approach a, are related to sampling depth in Figure 6.66 a). Although scattered between 4.2 and 30.7, sensitivity representing 63A, 65A (NGI 54mm) and 67A (NGI 86 mm) CRS tested materials corresponded well to those of lower quality IL oedometer specimens. Furthermore, results on CRS specimens of sublayer A corresponded well to fall cone test sensitivities obtained on STII and NGI 54 mm sampled material. Exceptions were high values characterising destructured 63A specimens that exceeded average NGI 54 mm result for ~10 units. Sensitivity values obtained on specimens of 63B NGI 54 mm sampled material were negligible, i.e. $S_t<12$. The results corresponded to those obtained on poorest quality IL oedometer specimens of sublayer B. Finally, most of the values representing 65C and 68C test groups were rather uniform, i.e. $16.1<S_t<30.7$. The results resembled the lowest values obtained on IL oedometer specimens and average fall cone test results obtained on STII material. In contrast, sensitivity values representing CRS specimens of 66C NGI 54 mm sampled quick clay were considerable, and ranged broadly from $97.2<S_t<175.7$. The results corresponded with the highest sensitivity results obtained on IL oedometer specimens.

Sensitivity obtained on CRS specimens using the approach b are presented in Figure 6.64 b). The results generally exceed values obtained on IL oedometer test specimens. Although highly scattered and characterised by limited amount of representable results, pattern of sensitivity values representing sufficiently destructured specimens complied with that based on fall cone and IL oedometer results. Values representing the highest quality specimens of 63A and 65C, exceeded those obtained by fall cone test on 86 mm samples for ~20 units. Indeed, values representing former group were characterised by $11<S_t<72$, while those of the latter group with $50<S_t<73$ were generally somewhat higher. Sensitivity values obtained on destructured specimens of 63B group ranged from 4 to 9, indicating severely disturbed specimens at the onset of the tests. Remaining results representing insufficiently destructured specimens were negligible, i.e. <10. Overall the highest sensitivity values broadly ranging from $12<S_t<122$ represented destructured 66C specimens of quick clay.

Figure 6.64 c) presents depth distribution of maximum sensitivity values obtained on CRS specimens using approach c. Despite being somewhat lower in magnitude, identical choice of reference compressibility of destructured material led to distribution of sensitivity values similar to that using approach a. Within sublayer A sensitivity ranged between $2.6<S_t<13.7$. The highest values of ~13 were obtained on destructured specimens of NGI 54 mm sampled 63A material. Those obtained in CRS test on 67A (NGI 86mm) and 65A (NGI 54 mm) were somewhat less, typically ~8. Thus, CRS test determined sensitivity values within sublayer A were significantly lower compared to those representing high quality IL oedometer specimens. Typically for disturbed specimens of sublayer B, values obtained on 63B NGI 54 mm sampled material were low, i.e. $S_t<5.9$. Finally, sensitivity values in sublayer C were highly scattered, i.e. $3.4<S_t<76.9$. Values above 58.9 characterised high quality specimens obtained

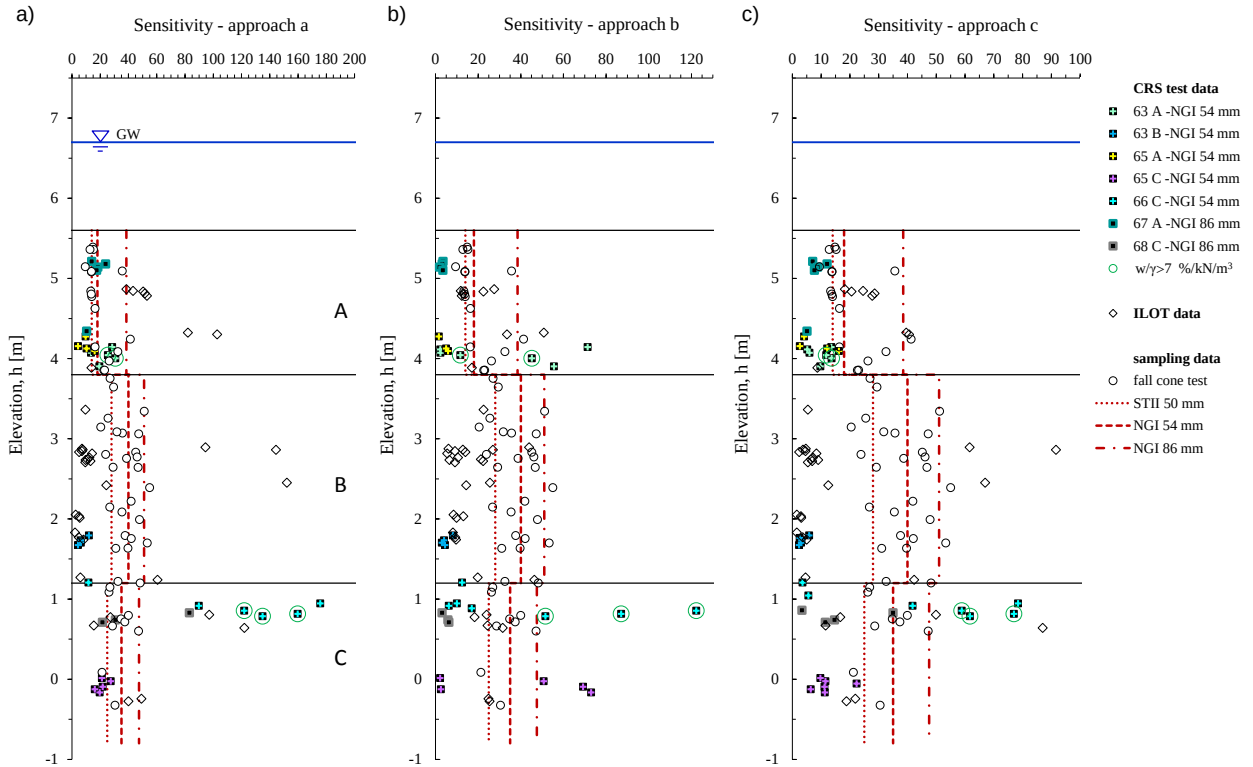

Figure 6.66 Sensitivity values of CRS and IL oedometer test specimens compared to values obtained using fall cone test after sampling; a) approach a, b) approach b, and c) approach c.

on 66C NGI 54 mm sampled material. Thus, sensitivity of high quality 66C quick clay specimens was 10 to 30 units higher compared to fall cone test average on NGI 86 mm material following the sampling. Although occasional sensitivity values were as high as 22.3 and 35.0, most of the results on 68C (NGI 86 mm) and 65C (NGI 54 mm) material were relatively low, i.e. S_t~11. The results were thus somewhat less than STII fall cone based average.

Considering approach c sensitivity results on IL and CRS specimens, two depth levels characterised by exceptionally high values emerge. Specimens at elevation from +2.45 to 2.89 absolute corresponding to sublayer B, exhibited sensitivity up to 91.6. Furthermore, specimens at elevation from +0.64 to 0.82 in upper portion of sublayer C, exhibited sensitivity as high as 87.0. Although differing in magnitude, high sensitivity values were spatially confirmed by results obtained using approach b, and in the case of highly sensitive zone of sublayer C, by approach a results. Provided that adequate attention is given to sampling, it is at these locations where highly sensitive quick clay material is.

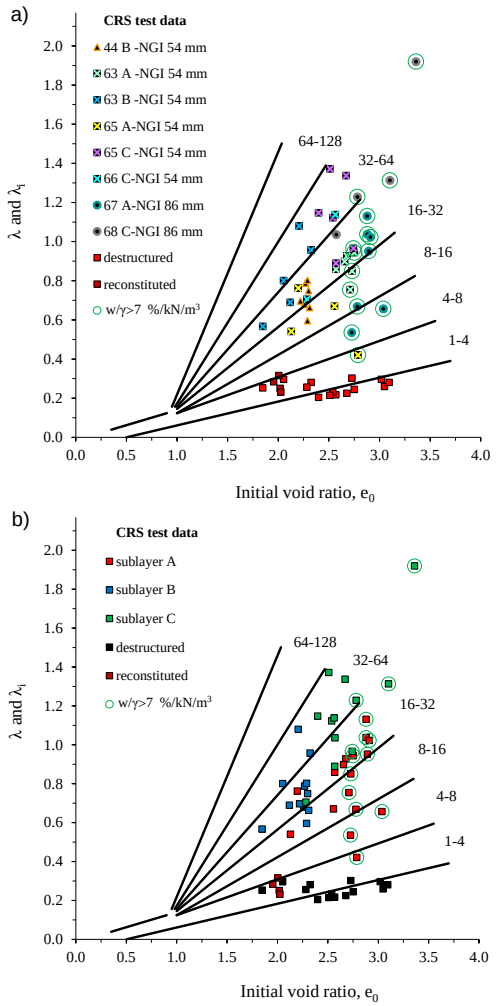

Figure 6.67 Sensitivity of CRS oedometer test specimens correlated from e_0 and λ (λ_i); a) related to sampling profile, and b) sublayer of origin [correlation after Leroueil et al. 1983].

To evaluate sensitivity values calculated with different approaches, resulting values were examined and compared to results of empirical correlation, relating sensitivity to initial void ratio and compression slope in NC stress range [Leroueil et al. 1983]. Unlike, a, b, and c interpretation approaches, estimation of sensitivity using empirical correlation did not necessitate complete destructuration of the specimen. Considering limited amount of CRS tests performed until sufficiently high strain levels, the correlated sensitivity values were of considerable importance for evaluation of both sampling and specimen preparation quality in CRS testing. Results obtained are in Figure 6.67 a) related to sampling profile, while in Figure 6.67 b) results are differentiated with respect to sublayer of origin. Considering material of sublayer A, most of the results were characterised with $16<S_t<32$. The highest sensitivity values were obtained on 67A material sampled with NGI 86, followed by 63A, and finally that of 65A sampled with NGI 54. Sensitivity values obtained on CRS specimens of sublayer B occurred within $8<S_t<64$. The highest sensitivity values $32<S_t<64$, were obtained on 63B material (NGI 54), while those of S-2009 44B exhibited $S_t<32$. Sensitivity values representing CRS specimens of sublayer C, were the highest. Sensitivity values ranging from 16 to 64 characterised NGI 54 sampled 65C specimens, and that of 68C sampled with NGI 86, with later characterised by somewhat higher e_o values. However, the values obtained on 66C NGI 54 sampled material were the highest overall. Indeed, sensitivity obtained on quick clay high quality specimens ranged from 64 to exceptionally high values >128.

Rate of destructuration

Sensitivity values determined using approach c, when related to vertical effective stress and void ratio, provide valuable information for evaluation of progressive destructuration process.

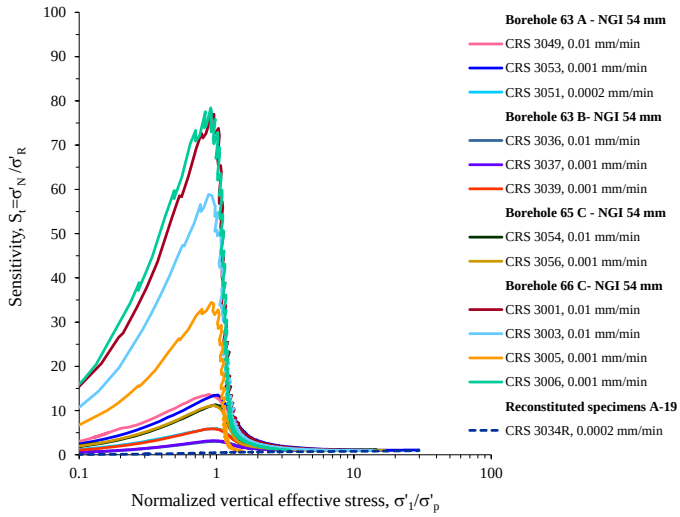

Figure 6.68 Sensitivity values in CRS oedometer test related to σ'_1/σ'_p.

In Figure 6.68 CRS test sensitivity data are related to vertical effective stress normalized with preconsolidation pressure. Entire set of curves regularly exhibited maximum sensitivity at preconsolidation stress level, i.e. at $\sigma'_1/\sigma'_p=1$, while at stress ratio levels corresponding to $\sigma'_1/\sigma'_p=3$, sensitivity was reduced to negligible values, i.e. $S_t<2$. Thus, for stress range following the yield, rate of destructuration was the highest. Advantage of continuous loading was clearly manifested if CRS test data are compared with results obtained on IL oedometer specimens in Figure 6.18. Resulting from IL procedure, sensitivity results following the yield were omitted. In contrast, CRS data accurately showed more rapid exponential decrease of sensitivity following the yield.

CRS sensitivity data are related to specific volumes in Figure 6.69. Maximum sensitivity values corresponded to specific volume at yield. An attempt to evaluate influence of specimen quality on rate of destructuration resulted with Equations 6.20 and 6.21. Complying with the conclusions derived for IL oedometer tests, rate of destructuration in CRS test was the most rapid for the highest quality specimens. Furthermore, compared to corresponding Equations 5.11 and 5.12 obtained in IL oedometer tests, rate of destructuration in CRS test was somewhat more pronounced.

$$S_{t\,HQ} = 0.0001\, e^{3.474v} \tag{6.20}$$

$$S_{t\,LQ} = 0.0011\, e^{2.513v} \tag{6.21}$$

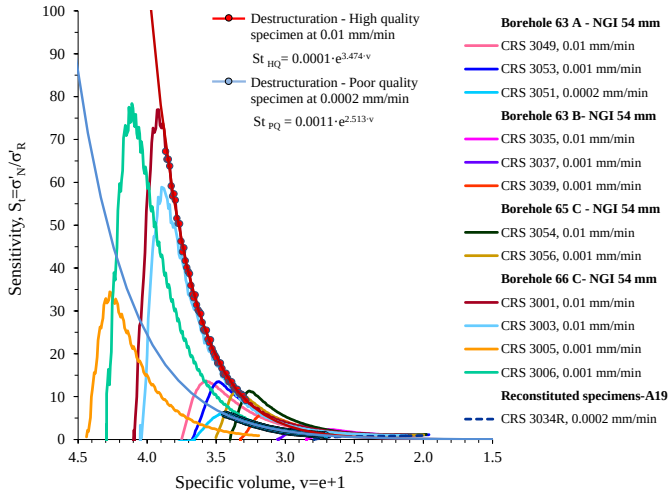

Figure 6.69 Sensitivity values in CRS oedometer test related to specific volume.

In Figure 6.70 $S_{t\,max}$ values obtained on CRS oedometer test specimens sufficiently destructured in testing ($\lambda_i/\lambda_R<25\%$) are shown vs. initial void ratio. The CRS test results showed exponential decrease in $S_{t\,max}$, representing initial structural characteristics, with decline of e_o of the specimens considered. In addition, Equation 6.22 defining CRS results was similar to that representing response of IL specimens. Thus, unlike those of other approaches, results of

approach c were compatible considering both IL and CRS oedometer test conditions.

$$S_{t\max} = 0.015\, e^{2.63 e_0} \tag{6.22}$$

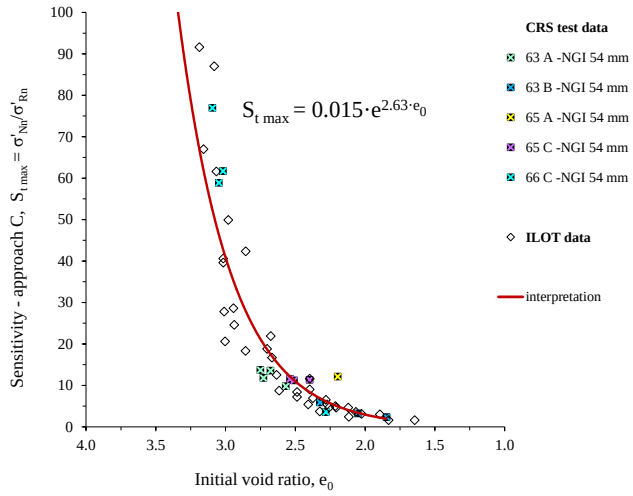

Figure 6.70 Maximum sensitivity values in CRS oedometer test related to initial void ratio.

6.2.8 Strain-rate parameters

Strain-rate coefficient β

In Figure 6.71, preconsolidation pressures in CRS tests on Perniö clay are related to strain-rate. Results on both natural and reconstituted specimens confirmed σ'_p being proportional to magnitude of strain-rate. To enable evaluation of response in distinctive soft clay materials, stain-rate dependency was examined in strain-rate vs. Log σ'_p/σ'_{vo} plane in Figure 6.72.

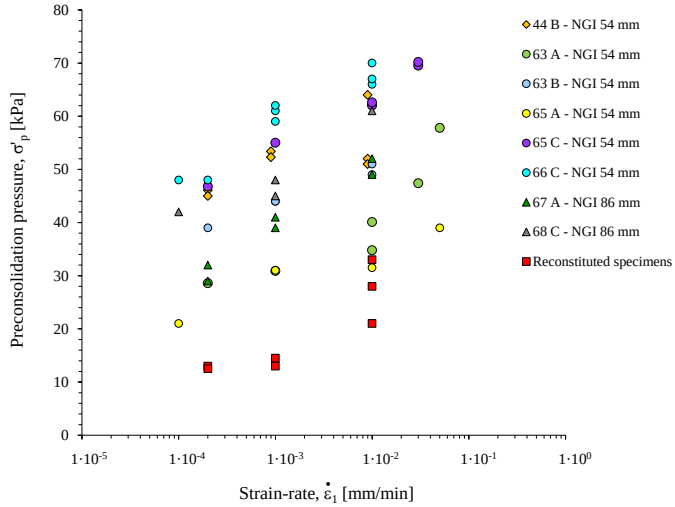

Figure 6.71 Influence of strain-rate on magnitude of σ'_p in CRS oedometer tests on Perniö clay.

Figure 6.72 a) presents CRS results on sublayer A material from profiles 63, 65 and 67. Reflecting the highest quality of specimens considered, results on NGI 86 sampled profile 67 exhibited the highest values of Log σ'_p/σ'_{vo} overall. The results were well represented by linear relation. Somewhat deviating from linear response were data on poor quality specimens tested at low strain-rate. Considering the highest quality 67A specimens characterised by average w/γ of 7.52 %/kN/m^3 and $\Delta e/e_o$ of 0.038, strain-rate dependency was expressed by linear relation of slope 0.0466, and rather high intercept 0.8964. In contrast to 67A results, Log σ'_p/σ'_{vo} values representing 63A NGI 54 sampled material were somewhat less. Although obtained on specimens of similar quality, results were fairly scattered. Considering results on selected specimens characterised by w/γ of 7.02 %/kN/m^3 and $\Delta e/e_o$ of 0.055, strain-rate influence was interpreted by linear relation defined by slope 0.0432 and intercept 0.6825. Among the tests on sublayer A material, results on 65A (NGI 54) were the most scattered, and marked by the lowest Log σ'_p/σ'_{vo} values overall. The results represented poor quality specimens with average w/γ of 6.14 %/kN/m^3 and $\Delta e/e_o$ of 0.052. Based on entire set of data, strain-rate dependence was interpreted by linear relation with slope of 0.0396 and intercept of 0.5678. Considering entire set of the results, slopes representing sublayer A material matched well. Intercept values however, differed considerably reflecting proportional relation to specimen quality.

CRS results obtained on sublayer B material of profiles 44 and 63, are shown in Figure 6.72 b). The 44B tests performed on NGI 54 sampled material in 2009, exhibited rather high values of Log σ'_p/σ'_{vo}. The effect was possibly related to smaller size of the specimens considered. With an exception of results at the highest strain-rate exhibiting relatively low Log σ'_p/σ'_{vo}, strain-rate effects on 44B specimens were well represented by linear relation with slope 0.0387 and intercept 0.6708. The results considered were marked by rather low average w/γ of 5.68 %/kN/m^3. Although characterised by specimens of poorer quality compared to 44B, results obtained on 63B (NGI 54) were less scattered. Furthermore, 63B results were represented by linear relation with somewhat lower slope of 0.0287. Reflecting relatively poorer specimen quality with average w/γ of 5.50 %/kN/m^3 and $\Delta e/e_o$ of 0.065, 63B results exhibited lower intercept, i.e. 0.4559.

Results obtained on sublayer C material are shown in Figure 6.72 c). The highest values of Log σ'_p/σ'_{vo} were obtained on high quality 66C specimens (NGI 54). With an exception of those at the lowest strain-rate, the results consistently exhibited linear proportionality. The slope identifying relation was relatively low 0.0274. Furthermore, reflecting very high quality of the specimens considered, i.e. average w/γ of 8.45 %/kN/m^3 and $\Delta e/e_o$ of 0.041, intercept of the relation was rather high 0.5226. Results obtained on NGI 86 sampled profile 68C were somewhat more scattered. The results were interpreted by linear relation characterised by slope 0.0363, and intercept 0.5664. Compared to 66C, quality of the specimens considered was somewhat less, i.e. average w/γ was 8.01 %/kN/m^3 and $\Delta e/e_o$ was 0.052. Finally, slope of 0.0301 identifying results on 65C corresponded rather well with those obtained for 66C and 68C. Reflecting relatively poorer quality of 65C specimens, i.e. w/γ of 6.31 %/kN/m^3 and $\Delta e/e_o$ of 0.054, resulting intercept was rather low 0.4782.

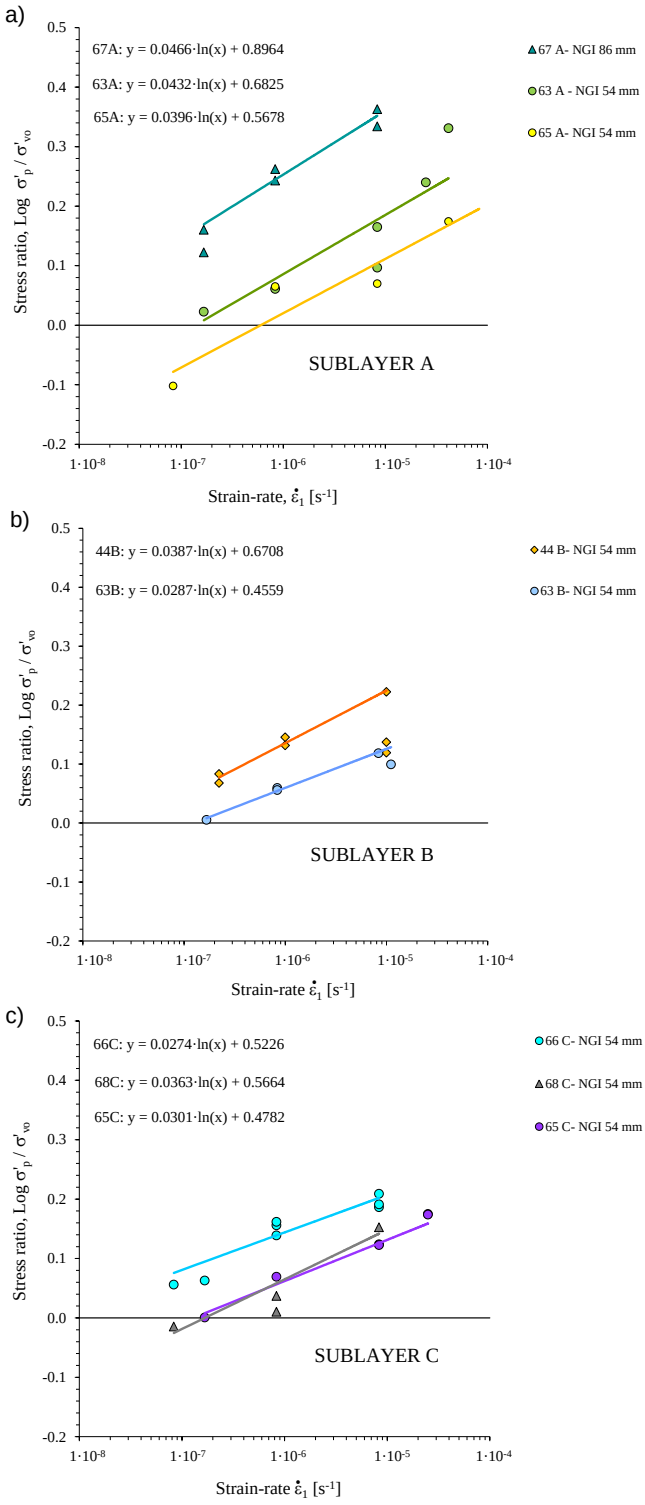

Figure 6.72 Strain-rate vs. σ'_p/σ'_{v0} in CRS oedometer tests; a) 63A, 65A and 67A, b) 44B and 63B, and c) 65C, 66C and 68C.

Figure 6.73 a) relates entire set of CRS results in strain-rate vs. Log σ'_p/σ'_{vo} plane. The results are distinctively displayed with respect to sublayer of origin. The slopes identifying linear strain-rate vs. Log σ'_p/σ'_{vo} relation in tests on sublayer A material were the highest. In addition, slopes identifying sublayer B and C materials corresponded in magnitude rather well. Furthermore, results on NGI 86 sampled 67A material of the highest sampling quality exhibited the highest intercept values overall. Influence of specimen preparation was reflected by results on NGI 86 profile 68C, characterised by Log σ'_p/σ'_{vo} values considerably less in magnitude. Considering NGI 54 sampled material, results on profiles 66C and 44B exhibited rather high Log σ'_p/σ'_{vo}, implying specimens of high quality. In contrast, results on NGI 54 sampled 63A, 63B, 65C and 65A material, characterised by relatively low Log σ'_p/σ'_{vo} values, indicated considerably disturbed low quality specimens.

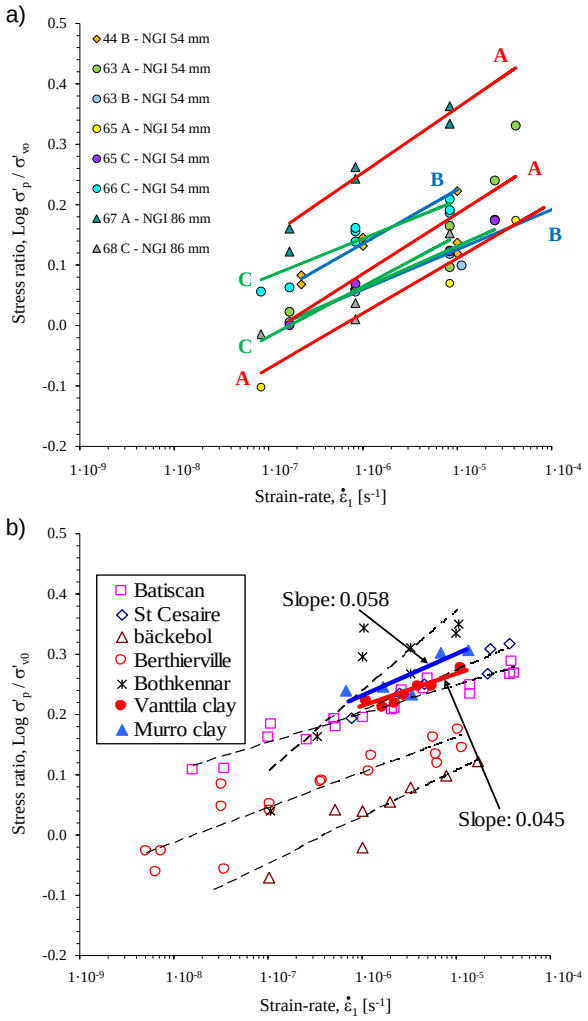

Figure 6.73 Comparison of Perniö clay strain-rate vs. σ'_p/σ'_{v0} data with results for other clays; a) results on Perniö clay, and b) results for other clays after Yin et al. [2001].

In Figure 6.73 b), strain-rate dependency results on Perniö clay are compared with data for other clays. CRS tests on 67A made on the highest quality NGI 86 sampled material, complied well with results obtained on Bothkennar clay. As well as Perniö clay of sublayer A, Bothkennar clay is generally characterised by relatively low sensitivity of 10. Due to sample disturbance remaining results on material of the same sublayer, i.e. NGI 54 sampled 63A and 65A, complied in slope, yet differed in magnitude of Log σ'_p/σ'_{vo}. Results obtained on high quality specimens of NGI 54 profiles 44 and 66, representing soft clay sublayers B and C, resembled those of Berthierville and Batiscan clay. Remaining results on sublayers B and C materials, i.e. profiles 63 and 65 (NGI 54), and 68 (NGI 86), complied in slope. However, reflecting the sample disturbance effects the results were more scattered and implied underconsolidation.

Considering CRS oedometer test, strain-rate coefficient β is defined as reciprocal value of slope identifying strain-rate dependency of the preconsolidation pressure in Log σ'_p/σ'_{vo} vs. strain-rate plane Yin et al. [2011]. In Figure 6.74 a), values of β measured in CRS tests on Perniö clay are related to sampling depth. Average values of β progressively rose with depth, amounting 23, 30 and 33 in sublayers A, B and C, respectively. Furthermore, β of 24.9 representing reconstituted A19 material corresponded well with average obtained on low sensitivity material of sublayer A. In Figure 6.74 b) and c), values of strain-rate coefficient β are related to corresponding parameter obtained in IL oedometer tests. According to Yin et al. [2011], β determined in CRS test should correspond with those based on IL oedometer results defined by Equations 6.12 and 6.13. As shown in Figure 6.74 b) and c) however, β in CRS oedometer tests were considerably higher. Namely, β_1 values obtained with Equation 6.12 amounted 9 in sublayer A, and rose with depth to 10.6 in sublayers B and C. Furthermore, β_2 defined by Equation 6.13 amounted 7.5, 8.5, and 9.5 in respective soft clay sublayers. Thus, despite similar response vs. depth, values of strain-rate coefficient in IL oedometer test were about three times less.

To examine validity of unique compression concept, stress levels identifying initial effective stress, compression stress and limit stress, were related to strain-rate. Values of σ'_o/σ'_{vo}, σ'_p/σ'_{vo}, σ'_C/σ'_{vo} and σ'_L/σ'_{vo}, examined in relation to strain-rate imposed in CRS test on 63A, 63B and 65C are presented in Figure 6.75. The results were characterised by progressive rise in slope, i.e. being the lowest for rate dependency of σ'_o/σ'_{vo}, somewhat higher for σ'_C/σ'_{vo}, and the highest for data identifying strain-rate response of σ'_L/σ'_{vo} values. Considering materials of all three sublayers, rate dependency of σ'_o/σ'_{vo} values was characterized with similar slope and intercept values. In contrast, those identifying strain-rate dependency of σ'_C/σ'_{vo} and σ'_L/σ'_{vo}, differed depending on sublayer of origin. Values identifying σ'_C/σ'_{vo} response were typically somewhat higher from those at σ'_p/σ'_{vo} level. Compared to σ'_p/σ'_{vo}, σ'_L/σ'_{vo} values were typically considerably higher, as well as values of slope identifying σ'_L/σ'_{vo} strain-rate dependency. Furthermore, values of slope identifying σ'_L/σ'_{vo} strain-rate dependency, highly differed with respect to sublayer of origin. The slope was the highest in sublayer A tests, followed by those on sublayer C materials, and the lowest in materials of sublayer B. The results thus indicated considerable variance of strain-rate influence with increase in strain.

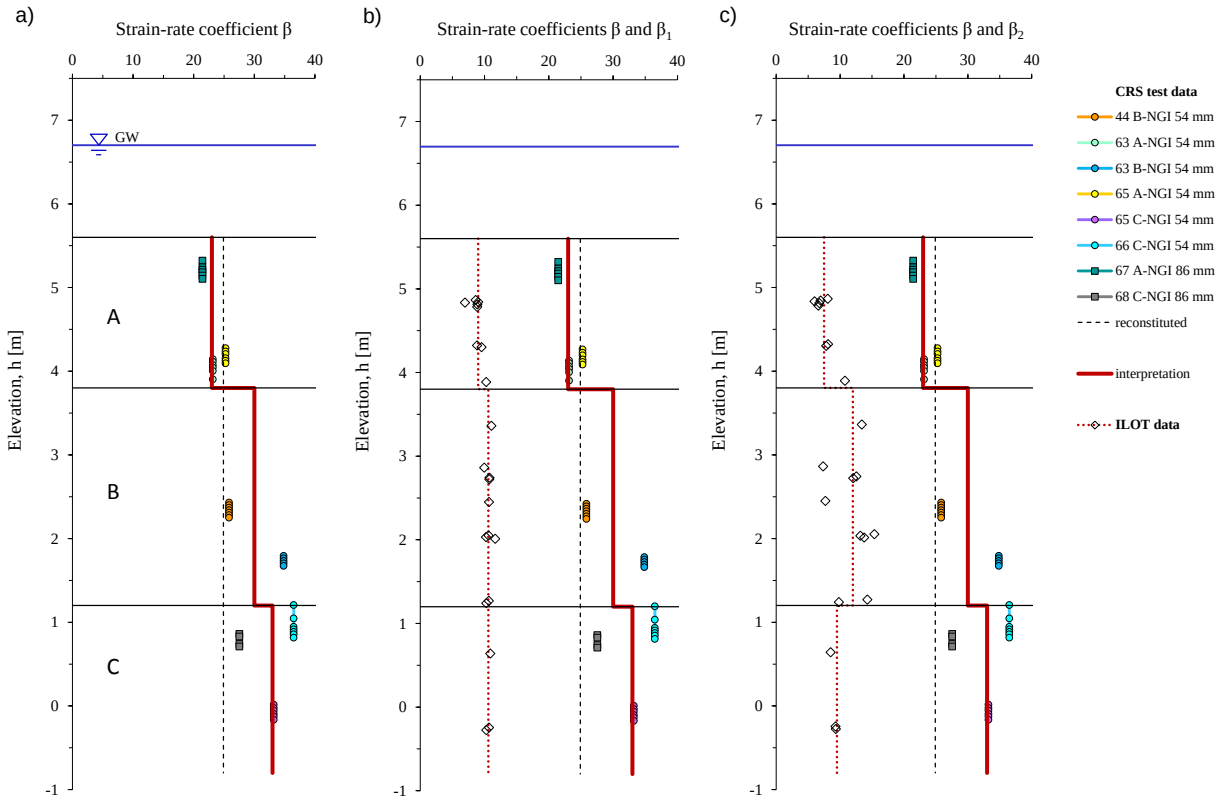

Figure 6.74 Strain-rate parameter in CRS oedometer tests; a) strain-rate coefficient β, b) comparison of β and β_1, and c) comparison of β and β_2.

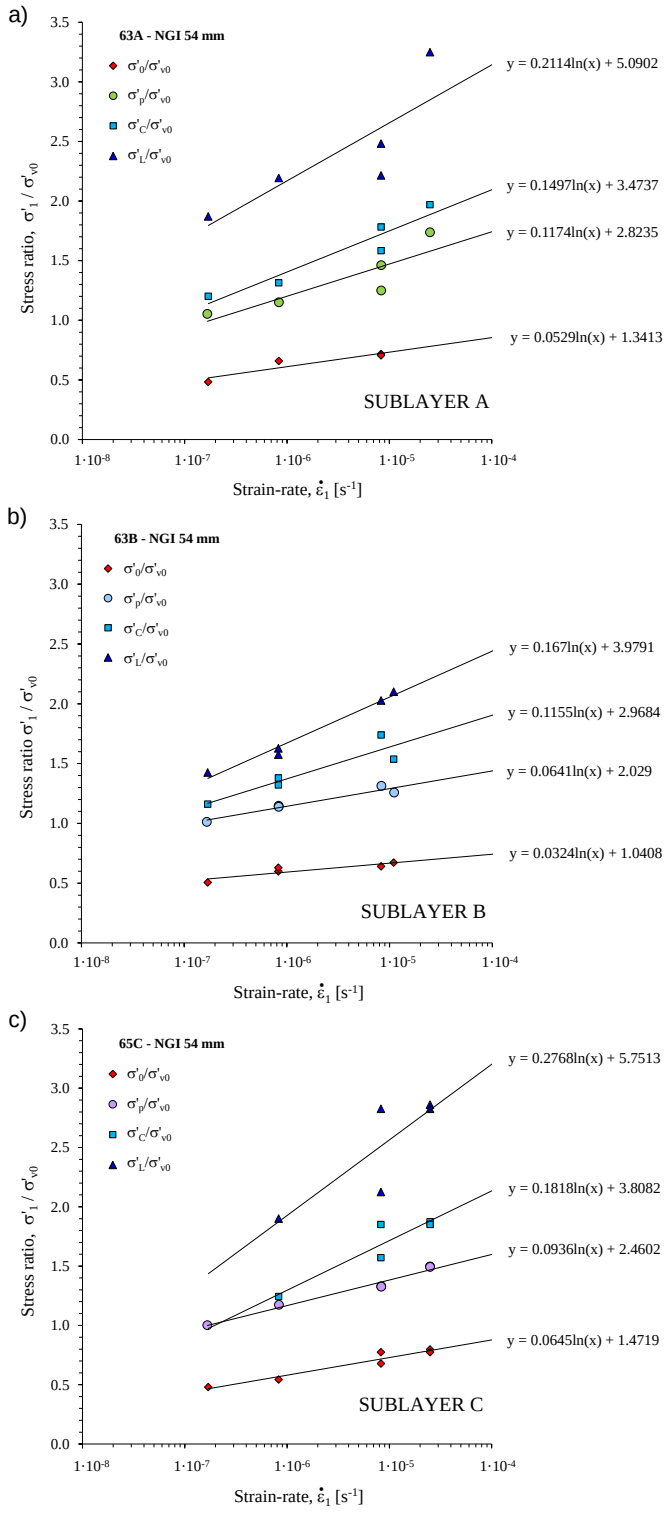

Figure 6.75 Values of σ'_0/σ'_{v0}, σ'_C/σ'_{v0} and σ'_L/σ'_{v0} related to strain-rate; a) 63A, b) 63B, and c) 65C material.

To conclude, validity of unique compression curve concept, based on normalisation of the compression response with respect to preconsolidation stress, postulates characteristic stress ratio levels σ'_o/σ'_{vo}, σ'_p/σ'_{vo}, σ'_C/σ'_{vo} and σ'_L/σ'_{vo} occurring on radially positioned lines in stress ratio vs. strain-rate plane. The concept thus takes into account change in viscous characteristics of the material with accumulated strain. The results obtained in CRS tests on Perniö clay in Figure 6.75, show slopes identifying rate dependence at characteristic stress levels being the lowest at σ'_o and the highest at σ'_L stress level, thus confirming the validity of the concept. To account for viscous behavior of structured clays, Yin et al. [2011] identified parameters; strain rate coefficient β representing slope, and fluidity index μ representing intercept of the preconsolidation pressure rate dependency in Log σ'_p/σ'_{vo} vs. strain-rate plane. The approach assumes influence of strain-rate, i.e. magnitude of the viscosity parameters, being constant for a certain material. Thus, perquisite for validity of the approach is magnitude of slope and intercept of Log σ'_p/σ'_{vo} strain-rate dependency being identical to those at characteristic stress levels prior and following the yield, i.e. Log σ'_o/σ'_{vo}, Log σ'_C/σ'_{vo} and Log σ'_L/σ'_{vo}. In other words, lines defining rate dependency of logarithm of characteristic stress levels normalized with σ'_{vo}, are assumed to be parallel. Based on the results obtained in CRS tests on Perniö clay, effects of the rate dependency on characteristic stress levels are to some extent compensated by logarithmic scale. However, strain-rate parameters as defined at preconsolidation stress level are not valid at stresses considerably lower and higher from preconsolidation. Indeed, results presented on Figure 6.75, point to stain-rate influence being strain dependent. Thus, the effects of sample disturbance and accumulated strain, i.e. effects of destructuration, should be taken into consideration when defining viscous properties of structured clays.

7. Triaxial testing

7.1 Triaxial consolidation test results CAD

7.1.1 General overview

Figure 7.1 presents stress paths in CAD tests performed on natural and reconstituted specimens of Perniö clay. Three groups of triaxial tests are distinguished with respect to material tested and consolidation procedure implemented. Stress path of continuously loaded K_o test on natural specimen is presented dotted. IL triaxial tests on natural specimens consolidated along radial stress paths η=0.4, 0.6 and 0.85, are presented by solid lines. Finally, stress paths of IL triaxial consolidation tests on reconstituted specimens at constant stress ratio, as well as those consolidated by simplified procedure are shown dashed.

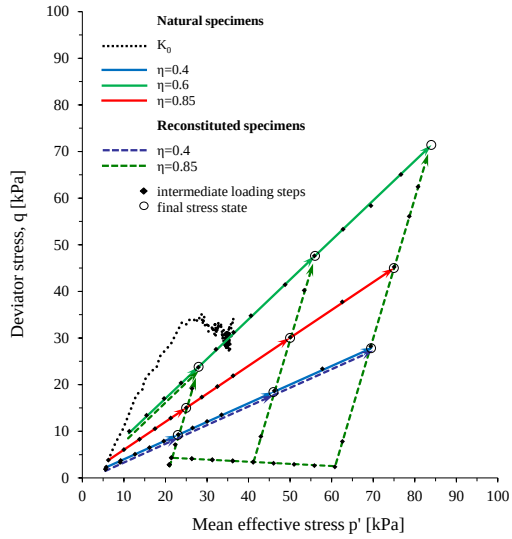

Figure 7.1 Stress paths in anisotropic consolidation tests on natural and reconstituted Perniö clay.

Triaxial test aiming determination of K_o^{NC} of Perniö clay was performed on natural specimen of 35 mm diameter and 80 mm height, under condition of ε_r=0 throughout the consolidation. Specimen was selected from NGI 54 profile 44, sampled in 2009. As shown in Figure 7.1, the K_o test revealed stress ratio response in reloading being rather high. Indeed, for ε_1<2 % stress ratio re-

mained fairly constant at η=1.38 (σ'_3/σ'_1=0.28). Following the yield at p'_p= 30.6 kPa however, stress ratio declined and stabilised at η=0.85 characterising NC response. Consequently, η_{Ko}^{NC}=0.85 (K_o^{NC}=0.46) was adopted in planning of subsequent CAD tests on Perniö clay.

Natural specimens of Perniö clay were loaded incrementally along constant stress ratio paths η=0.85, 0.6 and 0.4. CAD tests at η=0.4 and 0.6 were initiated from σ'_3=5.0 kPa, while those consolidated at η=0.85 were onset at σ'_3=8.0 kPa. Consolidation at each stress ratio included specimens being compressed to stress level limited by maximum σ'_3 of 20, 40 or 60 kPa. As presented in Table 7.1, σ'_1 corresponding to ultimate cell pressure in consolidation varied depending upon the η imposed. The tests were performed on specimens from NGI 54 mm profiles 43, 44 and 45 sampled in 2009, and profiles 65 and 66 sampled in 2010. With specimens being obtained by the same sampling method, comparison of the results on S-2009 and S-2010 material enabled evaluation of the effects of embankment load on compressibility response. To ensure comparability of the results, tests were made on specimens 100 mm in height and 50 mm in diameter. Repeatability was accounted for by at least two tests performed under identical consolidation conditions.

Table 7.1 Final stress conditions in CAD triaxial tests.

Consolidation stress ratio η	Consolidation stress ratio σ_3/σ_1	Cell pressure σ_3 [kPa]	Vertical effective stress σ'_1 [kPa]
0.85	0.459	20.0	43.6
		40.0	87.1
		60.0	130.7
0.6	0.571	20.0	35.0
		40.0	70.1
		60.0	105.1
0.4	0.687	20.0	29.1
		40.0	58.2
		60.0	87.3

Triaxial tests on reconstituted material considered specimens 100 mm in height and 50 mm in diameter, remoulded in batches R1, R2, R3 and R4. Although perceived to be consolidated as natural, consolidation of reconstituted specimens along constant stress ratio paths was only partly successful. Only tests at η=0.4 were characterised by constant stress ratio in consolidation. In consolidation at radial stress path of η=0.85 reconstituted specimens regularly failed. Indeed, consolidation at η=0.85=const. was successful only for R5886 performed until σ'_3=20 KPa. The result indicated remoulded material in reconstitution being subjected to lower η compared to Perniö clay in situ, as well as considerable effects of natural structure on deformability measured. Consequently, remaining reconstituted specimens were consolidated to η=0.85 using simplified anisotropic consolidation procedure. The specimens were firstly subjected to isotropic loading until final σ'_3, and latter axial load was increased in daily steps until η=0.85. Since η followed in consolidation was not constant,

results measured on the specimens are excluded from the analyses unless stated otherwise.

Figure 7.2 presents compressibility response in CAD test on natural and reconstituted specimens in σ'_1 vs. v plane. Results are firstly briefly outlined, and later specific features such as sample quality, compressibility, bonding and creep effects are examined in detail. In evaluation, emphasis is on influence of consolidation stress ratio imposed.

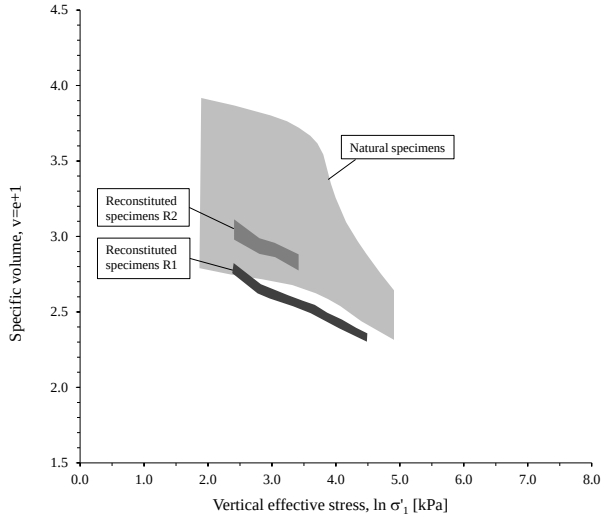

Figure 7.2 Compressibility of Perniö clay in anisotropic consolidation triaxial tests.

CAD results on reconstituted specimens

Average e_o of reconstituted specimens, i.e. 1.79, 2.04, 1.81 and 2.20, reflected water content of respective batches R1, R2, R3 and R4. As shown in Table 5.4, water content for R1 matched that of batch R3, while that of R2 was similar to those of batch R4 specimens. For simplicity, entire set of reconstituted specimens was reduced to groups R1,3 and R2,4 with respective w_o of 66.6 and 74.9% and e_o of 1.80 and 2.06. The tests on reconstituted specimens were initiated from σ'_3=8.0 kPa. Thus, vertical load at the onset of consolidation at η=0.4 amounted 12.1 kPa, while that at η=0.85 was 17.6 kPa. With the specimens consolidated in preparation under vertical load of 15 kPa, data on reloading at η=0.4 was limited to load steps of 12.1 and 16.5 kPa. Under these loads specimens exhibited high value of κ_o, averaging 0.327 for R1 and 0.269 for R2. Additional explanation for high κ_o can be traced in non-adequate contact between specimen, porous stones and cap/pedestal. The specimens consolidated at η=0.4 exhibited uniform λ values, well represented by average of 0.182 for R1, and 0.199 for R2. In R5886 consolidated at constant stress ratio path η=0.85, λ was somewhat higher, amounting 0.258. In tests consolidated to η=0.85 using simplified approach, isotropic portion in consolidation revealed average λ for R1,3 amounting 0.108, while that for R2,4 was 0.177. Table 7.2 summarises λ on reconstituted specimens in CAD, CRS and ILOT. λ values

obtained on η=0.85 consolidated R5886, complied with average λ measured in IL and CRS tests on reconstituted specimens R2,4. However, λ obtained in triaxial tests on R1 and R2 specimens consolidated along η=0.4, were considerably less than in IL and CRS oedometer tests. The results confirmed influence of w_o on slope in compression, and indicated proportional influence of stress ratio in consolidation on compressibility in NC stress range.

Table 7.2 λ of reconstituted specimens in ILOT, CRS and CAD tests.

	λ $R_{1,3}$ e_0=1.80	λ $R_{2,4}$ e_0=2.06
ILOT	-	0.259
CRS	0.231	0.270
CAD η=0.85	-	0.258
CAD η=0.40	0.182	0.199
CAD η~0	0.108	0.177

CAD results on natural specimens

High scatter in compressibility of natural specimens in CAD tests reflected natural variability, effects of sampling quality and specimen preparation, and variance in consolidation stress ratio conditions imposed. Although the natural specimens originated from soft clay sublayers A and B only, values of e_o varied broadly between 1.83 and 2.92. Values of reloading slope κ_o varied from 0.015 to exceptionally high 0.192. Considering specimens consolidated to σ'_3 of 40 and 60 kPa, slope of the normal compression line λ ranged from very low 0.212 to rather high 1.680. Despite the difference in consolidation conditions, i.e. free lateral boundary, λ measured were comparable to those identifying oedometer test specimens. Due to low magnitude of maximum σ'_1 in consolidation (see Table 7.1), final compression characteristics were not representable of intrinsic compressibility. Considering specimens consolidated to σ'_3 of 60 kPa, final slope in compression varied from 0.307 to 0.576, thus significantly exceeding λ_i values measured in oedometer testing.

Figure 7.3 relates preconsolidation pressures determined on natural specimens in CAD tests to sampling depth. Yield stresses were determined by modified bilinear approach, i.e. using linear plots of σ'_1 vs. v, and p' vs. v. Due to changes in anisotropy, usage of semi-logarithmic plots was not suitable [Koskinen et al. 2003]. Preconsolidation pressures generally complied with distribution of effective overburden and σ'_p obtained in CRS oedometer tests at low strain-rates. Evaluated at corresponding elevation however, magnitude of σ'_p varied up to ~10 kPa depending upon the stress ratio in consolidation and specimen quality. In tests at η=0.4 on NGI 54 specimens sampled in 2009, σ'_p/σ'_{vo} were the lowest, i.e. σ'_p/σ'_{vo} ~0.9. In contrast, the highest σ'_p/σ'_{vo} values identified S-2010 specimens consolidated at η=0.85, that in respective sublayers A and B amounted 1.55 and 1.30 at most. Considering high scatter of results, detail analyses on influence of structure, specimen quality, and consolidation stress ratio are necessary prior concise conclusions on CAD compression response under IL loading can be derived.

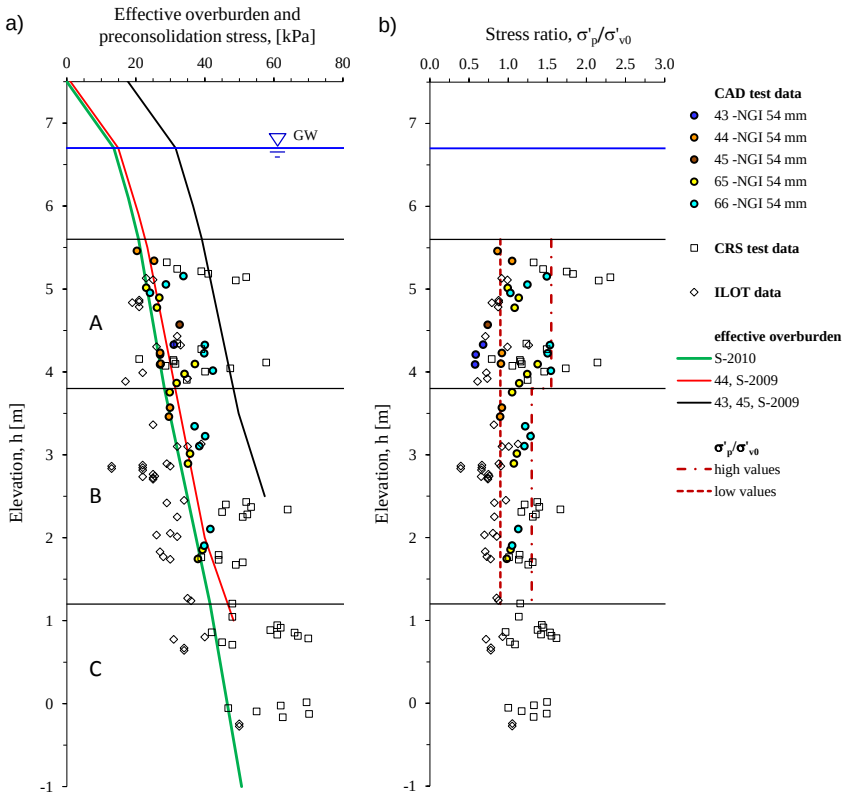

Figure 7.3 Overburden stress distribution and preconsolidation pressures in CAD triaxial tests.

7.1.2 Initial state parameters

Water content, initial void ratio and unit weight

Initial state parameters of CAD specimens complied with results obtained on oedometer specimens and following the sampling. Based on S-2010, w_o of CAD specimens were represented by 102.5 and 83.2 % in respective sublayers A and B (Figure 7.4 a). Correspondingly, average values of e_o in sublayer A and B were 2.8 and 2.2 (Figure 7.4 b). Finally, average γ in sublayers A and B were 14.2 and 15.0 kN/m^3, respectively (Figure 7.4 c). Furthermore, CAD results confirmed notable distinction of initial state parameters in S-2009. Namely, w_o and e_o in S-2009 exhibited similar pattern vs. depth as that characterising S-2010. However, values of the parameters in S-2009 were significantly less. In sublayer A, S-2009 specimens were represented by w_o of 88.0 %, while those of sublayer B amounted 75.0 %. Corresponding e_o values amounted 2.4 and 2.0, respectively. Finally, γ values representative of S-2009 were overall the highest, i.e. 14.8 and 15.2 kN/m^3 at elevation of sublayers A and B. Thus, examined at the corresponding elevation initial state parameters of S-2009 and S-2010 differed considerably. The effect was the most prominent in sublayer A, yet significant in sublayer B as well. The difference in magnitude of the parameters manifested effects of embankment load and sampling performance.

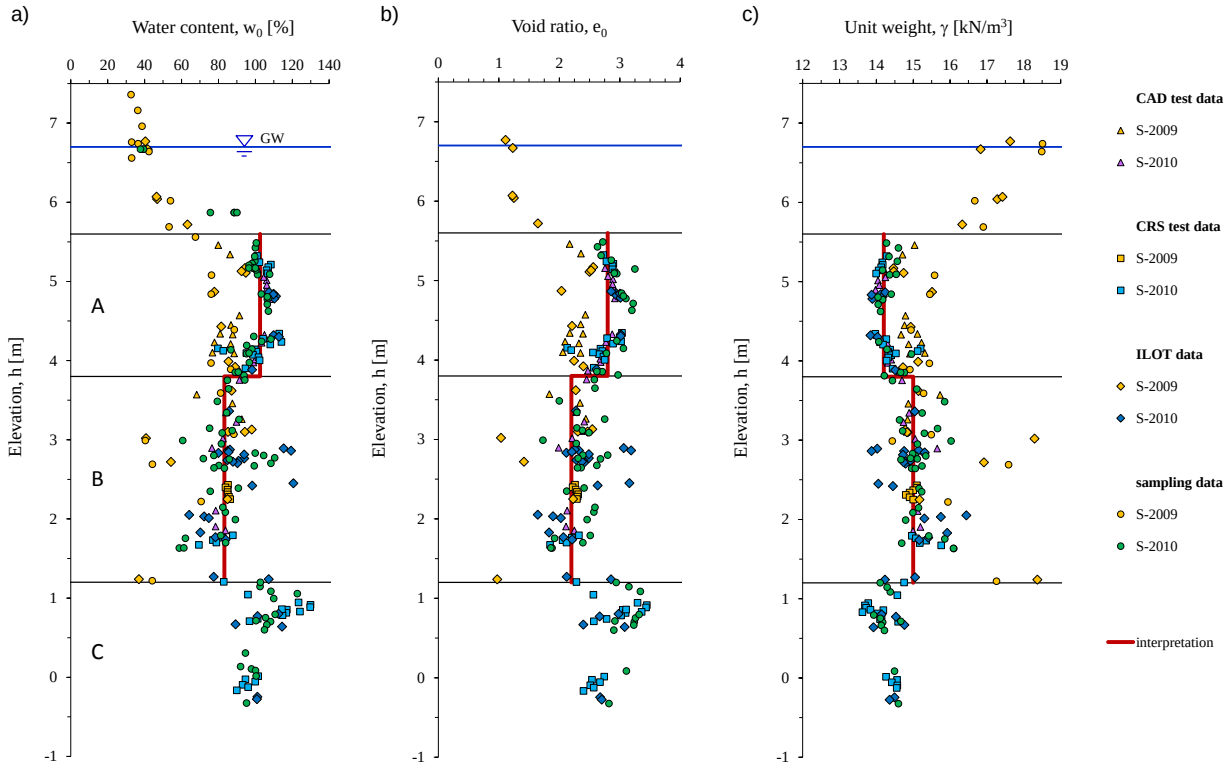

Figure 7.4 Initial state parameters of CAD triaxial specimens, a) water content, b) void ratio, and c) unit weight.

7.1.3 Sample quality

$\Delta e/e_o$ criteria

In Figure 7.5 a), Perniö clay specimens in anisotropic consolidation tests are examined using $\Delta e/e_o$ criteria. In the same figure, CAD specimens with $w/\gamma > 7.0$ %/kN/m³ are highlighted. Most of the CAD specimens exhibited $0.04 < \Delta e/e_o < 0.07$, indicative of good to fair specimen quality. In addition, occasional specimens of sublayer A exhibited very good to excellent quality satisfying $\Delta e/e_o < 0.04$. The $\Delta e/e_o$ values characterising poor quality specimens predominantly designated S-2009 material, i.e. profiles 43, 44 and 45. The $\Delta e/e_o$ results on CAD specimens outperformed those identifying IL oedometer specimens (see Figure 6.4 a), yet corresponded in range with those on CRS specimens influenced by strain-rate effects (see Figure 6.31 a). As in CRS testing, CAD specimens characterised by $\Delta e/e_o < 0.07$, often did not satisfy $w/\gamma > 7$ %/kN/m³ criteria. This was particularly notable within sublayer B. Both of these effects indicated $\Delta e/e_o$ being influenced by stress ratio in consolidation.

w/γ criteria

As shown in Figure 7.5 b), w/γ response representing CAD specimens complied with remaining results on Perniö clay. The w/γ characterising natural CAD specimens ranged from 4.3 to 7.7 %/kN/m³. Most of the results appeared within limits $4.9 < w/\gamma < 6.2$ %/kN/m³. Specimens of high quality with $w/\gamma > 7.0$ %/kN/m³ occasionally occurred on S-2010 profiles 65 and 66 (NGI 54). In contrast, w/γ values of reconstituted specimens occurred between 4.0 and 5.2 %/kN/m³.

In Figure 7.5 c), w/γ values obtained on CAD specimens are related to sampling depth. S-2010 CAD results in sublayers A and B were represented by average values of 7.2, and 5.5 %/kN/m³, respectively. The results complied well with data on S-2010 oedometer specimens. The highest values of 7.5 %/kN/m³ occurred on profiles 65 and 66 (NGI 54), in the mid of sublayer A. Within sublayer B, the highest w/γ values of 6.0 %/kN/m³ reflected generally poor sampling performance within the zone. In contrast to S-2010, CAD and oedometer results on S-2009 material were clearly less. According to w/γ criteria, all S-2009 specimens exhibited poor quality, i.e. $w/\gamma < 7$ %/kN/m³. Furthermore, although resembling distribution with depth obtained for S-2010, w/γ values of S-2009 specimens were offset toward ~1.2 %/kN/m³ lower values. The effect was explicit at elevations of sublayer A, and was caused by embankment load and poor sampling performance.

Comparison of $\Delta e/e_o$ and w/γ sampling quality criteria

CAD specimens with $\Delta e/e_o < 0.07$ are highlighted in Figure 7.5 c). Advantage of w/γ to that of $\Delta e/e_o$ criteria was exhibited by the fact of almost entire set of CAD specimens being characterised by $\Delta e/e_o < 0.07$. Same conclusion was valid for reconstituted CAD specimens. The outcome of $\Delta e/e_o$ based classification is thus questionable since it; failed to identify considerable difference in S-2009 and S-2010 sampling performance; neglected the influence of embankment load on specimen quality; and finally, failed to recognise influence of structure when results obtained on natural and reconstituted specimens were compared.

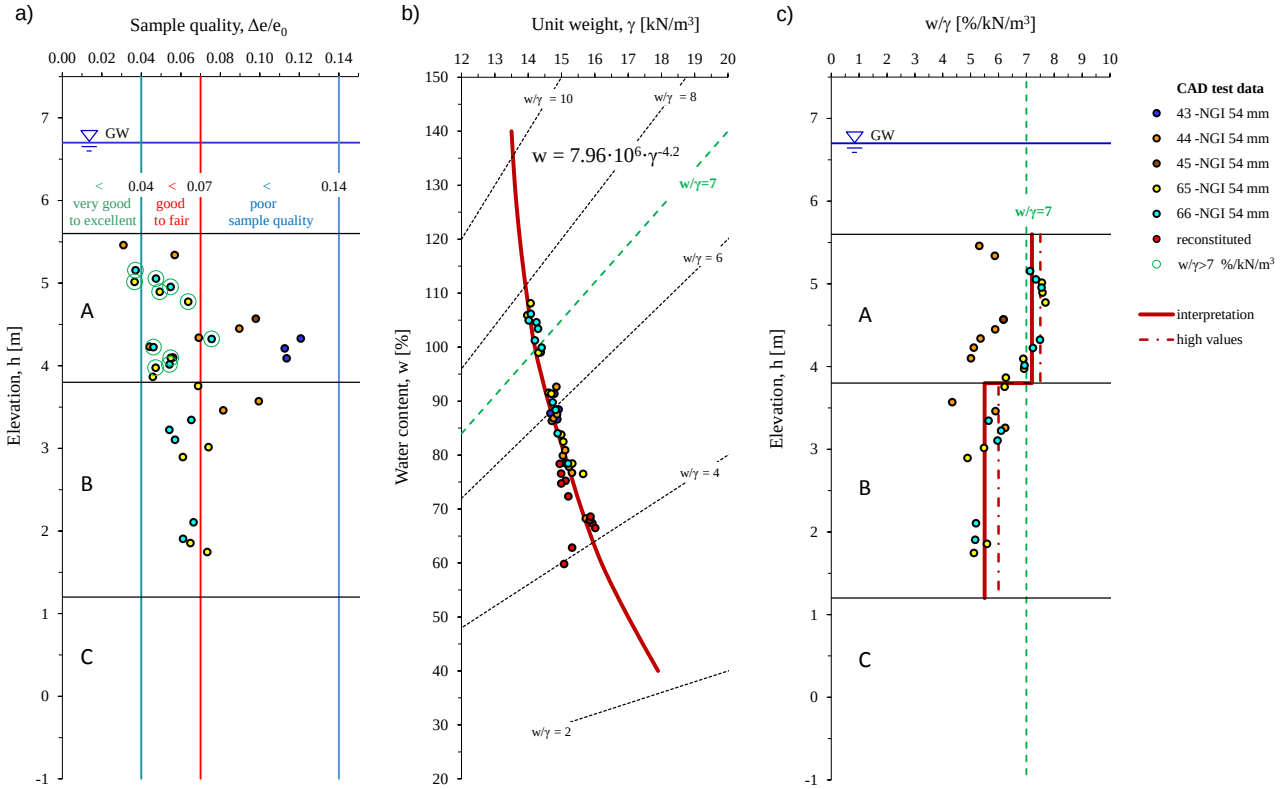

Figure 7.5 Specimen quality in CAD triaxial tests on Perniö clay; a) $\Delta e/e_0$ criteria, b) w/γ curve, and c) w/γ criteria.

7.1.4 Compressibility and preconsolidation pressure

Effects of consolidation stress ratio on compressibility curve

In Figure 7.6, compression curves on natural specimens are examined with respect to stress ratio in consolidation. Results are differed depending on sublayer of origin and analysed in σ'_1 vs. v plane. Compared with oedometer testing, CAD compression curves addressed limited compressibility range, i.e. maximum σ'_1 in consolidation was notably less. Due to free lateral boundary, compression curves were not as smooth as those obtained in oedometer testing. Non-adequate contact between specimen and top cap/pedestal influenced reloading segment of the compression curves.

Figure 7.6 a) shows compression curves obtained at $\eta_{K_o}^{NC}$=0.85. With an exception of final stress level reached, the results were obtained following identical consolidation conditions (see Table 7.1). The results were characterised with high compressibility similar to that measured in oedometer tests. Curves representing response of sublayer A plotted well above those on specimens of sublayer B. The scatter reflected considerable difference in v_o. With rise of vertical effective stress, the results exhibited asymptotic decrease in compressibility and tendency to merge. Overall, the specimens of sublayer B exhibited somewhat lower compressibility compared to those of sublayer A.

In Figure 7.6 b), compression curves obtained at η=0.6 are shown. The compression curves exhibited stiffer response compared to those measured at η=0.85. Furthermore, curves representing specimens of sublayer B were characterised with lower values of v_o and somewhat stiffer response compared to those on specimens of sublayer A. Overall, the curves obtained were relatively smooth while decrease in compressibility in NC stress range was negligible.

Compression curves obtained in consolidation at η=0.4 are presented in Figure 7.6 c). The results exhibited the lowest compressibility among CAD tests on natural specimens. Considering reloading response, the curves were significantly scattered. Compressibility response measured progressively declined until the end of loading. Due to considerable extent of destructuration in consolidation, yield was not well defined and the post-yield stiffness was high. In NC stress range, no clear distinction in compressibility of sublayer A and B specimens could be made.

Effects of sample disturbance on compressibility curve

In Figure 7.7, CAD compression curves measured on natural and reconstituted specimens are shown in σ'_1/σ'_p vs. v plane. To identify high quality natural specimens w/γ>7.0 %/kN/m^3 condition was used. Since in consolidation until σ'_3=20 kPa, preconsolidation pressures could not be determined, specimens consolidated to stress state limited by σ'_3= 40 or 60 kPa were considered only.

Among normalized compression curves in Figure 7.7 a) representing consolidation results at η=0.85, only specimens of sublayer A satisfied w/γ>7 %/kN/m^3. Shift of the compression curves toward lower values of specific volume was a clear manifestation of specimen disturbance. Reflecting the difference in initial water content, high quality specimens exhibited somewhat higher compressibility.

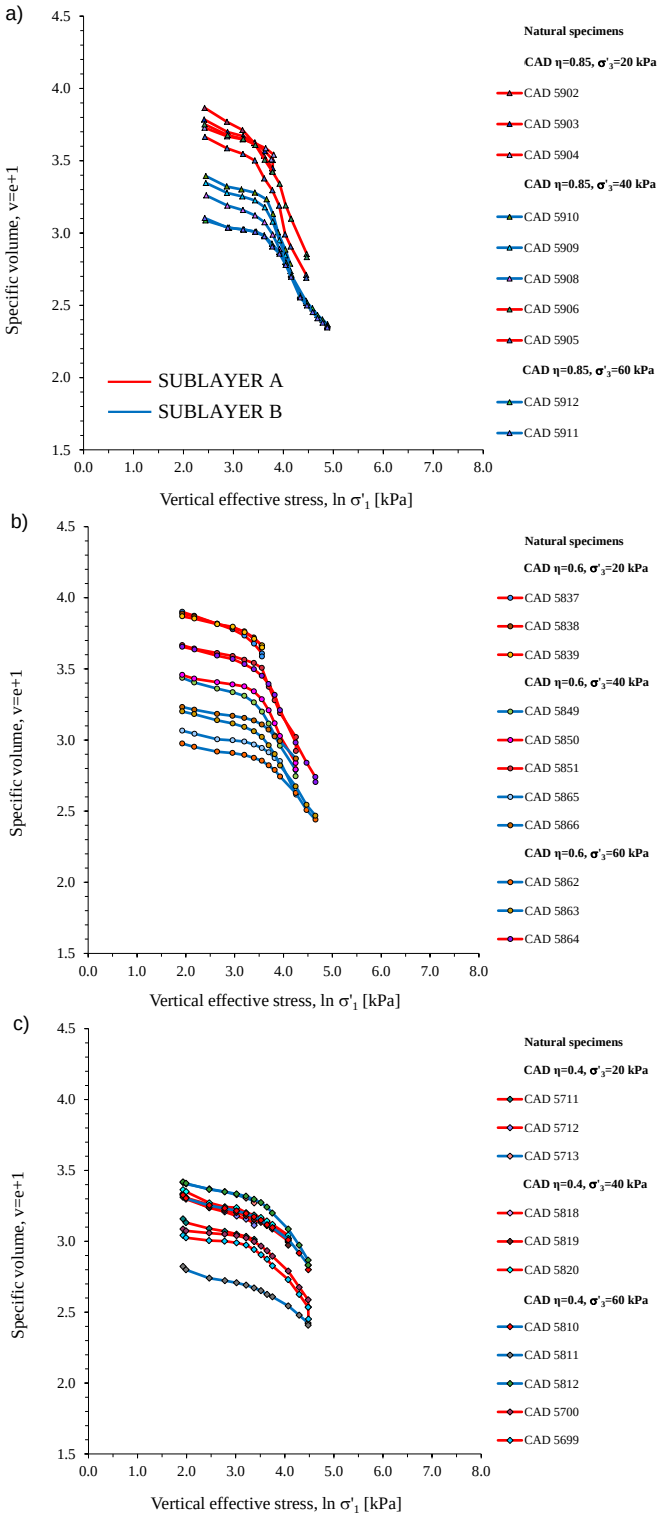

Figure 7.6 Influence of stress ratio in consolidation on compressive response of Perniö clay in CAD tests; a) η=0.85, b) η=0.6, and c) η=0.4.

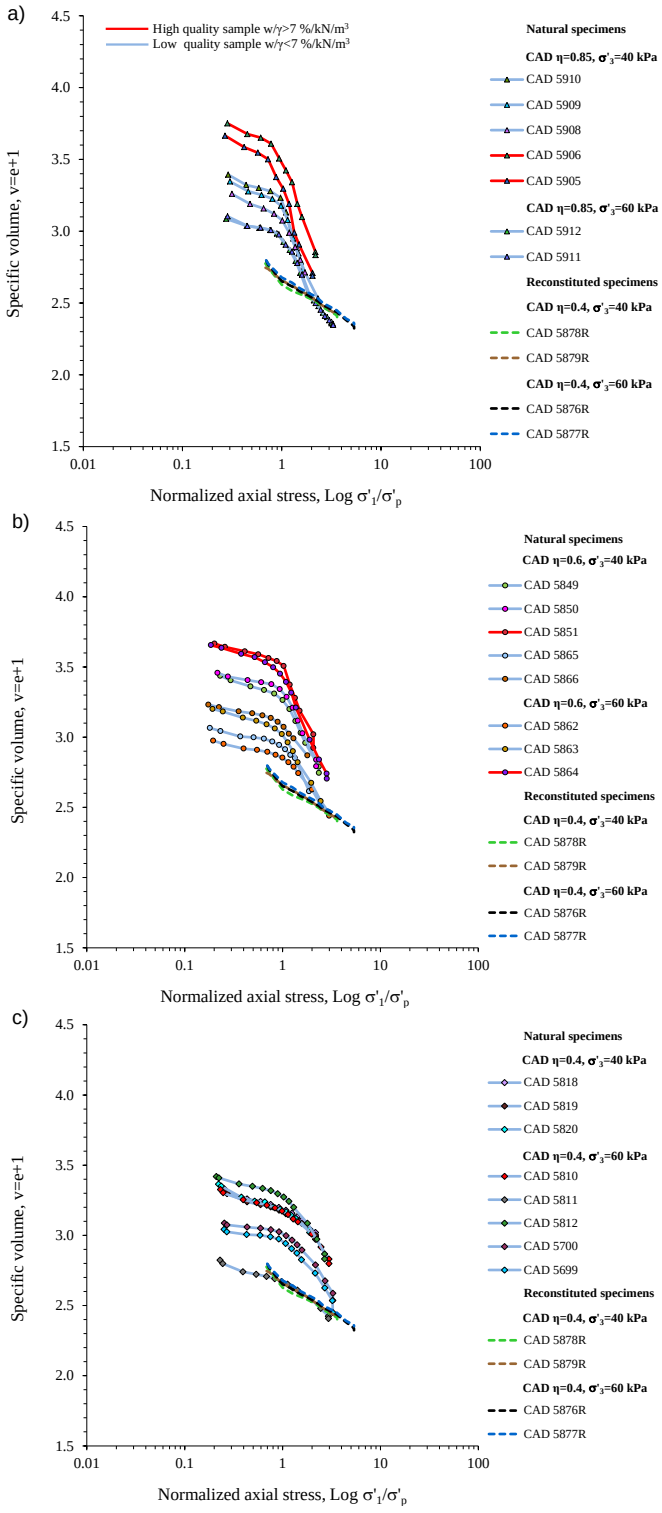

Figure 7.7 Influence of specimen quality on compression response of Perniö clay in CAD tests; a) η=0.85, b) η=0.6, and c) η=0.4.

Compared to response of reconstituted specimens, natural specimens of both high and poor quality exhibited much higher compressibility overall.

Normalized compression curves in consolidation at η=0.6 shown in Figure 7.7 b) directed to similar conclusions. Only a limited number of specimens originating from sublayer A satisfied w/γ>7 %/kN/m^3. Specimens characterised by lower v_o exhibited somewhat lower compressibility within NC stress ratio range.

Finally, Figure 7.7 c) shows normalized compression curves in consolidation at η=0.4. Entire set of the results was characterised by disturbed S-2009 specimens. Test 5811 performed on completely destructured specimen, exhibited compressibility corresponding to that of reconstituted specimens. The remaining results showed somewhat higher compressibility. However, overall response in consolidation at η=0.4 was characterised with significantly stiffer response compared to that measured in consolidation at η=0.6 and 0.85.

To conclude, despite considerable variation in initial properties and consequent disturbance effects, it was the stress ratio in consolidation that had the main influence on compression characteristics in NC stress range.

Effects of consolidation stress ratio on strain response

Reasons for difference in compressibility at various stress ratio conditions need to be traced in specimen strain response. Due to free lateral boundary, triaxial specimens exhibited both axial and radial strains. Thus, unlike in oedometer, ε_1 in CAD tests did not coincide with ε_v. Furthermore, magnitude of stress ratio in consolidation influenced radial strains ε_3, i.e. average lateral deformation along specimen height. Consequently, in consolidation along various η, resulting shear strains ε_d differed. Beside test conditions, both ε_v and ε_d were affected by specimen quality and localisation effects.

Figure 7.8 examines radial strains manifested in K_o and CAD tests on natural and reconstituted specimens at various magnitude of stress ratio in compression. K_o test represented by dotted line and performed under condition ε_3=0, indicated η_{Ko}^{NC}=0.85. In IL triaxial consolidation tests on natural specimens consolidated along η=0.85, ε_3 initially rose. Above yield however, ε_3 continuously declined and became negative at final stress levels. Throughout consolidation, radial strains remained within narrow limits -1<ε_3<+1 %. In consolidation at η=0.6, ε_3 initially rose at somewhat higher rate. In NC stress range however, ε_3 stabilised at fairly constant value of 2 %. Finally, in tests along η=0.4, ε_3 increased throughout the consolidation reaching considerable 2.7 % at final stress level. For comparison, ε_3 measured on reconstituted specimens consolidated at η=0.4 rose exponentially. Strain level reached however, corresponded with those obtained on natural specimens consolidated at the same stress ratio. In test on reconstituted specimen consolidated along radial stress path η=0.85, specimen rapidly attained negative values of ε_3, that aftermath stabilised at fairly constant level of -2.2 %. The results showed ε_3 measured on natural and reconstituted specimens being reciprocal to η imposed. Finally, the results indicated that in consolidation above η_{Ko}^{NC} radial strains attain negative values, while for η<η_{Ko}^{NC} radial strains are positive.

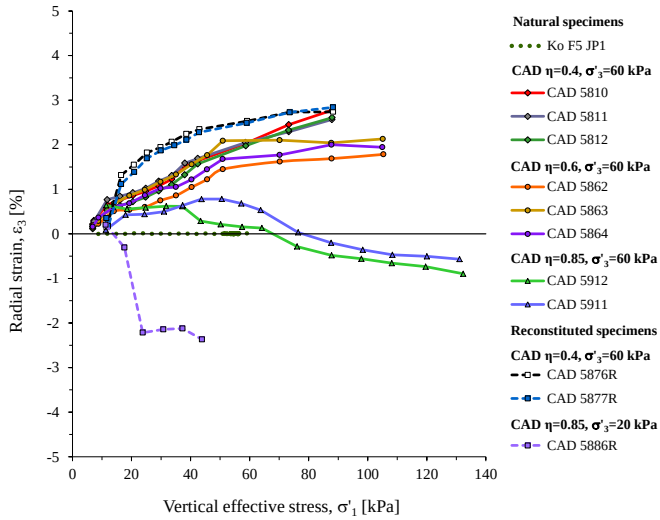

Figure 7.8 Radial strains in anisotropic consolidation triaxial tests.

To explain compressibility response in CAD tests, Figure 7.9 and Figure 7.10 examine strain paths measured on natural and reconstituted specimens in ε_v vs. ε_d plane. Figure 7.9 a) comprises results on natural specimens consolidated along η=0.85 as well as strain path measured in K_o test. In K_o test specimen was consolidated under condition ε_3=0. Consequently, in ε_v vs. ε_d plane the strain path exhibited inclination of 0.66. In IL CAD tests however, strain response was not restricted to $\varepsilon_d/\varepsilon_v$=0.66. At η=0.85, average slope of the strain path in reloading corresponded to ~0.50. For ε_v>5 % however, strain ratio progressively rose to stabilise at $\varepsilon_d/\varepsilon_v$=0.85. Thus, target values of strains depended on stress ratio in consolidation [Karstunen & Koskinen 2004]. Figure 7.9 b), examines characteristics of strain paths in consolidation at η=0.6. Prior yield, strain paths exhibited uniform strain ratio of ~0.30. Following the yield, strain ratio progressively increased towards target value of $\varepsilon_d/\varepsilon_v$=0.6 reflecting stress ratio conditions imposed. Similar response characterised strain paths in consolidation at η=0.4 shown in Figure 7.9 c). Changes in strain path gradient took part progressively. Since the initial strain ratio of ~0.25 fairly corresponded to target η, the effect was the least pronounced. Strain paths measured on reconstituted specimens at η=0.4 in Figure 7.10, were consistent with those on natural. For ε_v<5 %, strain paths exhibited $\varepsilon_d/\varepsilon_v$=0.14. For ε_v>10 % however, strain ratio measured reflected stress ratio conditions. Thus, deformability of natural and reconstituted specimens was strongly influenced by stress ratio conditions in consolidation. In reloading, gradient of strain paths was typically low, i.e. $\varepsilon_d/\varepsilon_v$~0.5 or less. Following the yield, gradient of the strain path was progressively modified approaching that of stress ratio conditions imposed. Thus, in contrast to that in reloading, results in NC stress range suggested associated flow response. Among various η implemented, the results characterised with least destructuration were indicative of stress ratio conditions in situ, i.e. η_{Ko}^{NC}=0.85 for natural Perniö clay. If stress ratio path differed from η_{Ko}^{NC}, destructuration effects were considerable.

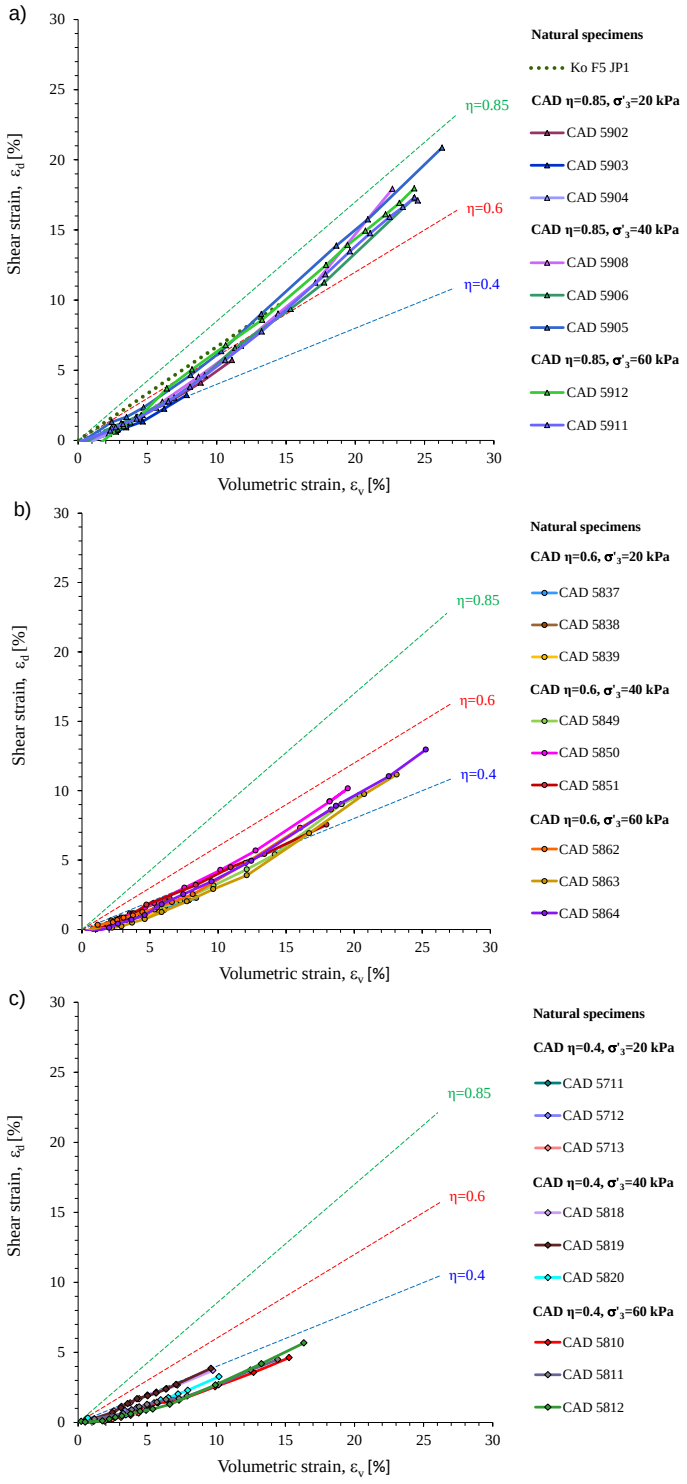

Figure 7.9 Strain paths in CAD tests on natural specimens of Perniö clay; a) η=0.85, b) η=0.6, and c) η=0.4.

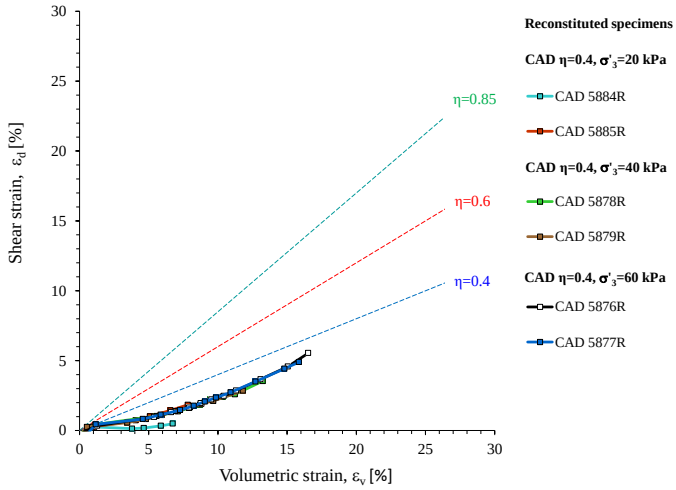

Figure 7.10 Strain paths in CAD tests on reconstituted specimens of Perniö clay at η=0.4.

Normalization of stress-strain curves

When normalized with stress at yield, compression curves obtained under identical test conditions on specimens of similar quality, should coincide. In Figure 7.11 CAD compression curves are examined in p'/p'_p vs. ε_v and p'/p'_p vs. ε_d planes. For clarity, stress-strain results at certain η are distinctively displayed. In tests performed along radial stress paths, $\sigma'_1/\sigma'_p=p'/p'_p=q/q_p$ is valid. Thus, conclusions derived for results in p'/p'_p vs. ε_v plane are valid for those in σ'_1/σ'_p vs. ε_v plane as well. To simplify the analysis, results obtained on high quality specimens with $w/\gamma>7.0$ %/kN/m³, are distinctively displayed.

In Figure 7.11 a) and b) results of tests at η=0.85 are shown. In p'/p'_p vs. ε_v plane, compression curves exhibited considerable slope in reloading. In NC range specimens exposed high compressibility that somewhat diminished with increase in p'/p'_p. If specimens of poor and high quality are separately considered, normalized compression curves exhibited rather uniform response. Considering p'/p'_p vs. ε_d plane, results showed similar response, yet compared to volumetric, shear strains were somewhat lower in magnitude. Furthermore, overall scatter of the results was somewhat more pronounced. Change in stress-strain characteristics at yield was clear. Reflecting low water content, poor quality specimens (sublayer B) exhibited higher volumetric and shear resistance in both reloading and NC stress range.

Normalization of stress strain curves following consolidation at η=0.6 in Figure 7.11 c) and d), produced fairly uniform results. Responding to η imposed, shear resistance in p'/p'_p vs. ε_d was considerably higher compared to volumetric resistance in p'/p'_p vs. ε_v plane. Concerning both volumetric and shear strain response, the results obtained on high quality specimens from sublayer A, complied. Although somewhat more scattered, and generally identified by higher compression and shear resistance, same conclusions was valid for response on poor quality specimens (mainly sublayer B).

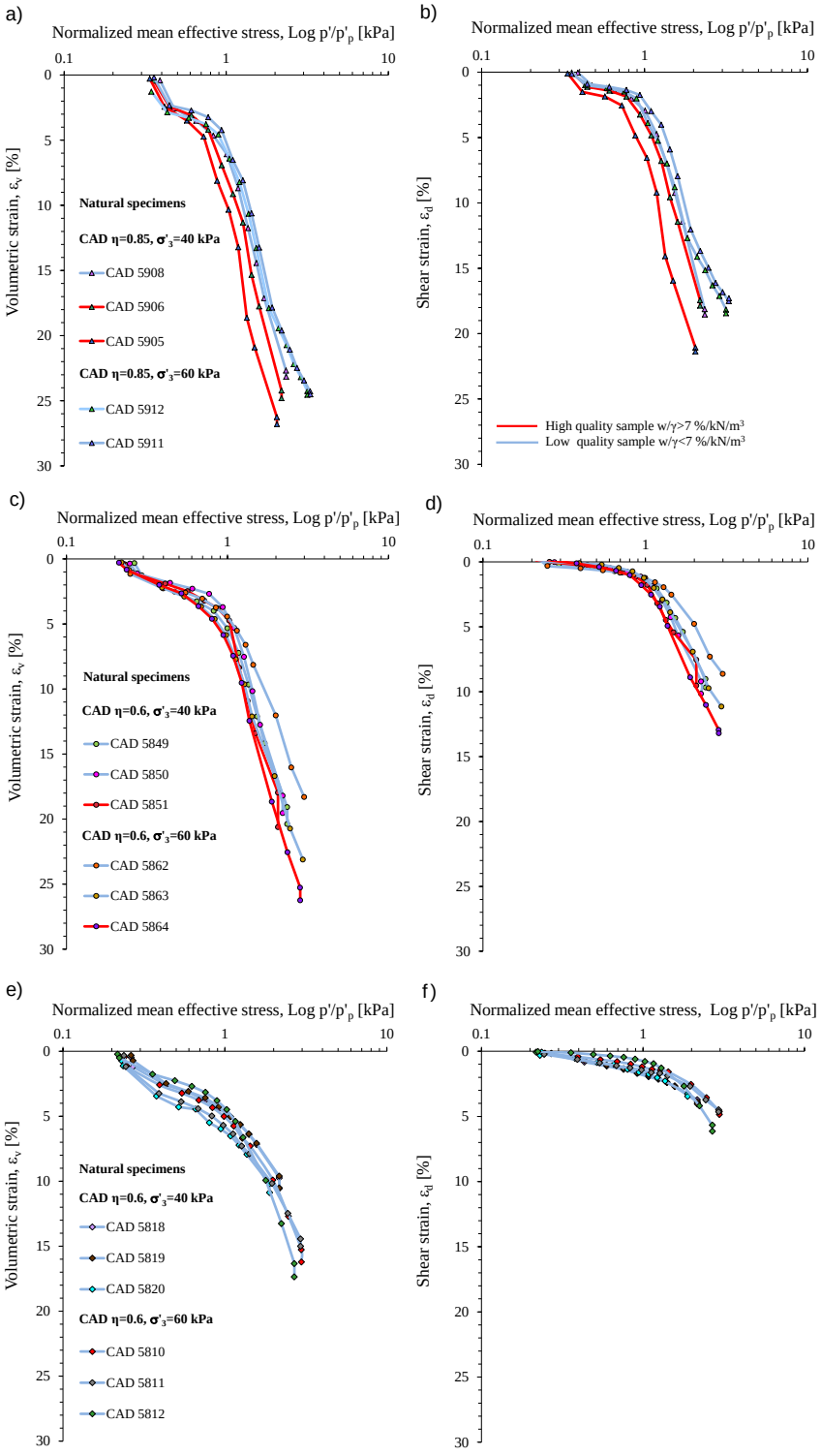

Figure 7.11 CAD test results in p'/p'$_p$ vs. ε_v and p'/p'$_p$ vs. ε_d planes examined with respect to specimen quality and stress ratio in consolidation; a) and b) η=0.85, c) and d) η=0.6, e) and f) η=0.4.

Normalized stress-strain curves following consolidation at η=0.4 are presented in Figure 7.11 e) and f). Entire set of the results was obtained on poor quality specimens. Nonetheless, considering specimens of similar initial water content, results of normalisation were fairly effective. Reflecting η=0.4, natural specimens exhibited the highest volumetric and shear resistance overall. Furthermore, both volumetric and shear resistance gradually decreased until the final stress level. As a consequence of the characteristics of the stress-strain response, yield was not well defined. Responding to relatively low stress ratio in consolidation, shear strains in p'/p'_p vs. ε_d plane remained rather low.

To conclude, if specimens of comparable stress history and initial water content were considered, normalization with respect to stress at yield produced similar response in terms of both volumetric and shear strains. In contrast, on specimens influenced by disturbance or variance in quality, scatter of the results was inevitable. Magnitude of shear and volumetric strains reflected stress ratio conditions in consolidation. Thus, rate of destructuration of natural clays depended on the stress path, seen as different gradients of the normal compression line [Koskinen & Karstunen 2004]. Specimens of relatively lower initial water content regularly exhibited higher compression and shear resistance.

Effect of stress ratio and sample disturbance on preconsolidation pressure

In Figure 7.12 values of σ'_p/σ'_{vo} are related to specimen quality defined by $\Delta e/e_o$ criteria. To account for changes in anisotropy values of σ'_p considered were defined using linear plots of σ'_1 vs. v, and p' vs. v [Koskinen et al. 2003]. Overall, CAD results complied well with those obtained in IL and CRS oedometer tests. The results confirmed specimens of poor quality with high $\Delta e/e_o$ values being characterised by the lowest σ'_p/σ'_{vo}. Specimens of the highest quality with $\Delta e/e_o$~0.05 exhibited σ'_p/σ'_{vo} value of ~1.5.

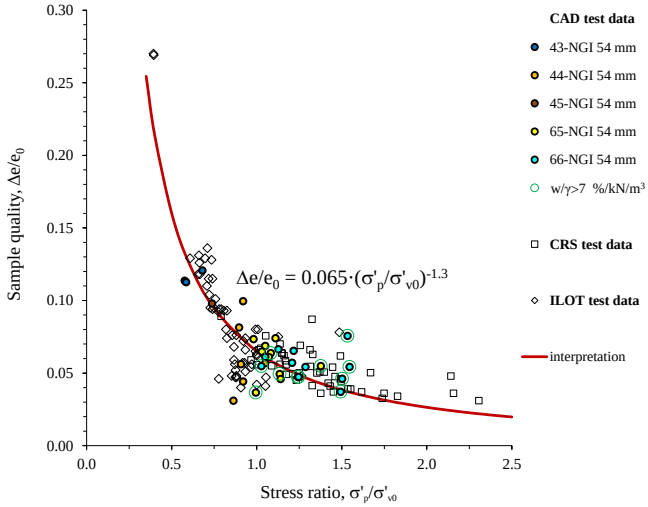

Figure 7.12 Preconsolidation pressure in CAD triaxial tests related to specimen quality.

Since $\Delta e/e_o$ values reflected specimen response in OC stress range, influence of stress ratio in consolidation on both $\Delta e/e_o$ and σ'_p/σ'_{vo} values was clearly

exposed. The S-2009 specimens consolidated along η=0.4 were destructured the most, i.e. characterised with $\sigma'_p/\sigma'_{vo}<1.0$. Specimens consolidated at η=0.6 generally showed $\sigma'_p/\sigma'_{vo}>1.0$. However, it was the specimens consolidated at η=0.85 that exhibited the highest σ'_p/σ'_{vo} and the lowest $\Delta e/e_o$ values. In the same Figure results characterised with $w/\gamma>7$ %/kN/m^3 are highlighted. Specimens with high w/γ generally exhibited high σ'_p/σ'_{vo} values. Thus, σ'_p/σ'_{vo} values were primarily dependent upon η imposed. The results confirmed destructuration of natural specimens in CAD test being the least at $\eta_{Ko}^{NC}=0.85$.

Yield surfaces of Perniö clay

In $p'_p/\sigma'_{vo,}$ vs. q'_p/σ'_{vo} plane on Figure 7.13, yield points in CAD tests at different stress ratios are plotted with yield surfaces interpreted. Yield values on specimens of stratigraphic units A and B are distinctively displayed. Systematic identification of yield of Perniö clay at various η enabled interpretation of yield surfaces representing sublayers A and B. Reflecting variance in quality of specimens, scatter of the normalized yield data at certain η was considerable. Influence of the specimen quality on shape and size of the yield surface was represented by response of poor quality destructured specimens. Based on results obtained, inclined elliptic yield surfaces reflecting anisotropy of Perniö clay were interpreted. Elliptic yield surfaces were defined by Equation 7.1:

$$f=(q-\alpha p')^2-(M^2-\alpha^2)(p'_m-p')p'=0 \tag{7.1}$$

where; α defines orientation of the yield curve, M is stress ratio at critical state, and p'_m defines the size of the yield curve [Dafalias 1986]. If Jaky's [1944] K_o formulation for NC soil is assumed, critical state stress ratio is related to in situ stress ratio at rest by Equation 7.2:

$$\eta_{K0}=\frac{3M_c}{6-M_c} \tag{7.2}$$

Anisotropic yield surfaces of Perniö clay were similar in the shape and orientation to those in previous studies of Finnish soft clays. As presented in Figure 7.12 the highest quality specimens were characterised with the highest $\sigma'_p/\sigma'_{vo,}$ values, and thus the highest values of $p'_p/\sigma'_{vo,}$ and q'_p/σ'_{vo}. Based on $\eta_{Ko}^{NC}=0.85$ and Equation 7.2, yield surfaces shown in Figure 7.13 corresponded to critical state of M=1.32. Yield surface representing response of high quality specimens of sublayer A was defined by size $p'_m=0.98$ and orientation α=0.82. Furthermore, yield surface defining high quality specimens of sublayer B was characterised by $p'_m=0.83$ and α=0.78. Additional yield surface D, representing yield response of poor quality specimens of both sublayers was defined by $p'_m=0.71$ and α=0.70. Despite identical magnitude of critical state M, yield surfaces interpreted differed in orientation α. Thus contrary to formulation in SClay1S, orientation of the yield surfaces in CAD tests on Perniö clay was modified to ensure reasonable compliance of yield points with the elliptic surfaces. α was the highest for high quality specimens of sublayer A, followed by high quality specimens of sublayer B, while the lowest α value characterised poor quality specimens of both sublayers. Based on the ellipses interpolated, maximum values of σ'_1/σ'_{vo} respectively corresponded to 1.59, 1.34 and 1.11.

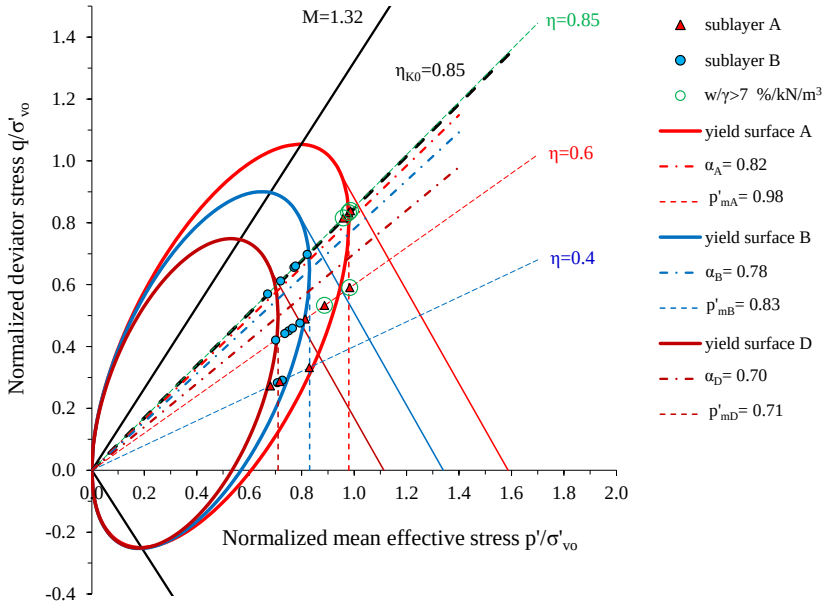

Figure 7.13 Yield curves of Perniö clay in p'_p/σ'_{v0}- q_p/σ'_{v0} plane, M=1.32.

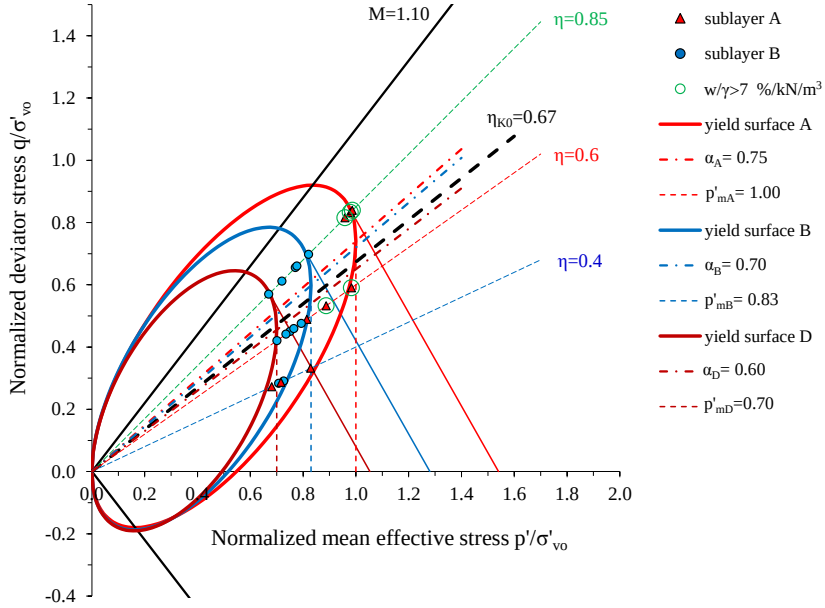

Figure 7.14 Yield curves of Perniö clay in p'_p/σ'_{v0}- q_p/σ'_{v0} plane, M=1.10.

The best compliance of the yield data with elliptic surfaces was obtained for M=1.10, as presented in Figure 7.14. Accordingly, ellipse representing high quality specimens of sublayer A was characterised by p'_m =1.0 and α=0.75, while that of high quality specimens of sublayer B was defined by p'_m =0.83 and α=0.70. Poor quality specimens of both sublayers were represented by yield surface D with p'_m =0.70 and α=0.60. With M=1.10, maximum values of

σ'_1/σ'_{vo} corresponded to 1.54, 1.28 and 1.05, respectively. The values complied with σ'_1/σ'_{vo} range in CRS and exceeded those on somewhat poorer quality IL oedometer specimens. Furthermore, by adopting M=1.10, the highest values of σ'_1/σ'_{vo} corresponded with response at $\eta_{K_o}^{NC}$=0.85. Thus clay anisotropy, i.e. shape and inclination of the yield surfaces, reflected initial quality of the specimens and progressive increase in destructuration with offset of radial stress path in consolidation from that representing conditions in situ. Characteristics of yield surfaces in Figure 7.13 and Figure 7.14 suggested main cause for difference in yield response of sublayer A and B specimens being extent of initial specimen disturbance. However, given the stress points through which yield surface is interpolated are rather close to each other, additional tests are needed to confirm the conclusions derived.

7.1.5 Compressibility-Cam-Clay parameters

Figure 7.15 examines compressibility of Perniö clay in triaxial consolidation tests using Modified Cam-Clay theory based parameters. The determination of the parameters was consistent with those in IL oedometer tests. Thus, to enable direct comparison with the results in IL and CRS oedometer tests, compressibility parameters in CAD tests were determined in v vs. ln σ'_1 plane (see Figure 6.7). The values on specimens with w/γ>7.0 %/kN/m^3 are highlighted.

Reloading behavior κ_o

In Figure 7.15 a), κ_o measured in CAD tests are related to sampling depth. Within sublayer A, κ_o varied broadly from 0.0150 to 0.192. However, majority of the values were well represented by average of 0.075. Specimens with w/γ>7.0 %/kN/m^3 generally exhibited high κ_o. Within sublayer B scatter was less. Altogether, κ_o in sublayer B were represented by average of 0.060, while the highest values identified upper section of the zone. Overall, the resulting κ_o values indicated proportionality with η imposed. Compared to those in oedometer tests, κ_o in CAD tests were more scattered. Furthermore, despite exhibiting the same pattern vs. depth in sublayers considered, average κ_o values exceeded those in CRS and IL oedometer testing.

Normal compression λ and intrinsic compression behavior λ_i

In Figure 7.15 b), λ values in CAD tests are related to depth. Only results on specimens consolidated to σ'_3=40 and 60 kPa are shown. Scatter of the λ values was high within both sublayers. Furthermore, λ were dependent upon the stress ratio in consolidation, being the highest in tests at η=0.85, followed by those at η=0.6, while values obtained at η=0.4 were extremely low. Considering high quality specimens consolidated at η=0.6 and 0.85, representable λ values in sublayers A and B amounted 1.0 and 0.75, respectively. Thus, λ in CAD exceeded those in oedometer tests, yet complied in pattern of response in respective sublayers. Specimens with high w/γ exhibited the highest λ values.

Figure 7.15 c), relates values of final slope reached in CAD tests to sampling depth. CAD tests performed until σ'_3=60 kPa were considered only. Average values amounted0.52 and 0.35 in sublayers A and B, respectively. Although re-

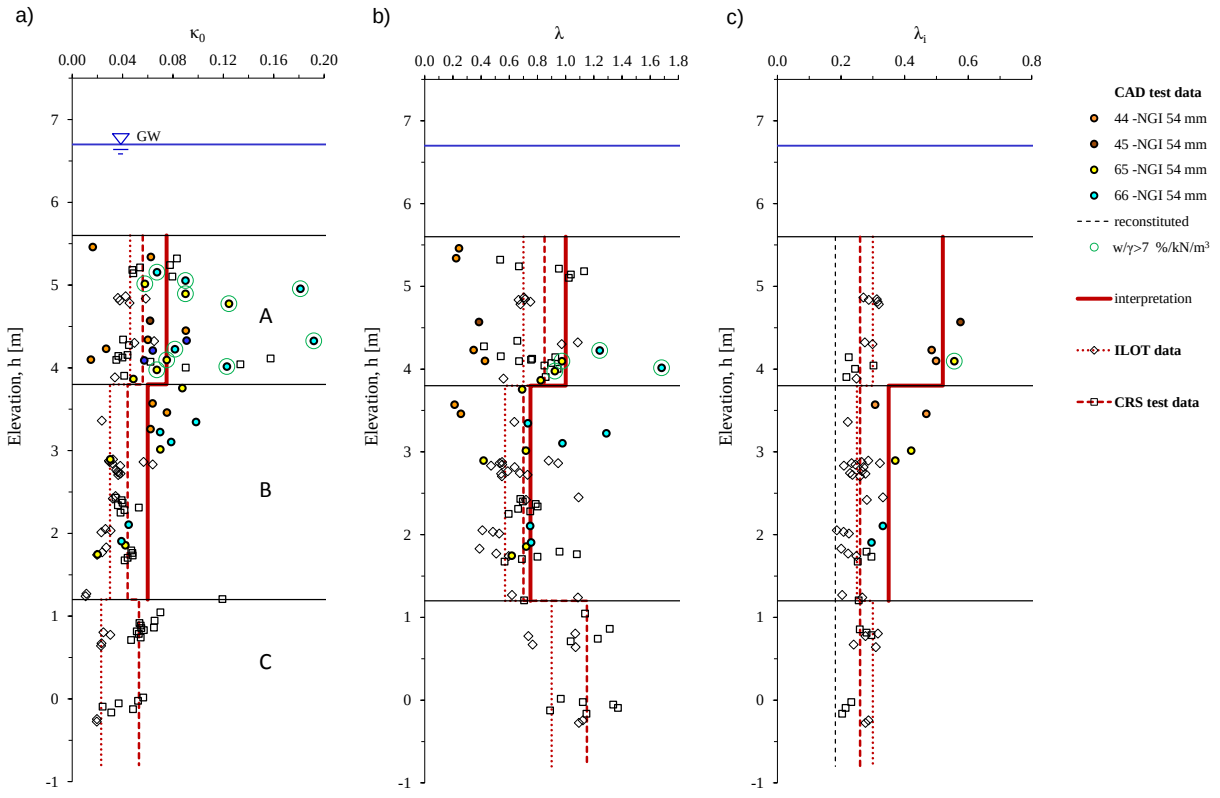

Figure 7.15 Cam-Clay theory based compression indices in CAD triaxial tests; a) reloading slope κ_0, b) slope of normal compression λ, and c) slope of final and intrinsic compression line.

sembling pattern of intrinsic compressibility in oedometer tests, results measured in CAD were much higher in magnitude. However, final slope in CAD tests was often not representable of intrinsic compressibility due to relatively low magnitude of σ'_i in consolidation (see Table 7.1). Stress ratio influence was marked by final slope reached at η=0.4 being the highest. In contrast, in tests on specimens consolidated at η=0.85 final slope in compression was markedly less, i.e. ~0.314. Later value corresponded to λ_i in oedometer tests, thus revealing sufficient level of destructuration. In contrast to those in oedometer tests, intrinsic compressibility in the CAD tests was reached at relatively lower level of strain. While oedometer test specimens reached λ_i level at ε_v~50 %, CAD specimens tested at η=0.85 showed corresponding compressibility at ε_v~35 %. The effect was possibly related to free lateral boundary test conditions. Figure 7.15 c) includes results on reconstituted specimens in CAD tests at η=0.4. Compared to those in oedometer tests, reconstituted specimens consolidated at η=0.4 exhibited somewhat lower slope in NC stress range, i.e. λ_R =0.188.

In Figure 7.16 a), λ values are related to stress ratio in consolidation. In triaxial stress space, the rate of destructuration depended upon the η imposed. Consequently, the values of λ for natural soil were influenced by η as well [Koskinen & Karstunen 2004]. Results on Perniö clay confirmed proportional relation of η and λ. Scatter of the λ values however, was very considerable. To examine effects of specimen disturbance, Figure 7.16 b) relates λ in CAD tests to w/γ. Among specimens consolidated at certain radial stress path, high quality specimens yielded with the highest λ values. For specimens consolidated at η=0.85, the w/γ to λ proportionality was the strongest. In contrast, those consolidated at η=0.4 and destructured specimens exhibited similar λ values independent of w/γ. Conclusion was valid for materials of both sublayers.

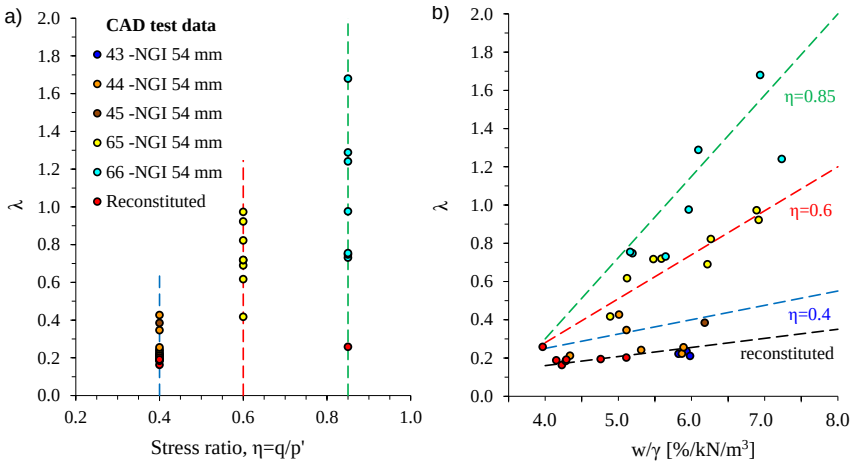

Figure 7.16 Evaluation of λ in CAD tests on Perniö clay, a) λ vs. η, and b) λ vs. w/γ.

Stress dependency of slope in compression

Figure 7.17 evaluates stress dependency of slope in compression in CAD tests on Perniö clay. The results are differed with respect to η in consolidation, while criteria w/γ>7.0 %/kN/m³ is used to identify high quality specimens.

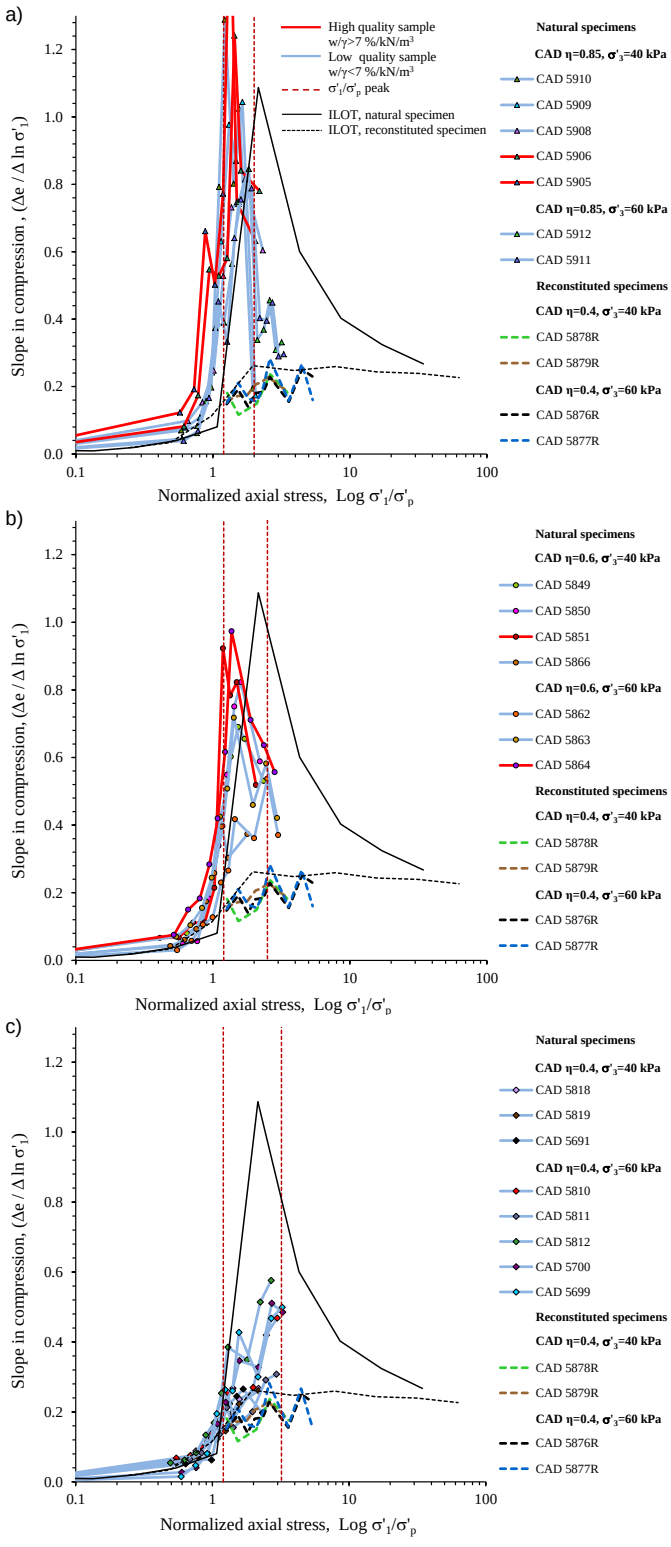

Figure 7.17 Slope in compression stress dependency in CAD tests on Perniö clay; a) η=0.85, b) η=0.6 and c) η=0.4.

The results obtained resembled corresponding curves measured in IL and CRS oedometer tests. However, effects of stress ratio in consolidation as well as those of triaxial test conditions were strongly exhibited. With specimens allowed to deform laterally, resulting curves were not smooth as in oedometer testing. Furthermore, η conditions imposed influenced both overall maximum and shape of the resulting curves. In reloading, the results were weighted by imperfections in the contact between the specimen and porous stones [Larsson & Sällfors 1986]. Compression response for the first load increment was considered as false and was restored by linear increase in reloading gradient at fairly low rate [Sandbaekken et al. 1987]. Slightly prior the yield, curves on natural specimens exhibited abrupt increase in compressibility. Independent of the η imposed, at $\sigma'_1/\sigma'_p=1$ majority of the specimens exhibited clear discontinuity in response manifested by the first peak. The effect was almost regularly exhibited by specimens of the highest quality, and was related to the onset of brittle failure. Following the first peak, values of slope in compression continued to rise and reached overall maximum corresponding to λ. Thereafter, compression gradient progressively declined, reflecting destructuration related decrease in compressibility within NC stress range. Curves obtained on specimens with $w/\gamma>7.0$ %/kN/m^3 generally plotted above those on poor quality specimens, thus showing higher reloading and virgin compression gradients overall. For comparison, data obtained on reconstituted specimens consolidated at η=0.4 are plotted as well. In NC stress range successive gradient values oscillated near the average of $\lambda_R=0.1875$.

Comparison of resulting curves revealed profound influence of η on consolidation characteristics in NC stress range. For consolidation results at η=0.85, increase in compression gradient following yield was the most rapid, while λ values reached were the highest. Slope in compression rose at somewhat lower rate in consolidation at η=0.6. Finally, at η=0.4 slope in compression increased at overall the lowest rate, while clear peak indicating λ was not reached within the vertical effective stress range imposed. Thus, depending upon the stress ratio in consolidation, values of maximum gradient in compression occurred within different normalized stress range, i.e. 1.2-2.0 at η=0.85, 1.2-2.5 at η=0.6, and 1.2-3.2 at η=0.4. Compared to equivalent curves obtained in IL oedometer test, CAD specimens consolidated at η=0.85, and η=0.6, exhibited more rapid increase in compression gradient following the yield.

7.1.6 Compressibility - Compression modulus parameters

Interpretation of parameters

In following compressibility of Perniö clay in triaxial consolidation test is examined using compression modulus theory. Firstly, CAD results are examined in the perspective of resistance to axial compression. Thus, compression modulus was defined in accordance with Equation 2.8 as the ratio of vertical effective stress and axial strain. Interpretation approaches used complied with those elaborated for IL oedometer tests presented in Figure 6.11. Unlike in IL oedometer test, under triaxial test conditions $\varepsilon_1 \neq \varepsilon_v$. For that reason results of triaxial consolidation test were evaluated in the perspective of volumetric re-

sistance as well. The values of bulk modulus were defined by the Equation 7.3:

$$K = \frac{dp'}{d\varepsilon_v} \tag{7.3}$$

where; dp' and $d\varepsilon_v$ are change in mean effective stress and volumetric strain, respectively. The values of bulk modulus were contrasted to shear resistance results. The values of shear modulus were defined by the Equation 7.4:

$$G = \frac{dq}{3 \cdot d\varepsilon_d} \tag{7.4}$$

where; dq and $d\varepsilon_d$ represented change in deviator stress and shear strain, respectively. Beside difference in moduli definition, interpretation approaches complied with those in oedometer testing. Volumetric resistance response was thus defined with parameters of initial bulk modulus $K_{Ø}$, limit bulk modulus K_L and bulk modulus number K', while transition from $K_{Ø}$ to K_L was defined with bulk destructuration line gradient $K'_{Ø}$. Accordingly, parameters defining shear modulus response were initial shear modulus G_o, limit shear modulus G_L, shear modulus number G', and shear destructuration line gradient G'_o. Information on both volumetric and shear resistance enabled comprehensive evaluation of specimen response under triaxial consolidation test conditions.

Initial M_o and limit compression modulus M_L

Figure 7.18 a) relates initial values of axial compression modulus M_o with depth. Within sublayer A, M_o values were scattered from 0.54 to 2.16 MPa, yet most of the results were well represented by 1.16 MPa. M_o values in sublayer B were represented by average of 1.55 MPa. However, results obtained within the sublayer were highly scattered, i.e. 0.97 to 2.12 MPa. Also, the M_o values rose in magnitude with sampling depth. Compared to results obtained in oedometer tests, triaxial specimens exhibited considerably higher M_o values overall.

Figure 7.18 b) presents values of limit modulus M_L in relation to depth. M_L values in CAD tests were highly scattered and strongly reflected reciprocal influence of η in consolidation. In sublayer A, M_L values ranged from 0.14 to 1.19 with representable average at 0.40. In sublayer B, M_L values were scattered from 0.13 to 0.99 with average at 0.45. Overall, values of M_L in triaxial consolidation tests were significantly higher than those measured in oedometer tests. M_L values in tests at η=0.85 and 0.6 however, corresponded fairly well with those of oedometer testing, i.e. 0.27 and 0.31 MPa in sublayers A and B.

Modulus number M'

Figure 7.18 c) examines axial compression resistance of triaxial specimens above σ'_L. Primary purpose of triaxial consolidation tests was specimen preparation for undrained shear at various consolidation stress levels. Consequently, amount of the specimens consolidated above σ'_L was limited. None of the tests were performed until sufficiently high stress levels for interpretation of parameter a. However, in several CAD tests at η=0.85 and 0.6 values of M' were found to vary between 0.008 and 0.017, thus complying fairly well with range of values identifying IL and CRS oedometer test results.

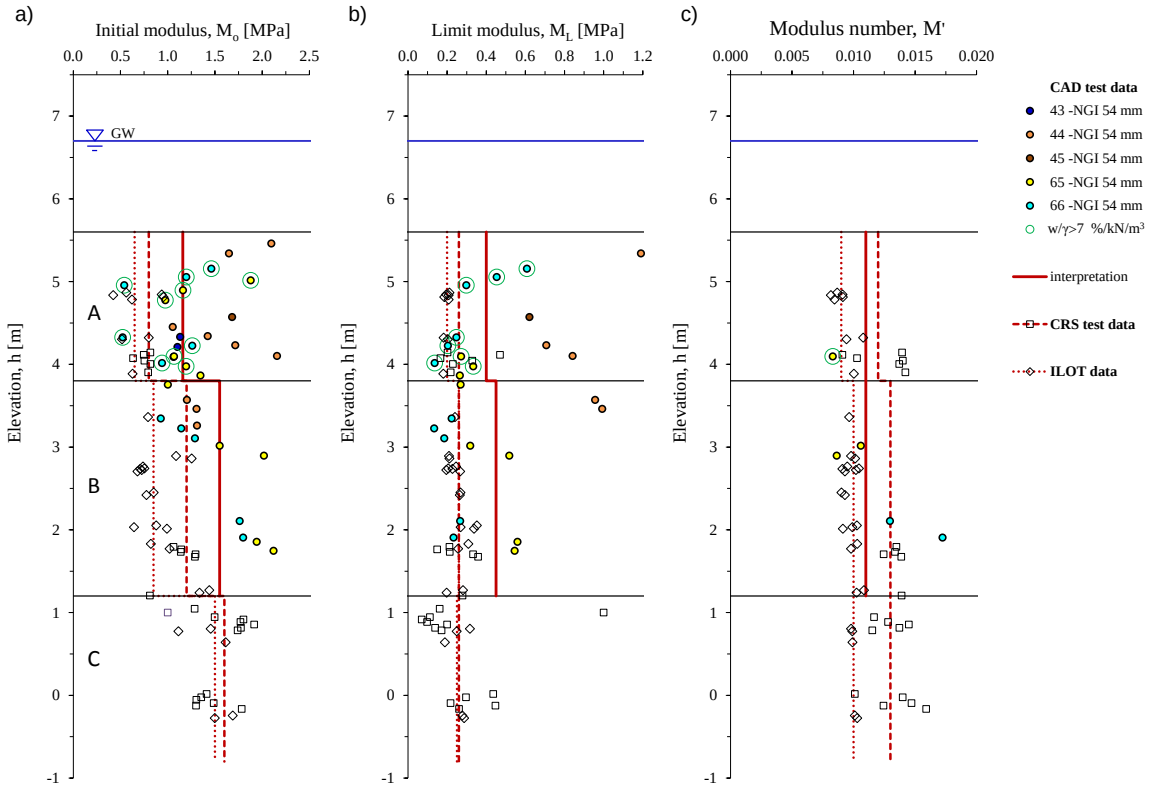

Figure 7.18 Compression modulus parameters in triaxial CAD tests on Perniö clay, a) Initial modulus M_o, b) limit modulus M_L, and c) modulus number M'.

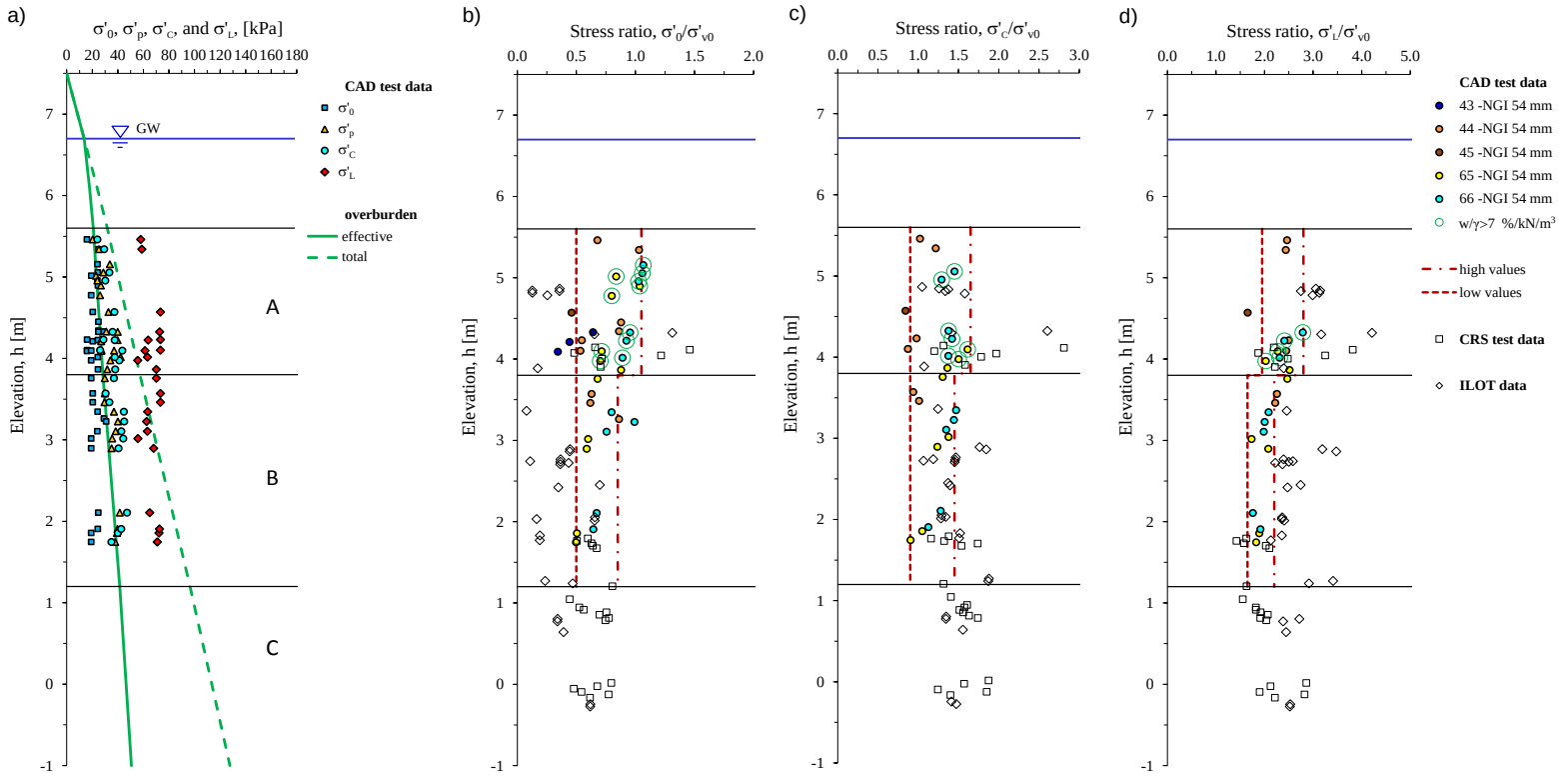

Figure 7.19 Evaluation of effective stress parameters characterising compression modulus curve in CAD triaxial tests; a) initial effective stress σ'_0, compression stress σ'_C, and limit stress σ'_L, b) σ'_0/σ'_{v0}, c) σ'_C/σ'_{v0}, and d) σ'_L/σ'_{v0}.

Effective stress parameters σ'_o, σ'_C and σ'_L

Figure 7.19 evaluates stress parameters characterising stages of specimen resistance to axial compression. Values of σ'_o continuously rose with sampling depth, resembling response measured in oedometer tests. With CAD specimens being compressed at fairly low strain-rate, the results exhibited less scatter compared to those in CRS oedometer tests. When normalized with effective overburden, the results were well represented by σ'_o/σ'_{vo} of 0.8 and 0.6 in respective sublayers A and B. Results of CAD tests confirmed σ'_C values representing upper limits of vertical effective stress at yield. Thus except of being somewhat higher in magnitude, σ'_C results resembled response elaborated for σ'_p. Representative values of σ'_C/σ'_{vo} in sublayers A and B amounted 1.55 and 1.27, respectively. Similar to the response measured in oedometer tests, σ'_L in CAD tests corresponded fairly well with distribution of total overburden stresses with depth. Again oscillations that occurred reflected response at yield. When normalized with effective overburden, the results were well represented by σ'_L/σ'_{vo} of 2.4 and 2.2 in sublayers A and B.

Effect of consolidation stress ratio on compression modulus curve

Figure 7.20 presents compression modulus response in CAD tests related to vertical effective stresses. Consolidation results at η=0.85, 0.6 and η=0.4 are distinctively displayed. Values of M_o exhibited considerable scatter independent of the consolidation conditions imposed, and generally exceeded values determined in oedometer testing. Majority of the M_o values occurred in limits from 1.02 to 1.94 MPa. Values of destructuration line gradient M'_o were somewhat less compared to those in IL oedometer testing. Influence of η in consolidation was manifested by different magnitude of M_L values in accordance with conclusions based on values of λ. Scatter of the M_L values was the most prominent in tests at η=0.4 being 0.62 to 1.19 MPa, followed by that at η=0.6, i.e. 0.27 to 0.56 MPa. Finally, M_L in tests at η=0.85 varied in relatively narrow limits from 0.13 to 0.30 MPa. The results showed triaxial specimens tested at η=0.85 being the least influenced by destructuration in consolidation. Amount of data on compression characteristic above σ'_L was limited. Based on the data available, M' values in tests at η=0.85, exceed those measured at η=0.6.

Initial $K_\emptyset$ and limit bulk modulus K_L

Figure 7.21 a) relates values of initial bulk modulus $K_\emptyset$ to sampling depth. The results are contrasted to values of initial compression modulus M_o determined in oedometer tests. $K_\emptyset$ results in sublayer A represented by 0.58 MPa revealed high scatter, i.e. 0.28 to 1.25 MPa. Evaluated at corresponding elevation values in tests at η=0.85 were the lowest. Within sublayer B, $K_\emptyset$ values were represented by 0.70 MPa. Again, the results were highly scattered and rose in magnitude with depth from 0.45 MPa in the upmost to 1.82 MPa in the lowest section of the zone. Considering results obtained on triaxial specimens of both sublayers, values identifying $K_\emptyset$ complied well with M_o results measured in IL and CRS oedometer tests. Compliance of the parameters indicate loading conditions in oedometer test prior to σ'_o being fairly isotropic, i.e. $p' \approx \sigma'_1$.

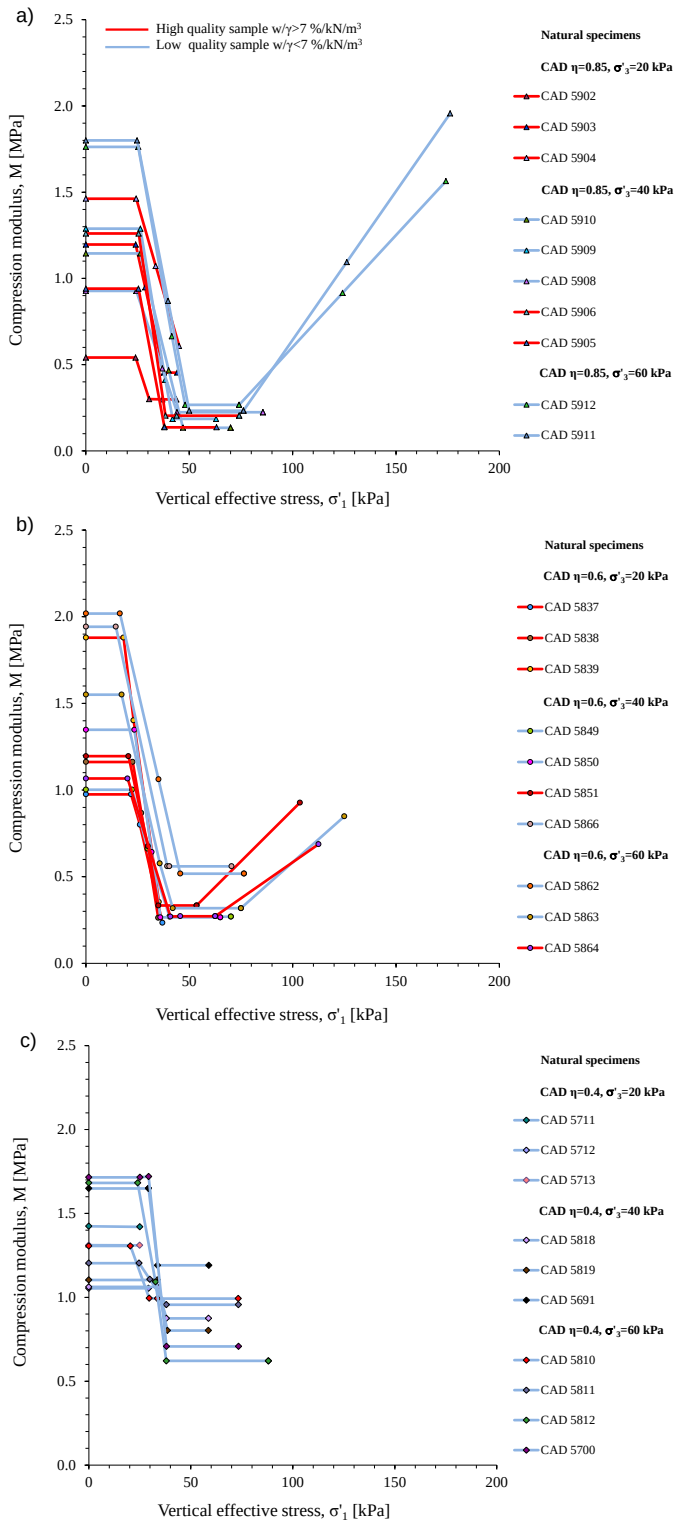

Figure 7.20 Compression modulus interpretation of CAD tests, a) η=0.85, b) η=0.6 and c) η=0.4.

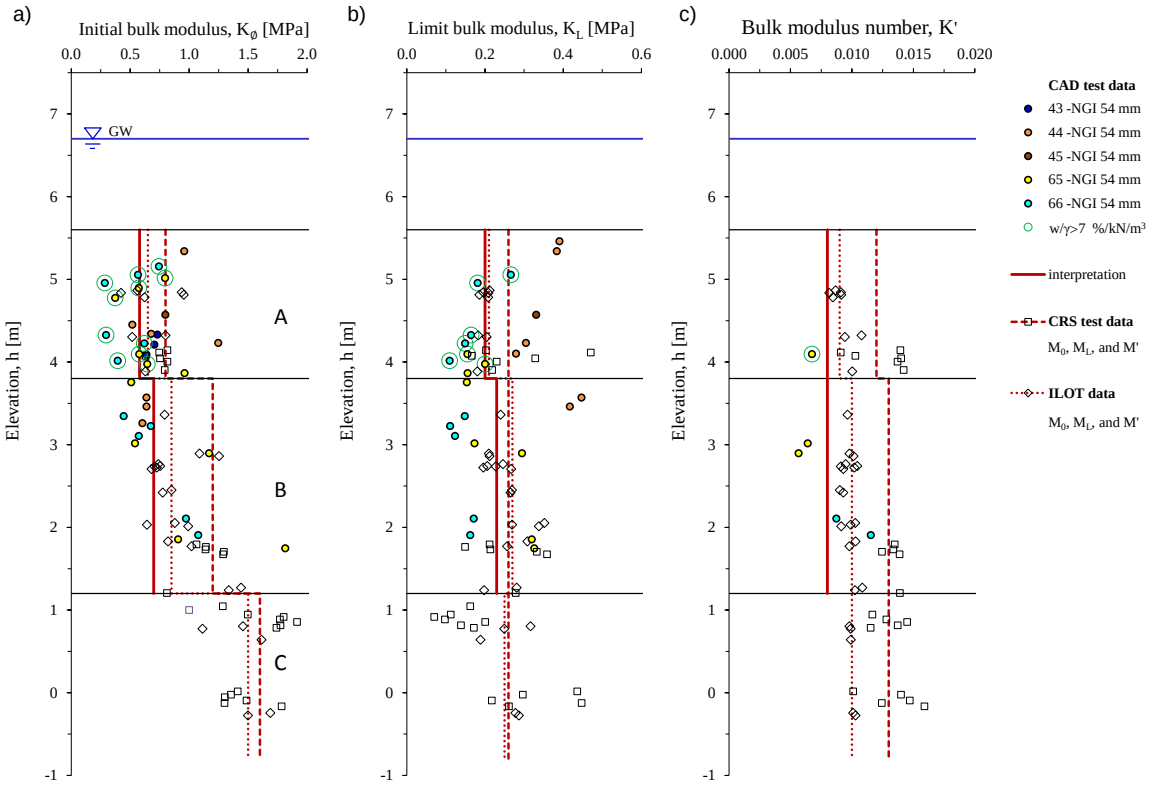

Figure 7.21 Bulk modulus parameters in triaxial CAD tests on Perniö clay, a) Initial bulk modulus $K_{ø}$, b) limit bulk modulus K_L, and c) bulk modulus number K'.

In Figure 7.21 b), values of limit bulk modulus K_L are presented in relation to sampling depth and compared with M_L results of oedometer testing. High scatter of K_L values reflected reciprocal influence of η in consolidation. In sublayer A, K_L ranged from 0.11 to 0.39 MPa, while in sublayer B scatter was from 0.11 to 0.44 MPa. Overall, representable K_L values measured on triaxial specimens were somewhat less compared to M_L in IL and CRS oedometer tests, i.e. 0.20 and 0.23 MPa in sublayers A and B. Both sublayers considered, the lowest values were identified on specimens consolidated at η=0.85. Indeed, in tests at η=0.85, representative K_L response in both sublayers was 0.15 MPa.

Bulk modulus number K'

Figure 7.21 c) shows parameter K' defining volumetric resistance of triaxial specimens above σ'_L. Based on limited amount of CAD test results at η=0.85 and 0.6, values of bulk modulus number K' varied between 0.006 and 0.012. Compared to M' values measured in oedometer testing, magnitude of the K' values was somewhat less.

Effects of consolidation stress ratio on volumetric resistance curves

In Figure 7.22, volumetric resistance in CAD tests is contrasted to vertical effective stress. Resulting curves in consolidation at η=0.85, 0.6 and η=0.4 are separately shown. Under respective test conditions the values of $K_Ø$ varied from 0.28 to 1.25. High scatter primarily reflected proportional influence of sampling depth. Furthermore, the $K_Ø$ values were typically less than half of M_o identified in the CAD tests. In contrast to highly scattered $K_Ø$, values of limit bulk modulus K_L measured at certain consolidation stress ratio were rather uniform. In tests at η=0.85, K_L varied from 0.11 to 0.18 MPa. Values obtained at η=0.6 were somewhat more scattered ranging from 0.15 to 0.33 MPa. Finally, in tests at η=0.4 values of K_L were between 0.30 and 0.45 MPa. Thus, reflecting the extent of destructuration magnitude of K_L was reciprocal to η in consolidation. Gradient of the volumetric destructuration line $K'_Ø$ somewhat exceeded M'_o in CAD tests. Limited number of results indicated bulk modulus number K' being proportionally related to consolidation η.

Initial G_o and limit shear modulus G_L

In Figure 7.23 a), values of $K_Ø$ and G_o in CAD tests are related to sampling depth and compared to M_o in IL and CRS oedometer tests. While $K_Ø$ values in CAD tests complied in response with M_o in oedometer testing, values identifying initial shear modulus G_o were significantly less. In sublayers A and B, G_o response was well represented by respective values of 0.29 and 0.35 MPa. Therefore, despite resembling distribution pattern vs. depth, magnitudes of G_o values were in average half of those identifying initial bulk resistances $K_Ø$.

Figure 7.23 b), examines K_L and G_L moduli in CAD tests. In sublayer A and B, G_L values were represented by values of 0.07 and 0.08 MPa. Thus, G_L response generally followed depth distribution of K_L values. Compared to K_L determined within the same tests however, G_L values were in average three times less, i.e. at limit stress range CAD results exhibited tendency toward $dq/d\varepsilon_d \sim dp'/d\varepsilon_v$.

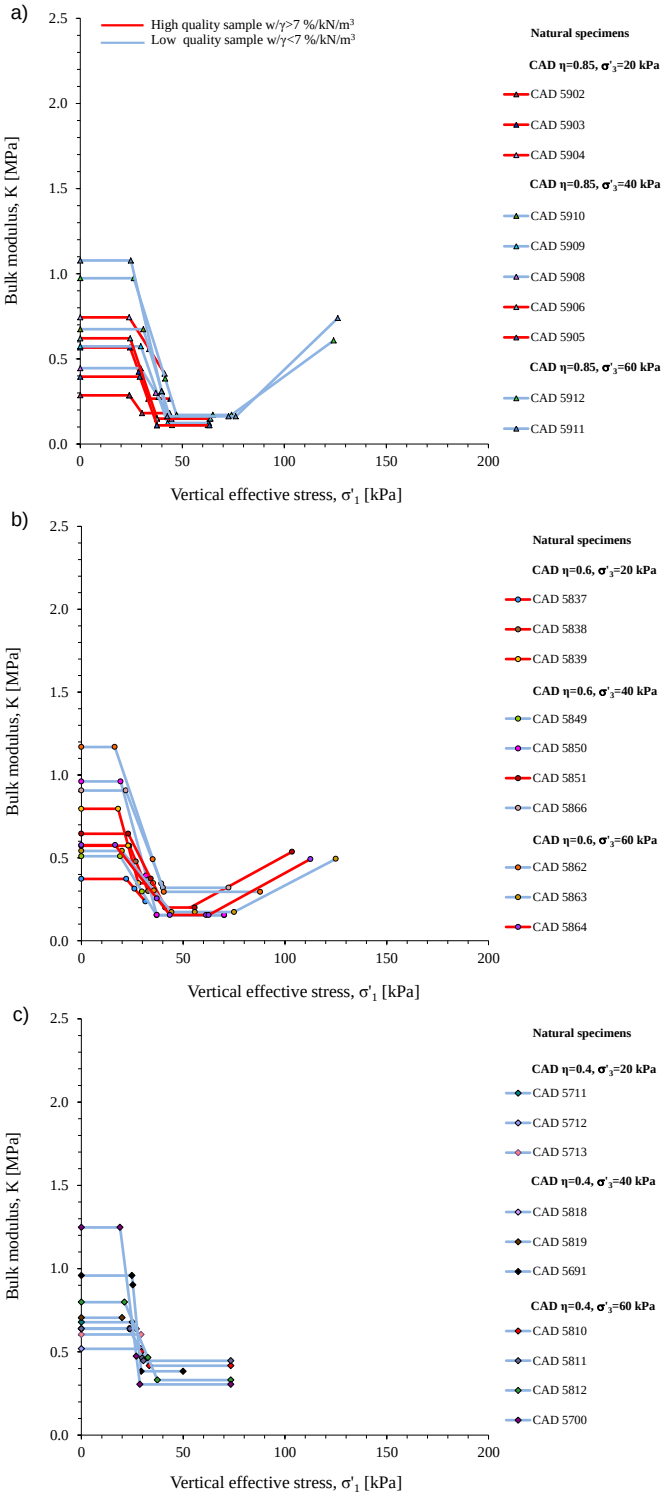

Figure 7.22 Compression modulus interpretation of volumetric resistance in CAD tests, a) η=0.85, b) η=0.6 and c) η=0.4.

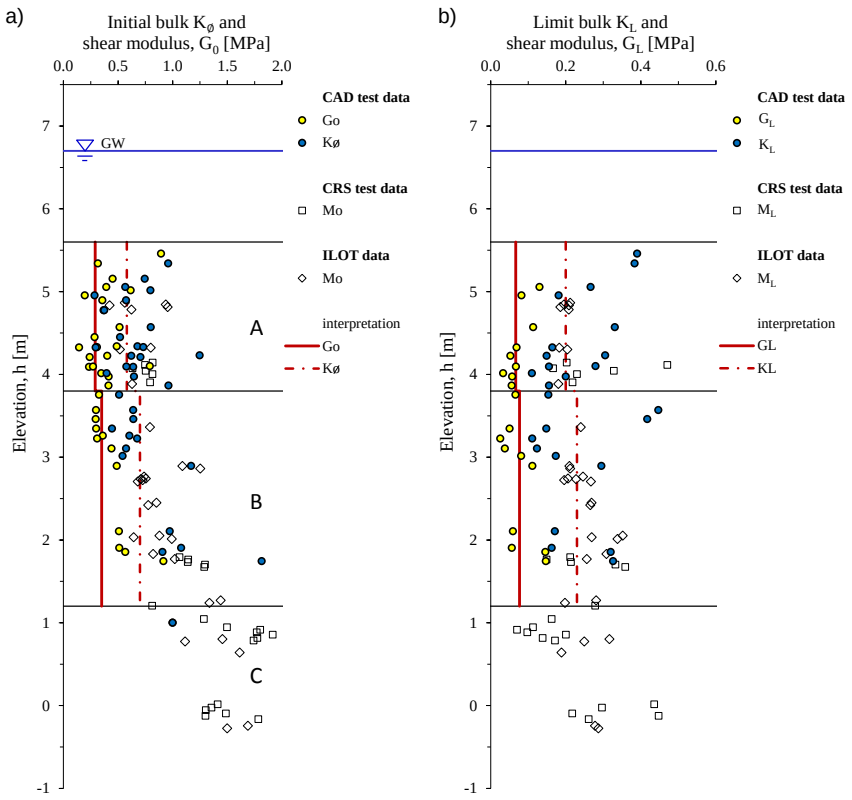

Figure 7.23 Volumetric and shear resistance parameters in triaxial CAD tests on Perniö clay, a) Initial bulk K_0 and shear modulus G_0, b) limit bulk K_L and shear modulus G_L.

Effects of consolidation stress ratio on shear resistance curves

Shear resistance results are contrasted to volumetric resistance response in Figure 7.24. Unlike that of bulk modulus, response in shear resistance was somewhat unclear. For that reason, several tests representing characteristic response at consolidation conditions implemented are selected and elaborated. Figure 7.24 a) presents response obtained on NC specimen 5911 at η=0.85. At η_{Ko}, shear resistance response was concise. Magnitude of G_o was less than half of $K_Ø$. Gradient G'_o defining transition from G_o to G_L, was somewhat less compared to that identifying reduction of bulk modulus in reloading. Above σ'_c, magnitude of shear modulus corresponded to 1/3 of bulk modulus, i.e. $dq/d\varepsilon_d \sim dp'/d\varepsilon_v$ was valid. Due to free lateral boundary some minor oscillations occurred within the limit modulus stress range, yet they influenced volumetric and shear resistance equally well. Shear resistance of NC specimen consolidated at η=0.6 is represented by test 5862 in Figure 7.24 b). Again, $K_Ø$ was more than twice higher than G_o. Bulk modulus destructuration rate in reloading was somewhat more rapid compared with that identifying shear modulus response, i.e. $K'_Ø > G'_o$. Within NC stress range, values of shear modulus corresponded fairly well to 1/3 of those identifying volumetric resistance, i.e. $dq/d\varepsilon_d \sim dp'/d\varepsilon_v$. In contrast to results at η=0.85 however, measured values of shear resistance in reloading oscillated. Similar response was measured in CAD 5812 on NC

specimen consolidated at η=0.4. Compared to results at η=0.85 and 0.6 however, values of shear modulus in reloading highly oscillated in value. Finally, test 5699 in Figure 7.24 d) presents response of OC specimen from profile 44 consolidated at η=0.4. Both $K_{Ø}$ and G_o were high in magnitude. While data representing volumetric resistance was rather concise, values identifying shear resistance oscillated strongly. The oscillations reflected negligible shear strains prior to σ'_L level, i.e. $\varepsilon_d \sim 0$. It was for $\sigma'_1 > \sigma'_L$ that values of shear modulus corresponded to 1/3 of bulk modulus leading to $dq/d\varepsilon_d \sim dp'/d\varepsilon_v$ condition being satisfied.

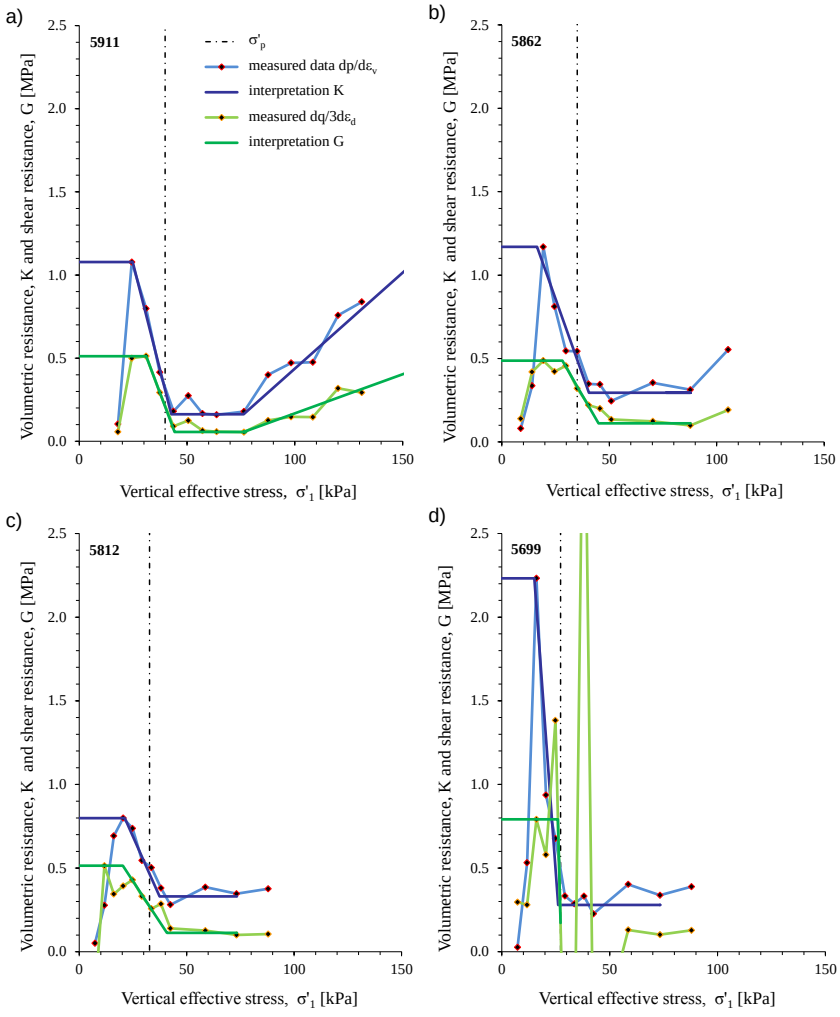

Figure 7.24 Comparison of shear and volumetric resistance in CAD tests; a) CAD 5911 at η=0.85, b) CAD 5862 at η=0.6, c) CAD 5812 at η=0.4, and d) CAD 5699 at η=0.4.

Oscillations in shear resistance reflected destructuration effects in CAD testing. In tests at η_{Ko}=0.85, radial strains were retained close to zero. Consequently, specimen structure in consolidation was preserved representable of that in situ, and oscillations in shear resistance were negligible. In contrast,

specimen consolidated at stress ratio condition differing significantly from η_{Ko} was subjected to prominent changes in structural characteristics manifested by high oscillations in shear resistance in reloading and reduction in compressibility within NC stress range.

Interpretation of shear and volumetric resistance in CAD tests provided valuable information for understanding of the destructuration process. Vertical effective stress characterising maximum shear resistance in reloading, did not necessarily correspond with stress level matching maximum bulk modulus, i.e. σ'_o at $K_{omax} \neq \sigma'_o$ at G_{omax}. Provided that CAD tests along constant stress ratio path are made using continuously loaded procedure, definition of q at G_{omax} and p' at K_{omax} would be feasible. Following normalization with effective overburden, the parameters could be used for definition of characteristic surface. Positioned within that of yield, the surface would define maximum compression/shear resistance in reloading. Consistently, deviator and mean isotropic stresses identifying limit stress state, i.e. p'_L and q_L, could be used to identify surface at limit state level. Thus, additionally to that at yield, specimen response in CAD test would be defined by surfaces characterising reloading and limit state response. Position and shape of the surfaces would provide additional data on destructuration and changes in anisotropy caused by stress release, as well as that induced by stresses above yield.

7.1.7 Bonding parameters

Sensitivity

Sensitivity of Perniö clay specimens in CAD test was examined using several approaches. Firstly, applicability of the sensitivity determination based on CAD compression curve characteristics was assessed. Results were compared with those obtained on oedometer test specimens and those determined by the fall cone test. Finally, values were contrasted to S_t correlated using the approach of Leroueil et al. [1983]. Free lateral boundary conditions in triaxial test and η in consolidation affected compression curve characteristics. Furthermore, accuracy of the interpretation approaches was influenced by magnitude of σ'_1 reached in consolidation. Due to relatively low σ'_1 implemented within the testing programme, intrinsic compression characteristics of CAD specimens were seldom reached. Consequently, sensitivity evaluations based on CAD compression curve characteristics need to be taken with caution.

Approach a

In approach a, CAD sensitivity values were calculated using the Equation 6.6. Thus, σ'_{pi} was defined at intersection of v_o=const. line with that representing compressibility of reconstituted specimen in NC range (see Figure 6.15). Reference compressibility of the reconstituted material was defined by adopting λ_R=0.259, measured under oedometric test conditions, while intercept $v_{R,}$ was determined using line of λ_R slope tangential to final portion of the CAD compression curve. Sensitivity values obtained using approach a are inFigure 7.25 a) related to sampling depth.

Approach b

In approach b, intersection of line representing final compressibility of natural specimen with that of initial specific volume defined intrinsic yield σ'_{pi} (see Equation 6.7 and Figure 6.15. Thus, resulting S_t values were directly related to final compressibility reached. Consequently, unless the natural specimen was completely destructured the results underrated true initial sensitivity. Approach b sensitivity results are shown in Figure 7.25 b).

Approach c

In approach c sensitivity of CAD specimens was defined by Equation 6.8. Thus, sensitivity was determined as ratio of compressibility of natural to that of reconstituted specimen at identical specific volume. Continuous S_t data obtained enabled evaluation of specimen destructuration with increase in strain. Maximum sensitivity values resulting from approach c are shown in Figure 7.25 c).

Comparison of sensitivity obtained in triaxial test and fall cone test

In Figure 7.25, sensitivity determined from CAD test results on Perniö clay are related to depth and compared to values representing oedometer test specimens and those obtained by fall cone test.

In Figure 7.25 a) sensitivity values determined with approach a are presented in relation to sampling depth. S_t values in sublayer A were low. The highest values, obtained on specimens tested at η=0.85, corresponded well with CRS tested specimens and fall cone test results on NGI 54 sampled material. Values on CAD specimens of sublayer B with S_t<10, complied with poor quality oedometer specimens, thus being considerably less than values determined by fall cone test. Calculated S_t values were strongly dependent upon σ'_1 reached in consolidation. Considering specimens consolidated to σ'_3= 40 and 60 kPa only, average S_t in tests at η=0.85, 0.6 and 0.4 were 19.6, 8.4, and 2.2 for sublayer A, while those for sublayer B specimens amounted 7.0, 4.1, and 2.0, respectively. The S_t values were determined assuming unique λ_R, thus neglecting the influence of η in consolidation. Namely, λ_R in triaxial consolidation at η=0.4, was considerably less, i.e. $\lambda_{R\ 0.4}$=0.188. Assuming linear λ_R to η relation and omitting the influence of w_o, λ_R amounted 0.259, 0.220 and 0.188 in tests at η=0.85, 0.6 and 0.4, respectively. Corresponding sensitivity values in tests at η=0.6 and 0.4 were thus somewhat higher, with average at η=0.6 amounting 14.5 and 6.2, while those at η=0.4 were 4.9 and 4.1 in sublayers A and B. Overall, the S_t values calculated were very low and did not adequately represent initial sensitivity of the specimens, but rather indicated relative magnitude of destructuration in consolidation.

Sensitivity values obtained on CAD specimens using approach b are related to sampling depth in Figure 7.25 b). Only specimens consolidated to stress level defined by σ'_3= 60 kPa were considered. Overall, S_t values calculated were negligible, amounting 3.5, 1.8 and 1.0 in tests at η=0.85, 0.6 and 0.4. Low St values reflected incomplete level of destructuration in consolidation. Namely, respective vertical effective stresses in consolidation at η=0.85, 0.6 and 0.4

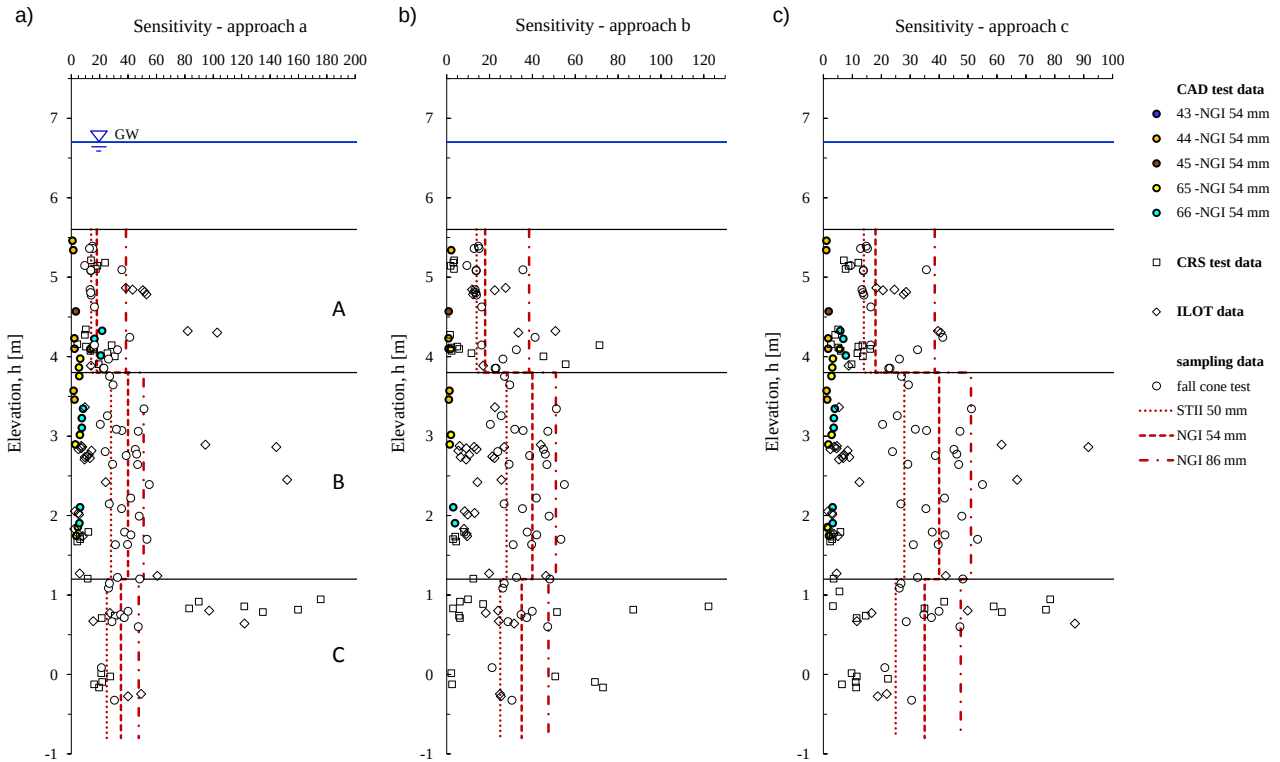

Figure 7.25 Sensitivity of CAD test specimens compared to values obtained in fall cone test; a) approach a, b) approach b, and c) approach c.

were σ'_1= 130.7, 105.1 and 87.3 kPa, while corresponding axial strains amounted ~20, 25 and 35 %. In comparison, perquisites for intrinsic compressibility in oedometer test were σ'_1~1000 kPa and ε_1~50 %. Although under free lateral boundary conditions intrinsic compressibility can be reached at relatively lower strains, S_t values obtained on CAD specimens were not representable.

In Figure 7.25 c), maximum sensitivity values obtained with approach c are related to sampling depth. Presented S_t results were determined by adopting reconstituted compressibility defined by unique slope λ_R=0.259. Due to similarities with approach a, maximum S_t obtained with approach c were just somewhat lower in magnitude. Considering specimens consolidated to σ'_3= 40 and 60 kPa only, values of maximum sensitivity in tests at η=0.85, 0.6 and 0.4 were represented by 6.8, 4.0, and 1.6 in sublayer A, while those in sublayer B amounted 3.5, 2.1, and 1.2, respectively. Due to consolidation to relatively low σ'_1 and omission of influence of η on reference reconstituted compressibility, maximum sensitivity of CAD specimens were overall negligible and complied with those obtained on poor quality oedometer specimens of sublayer A and B.

Sensitivity calculated on the basis of CAD compressibility response resulted with significantly lower values compared to those obtained by fall cone test following the sampling. In Figure 7.26, additional approach was examined, being that of empirical correlation between S_t, λ and e_o [Leroueil et al. 1983].

As shown in Figure 7.26 a), influence of η in consolidation on sensitivity values was clear. Results obtained on profile 66 specimens consolidated along η=0.85 were the highest, i.e. $16<S_t<128$. Furthermore, S_t values identifying specimens from profile 65 consolidated at η=0.6 occurred between 8 and 32. Finally, values obtained on specimens of profile 44 consolidated at η=0.4 were the lowest with $S_t<8$. Results on reconstituted CAD specimens complied with those obtained in oedometer testing, i.e. $S_t<4$.

In Figure 7.26 b), correlated sensitivity values are examined with respect to sublayer of origin. S_t on CAD specimens of sublayer B mainly occurred within $16<S_t<64$. The results exceeded values obtained on IL oedometer specimens, yet corresponded well with those representing specimens in CRS oedometer tests. Same conclusion was valid for CAD specimens of sublayer A. Compared with those in oedometer testing, S_t on CAD specimens were among the highest within the sublayer A. The results confirmed values obtained using approaches a, b and c, strongly underestimating initial S_t of the triaxial specimens.

To provide additional means for evaluation of the results, in Figure 7.27 sensitivity values in ILOT, CRS and CAD tests on Perniö clay are compared, and related to data identifying Eastern Canada clays reported by Leroueil [1997]. In relation to natural specimens in IL tests, CRS test specimens exhibited similar range of e_o, yet higher magnitude of λ. Consequently, correlated sensitivity values in CRS tests were generally higher. This fact can be related to higher initial quality of the CRS specimens, i.e. less disturbance in preparation of specimens aiming CRS test. However, the effect was probably related to influence of constant strain-rate test conditions. Sensitivity values characterising triaxial specimens generally exceeded those in IL oedometer tests as well.

Thus, despite somewhat lower range of e_o values, results obtained on CAD specimens corresponded with data on specimens in CRS oedometer tests. In addition, Figure 7.27 includes correlation of initial void ratio and compressibility of oedometer and triaxial specimens at the end of the tests. The approach enabled evaluation of specimen sensitivity following complete destructuration. The results identifying oedometer and triaxial specimens complied well and occurred within range of the lowest sensitivity. Occasional triaxial specimens indicated incomplete destructuration level at the end of consolidation. Compared to sensitivity values identifying Eastern Canada clays, Perniö clay results exhibited similar pattern, yet were clearly characterised by both higher e_o and λ values. Comparing the spatial position of the results however, Eastern Canada clays exhibit higher sensitivity. Considering relation of initial void ratio to sensitivity values defined in this study, the results indicate that true initial sensitivity of Perniö clay might be higher.

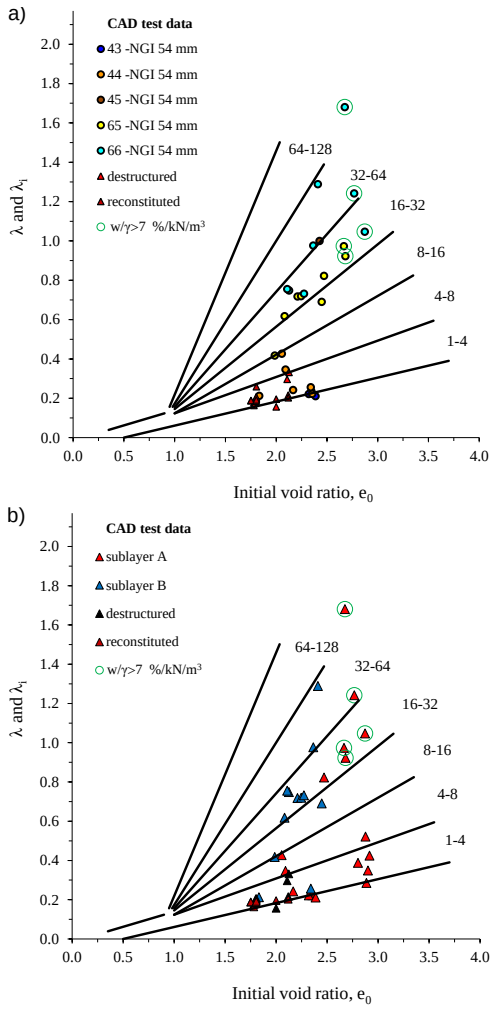

Figure 7.26 Sensitivity of CAD test specimens correlated from e_0 and λ (λ_i); a) related to sampling profile, and b) sublayer of origin [correlation after Leroueil et al. 1983].

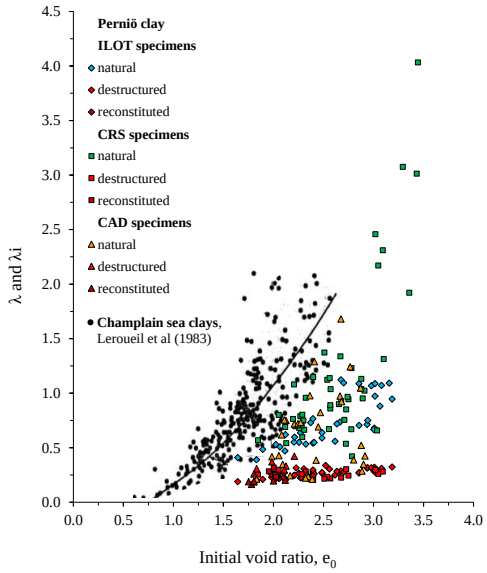

Figure 7.27 Sensitivity of Perniö and Eastern Canada clay [modified after Leroueil et al. 1983].

Rate of destructuration

Interpretation of sensitivity using approach c enabled evaluation of destructuration rate in CAD tests. In Figure 7.28, continuous sensitivity data are related to σ'_1/σ'_p. Although S_t values were not manifested in their full extent, the results confirmed conclusions based on oedometer testing. Altogether, curves exhibited maximum sensitivity values at yield, i.e. $0.9<\sigma'_1/\sigma'_p<1.15$. With further increase in vertical effective stresses S_t progressively declined reaching value equal to unity at the final stage of consolidation. As in oedometer testing, curves representing specimens of the highest quality merged with those on reconstituted specimens at σ'_1/σ'_p~3.0. In contrast to results on specimens

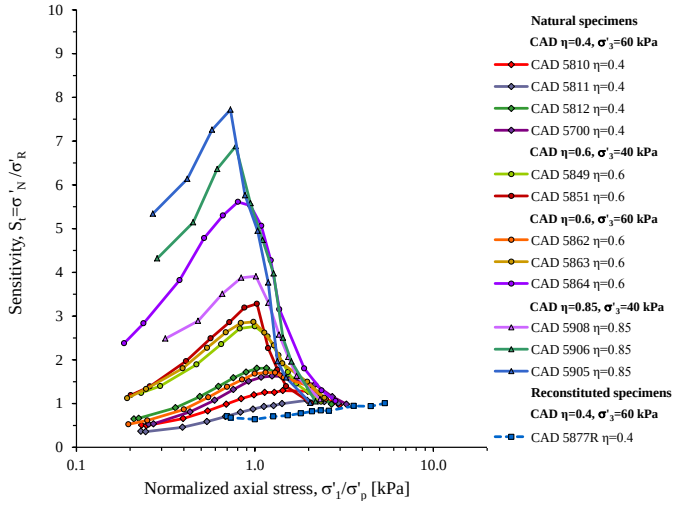

Figure 7.28 Sensitivity values in CAD triaxial tests in relation to σ'_1/σ'_p.

loaded to low σ'_1, sufficiently destructured specimens (e.g. 5911 and 5912) exhibited smooth transition when reaching unit sensitivity in the end of the test.

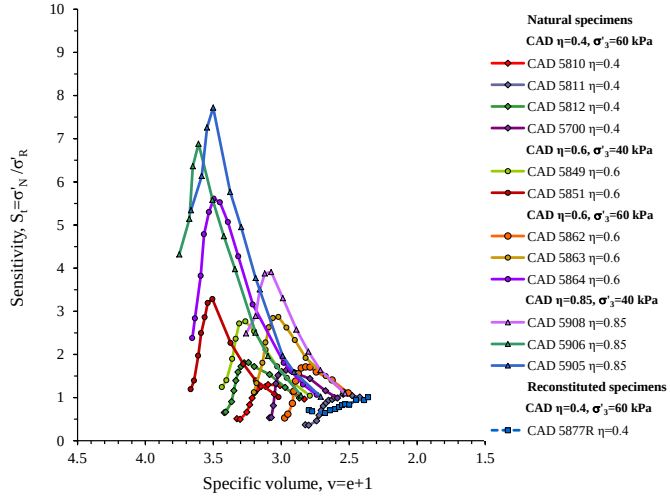

Figure 7.29 Sensitivity values in CAD triaxial tests in relation to specific volume.

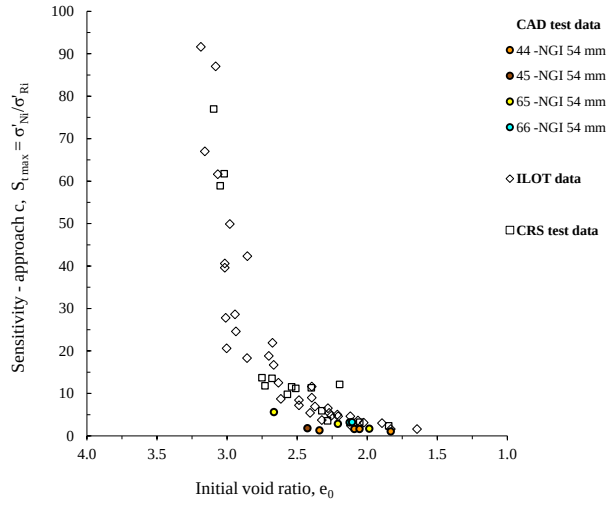

Figure 7.30 Maximum sensitivity values in CAD triaxial test related to initial void ratio.

In Figure 7.29, CAD sensitivity data are related to specific volume. The highest rate of destructuration was measured on specimens with the highest sensitivity and initial specific volume. Compared to those in oedometer testing, CAD sensitivity vs. specific volume results were significantly more scattered. Indeed, due to the characteristics of compressibility response, sensitivity values were proportionally influenced by stress ratio in consolidation. The main reason for discrepancy however, was in CAD specimens being consolidated to various generally low σ'_1, and intrinsic compressibility not being reached. Due to the reasons sensitivity values interpreted were low, while the rates of destructuration corresponded to those on oedometer specimens of poor quality.

In Figure 7.30 maximum S_t values determined on CAD test specimens using approach c are related to initial void ratio. Due to low strain level in consolidation, the $S_{t\,max}$ were more scattered compared to those on high quality IL and CRS oedometer specimens. Considering specimens consolidated to stress level defined by σ'_3= 60 kPa only, response of CAD specimens complied reasonably well. However, limited amount of data did not allow detail evaluation of the e_o influence on resulting $S_{t\,max}$ values. For the purpose, CAD tests on specimens with e_o>2.5 consolidated until sufficient level of destructuration were lacking.

7.1.8 Creep parameters

Secondary compression coefficient c_α

Digital measurements of specimen compressibility enabled determination of secondary compression coefficient in CAD tests at distinctive stress ratio levels. Interpretation approaches complied with those used for IL oedometer test (see Figure 6.21). Thus, the $c_{\alpha e}$ values were identified in e vs. log t plane for identical duration sequence from 6th to 24th h of each load step.

Figure 7.31 a) presents depth distribution of maximum values of secondary compression coefficient $c_{\alpha e\,max}$, determined in CAD tests at various η. Only results on specimens consolidated to σ'_3=40 and 60 kPa were considered. Creep

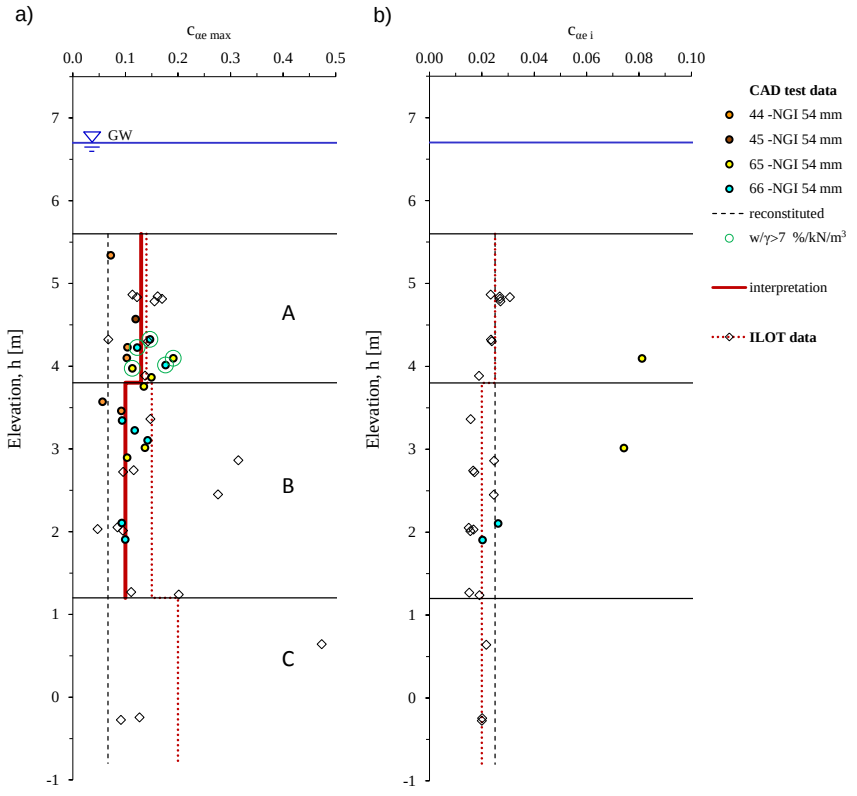

Figure 7.31 Secondary compression coefficient in CAD tests; a) maximum secondary compression coefficient $c_{\alpha e\,max}$, b) final and intrinsic secondary compression coefficient $c_{\alpha e\,i}$.

response in CAD test was characterised by moderate scatter. The highest values of $c_{\alpha e\ max}$ were obtained on specimens with high w/γ. Amounting 0.13 in average, $c_{\alpha e\ max}$ results within sublayer A complied well with those in IL oedometer test. Within sublayer B, CAD $c_{\alpha e\ max}$ values were well represented by average of 0.10. The result corresponded with those on poor quality specimens in oedometer tests, yet was significantly less compared to those measured on specimens of the highest quality. Average $c_{\alpha e\ max}$ representing reconstituted specimens consolidated at η=0.4 was 0.067.

Figure 7.31 b) compares depth distribution of final $c_{\alpha e}$ in CAD tests with $c_{\alpha e\ i}$ values obtained in IL oedometer test. Due to relatively low magnitude of vertical effective stresses in CAD, only specimens consolidated to σ'_3= 60 kPa were considered. Values obtained on specimens consolidated at η=0.85, complied with $c_{\alpha e\ i}$ in IL oedometer tests. Results on specimens consolidated at η=0.6 however, significantly exceeded intrinsic vales. The discrepancy was related to vertical effective stresses reached at η=0.6 (see Table 7.1). Final $c_{\alpha e}$ representing response of reconstituted specimens consolidated at η=0.4 was 0.025.

$c_{\alpha e}$ stress dependency

In Figure 7.32, values of coefficient of secondary compression determined in CAD tests are related to vertical effective stresses normalized with that at yield. Results obtained on natural specimens in consolidation at η=0.85, η=0.6 and η=0.4 are distinctively presented. Furthermore, $c_{\alpha e}$ stress dependency curves measured in CAD are examined with respect to w/γ specimen quality criteria, and contrasted to provisionally selected results obtained in IL oedometer tests, i.e. high quality natural specimen 5816, poor quality specimen 5835, and reconstituted specimen 5875R. Results identified in CAD tests exhibited same general features as those obtained in oedometer testing. Thus, despite oscillations and abrupt changes in $c_{\alpha e}$ values resulting from lateral strain related stress relaxation, it was possible to obtain meaningful $c_{\alpha e}$ stress dependency response in CAD tests at various η in consolidation. When approaching σ'_1/σ'_p of 1, secondary compression coefficients progressively rose in magnitude. Curves obtained at η=0.85 exhibited the most rapid increase in $c_{\alpha e}$ values. The rate of increase corresponded well with that measured on high quality oedometer specimen. In CAD tests on high quality specimens 5905 and 5906, $c_{\alpha e}$ was onset to rise at somewhat lower σ'_1/σ'_p compared to the rest. The $c_{\alpha e}$ stress dependency curves obtained at η=0.6 provided rather clear response resembling that of poor quality oedometer test specimen. Thus, rate of increase of $c_{\alpha e}$ values following the yield was somewhat less compared to that obtained at η=0.85. Finally in tests at η=0.4, $c_{\alpha e}$ stress dependency curves were characterised with the lowest rate of $c_{\alpha e}$ increase. Due to relatively low level of σ'_1 in consolidation, decrease of $c_{\alpha e}$ at high levels of σ'_1/σ'_p was captured in tests at η=0.85 and 0.6 only. Since the destructuration was not complete, intrinsic values of secondary compression coefficient were not reached. Overall, magnitudes of $c_{\alpha e}$ values proportionally reflected w/γ of the specimens considered. σ'_1/σ'_p range characterising maximum $c_{\alpha e}$ values was similar with that identifying maximum slope in compression λ.

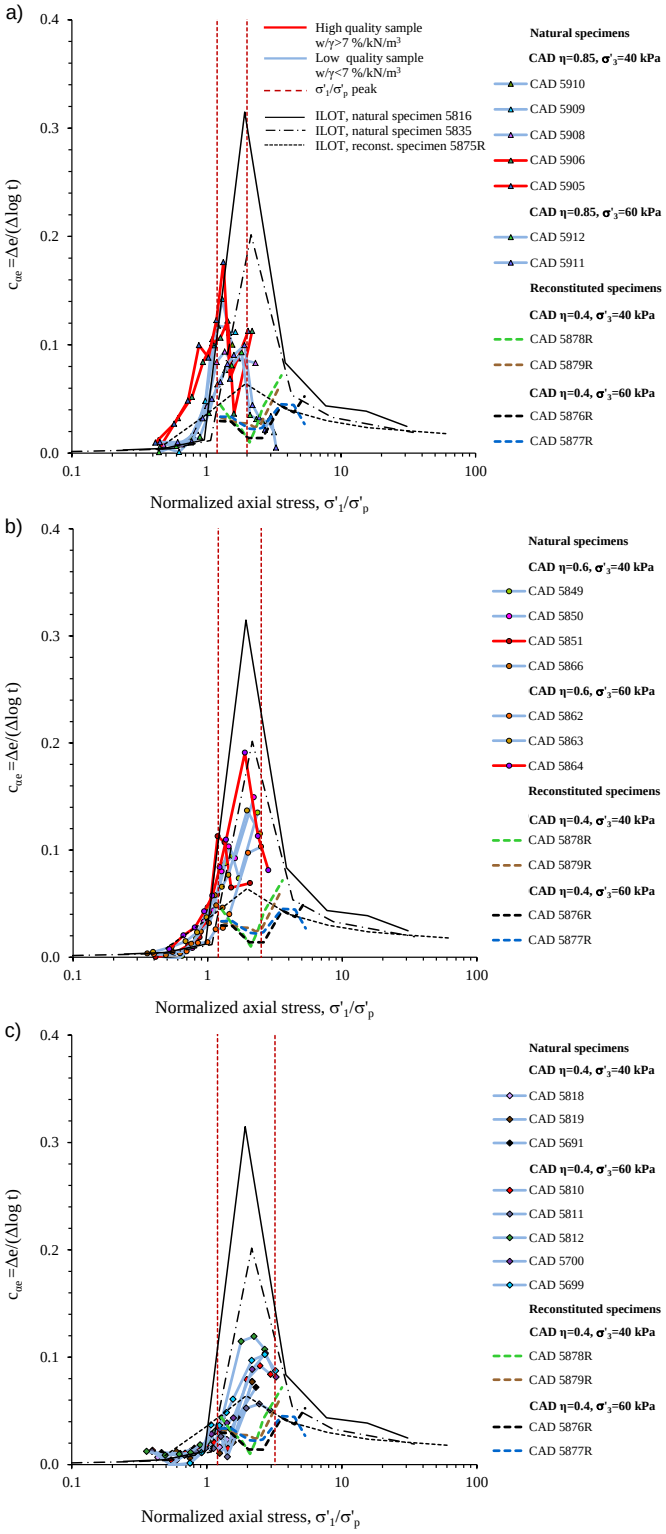

Figure 7.32 Stress dependency of secondary compression coefficient in CAD triaxial tests on Perniö clay; a) η=0.85, b) η=0.6 and c) η=0.4.

c_α/c_c parameter

Interrelation between compressibility and creep in CAD tests is examined in Figure 7.33. Maximum secondary compression coefficient and maximum compression gradient do not necessarily occur simultaneously. Consequently, adequate interrelation between compressibility and creep is that of both $c_{\alpha e}$ and c_c being determined for the same loading increment.

Related to sampling depth in Figure 7.33 a), maximum $c_{\alpha e}/c_c$ values were shown to range from 0.061 to 0.17. Influence of η in consolidation on magnitude of maximum $c_{\alpha e}/c_c$ was unclear. The resulting values appeared within the same general range in both sublayers considered. Overall, the values were represented by maximum $c_{\alpha e}/c_c$~0.10. Compared to corresponding parameter in IL oedometer test, maximum c_α/c_c values in CAD were generally less.

In Figure 7.33 b) final values of $c_{\alpha e}/c_c$ on CAD test specimens consolidated to σ'_3=60 kPa, are compared to intrinsic $c_{\alpha e}/c_c$ values obtained in IL oedometer test. Related to insufficient level of destructuration in CAD tests, only specimens of profile 66 consolidated at η=0.85 corresponded with those in IL oedometer tests, while remaining results were notably higher.

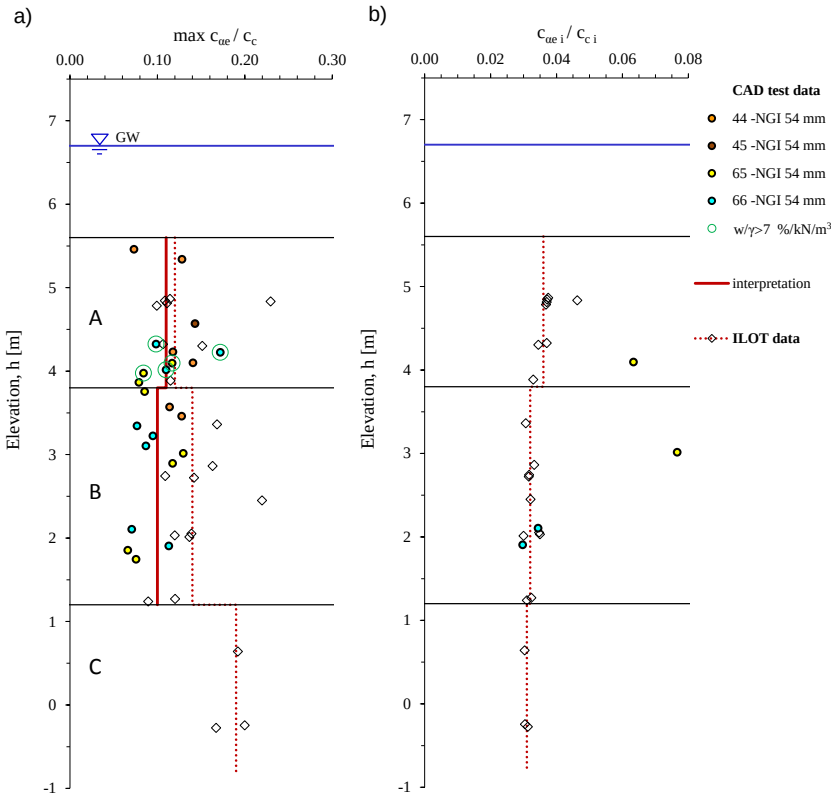

Figure 7.33 $c_{\alpha e}/c_c$ parameter in CAD tests; a) maximum values of $c_{\alpha e}/c_c$, and b) intrinsic $c_{\alpha e\,i}/c_{c\,i}$.

c_α/c_c stress dependency

Figure 7.34, relates $c_{\alpha e}/c_c$ values obtained in CAD tests on Perniö clay to vertical effective stress normalized with that at yield. The $c_{\alpha e}/c_c$ stress dependency

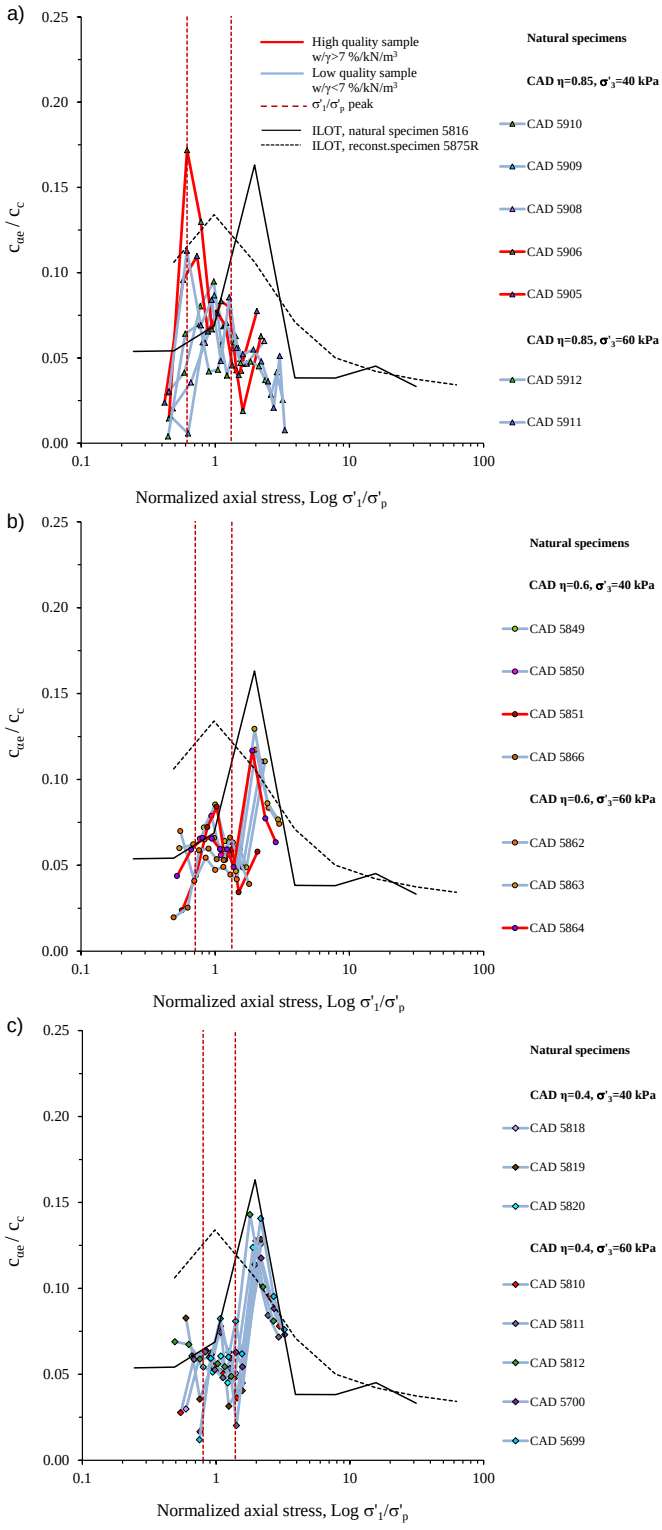

Figure 7.34 Stress dependency of c_α/c_c in CAD triaxial tests on Perniö clay; a) η=0.85, b) η=0.6 and c) η=0.4.

curves are distinctively displayed with respect to stress ratio imposed in consolidation. To allow for comparison, $c_{\alpha e}/c_c$ stress dependency curves were contrasted with results on natural and reconstituted specimens in IL oedometer tests 5816 and 5875R. Owing to triaxial consolidation conditions, resulting curves were characterised with abrupt oscillations and high scatter of $c_{\alpha e}/c_c$ values. In tests at η=0.85, growth in $c_{\alpha e}/c_c$ was onset at fairly low σ'_1/σ'_p of ~0.5. Maximum values were reached within $0.62<\sigma'_1/\sigma'_p<1.31$. Remaining results exhibited similar response with $c_{\alpha e}/c_c$ values progressively rising within $0.71<\sigma'_1/\sigma'_p<1.33$ at η=0.6, and $0.80<\sigma'_1/\sigma'_p<1.39$ in tests at η=0.4. Within the stated σ'_1/σ'_p range, peak $c_{\alpha e}/c_c$ values were fairly proportional to η, amounting 0.11, 0.08 and 0.06. Considering the response following the yield, in tests at η=0.85 $c_{\alpha e}/c_c$ values declined until the end of consolidation. The final ratio values reached corresponded to ~0.3. In tests at η=0.6 and 0.4 however, results exhibited abrupt increase in $c_{\alpha e}/c_c$ at σ'_1/σ'_p ~2.0. The $c_{\alpha e}/c_c$ values characterising second peak were overall the highest values reached throughout the CAD tests. Following the second peak the specimens exhibited decrease in $c_{\alpha e}/c_c$ values until the end of consolidation. To explain $c_{\alpha e}/c_c$ stress dependency response, consolidation conditions under radial stress path need to be recalled. In CAD consolidation tests, LIR was not constant. To enable accurate determination of yield, up to cell pressure of 29 kPa CAD specimens were consolidated in loading increments limited by $\Delta\sigma'_3$=3 kPa. Thereafter, cell pressure was increased in steps defined by $\Delta\sigma'_3$=10 kPa (see Figure 7.1). Abrupt increase in $c_{\alpha e}/c_c$ values corresponded with consolidation step in which LIR was increased. The effect revealed $c_{\alpha e}/c_c$ values being strongly dependent upon the LIR imposed. For comparison, in tests 5911 and 5912 consolidated at η=0.85, load increments in final stage of consolidation were limited by $\Delta\sigma'_3$=5 kPa. The lower increments were implemented to prevent specimens from failing in consolidation at η=0.85. In the tests, increase in $c_{\alpha e}/c_c$ values was less pronounced. Thus, maximum $c_{\alpha e}/c_c$ values overall occurred at rather high σ'_1/σ'_p ~2.0. However, $c_{\alpha e}/c_c$ values comparable with maximum values in IL oedometer test were those identifying first peak at lower level of σ'_1/σ'_p.

7.2 Undrained triaxial compression test results CAUC

7.2.1 General overview

Entire set of CAUC test results performed on reconstituted and natural specimens of Perniö clay are respectively presented in Figure 7.35 and Figure 7.36. The results were obtained on specimens following their triaxial consolidation elaborated in Chapter 7.1. In following, the results are briefly outlined. Latter, specific features such as undrained shear strength, pore pressure response, destructuration and strain-rate effects are examined in detail.

CAUC results on reconstituted specimens

The q-p' plane in Figure 7.35 comprises CAUC test results on reconstituted specimens remoulded in batches R1, R2, R3 and R4. The tests were performed in two series on specimens consolidated to stress ratio of η=0.4 and 0.85. Within each series, specimens consolidated to three different stress levels defined by σ'_3 of 20, 40 or 60 kPa, were sheared undrained at axial strain-rate of 0.1 or 0.01 mm/min, i.e. $1.7 \cdot 10^{-5}$ and $1.7 \cdot 10^{-6}$ s^{-1}. Void ratio values following consolidation e_s varied between 1.24 and 1.86, corresponding to water content from 42.7 to 67.5 %. The resulting stress paths were governed by magnitude of axial strain-rate and rate of pore pressure increase. Influence of consolidation stress ratio was considerable as well. Stress paths onset at η=0.85 were more abrupt at failure compared to those of η=0.4 consolidated counterparts. Although less ambiguous compared to that on natural specimens (see Figure 7.36), scatter in shear strength measured on reconstituted specimens shown in Figure 7.35, was rather high. Averaged strength envelope based on the entire set of maximum shear strength data identified friction angle of 25.4° and negligible cohesion. After considerable straining stress paths tended to converge, yet often exceed estimated critical state stress ratio of M=1.32.

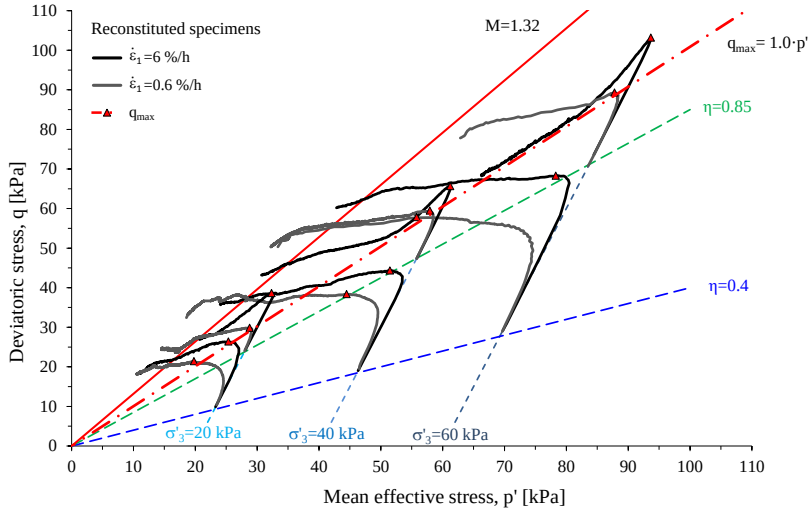

Figure 7.35 Stress paths in CAUC tests on reconstituted specimens of Perniö clay.

CAUC results on natural specimens

Figure 7.36 presents results of CAUC tests on natural specimens from NGI 54 mm profiles 43, 44 and 45 (S-2009), and profiles 65 and 66 (S-2010). The results comprise three test series performed on specimens consolidated under constant stress ratio of η=0.4, 0.6 and 0.85. Each series included three test groups identified by final cell pressure in consolidation σ'_3=20, 40 or 60 kPa. Specimens of each group were sheared undrained at three axial strain-rate levels of 0.1, 0.01 and 0.001 mm/min, i.e. $1.7 \cdot 10^{-5}$, $1.7 \cdot 10^{-6}$ and $1.7 \cdot 10^{-7}$ s^{-1}. The resulting stress paths reflected specimen structural characteristics, variance in consolidation conditions and strain-rate imposed. Reflecting the consolidation conditions, void ratio values in shear e_s ranged from 1.35 to 2.65 corresponding to broad range of water content from 50.4 to 97.4 %. The specimens consolidated at η=0.4 to stress level characterised by σ'_3=60 kPa were subjected to relatively high extent of destructuration and had low water content. Opposite was valid for specimens consolidated at η=0.85 to σ'_3=20 kPa. Variance in undrained shear response following consolidation to identical stress state manifested influence of strain-rate imposed, rate of pore pressure increase, and quality of the specimens. Consequently, shear strength measured differed considerably making the interpretation of natural Perniö clay strength parameters unreliable. Averaged strength envelope identified friction angle of 21.4° and cohesion of 5.5 kPa. Although generally converging in the final stage of undrained shear, stress ratio values characterising final segments of stress paths varied considerably and regularly exceed that of estimated critical state M=1.32. To define strain-rate and destructuration effects on undrained shear response, results of specific test groups need to be examined in detail.

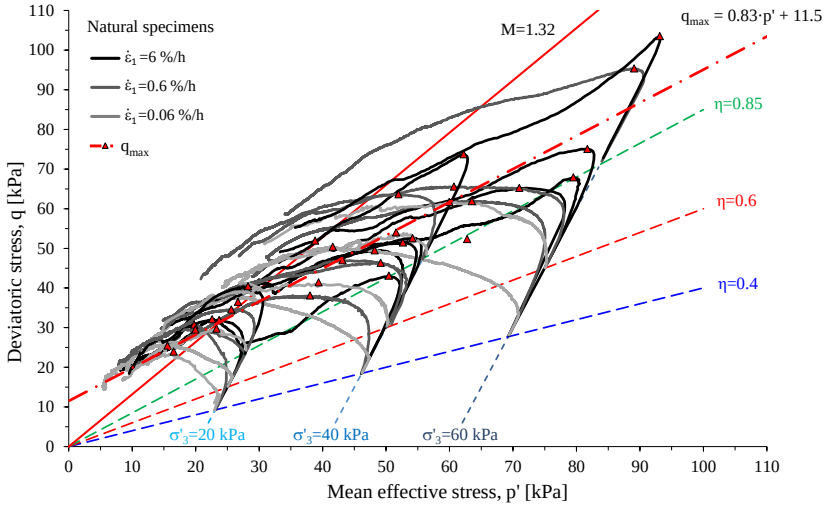

Figure 7.36 Stress paths in CAUC tests on natural specimens of Perniö clay.

7.2.2 Consolidation state parameters and sample quality

Effects of consolidation procedure on initial state parameters and specimen quality are examined in Figure 7.37. Properties of natural and reconstituted

specimens at the onset of undrained shear are shown in γ vs. w plane in Figure 7.37 a). Overall, the results complied with general response characterising Perniö clay materials. Reflecting the final stress conditions in consolidation, w/γ values at the onset of undrained shear were low, and corresponded to those on poor quality specimens following the sampling, i.e. w/γ<7.0 %/kN/m³. High values identified specimens of profiles 65 and 66 (NGI 54), consolidated to stress state defined by σ'_3=20 kPa. Remaining specimens consolidated to σ'_3=40 and 60 kPa exhibited w/γ<5 %/kN/m³. Finally, the values characterising reconstituted specimens were the lowest, w/γ<4.3 %/kN/m³.

In Figure 7.37 b), w/γ prior undrained shear are related to sampling depth. Despite large variance in final stress state in consolidation, it was the in situ conditions and consequent sampling disturbance effects that predominantly influenced w/γ in undrained shear. Thus, although less in magnitude, specimens subjected to undrained shear showed similar w/γ pattern vs. depth as that measured following the sampling. Average w/γ of specimens from sublayers A and B amounted 5.1 and 3.5 %/kN/m³, respectively. Considering specimens originating from sublayer A, the highest w/γ values of 6.5 %/kN/m³ identified specimens from profiles 65 and 66 (NGI 54) consolidated to σ'_3=20 kPa. Among sublayer B specimens, upper limit of w/γ of 4.1 %/kN/m³ marked specimens from profiles 44 and 65 (NGI 54) consolidated to σ'_3=20 or 40 kPa.

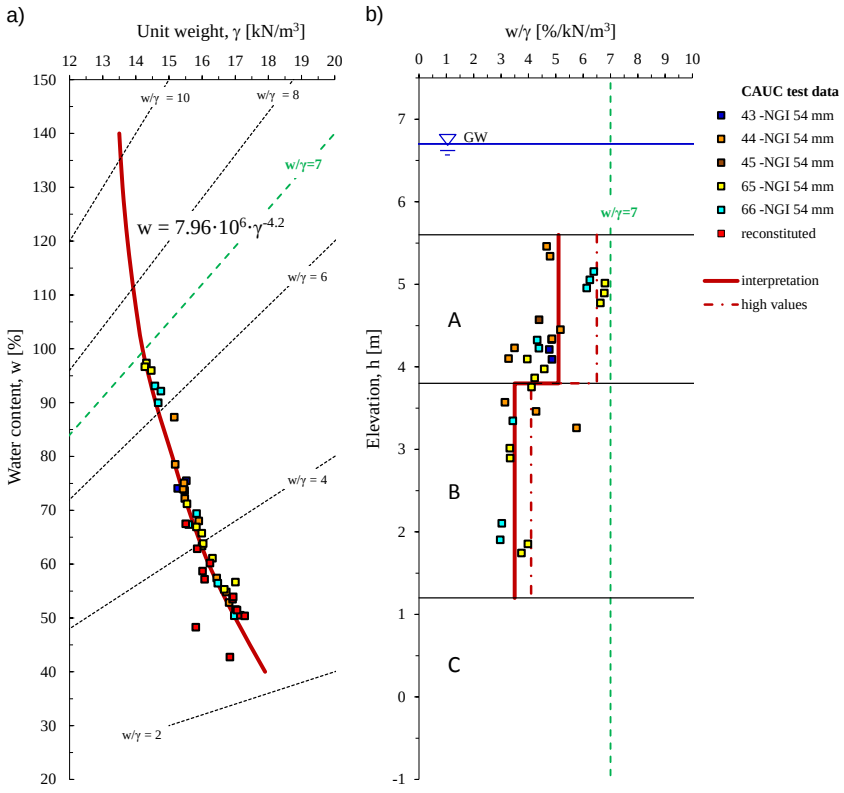

Figure 7.37 Specimen quality in CAUC triaxial tests on Perniö clay, a) w/γ curve, b) w/γ criteria.

7.2.3 Undrained shear characteristics

Effect of strain-rate on stress-strain response

Undrained triaxial compression results on natural and reconstituted specimens are presented in q vs. ε_1 plane in Figure 7.38 and Figure 7.39. The results are examined with respect to specimen quality, consolidation conditions and influence of strain-rate on shear strength, hardening and softening response.

The strength of the structured clay is greater than the strength of the same clay destructured by remoulding at the same void ratio [Bishop et al. 1965]. Consequently, shear resistance of natural specimen is influenced by the level of specimen disturbance in sampling and preparation, as well as by destructuration effects during the actual test, i.e. effects of consolidation and strain-rate. To derive unambiguous conclusions on shear strength and shear resistance, quality of the specimens needs to be accounted for. To define the reliability of undrained shear test on structured clay, the axial strain at failure was used. If the strain at failure in compression test exceeds 5 or 6 %, the sample is probably disturbed and shows reduced strength [Bjerrum 1954]. In the best samples of sensitive and quick clays, the strain at failure is only 1-3 % [Bjerrum 1954]. As an additional criteria influence of void ratio in shear was used. Thus, in evaluation of shear resistance of specimens tested under same consolidation and strain-rate conditions, influence of water content in shear was considered. Firstly, attention is given to analyses of strain-rate effects on undrained shear of natural specimens consolidated at η=0.85, 0.6 or 0.4, and subjected to various level of destructuration in consolidation. Later, the results on natural clay are contrasted with stress-strain response of reconstituted specimens following consolidation to η=0.85 or 0.4, and equivalent shear conditions.

Undrained shear results shown in Figure 7.38 a), were obtained following consolidation at η=0.85. The test series consisted of three test groups defined by final radial pressure in consolidation, i.e. σ'_3=20, 40 and 60 kPa. Influence of strain-rate on shear resistance was concise. Within each test group, peak strength q_{max} was proportional to magnitude of strain-rate. Axial strain at failure ε_{1F}, was reciprocal to strength of the specimens, thus influenced by both, radial pressure in consolidation and strain-rate in undrained shear. Overall, the values occurred within narrow limits ε_{1F}<1.5 %. Low average of 1.1 % indicated specimens of the series being of the highest quality. Stiffness in hardening, as well as the extent of post-peak softening, was proportional to specimens' strength. Consequently, peak strength was the most distinctive in shear at σ'_3=60 kPa. Reduction of shear resistance in softening was progressive, with influence of strain-rate on shear resistance, i.e. destructuration-rate, somewhat decreasing with strain. Post peak stress-strain curves on specimens consolidated to identical stress state were distinctive. Thus, effects of strain-rate and destructuration on extent of softening were consistent i.e. effects of variance in specimen quality on strain-softening response were minor. Rate of softening was somewhat less in shear at the lowest strain-rate. Overall, the results opposed condition of axial strain at failure being appropriate measure of specimen disturbance. Specimens consolidated far beyond effective overburden stress level indicated less destructuration in shear.

Stress-strain curves obtained following consolidation at η=0.6, are presented in Figure 7.38 b). Results of test groups at σ'_3 of 20, 40 or 60 kPa exhibited strength proportional to strain-rate in undrained shear. Overall, specimens of the series were well represented by average ε_{1F} of 1.7 %. Thus, compared to results of the previous series, in tests onset following consolidation at η=0.6 axial strains at failure were somewhat higher, i.e. ε_{1F}<3.2 %. Again, shear resistance in hardening was proportional to peak strength, resulting with fairly regular decrease of ε_{1F} with rise of consolidation cell pressure. Extent of softening was proportional to cell pressure in consolidation, and overall somewhat less than in test onset at η=0.85. Although influence of axial strain-rate on shear strength was clear, post-peak responses were somewhat less distinctive, especially in tests at the highest radial pressure. Effects of specimen quality and repeatability were examined by two pairs of tests at identical consolidation and strain-rate conditions, i.e. tests 5849 and 5865 sheared at 6%/h, and 5850 and 5866 at 0.6%/h. Despite almost identical peak strength, results 5866 and 5865 exhibiting higher ε_{1F}, identified specimens with lower e_s, and were thus assumed representable of response on more disturbed specimens. The results were characterised by somewhat higher extent of softening compared to their high quality counterparts.

Undrained shear results following consolidation to η=0.4 are shown in Figure 7.38 c). Reflecting poor initial quality of the specimens, as well as rather low stress ratio in consolidation, the results were less concise compared to those of former two series. The tests were performed on relatively disturbed specimens sampled in 2009, i.e. profiles 43, 44 and 45. Since consolidated at η differing significantly form that of in situ, initial structure of the specimens was strongly affected. Considering identically consolidated specimens, peak strength was proportional to strain-rate imposed. Resulting ε_{1F} indicated reverse proportionality to cell pressure in consolidation. Furthermore, the values were highly scattered with ε_{1F}<3.7 %, and rather high average of 2.5 %. Compared with the results of two previous series, extent of softening was somewhat less, while repeatability was poor, hence suggesting variations in sample quality. Due to large variation in undrained shear response, results of the test groups need to be examined in detail. In tests sheared at σ'_3=20 kPa, despite strain-rate related distinction in peak strength, stress-strain curve obtained at 0.6 %/h resembled that of test at 6%/h. Thus, due to higher void ratio in shear, hardening and softening response measured in 5713 complied with that in test 5711 at the highest strain-rate. Considering tests sheared at σ'_3=40 kPa, two tests were performed at identical consolidation and shear conditions, i.e. 5691 and 5819 at 6%/h. Despite identical void ratio in shear, 5691 exhibited overall higher shear resistance and significantly higher ε_{1F} compared to counterpart 5819. Distinction was related to the fact of specimen 5691 being sampled on profile 44, compared to remaining specimens of the group originating from profile 43. Finally, in tests at σ'_3=60 kPa, repeatability was examined in tests 5811 and 5699 at 6%/h. Results obtained were characterised with considerable variation in shear resistance. Result obtained on specimen 5699 with higher water content was characterised by lower ε_{1F} and higher peak strength.

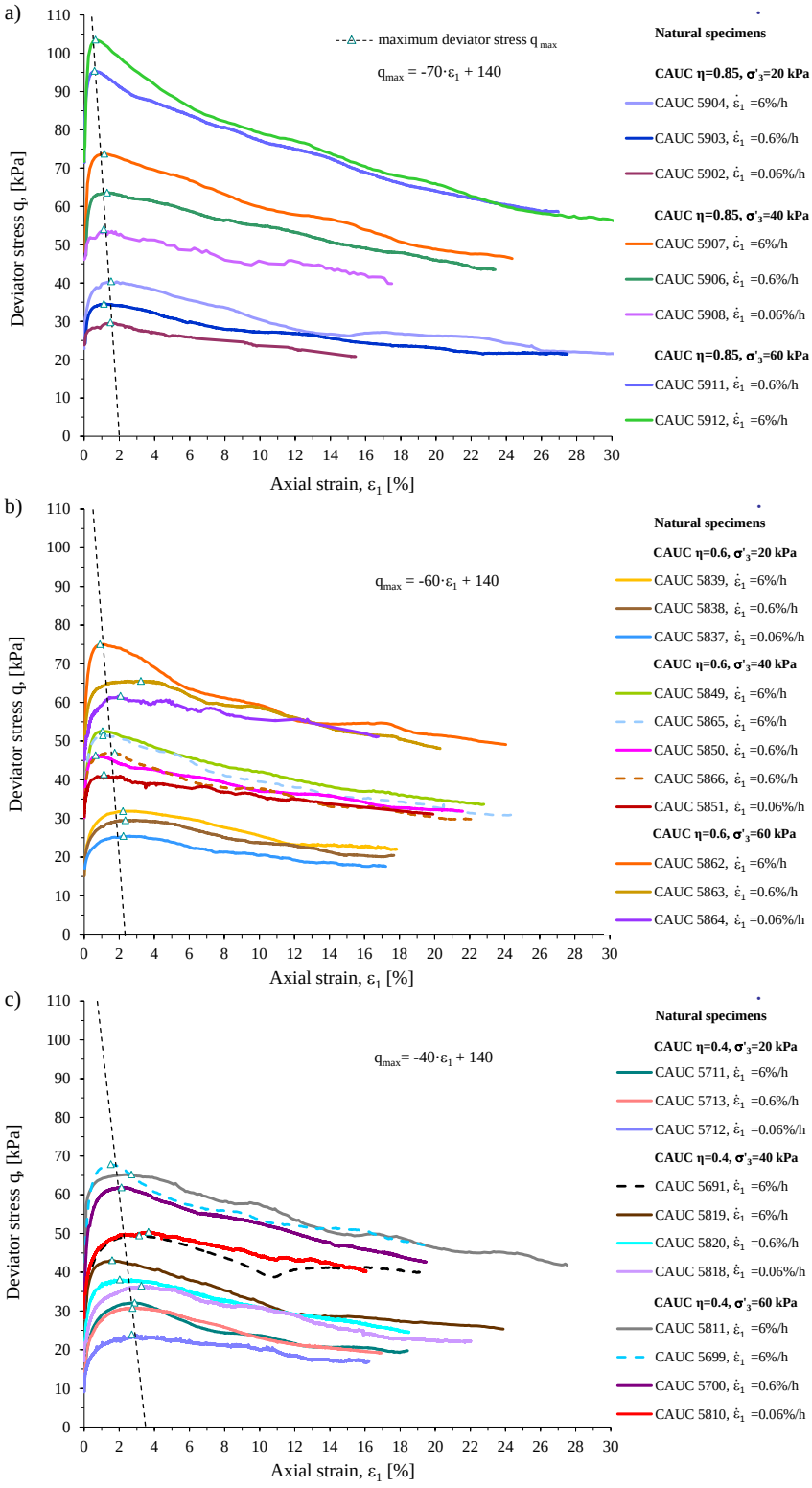

Figure 7.38 Undrained shear response of natural specimens in q vs. ε_1 plane; a) consolidation at η=0.85, b) η=0.6, and c) η=0.4.

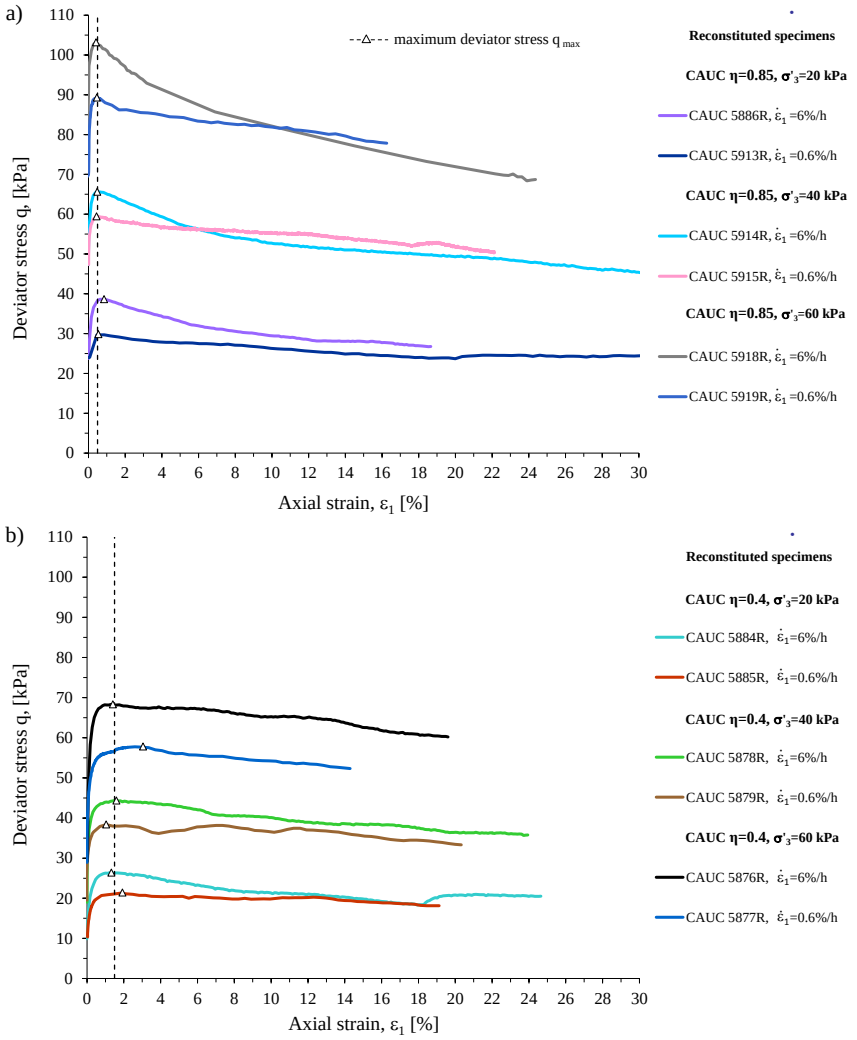

Figure 7.39 Undrained shear of reconstituted specimens in q vs. ε_1 plane; a) consolidation at η=0.85, and b) η=0.4.

Figure 7.39 a) presents undrained shear response measured on reconstituted specimens consolidated to η=0.85. Main conclusions complied with those elaborated for shear resistance of natural specimens. Specimens sheared following identical consolidation exhibited proportional influence of strain-rate on peak strength. Values of axial strain at peak strength were uniform and very low, i.e. ε_{1F}<0.9 %, with average at 0.5 %. Contrary to pattern exhibited by natural specimens, influence of cell pressure in consolidation on ε_{1F} was negligible. Hardening response was fairly proportional to peak strength, thus related to both radial pressure and strain-rate. Rate of softening lessened with increase of axial strain. Extent of softening was proportionally influenced by magnitude of cell pressure in consolidation. However, extent of softening was primarily governed by magnitude of axial strain-rate, i.e. being more pronounced in tests at high strain-rate. Additional effect was that of overlapping

of post peak responses at distinctive strain-rate levels.

Undrained shear results in Figure 7.39 b), onset following the consolidation along η=0.4, exhibited some distinctive features compared to those obtained on reconstituted specimens consolidated to η=0.85. Although fairly independent of the cell pressure in consolidation, values of axial strain at peak strength were considerable, i.e. ε_{1F}<3.0 %, and 1.7 % in average. Overall, the effects of strain-rate on extent of softening were consistent, i.e. characterised by distinctive post peak response. Furthermore, extent of strain softening was very low, with post-peak response being that of fairly linear decline in shear resistance.

Testing results allow comparison of reconstituted material response with that on natural specimens consolidated and shared under identical test conditions. With the exception of tests performed at σ'_3=60 kPa and the highest strain-rate, reconstituted specimens exhibited lower peak strength. Peak shear resistance of reconstituted material was in average ~4.0 kPa less compared to corresponding natural specimens. Considering both natural and reconstituted specimens, in tests at low radial pressure there was not much evidence of strain softening. In contrast, in tests onset following consolidation beyond effective overburden stress level, extent of softening increased. Magnitude of strain-rate influenced both peak strength and softening response. In tests onset following identical consolidation conditions, extent of softening was higher in tests at the highest strain-rate. Overall, extent and rate of softening measured on reconstituted specimens was considerably lower compared to that exhibited by their natural counterparts. Independent of the stress ratio in consolidation, natural specimens consolidated far beyond effective overburden stress level indicated ε_{1F} being relatively less. In addition, following identical consolidation and shear conditions, reconstituted specimens regularly exhibited lower level of ε_{1F}, i.e. 1.5 to 2.2 times less. Thus, usage of strain at failure in undrained shear as a measure of specimen disturbance is questionable. Instead, structural characteristics should be evaluated based on magnitude of void ratio in shear and specimen's response in softening. Indeed, strain softening characteristics were clearly distinctive feature of reconstituted compared to natural material behavior, suitable for quantification of influence of strain-rate on rate of destructuration in shear.

Effects of strain-rate on pore pressure

Stress state of the specimen in undrained triaxial compression is primarily dependent upon two quantities, axial load carried by the specimen defining deviator stress, and that of pore pressure response governing the magnitude of mean effective stress. Except for the part related to heave, influence of the pore pressure on deviator stress is negligible. Consequently, pore pressure response is of the major importance for analysis of stress path characteristics.

In Figure 7.40 pore pressures in undrained shear of natural specimens at distinctive cell pressure levels are related to axial strain. The pore pressure response in undrained shear was governed by radial pressure and axial strain-rate imposed. Overall, pore pressures rose progressively until the end of the tests, without levelling off as would be expected when critical state is reached.

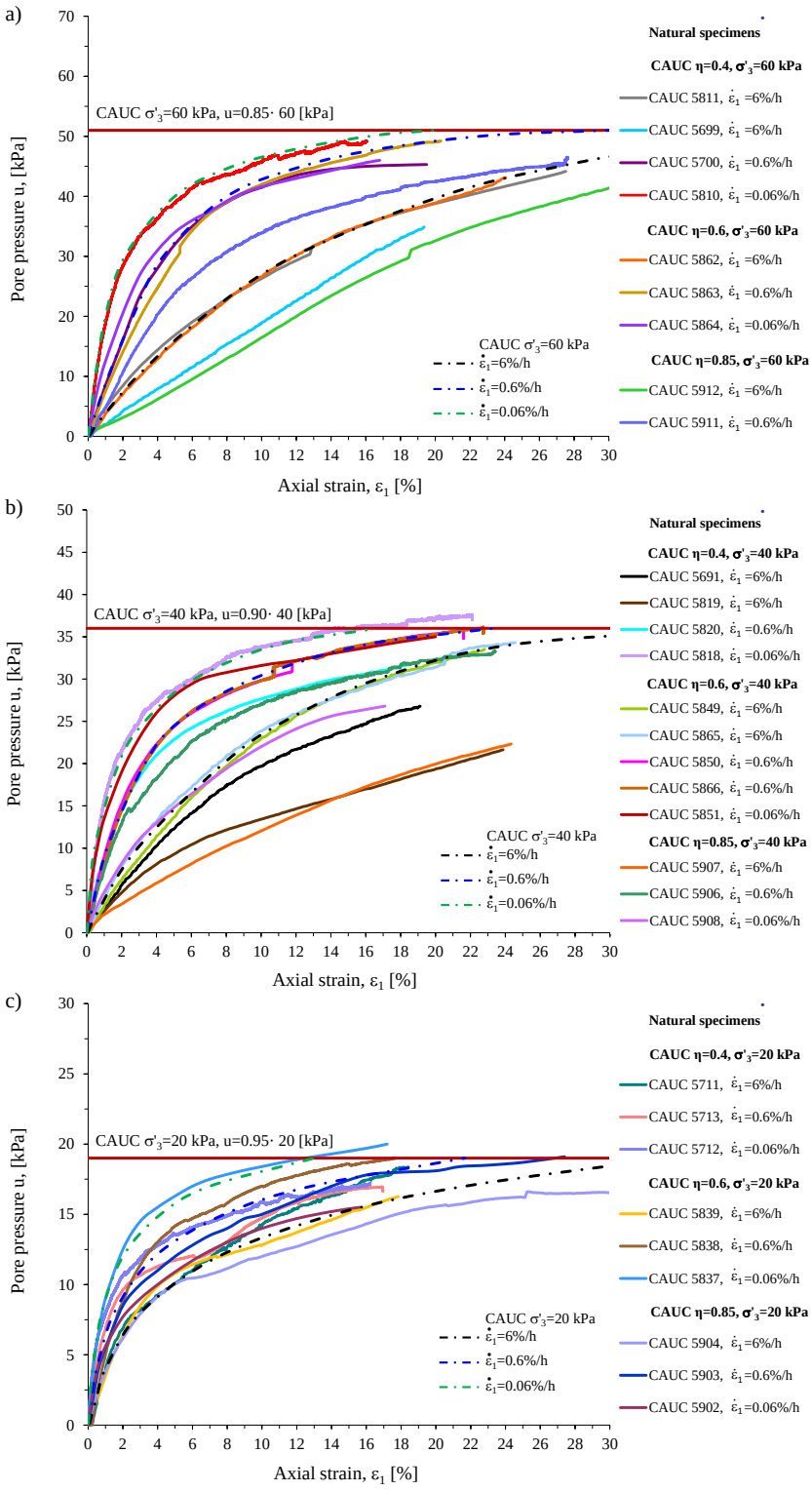

Figure 7.40 Axial strain vs. pore pressure in undrained shear of natural specimens at; a) σ'_3=60, b) σ'_3=40, and c) σ'_3=20 kPa.

Target pore pressure level was related to actual magnitude of the radial pressure. Thus, in tests at σ'_3=20, 40, and 60 kPa, pore pressure curves exhibited tendency toward respective target values of ~0.95, 0.90 and 0.85 times σ'_3. While the target pore pressure was primarily dependent upon the cell pressure in consolidation/shear, rate of the pore pressure increase was in addition to radial stress, influenced by axial strain-rate and void ratio. Despite considerable scatter, pattern of pore pressure response with rise of axial strain could be identified. Axial strain related rate of pore pressure increase was the highest in tests performed at the lowest axial strain-rate, and vice versa. Interpretation of strain related pore pressure response at distinctive strain-rates is presented with dash-dot curves. In interpretation, advantage was given to specimens exhibiting the highest rate of pore pressure increase with strain, as well as to repeatability. Most of the specimen sheared following the consolidation to stress state resembling effective overburden, i.e. at σ'_3=20 kPa, exhibited reduced gradient of pore pressure buildup at $2<\varepsilon_1<8$ %. The resulting pore pressure responses thus resembled those measured in CRS oedometer test.

In Figure 7.41 pore pressures measured in undrained shear of reconstituted specimens are related to axial strain. Results obtained at distinctive levels of radial pressure are separately shown. Overall, pore pressures rose until the end of the tests, with no sign of leveling off within the range of axial strains considered. Effects of strain-rate on rate of pore pressure increase were consistent. Pore pressure responses measured on identically consolidated specimens indicated tendency to merge at high strain levels, however, those sheared at higher axial strain-rate regularly exhibited higher pore pressure at certain axial strain. Unlike corresponding results on natural specimens, final pore pressures measured on reconstituted specimens were not clearly related to magnitude of cell pressure in consolidation/shear. In contrast, pore pressures reached were primarily governed by stress ratio conditions in consolidation. Considering tests performed at certain level of radial pressure, those sheared following consolidation at η=0.4 indicated higher target pore pressures compared to those in tests onset at η=0.85. The effect might have been related to difference in consolidation procedure implemented, i.e. simplified consolidation in tests toward η=0.85.

Pore pressure response in undrained shear of natural specimens was shown closely related to radial pressure in consolidation. With undrained shear phase of the tests being performed at constant rate of axial strain, pore pressure response should produce meaningful outcome when related to time. Such approach is shown in Figure 7.42 presenting tests results at radial pressures considered in semi-logarithmic plane. Additionally to results measured, interpreted pore pressure responses at distinctive axial strain-rates are presented as well. Thus, interpretation curves in Figure 7.42 correspond with those on Figure 7.40, scaled by magnitude of strain-rate. Rate of the pore pressure increase was strongly dependent upon the axial strain-rate. Specimens compressed at the highest rate reached target pore pressure level in significantly shorter period of time. In contrast, at low strain-rate, specimens exhibited lower rate of pore pressure buildup. Scatter in the pore pressure response at certain strain-rate was related to difference in void ratio of the specimens sheared e_s.

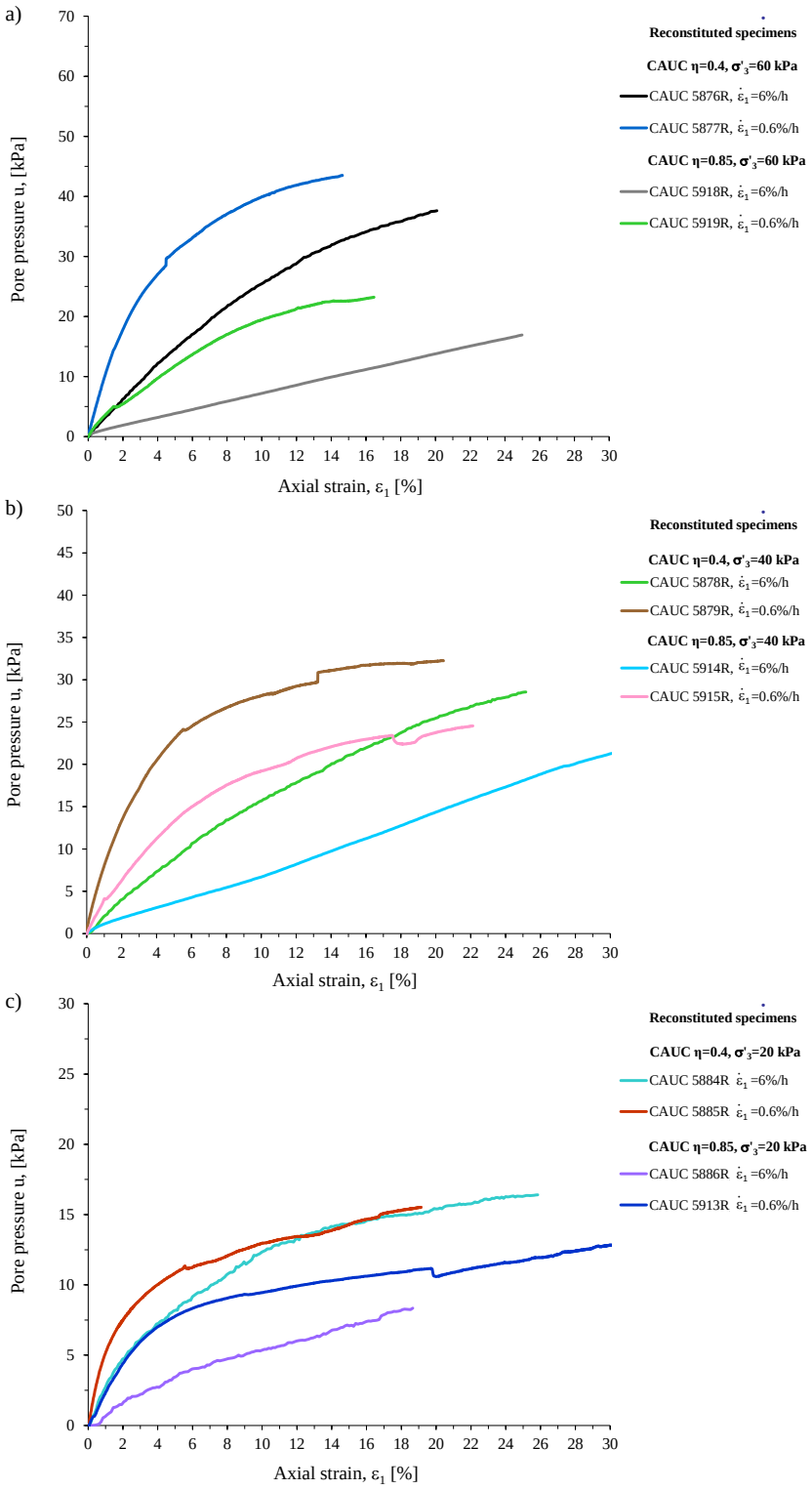

Figure 7.41 Axial strain vs. pore pressure in undrained shear of reconstituted specimens at; a) σ'_3=60, b) σ'_3=40, and c) σ'_3=20 kPa.

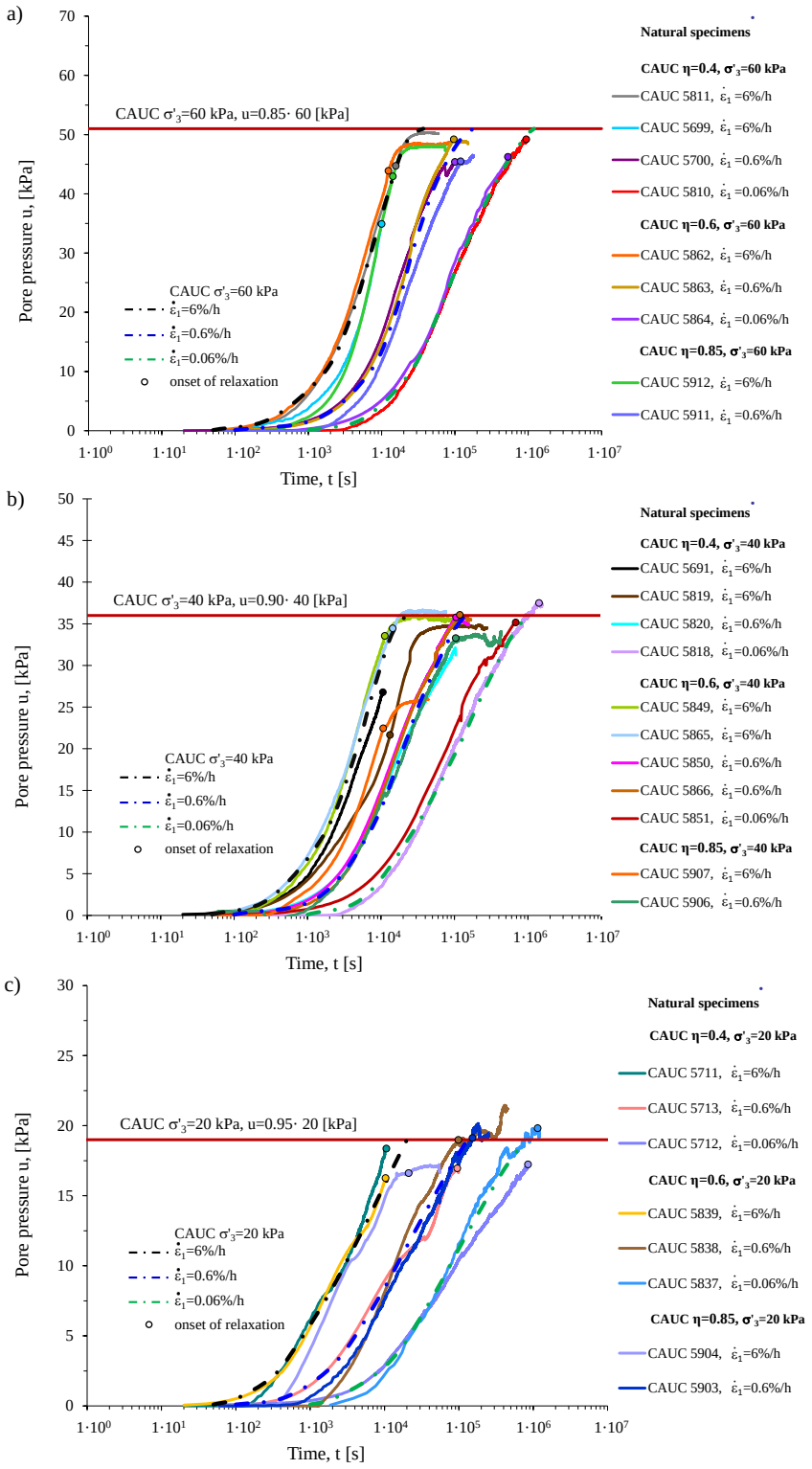

Figure 7.42 Time vs. pore pressure in undrained shear of natural specimens at; a) σ'_3=60, b) σ'_3=40, and c) σ'_3=20 kPa.

To distinct for the effects of radial pressure, interpreted pore pressure vs. time curves are presented on linear and semi-logarithmic plots in Figure 7.43. Overall, pore pressures were exponentially related to time (Figure 7.43 b). Rate of pore pressure buildup progressively decreased, being the least when reaching the target value. As shown in Figure 7.43 a), pattern of pore pressure response of specimens sheared at certain cell pressure was similar. Considering specimens axially strained at identical strain-rate, initial rate of pore pressure increase complied well independent of the cell pressure in consolidation/shear. Soon after however, curves diverged, with rate of pore pressure increase becoming proportionally related to cell pressure. Thus, specimens sheared at the highest radial pressure exhibited the highest rate of pore pressure build-up, followed by that obtained at σ'_3=40, while in tests at σ'_3=20 kPa pore pressure response in semi-log plot remained fairly linear. Above defined effects of cell pressure and strain-rate on pore pressure buildup mechanism are of primary importance for understanding characteristics of specimen response in undrained shear.

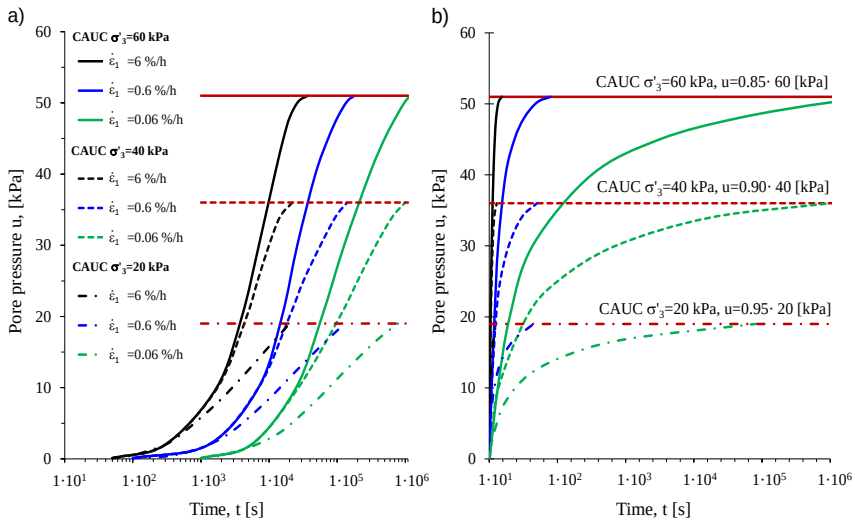

Figure 7.43 Interpreted pore pressure vs. time response of natural specimens; a) in semi-logarithmic, and b) in linear plot.

Effects of strain-rate on undrained stress path

In Figure 7.44, undrained stress paths measured on natural specimens consolidated to η=0.85, η=0.6 and η=0.4 are distinctively presented in q-p' plane. Results of nine test groups defined in Table 4.4 exhibited similar features linked to test conditions imposed. In following, the results obtained are examined with respect to strain-rate and consolidation conditions imposed.

Strain-rate conditions had the main influence on resulting stress paths. In test at the highest axial strain-rate, specimens failed at the highest level of deviator stress, q_{max} (see Figure 7.48). Prior to failure, the specimens exhibited high shear resistance manifested by rapid rate of deviator stress increase. Simultaneously, reflecting low rate of pore pressure increase with axial strain,

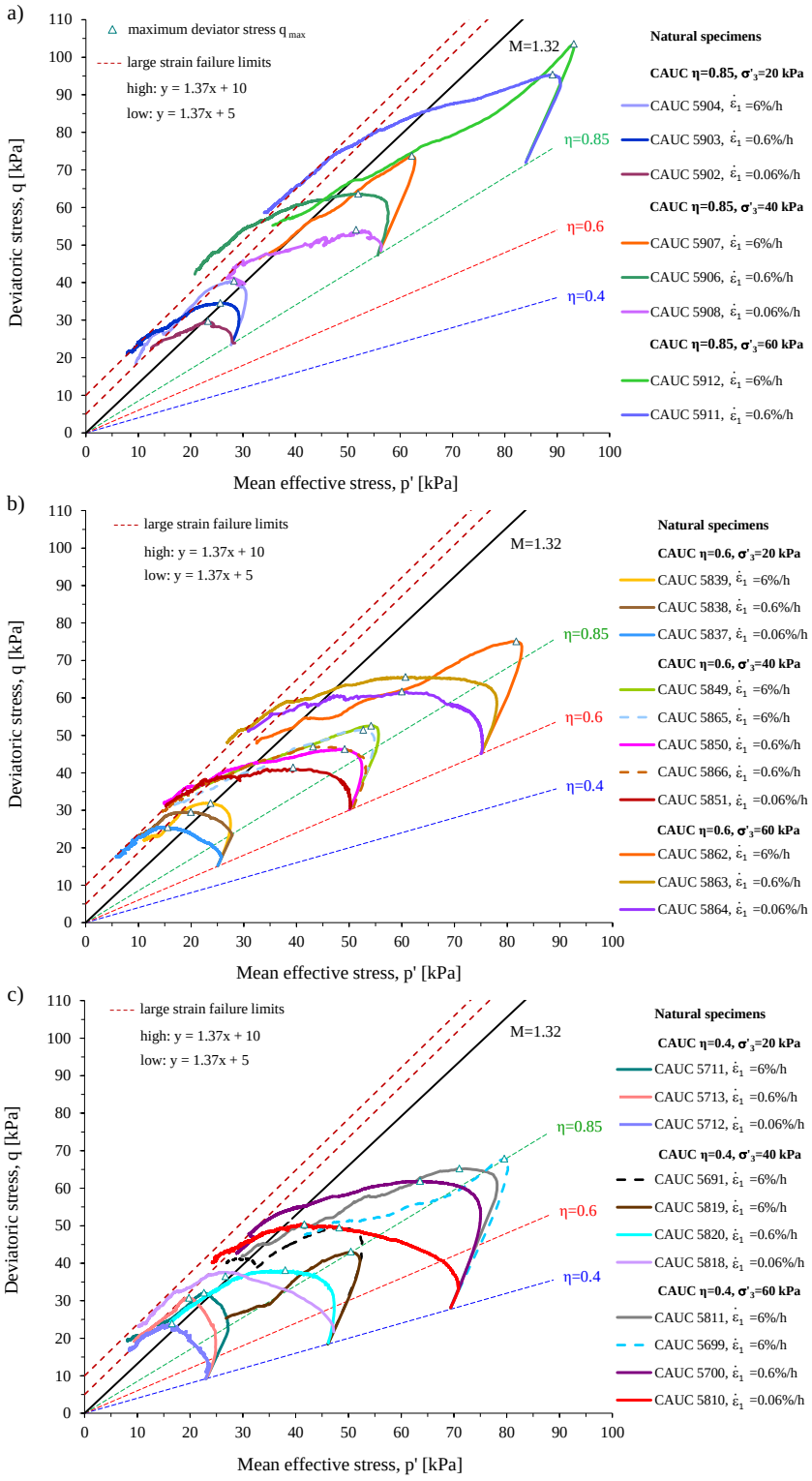

Figure 7.44 CAUC results on natural specimens in q vs. p' plane; a) consolidation at η=0.85, b) η=0.6 and c) η=0.4.

change in mean effective stress up to failure resembled that in drained tests. It was just prior failure when mean effective stress started to decline. The effect led to high magnitude of stress ratio η_α, identifying the highest level of mean effective stress p'_{max} (Figure 7.48). In contrast, in tests at the lowest strain-rate, axial strain related pore pressure increase was rapid, leading to substantial decrease of mean effective stress prior failure. Indeed, mean effective stress declined almost instantly, resulting with low magnitude of stress ratio η_α, just somewhat exceeding that in consolidation. Prior to failure, deviator stress increased at relatively the lowest rate, while peak shear resistance reached was overall the lowest. Thus, undrained shear strength of natural clay declined with decreasing strain-rate [Leroueil & Hight 2003b]. In tests at the highest strain-rate peak strength was high and distinctive, while in loading at the lowest strain-rate peak strength was relatively less with failure occurring progressively. The differences in strength and stress path characteristics were firstly, manifestation of difference in pore pressures at failure, and secondly, result of different rate of destructuration, both governed by magnitude of strain-rate.

With peak strength exceeded, stress paths tended to converge with increase of axial strain. In tests at the highest strain-rate characterised by the highest shear resistance, post failure stress paths exhibited high rate of deviator stress decrease. After large extent of straining however, stress response complied fairly well with that exhibited by specimens subjected to lower axial strain-rates. Thus, independent of the strain-rate or stress ratio in consolidation, ultimately, undrained shear resistance progressively declined at similar rate until the very end of the tests. Final segments of the stress paths overall exceed estimated critical state stress ratio of M=1.32. Instead, residual strength was fairly well represented by linear strength envelopes defined by effective friction angle of 33.9° and cohesion between 2.5 and 4.9 kPa. Difference in residual cohesion was result of destructuration rate related effects.

To highlight destructuration rate effects, consolidation conditions of specimens need to be considered. Specimens consolidated to stress state fairly corresponding to that of effective overburden, i.e. σ'_3=20 kPa along η=0.85, 0.6 or 0.4, exhibited the highest stress ratio at failure matching that of estimated critical state, i.e. η_F~1.32 (see Figure 7.48). In tests following consolidation to σ'_3=40 and 60 kPa however, values of stress ratio at failure were less, i.e. $0.92<\eta_F<1.22$. Considering specimens sheared at identical rate following consolidation to same radial pressure, yielding was somewhat more distinct in shear onset at η=0.85, while in tests at η=0.6 and η=0.4 it was more progressive. Water content in shear influenced peak strength measured. Specimens identically consolidated, yet characterized by considerable difference in water content, if shared at identical rate, exhibited difference in shear-strength.

In Figure 7.45 undrained stress paths on reconstituted specimens consolidated to stress ratio of η=0.85 and η=0.4 are shown. Main conclusions concerning strain-rate influence on undrained shear response of natural clay were valid for reconstituted specimens as well. Following identical consolidation, in tests at rapid strain-rate peak strength was high and distinctive, while in slow tests reconstituted specimen exhibited lower strength and failed progressively.

Specimens sheared at identical axial strain-rate and radial pressure exhibited more abrupt failure if shear was onset from η=0.85 compared with that started at η=0.4. In contrast to results on natural specimens, peak strength was typically less. Depending on the quality of the reference natural specimen, q_{max} measured on reconstituted specimens was up to 10 kPa less. In tests performed at identical consolidation and strain-rate conditions, reconstituted specimens exhibited exhibited lower magnitude of both η_α and η_F, as well as lower level of pore pressure at failure. Following the peak strength, shear resistance of reconstituted specimens declined at lower rate than that exhibited by corresponding natural specimens. Rate of the post failure decrease in shear resistance was proportional to both consolidation stress ratio and strain-rate. Finally, friction angle characterising residual strength envelope complied, i.e. φ'=33.9°, while cohesion was overall less than 2.5 kPa.

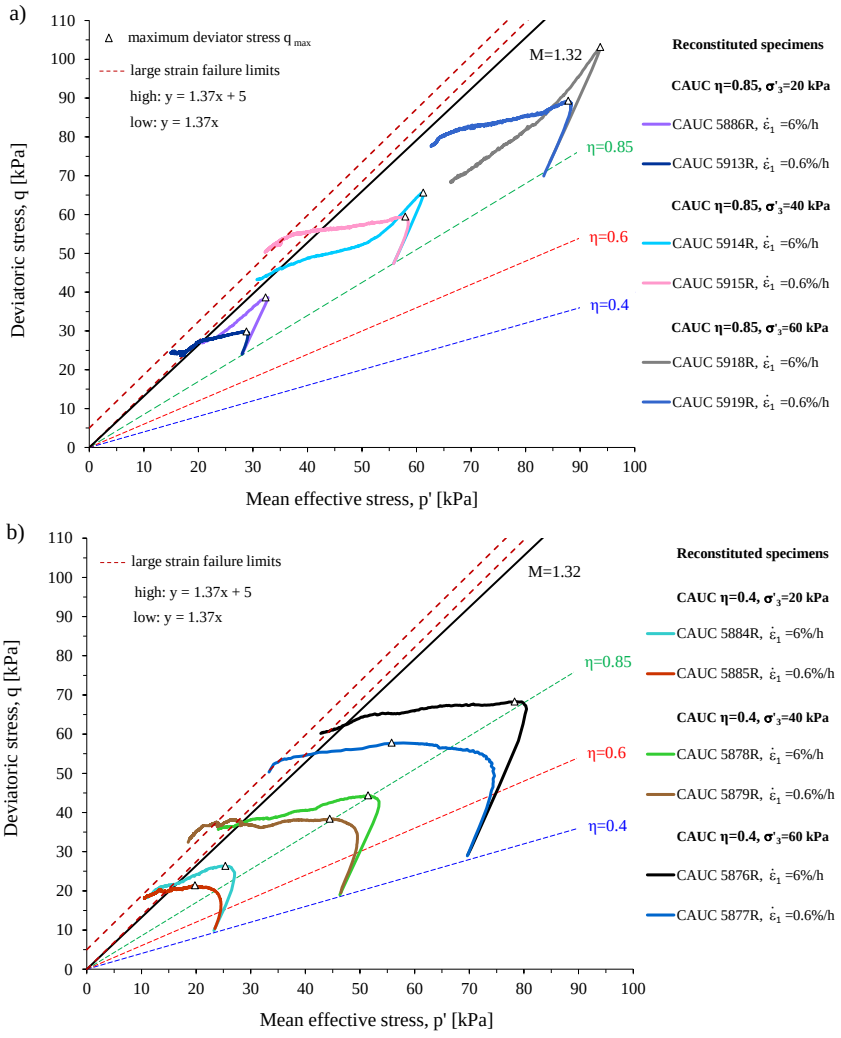

Figure 7.45 CAUC results on reconstituted specimens in q vs. p' plane; a) consolidation to η=0.85, and b) at η=0.4.

Evaluation of Critical State in compression

According to Critical State theory [Roscoe et al. 1958, Schofield & Wroth 1968], element of soil undergoing uniform shear distortion eventually reaches a critical state condition in which it continues to distort without further change of void ratio, deviator stress, or mean effective stress [Roscoe & Burland 1968]. In undrained triaxial compression test, such condition corresponds to constant stress ratio and constant pore pressure. Accordingly, following substantial extent of shear straining, specimen of structured clay should exhibit identical value of constant critical state stress ratio $\eta=M=q/p'$, independent of the consolidation and strain-rate conditions imposed.

In Figure 7.46 stress ratio response of natural specimens of Perniö clay is examined vs. deviatoric strains. The results are distinctively presented with respect to stress ratio conditions imposed in consolidation. At the end of undrained shear test, the natural specimens exhibited tendency toward target pore pressure related to magnitude of radial pressure in consolidation (see Figure 7.40). As presented in Figure 7.46 however, stress ratio response at the final stage of the tests considerably differed in magnitude. The stress ratio values generally intensified, even at the final stage of undrained shear. To elaborate the response, results of shear tests onset from specific η in consolidation need to be examined with respect to radial pressure and strain-rate imposed.

Figure 7.46 a) presents results of undrained shear tests on natural specimens initiated at $\eta=0.85$. Among tests performed at 6 %/h, the highest η values characterising final segment of the curve identified test 5904 at $\sigma'_3=20$ kPa. Somewhat lower η values were those in test 5907 at 40 kPa, and finally, generally the lowest were those in test 5912 performed at radial pressure of 60 kPa. Similarly, among tests at rate of 0.6 %/h, the highest η values at large strains were measured in test 5903 at radial pressure of 20 kPa, followed by those in 5906 at 40 kPa, and finally by those in 5911 at 60 kPa. Same conclusion was valid for final stress ratio response in tests at 0.06 %/h, i.e. η values in test 5902 performed at $\sigma'_3=20$ kPa exceeded those in 5908 at 40 kPa.

In Figure 7.46 b), results of undrained shear tests onset at $\eta=0.6$ are shown. Among tests at 6 %/h, the highest η values at large strains identified test 5839 at $\sigma'_3=20$ kPa, followed by 5849 and 5865 at 40 kPa, and finally those in 5862 performed at radial pressure of 60 kPa. Same pattern was observed in tests at 0.6 %/h. The highest η values characterised test 5838 at $\sigma'_3=20$ kPa, followed by those in 5850 and 5866 at 40 kPa, while those in 5863 performed at $\sigma'_3=60$ kPa were the lowest. Finally, in tests at 0.06 %/h, the highest η values were measured in test 5837 at $\sigma'_3=20$ kPa. Somewhat less were η values in 5851 at 40 kPa, and again, the least were those in test 5864 performed at $\sigma'_3=60$ kPa.

Figure 7.46 c) shows stress ratio vs. shear strain response of natural specimens in tests initiated at $\eta=0.4$. The results exhibited same general features. In tests at 6 %/h, the highest η values at large strains characterised respective tests 5711 and 5691 sheared at $\sigma'_3=20$ and 40 kPa, while the lowest η values were those obtained in tests performed at $\sigma'_3=60$ kPa, i.e. 5699 and 5811. Exception from the rule was test 5819 sheared at $\sigma'_3=40$ kPa. Considering tests at 0.6 %/h, the highest η were those in test 5713 at $\sigma'_3=20$ kPa. In remaining tests

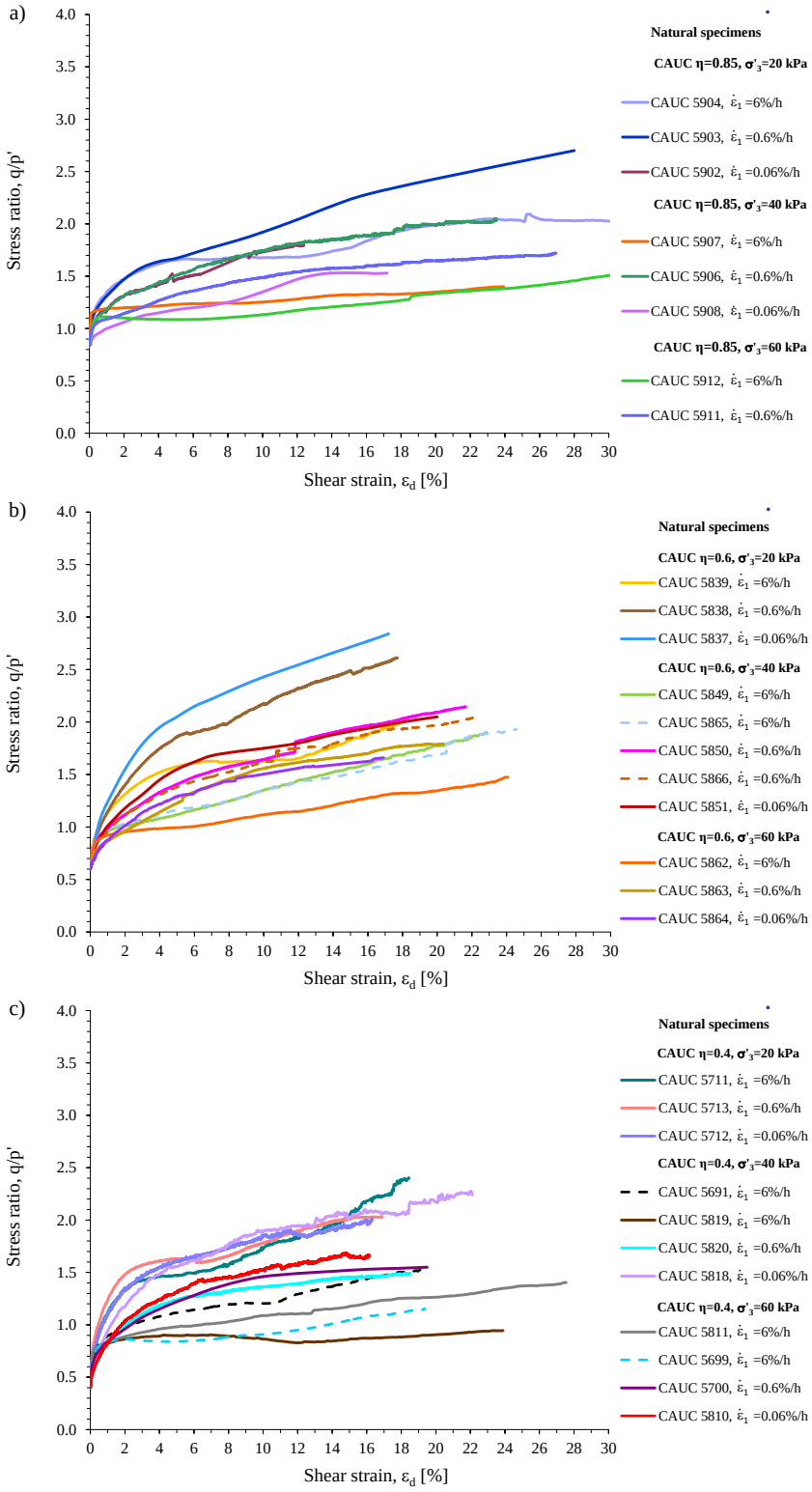

Figure 7.46 Change in stress ratio with shear strain in undrained compression of natural specimens onset at; a) η=0.8, b) η=0.6, and c) η=0.4.

at the same rate, final η values were notably less. Exceptionally, test 5700 at σ'_3=60 kPa exhibited somewhat higher final η than 5820 performed at 40 kPa. Lastly, in tests at 0.06 %/h, final η values in tests 5712 and 5818 at σ'_3=20 and 40 kPa were similar, while those in 5810 at σ'_3=60 kPa were significantly less.

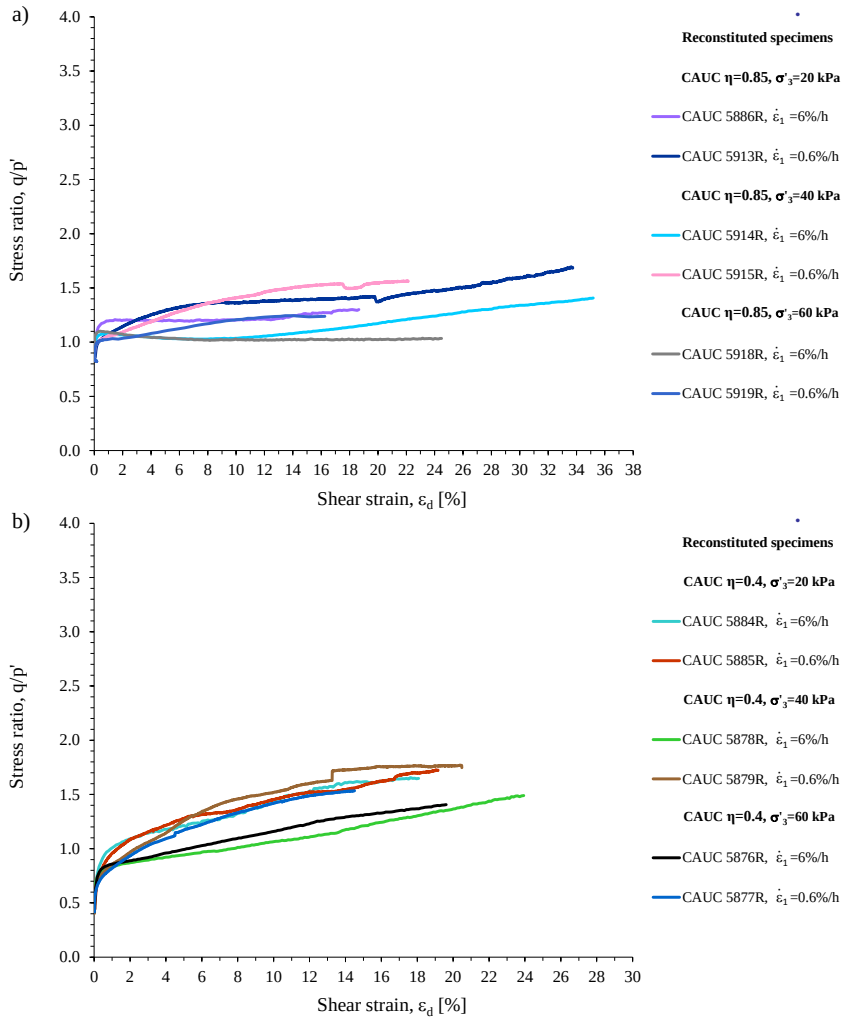

Figure 7.47 Change in stress ratio in undrained shear of reconstituted specimens onset at; a) η=0.85, and b) η=0.4.

Figure 7.47 a) presents stress ratio vs. shear strain results measured on reconstituted specimens sheared from η=0.85. Compared with results on natural, stress ratio values characterising response of reconstituted specimens at large strains were fairly stable. Furthermore, resulting pattern generally complied with that exhibited by natural material. Considering tests performed at identical strain-rate, specimens compressed at lower radial pressure generally exhibited somewhat higher η at large strains. Influence of strain-rate was significant, with specimens axially compressed at 0.6 %/h exhibiting generally higher η values compared to those in tests at 6 %/h.

Figure 7.47 b) presents results of undrained shear tests on reconstituted specimens initiated at η=0.4. Overall, the results were characterised with similar rate of stress ratio increase with shear strain. In comparison with test results of previous series, effects of radial stress on stress ratio response at large strains were reduced. Influence of strain-rate was however, yet again significant. Compared to those tested at 6 %/h, reconstituted specimens axially compressed at 0.6 %/h generally exhibited somewhat higher η values.

Despite sporadic exceptions related to effects of specimen quality and natural variability, the results on natural specimens revealed stress ratio values characterising final stage of undrained shear being significantly influenced by magnitude of radial pressure and axial strain-rate. Contrary to critical state theory, the specimens did not exhibit tendency towards uniform stress ratio values at large strains. Instead, η progressively increased at rate reciprocal to extent of destructuration. In tests performed at certain strain-rate, values of stress ratio at high strain were reciprocal to magnitude of radial pressure in shear. Compared to those on natural specimens, high strain η measured on reconstituted specimens identified relatively narrower range of values, while influence of radial pressure was less significant. Among reconstituted specimens, it was the axial strain-rate that controlled final magnitude of stress ratio, i.e. specimens shared at high strain-rates mostly exhibited lower η values.

7.2.4 Strain-rate parameters

Perniö clay specimens were shared undrained under the condition of constant axial strain-rate. As presented in Figure 7.48, along the undrained stress path several distinctive stages could be identified, i.e. point of maximum mean effective stress p'_{max} associated with stress ratio η_α, and point of maximum deviator stress q_{max} coupled with stress ratio at failure η_F. In following, stress and stress ratio conditions at the characteristic stages are analysed with respect to stress ratio and radial pressure in consolidation and axial strain-rate in shear.

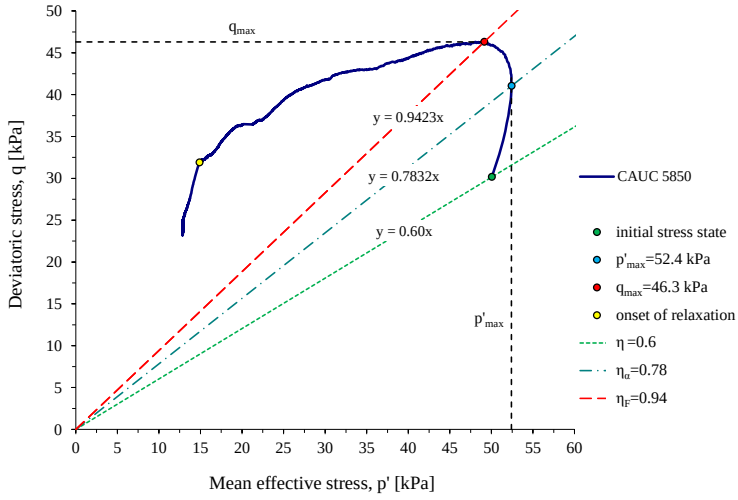

Figure 7.48 Characteristic stages of undrained stress path in q vs.p' plane, CAUC 5850.

Stress ratio η_α

In Figure 7.49, values of stress ratio η_α, characterising maximum mean effective stress in undrained shear tests, are related to axial strain-rate. For tests onset at certain consolidation stress ratio conditions, the η_α values occurred in narrow band revealing linear proportionality with logarithm of strain-rate. In tests onset at respective consolidation conditions of η=0.85, 0.6 and 0.4, rate effects on η_α values were well represented by Equations 7.5, 7.6, and 7.7:

$$\eta_{\alpha(\eta=0.85)} = 0.063\ln(\dot{\varepsilon}_1) + 1.30 \qquad (7.5)$$

$$\eta_{\alpha(\eta=0.6)} = 0.063\ln(\dot{\varepsilon}_1) + 1.09 \qquad (7.6)$$

$$\eta_{\alpha(\eta=0.4)} = 0.063\ln(\dot{\varepsilon}_1) + 0.96 \qquad (7.7)$$

where; $\dot{\varepsilon}_1$ is magnitude of axial stain-rate in mm/min. The same general relations were valid for both, natural and reconstituted specimens of Perniö clay.

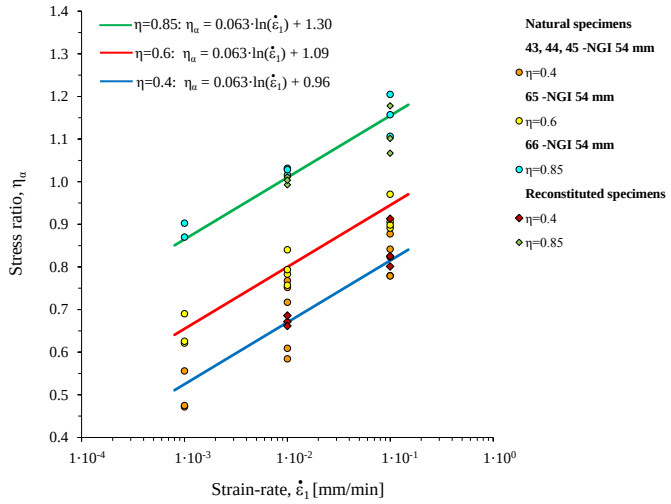

Figure 7.49 Influence of axial strain-rate on magnitude of stress ratio η_α in undrained shear,

Although strongly related to intensity of consolidation stress ratio and axial strain-rate, magnitude of η_α was fairly independent of cell pressure in shear. In fact, the values of η_α were proportional to consolidation stress ratio. Thus, tests characterised by high magnitude of η in consolidation exhibited generally higher values of η_α. In addition, influence of axial strain-rate was significant, yet fairly unrelated to consolidation conditions. Namely, linear proportionality of η_α to logarithm of strain-rate was well defined by unique slope of 0.063, uncontrolled by the magnitude of consolidation stress ratio. Based on the results at the strain-rates imposed, prior the value of η_α on certain stress path being reached, effects of structure on undrained shear response were minor.

Maximum mean effective stress p' $_{max}$

In Figure 7.50, values of maximum mean effective stress, measured in undrained shear on Perniö clay, are related to magnitude of axial strain-rate. Values of p'_{max} corresponding to stress ratio η_α, were in addition to strain-rate and consolidation stress ratio, governed by the intensity of radial stress in shear. Depending upon the cell pressure imposed, values of p'_{max} formed three distinctive groups. In tests at the lowest σ'_3, values of p'_{max} were overall the lowest, and vice versa. Furthermore, depending upon the η in consolidation, the results obtained at each level of radial pressure formed three bands, with p'_{max} values being proportionally related to magnitude of η. Influence of strain-rate was significant as well. Considering tests performed at identical cell pressure, values of p'_{max} exhibited linear proportionality when related to logarithm of axial strain-rate. For tests performed at identical radial pressure, linear proportionality was similar for specimens consolidated at various η levels. Overall however, slope defining rate-dependency intensified with increase of consolidation cell pressure. The results thus showed influence of axial strain-rate on specimen response intensifying with destructuration level. Indeed, the slopes identifying rate-dependency of p'_{max} were well represented by values of 0.6, 1.1 and 1.6, in undrained shear at σ'_3=20, 40 and 60 kPa, respectively. Conclusions were valid for both, natural and reconstituted specimens.

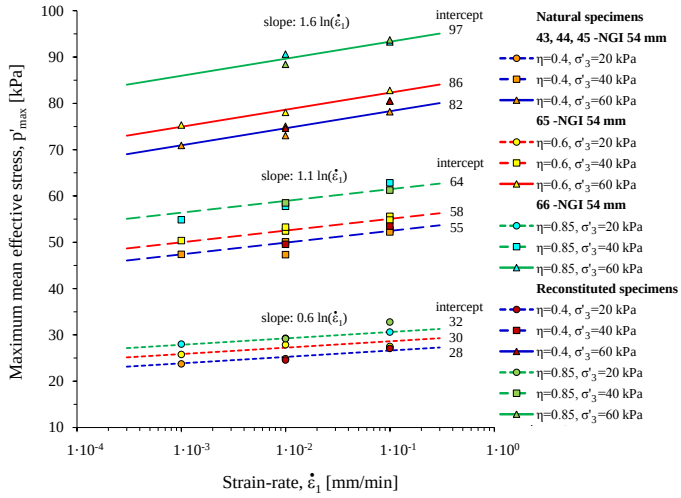

Figure 7.50 Influence of axial strain-rate on maximum mean effective stress in undrained shear

Figure 7.51 relates p'_{max} in undrained shear to corresponding void ratio of natural and reconstituted specimens. Values identifying natural specimens plotted above those measured on reconstituted material. General pattern exhibited was that of p'_{max} being the lowest in tests on specimens with the highest e_s. The effect primarily reflected stress-strain conditions in consolidation. Difference between mean effective stress following consolidation and p'_{max} in undrained shear was strain-rate dependent. Specimens consolidated to same level of σ'_3 however, occurred within narrow range of mean effective stresses.

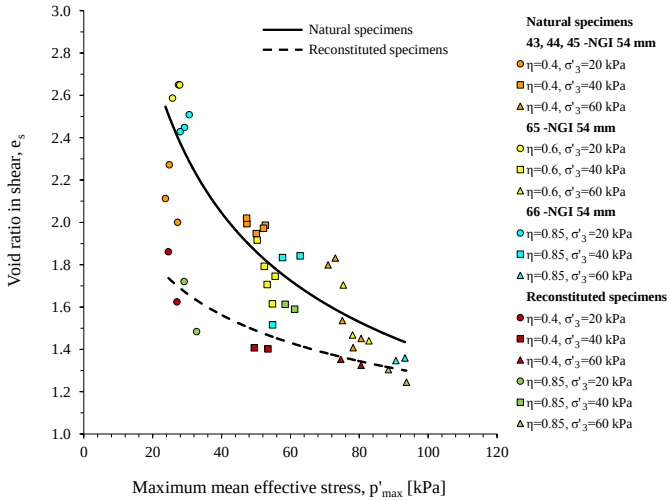

Figure 7.51 Influence of void ratio in undrained shear on maximum mean effective stress.

Stress ratio at failure η_F

Figure 7.52 presents stress ratio at failure exhibited by natural and reconstituted specimens of Perniö clay, related to axial strain-rate. Unlike stress ratio values characterising maximum mean effective stress, η_F values corresponding to peak deviator stress were highly scattered. The scatter reflected significant variance in quality of the natural specimens considered, as well as effects of destructuration caused by difference in consolidation conditions imposed. Natural specimens consolidated to stress state similar to effective overburden exhibited the highest η_F varying from 1.27 to 1.64 (see Figure 7.52 a). In average, the values corresponded fairly well with that of estimated critical state, i.e. η_F~1.34. In tests at σ'_3=40 kPa, failure stress ratio values were somewhat less, i.e. $0.94<\eta_F<1.41$. Finally, in undrained shear tests at σ'_3=60 kPa, the natural specimens exhibited overall the lowest stress ratio at failure, i.e. $0.82<\eta_F<1.21$. Similar pattern was measured on reconstituted specimens (see Figure 7.52 b),

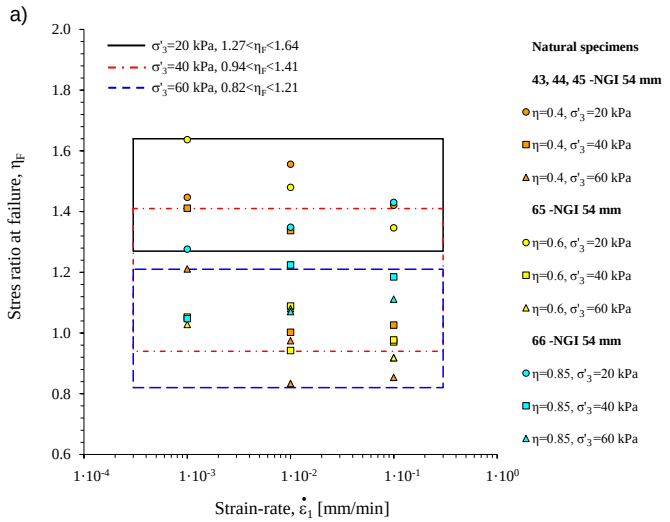

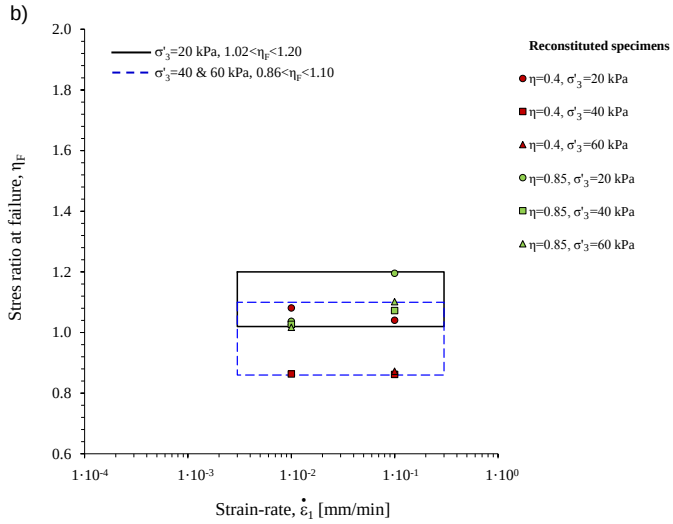

Figure 7.52 Influence of axial compression rate and radial pressure on stress ratio at failure in undrained shear; a) natural and b) reconstituted specimens.

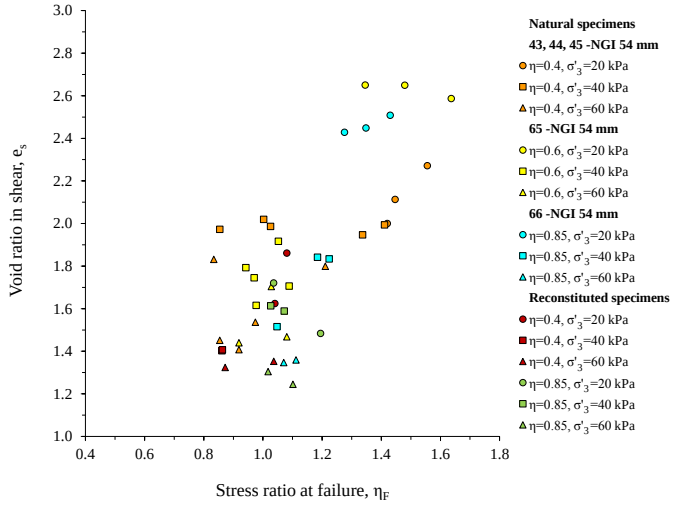

Figure 7.53 Influence of void ratio in undrained shear on stress ratio at failure.

yet the η_F values were overall less in magnitude and less scattered. In tests at σ'_3=20 kPa, η_F values varied between 1.0 and 1.2, while in tests at σ'_3=40 and 60 kPa, η_F occurred in a range from 0.86 to 1.1. With failure at the lowest level of strain-rate being characterised by fairly uniform magnitude of q over wide range of p', corresponding η_F values were the least reliable. Despite considerable scatter, resulting η_F values indicated reciprocal relation with radial pressure in undrained shear, i.e. extent of destructuration. Furthermore, η_F values plotted vs. magnitude of e_s in Figure 7.53 indicated proportional relation of stress ratio at failure with water content of the specimens considered. With the magnitude of e_s reflecting the extent of specimen destructuration in consolidation, the results showed values of stress ratio at failure being influenced by quality of the specimens tested.

Maximum deviator stress q_{max}

In Figure 7.54, values of maximum deviator stress in undrained shear are related to axial strain-rate. Strain-rate dependency of q_{max} was strongly influenced by both η in consolidation and σ'_3 in shear. At the state of maximum shear strength being mobilized, effects of specimen disturbance were very pronounced. Consequently, the results were less decisive compared to those defining p'_{max} in Figure 7.50. The values of q_{max} were proportionally influenced by magnitude of σ'_3 in shear. Thus, depending upon the radial pressure, three groups of undrained shear strength results could be distinguished. However, region of q_{max} values obtained at σ'_3=40 kPa, overlapped with that identifying results at σ'_3=60 kPa. Considering tests performed at identical level of σ'_3, values of q_{max} at certain axial strain-rate were generally proportional to magnitude of η in consolidation. Thus, to define influence of strain-rate on q_{max}, both consolidation η as well as σ'_3 in shear needed to be taken into account.

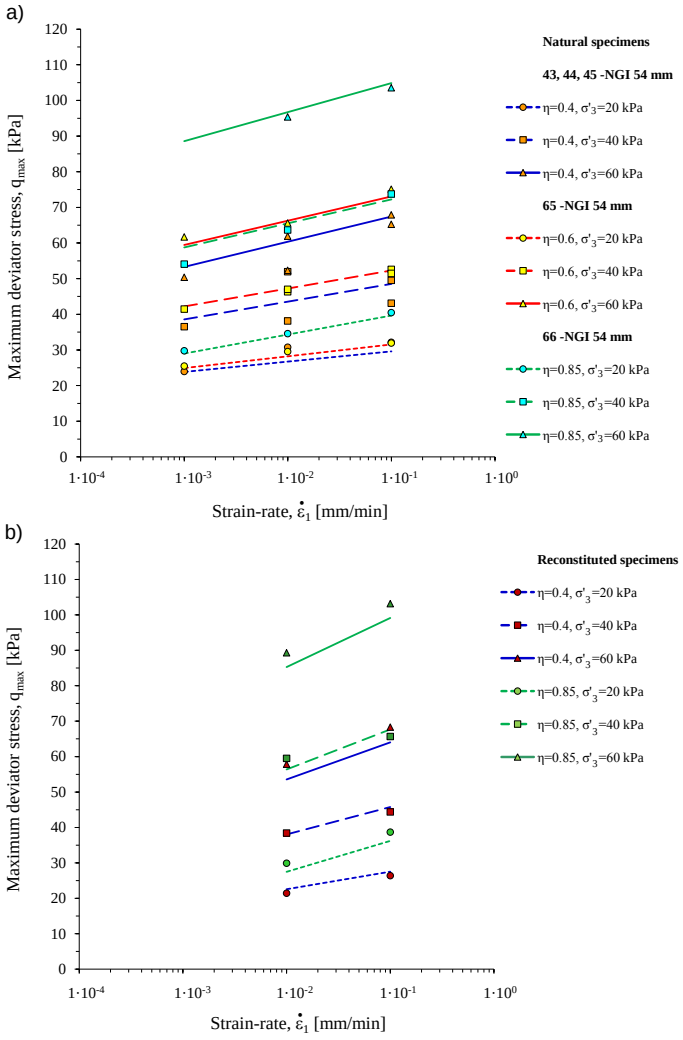

Figure 7.54 Influence of axial compression-rate on maximum deviator stress in undrained shear; a) natural and b) reconstituted specimens.

Interpretation of strain-rate influence on shear strength is presented in Table 7.3. It was based on linear relation between strain-rate and shear strength in semi logarithmic plane. Considering specimens consolidated at identical η, slope of the line defining rate-dependency of q_{max} was the lowest for specimens sheared at σ'_3=20 kPa. Somewhat higher was the slope identifying rate-dependence of specimens sheared at σ'_3=40 kPa. Lastly, for specimens sheared at the highest radial pressure of 60 kPa, slope defining rate-dependence of q_{max} was the highest. Conclusions were valid for both, natural and reconstituted specimens. Interpretation of strength vs. strain-rate response identified intercept of the relations being dependent primarily upon the σ'_3 in shear. Slope of the relations however, was highly influenced by specimen structural characteristics. Namely, under identical conditions of consolidation and shear, reconstituted specimens exhibited higher slope identifying strength vs. strain-rate response. Thus, maximum available strength exhibited at certain strain-rate was proportionally related to the magnitude of consolidation stress ratio and radial pressure in shear.

Table 7.3 Influence of axial compression-rate on maximum shear strength; q_{max}=slope·ln($\dot{\varepsilon}_1$)+intercept.

Stress ratio	Cell pressure [kPa]	Natural specimens		Reconstituted specimens	
		slope	intercept	slope	intercept
η=0.85	60	3.54	113	6.023	113
	40	2.93	79	4.917	79
	20	2.32	45	3.811	45
η=0.6	60	2.948	79.83	-	-
	40	2.192	57.33	-	-
	20	1.436	34.83	-	-
η=0.4	60	3.072	74.5	4.553	74.5
	40	2.162	53.5	3.357	53.5
	20	1.253	32.5	2.161	32.5

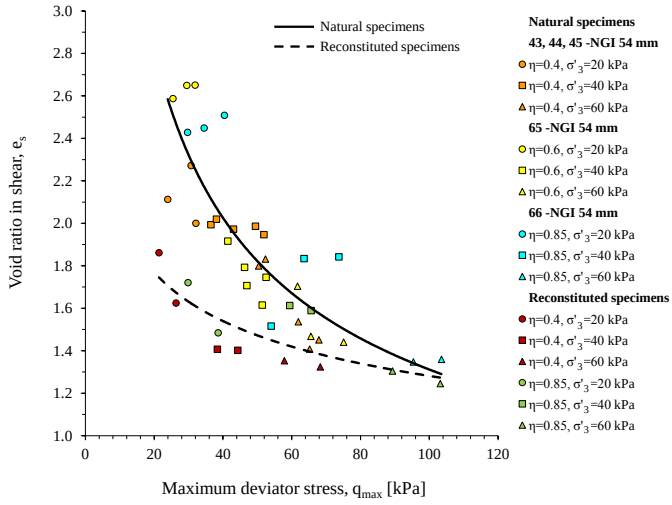

Figure 7.55 Influence of void ratio in undrained shear on deviator stress at failure.

In Figure 7.55, values of q_{max} are related to magnitude of void ratio in shear. Despite high scatter reflecting the variation in test condition imposed, values of q_{max} were clearly reciprocal to e_s. The effect reflected stress-strain conditions in consolidation. For highly destructured natural specimens tested at σ'_3=60 kPa, q_{max} complied well with those on reconstituted material. In tests at σ'_3=20 kPa however, q_{max} on natural specimens exceeded those on reconstituted, and were related to significantly higher values of e_s. In tests performed at the same level of e_s, offset in q_{max} was related to magnitude of axial strain-rate.

7.2.5 Normalization of stress paths and failure envelopes

Examined in q-p' plane (see Figure 7.44), final segments of stress paths, representing residual undrained shear resistance of natural Perniö clay specimens, were highly scattered making the interpretation of critical state stress ratio difficult and unreliable. However, following normalization of stress invariants characterising undrained stress paths, with maximum vertical effective stress reached in consolidation σ'_{1C}, the stress paths measured became meaningful.

As shown in Figure 7.56, with stress invariants normalized by σ'_{1C}, final stress states in consolidation test at identical stress ratio were reduced to a single point. Consequently, effects of axial strain-rate and destructuration on undrained shear response could be clearly examined. With onset of undrained shear at different strain-rates, normalized stress paths diverged. The difference in undrained shear response was primarily related to magnitude of axial strain-rate imposed. Stress paths obtained at the highest strain-rate exhibited rapid increase in normalized mean effective stress and deviator stress, and the highest value of normalized shear strength. Opposite was valid in tests at low strain-rate. However, with maximum value of normalized deviator stress level exceeded, normalized stress paths exhibited tendency to converge.

Beside strain-rate, characteristics of the normalized stress paths were highly influenced by the level of radial stress in consolidation, i.e. extent of destructuration process prior undrained shear. Figure 7.56 a) comprises results of undrained shear tests onset after consolidation to stress state defined by σ'_3=20 kPa. With peak deviator stress level exceeded, normalized stress paths converged toward linear failure envelope with slope of 1.1. Some scatter of the stress path characteristics at large strains was manifested by variance in intercept values, i.e. 0.25 to 0.32. In tests onset from consolidation states defined by σ'_3=40 and 60 kPa respectively shown in Figure 7.56 b) and c), final portion of stress paths converged as well. In these tests however, linear failure envelope was characterised by reduced slope of 0.47, and intercept values mainly between 0.35 and 0.42. Reason for the variance in the final portion of normalized stress path characteristics, i.e. position of the failure envelope, was related to structural characteristics of the specimens. Stress states of the specimens consolidated until σ'_3=20 kPa corresponded rather well with that of effective overburden. Consequently, prior undrained shear destructuration of the specimens was minor. In contrast, stress states of the specimens in consolidation characterised with σ'_3=40 or 60 kPa considerably exceeded that in situ. The specimens were thus subjected to relatively higher extent of destructuration prior undrained shear.

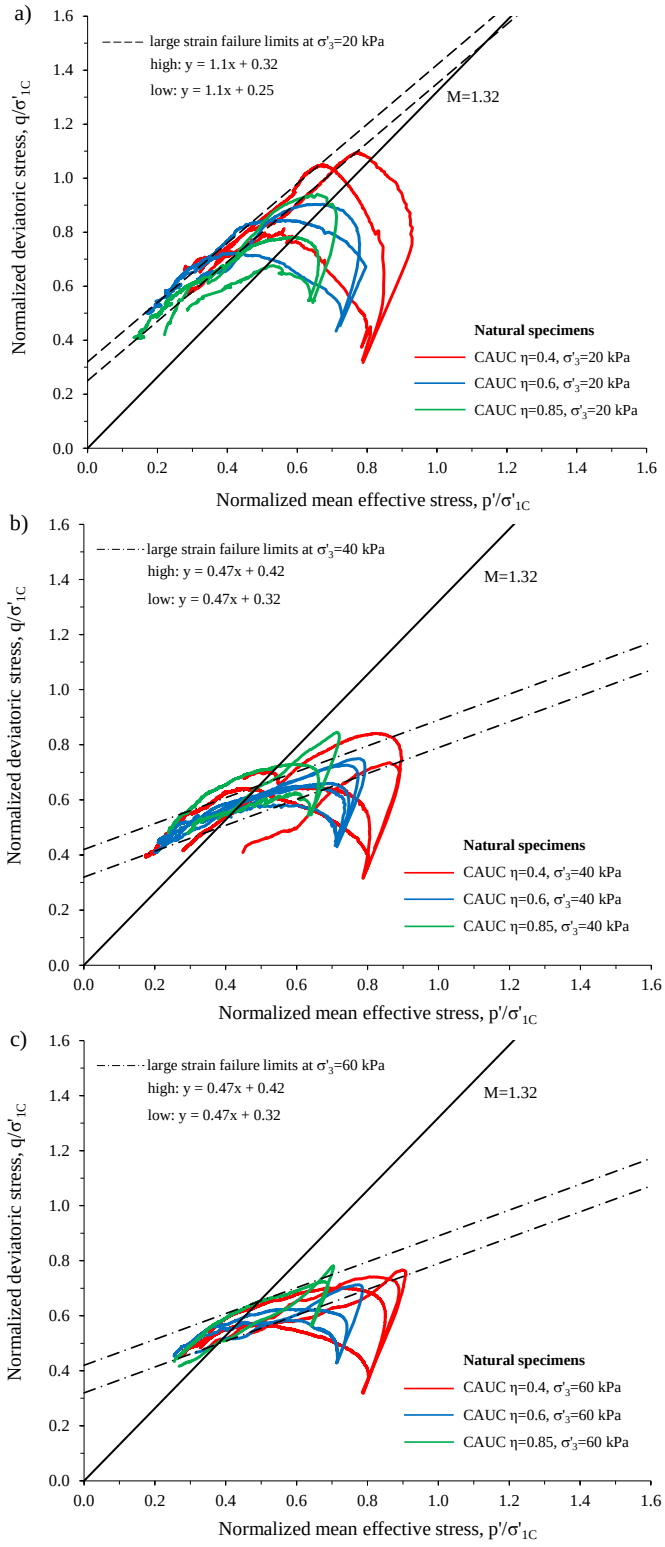

Figure 7.56 Undrained stress path on natural specimens normalized with vertical effective stress in consolidation; a) tests at σ'$_3$=20 kPa, and b) tests at σ'$_3$=40 and 60 kPa.

In Figure 7.57 results of normalization of undrained shear tests on natural specimens are examined in detail. The results following consolidation at η=0.85, 0.6 and 0.4 are separately shown. Furthermore, the undrained shear results, together with large strain failure envelopes interpreted, are related to yield surfaces identifying response of corresponding specimens in triaxial consolidation tests. Characteristics of the natural specimens, as well as details of triaxial consolidation and undrained shear conditions are listed in Table 7.4.

Figure 7.57 a), presents results of normalization of undrained shear tests onset at η=0.85. Following normalization, initial stress state in the shearing tests was positioned within the smallest in size yield surface D, representing response of the poorest quality specimens of sublayers A and B. Final segments of normalized stress paths measured on specimens tested at σ'_3=20 kPa were bound by lines with slope of 1.1 and intercepts in range from 0.25 to 0.32. The specimens were characterised with $\sigma'_{1c}/\sigma'_{V0}$ values of 1.9. In tests on specimens sheared at σ'_3=40 and 60 kPa, the final stress conditions were bound by lines with slope 0.47 and intercept values ranging from 0.35 to 0.42. Scatter of the intercept values was related to effects of specimen disturbance, i.e. lower intercepts characterised specimens with relatively lower water content in shear.

Considering stress paths obtained in tests on natural specimens consolidated at η=0.6 shown in Figure 7.57 b), results of normalization were the most consistent. The tests were onset at stress state positioned on yield surface D, and thus, well within yield surfaces identifying yielding of the highest quality specimens of sublayers A and B. In tests on specimens sheared at σ'_3=20 kPa, final segments of normalized stress paths were bound by lines with slope 1.1 and intercepts between 0.25 and 0.32. The specimens were marked with $\sigma'_{1c}/\sigma'_{V0}$ of 1.5. Furthermore, values of normalized peak strength resembled those on specimens sheared at the same strain-rates and radial pressure, yet onset at η of 0.85. In tests at σ'_3=40 and 60 kPa, final stress characteristics were that of 0.47 in slope, and intercepts in range from 0.32 to 0.39. In tests performed at the highest strain-rate, stress paths converged with failure envelope at higher level of normalized mean effective stress. In contrast, stress paths in slow tests merged with failure envelope at the final stage of the tests.

Normalized stress paths representing natural specimens consolidated at η=0.4 in Figure 7.57 c), were fairly scattered. Initial stress state positioned closely to yield surface B, identifying yield of the highest quality sublayer B specimens. In tests at σ'_3=20 kPa, normalized stress paths yet again converged toward linear response characterised by slope of 1.1 and intercepts between 0.25 and 0.32. Furthermore, the results exhibited the highest level of normalized peak strength. Indeed, in tests at rates of 6 and 0.6 %/h, normalized peak strength corresponded well with yield response identifying the highest quality specimens of sublayer A. The effect was related to relatively the lowest values of $\sigma'_{1c}/\sigma'_{V0}$ characterising the specimens, i.e. $\sigma'_{1c}/\sigma'_{V0}$ of 1.0. In tests at σ'_3=40 and 60 kPa, large strain characteristics converged with linear response characterised by slope of 0.47, and considerable range of intercept values between 0.32 and 0.42. High scatter in intercept values reflected considerable extent of disturbance of the specimens considered.

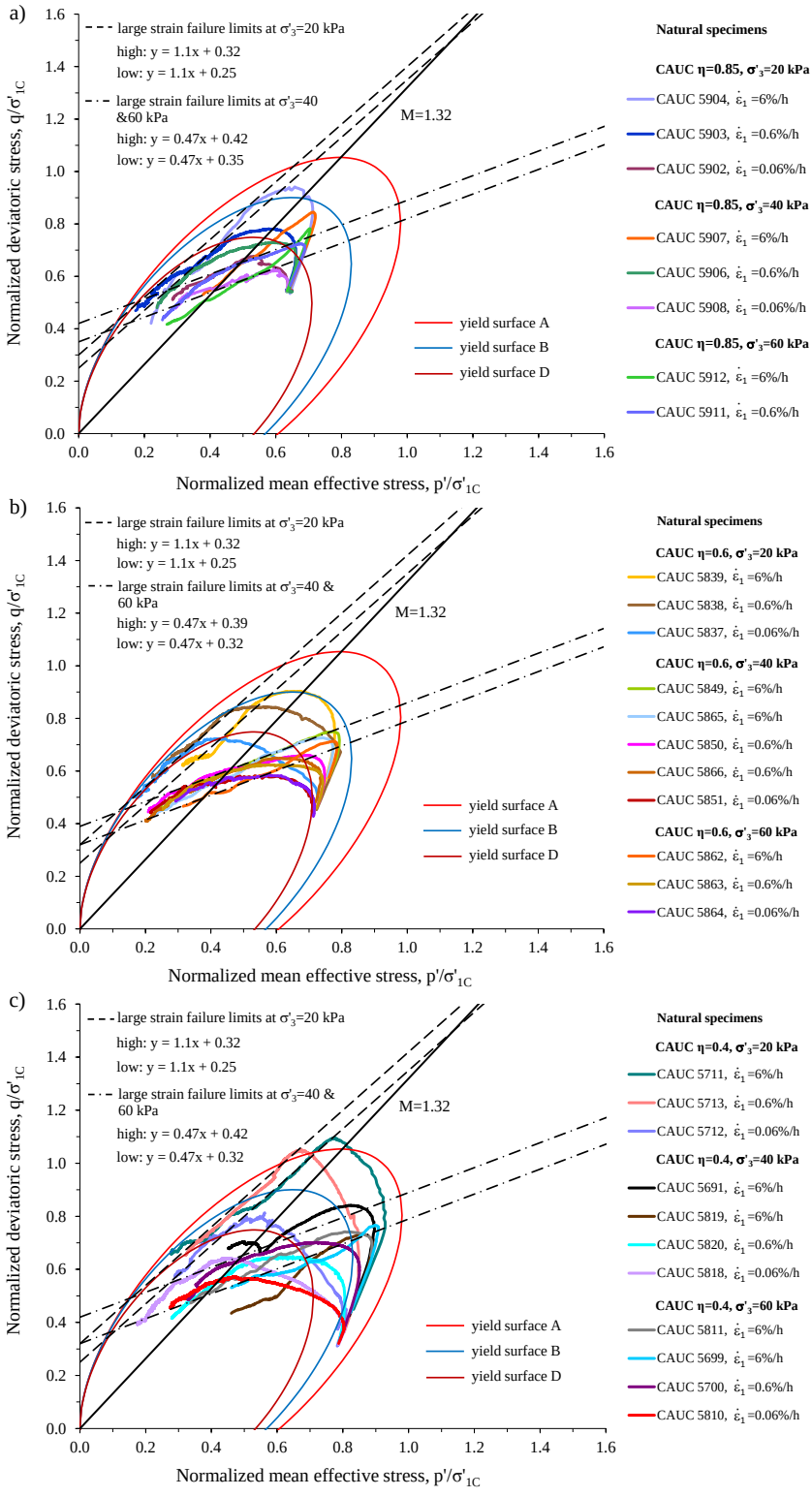

Figure 7.57 Undrained stress paths on natural specimens normalized with vertical effective stress in consolidation at; a) η=0.85, b) η=0.6, and c) η=0.4.

Normalized stress paths of undrained shear tests on reconstituted specimens are shown in Figure 7.58. Characteristics of the reconstituted specimens and triaxial test conditions are listed in Table 7.5. The $\sigma'_{1c}/\sigma'_{vo}$ values identifying tests on reconstituted specimens were generally higher. However, independent of the magnitude of stress ratio and radial stress in consolidation, normalized stress paths at large strains exhibited tendency toward linear response defined with 0.47 in slope and intercepts from 0.32 to 0.43. Therefore, in contrast to those on natural, results on reconstituted specimens did not exhibit significant destructuration effects. Thus normalized stress paths in undrained shear tests at σ'_3=20 kPa, resembled those in undrained shear at higher levels of radial pressure, i.e. σ'_3=40 and 60 kPa. Strain-rate effects of on normalized stress path characteristics remained yet were less significant than in tests on natural specimens.

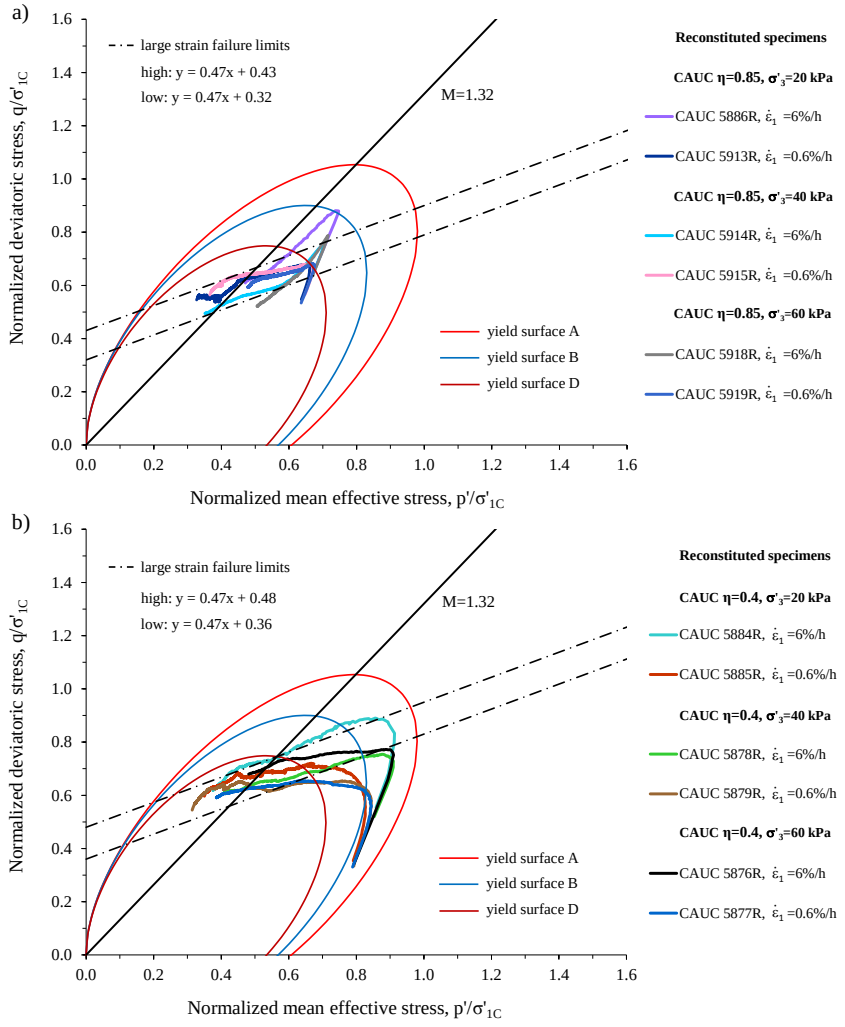

Figure 7.58 Undrained stress paths on reconstituted specimens normalized with vertical effective stress in consolidation at; a) η=0.85, b) η=0.4.

Table 7.4 Characteristics of natural specimens in undrained shear tests.

Stress ratio	Cell pressure [kPa]	Strain rate [mm/min]	Test no.	Sublayer	Void ratio in shear e_s	OCR $\sigma'_{1C}/\sigma'_{V0}$	Normalized peak strength q_F/σ'_{1C}
η=0.85	20	6	5904	A	2.51	1.9	0.93
		0.6	5903	A	2.49	1.9	0.78
		0.06	5902	A	2.43	1.9	0.68
	40	6	5907	A	1.84	3.3	0.84
		0.6	5906	A	1.83	3.3	0.73
		0.06	5908	B	1.52	2.8	0.62
	60	6	5912	B	1.36	3.5	0.78
		0.6	5911	B	1.35	3.5	0.72
η=0.6	20	6	5839	A	2.65	1.5	0.90
		0.6	5838	A	2.65	1.4	0.84
		0.06	5837	A	2.59	1.5	0.72
	40	6	5849	B	1.75	2.5	0.75
		6	5865	B	1.62	1.8	0.73
		0.6	5850	A	1.79	2.5	0.66
		0.6	5866	B	1.71	1.9	0.65
		0.06	5851	A	1.92	2.6	0.58
	60	6	5862	B	1.44	3.2	0.71
		0.6	5863	B	1.47	3.3	0.62
		0.06	5864	A	1.70	3.9	0.58
η=0.4	20	6	5711	A	2.00	1.0	1.09
		0.6	5713	B	2.27	0.9	1.05
		0.06	5712	A	2.11	1.0	0.82
	40	6	5691	A	1.99	2.4	0.84
		6	5819	A	1.92	1.3	0.73
		0.6	5820	A	2.02	1.3	0.65
		0.06	5818	A	1.99	1.3	0.64
	60	6	5811	B	1.41	2.7	0.74
		6	5699	A	1.45	3.0	0.77
		0.6	5700	A	1.54	3.0	0.70
		0.06	5810	B	1.80	2.7	0.57

Table 7.5 Characteristics of reconstituted specimens in undrained shear tests.

Stress ratio	Cell pressure [kPa]	Strain rate [mm/min]	Test no.	Void ratio in shear e_s	OCR $\sigma'_{1C}/\sigma'_{V0}$	Normalized peak strength q_F/σ'_{1C}
η=0.85	20	6	5886R	1.48	2.9	0.88
		0.6	5913R	1.73	2.9	0.68
	40	6	5914R	1.59	5.8	0.75
		0.6	5915R	1.61	5.8	0.68
	60	6	5918R	1.25	8.7	0.78
		0.6	5919R	1.30	8.7	0.68
η=0.4	20	6	5884R	1.62	2.0	0.88
		0.6	5885R	1.86	2.0	0.72
	40	6	5878R	1.40	3.9	0.75
		0.6	5879R	1.41	3.9	0.65
	60	6	5876R	1.32	5.9	0.77
		0.6	5877R	1.35	5.9	0.65

To conclude, CAUC results on Perniö clay revealed destructuration and strain-rate effects having a strong impact on undrained shear resistance of natural clay. With stress invariants normalized by final vertical effective stress in consolidation, stress paths converged towards the end of the test. The response was well represented by linear failure envelopes. Specimens with quality representable of that in situ exhibited the highest normalized shear resistance marked by steep failure envelope. Specimens consolidated well beyond effective overburden showed reduced normalized shear resistance, reflecting higher extent of destructuration. In contrast, the effects of destructuration on response of reconstituted specimens were insignificant. Considering specimens of comparable structural qualities, stress paths in tests at high strain-rates reached failure envelope at high level of normalized mean effective and deviator stresses. In tests at low strain-rates, stress paths reached failure envelope at low level of normalized stress invariants, i.e. those characterising specimen response at large strain.

8. Conclusions and recommendations

The quality of a constitutive model is reflected in its ability to represent real soil behavior. In development and evaluation of advanced constitutive models it is essential to validate the model formulation and the model response with high quality in situ and laboratory test results. Furthermore, application of constitutive models in geotechnical design necessitates accounting for extent of sample disturbance and consequent effects on results of laboratory tests. For that reason, the main emphasis of this research work was on experimental evaluation of soil sampling and subsequent testing of structured clays.

Constitutive modelling of soil behavior requires the highest quality sampling to ensure representativeness of laboratory results. This study evaluated performance of three available sampling techniques. Among the sampling techniques used, only NGI 86 mm sampler had suitable characteristics for sampling of soft structured clay. The sampler in its present form however, lacked valve for securing sample retrieval. Due to the importance of sampling quality on laboratory test results aiming concise interpretation of stratigraphic conditions and providing high quality specimens suitable for advanced laboratory testing, availability of an adequate sampler is of high importance. For sampling of structured clays development of large diameter sampler with an adequate cutting and sample retaining mechanism is essential.

Laboratory tests aiming for development and calibration of constitutive models need to be designed to target those particular aspects of the soil behavior that are perceived as the most important. The testing techniques should enable accurate, consistent and efficient performance of the equipment and representativeness of the results. During this work, the data acquisition for one dimensional and triaxial test conditions was automated. This improvement, combined with improved test methodology enabled enhancement of the interpretation approaches and comprehensive examination of destructuration and strain-rate effects. Considering the testing equipment used at Aalto University, ongoing enhancement of the present state of triaxial testing is very important. Development and implementation of computer controlled incremental and continuous loading triaxial test devices suitable for advanced triaxial consolidation and undrained shear testing is crucial.

The comprehensive testing programme in this thesis comprised of considerable number of oedometer and triaxial tests on natural and reconstituted specimens of Perniö clay. Based on the experimental results, the compressibility, the apparent strength and the rate dependency of the clay response under one-dimensional and triaxial test conditions are strongly related to sample disturb-

ance and consolidation stress history. Study explained effects of structure and sample disturbance on compressibility and creep response in oedometer and triaxial consolidation tests. Effects of strain-rate and specimen quality during one-dimensional compression and triaxial undrained shear are clarified. Methods in formulating rate dependent effects for constitutive modelling of structured clays are enhanced. Approaches used in interpretation of the experimental results were based on Modified Cam-Clay theory [Roscoe et al. 1958, Schofield & Wroth 1968, Roscoe & Burland 1968], Compression Modulus theory [Janbu 1963, Janbu 1967], and that of Isotache concept [Šuklje 1957, Tavenas & Leroueil 1977, Leroueil et al. 1979]. Deductions of the interpretation of Perniö clay experimental behavior were consistently contrasted to formulation of advanced constitutive models SCLAY1S [Karstunen et al. 2005] and AniCreep [Yin et al. 2011]. Despite being among the most sophisticated constitutive models for representing effects of anisotropy, bonding and rate dependence of soft structured clays, formulation of the models still needs improvement. The dissertation contributes to research on soft structured clays in subsequent ways:

Effects of sensitivity and destructuration rate on compressibility and creep
A key research question was how to define and determine sensitivity of the specimen in consolidation test. Based on this study, appropriate definition of the specimen-specific sensitivity is that of ratio of vertical effective stresses carried by natural and reconstituted specimen at the same magnitude of specific volume, i.e. approach c in the thesis. The sensitivity interpretation approach was proven to be applicable for both oedometric and triaxial compression, including studying the changes in the sensitivity during testing. The proposed approach has also the advantage that it complies with the theoretical definition used for the concept of intrinsic yield surface [Gens and Nova 1993] adopted in advanced constitutive models SCLAY1S [Karstunen et al. 2005] and AniCreep [Yin et al. 2011].

The proposed interpretation of sensitivity enabled introduction of the concept of the destructuration curve, which allowed evaluating the rate of destructuration during consolidation. Above yield, high quality specimens were shown to be subjected to notably higher rates of destructuration compared to those experienced by poor quality specimens. Furthermore, the initial sensitivity was shown to be exponentially related to initial void ratio of saturated specimen, i.e. the amount of water the specimen contains. This finding was used to develop consistent approach for quantification of sample disturbance following sampling, independent of the testing conditions. The method, demonstrated successfully for the evaluated deposit, is based on w/γ, i.e. ratio of water content over bulk unit weight. The methodology enables to assess the quality of the samples before expensive and time-consuming testing. The differences in fundamental properties, such as specific gravity, require re-calibration of this metric for other Scandinavian clays.

Preconsolidation pressure and compressibility characteristics following yield were shown to be related to specimen quality and destructuration effects, as

was expected based on previous research findings. The magnitude of the stress ratio in consolidation was proven decisive for compressibility and destructuration response. The highest compressibility following yield was measured on high quality specimens consolidated at stress ratio corresponding to the estimated coefficient of earth pressure at rest. In loading at stress paths with stress-ratios that significantly differed from the effective stress conditions in-situ, the changes in soil structure were found to be considerable. This can be explained by re-arrangement of the initial anisotropic structure in order to comply with the conditions imposed by the stress ratio during the tests. Given the consolidation tests along constant stress ratio paths were made using small load increments, it was also feasible to identify bulk and shear moduli and their evolution during loading. Volumetric and shear resistances were found to be consistently related to the destructuration mechanism. These observations are in line with the SCLAY1S [Karstunen et al. 2005] model formulation.

Effects of sample disturbance and stress level on creep response were explained in detail. Peak magnitude of c_α was proven to be proportionally related to initial quality of the specimen, proving that the measured creep rates are largely a function of the amount of destructuration during the test. The commonly accepted paradigm of c_α/c_c being constant under conventional one dimensional consolidation conditions was proven wrong, confirming the findings in contemporary research. Analogously to 1D condition, creep and c_α/c_c response was interpreted under triaxial test conditions and proven to be related to specimen quality, consolidation stress ratio and load increment ratio. Most encouragingly, the intrinsic creep rates of Perniö clay in 1D and triaxial consolidation appear to be identical, which suggests that modelling creep, as done in the AniCreep model [Yin et al. 2011] is qualitatively appropriate.

The results suggest that the anisotropic consolidation response at yield is related to the sensitivity characteristics of the clay specimens. The numerous natural specimens were tested at identical test conditions at several radial stress paths. Yield surfaces representing poor quality specimens were less inclined and size-wise smaller than the surface representing the results from the specimens of the highest quality. The elliptic shape of the yield surface was directly related to initial sensitivity characteristics and the destructuration at certain radial stress path. The highest yield pressure was identified in consolidation tests at stress ratio conditions corresponding to those in situ. With offset of the test stress ratio conditions, resulting magnitude of yield descended. The highest yield pressure measured on specimens of poor quality reflected changes in stress conditions of the specimen as the result of stress release and specimen disturbance. Hence, the stress release and specimen disturbance may also affect the initial anisotropy of the sample, and not just reduce the amount of apparent bonding and sensitivity.

Strain path analyses were proven crucial for understanding effects of change in anisotropy. Provided that CAD tests along constant stress ratio paths were made using continuously loaded procedure, definition of stresses identifying maximum compression and shear resistance in reloading would be feasible. Following normalization with effective overburden, the parameters could be

used for definition of characteristic surfaces. Positioned within that of yield, the surfaces would coincide with the notable drop in the apparent moduli caused by destructuration. Consistently, deviator and mean isotropic stresses identifying limit stress state could be used to identify surface at limit state level. Thus, additionally to that at yield, specimen response in CAD test could be defined by surfaces characterising reloading and limit stress state response. The position and shape of the surfaces would provide additional data on destructuration and change in anisotropy caused by stress release, as well as that induced by stresses above yield.

Effects strain-rate on compressibility and undrained shear response

Effects of strain-rate on oedometric compressibility are commonly defined by considering rate dependency of the preconsolidation stress. Compression curves measured at various strain rates tend to collapse to one curve if normalised with the effective stresses at yield. However, difference in initial quality of the specimens affected performance of the normalization of the results. In this study, effects of strain-rate were evaluated at stresses characterising maximum bulk resistance in reloading, at yield, and that at limit stress level. Evaluated in semi-logarithmic stress ratio vs. strain-rate plane, the characteristic stresses were positioned on radial lines when related to strain-rate in compression. This result is in line with the validity of unique compression curve concept [Leroueil et al. 1985]. The approach revealed that the viscosity of the specimen is influenced by the initial quality, as well as the rate dependent destructuration process.

Approaches used for evaluation of the stress dependency of the slope in compression were shown to provide adequate basis for deriving concise conclusions on destructuration rate under CRS oedometric conditions. Additionally to the yield stress, the slope in compression was shown to be strain-rate dependent as well. Above yield, sensitive specimens compressed at high strain–rates exhibited relatively lower rates of destructuration due to degradation of apparent bonds, demonstrated by lower compressibility following the yield. Based on this, derivation of stiffnesses and preconsolidation pressure parameters from CRS results aiming settlement predictions of sensitive clays should be based on tests at low strain-rates.

Effects of strain-rate on one dimensional compressibility were clarified by defining destructuration rate in reloading. Namely, interpretation of the stress dependency of the compression modulus was enhanced by definition of strain-rate effects on response in reloading using a parabola and destructuration rate coefficient. The extent of destructuration in reloading was shown to be reciprocal to strain-rate, manifested by the highest rate of compression modulus decline prior yield, i.e. the lowest values of destructuration rate coefficient. Thus, the initial structural characteristics of the specimens loaded to yield at the lowest strain-rate were the most preserved.

The mobilized undrained shear resistance and strength were found to be influenced both by the strain-rate and destructuration process. In tests onset at identical consolidation conditions, apparent strength and extent of softening

were proportional to strain-rate. Compared to their natural counterparts, reconstituted specimens exhibited lower apparent strength and reduced extent of softening. Considering both natural and reconstituted specimens, in tests at low radial pressure there was not much evidence of strain softening. Natural specimens consolidated far beyond effective overburden stress level were shown to exhibit reduced values of axial strain at failure, while those measured on reconstituted specimens were overall the lowest. Thus, instead of strain at failure, specimen disturbance in undrained shear should be evaluated based on magnitude of void ratio in shear and response in softening.

Effects of strain-rate on pore pressure response were proven decisive for undrained shear response. Target pore pressure level in tests on natural specimens was related to magnitude of the radial pressure in consolidation. Specimens compressed at the highest strain-rate reached target pore pressure level in significantly shorter period of time. In contrast, at low strain-rates, specimens exhibited lower rate of pore pressure buildup. Thus, if the purpose of the testing is to reach condition of pore pressures levelling off, it is preferred to use rather high strain-rates combined with low confining pressures. The tests under such preferences involve shearing to very high axial strain levels.

On the basis of characteristic points, an approach for defining strain-rate effects on undrained shear response was introduced. Effects of strain-rate were defined at characteristic points, coinciding with the levels of maximum mean effective stress and maximum deviator stress, considering also the corresponding stress ratio values. Besides being influenced by rate of undrained shearing, the characteristic conditions were found to be consistently related to the stress ratio and the radial pressure in consolidation, i.e. the test parameters that affect destructuration.

Specimens subjected to high destructuration level during the consolidation phase were shown to exhibit reduced undrained shear resistance. Following normalization of stress paths with maximum vertical effective stress in consolidation, i.e. in q/σ'_{1C} vs. p'/σ'_{1C} plane, soft structured Perniö clay in undrained shear exhibited failure envelopes whose position depended upon the extent of destructuration in consolidation. Specimens with quality representative of that in situ exhibited high shear resistance marked by steep failure envelope. Specimens consolidated well beyond the effective overburden stress level showed reduced shear resistance reflecting higher extent of destructuration. Considering specimens of comparable structural qualities, stress paths in tests at high strain-rates reached failure envelope at higher levels of mean effective and deviator stress. Opposite was valid in tests at low strain-rates. All this demonstrates how intricately interlinked the destructuration and rate-effects are. Following work should focus on using the data created by this project in advanced model simulations, to see if quantitative rather than qualitative predictions of the mobilised undrained strength can be made.

In conclusion, the comprehensive experimental programme highlights a number of issues related to the analyses and constitutive modelling of the rate-dependent response of soft structured clays. To account for rate dependent effects on compressibility and apparent strength, it is important to consider

features of sample disturbance, geological history as well as consolidation stress history. The latter refers to both construction related consolidation history, such as loading by old embankment in the case of Perniö, and the consolidation history during the actual tests conducted in laboratory. So not only is sampling important, but equally important is to appreciate that the clay structure can be disturbed in specimen preparation, as well as by the stress paths imposed on the specimen during testing. The latter makes studying the effects of structure and sample disturbance on compressibility and creep response particularly challenging.

To study sample disturbance and its effects, the variability due to different soil layers having different geological history need to be first eliminated. In the case of Perniö, this meant dividing the deposit into three main representative layers. Within the layers, there was evidence of natural variability, combined with sampling and testing induced variability. Thus the next step was to separate natural variation due to geological origin from the apparent variation due to sample disturbance. The natural variability, manifested by scatter of the results obtained on high quality specimens, appeared to be significantly smaller than the variability due to sample disturbance. The results thus revealed that what commonly is perceived as natural variability, is obscured by variability in the measured response due to sample disturbance. In reality, geotechnical design based on the highest quality specimens is rarity. Indeed, usage of constitutive models in geotechnical engineering is often based on parameters interpreted from laboratory tests performed on relatively disturbed specimens such as those sampled by NGI 54 and STII. Without clarity in definition of the effects of sample disturbance in the formulation of the constitutive models, i.e. in a form of an input parameter, outcomes of the geotechnical analyses can be unreliable. The data from this study can be used in the future to understand the relationship for the latter phenomena, as for the first time there is enough of high quality data to represent natural variation separate from the scatter due to sampling and testing induced variability.

Much more challenging than dealing with variation in the context above is to ensure that the stiffnesses and the apparent strengths that are measured in the laboratory, using high quality specimens, actually correspond to the in situ stress conditions. Hence, the starting point for any triaxial test for practical purposes should be consolidating the specimen to its in situ conditions. The recommended consolidation procedure is that of continuous loading at the lowest rates, ensuring negligible pore pressures and least impact on structural characteristics in reloading. The method proposed for assessing specimen-specific sensitivity during consolidation enables to assess sample quality during the tests. Once adequately reconsolidated, the specimens can be subjected to any stress/strain probing and/or shearing to failure from that point. This is in contrast to the majority of the advice given for users of standard constitutive models available in geotechnical FE codes. In order to account for the evolution of anisotropy during construction and consolidation, it would be advisable to perform shearing of a pair of specimens in triaxial compression and triaxial extension. To account for the destructuration effects on shear strength, addi-

tional pair of triaxial tests is advised by considering specimens consolidated well beyond effective overburden stress level. The rate effects in triaxial shearing can be evaluated by using an advanced rate dependent constitutive model in the interpretation of the results. To account for creep and settlement predictions, incrementally loaded oedometer tests are indispensable. If based on CRS results, stiffnesses and preconsolidation pressure parameters should strictly consider test at very low strain-rates only. Finally, extra care should be taken in the process of specimen preparation for both oedometer and triaxial testing, as this process can introduce significant sample disturbance which was evidenced in the results presented in the thesis.

References

Alén, C. (2009). What can we learn from CRS test? *3rd CREBS Workshop-Creep Behavior of Soft Soils*, 3-4 June, 2009, Gothenborg, Sweeden.

Andresen, A., Bjerrum, L., DiBiago, E. & Kjærnsli, B. (1957). Triaxial equipment developed at the Norwegian Geotechnical Institute. *Norwegian Geotechnical Institute,* Publication No. 21, pp. 1-31. Oslo: NGI.

Andresen, A. & Kolstad, P. (1980). The NGI 54-mm samplers for undisturbed sampling of clays and representative sampling of coarser material. *Norwegian Geotechnical Institute,* Publication No. 130, pp. 1-9. Oslo: NGI.

Atterberg, A. (1911). Lerornas förhållande til vatten, deras plasticitetsgränser och plasticitetsgrader. *Kungliga Lantbruksakademiens Handlingar och Tidskrift*, **50,** No. 2, 132-158.

Åhnberg, H. (2006). Strength of stabilised soils. PhD thesis, 80 p., *Swedish Deep Stabilization Research Centre*, Report 16, Linköping, Sweden.

Baligh, M. M., Azzouz, A. S. & Chin, C. T. (1987). Disturbances due to ideal tube sampling. *J. Geotech. Engng. Div., Am. Soc. Civ. Engrs.* **113**, No. 7, 739-757.

Battelino, D. (1973). Oedometer testing of viscous soil. *Proc. 8th Int. Conf. Soil Mech. Fnd. Engng. Moscow* **1,** No.1, 25-30.

Berre, T., Schjetne, K. & Sollie, S. (1969). Sampling disturbance of soft marine clays. *Proc. 7th Int. Conf. Soil Mech. Fnd. Engng. Mexico City*, Speciality Session I, 21-24.

Bishop, A. W. & Henkel, D. J. (1957). *The measurement of soil properties in the triaxial test.* 190 p. London: Edward Arnold.

Bishop, A. W., Webb, D. L., Lewin, P. I. (1965). Undisturbed samples of London clay from the Ashford Common shaft: strength-effective stress relationships. *Géotechnique*, **15**, No.1, 1-31.

Bjerrum, L. (1954). Geotechnical properties of Norwegian marine clays. *Geotechnique* **4**, No. 2, 49-69.

Bjerrum, L. (1967). The Seventh Rankine Lecture. Engineering geology of Norwegian normally consolidated marine clays as related to settlements of buildings. *Géotechnique* **17,** No. 2, 81-118.

Bjerrum, L. (1973). Problems of soil mechanics and construction on soft clays. *Proc. 8th Int. Conf. Soil Mech. Fnd. Engng. Moscow* **3,** State of the Art Report to Session IV, 111-159.

Burland, J. B. (1990). On the compressibility and shear strength of natural clays. *Géotechnique* **40,** No. 3, 329–378.

Brand, E. W. & Brenner, R. P. (eds.) (1981). *Soft clay engineering*. 779 p. Amsterdam: Elsevier.

Casagrande, A. (1932). Research on the Atterberg limits of soils. *Public Roads* **8**, 121-130.

Casagrande, A. (1936). Determination of the preconsolidation load and its practical significance. *Proc. 1st Int. Conf. Soil Mech. Found. Engng., Cambridge* **3**, 60–64.

Claeson, P. (2003). Long term settlements in soft clays. PhD thesis, 195 p., *Chalmers University of Technology*, Gothenburg, Sweeden.

Clausen, C.-J. F., Graham, J. & Wood, D. M. (1985). Yielding in soft clay at Mastemyr, Norway. *Géotechnique* **34,** No. 4, 581-600.

Clayton, C. R. I., Matthews, M. C. & Simons, N. E. (1982). *Site investigation,* second edition. 424 p. New York: Halsted Press.

Crawford, C. B. (1964a). Resistance of soil structure to consolidation. *Can. Geotech. J.* **2,** No. 2, 90-115.

Crawford, C. B. (1964). Interpretation of consolidation tests. *J. Soil Mech. Fdns. Div., Am. Soc. Civ. Engrs.* **90,** No. 5, 87-102.

Crawford, C. B. (1968). Quick clays of eastern Canada. *Engng. Geology* **2**, No. 4, 239-265.

Crawford, C. B. (1986). State of the Art: Evaluation and interpretation of soil consolidation tests. *Consolidation of soils; testing and evaluation*, Young & Townsend (eds.). ASTM Special Technical Publication 892, pp. 71-103. Philadelphia: American Society for Testing and Materials.

Dafalias, Y. F. (1986). An anisotropic critical state soil plasticity model. *Mechanics Research Communications* **13**, No. 6, 341-347.

Dafalias, Y. F. & Manzari, M. T. (2006). SANICLAY: simple anisotropic clay plasticity model. *Int. J. Num. Analytical Meth. Geomech.* **30**, No.12, 1231-1257.

Den Haan, E. J. (2001). Sample disturbance of a soft organic Dutch clay. *Strategic Research Department GeoDelft*, Research report, 50 p. Delft: GeoDelft.

Degago, S. A., Grimstad, G., Jostad, P. H., Nordal, S. & Olsson, M. (2011). Use and misuse of isotache concept with respect to creep hypotheses A and B. *Géotechnique* **61**, No. 10, 897 –908.

Fearon, R. E. & Coop, M. R. (2000). Reconstitution: what makes an appropriate reference material? *Géotechnique* **50**, No. 4, 471-477.

Gardemeister, R. (1975). On engineering-geological properties of fine-grained sediment in Finland. PhD thesis, 91 p., *Tech. Research Centre of Finland,* Building technology and community development, Publication 9, Helsinki, Finland.

Gens, A. & Nova, R. (1993). Conceptual bases for a constitutive model for bonded soils and weak rocks. *Int. Symp. Hard soils-soft rocks*, Athens, 485-494.

Germaine, J. T. & Ladd, C. C. (1988). Triaxial testing of saturated cohesive materials. *Advanced triaxial testing of soil and rock*, Donaghe et al. (eds.). ASTM Special Technical Publication 977, pp. 421-459. Philadelphia: American Society for Testing and Materials.

Graham, J., Crooks, J. H. A. & Bell, A. L. (1983). Time effects on the stress strain behavior of natural soft clays. *Géotechnique* **33,** No. 3, 327-340.

Graham, J. (2006). The 2003 R. M. Hardy Lecture: Soil parameters for numerical analysis in clay. *Can. Geotech. J.* **43**, 187-209.

Hamilton, J. J. & Crawford, C. B. (1959). Improved determination of preconsolidation pressure of a sensitive clay. ASTM Special Technical Publication 254, pp. 254-271. Philadelphia: American Society for Testing and Materials.

Hawley, J. G. & Borin, D. L. (1973). A unified theory for consolidation of clays. *Proc. 8th Inter. Conf. Soil Mech. Fnd. Engng. Moscow* **1,** No. 3, 107-119.

Head, K. H. (1986). *Manual of soil laboratory testing*. Vol. 3: Effective stress tests. 1238 p. London: ELE International Limited.

Hight, D. W., Jardine, R. J. & Gens, A. (1987). *The Behavior of soft clays*. Chapter 2, Embankments on soft clays, pp. 33-157. Athens: Public Works Research Center of Greece.

Hinchberger, S. D. (1996). The behavior of reinforced and unreinforced embankments on soft rate sensitive foundation soils. PhD thesis, 537 p., *University of Western Ontario*, London, Ontario, Canada.

Hong, Z., Yin, J. & Cui, Y (2010). Compression behavior of reconstituted soils at high initial water contents. *Géotechnique* **60**, No. 9, 691-700.

Hong, Z.-S., Zeng, L.-L, Cui, Y.-J., Cai, Y.-Q. & Lin, C. (2012). Compression behavior of natural and reconstituted clays. *Géotechnique* **62**, No. 4, 291-301.

Hvorslev, M. J. (1949). *Subsurface exploration and sampling of soils for civil engineering purposes.* Report on the Research Project of the Committee on Sampling and Testing, Soil Mech. Fnd. Div., Am. Soc. Civ. Engrs., 521 p. Mississipi: Waterways Experiment Station, Vicksburg.

Jakobson, B. (1954). Influence of sampler type and testing method on shear strength of clay samples. *Roy. Swedish Geotech. Inst. Proc.* No. 8, 1-59. Stockholm: KTH.

Jaky, J. (1944). The Coefficient of Earth Pressure at Rest, *J. Soc. Hungarian Arch. & Eng*., 355–358.

Janbu, N. (1963). Soil compressibility as determined by oedometer and triaxial tests. *Proc. 2nd Eur. Conf. Soil Mech. Fnd. Engng, Wiesbaden* **1,** 19-25.

Janbu, N. (1967). Settlement calculations based on the tangent modulus concept. Lectures given at the Moscow State University. *NTH Publication*, Bulletin 2, Three lectures; 20p+17 p+56p. Trondheim: NTNU.

Janbu, N. (1969). The resistance concept applied to deformations of soils. *Proc. 7th Int. Conf. Soil Mech. Fnd. Engng. Mexico City* **1,** 191-196.

Janbu, N., Tokheim, O. & Senneset, K. (1981). Consolidation tests with continuous loading. *Proc. 10th Int. Conf. Soil Mech. Fnd. Engng. Stockholm* **1,** 645-654.

Janbu, N. (1998). Sediment deformations-A classical approach to stress-strain-time behavior of granular media as developed at NTH over a 50 year period. *NTNU Publication*, Bulletin 35, pp. 1-86. Trondheim: NTNU.

Kallstenius, T. (1971). Secondary mechanical disturbance. Effects in cohesive soil samples. *Proc. 4th Asian Conf. Soil Mech. Fnd. Engng., Bangkok*, Speciality Session on Quality in Soil Sampling, 30-39.

Karstunen, M. & Koskinen, M. (2004). Undrained shearing of soft natural clays. *Proc. 9th International Symposium on Numerical Models in Geomechanics (NUMOG IX),* Pande & Pietruszczak (eds.), 25-27 August 2004, Ottawa, Canada, pp. 173-179. London: Taylor & Francis Group.

Karstunen, M., Krenn, H., Wheeler, S., Koskinen, M., Zentar, R. (2005). Effect of anisotropy and destructuration on the behavior of Murro test embankment. *Int. J. Geomech., Am. Soc. Civ. Engrs.* **5**, No. 2, 87-97.

Karstunen, M. & Koskinen, M. (2008a). Plastic anisotropy of soft reconstituted clays. *Can. Geotech. J.* **45,** No. 3, 314-328.

Karstunen, M., Yin, Z. Y., Koskinen, M., Leoni, M. & Vermeer, P. A (2008b). Some recent developments in constitutive modelling of soft clays. *12th Int. Conf. of Int. Ass. for Computer Methods and Advances in Geomechanics (IACMAG)*, 1st-6th October, 2008. Goa, India. pp. 966-975.

Kenney, T. C. (1976). Formation and geotechnical characteristics of glacial-lake varved soils. *Norwegian Geotechnical Institute,* Laurits Bjerrum Mem. Vol., Janbu, Jostad & Kjærnsli (eds.), pp.15-39. Oslo: NGI.

Kobayashi, M., Furudoi, T., Suzuki, S., Watabe, Y. (2005). Modeling of consolidation characteristics of clays for settlement prediction of Kansai International Airport. *Proc. Symp. Geotech. Aspects Kansai Int. Airport*, 65-76.

Kolisoja, P. (1990). Developments in laboratory automation. Licentiate thesis, 197 p., *Tampere University of Technology*, Tampere, Finland.

Kolisoja, P., Sahi, K. & Hartikainen, J. (1987). Automated oedometer device. *Proc. 9th Eur. Conf. Soil Mech. Fun. Engng. Dublin*, 67-70.

Kolisoja, P. & Halkola, H. (1988). Compressibility determination with an automatic oedometer device. *Proc. 6th Baltic Soil Mech. Fun. Engng. Tallin.*

Kolisoja, P., Sahi, K. & Hartikainen, J. (1989). An automatic triaxial-oedometer device. *Proc. 12th Int. Conf. Soil Mech. Fnd. Engng., Rio de Janeiro* **1**, 61-64.

Korhonen, K. H. & Lojander, M. (1987). Yielding of Perno clay. *Proc. Const. Laws Engng. Materials: Theory and Applications*, Desai et al. (eds.), Vol. 2. pp. 1249-1255. Amsterdam: Elsevier.

Koskinen, M., Karstunen, M. & Wheeler, S. J. (2002). Modelling destructuration and anisotropy of a natural soft clay. *Proc. 5th Eur. Conf. Num. Meth. in Geotech. Engng. (NUMGE)*, Maestat (ed.). 4-6 September 2002, Paris, France. pp. 11-19. Paris: Presses de I´ENPC/LCPS.

Koskinen, M., Karstunen, M. & Lojander, M. (2003). Yielding of "Ideal" and Natural Anisotropic Clays. *Proc. Int. Workshop on Geotechnics of Soft Soils- Theory and Practice*,17th-19th September 2003, Noordwijkerhout, The Netherlands, pp. 197-204. Essen: Verlag Glückauf Essen.

Koskinen, M. & Karstunen, M. (2004). The effect of structure on the compressibility of Finnish clays. *Proc. 14th Nordic Geotechnical Meeting (NGM04),* 19th-21st May 2004, Ystad, Sweden, Vol. 1, A11–A22. Swedish Geotechnical Society: Report 3:2004.

Koskinen, M. (2014). Plastic anisotropy and destructuration of soft Finnish clays. PhD thesis, 409 p., *Aalto University,* Helsinki, Finland.

Kuwano, J., Katagiri, M., Kita, K., Nakano. M. & Kuwano R. (1999). A review of Japanese strandards for laboratory shear test. *Inter. workshop on recent advances related to terms of reference of TC-29 of ISSMGE,* September 1999, Torino, Italy, pp. 1-12.

Ladd, C. C. (1971). Settlement analysis of cohesive soil. *Massachusetts Institute of Technology*, Department of Civil Engineering, Research report R71-2.

Ladd, C. C. (1972). Clay behavior. MIT Summer school.

Lambe, T. W. & Whitman, R. V. (1969). *Soil Mechanics*. 563 p. New York: John Wiley & Sons.

Lancellotta, R. (1995). *Geotechnical Engineering*. 436 p. Rotterdam: Balkema.

Landva, A. (1964). Equipment for cutting and mounting undisturbed specimens of clay in testing devices. *Norwegian Geotechnical Institute,* Publication No. 56, pp. 1-5. Oslo: NGI.

La Rochelle, P., Sarrailh, J., Tavenas, F., Roy, M. & Leroueil, S. (1981). Causes of sampling disturbance and design of a new sampler for sensitive soils. *Can. Geotech. J.* **18**, No. 1, 52-66.

Larsson, R. & Sällfors, G. (1986). Automatic continuous consolidation testing in Sweden. *Consolidation of soils; testing and evaluation*, Young & Townsend (eds.). ASTM Special Technical Publication 892, pp. 299-328. Philadelphia: American Society for Testing and Materials.

Larsson, R., Bengtsson, P-E. & Eriksson, L. (1997). Prediction of settlements of embankments on soft, fine-grained soils. Calculation of settlements and their course with time, *Swedish Geotechnical Institute,* Information No. 13E, 52 p. Linköping: SGI.

Länsivaara, T. (1993). Stress path testing with an automated triaxial testing device. *Proc. 7th Young Geotech. Enging. Conf.,* Böblingen, Germany.

Lefebvre, G. & Poulin, C. (1979). A new method of sampling in sensitive clay. *Can. Geotech. J.* **16**, No.1, 226-233.

Lefebvre, G., Ladd, C. C., Pare, J-J. (1988). Comparison of field vane and laboratory undrained shear strength in soft sensitive clays. *Vane Shear Testing in Soils: Field and lab. stud.,* Richards (eds.). ASTM Special Technical Publication 1014, pp. 233-246. Philadelphia: American Society for Testing and Materials.

Lehtonen, V. (2011). Instrumentation and analysis of a railway embankment failure experiment. *Finnish Transportation Agency,* Research report 29/2011, 62 p. Helsinki: Liikennevirasto.

Leonards, G. A. & Girault, P. (1961). A study of one-dimensional consolidation test. *Proc. 5th Int. Conf. Soil Mech. Fnd. Engng. Paris* **1,** 213-218.

Leroueil, S., Tavenas, F., Brucy, F., La Rochelle, P. & Roy, M. (1979). Behavior of destructured natural clays. *J. Geotech. Engng. Div., Am. Soc. Civ. Engrs.* **105,** No. 6, 759-778.

Leroueil, S., Samson, L. & Bozozuk, M. (1983). Laboratory and field determination of preconsolidation pressure at Gloucester. *Can. Geotech. J.* **20,** No. 3, 477-490.

Leroueil, S., Kabbaj, M., Tavenas, F. & Bouchard, R. (1985). Stress-strain-strain rate relation for the compressibility of sensitive natural clays. *Géotechnique* **35**, No. 2, 159-180.

Leroueil, S., Tavenas, F., La Rochelle, P. & Tremblay, M. (1988a). Influence of filter paper and leakage on triaxial testing. *Advanced triaxial testing of soil and rock*, Donaghe et al. (eds.). ASTM Special Technical Publication 977, pp. 189-201. Philadelphia: American Society for Testing and Materials.

Leroueil, S., Kabbaj, M., & Tavenas, F. (1988b). Study of the validity of a σ_v'-ε_v-$\dot{\varepsilon}_v$ model in in situ conditions. Soils & Fdns. **28**, No. 3, 13-25.

Leroueil, S. (1988). Tenth Canadian Geotechnical Colloquium: Recent developments in consolidation of natural clays. *Can. Geotech. J.* **25**, No.1, 85-107.

Leroueil, S. & Vaughan, P. R. (1990). The general and congruent effects of structure in natural soils and weak rocks. *Géotechnique* **40**, No.3, 467–488.

Leroueil, S., Magnan, J.-P. & Tavenas, F. (1990). *Embankments on soft clays.* 360 p. New York, London: Ellis Horwood.

Leroueil, S. Jamiolkowski, M. (1991). Exploration of soft soil and determination of design parameters. *Proc. Geo-Coast '91*, Yokohama, Japan, Vol. 2, pp. 969-998. Port & Harbour Research Institute.

Leroueil, S. (1997). Geotechnical characteristics of eastern Canadian clays. *Proc. Int. Symp. Characterization of Soft Marine Clays-Bothkennar, Drammen, Quebec and Ariake Clays*, Tsuchida & Nakase (eds.), 26th-28th February 1999, Yokosuka, Japan, pp. 3–32. Rotterdam: Balkema.

Leroueil, S. & Hight, D.W. (2003). Characteriation of soils for engineering purposes. *Characterization and engineering properties of natural soils*, Tan et al. (eds.), Vol. 2, pp. 255-360. Lisse: Swets & Zeitlinger.

Leroueil, S. & Hight, D. W. (2003b). Behavior and properties of natural soils and soft rocks. *Characterization and engineering properties of natural soils*, Tan et al. (eds.), Vol. 1, pp. 29-254. Lisse: Swets & Zeitlinger.

Leroueil, S. (2006). The isotache approach. Where are we 50 years after its development by Professor Šuklje? *Proc.13th Danube Eur. Conf. Geotech. Engng. Ljubljana* **1,** 55–58.

L'Heureux, J. S., Locat, A., Leroueil, S., Demers, D. & Locat, J. (eds.) (2014). Landslides in Sensitive Clays - From Geosciences to Risk Management. 418 p. New York: Springer.

Locat, J. & Demers, D. (1988). Viscosity, yield stress, remoulded strength, and liquidity index relationships for sensitive clays. *Can. Geotech. J.* **25**, No.4, 799-806.

Lunne, T., Berre, T. & Strandvik, S. (1997). Sample disturbance effects in soft low plasticity Norwegian clay. *Proc. Conf. Recent Developments in Soil and Pavement Mechanics,* Rio de Janeiro, Brazil, 81-102.

Lunne, T., Berre, T., Andersen, K.H., Strandvik, S., Sjursen, M. (2006). Effects of sample disturbance and consolidation procedures on measured shear strength of soft marine Norwegian clays. *Can. Geotech. J.* **43**, No.7, 726-750.

Mansikkamäki, J., Lehtonen, V., Länsivaara, T. & Luomala, H. (2011). Full scale failure test on a railway embankment; extensive instrumentation and real time monitoring. *Proc. 15th Eur. Conf. Soil Mech. Geotech. Engng., Athens* **2**, 1165-1170.

Mansikkamäki, J. (2015).Effective stress finite element analysis of an old railway embankment on soft clay. PhD thesis, 165 p., *Tampere University of Technology*, Tampere, Finland.

Marques, M.E.S. (1996). *Influencia da velocidade de deformacao O e da temperature no adensamento de argilas naturais.* M.Sc. thesis, Ressearch performed at Universite Laval, Ste-Foy, Canada in cooperation with COPPE-Federal University of Rio de Janeiro, Brazil.

Mesri, G. & Godlewski, P. M. (1977). Time and stress compressibility interrelationship. *J. Geotech. Engng. Div., Am. Soc. Civ. Engrs.* **103**, GT5, 417-430.

Mesri, G. & Castro, A. (1987). The C_α/C_c concept and K_o during secondary compression. *J. Geotech. Engng. Div., Am. Soc. Civ. Engrs.* **113,** No.3, 230-247.

Mesri, G., Stark, T.D., Ajlouni, M. A. & Chen, C. S. (1997). Secondary compression of peat with or without surcharging. *J.Geotech. Geoenviron. Engng., Am. Soc. Civ. Engrs.* **123,** No. 5, 411-421.

Mitchell, J. K. (1976). *Fundamentals of soil behavior.* 422 p. New York: John Wiley & Sons.

Nash, D. F. T. (2010). Influence of destructuration of soft clay on time dependent settlements. *Proc. 7th Eur. Conf. Num. Meth. in Geotech. Engng. (NUMGE)*, Benz & Nordal (eds.), 2nd - 4th June 2010, Trondheim, Norway. pp. 75-80. London: Taylor and Francis group.

Näätänen, A. & Lojander, M. (2000). Modelling of anisotropy of Finnish clays. *Proc. 7th Finnish Symp. Mech.,* pp. 589-598. Tampere University of Technology.

Osterman, J. (1964). Studies on the properties and formation of quick clays. *Swedish Geotechnical Institute,* Reprints and preliminary reports, No. 8, pp. 87-108. Stockholm: SGI.

Perzyna, P. (1963). The constitutive equations for work-hardening and rate sensitive plastic materials. *Proc. Vibration Problems*, Warsaw, Vol. 4, No 3. pp. 281–290.

Potts, D. M. & Zdravković, L. (1999). *Finite element analysis in geotechnical engineering-theory,* Vol.1, 440 p. London: Thomas Telford Limited,

Rankka, K., Andersson-Sköld, Y., Hulten, C., Larsson, R., Leroux, V. & Dahlin, T. (2004). Quick clay in Sweden. *Swedish Geotechnical Institute,* Report 65, 145 p. Linköping: SGI.

Rendulic, L. (1937). Ein Grundgesetz der Tonmechanik und sein experimenteller Beweis. *Der Bauingenieur* **18,** 459-467.

Rosenqvist, I. T. (1946). Om leirers kvikkagtighet. *Norvegian Public Road Administration,* Veglaboratoriet Meddelelse Nr 4, 29–36. Oslo: Statens Vegvesen.

Rosenqvist, I. T. (1953). Considerations on the sensitivity of Norwegian quick-clays. *Géotechnique* **3**, No.5, 195-200.

Rosenqvist, I. T. (1955). Investigations in the clay-electrolyte-water system. *Norwegian Geotechnical Institute,* Publication No. 9, 125 p. Oslo: NGI.

Rosenqvist, I. T. (1978). A general theory for the sensitivity of clays. *Proc. Interdiscip. Conf. Univ. Luleå,* Permont Press.

Roscoe, K. H., Schofield, A. N., & Wroth, C. P. (1958). On the yielding of soils, *Géotechnique,* **8**, No.1, 22-53.

Roscoe, K. H. & Burland, J. B. (1968). On the generalized behavior of wet clay. *Engineering Plasticity*, Heyman and Leckie (eds.), pp. 535-609. Cambridge: Cambridge University Press.

Samuels, S. G. (1975). Some properties of the Gault Clay from the Ely-Ouse Essex water tunnel. *Géotechnique* **25**, No. 2, 239-264.

Sandbaekken, G., Berre, T. & Lacasse, S. (1986). Oedometer testing at the Norwegian Geotechnical Institute. *Consolidation of soils; testing and evaluation*, Young & Townsend (eds.). ASTM Special Technical Publication 892, pp. 229-353. Philadelphia: American Society for Testing and Materials.

Sällfors, G. (1975). Preconsolidation pressure of soft, high-plastic clays. PhD thesis, 231 p., *Chalmers University of Technology,* Gothenburg, Sweeden.

Schofield, A. N. & Wroth, C. P. (1968). *Critical State Soil Mechanics*. 310 p. London: McGraw-Hill.

Shibata, T. & Nishihara, A. (1999). Mechanical behavior of remoulded reconstituted clays related to physical properties of soils. *Proc. Int. Symp. Characterization of Soft Marine Clays-Bothkennar, Drammen, Quebec and Ariake Clays*, Tsuchida & Nakase (eds.), 26th-28th February 1999, Yokosuka, Japan, pp. 133-144. Rotterdam: Balkema.

Skempton, A. W. & Northey, R. D. (1952). The sensitivity of clays. *Géotechnique* **3**, No.1, 30-53.

Skempton, A. W. (1953). The colloidal activity of clays. *Proc. 3rd Int. Conf. Soil Mech. Fnd. Engng. Zurich* ***1,*** *57-61.*

Skempton, A. W. (1967). The consolidation of clays by gravitational compaction. *Quarterly Journal of the Geological Society,* **125**, 373-411.

Söderblom, R. (1969). Salt in Swedish clays and its importance for quick clay formation. *Swedish Geotechnical Institute,* Proc. No. 22, 63 p. Stockholm: SGI.

Šuklje, L. (1957). The analysis of the consolidation process by the isotache method. *Proc. 4th Int. Conf. Soil Mech. Fnd. Engng, London* **1,** 200-206.

Talme, O. (1968). Clay sensitivity and chemical stabilisation. *National Swedish Institute for Building Research,* Rapport 56. Stockholm: Byggforskningsrådet.

Tanaka, H. (2000). Sample quality of cohesive soils: Lessons from three sites, Ariake, Bothkennar and Drammen. *Soils and Fdns*. **40,** No. 4, 57-74.

Tavenas, F. & Leroueil, S. (1977). Effects of stresses and time on yielding of clays. *Proc. 9th Int. Conf. Soil Mech. Fnd. Engng., Tokyo* **1,** 319-326.

Tavenas, F., Blanchet, R., Garneau, R. & Leroueil, S. (1978). The stability of stage-constructed embankments on soft clays. *Can. Geotech. J.* **15,** No. 2, 283-305.

Tavenas, F. & Leroueil, S. (1979). Clay behavior and the selection of design parameters. *Proc 8th Eur. Conf. Soil Mech. Fnd. Engng. London* **1,** 281-291.

Tavenas, F. (1981). Some aspects of clay behavior and their consequences on modelling techniques. *ASTM Special Technical Publication* 740, pp. 667-677. Philadelphia: American Society for Testing and Materials.

Tavenas, F. & Leroueil, S. (1985). Disscusion. *Proc. 11th Int. Conf. Soil Mech. Fnd. Engng., San Francisco* **5**, 2693-2694.

Tavenas, F. & Leroueil, S. (1987). State of the art on laboratory and in situ stress-strain-time behavior of soft clays. *Int. Symp. Geotech. Engng. Soft Soils*, Mexico City **2**, 1-46.

Taylor, D. W. (1942). Research on consolidation of clays. *Massachusetts Institute of Technology,* Department of Civil and Sanitary Engineering, Publ. Serial 82, 147 p.

Terzaghi, K. (1925). Settlement and consolidation of clay. *Engineering News-Record*, 874-878.

Terzaghi, K. (1936). Stability of slopes of natural clays. *Proc. 1st Int. Conf. Soil Mech. Fnd. Engng. Harvard* **1**, 161-165. Cambridge, Mass: Harvard University Graduate School of Engineering.

Terzaghi, K. (1944). Ends and means in soil mechanics. *Grad. School Eng. Publ.* No. 402, Harvard University.

Thakur, V., Oset, O., Degago, S. A., Berg, P. O., Aabøe, R., Wiig, T., Elisabeth, E. D., Lyche, E., Sæter, M. B. & Robsrud, A. (2011). A critical appraisal on the definition of Brittle clays. *Proc. 16th Nordic Geotechnical Meeting (NGM12),* 9th-12th May 2012, Copenhagen, Denmark, Vol. 1, pp. 451-462. London: Taylor & Francis Group.

Tokheim, O. & Janbu, N. (1976). A continuous consolidation test. Internal report, *NTH Publication*, Bulletin 9, pp. 1-31.

Torrance, J. K. (1974). A laboratory investigation of the effect of leaching on the compressibility and shear strength of Norwegian marine clays. *Géotechnique* **24**, No. 2, 155-173.

Torrance, J. K. (1979). Post depositional changes in the pore water chemistry of the sensitive marine clays of the Otawa area, Eastern Canada. *Engng. Geology* **14**, No. 2-3, 135-147.

Torrance, J. K. (1983). Towards a general model of quick clay development. *Sedimentology* **30**, No. 4, 547-555.

Vaid, Y. P. & Campanella, R. G. (1977). Time-dependent behavior of undisturbed clay. *J. Geotech. Engng Div., Am. Soc. Civ. Engrs.* **103,** No.7, 693-709.

Yin, Z. Y., Karstunen, M., Chang, C. S., Koskinen, M. & Lojander, M. (2011). Modeling time-dependent behavior of soft sensitive clay. *J. Geotech. Geoenviron. Engng., Am. Soc. Civ. Engrs.* **137,** No. 11, 1103-1113.

Watabe, Y., Udaka, K., Nakatani, Y. & Leroueil, S. (2012). Long term consolidation behavior interpreted with isotache concept for worldwide clays. *Soils Fdns* **52,** No. 3, 449-467.

Watabe, Y. & Leroueil, S. (2012). Modelling and implementation of isotache concept for long-term consolidation behavior. *Int. J. Geomech.* **15**, No.5.

Wheeler, S. J., Näätänen, A., Karstunen, M. & Lojander, M. (2003). An anisotropic elastoplastic model for soft clays. *Can. Geotech. J.,* **40**, No. 2, 403-418.

Whittle, A. J. & Kavvadas, M. J. (1994). Formulation of MIT-E3 constitutive model for overconsolidated clays. *J. Geotech. Engng., Am. Soc. Civ. Engrs.* **120**, No. 1, 173-198.

Wroth, C. P. & Wood, D., M. (1978). The correlation of index properties with some basic engineering properties of soils. *Can. Geotech. J.* **15**, No. 2, 137-145.

Finnish Standards: Geotechnical Investigation and Testing. Sampling Methods and Groundwater Measurements. Part 1. Technical Principles for Execution, SFS-EN ISO 22475-1:2006E, 120 p.

ISO 14688-2:2004 Geotechnical investigation and testing, Identification and classification of soil, Part 2: Principles for a classification.

Appendices

Appendix 1:

Maps of the Perniö sampling site.

Appendix 2:

Plan view of the Perniö embankment and location of cross sections: A-A', B-B', C-C', D-D', E-E', F-F'.

Appendix 3:

Cross sections of the Perniö embankment: A-A', B-B', C-C', D-D', E-E', F-F'.

Appendix 4:

GPS coordinates of the sampling profiles.

Appendix 1

Maps of the Perniö sampling site.

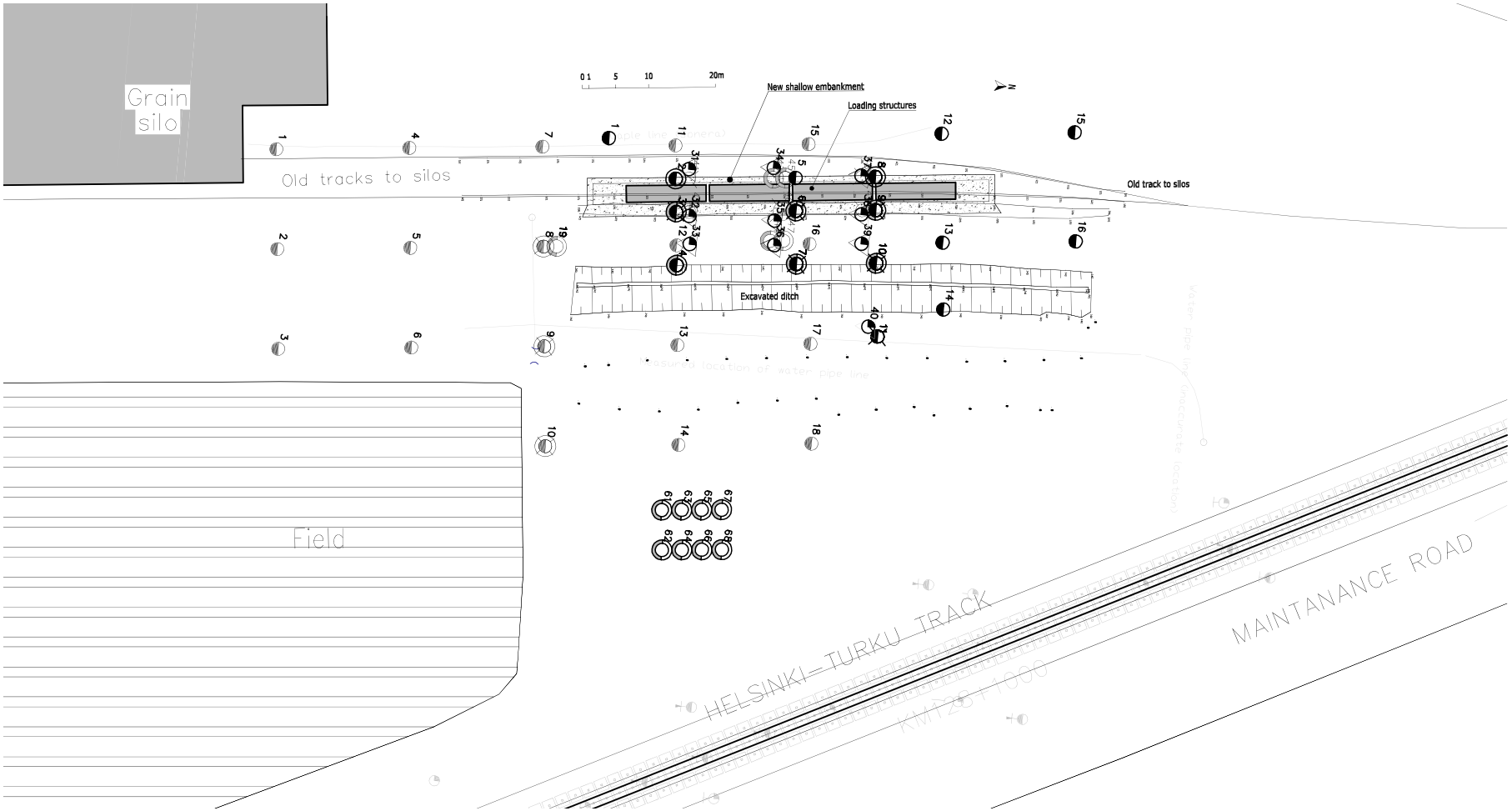
Grain silo
0 1 5 10 20m
New shallow embankment
Loading structures
N
Old tracks to silos
Old track to silos
Excavated ditch
Field
HELSINKI–TURKU TRACK
MAINTANANCE ROAD

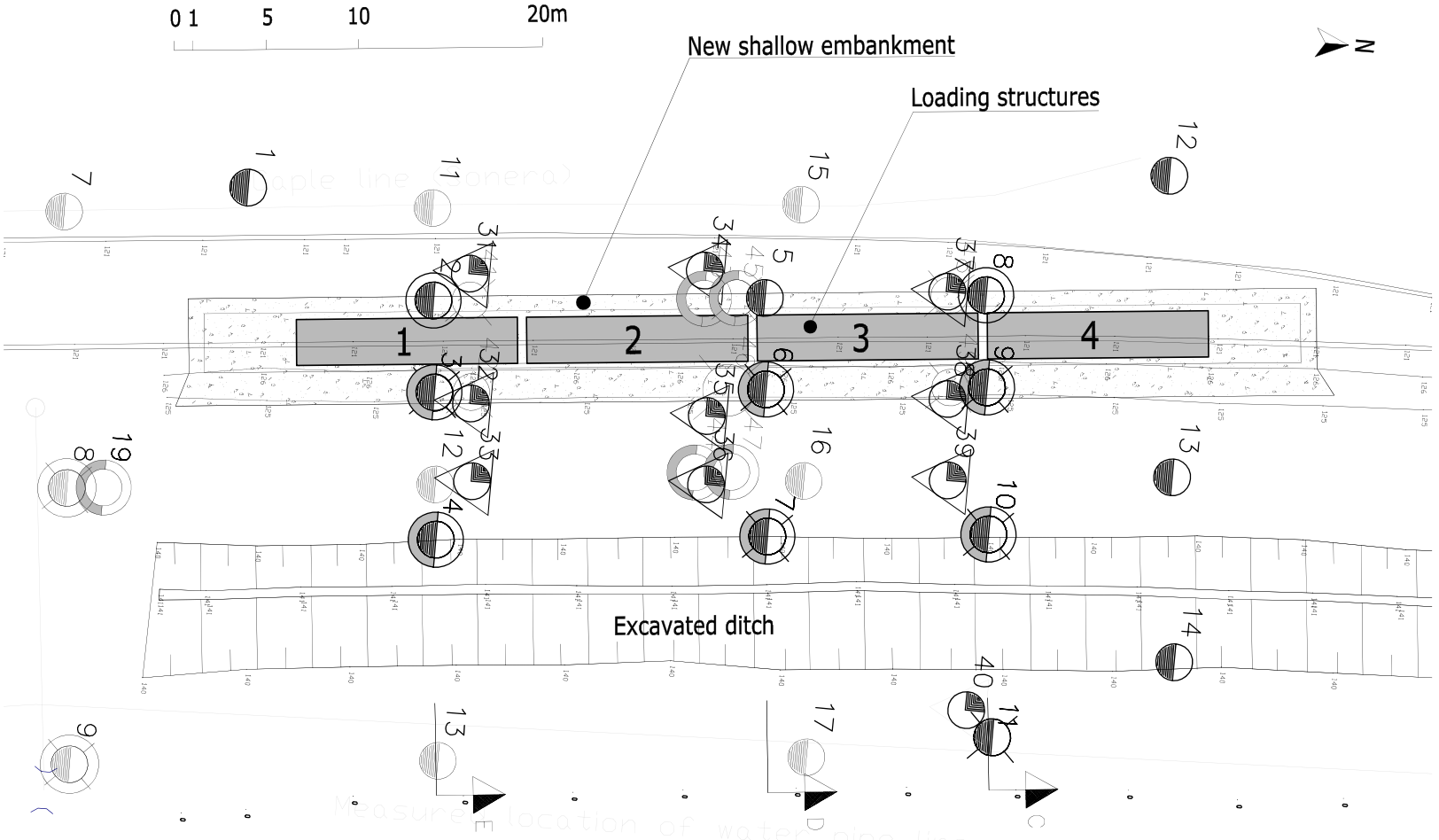
0 1 5 10 20m
New shallow embankment
Loading structures
N
1
2
3
4
Excavated ditch
A
B
C
D

Appendix 2

Plan view of the Perniö embankment and location of cross sections: A-A', B-B', C-C', D-D', E-E', F-F'.

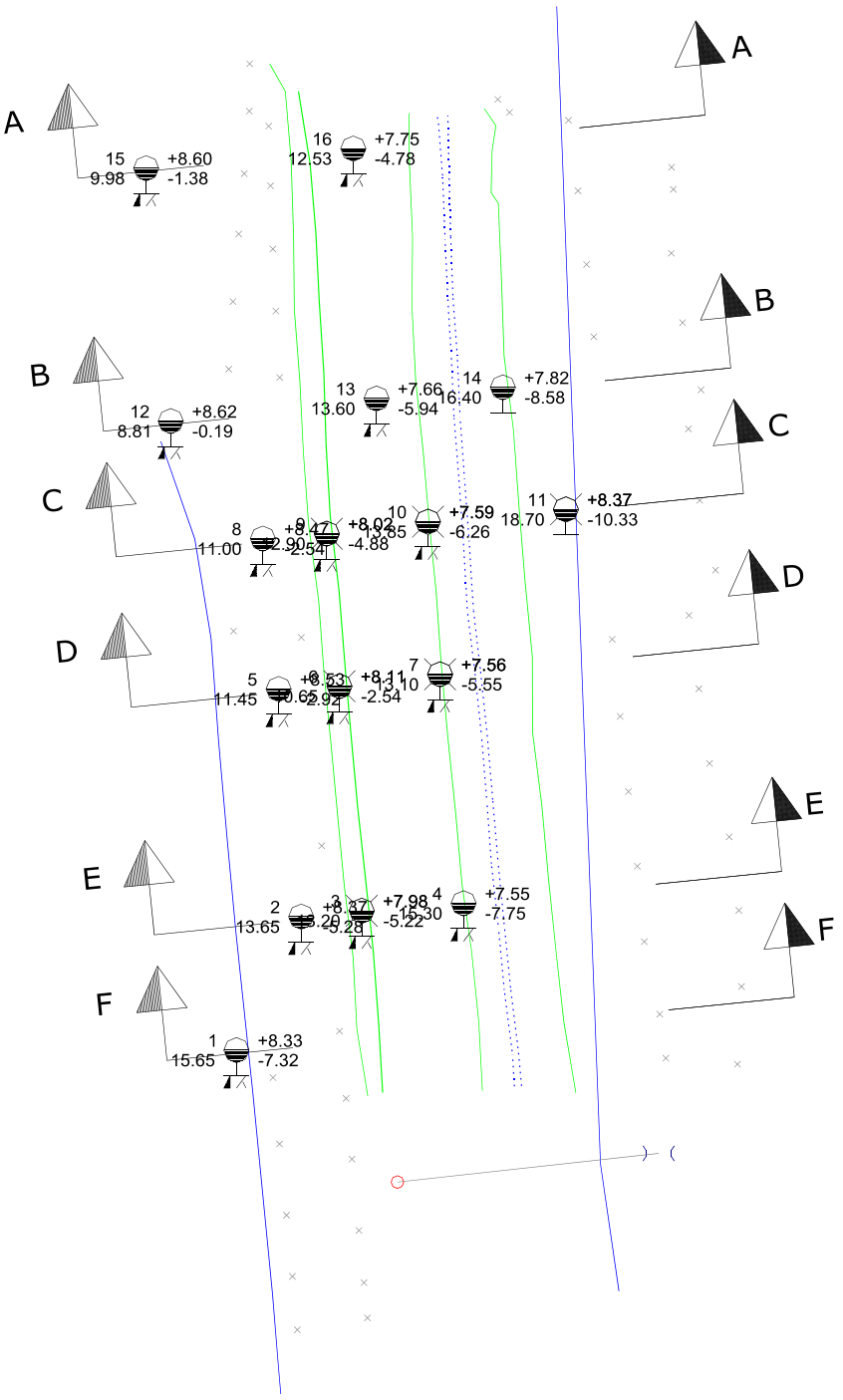
A
A
15
9.98
+8.60
-1.38
16
12.53
+7.75
-4.78
B
B
12
8.81
+8.62
-0.19
13
13.60
+7.66
-5.94
14
16.40
+7.82
-8.58
C
C
8
11.00
+8.47
-2.90
9
+8.02
-4.88
10
+7.59
-6.26
11
18.70
+8.37
-10.33
D
D
5
11.45
+8.53
-2.54
7
+7.56
-5.55
E
E
2
13.65
+8.37
-5.28
4
+7.55
-7.75
F
F
1
15.65
+8.33
-7.32

Appendix 3

Cross sections of the Perniö embankment: A-A', B-B', C-C', D-D', E-E', F-F'.

LEIKKAUS A - A
1:200/1:200

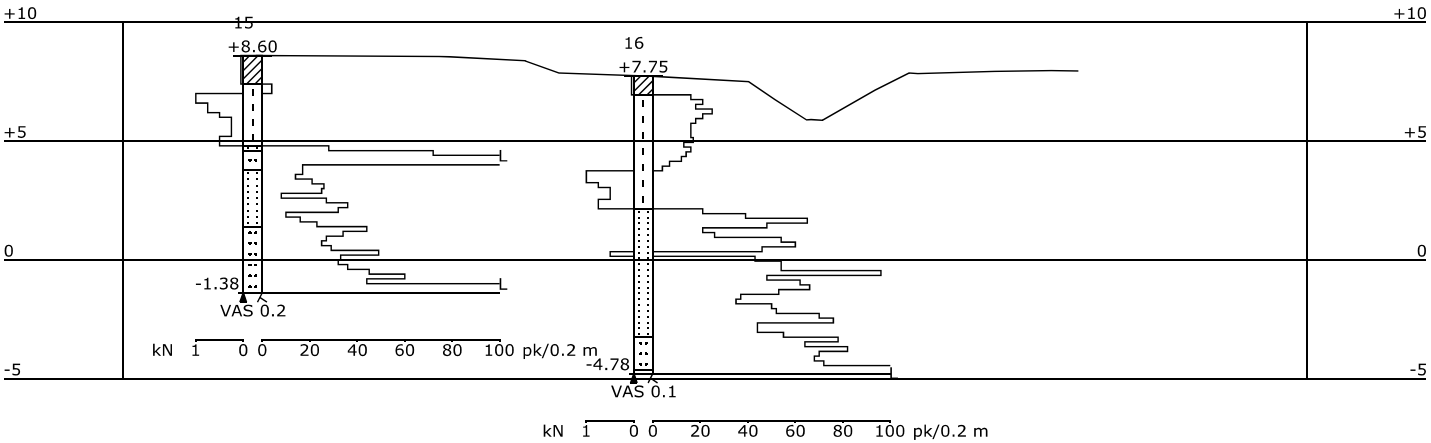

LEIKKAUS B - B
1:200/1:200

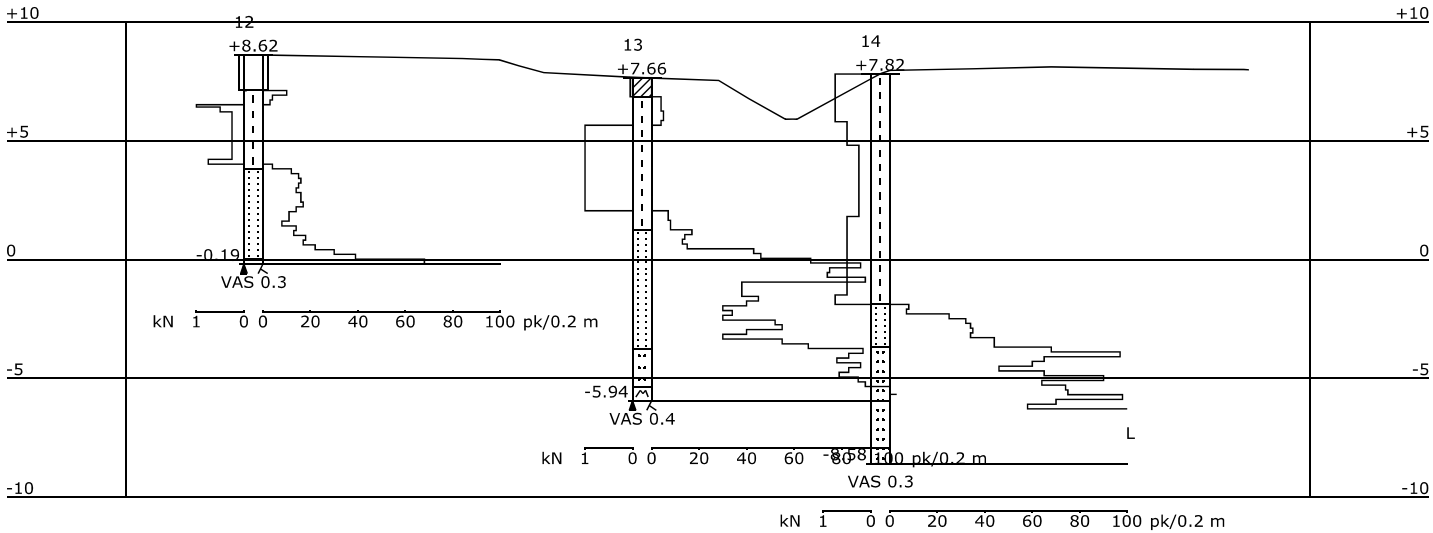

LEIKKAUS C - C
1:200/1:200

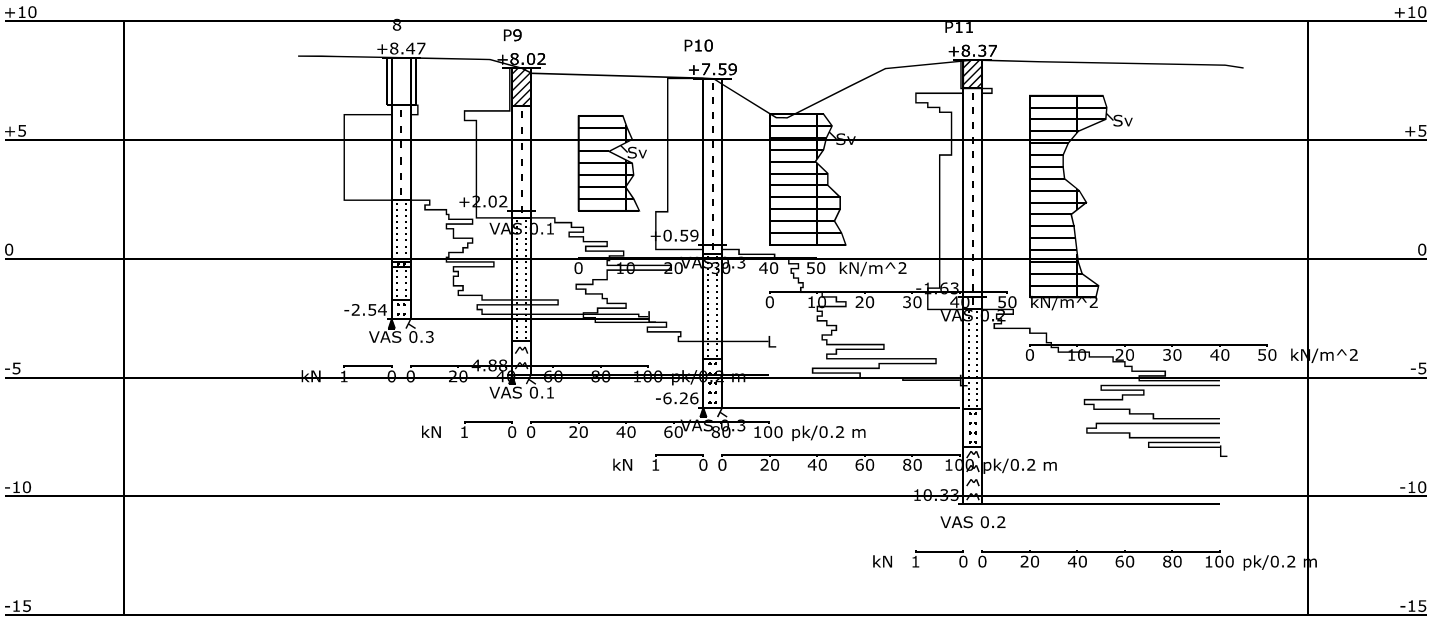

LEIKKAUS D - D
1:200/1:200

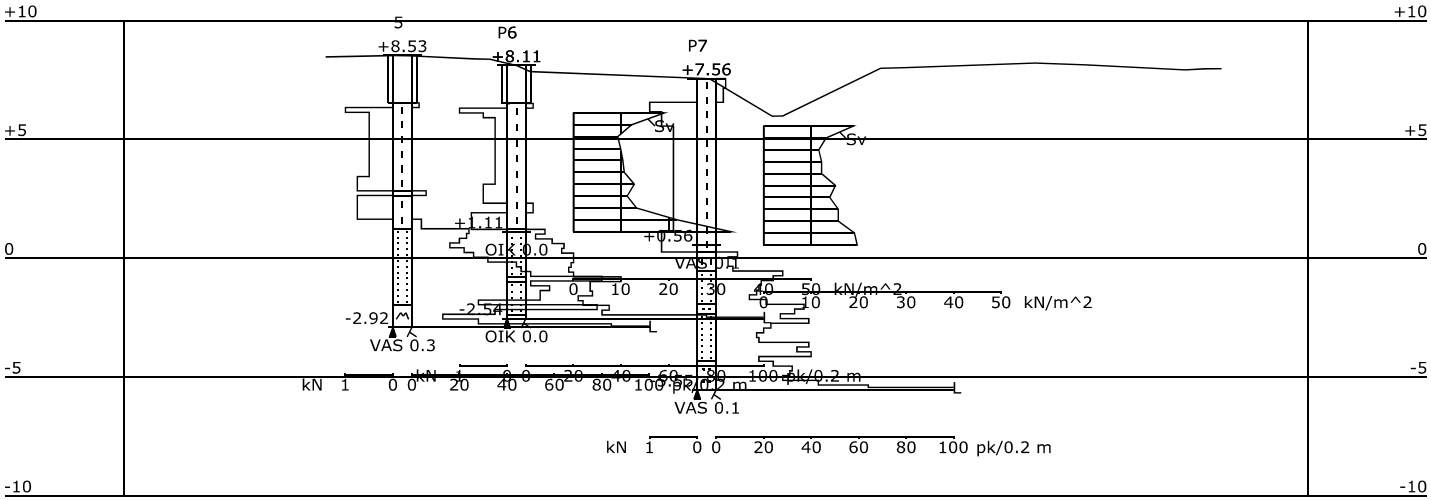

LEIKKAUS E - E
1:200/1:200

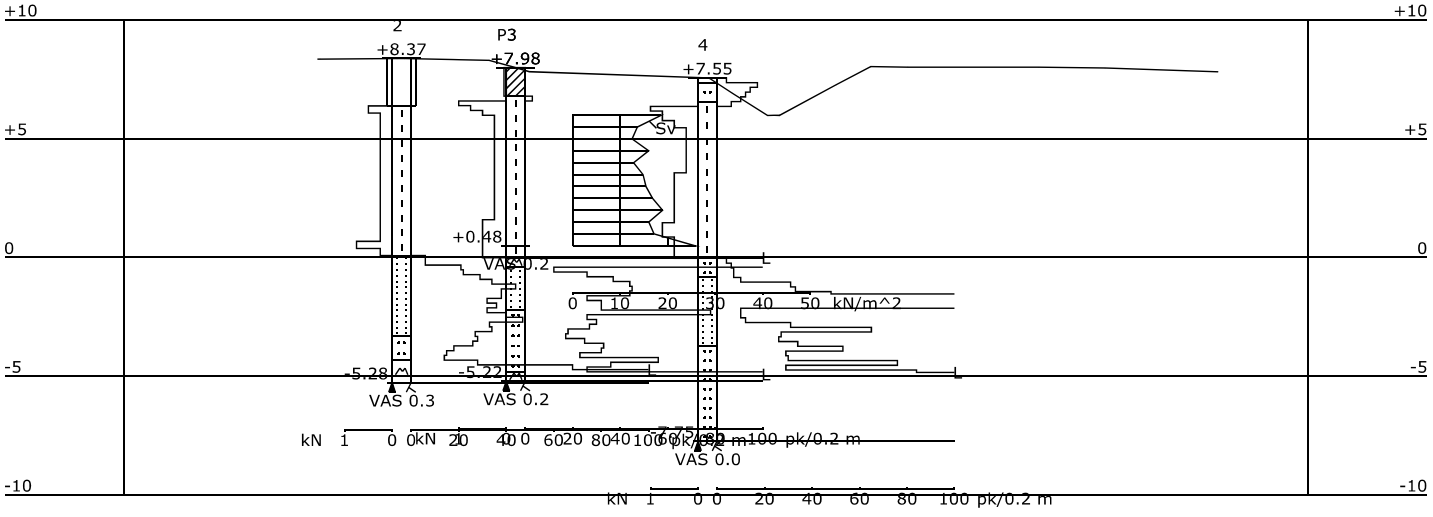

LEIKKAUS F - F
1:200/1:200

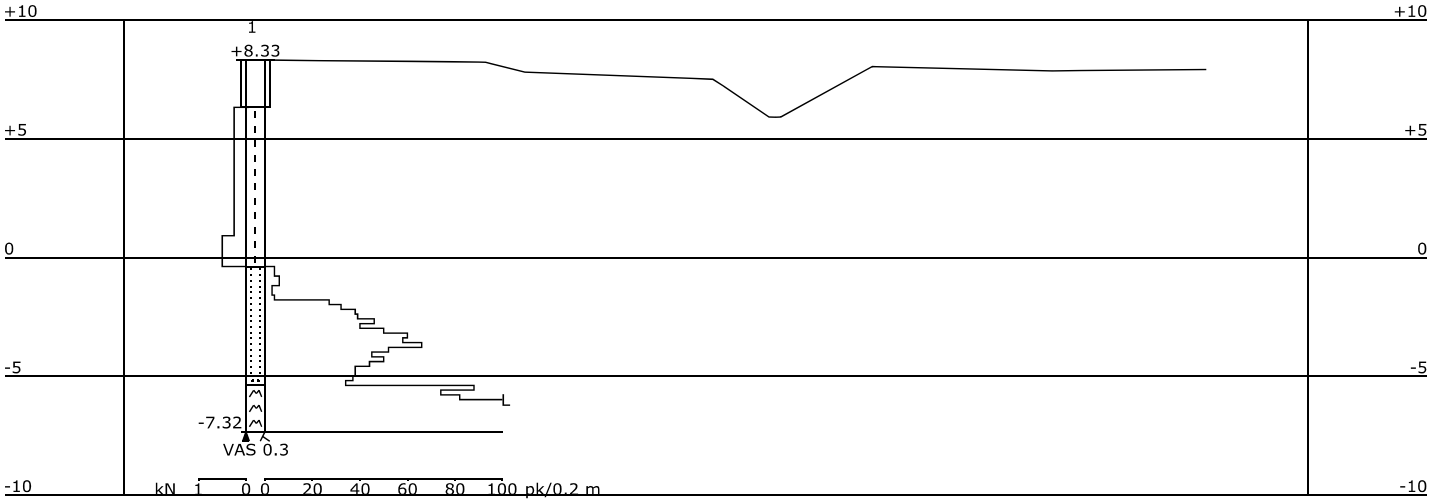

Appendix 4

GPS coordinates of the sampling profiles.

Perniö sampling research 17.-18. 09. 2009

Borehole coordinates S-2009

Borehole No.	x	y	z	Sampling method
43	6684560	2452071	8.530	NGI 54 mm
44	6684560	2452081	7.560	NGI 54 mm
45	6684562	2452071	8.530	NGI 54 mm
47	6684562	2452080	7.560	NGI 54 mm

Perniö sampling research 10.-16. 09. 2010

Borehole coordinates S-2010

Borehole No.	x	y	z	Sampling method
61	6684547	2452122	7.426	STII 50 mm
62	6684548	2452128	7.486	STII 50 mm
63	6684550	2452122	7.473	NGI 54 mm
64	6684551	2452128	7.502	NGI 54 mm
65	6684553	2452122	7.475	NGI 54 mm
66	6684554	2452128	7.505	NGI 54 mm
67	6684556	2452122	7.502	NGI 86 mm
68	6684557	2452127	7.470	NGI 86 mm

The thesis evaluates the effects of structure and rate dependency on the behavior of soft, sensitive clay. The comprehensive sampling and laboratory testing programmes on soft sensitive Perniö clay comprised of three sampling techniques and numerous advanced oedometer and triaxial tests on natural and reconstituted specimens, resulting in a unique experimental database. Experimental results were interpreted in terms of physical parameters enabling detailed evaluation of the key features of soft soil behavior.Based on experimental results on Perniö clay, creep and strain-rate characteristics in one-dimensional and triaxial test conditions are strongly related to sample disturbance and consolidation stress history. This is important to account for in any future sampling and testing programmes, in particular if the testing is aimed at improving advanced constitutive modelling of soft natural clays.

Aalto-DD 8/2016

ISBN 978-952-60-6617-2 (printed)
ISBN 978-952-60-6618-9 (pdf)
ISSN-L 1799-4934
ISSN 1799-4934 (printed)
ISSN 1799-4942 (pdf)

Aalto University
School of Engineering
Department of Civil Engineering
www.aalto.fi

BUSINESS + ECONOMY

ART + DESIGN + ARCHITECTURE

SCIENCE + TECHNOLOGY

CROSSOVER

DOCTORAL DISSERTATIONS